Genetically Encoded Discovery of Proteolytically Stable Macrocyclic Peptides

by

Ying Kit Jeffrey Wong

A thesis submitted in partial fulfillment of the requirements for the degree of

Doctor of Philosophy

Department of Chemistry
University of Alberta

Abstract

Phage display libraries bearing natural amino acids are commonly used for discovering potential therapeutic macrocycles; however, direct application of those linear peptides often leads to poor pharmacokinetics, including low serum stability, lower cell membrane permeability, and rapid renal clearance. Chemical macrocyclization of readily accessible phage display libraries can potentially improve the pharmacokinetic properties of peptides. In this thesis, I aim to expand the current chemical space of the phage displaying peptides with chemical post-translational modifications to discover bioactive ligands for therapeutically important proteins with modified phage display libraries.

In chapter 1, I briefly review the current state of the art in macrocyclization for peptide phage-displayed libraries. In Chapter 2, I develop a two-fold symmetric linchpin (**TSL**) that converts readily available phage-displayed peptide libraries made of 20 natural amino acids to genetically encoded bicyclic libraries. **TSL** combines an aldehyde-reactive group and two thiol-reactive groups by bridging two side chains of cysteine C with an N-terminal aldehyde group derived from an N-terminal serine S, yielding a novel bicyclic topology that lacks a free N-terminus. Phage display library of SXCX$_6$C sequences, where X is any amino acid but cysteine, were converted into a library of bicyclic **TSL**-SXCX$_6$C peptides in 45 ± 15% yield. Using this library and protein morphogen NODAL as a target, we discovered bicyclic macrocycles that specifically antagonize NODAL-induced signalling in cancer cells. At 10 μM concentration, two discovered bicyclic peptides completely suppressed NODAL-

induced phosphorylation of SMAD2 in P19 embryonic carcinoma cells. The **TSL**-SYCKRAHKNC bicycle inhibited NODAL-induced proliferation of NODAL-TYK-nu ovarian carcinoma cells with an apparent IC_{50} of 1 μM. The same bicycle at 10 μM concentration did not affect the growth of the control TYK-nu cells. **TSL**-bicycles remained stable over the course of the 72 hour-long assays in a serum-rich cell-culture medium. We further observed general stability in mouse serum and in a mixture of proteases (Pronase™) for 21 diverse bicyclic macrocycles of different ring sizes, amino acid sequences, and cross-linker geometries. **TSL**-constrained peptides to expand the previously reported repertoire of phage display bicyclic architectures formed by cross-linking cysteine side chains. We anticipate that the **TSL** will aid in the discovery of proteolytically stable bicyclic inhibitors for a variety of protein targets.

In Chapter 3, I describe discovery of a low molecular-weight, chemically modified macrocyclic peptide that binds to albumin with low micro-molar affinity for prolong circulation time. We modified SX_nCX_mC phage-displayed libraries, where X is any amino acid but cysteine, n = 1 and m = 3-5 amino acids, with decafluoro diphenylsulfone (**DFS**). Using these macrocyclic libraries and human serum albumin (HSA) as bait, we identified 8 macrocyclic peptides through three different discovery campaigns. The peptides were modified with **DFS** and a more stable linchpin pentafluorophenyl sulfide (**PFS**). The poly-fluorobenzene groups in the **DFS** and **PFS** modified peptides made it possible to a use ^{19}F NMR binding assay to determine and rank their bindings capacities. **PFS**-SICRFFC binds the strongest to HSA, and **PFS**-SICQGEC binds the

weakest to HSA. I determined the **PFS**-SICRFFC binds to HSA with an affinity of K_d = 6 μM via fluorescence polarization.

Preface

Chapter 1 of this thesis is part of an unpublished invited review entitled "Phage Display Macrocyclic Libraries." for *Chemical Reviews*. R. Derda and I co-wrote this review.

Chapter 2 of this thesis was published by Wong, J. Y.-K.; Mukherjee, R.; Miao, J.; Bilyk, O.; Triana, V.; Miskolzie, M.; Henninot, A.; Dwyer, J. J.; Kharchenko, S.; Iampolska, A.; Volochnyuk, D. M.; Lin, Y.-S.; Postovit, L.-M.; Derda, R., Genetically-encoded discovery of proteolytically stable bicyclic inhibitors for morphogen NODAL. *Chem. Sci.* **2021**, 12 (28), 9694–9703. I performed the experiments for phage modification and quantification, library screening, peptide synthesis and modification, cell-based validation experiments and proteolytic studies. I wrote the main manuscript with R. Derda's advice. R. Mukherjee designed and synthesized the **TSL** linchpins and performed proteolytic studies. V. Triana performed the phage modification and quantification partially. O Bilyk provided TYK-nu -NODAL and -GFP cell line. J Miao and Y.-S. Lin performed dynamic molecular simulations. M. Miskolzie performed the characterization of the **TSL**-modified peptides. S. Kharchenko, A. Iampolska and D. Volochnyuk optimized the scale-up **TSL**-peptide modifications. R. Derda, L.-M. Postovit, A Henninot and J. Dwyer contributed to the design of experiments. R. Derda conceived and designed the project and assisted in the preparation of the manuscript.

Chapter 3 of this thesis has not been submitted for publication. I designed and performed one screening campaign, analysis, ITC binding assay, ^{19}F NMR

binding assay, fluorescence polarization assay, and the *in vivo* experimental analysis. S. Kirberger and R. Qiu performed the ^{19}F NMR binding assay. E. Alvizo-Paez performed the screening campaign and the analysis. S. Kalhor-Monfared performed the **DFS** stability experiments. J Miao and Y.-S. Lin performed the dynamic molecular simulations. S. Sarkar performed the *in vivo* experiment. R. Derda, W. Pomerantz, and J. Dwyer contributed to the design of experiments.

Acknowledgments

The path to Ph.D. was full of surprises, despair, and joy. The journey would be difficult without my friends and families who supported and believed in me along the way.

I would like to express my deepest gratitude to my mother, Gloria F-K Wong, and my brother, Michael L-K Wong, who always believed in and supported me in all my journeys. I want to give my mother special thanks for all her hard work and sacrifice over the course of my early life to nurture and provide for me an excellent environment to explore and grow. I am forever in her debt.

I want to thank Prof. Ratmir Derda for being a great mentor throughout my undergraduate and Ph.D. studies. With his patience, support, trust, and guidance, I have overcome many complex challenges and obstacles during the numerous years under his supervision. I am grateful for the opportunities and training that he has provided me.

I am thankful to Prof. Todd Lowary and Prof. Robert Campbell for being my supervisory committee members and providing advice over the course of my Ph.D. studies. I would also like to thank Prof. Julianne Gibbs for being my arm's length examiner in my candidacy exam and thesis defense. I am grateful to Prof. Philip Dawson for taking time to be my external examiner.

The life of a Ph.D. student would be bland and dull if not for my dear friends: Vitor Cunha, Ryan Sweeney, Samantha Kwok and Wayne Vuong. I am

forever thankful for their friendships and inspirations; they have filled my life outside of my Ph.D. studies with great adventures and memories.

I want to thank the current and past Derda lab members, especially Mirat Sojitra, Yuki Kamijo, Nicholas Bennett, Arunika Ekanayake, Revathi Reddy, and Jessica Wickware, for all their advice and support inside and outside of the laboratory.

At last, I would like to thank the department of chemistry's fantastic support staff for all their assistance: Dr. Randy Whittal, Bela Reiz, Gareth Lambkin, Mark Miskolzie, Ryan Lewis and Michael Barteski.

Table of contents

List of figures

List of tables

List of abbreviations

AOB	aminooxy-biotin
BIA	biotin-PEG2-iodoacetamide
Boc	*tert*-butyloxycarbonyl
BODIPY	4,4-difluoro-4-bora-3a,4a-diaza-s-indacene
BSH	biotin-thiol
Calc	calculated
COSY	correlation spectroscopy
Da.	daltons(s)
DBMB	α,α′-Dibromo-m-xylene
DBU	1,8-Diaza-bicyclo (5.4.0) undec-7-en
DCM	dichloromethane
DFS	decafluoro diphenylsulfone
DMF	N, N-Dimethylformamide
EDT	1,2-ethanedithiol
eq.	equivalent(s)
ESI	electrospray ionization
h	hour(s)
HPLC	high performance liquid chromatography
HRMS	high-resolution mass spectrometry
HSA	human serum albumin
ITC	isothermal titration calorimetry
LC–MS	liquid chromatography mass spectrometry
MHz	megahertz
min	minute(s)
mL	milliliter(s)
mM	millimolar
mmol	millimoles
MSA	mouse serum albumin
MsCl	methanesulfonyl chloride

NMR	nuclear magnetic resonance
NOESY	nuclear overhauser effect spectroscopy
O/N	over night
PBS	phosphate buffered saline
PCR	polymerase chain reaction
PFS	pentafluorophenyl sulfide
ppm	parts per million
ROESY	rotating frame overhauser effect correlation spectroscopy
RSA	rat serum albumin
rt	room temperature
TBMB	1,3,5-Tris(bromomethyl)benzene
TBS	tris-buffered saline
TBST	tris-buffered saline, w. 0.1% Tween 20
TCEP	tris(2-carboxyethyl)phosphine)
TFA	trifluoroacetic acid
TIPS	triisopropylsilane
TLC	thin layer chromatography
TOCSY	total correlation spectroscopy
Tris	tris(hydroxymethyl)aminomethane
TSL	two fold symmetric tridentate lincpin
v/v	volume/volume

Chapter 1: Overview of genetically encoded peptides' architecture on M13 phage display libraries

1.1 Introduction:

Macrocycles derived from peptides have emerged as attractive, simple-to-synthesize molecular entities that can be employed to solve diverse problems in molecular recognition. Molecular recognition events can take place between the macrocyclic **ligand** and ground state molecular **receptors** such as: (i) individual atoms and ions; (ii) small organic and inorganic molecules; (iii) well-defined soluble macromolecules such as proteins, nucleic acids, and glycans; (iv) colloidal macromolecular assemblies such as protein aggregates, lipid membranes, and peptidoglycan polymers at the surface of bacteria cells and (v) solid interfaces, such as the surfaces of crystalline or amorphous solids and, the surfaces of organic and inorganic polymers. Interactions can also take place between macrocyclic ligands and transient receptors; an example of the latter are (i) macrocycles that interact with the transition state of a reaction and influence the rate or the outcome of chemical reactions and (ii) macrocycles that interact with the photoexcited state of a molecule and influence the photophysical outcome.[1]

Some molecular recognition problems listed above, such as the identification of a ligand for a metal ion, can be solved with molecules of both small (e.g., EDTA) and large molecular areas (e.g., metal-binding proteins). Other recognition problems mandate the use of molecules of large area; an

example is specific recognition of "hot spots" on the extended surface of a folded protein. In solving the latter recognition problems, macrocyclic topology is often quoted as "advantageous" when compared to linear or branched topologies.[2] The overarching physicochemical advantage of cyclic molecules is their depleted ground state conformational ensemble when compared to a conformational ensemble of linear or branched molecules with a similar number of atoms and of a similar molecular area. The depleted ensemble is the origin of the biophysical advantages such as high affinity and specificity of the interaction and the downstream practical advantages such as proteolytic stability and bioavailability. The depleted conformational state is one of the privileged properties of molecules in other fields such as catalysis and the design of macromolecular materials. Not all molecular recognition problems are suitable for molecules of macrocycles topology. For example, linear oligomers (e.g., DNA) are nature's best solution for the storage and transfer of hereditary information. Hyperbranched topologies, such as those observed in natural glycans, are employed in all kingdoms of life to solve self-versus non-self-recognition and other molecular recognition problems are not yet completely understood.

A general molecular recognition problem can be formulated as "find a macrocycle of a specific atomic composition that serves as a potent and specific ligand for a given receptor." Theoretically, a first-principal approach should be able to compute what type of atoms should be connected in what sequence to form a cycle that has the desired molecular shape with the desired properties. Peptide macrocycles made of well-defined amino acid building blocks make this

problem simpler and chemically tractable. One needs to find what amino acid building blocks should be connected in what sequence to form a cyclic or multi-cyclic topology. One of the experimental approaches that allow finding ligands for well-defined, stable molecular receptors by methods is known as *genetically-encoded macrocyclic peptide libraries*. This chapter focuses on a sub-set of such macrocyclic libraries displayed on bacteriophage particles and encoded in the genome of the bacteriophage.

1.2 Genetically encoded libraries: linking of genotype and phenotype

Figure 1-1 describes a prototypical phage-displayed, genetically-encoded macrocyclic peptide library. A particle of the bacterial virus, bacteriophage M13 is composed of a number of "coat" proteins, five pIII in the case of M13 (Figure 1-1A). A bacterial genome encodes these and a few additional genes/proteins. The genome is packaged inside the phage particle and protected by the coat proteins (Figure 1-1B). Introduction of the foreign DNA into the specific location of the gene *gIII* of the bacteriophage allows the production of phage particles that contain foreign amino acid sequences added to the sequence of protein pIII (Figure 1-1C). In these phage particles, the foreign peptide is "displayed" on the surface of the phage particle, and the composition of this peptide is "stored" in the DNA in the same phage particle. The structure of the peptide (phenotype) is linked to the sequence of the DNA (genotype) that is encoded.

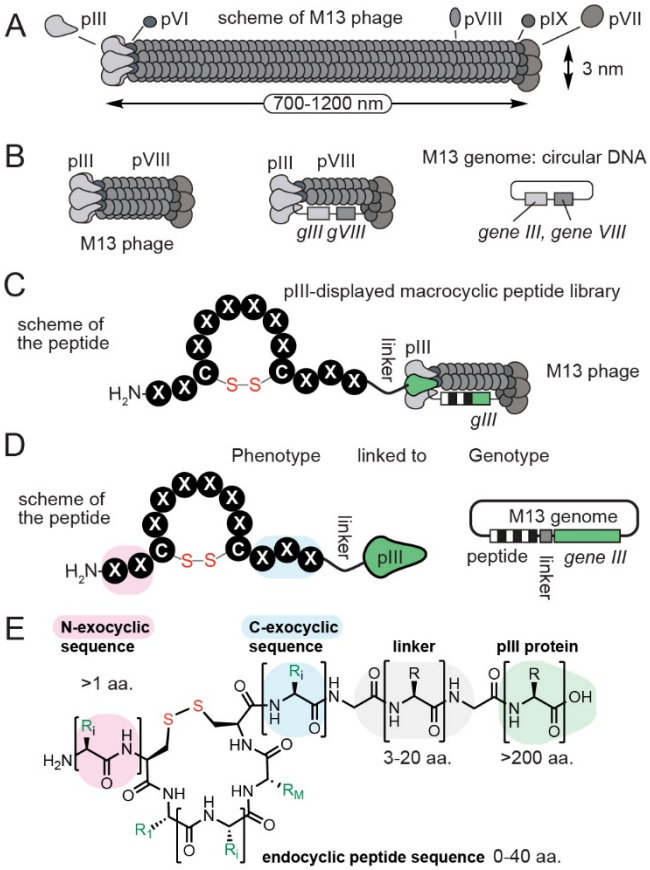

Figure 1-1. A typical phage display library. (A) Phage coat protein on the phage. (B) M13 phage PIII and PVIII displayed with phagemid. (C) A peptide expressed on the pIII phage protein with the *gIII* gene. (D) A structural representation of the pIII peptide expressed on the phage. (E) Chemical structure of the pIII peptide display.

As the foreign peptide sequence, an in-frame fusion to the sequence of naturally occurring protein, the structure and location of the peptide is defined unambiguously by the design of the DNA sequence (Figure 1-1D). I focus on displayed peptides with cysteine residues; for example, a peptide with one, two three or more disulfide bridges forming mono-, bi-, and tri-cyclic architectures (Figure 1E), as well as libraries in which natural disulfide bridges have been replaced, post-translationally by other linkages.

1.3 Library design

The physical library of DNA molecules is a critical starting point to generate any phage display library. These libraries have either synthetic or biological origins. DNA libraries of biological origin are produced by error prone PCR amplification from natural DNA or mRNA libraries.[3] In this review, we focus on peptide libraries that in nearly all cases, originate from synthetic DNA. Original phage display approaches were built on fully or partially randomized libraries created as a sequence of a mixture of nucleotides: N (A+T+C+G), K (G+T), S (G+C), W (A+T), or R(A+G).[4-7] An uniform mixture of pre-synthesized trinucleotide codons (TriNuc),[8] can yield higher quality libraries than those created by NNK or NNS codons; for example, the amino acids Ser is encoded by 6 NNK combinations and, Pro by 4 NNK combinations, whereas Trp is encoded by only NNK combination. In NNK-libraries, the ratio of the amino acids for Pro : Ser : Trp are 6:4:1, but in TriNuc libraries, the ratio is closer to 1:1:1.[9] The second critical step in the production of phage libraries is the integration of the synthetic DNA libraries into the genome of the bacteriophage. Techniques for such integration use ligation of PCR amplification,[10] or Kunkel mutagenesis[11]. The resulting DNA construct needs to be transformed into bacteria to allow the bacterial host to transcribe the phage components and package them into the virion. Although the first phage display vector was reported in 1985,[12] efficient production of diverse libraries was not possible. Chemical transformation of DNA into bacteria limited diversity of produced libraries to 10^5.[13] The invention

of a high-efficiency transformation protocol by electroporation in 1990 enabled large-scale, diverse phage display libraries.[14] Since then, electroporation has been ubiquitously used in the production of phage display libraries.

1.4 Phage display technology

Phage display library design involves the presentation of the peptides, the display carrier, the topology of the resulting peptides, the composition of the peptide libraries, and the diversity of the library. The phage display peptide is expressed as either the N or C-terminal fusion to the coat protein of the bacteriophage. Intra-protein presentation is also possible.[15] Genetic engineering technologies permit display on protein pIII,[15] truncated pIII, the N-terminus of pVIII, the C-terminus of pVIII,[16-18] pVII and pIX,[19-21] pIX,[22-23] of phage M13, protein X of T4,[24] protein 10 of T7, the tail protein of T7,[25-26] bacteriophage lambda,[27-32] bacteriophage P22,[33-35] bacteriophage MS22,[36-37] *bacillus thuringiensis* spores,[38] FliTrx random cyclic dodecapeptide,[39] and Novagen's T7 select phage display system. Phage-displayed peptides that are also displayed as fusion on constant proteins such as beta-lactamase.[40] Ligation of synthetic peptides to phage is also possible[41], and while such a system has no obvious advantage over the genetic display, such ligation has been used to display glycans[42] and protein oligomers.[43]

Exhaustive comparison of display platforms is beyond the scope of this chapter but for representative examples of comparison, consult Bradbury and co-workers who compare the expression of GFP on three different M13 proteins in

nine different display systems.[44] Line and co-workers, who compared the T7 and lambda display systems;[45-46] and as well as Makowski and Mori, who compared the M13 and T7 phage display system.[47]

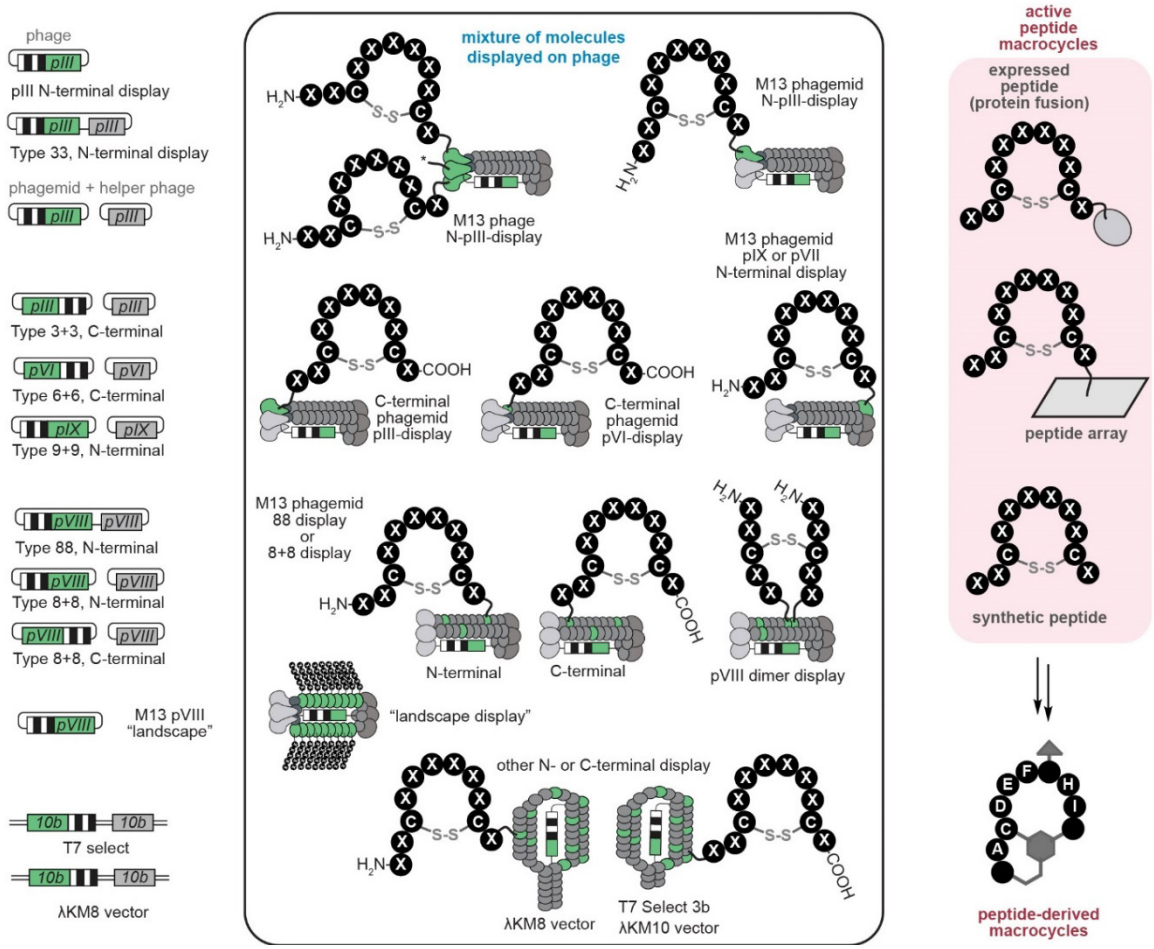

Figure 1-2. Types of display system on M13 phage.

Valency of the display is important: the carrier can display exactly one copy (monovalent display) or multiple copies (multivalent display). *Bonafide* monovalent display is simple to achieve in mRNA and DNA-display technologies where the information carrier has only one attachment point. In phage display technologies, the copy number of phage proteins on which the

peptide is displayed is always greater than one. Thus, many phage display platforms are multivalent displays. Monovalent display on phage carrier can be achieved by "mosaic display" technology dubbed by Smith and others as "X+X systems", where X is the identity of the protein on which the library is displayed (Figure 1-2).[48] In the 3+3, 6+6 or 8+8 systems, the virion contains the pIII, pVI or pVIII proteins both with and without the fusion polypeptide. For example, simultaneous expression of the pIII protein and the pIII-peptide gives rise to a low copy number display. In a typical display, 90% of the particles contain no displayed peptide and 10% of the particles display one or more copies.[48] Such a 3+3 system is considered monovalent because the probability of displaying two or more copies is low. Proteolytic cleavage of peptides, either natural or introduced artificially, also reduces the copy number of the displayed polypeptides. For example, the copy number in the M13 phage of proteins pIII is 3-5, but the copy number of displayed peptides can be significantly lower than 3. The proteolysis of peptides depends on the length, the charge and the sequence of the peptide.[49]

1.5 Macrocyclic architectures displayed on phage carriers

In 1996 the first comprehensive report of peptide libraries by Burrit et al[50] reported 23 peptide libraries in nine different vectors displayed on pIII: fUSE5, fAFF1, M13LP67, M13KBst, MKTN, m666, M13PL-6 and on pVIII proteins in vector PC89 and fdH.[50] In 1997, a comprehensive review by Smith and Petrenko

quoted the production of 60 peptide libraries and 50 protein display libraries displayed on phage.[48]

After many years, the true number of libraries produced worldwide is difficult to estimate; however, an estimate can be assessed from the BioPanning Database: 517 peptide library types, 3000 peptides in 1600 entries. In this chapter, I am focused on covalently cyclized macrocyclic libraries displayed on phage. To the best of our knowledge, all cyclic libraries formed spontaneously during their expression in bacteria are formed through a disulfide bond. Another class of libraries is diversified after their expression via chemical post-translational modifications (cPTM) with a synthetic cross-linker called "linchpin." Linchpins are commonly used to constrain the secondary structure or introduce unnatural properties not found in natural amino acids, such as light responsiveness or additional biorthogonal functionalities.[51] All monocyclic libraries with two cysteines can be abbreviated as $X_n\underline{C}X_m\underline{C}X_l$, where *n*, *m* and *l* are integers. To date, 48 diverse architectures are represented by 48 unique combinations of [*n*, *m*, *l*] (section 1.5.3). Libraries with four cysteines $X_n\underline{C}X_m\underline{C}X_l\underline{C}X_k\underline{C}X_i$, are known as well, but the published diversity of the architectures is limited (section1.5.5). Libraries with a larger even number of cysteines are theoretically possible to produce but are limited (section 1.5.5). Libraries with odd numbers of cysteines can also form libraries, but one of the cysteines forms a disulfide bond with external thiols. For example, libraries with three cysteines, $X_n\underline{C}X_m\underline{C}X_l\underline{C}X_k$ has been expressed for a diverse number of [*n*, *m*, *l*, *k*] combinations (section 1.5.8).

1.5.1 Phage displaying linear peptides: X_n

The most widely used phage display library is expressed with linear peptide: X_n, where X can be any amino acid and n = 3-30 amino acids. Although the libraries are often referred to as the library of "linear motifs," the presence of cysteine makes it possible to find disulfide macrocycles that are expressed as part of the library. If selection pressure can enrich disulfide cyclized peptides, such cyclic peptides can commonly be discovered from a "linear" library.

For example, Ruoslathi and co-workers used a X_6 library and integrin $\alpha_V\beta_3$ as bait to identify disulfide constrained peptide sequence: CRGDCA. They identified a sequence bound to $\alpha_V\beta_3$ with an IC_{50} of 10 μM.[52] Patthy and co-workers used an X_{15} library and fibronectin type II modules of matrix metalloproteinase 2 as bait.[53] Panning selected the peptide sequence: ACGYTYHPPCARLTV. Unfortunately, Patthy and co-workers were unable to validate the bio-activity of the peptide due to poor solubility.[53] Wang and co-worker used an X_{15} library and monoclonal antibody that recognized the antimicrotubular phomopsin mycotoxin as bait. They isolated a cyclic motif of CVALC with the sequences of CTVALCNMYFGAKLD as the strongest binder.[54] Kopeček and co-workers used the X_{15} library selected against the CD21 receptor, and selected to 2 different ring sizes of disulfide cyclized peptides: One with 4 amino acids: PNLDFSPTCSFRFGC and one with 8 amino acids RLAYWCFSGLFLLVC.[55]

1.5.2 Phage displaying peptides that contain one cysteine: X_nCX_m

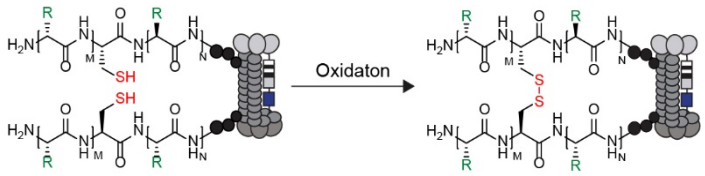

Figure 1-3. A representative example of a peptide with X_nCX_m motif expressed on M13 phage display.

The display of a linear peptide with a single cysteine, X_nCX_m, on the phage is possible.[56] The linear peptide dimerized with a neighboring peptide resulting in a macrocycle. These peptide architectures are expressed on the pVIII or pIII of the M13 phage (Figure 1-3). Scott and co-workers displayed the peptide libraries with X_8CX_8, $X_{15}CX$ and XCX_{15} motif on the phage pVIII protein.[56] Their libraries were shared with other researchers and screened against anti-HIV-1 gp120 monoclonal anti-body[57], malarial antigen antibody[58], carbohydrate-binding antibodies[59-60], anti- *T. saginata* antibody[61], anti-African horse sickness virus serotype 3 antibody[62] and injured vascular endothelial cells[63].

Recently, Kay and co-workers expressed a phage display library with the architecture of X_8CX_2 and $X_{10}C$ on the pIII proteins.[64] The macrocyclic libraries were subsequently screened against human factor H[65] and *Streptococcus pneumoniae*'s Ser/Thr kinases.[66]

1.5.3 Phage displaying peptides that contain two cysteines: $X_nCX_mCX_l$

The monocyclic, $X_nCX_mCX_l$, peptide phage displayed libraries are commonly expressed. As phage proteins assemble in the periplasm, the displayed cysteines are oxidized and form a disulfide bond. The amino acid is X_m where X

is any natural amino acid, but cysteine and *m* is any number of random amino acids from 1 to 15. Table 1-1 to Table 1-13 highlights phage display libraries with different ring sizes used in panning. The 48 various motif libraries were either expressed on the pVIII or pIII protein.

Table 1-1. Table of phage display libraries with X_nCXCX_l

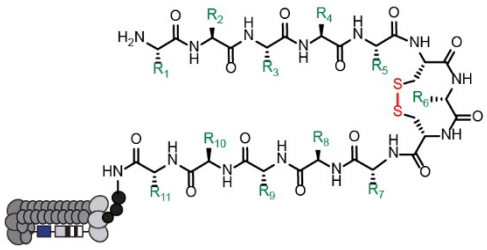

Motifs	Length (ref. #)
XXXXXCXCXXXXX	13 (ref. [67])

Table 1-2. Table of phage display libraries with $X_nCX_2CX_l$

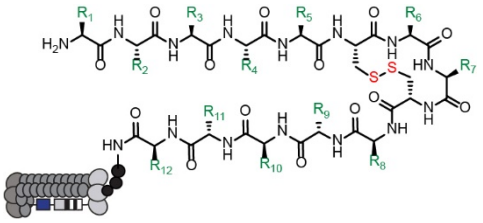

Motifs	Length (ref. #)
XXCXXCXX	8 (ref.[68])
XXXXXCXXCXXXXXX	14 (ref. [69-70])

Table 1-3. Table of phage display libraries with $X_nCX_3CX_l$

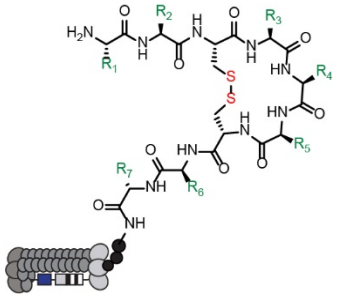

Motifs	Length (ref. #)
XXCXXXCXX	9 (ref. [7, 68, 71])
XXXCRGDCXXX	11 (ref. [72])
DGXXXCRGDCXXX	12 (ref. [72])
XXXXXCXXXCXXXX	14 (ref. [70])

Table 1-4. Table of phage display libraries with $X_nCX_4CX_l$

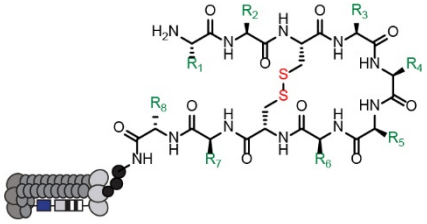

Motifs	Length (ref. #)
CXXXXC	6 (ref. [73-74])
XCXXXXCX	8 (ref. [75-76])
XXCXXXXCX	9 (ref. [77])
XXCXXXXCXX	10 (ref. [78])
XXXCXXXXCXXX	12 (ref. [79])
XXXXCXXXXCXXXX	14 (ref. [60, 80-81])
XXXXCXXXXCXXXXX	15 (ref. [70, 82])

Table 1-5. Table of phage display libraries with $X_nCX_5CX_l$

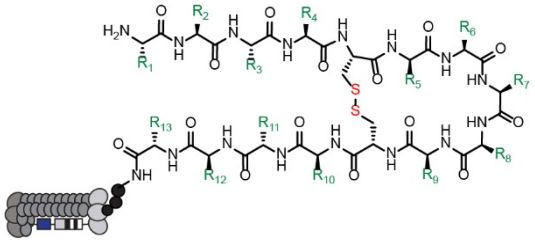

Motifs	Length (ref. [#])
CXXXXXC	7 (ref. [74, 83-87])
XCXXXXXCX	9 (ref. [88-89])
AXCXXXXXCX	10 (ref. [90])
XXCXXXXXCXX	12 (ref. [88])
XXXXCXXXXXCXXXX	15 (ref. [91-92])
XXXXXXCXXXXXCXXXXX	18 (ref. [93])

Table 1-6. Table of phage display libraries with $X_nCX_6CX_l$

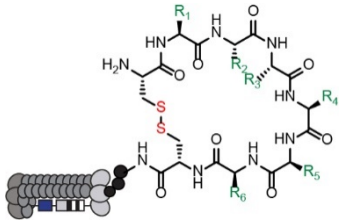

Motifs	Length (ref. [#])
CXXXXXXC	8 (ref. [47, 74, 77, 83-87, 94-112])
XCXXXXXXCX	10 (ref. [60, 70, 75])
XXCXXXXXXCXX	12 (ref. [7, 113])
XXXXCXXXXXXCXXXX	16 (ref. [70, 114-121])

Table 1-7. Table of phage display libraries with $X_nCX_7CX_l$

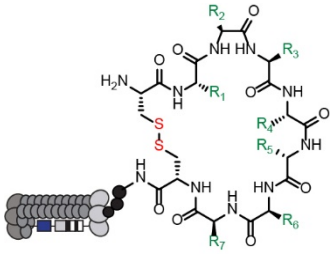

Motifs	Length (ref. [#])
CXXXXXXXC	9 (ref. [71, 77-81,122-130])
ACXXXXXXXC	10 (ref. [89, 131])
XXCXXXXXXXCXX	13 (ref. [132-133])
XXXCXXXXXXXCXXX	15 (ref. [134])

Table 1-8. Table of phage display libraries with $X_nCX_8CX_l$

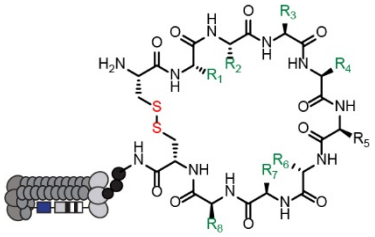

Motifs	Length (ref. [#])
CXXXXXXXXC	10 (ref. [135-147])
XCXXXXXXXXCX	12 (ref. [60, 148-156])
XXCXXXXXXXXCXX	14 (ref. [157])
XXXCXXXXXXXXCXXX	16 (ref. [79, 158-159])
XXXXXCXXXXXXXXCXXXXX	20 (ref. [7])

Table 1-9. Table of phage display libraries with $X_nCX_9CX_l$

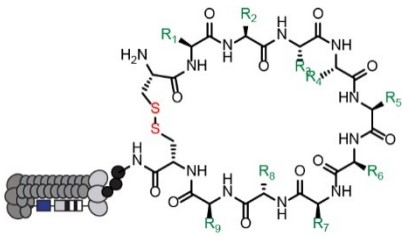

Motifs	Length (ref. [#])
CXXXXXXXXXC	11 (ref. [160-164])
XXXXXCXXXXXXXXXCXXXX	20 (ref. [7, 68])

Table 1-10. Table of phage display libraries with $X_n\underline{C}X_{10}\underline{C}X_l$

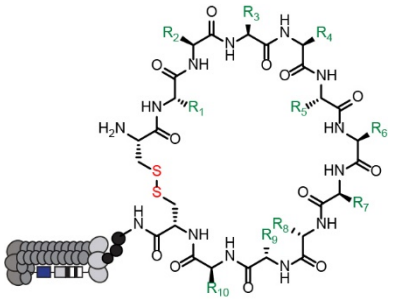

Motifs	Length (ref. [#])
CXXXXXXXXXXC	12 (ref. [110, 147-148, 165-180])
XXCXXXXXXXXXXCXX	16 (ref. [7])
XXXCXXXXXXXXXXCXXX	18 (ref. [79])
XXXXCXXXXXXXXXXCXXXX	20 (ref. [181-182])

Table 1-11. Table of phage display libraries with $X_n\underline{C}X_{12}\underline{C}X_l$

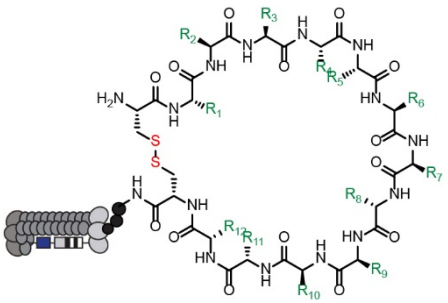

Motifs	Length (ref. [#])
CXXXXXXXXXXXXC	14 (ref. [57, 183-185])
XXXCXXXXXXXXXXXXCXXX	20 (ref. [186])

Table 1-12. Table of phage display libraries with $X_nCX_{13}CX_l$

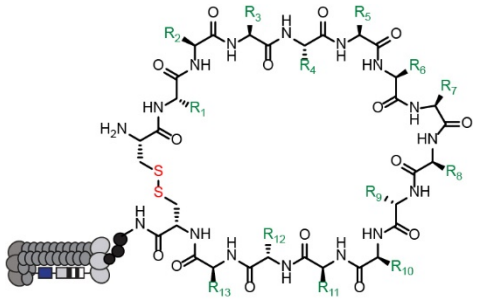

Motifs	Length (ref. #)
CXXXXXXXXXXXXXXC	16 (ref. [136])
XXXCXXXXXXXXXXXXXXCXXX	22 (ref. [86, 187-188])

Table 1-13. Table of phage display libraries with $X_nCX_{15}CX_l$

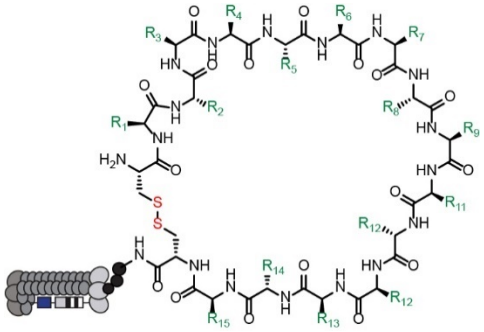

Motifs	Length (ref. #)
CXXXXXXXXXXXXXXXC	17 (ref. [136, 189-191])

1.5.4 Phage displaying peptides that contain three cysteines: $X_nCX_mCX_lCX_k$

Phage displayed libraries can express peptides containing 3 cysteines; however, those libraries were intended for post-translational modification with a linchpin to from bicycles.[192] More detailed discussion of the modified tri-cysteines phage displayed libraries can be found in the section: 1.5.8.

1.5.5 Phage displaying peptides that contain four cysteines or more

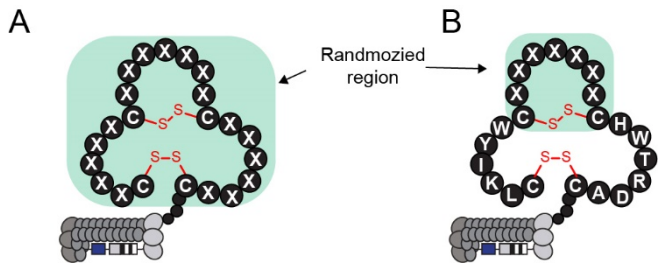

Figure 1-4. A representative model of a peptide with 4 or more cysteine motifs expressed on M13 phage display. (A) The peptide displayed on the phage is all randomized except cysteine. (B) A selected region of the displayed peptide is randomized on the phage.

A phage display library with more than 4 cysteines or disulfide-rich peptides is typically employed for creating serum stable bioactive peptides and small proteins. Typically, there are two architectures to display peptides that contain 4 or more cysteine: i) all the amino acids in the rings are randomized for *de novo* discovery (Figure 1-4A) or ii) only one or two rings' amino acids are randomized (Figure 1-4B).

Ruoslathi and co-workers expressed bicycles phage displayed libraries that contains 4 cysteines. Their phage libraries contain $\underline{C}X_3\underline{C}X_3\underline{C}X_3\underline{C}$ and $\underline{C}X_3\underline{C}X_4\underline{C}X_2\underline{C}$ motif to identify peptide ligands with prostate-specific antigen[166], solid breast tumor[90] and *in vivo* vascular endothelium.[77] The most noticeable work from Ruoslathi and co-workers was used the $\underline{C}X_3\underline{C}X_3\underline{C}X_3\underline{C}$ peptide motif on the phage and screened against solid tumors. They discovered that the peptide CNGRCVSGCAGRC showed tumor selectivity and identified the motif CNGRC for cancer therapeutics.[90]

In a recent example, Klok and co-workers displayed bicycles libraries with X$\underline{C}$X$_n$$\underline{C}X_l$$\underline{C}X_k$$\underline{C}$X motif ($n$ + l +k = 3, 4, 5, 6, 7 or 8; where X indicates random amino acids expect cysteine) on phage and to identify ice-binding peptides. They selected a peptide K$\underline{CC}$TKN$\underline{C}$DSTAH$\underline{C}$T that showed to have ice recrystallization inhibition activities.[193]

Wu and co-workers displayed $\underline{C}$X$\underline{C}$X$_5$$\underline{C}X_5$$\underline{C}$ peptides on phage's pIII protein. They used the library to screen against Kelch-like ECH-associated protein 1 and identified G$\underline{C}$G$\underline{C}$AGWRD$\underline{C}$ESGER$\underline{C}$ as the most potent binder. Through a fluorescence polarization competition assay, one of the isomers exhibited an inhibition activity with K_i of 0.36 μM, and the other isomer exhibited weak binding affinity with K_i of 37.2 μM.[194]

One of the drawbacks of expressing a peptide library containing multiple cysteines in the peptide is multiple regional isomers. The numerous regioisomers create a laborious follow-up in the validation and increase the difficulty of the peptide synthesis to isolate the bioactive isomer. Wu and co-workers expressed a tri-cyclic peptide library with six cysteines on the phage to control the disulfide crosslinking: $\underline{C}$PP$\underline{C}$X$_5$$\underline{C}X_5$$\underline{C}X_5$$\underline{C}PP\underline{C}$. The expression of the $\underline{C}$PP$\underline{C}$ motif guides the disulfide pairing to a predictable conformation and reduces the number of regioisomers displayed on the phage or during synthesis and validations.[195]

Researchers used known small proteins containing four or more cysteines to engineer and design small proteins. The whole protein or part of the protein was expressed on the phage surface. Only some of the protein sequences were randomized to engineer a stronger binder or a better inhibitor.[196]

Hudson and co-workers expressed the Min-23 protein, a small four cysteine-stabilized peptide scaffold on the phage. Min-23 is included with random decameric amino acid ring: LMRCKQDSDCLAGSVCX_{10}FC.[197] Later, a similar approach was used by Haberkorn and co-worker to express LMRCKQDSDCLAGSVCX_8FC on the phage; they were able to select the delta-like-ligand 4 binder, LMRCKQDSDCLAGSVCLFHLFIYIFC with a K_d of 22 nM.[198]

1.5.6 Chemical post-translational modification with peptide displayed on phage that contains one cysteine: X_nCX_m

Post-translation medication of

Most linchpins rely on crosslinking two or more cysteines expressed on the phage. The chemistry was limited to bio-orthogonal and thiol related chemistry. To cyclize peptide containing a single cysteine, researchers have used two bio-orthogonal site-specific reactions to cyclize the peptide or displayed the peptide containing an unnatural amino acid on the phage that consumed the free thiol to cyclize it (Section 1.5.10).[199-200]

In a recent example, Mayer and co-workers used linchpins that relied on a cysteine and the N-terminal amine to create head-to-tail macrocycles (Figure 1-5). The asymmetric linchpins contain two reactive groups: i) a reactive thiol group for cysteine and ii) an aldehyde group for the N-terminal amine to create head-to-tail architecture. The advantage of 2 different bio-orthogonal reactive groups on the asymmetric linchpins were to avoid creating 2 regioisomers. They used three different asymmetric linchpins to modify the unprotected sulfide-

peptide to a head-to-tail macrocyclic peptide. They modified a monoclonal peptide displayed on phage with the three asymmetric linchpins into the head to tail macrocycle (Figure 1-5).[201]

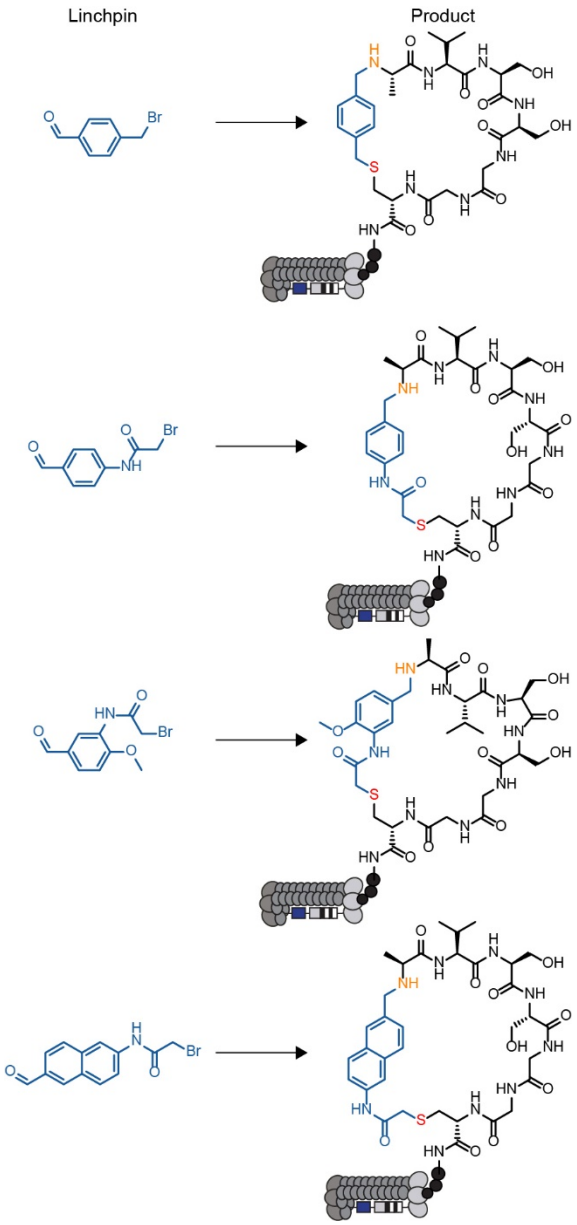

Figure 1-5. Asymmetric linchpins modified AVSSGGC peptide displayed on phage.

1.5.7 Chemical post-translational modification with phage display libraries that contain two cysteines: $X_nCX_mCX_l$

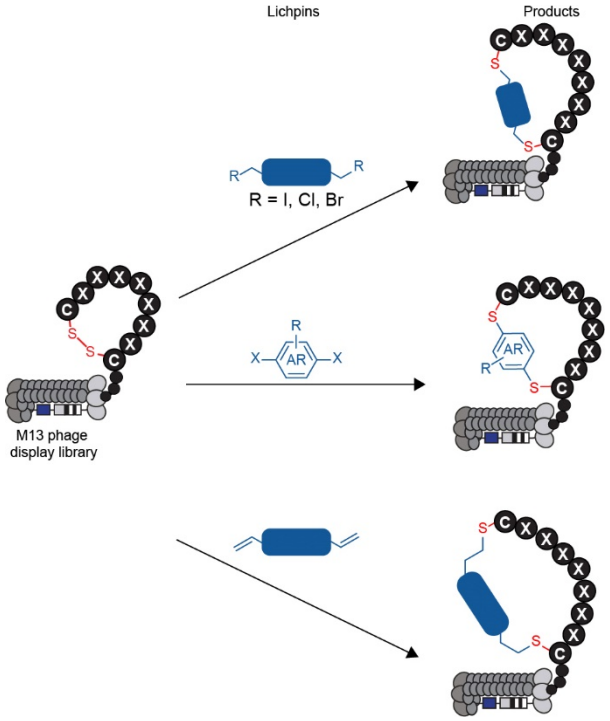

Figure 1-6. Type of reactions for modifying disulfide phage displayed library.

The chemical modification of disulfide phage-displayed libraries is an attractive strategy because reactive thiol linchpins are known for stapling peptides or proteins.[202] Those linchpins are readily available to modified disulfide peptides phage library to generate billions of unique macrocycles simultaneously via S_N2 reaction, S_NAr reaction or Michael addition (Figure 1-6).[202] Most linchpins mimic disulfide bond to constrain the peptide and are not susceptible to reduction and exchange. Replacing disulfide bonds with a linchpin can preserve the activity of the peptides and enhance the peptides' pharmacokinetics, such as

by increasing resistance to enzymatic hydrolysis, cell membranes permeability, or penetration of the blood-brain barrier.[203-209]

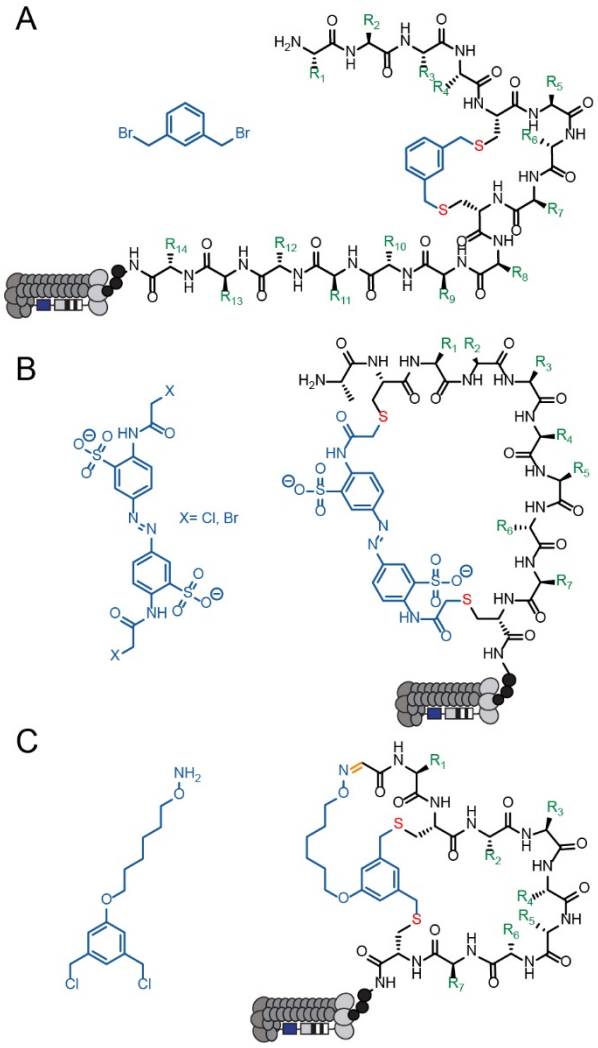

Figure 1-7. Linchpins that exploit the S_N2 reaction to staple disulfide peptides phage-displayed library.

Stapling peptides via S_N2 reaction is fast and selective between cysteine and a halo-acetamide or halo-benzyl linchpin. An example of a linchpin that uses an S_N2 reaction is **DBMB**. Initially, **DBMB** was developed by Timmerman and co-workers to stabilize proteins and short peptides.[210] Later, Heinis and co-

workers adopted the same linchpin for installation onto a disulfide peptide phage-displayed library to generate α-helical peptides (Figure 1-7A).[211]

A linchpin with azobenzene functionalization was used to modify phage display libraries. Two variants of the azobenzene linchpin have been published. Heinis and co-workers used the azobenzene with a bromo-acetamide group (**BSBBA**) to modify the phage display library and streptavidin as bait. They identified a ligand that was actively bound to streptavidin as the *cis* isomer and had reduced activity as the *trans* isomer.[89] In a similar fashion, Derda and co-workers used an azobenzene with a chloro-acetamide group (**BSBCA**) to modify a A$\underline{C}X_7\underline{C}$ phage-displayed library and streptavidin as bait to identify a light-responsive ligand. The identified ligand was active as the *trans* isomer and inactive as the *cis* isomer (Figure 1-7B).[212]

In Chapter 2, I functionalized a disulfide phage displayed library with the motif SX$\underline{C}X_6\underline{C}$ and a linchpin containing a chlorobenzyl group to react with cysteines to bicycles. The library was used to screen an oncogenic morphogen NODAL and result in a 1-10 μM bicyclic peptide that could disrupt the NODAL signaling pathway (Figure 1-7C).[213]

Linchpins can cyclize disulfide peptides and add a bio-orthogonal functional group on a natural express peptide to bypass the need for unnatural amino acid incorporation. This technique has proven to be a powerful tool for fragment-based discovery with known pharmacophores.

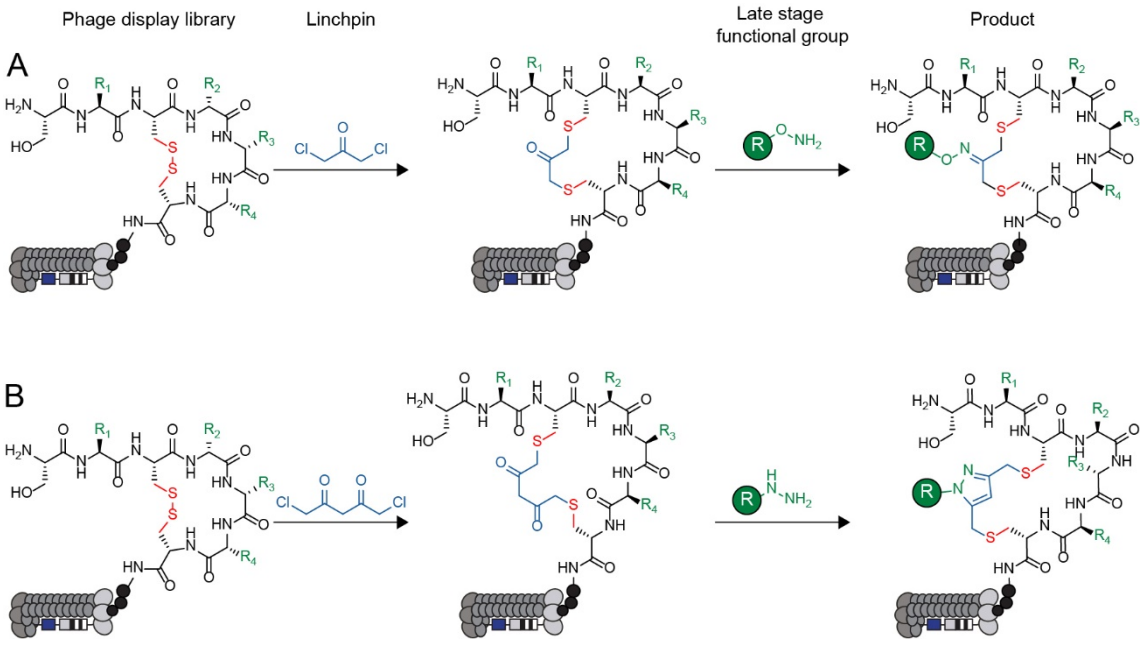

Figure 1-8. Late-stage functionalization linchpins on phage display library.

Derda and co-workers described a late-stage functionalization on the phage display library with the linchpin of 1,3-dichloroacetone.[214] The reaction of 1,3-dichloroacetone with thiol was relatively fast; however, the late-stage reaction between the aminooxy and the acetone group was relatively slow and reversible. The reaction only proceeds to completion overnight (Figure 1-8A).[215] To circumvent the slow reaction of the late-stage functionalization, Derda and co-workers described another late-stage functionalization method on the phage display library with the linchpin that used the Knorr pyrazole reaction.[216] The reaction that uses the 1,5-dichloropentane-2,4-dione linchpin to yield 1,3-diketone modified macrocyclic peptides phage-displayed library. The 1,3-diketone macrocycles then react with hydrazine-based pharmacophores to form pyrazole in 1 hour (Figure 1-8B).[217]

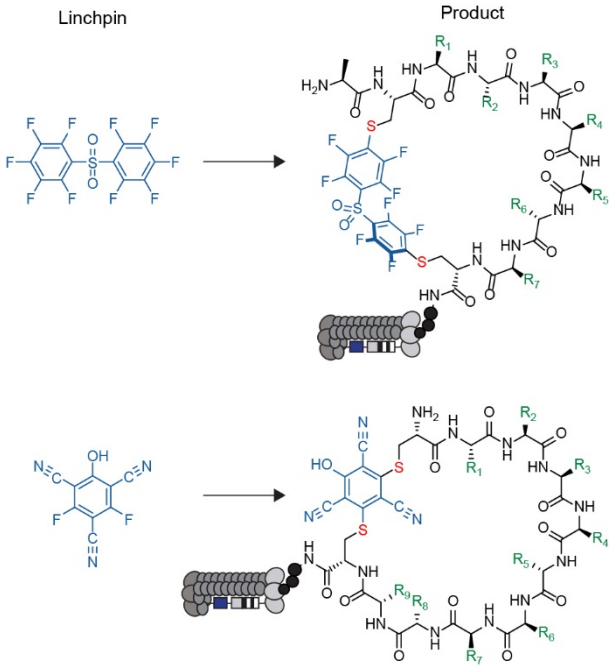

Figure 1-9. Linchpins that use S_NAr to staple disulfide peptide libraries displayed on phage.

Using S_NAr to modify proteins is well described. The most recent example is from the Pentelute and Buchwald groups who used it to staple proteins. Most S_NAr reagents are highly insoluble in aqueous media.[218] The reaction is done in a pure organic solvent or a mixture of water and a high percentage of organic solvent. Due to this limitation, there are limited S_NAr reactions used to modify a phage display library. To circumvent this limitation, the Dedra group identified a deafluorobiphenlysulfone (**DFS**) linchpin for cyclizing peptides. **DFS** was sufficient to react in primarily aqueous conditions with 5 % DMF. Using a low percentage of DMF as co-solvent, they modified the phage display library in 0.5 mM **DFS** at pH 8.5 with 5% DMF for 1-2 hour.[219]

Wu and co-workers further removed the need for organic solvent with the linchpin: 2,4-difluoro-6-hydroxy-1,3,5-benzenetricarbonitrile (**DFB**). The

reaction proceeds in neutral pH with no organic solvent and quantitative conversion in 5-30 min to modify unprotected peptides. The reaction conditions were used to modify the ACX_9C phage-displayed library in 0.1 mM **DFB** at neutral pH for 1 hour.[220]

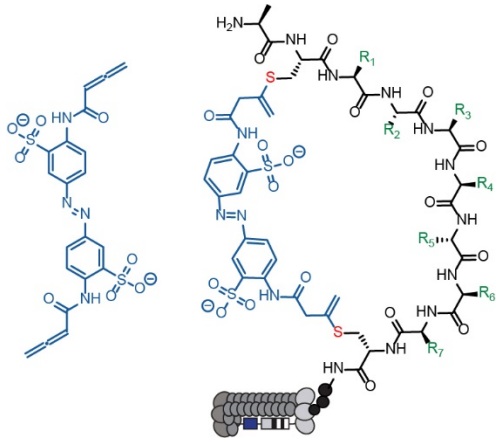

Figure 1-10. Linchpins that use Michael addition to staple disulfide peptide libraries displayed on phage.

There is currently one linchpin that uses Michael addition to a staple disulfide peptide on phage display library. Derda and co-workers developed another azobenzene linchpin to modify the ACX_7C phage-displayed library. They found that the azobenzene with the new allenamide functional group is two or three times faster than the previous alkyl halide (Figure 1-10).[221]

1.5.8 Chemical post-translational modification with phage display libraries that contain three cysteines: $X_nCX_mCX_lCX_k$:

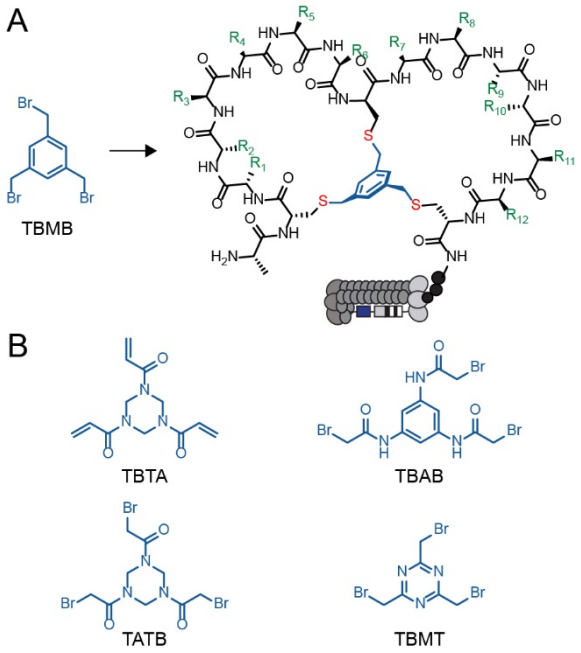

Figure 1-11. Representation of post-translational modification for a phage display library with 3 cysteines with (A) **TBMB** and (B) other linchpins.

Heinis, Winter, and co-workers created a tri-cysteine library specifically for a set of reactive thiol linchpins (Figure 1-11). They were also the first to introduce a chemical modification to generate millions of bicyclic macrocycles on a phage display library. The bicyclic phage-displayed library modified with **TBMB** was used to discover a plasma kallikrein inhibitor with K_i = 1.5 nM.[222-223]

The same modification had been applied to the different tri-cysteine libraries (Table 1-14) to discover binders or inhibitors against the Notch1 receptor,[224] human RNA-decapping enzyme DCP2,[225] G-Quadruplex,[226] and serine protease urokinase-type plasminogen activator.[227]

Table 1-14. TBMB post-translational modification for the phage display libraries with $X_nCX_mCX_lCX_k$

Motifs	Length (ref. #)
CXXXCXXXC	9 (ref. [222, 226])
XCXXXCXXXCX	11(ref. [222, 227])
CXXXXCXXXXC	11(ref. [226])
XCXXXXCXXXXCX	13(ref. [227])
CXXXXXCXXXXXC	13(ref. [223])
CXXXXXCXXXXXXC	14(ref. [222])
CXXXXXXCXXXXXXC	15(ref. [225])
ACXXXXXXCXXXXXXCA	16(ref. [228-229])

Other **TBMB** like linchpins were also developed and modified tri-cysteine peptide phage-displayed library (Figure 1-11B). However, **TBMB** is the most used for identifying bicycles ligands.[227, 230-232]

1.5.9 Chemical post-translational modification with a phage display library that contain four cysteines and more

Peptides with four cysteines are displayed on phage that have a bicyclic architecture and can be further modified with thiol reacting linchpins to increase protease-resistance or to discover orally available peptide.[233]

Heinis and co-workers applied a set of 10 thiol-reactive reagents to modify the $XCX_mCX_lCX_kCX$ phage-displayed library, where $m + l + k = 3\text{-}8$ and X indicates any random natural amino acids but cysteine (Figure 1-12). The modified library was incubated with porcine pancreatin to mimic protease pressure in the intestine, then selected against coagulation Factor XIa. They identified that one of the isomers from the di-bromoacetone modified peptide, TCVNIMCCRFP, was able to resist porcine pancreatin degradation and inhibit coagulation Factor Xia with a K_i of 19 nM simultaneously.[233]

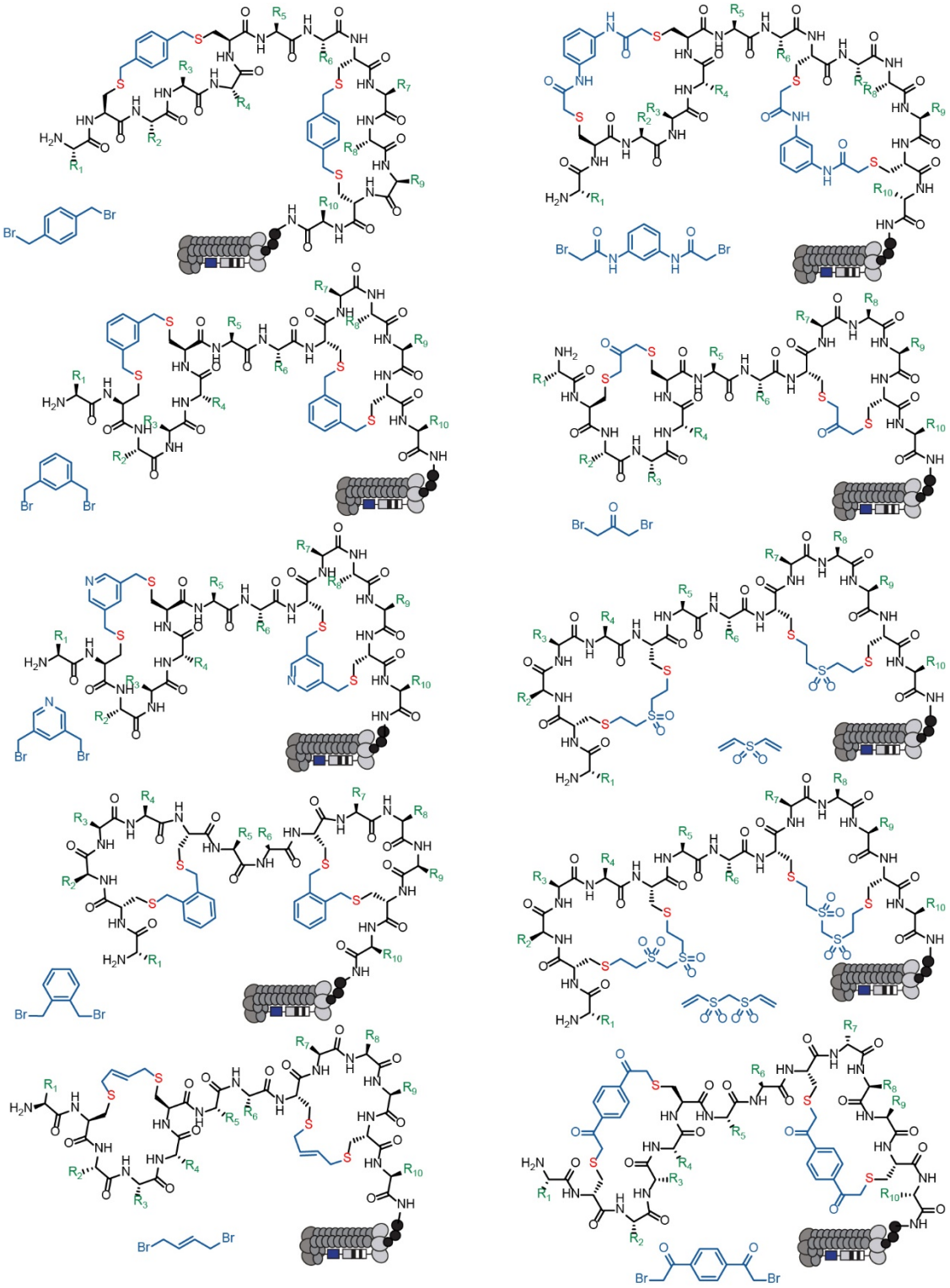

Figure 1-12. A representative 10 reactive thiol reagents modifying $X\underline{C}X_m\underline{C}X_l\underline{C}X_k\underline{C}X$ phage-displayed libraries.

1.5.10 Expressing unnatural amino acid on the phage display libraries: $X_n\underline{C}X_m$[UAA] / [UAA]X_nCX_m

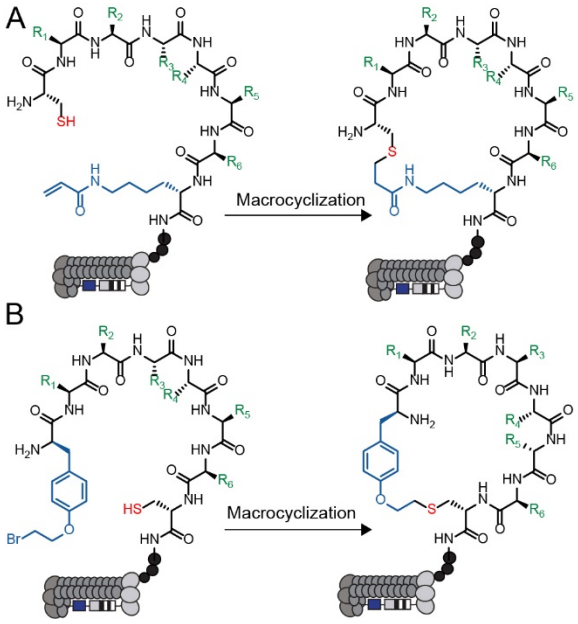

Figure 1-13. Unnatural amino acid-bearing macrocycles on phage display libraries.

It is possible to display a head-to-tail architecture on the phage without linchpins' modification; however, this requires incorporating an unnatural amino acid (UAA),[234-235,] which has been used to generate a macrocyclic library.[199-200] (Figure 1-13)

Liu and co-workers displayed a cysteine-reactive unnatural amino acid, *N*$^{\varepsilon}$-acryloyl-lysine (AcrK), and a proximal cysteine to generate macrocycles on phage. (Figure 1-13A) This platform produced a phage display library with the motif $\underline{C}X_{5\text{-}7}$[AcrK]. The library was screened against TVE protease and HDAC8 to identify cyclized peptides with a higher affinity than the linear peptides.[199]

Fasan and co-workers displayed a cysteine-reactive unnatural amino acid O-(2-bromomethyl)-tyrosine (O2beY) and a proximal cysteine residue to generate a macrocyclic peptide phage-displayed library. (Figure 1-13B) This platform was used to produce peptides with the motif of [O2beY]X_{6-7}C, CX_{6-7}[O2beY], X_4[O2beY]X_{6-7}CX_4, and X_4CX_{6-7}[O2beY] X_4 on the phage's pIII protein and screened against three different protein targets, resulting in a macrocycle that bounds to streptavidin with K_d = 20 nM, to Sonic Hedgehog with K_d = 550 nM and to Kelch-like ECH-associated protein 1 with K_d = 40 nM.[200]

1.6 Scope of the thesis

Phage display is a platform that can generate a diverse peptides library of natural amino acids for discovering macrocyclic ligands. The most common macrocyclic architecture is a monocyclic peptide which is generated from the oxidation of disulfide peptide. Chemical post-translational modification and or incorporation of unnatural amino acids are also used to diversify the architecture of macrocycles displayed on phage. The incorporation of unnatural amino acids in phage display is not well established; therefore, researchers have turned to chemical post-translational modification to bypass the complexity of unnatural amino acid incorporation. Linchpins for chemical post-translation modification rely on three primarily thiol specific reactions to diversify disulfide macrocyclic libraries displayed on phage: S_N2, S_NAr, and Michael addition. Introducing bio-orthogonal chemistry for natural amino acids other than thiol reactions needs to fulfill two requirements: i) the reaction must not reduce the diversity of the

peptide library, and ii) the reaction reagents and solvents must not denature the phage to converse the genotype and phenotype linkage. Most orthogonal reactions for natural amino acids cannot meet the requirements above. In this thesis, I describe a new linchpin that combines a non-thiol bio-orthogonal reactive group with a thiol-reactive group to generate bicyclic peptides on a phage display library.

In chapter 2, I describe a method of using **TSL**s to generate bicycles by combining a non-thiol bio-orthogonal reaction for N-terminal serine and thiol reaction to generate a bicyclic motif. The method was compatible with SX_nCX_mC peptide phage-displayed libraries. The **TSL-6** bicyclic library was used to elucidate an inhibitor of the NODAL signaling pathway.

In Chapter 3, I describe the discovery a 4 μM binder of human serum albumin (HSA) with **DFS** modified macrocycles phage-displayed libraries. We expect the HSA ligand to enhance the circulation half-life of peptides with known poor pharmacokinetics.

Chapter 2: Genetically encoded discovery of proteolytically stable bicyclic inhibitors for morphogen NODAL

2.1 Introduction

This chapter was published in its' current form in the *Chemical Science*: Wong, J. Y. K.; Mukherjee, R.; Miao, J.; Bilyk, O.; Triana, V.; Miskolzie, M.; Henninot, A.; Dwyer, J. J.; Kharchenko, S.; Iampolska, A.; Volochnyuk, D. M.; Lin, Y.-S.; Postovit, L.-M.; Derda, R., Genetically-encoded discovery of proteolytically stable bicyclic inhibitors for morphogen NODAL. *Chem. Sci.* **2021**, 12 (28), 9694-9703., and the text was reformatted into thesis format with only minor modifications. For consistency, all procedures from the publications were included in my thesis. The following sections have been performed entirely by the co-authors:

- Dr. Raja Mukherjee: Sections 2.4.1-2 and 2.4.1-7
- Dr. Jiayuan Miao and Dr. Yu-Shan Lin: Section 2.4.5
- Dr. Olene Bilyk: Sections 2.4.3-11
- Mark Miskolzie, M.Sc.: Appendix A-6.2 and Appendix A-6.3
- Dr. Serhii Kharchenko: Sections 2.4.1-10,2.4.1-11 and 2.4.1-12

Peptide macrocycles constitute a significant fraction of approved peptide therapeutics, as around 30 out of 80 peptide drugs on the global market; macrocyclic topologies, and they prevalent among 150 peptides in clinical development and in the 400–600 peptides undergoing preclinical studies.[236-239] Macrocyclization of peptides increases binding affinity, improves permeability

through the cell membrane, and increases stability towards enzymatic hydrolysis compared to linear peptides.[203-207] The large surface area of macrocycles has been critical for identifying molecules that bind extended protein surfaces and inhibit protein-protein interactions.[2] The introduction of a bridgehead into the macrocyclic topologies to form so-called bicyclic peptides could further decrease conformational flexibility and increase stability or binding potency.[203, 240] Bioactive bicyclic peptides that have been reported thus far originate from natural products,[241] computational approaches,[242-244] cyclization of known bioactive peptides,[210, 245-247] or screening of combinatorial libraries.[248-250] To fuel the last method, synthesis on the solid support can yield libraries of 10^2–10^5 diversity,[248-250] whereas late-stage chemical diversification of biosynthesized peptides displayed on mRNA[240, 251-253] or phage[192, 254] can give rise to bicyclic libraries with 10^9–10^{12} diversity. DNA-encoded libraries (DELs) have been used extensively to synthesize mono-cyclic libraries of 10^4–10^8 members[255-258] and recently 10^{12} members;[259] although, there are no published examples of bicyclic DELs, the late-stage chemical diversification used in phage and mRNA display can be applied to DELs to generate such libraries.[260] Development of new approaches for late-stage chemical diversification of encoded libraries[261-263] make it possible to screen and discover new macrocyclic and bicyclic topologies with value-added properties.

There are currently two strategies for synthesizing chemically-modified phage-displayed bicyclic libraries. Both employ crosslinking of Cys side chains with electrophiles (Figure 2-1A). The first approach pioneered by Winter and

Heinis cross-links three Cys residues with a C_3-symmetric electrophile to yield bicycles displayed on phage (Figure 2-1A).[192] This approach was developed extensively by Heinis group[227, 229] and researchers at Bicyclic Therapeutics[223, 232] and employed recently by Slavoff and co-workers[225] and Wales, Balasubramanian and co-workers.[226] The second approach published recently by Heinis group employs cross-linking of four Cys residues with C_2-symmetric electrophiles to yield a mixture of three regioisomeric bicycles displayed on phage (Figure 2-1A).[233, 254] Bicyclic libraries have also been synthesized in mRNA display libraries using the strategy (i),[252] via incorporation of two pairs of orthogonal reactive unnatural amino acids (UAAs) into mRNA display libraries,[253] or via a combination of the two approaches.[240, 264]

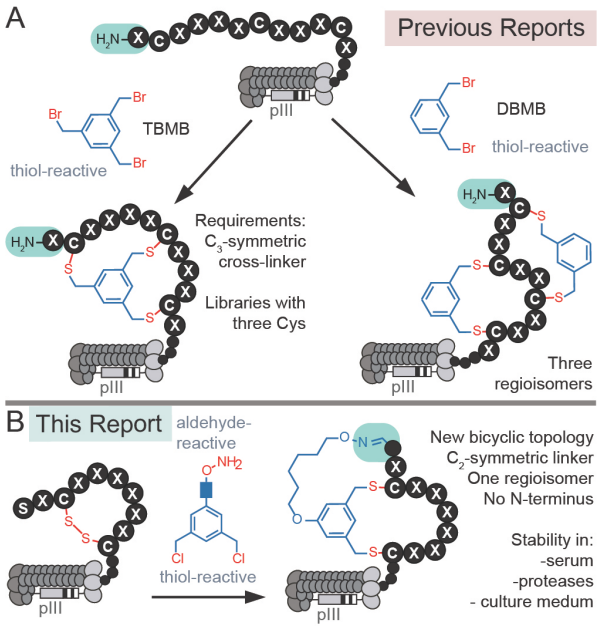

Figure 2-1. Overall view of current bicyclic strategies: (A) Previous reports of synthesis of bicyclic phage displayed peptide libraries. (B) Synthesis of bicyclic phage-displayed peptide libraries described in this report.

Incorporation of UAAs into phage-displayed peptide libraries is possible,[234-235] and UAAs have been used to generate phage-displayed macrocyclic libraries.[199-200]

In this manuscript, we sought to devise the modification approach that uses peptide libraries made of 20 natural amino acids. Bypassing the complexity of UAA incorporation avoids biases that might result from the incorporation of such UAAs in the phage library.[265] We combined modifications of N-terminal Ser and Cys-side chains to generate a novel genetically-encoded bicyclic topology (Figure 2-1B). Contrast to previous topologies (Figure 2-1A), this topology does not display a free Cys-side chains to generate a novel genetically-encoded bicyclic topology (Figure 2-1B). N-terminus and unlike strategies that modify four Cys residues,[233, 254] this cyclization strategy yields a single regioisomer (Figure 2-1B).

Aldehyde is a versatile bio-orthogonal handle. In proteins, aldehydes can be incorporated by periodate oxidation of N-terminal Ser.[266-267] This method has been used for PEGylation of clinically relevant growth factors,[268] for improving the stability of cytokines in preclinical studies,[269] and for the synthesis of antibody-drug conjugates.[270] Libraries with N-terminal Ser have been previously converted to peptide-aldehydes and modified by oximes and hydrazines,[271] benzamidoxime,[272] or Wittig reaction,[273] and used for the selection of diverse chemically-modified peptide ligands.[274-278] Our group has previously demonstrated that the bicyclic topology akin to the one described in Figure 2-1B can be introduced into synthetic peptides using C_2-symmetric azobenzene linkers

with an aldehyde reactive oxime functionality and two thiol-reactive chlorobenzyl functionalities.[279] We demonstrated the feasibility of such bicyclization in several unprotected synthetic peptides with N-terminal Ser and two Cys residues in aqueous and organic solvents.[279] In this report, we extend the previously published concept other classes of linkers biocompatible aqueous environment. We then provide the first example of using this technology for bicyclization of bacteriophage displayed libraries with N-terminal aldehyde residues (Figure 2-1B). To demonstrate the value of such a library in discovering new bioactive bicycles, we employed this library to discover inhibitors of protein NODAL and antagonists of NODAL-induced signaling.

The extracellular embryonic morphogen NODAL belongs to the transforming growth factor-beta (TGF-β) superfamily.[280] It is a stem-cell-associated factor that has emerged as a putative target for the treatment of cancer.[281-282] NODAL is normally restricted to embryogenesis, wherein it maintains pluripotency in the epiblast and governs the formation of the body axis and left-right asymmetry.[280] After development, NODAL is relatively restricted to reproductive cell types and is not detectable in most normal adult tissues.[283] However, NODAL expression re-emerges in a large number of divergent cancers.[284-294] It also supports self-renewal in pancreatic and breast cancer stem cells and is enriched in melanoma and colon cancer cells with stem cell properties.[284-286] In almost every cancer studied thus far, the acquisition of NODAL expression is associated with increased tumorigenesis, invasion, and metastasis. NODAL exerts its function by binding to and activating the cell

surface receptors Alk4 and Alk7 in cooperation with the co-receptors Cripto-1 (FDGF1) or Cryptic (CFC1) to form a ligand–receptor complex that leads to the phosphorylation of Smad2/3 and the transcription of target genes, including NODAL itself.[288] The only available inhibitor of NODAL to date, monoclonal anti-NODAL antibody 3D1,[295-296] has demonstrated success in preclinical models of melanoma and is currently undergoing further preclinical evaluation. Recently, Mandomenico and co-workers designed a bicyclic peptide that inhibited the interaction between ALK4 and Cripto-1.[243] In this manuscript, we employed bicyclic phage libraries to discover the first-in-class bicyclic ligands for NODAL protein. These ligands antagonize NODAL-induced signaling and specifically suppress NODAL-promoted proliferation of cancer cells. Evaluation of these antagonists benefited from the unique topology of the macro-bicycles that masked the N-terminus and equipped these macro-bicycles with multi-day stability in serum-rich cell culture media.

2.2 Results and discussion

2.2.1 Optimization of bicyclization on unprotected synthetic peptides

The chemical linkers **TSL-1**, **TSL-3**, and **TSL-6**, containing aminooxy and benzyl chloride functional groups were synthesized by post-doctoral fellow in Derda Lab (Dr. Raja Mukherjee) (Figure 2-2 and Figure 2-3A) and tested for their ability to modify a series of unprotected peptides of structure SX_nCX_mC where X is any amino acids except Cys and n+m ranges from 4 to 11. To mimic the conditions that would be suitable for modification of phage display library of

peptides, we used model peptides at a micromolar concentration in aqueous buffers and treated them with super-stoichiometric reagents (Figure 2-3B).

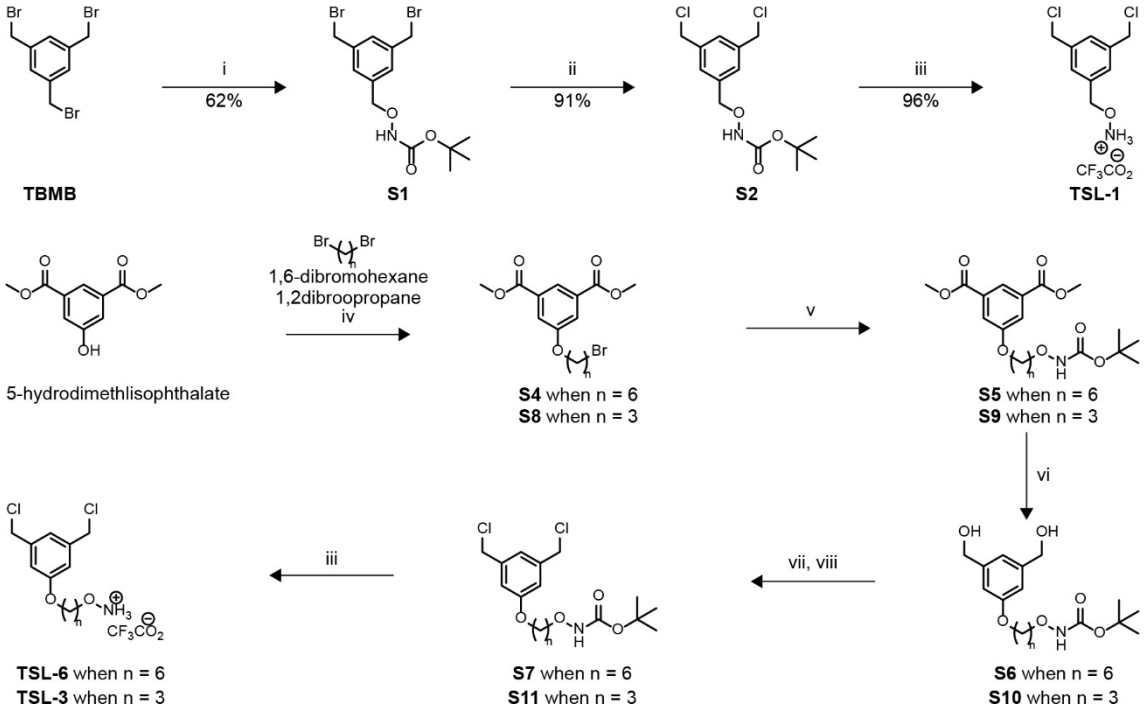

Figure 2-2. Synthetic procedures for the linchpins **TSL-1**, **TSL-3** and **TSL-6**: Reagents and conditions: i) BocNHOH, DBU, DCM, 3 h; ii) LiCl, DMF, 10 h; iii) TFA, DCM; iv) 1,6-dibromohexane or 1,3-dibromopropan, K_2CO_3, CH_3CN, reflux, 72 h; v) BocNHOH, DBU, DCM, 5 h; vi) $LiAlH_4$, THF, 0 °C to rt, 1 h; vii) MsCl, Et_3N, 0 °C to rt, 5 min; viii) LiCl, DMF, 10 h.(This synthesis was performed by Dr. Raja Mukherjee.)

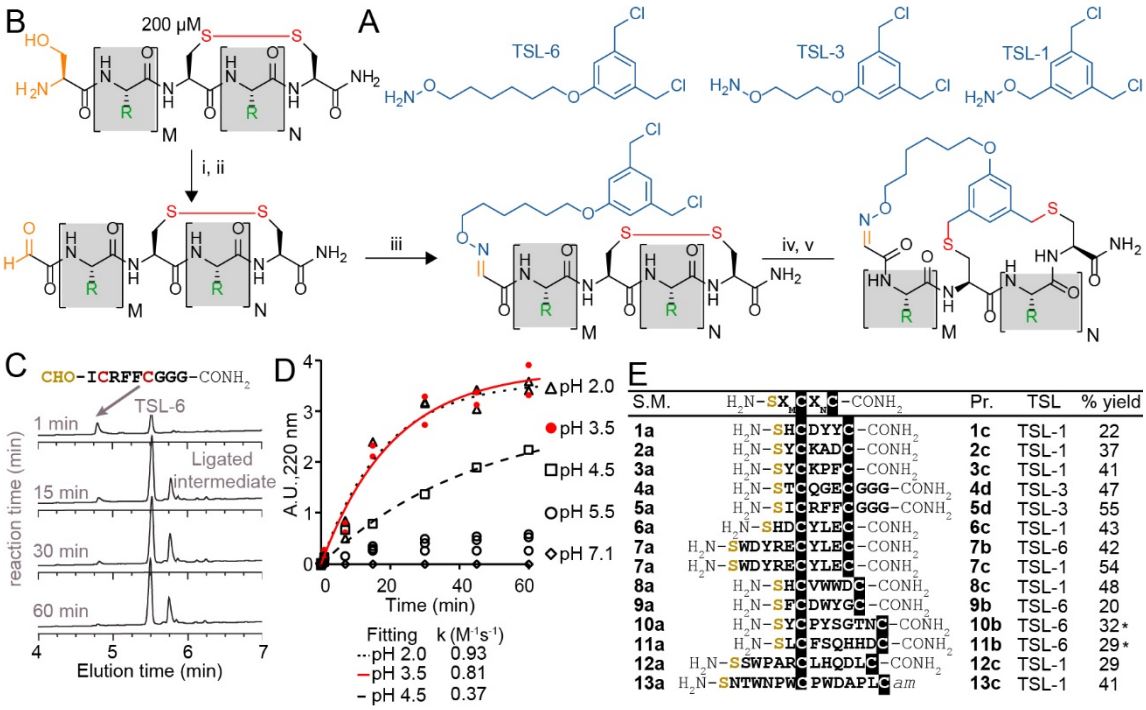

Figure 2-3. Macrocyclization reaction of bicycles with model peptides. (A) Chemical structure of **TSL**s. (B) Ligation of disulfide peptides with **TSL-6** at pH 3.5 and further macrocyclization into bicyclic peptides at pH 10. (i) 0.06 mM $NaIO_4$, pH 7.9, 9 min, ice. (ii) 0.5 mM Met, 20 min, r.t. (iii) 1 mM **TSL-6**, 10% MeCN, 0.1% TFA, 1 h, r.t. (iv) 1 mM TCEP in 10 mM NaAc buffer, pH 4.6, 30 min. Increase the pH to 10 by adding 1 M $NaHCO_3$ and incubate for 3 h, r.t. (C) Liquid chromatography traces at 220 μM for the reaction between oxidated **5a** and **TSL-6**. The reaction reaches 95% completion in 1 hour. (D) Kinetic traces of the reaction between oxdized **5a** and **TSL-6** at different pH. Reaction rates at pH 2.0, pH 3.5, and pH 4.5 were fit to pseudo first order kinetic equation to determine *k* values. (E) Isolated yields of bicyclic peptides with various sequences and different **TSL**s. The bicycles modified with **TSL-6**, **TSL-1** and **TSL-3** were denoted as #**b**, #**c** and #**d** respectively. (*see Experimental procedure **2.4.1-11** and **2.4.1-12** for details of the modification protocol)

Figure 2-3C–D describe monitoring of the oxime formation progress. A representative model peptide SICRFFCGGG (200 μM) and $NaIO_4$ (2.4 mM) reacted to form the N-terminal oxoaldehyde. Quenching the excess of $NaIO_4$ with an excess of methionine, and addition of 1 mM **TSL-6** while decreasing the pH, led to the formation of the oxime (Figure 2-3B). At pH ranging from 2.0 to 3.5, the rate constant of this ligation was k = 0.81–0.93 $M^{-1}s^{-1}$ (Figure 2-3C–D). In these conditions, oxime ligation went to completion within 1 hour. Increasing the pH to 4.5 decreased the rate (k = 0.37 $M^{-1}s^{-1}$) and led to partial completion in 1 hour (Figure 2-3D). Little to no oxime was formed at a pH higher than 5.5 (Figure 2-3D). We note that aniline can catalyze oxime reactions[271, 297]; however, we avoided aniline and other nucleophilic catalysts to prevent the formation of byproducts with **TSL**s.[279] The addition of 1 mM TCEP to the ligated product reduced the disulfide linkage. Raising the pH to 10 led to the bicyclization of peptides in 3 hours. We note that this specific sequence of reactions—oxidation and aldehyde ligation followed by bicyclization via S_N2 reaction between the thiols and chlorobenzyl—was based on a previously optimized route to bicyclic peptides.[279] Switching the order of steps is possible but it should be done with caution: When oxidation of the N-terminal Ser to aldehyde is performed after formation of thioether the oxidation of relatively electron rich benzyl thioethers to sulfoxides may take place.[279, 298] We also observed sluggish linker- and sequence-dependent bicyclization when oxime ligation was used in place of thioether formation as the last ring-closing step.[279] The reaction sequence described in Figure 2-3B successfully produced 14 unique bicycles of different

spacing between the Ser and Cys residues with an average isolated yield of 40% (Figure 2-3E). Monitoring of the step-by-step synthesis for these and other bicycles are available in Appendix A (Appendix A-Scheme 1-35) and are summarized in Appendix A-Table1. We note that bicyclization of peptides can proceed at pH 10 (Appendix A-Scheme 6-9, 21-31), pH 8.5 (Appendix A-Scheme 2-6, 10-18, 32-35) as well as pH 8.0 (Appendix A-Scheme 18-Appendix A-Scheme 19). The model peptides were either chosen at random (**1a**–**3a**, **6a**–**7a**) or selected from the phage-displayed peptide library (**4a–5a,** and **10a–11a**). Two peptides (**12a–13a**) were adapted from a previous publication.[223] Appendix A-Table2 further highlights the various physicochemical properties of these peptides. We compared the yields of this reaction to modification of peptides with other reagents such as pentafluorophenyl-sulfide (**PFS**),[299] 1,3,5-tris(bromomethyl)benzene (**TBMB**)[192] and α,α′-dibromo-m-xylene (**DBMB**).[210] **PFS** cyclized peptides had an average yield of 35.5% (Appendix A-Scheme S36 and Appendix A-Table3). **TBMB** cyclized peptides had an average yield of 35% (Appendix A-Schemes S37–S38, Appendix A-Table3). **DBMB** cyclized peptides had an average yield of 31% (Appendix A-Table3). In conclusion, the aqueous biocompatible modification of peptides with **TSL** effectively produced bicyclic peptides with comparable yields with other reagents used in peptide cyclization or bicyclization. Although oxime linker is known to be reversible, we observed these bicycles to be stable in aqueous ammonium acetate (pH 4.7), in PBS (pH 7.4), and in Tris buffers (pH 8.5) for a month at room temperature (Figure 2-4).

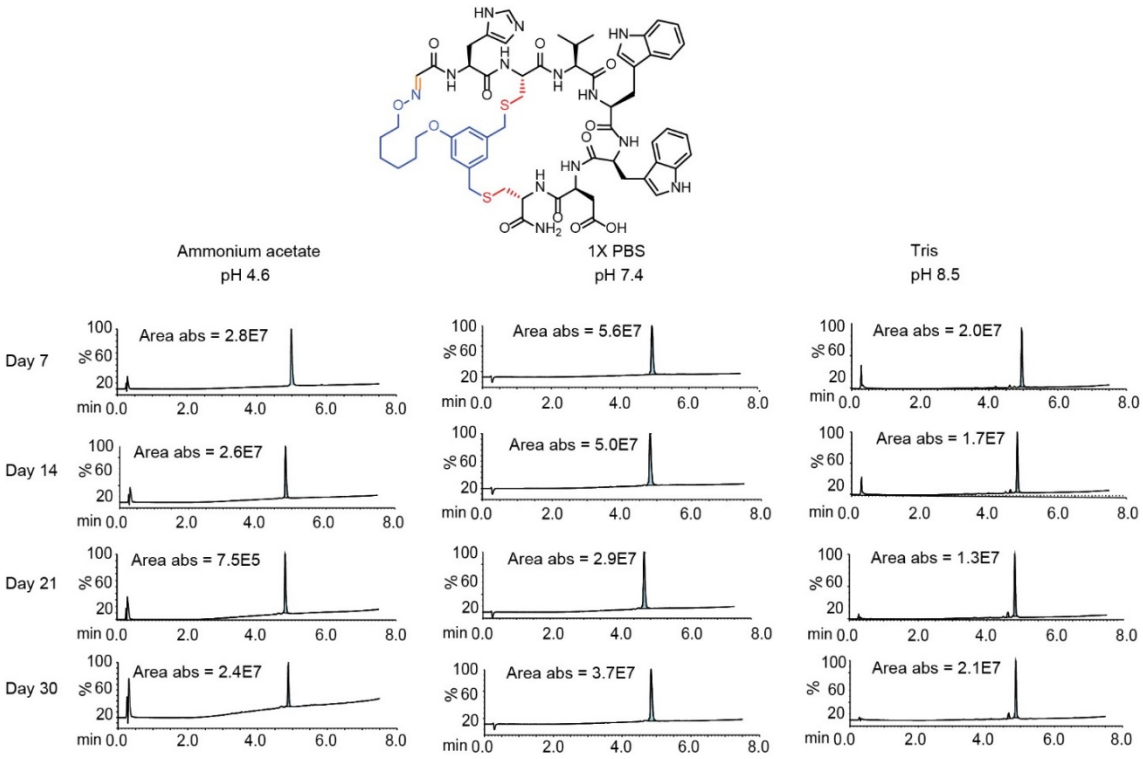

Figure 2-4. Stability analysis of bicyclic peptide **TSL-6-**SHCDYYC over 30 days in buffers of different pH

2.2.2 Modification of phage display libraries

The bicyclization approach described above was compatible with the modification of the phage-displayed peptide libraries. To quantify the efficiency of the bicyclization reaction in the phage libraries, we employed biotinylation and phage capture steps with similar approaches as in previous publications (Figure 2-5).[271, 273-275, 300] Previously, the formation and reactivity of aldehyde in phage libraries were quantified by exposing the library to an aldehyde-reactive aminooxybiotin (AOB) and counting the number of biotinylated particles captured by streptavidin paramagnetic particles ("AOB capture," Appendix A-Figure 1C).[271] Using the reported oxidation conditions, we exposed a phage displaying $SX_1CX_2X_3X_4X_5X_6X_7C$ library with a diversity of ~10^9 peptides to an ice-cold solution of $NaIO_4$ (60 μM in PBS) for 9 min, quenched the oxidation by 0.5 mM methionine for 20 min and used AOB capture to confirm that 93±11% of the library was converted to aldehyde. Reacting with 1 mM solution of **TSL-6** at pH 3.5 for 1 hour consumed most of the aldehyde functionalities (Appendix A-Figure 2E). After removing excess **TSL-6** by size exclusion spin column, we exposed the phage to a biotin-thiol reagent (BSH, Figure 2-5E) and captured the biotinylated clones by streptavidin paramagnetic particles. This "BSH capture" confirmed that 52±4% of the library contained thiol-reactive benzyl chloride groups (Figure 2-5B). Exposure of phage to TCEP and then pH 10 buffer completed bicyclization as evidenced by the decrease in BSH capture.

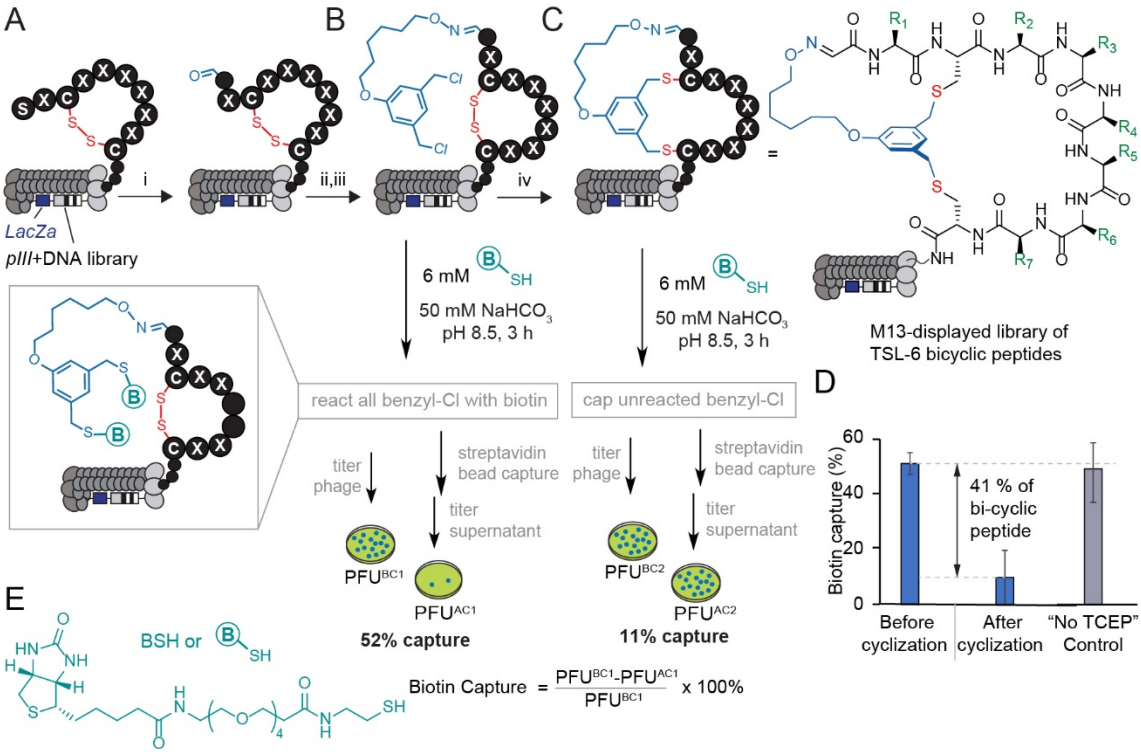

Figure 2-5. Modification of the library with a diversity of ~10^9 peptides displayed on phage by the **TSL-6**. (A–B) M13 phage-displayed disulfide library was oxidized and ligated with **TSL-6**. Reaction conditions: (i) 0.06 mM $NaIO_4$, pH 7.9, 9 min, ice. 0.5 mM Met, 20 min, r.t.(ii) 1 mM **TSL-6**, 10% MeCN, 0.1% TFA, 1 h, r.t. (iii) Zeba^{TM} column, elute with 10 mM NaOAc buffer, pH 4.6 (iv) 1 mM TCEP in 10 mM NaAc buffer, pH 4.6, 30 min. Increase the pH to 10 by adding 1 M $NaHCO_3$ and incubate for 3 h, r.t. (C) The **TSL-6** ligated peptides were further converted into bicyclic peptides. (D) Quantification of the phage with thiol-reactive groups before and after cyclization. Control incubation of **TSL-6**-ligated phages in pH 10 buffer for 3 h did not lead to a significant decrease of thiol-reactive group content. (E) Chemical structure of the biotin-thiol (BSH) probe.

In the control condition, incubation of the **TSL-6** ligated library at pH 10 in the absence of TCEP did not lead to any decrease in BSH capture, indicating that the number of benzyl chloride groups on phage remained unchanged in the absence of TCEP. We estimated 41±13% of the library to be converted to the **TSL6**-bicyclic library (Figure 2-5D). Detailed calculation of the conversion percentage

can be found in Appendix A-Figure 2. Similar monitoring the modification of the $SX_1CX_2X_3X_4X_5X_6X_7C$ library with **TSL-1** and **TSL-3** (Appendix A-Figure 3) and the $SX_1CX_2X_3X_4C$ phage with **TSL-6** (Appendix A-Figure 4) demonstrated a generality of this approach. Although modification of synthetic peptide proceeds effectively in pH 8.0-10.0 range, we observed that modification of libraries at pH 10 was more reliable. The ligation condition showed minor effects on the infectivity of the phage (Appendix A-Figure 1F). To confirm the chemical modification did not compromise the integrity of the phage DNA; we performed PCR (Appendix A-Figure 5 and Appendix A-Figure 6) of the library and deep sequenced the PCR amplicons to monitor the sequence diversity of the library before and after chemical modification. If chemical modification significantly damaged the DNA, we anticipated observing a change in the library composition. As the composition of the library before and after the modification remained the same (Appendix A-Figure 7-10), we concluded that the modification did not impact the diversity of the phage library and did not impact the integrity of the phage DNA. These studies collectively demonstrate the construction of a bicyclic library that offers the potential for discovering bicyclic ligands for any target using canonical selection approaches.

2.2.3 Selection of bicycles that bind to NODAL

We applied a **TSL-6**-modified phage-displayed $SX_1CX_2X_3X_4X_5X_6X_7C$ library to discover a ligand for the morphogen NODAL. We performed three rounds of phage selection using His_6-tagged NODAL protein as bait. In between rounds of selection, we raised the stringency by increasing the number of washes

and reducing the amount of immobilized NODAL protein (Figure 2-6A). In round 3, we also performed two control selections; in the first control, we panned the unmodified R3 library against the NODAL protein (R3-UN) and in the second control, we panned the **TSL-6**- modified R3 library against unrelated His_6-tagged protein (R3-TG). Phage recovery increased by 4-fold in R3 when compared to R1 and R2. This recovery was ablated by 20-fold when the unmodified round 3 library was panned against NODAL (R3-UN) and when the **TSL-6**-modified library was panned against an unrelated protein (R3-TG) (Figure 2-6C). Deep sequencing the output of all selection rounds and the control experiments identified families of sequences that exhibited high normalized abundance in R3 and low normalized abundance in R1, R2, and control experiments R3-UN, and R3-TG (Figure 2-6B and Appendix A-Figure 10). From these families, we selected six representative sequences for further validation (**14a**–**19a**; Figure 2-6B and Appendix A-Figure 10).

2.2.4 Validation of NODAL bicyclic inhibitors

The bicycles **14b**–**19b** were chemically synthesized and tested for their ability to antagonize NODAL-induced signaling in the P19 cells: a model cell line known to respond to NODAL.[301] Stimulations of the P19 cells with rhNODAL at 100 ng/mL for 1 hour led to the phosphorylation of SMAD2 (Figure 2-6D, column 3). This phosphorylation was inhibited by ALK4/7 kinase inhibitor SB431542 (Figure 2-6D, column 4), as previously reported.[301]

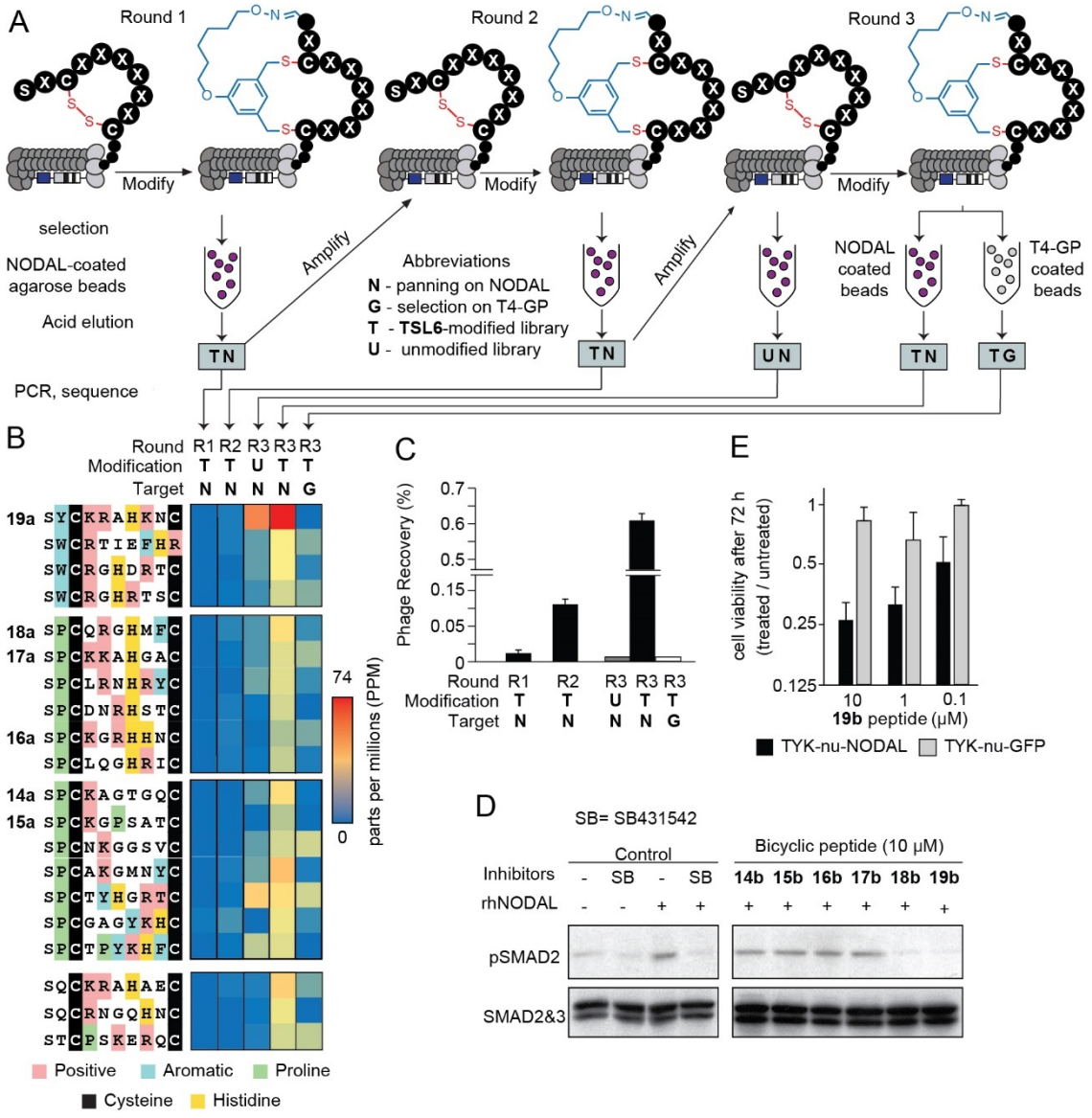

Figure 2-6. Bio-panning against the NODAL protein. (A) A scheme of three-rounds panning against NODAL and negative controls. (B) The top 20 sequences from the deep sequencing results were clustered into 4 groups and 6 of them were chemically synthesized. (C) Percentage of the phage recovery after each round of bio-panning. (D) Western blot validation with p-SMAD2 in response to treatment with rhNODAL and inhibitors in P19 cells. Total SMAD used as control (E) Cell viability assay of TYK-nu cell line transfected with rhNODAL or GFP and treated with **19b** at various peptide concentrations for 72 hours.

Bicyclic peptides **14b**–**19b** at 100 μM were able to inhibit rhNODAL-induced phosphorylation of SMAD2 (Appendix A-Figure 11A). At the concentration of 10 μM, bicyclic peptides **18b** and **19b** inhibited phosphorylation of SMAD2 (Figure 2-6D, columns 9 and 10), whereas bicyclic peptides **14b**–**17b** exhibited no inhibition (Figure 2-6D, columns 5–8 and Appendix A-Figure 11B). As **19b** exhibited robust and reproducible inhibition of phosphorylation (Appendix A-Figure 11B), we further tested the ability of **19b** to suppress the NODAL-induced proliferation of ovarian cancer cells. We transfected ovarian cancer cells (TYK-nu) with a plasmid vector containing human NODAL and used a GFP transfected TYK-nu cell line as an isotype control. TYK-nu-NODAL and TYK-nu-GFP cell lines were cultured in the presence and absence of **19b** for 72 hours (Appendix A-Figure 12-14). Treatment of TYK-nu-GFP cell with **19b** at 10 μM had no effect on the proliferation, whereas the viability of TYK-nu-NODAL cells was reduced to 23% compared to untreated TYK-nu-NODAL cells (Figure 2-6E). The response to **19b** was dose-dependent with apparent IC_{50} between 0.1 and 1 μM **19b** (Figure 2-6E and Appendix A-Figure 12). The discovery of **19b** served as a promising starting point for developing more potent NODAL antagonists.

2.2.5 Proteolytic stability of bicycles

Intrinsic proteolytic stability of the bicyclic scaffold was critical to the evaluation of the NODAL antagonist in the aforementioned cell-based assays. Specifically, we found that 64% of the bicyclic peptide antagonist **19b** remained intact after 72 hours of incubation at 37 °C in a serum-rich culture medium (Figure 2-7).

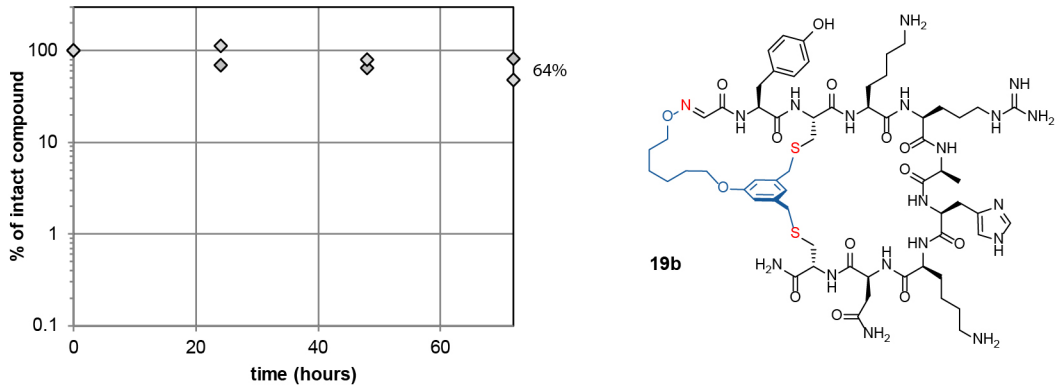

Figure 2-7. Peptide stability in active P19 cell culture for 72 hours of **19b**.

We followed up on this observation and tested the stability of a panel of bicyclic scaffolds in two proteolytic degradation conditions (Figure 2-8). In the first condition, we exposed the bicycles for 5 hours at 37 °C to Pronase™: a mixture of endo- and exo-proteases known to cleave proteins into individual amino acids. The analysis of 21 other **TSL**s bicycles (Figure 2-8A) highlighted that 25–90% of the bicycles remained intact after 5 hours of exposure to Pronase™ (Appendix A-Figure 14-26). In these conditions, all the tested linear and monocyclic disulfides degraded to <1%. In the second condition, nine of these bicycles were exposed to fresh mouse serum at 37 °C. On average, 72% of the starting peptide amount was intact after 5 hours (Figure 2-8A, and Appendix A-Figure 23–Appendix A-Figure 27). Monocyclic peptides formed by modifying peptides with **DBMB**,[210, 302] which have the same topology as one of the rings in **TSL**-modified bicycles.

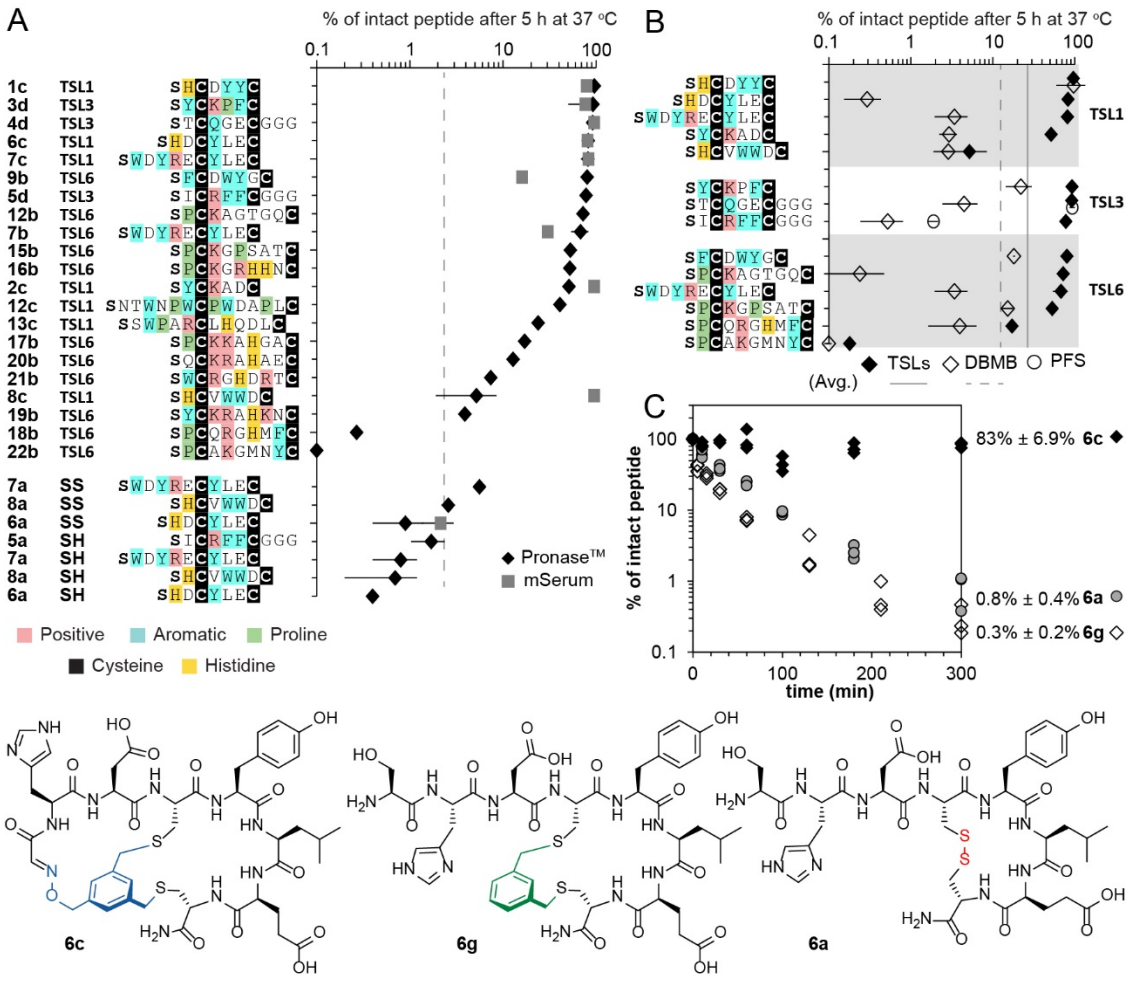

Figure 2-8. Proteolytic stability of bicycles and controls. (A) Stability of **TSL**s bicycles, disulfide constrained peptides, and linear peptides in the presence of Pronase™ and mouse serum for 5 hours at 37 ºC. (B) Stability of peptides modified with **TSLs**, **DBMB** and **PFS** in the presence of Pronase™ for 5 hours at 37 ºC. (C) Stability of **6a** (disulfide-bonded), **6c** (bicycled with **TSL-1**), and **6g** (macro-cyclized with **DBMB**) in the presence of Pronase™.

We observed that on average, 13% of the **DBMB** macrocycles remained intact after 5-hour treatment by Pronase™, compared to 62% from the **TSL**s-modified set (Figure 2-8B and Appendix A-Figure 28–Appendix A-Figure 33, the values represent average from the set of n = 14 sequences modified by both **DBMB** and **TSL**s). Figure 2-8C represents an example of bicycle **6b** that remained 83±6.9% intact after 5 h of incubation in Pronase™; the **DBMB** macrocycle **6g** and the disulfide precursor **6a** degraded to <1% under the same conditions. We tested the stability of two sequences modified with the **PFS** cross-linker developed by the Pentelute Lab.[299] In Pronase™, macrocycle **PFS**-STCQGECGGG and bicycle **TSL-3**-STCQGECGGG exhibited similar stabilities, whereas macrocycle **PFS**-SICRFFCGGG exhibited lower stability than bicycle **TSL-3**-SICRFFCGGG (Figure 2-8B, Appendix A-Figure 34 and Appendix A-Figure 35). Due to differences in the shape of the cross-linkers resulting in different conformations of peptides, the results were difficult to interpret, and we did not expand on this comparison further. In general, it is not trivial to quantify the advantages of a peptide cross-linkers in comparison to the other available cross-linkers to-date; however, a comparison of a set, n = 14, peptides modified with closely related **DBMB** and **TSL** linkers indeed suggests that the bicyclization yields a significant improvement in stability.

2.2.6 Molecular dynamics simulation of bicycle structures.

In testing the stability of a large, diverse set of bicycles, we observed preliminary linker-dependent and sequence dependent trends in degradation. For example, Pronase™ degradation of peptide SWDYRECYLEC modified with

TSL-1, or **TSL-6** linker yielded minor but statistically significant differences: 82±13% and 68±14% intact bicycles after 5 hours (Figure 2-8A). To explore these differences, we employed molecular dynamics (MD) simulation of the conformational ensemble of these bicycles by Dr. Jiayuan Miao and Dr. Yu-Shan Lin at Tufts University. The penultimate amino acids in **TSL-1**-SWDYRECYLEC and **TSL-6**-SWDYRECYLEC bicycles yielded different Ramachandran plots describing the dihedral angles for -WDYR- sequences in the first ring. On the other hand, the dihedral angle populations for the -CYLEC- sequence in the second ring were similar (Figure 2-9). The MD simulation suggested that conformations of two rings are decoupled from one another. Thus, differences in degradation for two bicycles, might originate from the enhanced flexibility in one of the rings. Similar decoupling was observed in **TSL-1**-SHCVWWDC and **TSL-6**-SHCVWWDC bicycles. The penultimate amino acid, His, exhibited different clustering of the dihedral angles. On the other hand, -VWWD- sequence in the second ring had similar backbone conformations in both bicycles (Figure 2-9). These studies provide an important starting point for understanding the ground-state conformational ensemble of these molecules.

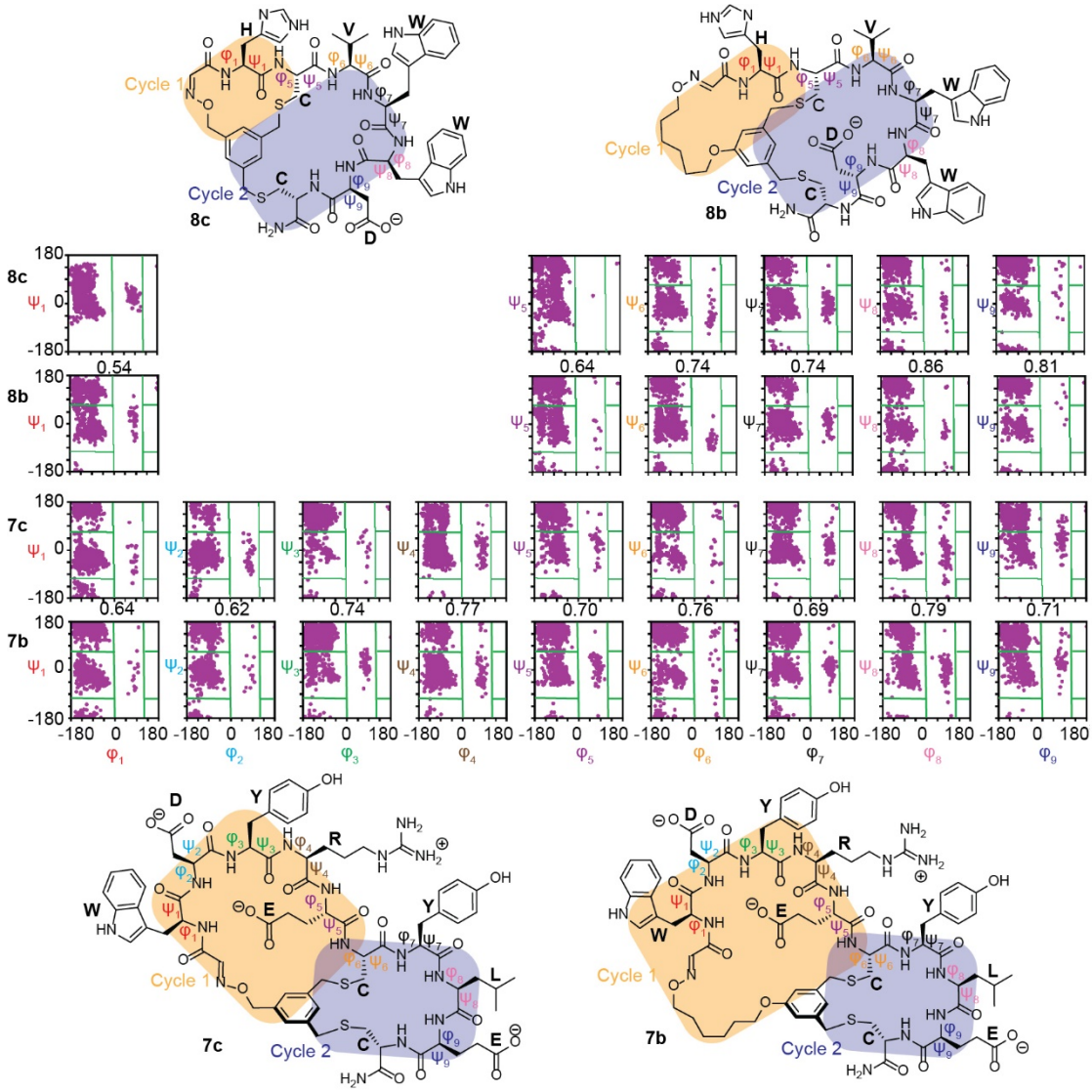

Figure 2-9. Ramachandran plot of the cyclic peptide backbone for **8c**, **8b**, **7c** and **7b**: Green lines indicate the binning boundaries used in the cluster analysis. The numbers shown between the Ramachandran plots of **8c** and **8b,** and between those of **7c** and **7b** are the normalized integrated product (NIP) calculated as $\mathrm{NIP} = \frac{2\sum_i \rho_{i,\mathrm{peptide1}}\rho_{i,\mathrm{peptide2}}}{\sum_i \rho_{i,\mathrm{peptide1}}{}^2 + \sum_i \rho_{i,\mathrm{peptide2}}{}^2}$.[303] NIP takes a value between 0 and 1, with 0 indicating no overlap between the two distributions and 1 indicating the two distributions are identical. The molecular dynamic was performed by Dr. Jiayuan Miao and Dr. Yu-Shan Lin at Tufts University.

2.3 Conclusions

In conclusion, two-fold symmetric tridentate linchpins that contain aldehyde and two thiol-reactive groups enable a robust one-pot bicyclization of peptides SX_nCX_mC. Such libraries can be used to discover productive antagonists of protein–protein interactions. The bicycles show good stability in digestive conditions. Although the 21 bicyclic peptide sequences tested do not exhaustively sample all possible combinations, the tested peptides included all the potentially problematic amino acids (Lys, Arg, His, Tyr, Trp, Asp/Glu, Ser/Thr). Proteolytic stability of bicyclic architecture sans a free N-terminus is significantly improved when compared to closely-related **DBMB**-cross-linked monocycles. As the strategy is compatible with phage display libraries containing the SX_nCX_mC motif, we anticipate that other peptide libraries that contain this motif will be amenable to such late-stage functionalization. We noted that many genetically-encoded libraries do not contain N-terminal Ser and instead have an N-terminal Met or Met analogs encoded by AUC starting codon. However, it is possible to introduce an N-terminal Ser into these systems by expressing a library with N-terminal TEV-cleavable sequence: H-MENLYFQ\S (where \ denoted as the cleavage site). A conceptually similar approach has been recently demonstrated by Jianmin Gao and co-workers who expressed ENLYFQ\C in phage displayed peptide libraries and used TEV cleavage to expose the N-terminal Cys.[304] Finally, the lower symmetry of the **TSL**-style linkers allows their diversification with any chemotype of C_2-symmetry.[279] It offers a significant expansion of the

bicyclization repertoire beyond traditional architectures produced from three-fold symmetric cross-linkers.

2.4 Experimental procedures

2.4.1 Chemistry methods

2.4.1-1 General chemistry information

Chemical reagents and solvents were purchased from Sigma-Aldrich or Fisher Scientific unless noted otherwise. 5-hydroxydimethyl isophthalate, 1,6-dibromohexane and 1,3-dibromopropane were purchased from TCI America. 1,3,5-Trisbromomethyl benzene was purchased from Synthonix. TCEP was purchased from Soltech Ventures. Pronase was purchased from Roche Diagnostics GmbH. Reagents for peptide synthesis were purchased from ChemPep. Reactions were monitored by TLC which was carried out on silica gel 60 F_{254} (Merck) plates and visualized by UV-light (λ = 254 nm) and/or by spraying potassium permanganate, anisaldehyde followed by heating. Flash column chromatography was performed using silica gel 60 (40-63 μm). The subsequent evaporation of solvents *in vacuo* was performed using IKA RV10 rotary evaporator. Analytical and preparative HPLC was conducted using Waters 1525 Binary pump equipped with a Waters Symmetry prep 19×50 mm C18 Columns and Waters 2489 UV detector. Removal of aqueous solvents was performed using Labconco Freezone 2.5w system.

Proton (^{1}H NMR) and Carbon (^{13}C NMR) nuclear magnetic resonance spectra were recorded on an Agilent/Varian VNMRS two channel 500 MHz or

Agilent/Varian Inova two-channel 400 MHz spectrometer. The chemical shifts are given in part per million (ppm) on the delta scale. The solvent peak was used as reference values. For ^{1}H NMR: $CDCl_3$= 7.26 ppm and for ^{13}C NMR: $CDCl_3$= 77.16 ppm. The following abbreviations have been used: s, singlet; d, doublet; t, triplet; m, multiplet. LC–MS analysis of peptide modifications was obtained on Agilent Technologies 6130 LC–MS. A gradient of solvent A (MQ water) and solvent B (MeCN/H_2O 95/5) was run at a flow rate of 0.5 mL/min (0-4.0 min 5% B; 4.0-5.0 min 5%→60% B; 5.0-5.5 min 60%→100% B; 5.5-7.5 100% B, 7.5-11 min 100%→5% B). LC–MS studies of stability of peptides in proteases and serum were performed in Hewlett Packard 1100 series instrument using a Phenomenex Jupiter C4 protein column (300 Å, 2×50 mm, 0.3 mL/min, A: 0.1% formic acid in water, B: 0.1% formic acid in acetonitrile (0 min 2% B, 0→10 min 2%→70% B, 10→15 min 70% B, 15→20 min 70%→2% B). The amount of peptide remaining was calculated with the area under the curve of SIM (Selected Ion Monitoring) peak in LC–MS. All the sequencing results will able available on 48 Hour Discovery cloud: https://48hd.cloud/. All the 20×20 plots were generated on the 48 Hour Discovery cloud: https://48hd.cloud/.

2.4.1-2 Synthetic procedures for the linchpins TSL-1, TSL-3 and TSL-6

This section was performed entirely by Dr. Raja Mukherjee.

tert-Butyl ((3,5-bis(bromomethyl)benzyl)oxy)carbamate **S1**

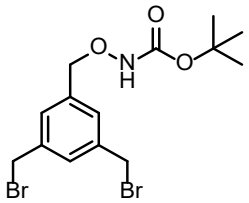

To a solution of 1,3,5-Trisbromobenzylbenzene (**TBMB**) (2.5 g, 7 mmol) in DCM (30 mL), an equimolar solution of N-Boc-hydroxylamine (306 mg, 2.3 eq.) and DBU (0.3 mL, 2.3 eq.) in DCM (5 mL) was added over the course of 30 min and the resulting solution was stirred for 3 h. The solvent was removed on a rotary evaporator and the crude residue was purified over silica gel chromatography using ethyl acetate-hexanes (1:4) as eluent producing the title compound **S1** as a white solid (707 mg, 25%): ^{1}H NMR (500 MHz, CDCl3) δ = 7.37 (s, 1 H), 7.34 (s, 1 H), 7.33 (s, 2 H), 4.82 (s, 2 H), 4.44 (s, 4 H), 1.47 (s, 9 H). ^{13}C NMR (125 MHz, CDCl3) δ = 156.73, 138.65, 137.18, 129.59, 129.38, 81.89, 77.58, 32.48, 28.20. HRMS (ESI) calculated for $C_{14}H_{19}Br_2NO_3Na$ [M+Na]+ m/z=429.9629, found 429.9226.

tert-Butyl ((3,5-bis(chloromethyl)benzyl)oxy)carbamate **S2**

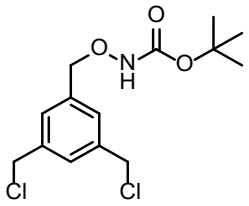

Lithium chloride (196 mg, 3 eq.) was added to a solution of **S1** (707 mg, 1.72 mmol) in DMF (10 mL) and the solution was stirred for 10 h. The reaction mixture was partitioned between ethyl acetate and water. The combined organic layers were washed with water and brine. The organic layer was dried over anhydrous sodium sulfate. After removing the solvent on a rotary evaporator, the crude residue was purified over silica gel chromatography using ethyl acetate-hexanes (1:4) as eluent producing the title compound **S2** as colorless oil (457 mg, 83%). ^{1}H NMR (400 MHz, $CDCl_3$) δ = 7.46 (s, 1 H), 7.37 (s, 1 H), 7.36 (s, 2 H), 4.82 (s, 2 H), 4.53 (s, 4 H), 1.46 (s, 9 H). ^{13}C NMR (100 MHz, $CDCl_3$) δ = 156.99, 138.51, 137.29, 129.14, 128.86, 82.04, 77.85, 45.70, 28.39. HRMS (ESI) calculated for $C_{14}H_{19}Cl_2NO_3Na$ $[M+Na]^+$ m/z=342.0640, found 342.0632.

O-(3,5-bis(chloromethyl)benzyl)hydroxylammonium 2,2,2-trifluoroacetate

TSL-1

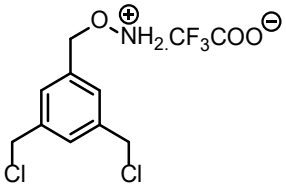

To a solution of **S2** (450 mg, 1.4 mmol) in DCM (10 mL), TFA (0.5 mL, 5 eq.) was added and the mixture was stirred for 1 h. The volatiles were removed on a rotary evaporator. Residual TFA was azeotropically removed by repeatedly dissolving the resulting oil in toluene and evaporation on a rotary evaporator to produce the title compound **TSL-1** as white viscous liquid (416 mg, 89%). To obtain product of higher purity 300 mg of crude **TSL-1** was purified by semi preparative RP-HPLC and lyophilized to yield **TSL-1** as light-yellow powder (212 mg, 71%). ^{1}H NMR (400 MHz, CD_3OD) δ = 7.56 (s, 1 H), 7.49 (d, 2 H, *J* = 1.6 Hz), 5.06 (s, 2 H), 4.70 (s, 4 H). ^{13}C NMR (100 MHz, CD_3OD) δ = 141.5, 136.7, 131.7, 131.1, 78.3, 46.49. HRMS (ESI) calculated for $C_9H_{12}Cl_2NO$ $[M+H]^+$ m/z=220.0290, found 220.0289.

Dimethyl 5-((6-bromohexyl)oxy)isophthalate **S4**

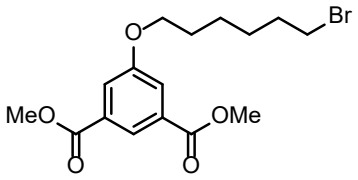

To a solution of 5-hydroxydimethylisophthalate (Sigma-Aldrich Cat# 371785-10G) (4.2 g, 20 mmol) and 1,6-dibromohexane (Sigma-Aldrich Cat# D41007-25G) (9.2 mL, 3 eq.) in CH_3CN (50 mL), potassium carbonate (8.3 g, 3 eq.) was added and the mixture was refluxed for 12 h. The reaction mixture was cooled to room temperature, diluted with water (50 mL) and extracted with ethyl acetate (3×20 mL). The combined organic layer was washed with water (50 mL) and brine (50 mL). Ethyl acetate was removed by rotary evaporator. Chromatography of the residue on silica gel using ethyl acetate-hexanes (7:1) as eluent produced the title compound **S4** as white solid (5.3 g, 70%): ^{1}H NMR (500 MHz, $CDCl_3$) δ = 8.23 (s, 1 H), 7.71 (s, 2 H), 4.02 (t, 2 H, *J* = 6.5 Hz), 3.92 (s, 6 H), 3.40 (t, 2 H, *J* = 6.5 Hz), 1.89-1.80 (m, 4 H), 1.51-1.48 (m, 4 H). ^{13}C NMR (125 MHz, $CDCl_3$) δ = 166.43, 159.40, 132.00, 123.09, 120.07, 68.60, 33.95, 32.91, 29.18, 28.13, 25.48. HRMS (ESI) calculated for $C_{16}H_{21}BrO_5Na$ $[M+Na]^+$ m/z=395.0465, found 395.0472.

Dimethyl 5-((6-(((tert-butoxycarbonyl)amino)oxy)hexyl)oxy)isophthalate **S5**

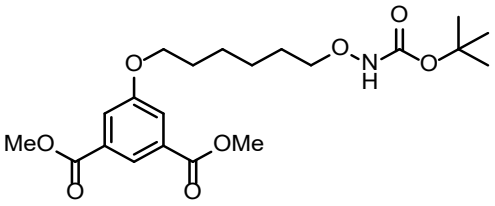

To a mixture of **S4** (5.3 g, 14 mmol) and N-Boc hydroxylamine (1.8 g, 1.2 eq.) in DCM (30 mL), DBU (1.7 mL, 1.2 eq.) was added drop wise and the solution stirred for 5 h. DCM was evaporated on a rotary evaporator and the crude residue was subjected to chromatography over silica gel with ethyl acetate-hexanes (4:1) produced the title compound **S5** as colorless oil (2.6 g, 43%). ^{1}H NMR (500 MHz, $CDCl_3$) δ = 8.24 (s, 1 H), 7.71 (s, 2 H), 7.15 (s, 1 H), 4.02 (t, 2 H, *J* = 6.5 Hz), 3.92 (s, 6 H), 3.85 (t, 2 H, *J* = 6.5 Hz), 1.80-1.64 (m, 4 H), 1.50-1.44 (m, 17 H). ^{13}C NMR (125 MHz, $CDCl_3$) δ = 166.50, 159.49, 157.22, 132.07, 123.11, 120.13, 81.86, 68.75, 29.27, 28.53, 28.49, 28.26, 26.13, 25.97. HRMS (ESI) calculated for $C_{21}H_{31}NO_8Na$ $[M+Na]^+$ m/z=448.1942, found 448.1940.

tert-Butyl ((6-(3,5-bis(hydroxymethyl)phenoxy)hexyl)oxy)carbamate **S6**

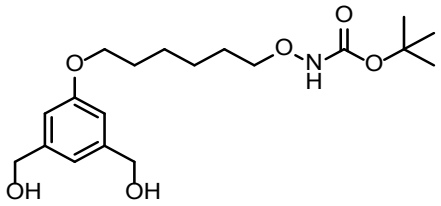

A solution of lithium aluminum hydride (713 mg, 18.3 mmol) in THF (10 mL) was added to an ice cold solution of **S7** (2.6 g, 6.1 mmol) in THF (25 mL) drop wise via cannula and the mixture was stirred for 3 h. Water was added very carefully until the evolution of hydrogen ceased. The white precipitate was filtered off and the solution was partitioned between ethyl acetate (3×30 mL) and water. The combined organic layers were washed with water, brine and dried over anhydrous sodium sulfate. Ethyl acetate was evaporated on a rotary evaporator and chromatography over silica gel of the crude residue with ethyl acetate-hexanes (1:1) produced the title compound **S6** as a colorless gum (1.5 g, 66 %): ^{1}H NMR (500 MHz, $CDCl_3$) δ = 7.15 (s, 1 H), 6.92 (s, 1 H), 6.84 (s, 1 H), 4.65 (s, 4 H), 3.98 (t, 2 H, *J* = 6.5 Hz), 3.86 (t, 2 H, *J* = 6.5 Hz), 2.03 (bs, 2 H), 1.82-1.76 (m, 2 H), 1.69-1.64 (m, 2 H), 1.52-1.43 (m, 13 H). ^{13}C NMR (125 MHz, $CDCl_3$) δ = 159.61, 156.96, 142.81, 117.36, 112.17, 81.63, 76.70, 67.87, 65.13, 29.05, 28.23, 27.92, 25.83, 25.61. HRMS (ESI) calculated for $C_{19}H_{31}NO_6Na$ $[M+Na]^+$ m/z=392.2044, found 392.2046.

tert-Butyl ((6-(3,5-bis(chloromethyl)phenoxy)hexyl)oxy)carbamate **S7**

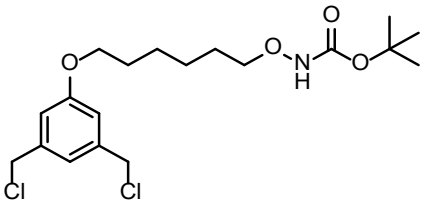

To an ice-cold solution of **S6** (1.5 g, 4 mmol) and triethylamine (1.7 mL, 3 eq.) in DCM (20 mL), methane sulfonyl chloride (0.8 mL, 2.5 eq.) was added dropwise and the solution was stirred for 30 min. Without further purification THF (10 mL) and lithium chloride (500 mg, 3 eq.) was added subsequently. The ice bath was removed, and the reaction stirred for 12 h. The solvent was removed in a rotary evaporator and the crude residue was purified by chromatography over silica gel using ethyl acetate-hexanes (7:1) as eluent to produce the title compound **S7** was as colorless oil (1.2 g, 74%). ^{1}H NMR (500 MHz, $CDCl_3$) δ = 7.15 (s, 1 H), 6.97 (s, 1 H), 6.87 (s, 2 H), 4.53 (s, 4 H), 3.96 (t, 2 H, *J* = 6.5 Hz), 3.86 (t, 2 H, *J* = 6.5 Hz), 3.92 (s, 6 H), 3.40 (t, 2 H, *J* = 7.0 Hz), 1.89-1.63 (m, 4 H), 1.51-1.48 (m, 4 H). ^{13}C NMR (125 MHz, $CDCl_3$) δ = 159.61, 156.91, 139.29, 120.69, 114.72, 81.60, 68.04, 52.57, 45.86, 29.02, 28.25, 27.97, 25.88, 25.69. HRMS (ESI) calculated for $C_{19}H_{29}Cl_2NO_4Na$ $[M+Na]^+$ m/z=428.1366, found 428.1372.

O-(6-(3,5-bis(chloromethyl)phenoxy)hexyl)hydroxylammonium 2,2,2-trifluoroacetate

TSL-6

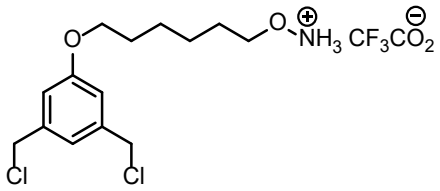

TFA (1.1 mL, 5 eq.) was added to a solution of **S7** (1.2 g, 2.9 mmol) in DCM (15 mL) and stirred for 1 h. TFA and DCM was removed on a rotary evaporator. Residual TFA was azeotropically removed by repeatedly dissolving the resulting oil in toluene and evaporation on the rotary evaporator to produce the title compound **TSL-6** as white viscous liquid (1.1 g, 89%). To yield a product of higher purity 100 mg of this compound was purified by RP-HPLC and lyophilized to produce the title compound **TSL-6** as white powder (62 mg, 62%). ^{1}H NMR (500 MHz, CD_3OD) δ = 7.05 (s, 1 H), 6.95 (s, 2 H), 4.61 (s, 4 H), 4.08-4.01 (m, 4 H), 1.82-1.68 (m, 4 H), 1.57-1.46 (m, 4 H). ^{13}C NMR (125 MHz, CD_3OD) δ = 161.81, 141.94, 122.82, 116.44, 77.12, 69.81, 47.29, 30.94, 29.48, 27.56, 27.23. HRMS (ESI) calculated for $C_{14}H_{22}Cl_2NO_2$ $[M+H]^+$ m/z=306.1028, found 306.1026.

Dimethyl 5-(3-bromopropoxy)isophthalate **S8**

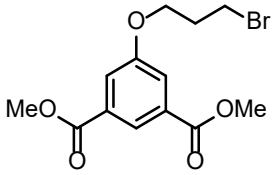

To a solution of 5-hydroxydimethylisophthalate (900 mg, 2.3 mmol) and 1,3-dibromopropane (0.31 mL, 1.5 eq.) in CH_3CN (20 mL), potassium carbonate was added and the mixture was refluxed for 12 h. The reaction mixture was allowed to cool down to room temperature, diluted with water (60 mL) and extracted with ethyl acetate (3×20 mL). The combined organic layer was washed with brine (50 mL). Ethyl acetate was removed on a rotary evaporator. Chromatography of the residue on silica gel in ethyl acetate-hexanes (7:1) produced the title compound **S8** as white solid (980 mg, 85%): ^{1}H NMR (500 MHz, $CDCl_3$) δ = 8.27 (s, 1 H), 7.74 (s, 2 H), 4.18 (t, 2 H, *J* = 6.0 Hz), 3.92 (s, 6 H), 3.60 (t, 2 H, *J* = 6.0 Hz), 2.33 (p, 2 H, *J* = 6.0 Hz). ^{13}C NMR (125 MHz, $CDCl_3$) δ = 166.43, 159.13, 132.20, 123.56, 120.17, 66.23, 52.78, 32.48, 29.96. HRMS (ESI) calculated for $C_{13}H_{15}BrO_5Na$ $[M+Na]^+$ m/z=353.9995, found 353.0002.

Dimethyl 5-(3-(((tert-butoxycarbonyl)amino)oxy)propoxy)isophthalate **S9**

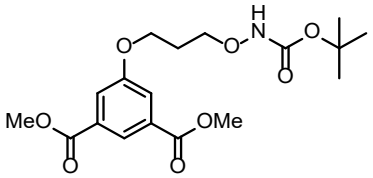

To a mixture of **S8** (3 g, 9 mmol) and N-Boc hydroxylamine (1.4 g, 1.2 eq.) in DCM (20 mL), DBU (1.6 mL, 1.2 eq.) was added dropwise and the solution stirred for 5 h. DCM was evaporated on a rotary evaporator and the crude was subjected to chromatography over silica gel with ethyl acetate-hexanes (4:1) produced the title compound **S9** as colorless oil (1.25 g, 36%). ^{1}H NMR (500 MHz, $CDCl_3$) δ = 8.26 (s, 1 H), 7.74 (s, 2 H), 7.21 (s, 1 H) 4.18 (t, 2 H, *J* = 6.0 Hz), 4.04 (t, 2 H, *J* = 6.0 Hz), 3.93 (s, 6 H), 2.14 (p, 2 H, *J* = 6.0 Hz), 1.47 (s, 9 H). ^{13}C NMR (125 MHz, $CDCl_3$) δ = 166.19, 159.03, 157.04, 131.81, 123.06, 119.91, 81.87, 73.14, 65.29, 52.44, 28.25, 28.05. HRMS (ESI) calculated for $C_{18}H_{25}NO_8Na$ $[M+Na]^+$ m/z=406.1472, found 406.1468.

tert-Butyl (3-(3,5-bis(hydroxymethyl)phenoxy)propoxy)carbamate **S10**

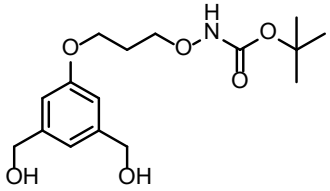

A solution lithium aluminium hydride (129 mg, 3 eq.) in THF (2 mL) was added to an ice cold solution of **S9** (1.25 g, 3.2 mmol) in THF (10 mL) via cannula drop wise and the mixture was stirred for 3 h. Water was added carefully until the evolution of hydrogen ceased. The white precipitate was filtered off and the filtrate was extracted with ethyl acetate (3×30 mL). The combined organic layer was washed with water, brine and dried over anhydrous sodium sulfate. Ethyl acetate was evaporated on a rotary evaporator and purification of the crude residue by chromatography over silica gel with ethyl acetate-hexanes (1:1) as eluent produced the title compound **S10** as a colorless gum (1.23 g, 86 %). ^{1}H NMR (500 MHz, $CDCl_3$) δ = 7.39 (s, 1 H), 6.87 (s, 1 H), 4.59 (s, 4 H), 4.18 (t, 2 H, *J* = 6.0 Hz), 4.04 (t, 2 H, *J* = 6.0 Hz), 3.93 (s, 6 H), 2.14 (t, 2 H, *J* = 6.5 Hz), 1.47 (s, 9 H). ^{13}C NMR (125 MHz, $CDCl_3$) δ = 159.63, 157.36, 143.14, 117.89, 112.48, 82.10, 73.61, 65.28, 65.01, 28.54, 28.42. HRMS (ESI) calculated for $C_{16}H_{25}NO_6Na$ $[M+Na]^+$ m/z=350.1574, found 350.1569.

tert-Butyl (3-(3,5-bis(chloromethyl)phenoxy)propoxy)carbamate **S11**

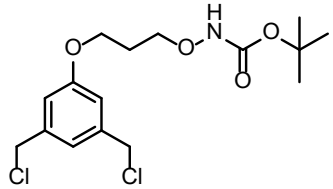

To an ice-cold solution of **S10** (1.2 g, 3.7 mmol) and trimethylamine (1.5 mL, 3 eq.) in DCM (15 mL), methane sulfonyl chloride (0.7 mL, 2.5 eq.) was added dropwise and the solution was stirred for 30 minutes. Without further purification THF (5 mL) and lithium chloride (421 mg, 3 eq.) was added subsequently. The ice bath was removed and the reaction mixture was stirred for 12 h. The volatiles were evaporated on a rotary evaporator and the crude residue was subjected to chromatography over silica gel using ethyl acetate-hexanes (1:6) as eluent to produce the title compound **S11** as colorless oil (900 mg, 65%). ^{1}H NMR (500 MHz, $CDCl_3$) δ = 6.99 (s, 1 H), 6.90 (s, 2 H), 4.54 (s, 4 H), 4.31 (t, 2 H, *J* = 6.0 Hz), 4.13 (t, 2 H, *J* = 6.0 Hz), 2.15 (p, 2 H, *J* = 6.0 Hz), 1.48 (s, 9 H). ^{13}C NMR (125 MHz, $CDCl_3$) δ = 159.49, 151.69, 139.51, 121.14, 114.92, 86.19, 76.23, 45.97, 38.76, 28.27. HRMS (ESI) calculated for $C_{16}H_{23}Cl_2NO_4Na$ $[M+Na]^+$ m/z=386.0896, found 386.0902.

O-(3-(3,5-bis(chloromethyl)phenoxy)propyl)hydroxylammonium 2,2,2-trifluoroacetate **TSL-3**

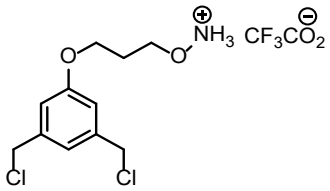

TFA (0.9 mL, 5 eq.) was added to a solution of **S11** (900 mg, 2.4 mmol) in DCM (10 mL) and stirred for 1 h. TFA and DCM was removed on a rotary evaporator. Residual TFA was azeotropically removed by repeatedly dissolving the resulting oil in toluene and evaporation, which produced the title compound **TSL-3** as white gummy liquid (725 mg, 80%). To obtain a product of higher purity, 300 mg of the title compound was purified in RP-HPLC and lyophilized to get a white powder (202 mg, 67%). ^{1}H NMR (400 MHz, CD_3OD) δ = 7.08 (s, 1 H), 6.98 (s, 2 H), 4.63 (s, 4 H), 4.27 (t, 2 H, *J* = 6.0 Hz), 4.14 (t, 2 H, *J* = 6.0 Hz), 2.20 (p, 2 H, *J* = 6.0 Hz).^{13}C NMR (100 MHz, CD_3OD) δ = 161.3, 142.1, 123.3, 116.5, 73.9, 65.9, 29.7. HRMS (ESI) calculated for $C_{11}H_{16}Cl_2NO_2$ $[M+Na]^+$ m/z=264.0553, found 264.0551.

2.4.1-3 General procedure for peptide synthesis

Peptides were synthesized on an automated peptide synthesizer (Prelude®X; Gyros Protein Technology) using standard solid phase amide coupling. After synthesis the resin was transferred to a Poly-Prep column (Biorad) and washed with DCM (10 mL) and dried in vacuum. The resin was then treated with a cleavage cocktail (7 mL) containing TFA/H_2O/TIPS/EDT, 90/2.5/5/2.5 (v/v/v/v) for the global deprotection and cleavage of the peptide from the resin. After 4 h the flow through from the column was collected and the resin was rinsed with TFA (1 mL). The combined cleavage mixture reduced in volume to 2 mL by means of gently bubbling nitrogen through it and was added drop-wise to cold diethyl ether (10 mL) in a 15 mL polypropylene centrifuge tube (Falcon, Thermo Fisher). The precipitate formed was separated by centrifugation (5 min, 3000 rpm). Supernatant was decanted and the precipitates were washed with cold diethyl ether (10 mL). The centrifugation and washing steps were repeated for two more cycles. The precipitates were air-dried. For HPLC purification, crude peptide powder was dissolved in MeCN and water; addition of acetic acid was necessary in some cases to dissolve the peptide. The solution was injected into a semi preparative RP-HPLC system. The fractions corresponding to the main peak were collected. CH_3CN was removed in Speed Vac (Savant SPD111V). The aqueous solution was lyophilized to yield the peptide as white powder.

2.4.1-4 Protocol 1: bicyclization of peptides SX_nCX_mC with TSL using C18 spin column.

Procedure (analytical scale: 25 nanomole or 25 μg of 1000 Da peptide):	Vol. (μL):
1. In a 0.6 mL Eppendorf tube, combine peptide (5 μL from 5 mM stock) and 45 μL PBS to a final concentration of peptide 0.5 mM.	45+5=50
2. Take 1 μL out to check the purity of the starting material and serve as reference (mix 1 μL with 9 μL 0.1% TFA and inject 5 μL in the LC–MS)	50-1=49
3. Add sodium periodate (1.2 eq., 0.6 mM, 1 μL from 30 mM stock) and incubate for 5 min in the dark.	49+1=50
4. Load the resulting solution onto an equilibrated C18 desalting spin column. Wash the column with 2×50 μL of 20% acetonitrile containing 0.1% TFA and elute the peptide with 2×20 μL of 70% acetonitrile. A typical volume collected at this step is 40 μL	40
5. Remove excess of acetonitrile in the speed-vac. A typical volume after this step is 12 μL. Then add 28 μL mQ water.	12+28=40
6. To solution from 5, add (in this order!): 8 μL acetonitrile, then 1 μL of 5% TFA (final TFA concentration = 0.1%) and then 1 μL of 30 mM stock solution of **TSL** (1.2 eq., final concentration 0.6 mM). Incubate for 1 h.	40+1+8+1=50
7. If necessary, monitor the progress of the reaction by withdrawing 1 μL and quenching is with 9 μL of 0.1% TFA and injecting 5 μL in the LC–MS.	50-1=49
8. To the resulting oxime, add TCEP (5 eq., 1 μL from 125 mM stock solution, final concentration 2.5 mM) and incubate for 30 minutes.	49+1=50
9. Add 30 μL mQ water followed by addition of 20 μL 500 mM Tris of pH 8.5 (final Tris concentration 100 mM) and incubate for an hour.	50+30+20=100
10. To confirm the formation of the product, withdraw 1 μL of reaction mixture, quenching with 9 μL 0.1% TFA and injecting 5 μL in the LC–MS	100-1=99

Materials:

- Solution of 5 mM peptide (SX_mCX_nC) in water
- 30 mM stock of **TSL** in water: acetonitrile (1:1)
- 30 mM stock of $NaIO_4$ solution in water
- 125 μM stock solution of TCEP in water
- C18-desalting spin column (Thermo Scientific ,#89870 Pierce C-18 spin column)
- MiliQ (mQ) water and HPLC grade acetonitrile
- 500 mM Tris, pH 8.5
- 5% TFA solution in mQ water.
- PBS (50 mM K_2HPO_4, 150 mM NaCl, pH 7.4)
- 0.6 mL Eppendorf tubes, pipettes and tips
- LC–MS instrument and auto-sampler vials for LC–MS

2.4.1-5 Protocol 2: bicyclization of peptides SX_nCX_mC with TSL using methionine as quencher

Procedure (analytical scale: 25 nanomole or 25 μg of 1000 Da peptide):	Vol. (μL):
1. In a 0.6 mL epi, combine peptide (1 μL from 25 mM stock) 39 μL PBS pH 7.4 and 10 μL acetonitrile to a final concentration of 0.5 mM.	1+39+10=50
2. Take 1 μL out to check the purity of the starting material and serve as reference point (mix 1 μL with 9 μL 0.1% TFA and injecting 5 μL in the LC–MS)	50-1=49
3. Add sodium periodate (1.0 eq., 0.5 mM, 1 μL from 25 mM stock) and incubate for 5 min in the dark.	49+1=50
4. Take 1 μL out to check LC–MS	50-1 = 49
5. To the resulting solution add methionine (5.0 eq., 2.5 mM, from 125 mM stock) and incubate for 15 min	49+1 = 50
6. To the solution then add 1 μL of 5% TFA (final TFA concentration = 0.1%) and 1 μL of 30 mM stock solution of **TSL** (1.2 eq., final concentration 0.6 mM). Incubate for 1 h.	50+2 = 52
7. Monitor the progress of the reaction by withdrawing 2 μL in 18 μL of 0.1% TFA and injecting 5 μL in the LC–MS.	52-2 = 50
8. To the resulting oxime, add TCEP (5 eq., 1 μL from 125 mM stock solution, final concentration 2.5 mM) and incubate for 30 minutes.	50+1=51
9. Add 10 μL acetonitrile, 29 μL mQ water, followed by addition of 10 μL 1000 mM Tris of pH 8.5 (final Tris concentration 100 mM) and incubate for an hour.	51+10+29+10 =100
10. To confirm the formation of the product, withdraw 1 μL of reaction mixture, quenching with 9 μL 0.1% TFA and injecting 5 μL in the LC–MS.	100-1=99

Materials:

- Solution of 25 mM peptide (SX_mCX_nC) in water
- 25 mM stock of $NaIO_4$ solution in water
- 125 mM methionine in water
- 30 mM stock of **TSL** in water: acetonitrile (1:1)
- 125 μM stock solution of TCEP in water
- MiliQ (mQ) water and HPLC grade acetonitrile
- 1000 mM TRIS of pH 8.5

- 5% TFA solution in mQ water.
- 1×PBS, (50 mM phosphates, 150 mM NaCl, pH 7.4)
- 0.6 mL epi tubes, pipettes and tips
- LC–MS instrument and auto-sampler vials for LC–MS

2.4.1-6 General procedure for one-pot bicyclization on semi-preparative scale

In a 50 mL poly-propylene falcon tube, 10 mg of peptide (NH_2-SYCKPFC-$CONH_2$, MW = 846 Da, 12 μmol) was dissolved in 20.8 mL PBS (pH 7.4) containing 2.36 mL of acetonitrile. To the resulting solution, sodium periodate (1.2 eq., 236 μL of 500 mM in water) was added and mixed on a rocker for 5 minutes in the dark. A solution of methionine in water (5 eq., 9 mg, 0.06 mmol) was added to quench the residual oxidizing agent (periodate/iodate). After 15 minutes, neat TFA was added to the reaction (23.6 μL to a final concentration of 0.1%) followed by the addition of **TSL-1** in acetonitrile (2 eq., 26.6 μL from 1 M stock). As oxo-aldehyde and formaldehyde are generated simultaneously, an excess of **TSL** was needed in this step (Appendix A-Scheme 1). After incubation for 1 h, solution of TCEP in water (5 eq., 15 mg, 0.06 mmol) was added and rocked for 30 minutes to reduce the disulfide bond. The reaction mixture was diluted by 16.5 mL of water and 2.36 mL of acetonitrile followed by the addition of sodium bicarbonate at pH 10 (4.7 mL from 1 M stock to a final concentration of 100 mM) and rocked for 3 h. Completion of bicyclization can be confirmed by sampling an aliquot and analyzing it by LC–MS. The reaction was purified in semi preparative RP-HPLC to yield a bicyclic peptide **TSL-1**-SYCKPFC (5 μmol, 4.6 mg, 42%).

2.4.1-7 General protocol for bicyclization with TBMB

This section was performed entirely by Dr. Raja Mukherjee.

Peptide **12a** (10 mg, 5.4 μmol) was dissolved in 5.4 mL bicarbonate buffer (100 mM, pH 10) containing 10% acetonitrile. A solution of TCEP (2.5 eq, 27 μL of 500 mM stock, to a final concentration 2.5 mM) was added, follow with a solution of TBMB was added (1 eq, 11 μL of 500 mM in acetonitrile) and the reaction mixture was mixed on a rocker for 20 h. Upon consumption of all the starting material (as confirmed by LC–MS) the reaction mixture was directly purified on RP-HPLC and freeze-dried to yield **12f** as light yellow powder (4.3 mg, 41%).

2.4.1-8 General protocol for cyclization with pentafluorophenylsulfide (PFS)

Peptide **5a** (10 mg, 10 μmol) was dissolved in 5.0 mL DMF in a glass vial and a solution of perflurodiphenylsulfide (4 eq, 14 mg, 40 μmol) was added to this solution. 560 μL of 50 mM Tris base (final concentration of Tris is 5 mM/DMF) were added into the vial. The mixture was vortexed for 30 sec and incubated at rt for 1 h. After 1 h, the reaction was quenched by diluting 10 times with 50% aq. acetonitrile containing 0.1% TFA. The product was purified with RP-HPLC, freeze dried to obtain **5e** as white powder (5 mg, 40%).[219]

2.4.1-9 General protocol for cyclization with α,α′-dibromo-m-xylene (DBMB)

Peptide **5a** (10 mg, 10 μmol) was dissolved in 5.0 mL H_2O/ACN 50% in a glass vial and a solution of α,α′-Dibromo-m-xylene in acetonitrile (1.2 eq) was added to this solution. 500 μL of 500 mM Tris-HCl buffer at pH 8.5 (final concentration of Tris-HCl buffer 50 mM) were added into the vial. The mixture was vortexed for 30 sec and incubated at rt for 1 hour. After 1 hour, the reaction was purified with RP-HPLC, freeze dried to obtain **5g** as white powder (5.1 mg, 46%).

2.4.1-10 General bicyclization analytical procedure for 10b and 11b

Materials

Procedure (analytical scale: 25 nanomole or 25 μg of 1000 Da peptide):		Vol. (μL):
1.	In a 0.6 mL Eppendorf tube, combine peptide (5 μL from 5 mM stock) and 45 μL PBS to a final concentration of peptide 0.5 mM.	45+5=50
2.	Take 1 μL out to check the purity of the starting material and serve as reference (mix 1 μL with 9 μL 0.1% TFA and inject 5 μL in the LC–MS)	50-1=49
3.	Add sodium periodate (1.2 eq., 0.6 mM, 1 μL from 30 mM stock) and incubate for 5 min in the dark. Add methionine (12 eq., 6 mM, 1 μL from 300 mM stock) and incubate for an hour	49+2=51
4.	Load the resulting solution onto an equilibrated C18 desalting spin column. Wash the column with 2 × 50 μL of 20% acetonitrile containing 0.1% TFA and elute the peptide with 2×20 μL of 70% acetonitrile. A typical volume collected at this step is 40 μL	40
5.	Remove excess of acetonitrile in the speed-vac. A typical volume after this step is 12 μL. Then add 28 μL miliQ water.	12+28=40
6.	To solution from 5, add (in this order): 8 μL acetonitrile, then 1 μL of 5% TFA (final TFA concentration = 0.1%) and then 1 μL of 30 mM stock solution of TSL (1.2 eq., final concentration 0.6 mM). Incubated for 1 h.	40+1+8+1=50
7.	If necessary, monitor the progress of the reaction by withdrawing 1 μL and quenching is with 9 μL of 0.1% TFA and injecting 5 μL in the LC–MS.	50-1=49
8.	To the resulting oxime, add TCEP (5 eq., 1 μL from 125 mM stock solution, final concentration 2.5 mM) and incubate for 30 minutes.	49+1=50
9.	Add 30 μL mQ water followed by addition of 20 μL 500 mM $KHCO_3$ of pH 8.0 (final $KHCO_3$ concentration 100 mM) and incubate for an hour.	50+30+20 =100
10.	To confirm the formation of the product, withdraw 1 μL of reaction mixture, quenching with 9 μL 0.1% TFA and injecting 5 μL in the LC–MS	100-1=99

2.4.1-11 Protocol for 10b scale up synthesis

This section was performed entirely by Dr. Serhii Kharchenko

Peptide **10a** (10 mg, 0.0084 mmol) was dissolved in water: acetonitrile (1.67 mL, v/v 7:3) and buffered with PBS (14.98 mL, 50 mM K_2HPO_4, 150 mM NaCl, pH 7.4). 1 µL of the solution was sampled for LC–MS (mixed 1 µL with 9 µL of 0.1% TFA and injected 5 µL in the LC–MS). A solution of $NaIO_4$ in water (336 µL, 1.2 eq, 2.16 mg, 0.01 mmol) was added to the reaction and incubated at 20 °C in the dark for 5 min. To quench the oxidation, a solution of methionine in water (336 µL, 12 eq, 14.86 mg, 0.01 mmol) was added to the reaction and incubated for 1 h. The resulting solution was loaded onto an equilibrated C18 desalting spin column (pre-washed the column with 2×2.5 mL of 20% acetonitrile containing 0.1% TFA) and eluted the peptide with 2×500 µL of 70% acetonitrile without TFA. A typical volume collected at this step is 13.4 mL. The excess acetonitrile was removed in the speed-vac and the typical volume after this step was ~4 mL. MiliQ water was added to a final volume of 13.4 mL and 1 µL of the solution was sampled to check the purity of the eluent to serve as a reference (mix 1 µL with 9 µL 0.1% TFA and inject 5 µL in the LC–MS). To the eluent, we added acetonitrile in water:acetonitrile v/v 1:1 (2.67 mL), 5% TFA (336 µL) and then a solution of **TSL-6** (336 µL, 1.2 eq, 4.2 mg, 0.01 mmol,) was added. The reaction mixture stirred for 2 h at 30 °C. The progresses of the reaction were monitored by withdrawing 1 µL, quenching with 9 µL of 0.1% TFA and injecting 5 µL in the LC–MS. When the reaction was completed, a solution of TCEP in water (336 µL, 5 eq, 12.02 mg, 0.043 mmol) was added to

the reaction and stirred for 1 h (1 µL of the reaction was sampled, mixed with 9 µL of 0.1% TFA and injected 5 µL in the LC–MS as a reference). The reaction mixture was then supplemented with mQ water (10.05 mL), adjusted the $KHCO_3$ buffer to a final concentration of 100 mM (6.6 mL from 500 mM $KHCO_3$ of pH 8.0 stock) and incubated for 3 h. The progress of the reaction was monitored by withdrawing 1 µL, quenching with 9 µL of 0.1% TFA and injecting 5 µL in the LC–MS. Then, the reaction mixture was concentrated by lyophilization and was purified by LC–MS. The yield of the bicyclization is 3.5 mg, 32% from 10 mg starting material.

2.4.1-12 Protocol for 11b scale up synthesis

This section was performed entirely by Dr. Serhii Kharchenko

Peptide **11a** (10 mg, 0.0066 mmol) was dissolved in water:acetonitrile (1.32 mL, v/v 7:3) and buffered with PBS (11.88 mL, 50 mM K_2HPO_4, 150 mM NaCl, pH 7.4). 1 µL of the solution was sampled for LC–MS (mixed 1 µL with 9 µL of 0.1% TFA and injected 5 µL in the LC–MS). A solution of $NaIO_4$ in water (264 µL, 1.2 eq, 1.7 mg, 0.0079 mmol) was added and the reaction was incubated at 20 °C in the dark for 5 min. To quench the oxidation, a solution of methionine in water (264 µL, 12 eq, 11.7 mg, 0.079 mmol) was added and the reaction was incubated for 1 h. The resulting solution was loaded onto an equilibrated C18 desalting spin column (pre-washed the column with 2×2.5 mL of 20% acetonitrile containing 0.1% TFA). The peptide was eluted with 2×500 µL of 70% acetonitrile. A typical volume collected at this step is 10.5 mL. The excess acetonitrile was removed in the speed-vac and the typical volume after this step

was ~ 3 mL. MiliQ water was added to a final volume of 10.5 mL. 1 µL of the solution was sampled to check the purity of the eluent and to serve as a reference (mixed 1 µL with 9 µL of 0.1% TFA and injected 5 µL in the LC–MS). To the reaction mixture, we added acetonitrile (2.1 mL), 5% TFA (336 µL) and then a solution of **TSL-6** in water:acetonitrile v/v 1:1 (264 µL, 1.2 eq, 3.18 mg, 0.0079 mmol,) was added to the reaction. The reaction mixture was stirred for 2 h at 30 °C. The progresses of the reaction were monitored by withdrawing 1 µL, quenching with 9 µL of 0.1% TFA and injecting 5 µL in the LC–MS. When the reaction was completed, a solution of TCEP in water (264 µL, 5 eq, 9.47 mg, 0.0339 mmol) was added to the solution, and stirred for 1 h (1 µL of the reaction was sampled, mixed with 9 µL of 0.1% TFA and injected 5 µL in the LC–MS as a reference). Reaction mixture was then supplemented with miliQ water (7.92 mL), adjusted the $KHCO_3$ buffer to a final concentration of 100 mM (5.2 mL from 500 mM $KHCO_3$ of pH 8.0 stock) and incubated for 3 h. The progress of the reaction was monitored by withdrawing 1 µL, quenching with 9 µL of 0.1% TFA and injecting 5 µL in the LC–MS. Then, the reaction mixture was concentrated by lyophilization and was purified by LC–MS. The yield of the bicyclization was 2.9 mg, 28% from 10 mg starting material.

2.4.2 Phage modification methods

2.4.2-1 Preparation of $SXCX_6C$ phage libraries

The procedures have been adopted and modified from previously described in two publications that produced the M13-displayed SXCXXXC library[305] and M13-SDB vector.[306] In short, the vector SB4 QFT*LHQ was digested with Kpn I HF (NEB cat# R3142S) and Eag I HF (NEB cat# R3505S). A primer/template pair consisting of primer 5'-CAT GGC GCC CGG CCG AAC CTC CAC C-3' and template 5'-CC CGG GTA CCT TTC TAT TCT CAC TCT TCT X TGT XXXXXX TGT GGT GGA GGT TCG GCC GGG CGC TTG ATT -3' with the 'X' representing a trinucleotide was formed by annealing. The primer/template was then extended using Klenow DNA polymerase (NEB) according to the manufacturer's instructions. The insert fragment was then digested with Kpn1 HF and Eag1 HF, gel purified and ligated into the cut vector. The ligation products were then transformed into electrocompetent *E.coli* cells and the transformants were grown overnight on *E.coli* TG1 to allow for phage production. Phage cultures were then centrifuged to remove cells and debris and then the phage was precipitated by PEG precipitation (5% PEG 0.5 M NaCl). We sequenced the naïve libraries by Illumina sequencing and the naïve library of SB4-SXCXXXXXXC composition are publicly available at the following links: https://48hd.cloud/file/1470

2.4.2-2 General protocol for modification of $SXCX_6C$ phage library

$SXCX_6C$ phage displayed peptide library was used. We observed that the further cleanup of phage-associate lipopolysaccharide (LPS) improved the chemical modification. To remove the LPS, the phage solution (10^{13} PFU/mL) was combined with Triton X-100 to 10% final amount and incubated for 1 hour at room temperature. The phage was then re-purified using PEG-NaCl precipitation and resuspended to original volume with PBS (50 mM, pH 7.4). The resuspended phage then dialyzed at 4 ˚C against 4 L of PBS (50 mM, pH 7.4) for 12 hours using 10K MWCO membrane. All the incubation in the chemical modification were performed by gentle agitation with a rotator, as prolonged vortex-shaking of phage is detrimental to infectivity of phage.

Oxime Ligation: To a cleaned phage library (100 µL, ~3×10^{13} pfu/mL), we added sodium periodate (1 µL of 6 mM $NaIO_4$ in water to a final concentration of 60 µM) and incubated on ice in the dark for 9 min. The oxidation was quenched with methionine (1 µL of 500 mM methionine in water to a final concentration of 0.5 mM) and incubated for 20 minutes at rt. To the oxidized library, we added **TSL-6** linchpin (100 µL of 2 mM **TSL-6** in 20% aq. CH_3CN containing 0.2% TFA; final concentrations: 2 mM of **TSL-6**, 10% CH_3CN, 0.1% TFA) and incubated for 1 h at rt. To monitor the oxidation and oxime ligation reactions, we used previously described biotin capture assay.[271] Briefly, 5 µL of the oxidized or 5 µL of the oxime-ligated phage solutions were combined with 1 mM (5 µL of 2 mM AOB in 200 mM anilinum acetate buffer,

pH 4.6) for 1 h. AOB modified phage was diluted 10^6 fold, captured with streptavidin magnetic beads; supernatant was tittered before and after capture.

Reduction and bicyclization: The **TSL**-ligated library was purified using Zeba™ Spin Desalting Columns (7K MWCO, 0.5 mL, cat# 89882) using sodium acetate (50 mM NaAc, pH 5) as eluent. To 100 µL of the purified library, we added TCEP (2 µL of 50 mM TECP in water, final concentration 0.5 mM) and incubated for 30 mins. Increase of the pH to 10 by addition of bicarbonate buffer (25 µL of 1 M bicarbonate buffer, pH 10) and incubation for 3 h led to cyclization. The modified library supplemented with PBS (20 µL of 500 mM PBS, pH 7.4) and purified using Zeba column prior to storage or panning. To monitor the cyclization reaction, 5 µL of the reaction mixture was sampled at various steps (before and after addition of TCEP, control experiments with TCEP) and combined thiol-biotin (BSH) at pH 8.5 (2 µL of 4 mM BSH in MiliQ water), supplemented with 5 µL of 500 mM Tris-HCl pH 8.5 and 38 µL water and incubated for 3 hours. The phage treated with BSH was captured with biotin-capture assay as described above. Typically, over 40% of the phage library was successfully bicyclized.

2.4.3 General selection and validation methods

2.4.3-1 General setting for panning on KingFisher Sample Purification System

The protein immobilized beads suspension and other reagents were added to a 96 Deepwell Plate (Thermo Fisher, #95040450) as follows:

Row A: Protein coated magnetic beads (1 mL in in PBS Buffer)

Row B: Reserved for 12-tip Deepwell magnetic comb (Thermo Fisher, #97003500)

Row C: Wash Buffer (1 mL, PBS buffer)

Row D: Blocking Buffer (1 mL, 2% BSA (w/v) in PBS Buffer)

Row E: Solution of **TSL-6**-SXCX$_6$C libraries (1 mL, 10^9 PFU/mL in PBS Buffer)

Row F: Wash Buffer (1 mL, 0.1% Tween-20 (v/v) in PBS Buffer)

Row G: Wash Buffer (1 mL, 0.1% Tween-20 (v/v) in PBS Buffer)

Row H: Wash Buffer (1 mL, 0.1% Tween-20 (v/v) in PBS Buffer)

Following steps were performed using a KingFisher™ Duo Prime Purification System with a magnetic comb to transfer the beads. The program is as follows: a) collect comb from row B b) Collect beads from row A on comb, c) Wash beads in row C – 30 s, d) Block in row D – 1 h, e) Phage binding in row E – 1.5 h, f) Wash beads in row F – 1 min, g) Wash beads in row G – 1 min, h) Wash beads in row H – 1 min. At the end of the program, the protein coated beads with phage bound were in wells in the Row H. The content of each well from row H was transferred to individual Eppendorf™ tube, and process for next

round panning described in **2.4.3-2** and for Illumina deep sequencing described in **2.4.3-3**.

2.4.3-2 Bio panning of NODAL protein

First round of selection: (Denoted as R1-NT) In a 1.7 mL centrifuge tube, 20 µL of Ni-NTA magnetic beads (Thermo Fisher Scientific cat # 10104D) were incubated with 5 µg of His-tagged NODAL (Proteintech cat # Ag21882) overnight in 100 µL of 1×PBS at 4 °C. In parallel, **TSL-6** modified library was incubated with 20 µL of empty Ni-NTA magnetic beads over at 4 °C to remove beads specific binding. After immobilizing, the beads were wash with 1×PBS 3 times and blocked with blocking solution (1 % BSA in 1×PBS) at rt for 1 hour. In parallel, **TSL-6** modified library was incubated with 20 µL of empty Ni-NTA magnetic beads in the present of blocking solution (1 % BSA in 1×PBS) at rt for 1 hour. After blocking the NODAL immobilized beads, pre-selected **TSL-6** modified library was incubated with NODAL immobilized beads for 2 hours at rt. The beads were captured with magnetic rack and washed once with 1×PBS with 0.1% (v/v) Tween-20 to remove unbound phage. Phage remaining on the beads were eluted with 200 µL of glycine elution buffer (Glycine-HCl pH 2.2, 0.1% BSA) for 9 min. The elution buffer was transferred into a new 1.7 mL microcentrifuge tube and neutralized with 20 µL of 1 M Tris-HCl (pH 9.1). The recovered phage solution was amplified for next round of bio panning and for deep sequencing.

Second round of selection: (R2-NT) Amplified phage recovered from R1-NT was modified with **TSL-6 a**s described in section 2.4.2-2. In a 1.7 mL centrifuge tube, 20 µL of Ni-NTA magnetic beads were incubated with 5 µg of His-tagged NODAL overnight in 100 µL of 1×PBS at 4 °C. In parallel, **TSL-6** modified library was incubated with 20 µL of empty Ni-NTA magnetic beads over at 4 °C to remove beads-specific binders. The blocking, panning and washing were performed in Kingfisher Instrument. The NODAL immobilized beads, phage library, blocking buffer and washing buffer were added into King Fisher Plate in the corresponding well. The panning solution after Kingfisher Instrument were transfer into 1.7 mL centrifuge tube. Phage remaining on the beads were eluted with 200 µL of glycine elution buffer (Glycine-HCl pH 2.2, 0.1% BSA) for 9 min. The elution buffer was transferred into a new 1.7 mL microcentrifuge tube and neutralized with 20 µL of 1 M Tris-HCl (pH 9.1). The recovered phage solution was amplified for next round of bio panning and for deep sequencing.

Third round of selection: Amplified phage recovered from R2-NT was modified with **TSL-6**. In each 1.7 mL centrifuge tube, 20 µL of Ni-NTA magnetic beads were incubated with 2.5 µg of His-tagged NODAL and His-tagged T4-GP overnight in 100 µL of 1×PBS at 4 °C. In parallel, of second round selected **TSL-6** modified library and second round selected un-modified library was incubated with 20 µL of empty Ni-NTA magnetic beads over at 4 °C to remove beads specific binding. The panning against NODAL were performed in Kingfisher Instrument. (R3-NT) In control panning, **TSL-6** library against T4-GP

(R3-TG) and unmodified library that amplified phage from R2-NT against NODAL (R3-UN) were also performed in parallel. The proteins immobilized beads, phage library, blocking buffer and washing buffer were added into KingFisher Plate in the corresponding well. The panning solution after KingFisher Instrument were transfer into 1.7 mL centrifuge tube. Phage remaining on the beads were eluted with 200 µL of glycine elution buffer (Glycine-HCl pH 2.2, 0.1% BSA) for 9 min. The elution buffer was transferred into a new 1.7 mL microcentrifuge tube and neutralized with 20 µL of 1 M Tris-HCl (pH 9.1). The recovered phage solution was amplified for next round of bio panning and for deep sequencing.

2.4.3-3 General PCR amplification protocol for Illumina deep sequencing

Take 25 µL of eluted or amplified phage solution was used as a template for PCR with total volume of 50 µL (Appendix A-Figure 5).

A Typical 50 µL PCR mixture contained:

1.	5×Phusion buffer	10 µL
2.	10 mM dNTPs	10 µL
3.	Phusion® High-Fidelity DNA Polymerase (NEB, cat#M0530S)	0.5 µL
4.	Forward primer (3'-CAAGCAGAAGACGGCATACGAGATCGGTCTCGGCATTCCTGCTGAACCGCTCTTCCGATCTXXXXXCCTTTCTATTCTCACTCT-5', 10 µM)	2.5 µL
5.	Reverse primer (3'-AATGATACGGCGACCACCGAGATCTACACTCTTTCCCTACACGACGCTCTTCCGATCTXXXXACAGTTTCGGCCGA-5', 10 µM)	2.5 µL
6.	Template solution	25 µL
7.	Nuclease free water	8.5 µL

Thermocycler was preformed using the following setting:

a) 95 °C for 30 sec

b) 95 °C for 30 sec

c) 60.5 °C for 15 sec

d) 72 °C for 30 sec

e) Repeat step b) to d) 25 times

f) 72 °C for 5 min

g) hold at 4°C

2.4.3-4 Illumina sequencing of samples before and after panning

The PCR products were produced by PCR as described in Section 2.4.3-3 with one exception: in amplification of libraries before panning (input), volume of template (phage solution) was 2 µL. All products were quantified by 2% (w/v) agarose gel in Tris-Borate-EDTA buffer at 100 volts for ~35 min using a low molecular weight DNA ladder as standard (NEB, #N3233S). PCR products that contain different indexing barcodes were pooled allowing 10 ng of each product in the mixture. The mixture was purified by eGel, quantified by quBit and sequenced using the Illumina NextSeq paired-end 500/550 High Output Kit v2.5 (2×75 cycles). Data was automatically uploaded to BaseSpace™ Sequence Hub. Processing of the data is described in section "2.4.3-6 Processing of Illumina data".

2.4.3-5 General data processing methods

Data analysis of Illumina data at Appendix A-Figure 10 was performed in Microsoft Excel. All the 20×20 plots were generated on the 48 Hour Discovery cloud: https://48hd.cloud/. Linear regression analysis of Appendix A-Figure 12 and Appendix A-Figure 13 were performed in Studio R script.

2.4.3-6 Processing of Illumina data

The Gzip compressed FASTQ files were downloaded from BaseSpace™ Sequence Hub. The files were converted into tables of DNA sequences and their counts per experiment. Briefly, FASTQ files were parsed based on unique multiplexing barcodes within the reads discarding any reads that contained a low-quality score. Mapping the forward (F) and reverse (R) barcoding regions,

mapping F and R priming regions allowing no more than one base substitution each, and F-R read alignment allowing no mismatches between F and R reads yielded DNA sequences located between the priming regions. The files with DNA reads, raw counts, and mapped peptide modifications were uploaded to http://48hd.cloud/ server. Each experiment has a unique alphanumeric name (e.g., 20181108-16TSooPA-YW) and a unique static URL:

	R1	R2	R3
Un-Modified	http://48hd.cloud/file/2363	https://48hd.cloud/file/2326	https://48hd.cloud/file/2600
TSL-6 Modified	https://48hd.cloud/file/2320	https://48hd.cloud/file/2602	https://48hd.cloud/file/2609
Elution	https://48hd.cloud/file/2322	https://48hd.cloud/file/2601	https://48hd.cloud/file/2608
Amplification	https://48hd.cloud/file/2326	https://48hd.cloud/file/2600	https://48hd.cloud/file/2607

2.4.3-7 General protocol for protein extraction

All samples in the protein extraction protocol were done on ice. All cell samples were scrapped and treated with M-PER™ Mammalian Protein Extraction Reagent (Thermo Scientific, cat# 78501). Then, the treated sample sonicated for 4 sec and centrifuging with ~15,000×g for 10 mins at 4 °C to remove cell debris. The supernatant then transferred to a new tube and store at -20 °C for further analysis

2.4.3-8 Western blotting protocol for detecting pSMAD2 protein level

All cell lysate samples were mixed with 4×Laemmli sample buffer (Biorad, cat# 1610747) and 5% (v/v) 2-mercaptoethanol (Sigma-Aldrich, cat# M6250). All sample were boiled for five minutes at 95 °C. SDS-PAGE were run with 10% Acrylamide gels with 4 % staking layer. Proteins were transfer to nitrocellulose membrane, 0.45 µm (Biorad, cat# 1620115) with setting of 80 V for 75 mins in 4 ºC. After western blot transfer, all the membranes were blocked with 6% milk in 1×TBS with 0.1% Tween 20 in room temperature for 1 h. All membranes were incubated with primary antibodies in 1×TBS, 0.1% Tween 20 and 3% BSA at 4 °C O/N. For detecting pSMAD2, rabbit anti-smad2 (phospho S423 + S425) antibody (Cell signaling Technology, cat# 3108) was used at the dilution of 1/1000. For detecting SMAD2/3, Anti-Smad2 + Smad3 antibody (Cell signaling Technology, cat# 8685) was used at the dilution of 1/1000. For detecting Nodal, Human Nodal Antibody (R&D system, cat# MAB3218) was used at the dilution of 1/1000. After O/N primary antibody incubation, all membranes were washed 3 times with 1×TBS and 0.1% Tween 20 in room

temperature for 5 mins. All the membranes then incubated with corresponding seconding antibody anti-Mouse or anti-Rabbit that conjugate with HRP at the dilution of 1:7000. For imaging, the membranes were treated with Clarity™ Western ECL Substrate (Biorad, cat# 1705060) for 1 min and then exposed to X-ray film (Fuji Super RX) accordingly.

2.4.3-9 General protocol P19 cell culture

P19 Cell were obtained from ATCC cell bank and culture in alpha minimum essential medium with ribonucleotide and deoxyribonuclease with 7.5% bovine calf serum and 2.5% fetal bovine serum at 37 °C with 5% CO_2 supplementation.

2.4.3-10 Inhibition of pSMAD assay with P19 cell

P19 Cells were seeded in 6 wells plate with 200,000 cells/well and were grew in full media contain 10 μM of SB341542 to suppress pSMAD signals O/N. Then, the cells were washed with warm serum free Alpha Minimum Essential medium 3 times and were co-treated the cells with peptides at 10 μM and rhNODAL 100 ng/mL (R&D system, cat# 3218-ND/CF) in serum free Alpha Minimum Essential medium for 1 hour at 37 °C with 5% CO_2 supplementation**.** After 1 hour of treatment, cells washed and lysed (2.4.3-7 General protocol for protein extraction). All the samples were stored at -20 °C for further western blotting analysis (2.4.3-8 Western blotting protocol for detecting pSMAD2 protein level).

2.4.3-11 Transfection of TYK-nu cell with constitutive NODAL and GFP

This section was performed entirely by Dr. Olene Bilyk

TYK-nu ovarian cancer cells were obtained from JCRB cell bank and cultured in Eagle's minimal essential medium with 10% fetal calf serum (Gibco/Thermo Fisher; Waltham, Massachusetts, USA) at 37 °C with 5% CO_2 supplementation. To express the constitutive NODAL, a plasmid vector for human NODAL open reading frame (not including the stop codon) was cloned into pCMV6-Entry vector in frame with a tandem MYCDYK (FLAG) tag (Origene, cat# RC211302). The pCMV6 plasmid containing a GFP insert was used as a negative control. TYK-nu cells were transfected with desired plasmids using GeneIn (GlobalStem) following the manufacturer's protocol. Cells were stably selected with G418 (Thermo Fisher) at 250 μg/mL starting 48 hours after transfection for 10 days, and then maintained at 100 μg/mL. Nodal overexpression in TYK-nu cells was confirmed by Western blotting.

2.4.3-12 Cell Viability assay with TYK-nu-NODAL and TYK-nu-GFP

Cells were seeded in three 96 wells plates with 600 cells/well or 6000 cells/well and grow in full media with G418 at 100 μg/mL O/N. The next day the media was changed to contain **19d** peptide (10 μM, 1 μM and 0.1 μM) and without G418. Cells viability was measured every 24 hours with CellTiter-Glo® Luminescent Cell Viability Assay (Promega cat# G7572) over the course of 72h.

2.4.4 Proteolytic stability methods

2.4.4-1 Protocol for measurement of proteolytic stability in cell assay

10 μL of the solution was sampled from the cell media and quenched with 190 μL of 50% aq. CH_3CN. The mixture was vortexed and centrifuged in a bench top centrifuge at max speed to precipitate any proteins. The supernatant was maintained at 4 °C until analysis by LC–MS.

2.4.4-2 Protocol for measurement of proteolytic stability in Pronase™

In a 600 μL Eppendorf tube, we combined 196 μL PBS (pH 7.4), 2 μL of corresponding peptide solution (from 10 mM stock) and 2 μL of 0.1 mg/mL Pronase™. The mixture was vortexed and incubated at 37 °C. At indicated time points, 10 μL of the solution was sampled, quenched with 190 μL of 50% aq. CH_3CN and maintained at 4 °C until analysis by LC–MS.

2.4.4-3 Protocol for measurement of proteolytic stability in fresh mouse serum

In a 600 μL Eppendorf tube, we combined 198 μL fresh mouse serum, 2 μL of corresponding peptide solution (from 10 mM stock). The mixture was vortexed and incubated at 37 °C. At indicated time points, 10 μL of the solution was sampled, quenched with 190 μL of 50% aq. CH_3CN. The mixture was vortexed and centrifuged in a bench top centrifuge at 14000 RPM to precipitate the serum protein. The supernatant was maintained at 4 °C until analysis by LC–MS.

2.4.5 Molecular dynamics simulation

This section was performed entirely by Dr. Jiayuan Miao and Dr. Yu-Shan Lin at the Tufts University

Molecular dynamics (MD) simulations were performed for four bicyclic peptides (**8c**, **8b**, **7c**, and **7b**; Figure 2-9). The initial structure of each peptide was built using the Maestro 11.7 software of Schrödinger.[307] The topology file for each peptide was generated using the Schrödinger utility ffld_server and converted to the GROMACS format using the ffconv.py script.[308] All MD simulations in this study were performed using the GROMACS 4.6.7 suite[309] with the OPLS 2005 force field and the TIP4P water model.[310-311] The initial structure was first energy minimized for 1000 steps and then solvated in a cubic box of water molecules. The box size was chosen such that the distance between the peptide and the box wall was at least 1.5 nm. Minimal explicit counter ions were also added to neutralize the net charge of the system. With all heavy atoms of the linker restrained, the solvated system was further energy minimized for 5000 steps. Each initial structure was subjected to 1000 independent runs starting from different initial velocities. With all the heavy atoms of the linker remained restrained to their initial coordinates, a 50 ps NVT (isochoric-isothermal) equilibration at 300 K was performed for each of the 1000 runs, followed by a 50-ps NPT (isobaric-isothermal) equilibration at 300 K and 1 bar to adjust the solvent density. The equilibrated system then underwent a simulated annealing process in the NVT ensemble. The system temperature was first increased to 600 K in 500 ps and maintained at 600 K for additional 500 ps. The temperature was

then decreased gradually to 300 K in 1 ns. During the simulated annealing, the position restraints for the linker were removed. In all the simulations, the temperature was regulated using the v-rescale thermostat[312] with a coupling time constant of 0.1 ps. To avoid the "hot solvent/cold solute" artifacts,[313-314] two separated thermostats were applied to the solvent (water and ions) and the peptide. Then, the system underwent a 1 ns equilibration process at 300 K and 1 bar without position restraints, followed by a 5 ns production simulation also at 300 K and 1 bar. For the NPT simulations, the pressure was maintained using the isotropic Berendsen barostat[315] with a coupling time of 2.0 ps and compressibility of 4.5×10^{-5} bar^{-1}. For all the MD simulations, bonds involving hydrogen were constrained using the LINCS algorithm.[316] A 2-fs time step was used with the leapfrog integrator.[317] The nonbonded interactions (Lennard-Jones and electrostatic) were truncated at 1.0 nm. Long-range electrostatic interactions were treated using the Particle Mesh Ewald summation method.[318-319] A long-range analytic dispersion correction was applied to both the energy and pressure to account for the truncation of Lennard-Jones interactions. The last frame of each production run was used for further analysis. The 1000 final structures for each system could be found in the MD_movies.zip provided in the Supporting Information.

Cluster analysis was performed for the peptide backbone by binning the torsional angles within the ring structures; however, the ω dihedrals describing the peptide amide bonds were not included as they were all in the *trans*

conformation. The bicyclic peptides had two cycles in each molecule. Cycle 1 was defined as the cycle containing the *N*-terminal residues up to the first Cys (orange circles in Figure 2-9). Cycle 2 was defined as the cycle containing the residues between the first and the second Cys's (blue circles in Figure 2-9). The cluster analysis was performed on each of the two cycles. The populations of the top 10 clusters for the two cycles for **8c**, **8b**, **7c**, and **7b** are shown in the Table 2-1 and Table 2-2 below. In Figure 2-9, the binning boundaries for each residue are shown as green lines.

In general, the bicyclic peptides linked with **TSL-1** were better structured than its counterpart linked with **TSL-6** in cycle 1 (orange circles in Figure 2-9). As observed in the Table 2-1 below, when clustering based on the conformations of cycle 1, **8c** (bicyclized with **TSL-1**) showed two clusters that have significant populations (> 20%), while the populations of the top clusters of **8b** (bicyclized with **TSL-6**) were all relatively small (~2%). Similarly, when clustering based on the conformations of cycle 1, the top cluster of **7c** (bicyclized with **TSL-1**) had a population of 16.3%, but the population of the top cluster of **7b** (bicyclized with **TSL-6**) was only 1.2%. Overall, bicyclic peptides linked by **TSL-6** seemed to be quite flexible in cycle 1, as there were no structures with significant populations. However, the difference in cycle 2 (the cycle containing residues between the two Cys's; blue circles in Figure 2-9) was much smaller between bicyclic peptides linked with **TSL-1** and that linked with **TSL-6**, as shown in the Table 2-2 below, likely because cycle 2 of both the **TSL-1**-linked and the **TSL-6**-linked compounds shared the same molecular topology. It was also found that when

comparing the Ramachandran plots between **8c** and **8b**, and similarly between **7c** and **7b**, the residue(s) near the *N*-terminus exhibited different distributions of backbone dihedral angles when the peptide was linked by **TSL-1** vs. **TSL-6**, as indicated by smaller normalized integrated products[303] between the two sets of Ramachandran plots (Figure 2-9). Specifically, compared to the other resides, the His residue showed a larger difference in the (ϕ, ψ) distribution between **8c** and **8b**; similarly, compared to the other resides, the Trp and Asp residues showed a larger difference in the (ϕ, ψ) distribution between **7c** and **7b**.

Table 2-1. Populations of the top 10 clusters of **8c**, **8b**, **7c**, and **7b** using the torsional angles in cycle 1 in the cluster analysis.

Cluster #	8c	8b	7c	7b
1	21.8%	2.3%	16.3%	1.2%
2	21.5%	2.1%	7.0%	0.4%
3	9.5%	1.8%	3.1%	0.4%
4	9.4%	1.8%	2.6%	0.3%
5	6.3%	1.7%	2.2%	0.3%
6	4.9%	1.7%	1.5%	0.3%
7	4.1%	1.0%	1.3%	0.3%
8	3.6%	1.0%	1.2%	0.3%
9	2.1%	1.0%	1.2%	0.3%
10	2.0%	0.7%	1.0%	0.3%

Table 2-2. Populations of the top 10 clusters of **8c**, **8b**, **7c**, and **7b** using the torsional angles in cycle 2 in the cluster analysis.

Cluster #	8c	8b	7c	7b
1	7.6%	12.7%	7.3%	9.9%
2	5.4%	3.7%	5.4%	3.9%
3	4.4%	2.2%	4.7%	2.6%
4	4.1%	2.2%	3.9%	2.2%
5	2.6%	2.1%	3.9%	2.2%
6	2.5%	2.0%	3.6%	2.0%
7	2.5%	1.9%	3.0%	1.9%
8	2.1%	1.7%	3.0%	1.8%
9	2.0%	1.7%	2.8%	1.6%
10	1.6%	1.5%	2.0%	1.3%

Chapter 3: Genetically encoded discovery of albumin-binding pentafluorophenyl-sulfide peptide macrocycle

3.1 Introduction

There are around 80 peptide drugs on the global market; more than 150 peptides are in clinical development and another 400–600 peptides undergoing preclinical studies.[236] The large surface area of peptides (900 Da to 60 kDa), compared to a typical small molecule drug (< 900 Da) equip peptide ligands with advantageous properties such as high affinity binding due to the extended areas of proteins and other biomolecules. Such extended binding interfaces are commonly found in protein-protein interactions (PPI), in the shallow binding pockets of protein-carbohydrate interactions, protein-DNA interactions. These extended binding areas are a hallmark of "undruggable targets" because they are significantly more challenging to target using conventional small therapeutic molecules when compared to traditional "druggable targets." Examples of the latter are enzymes that possess a small-volume, deep binding pockets and receptors that naturally evolve to bind small-molecule metabolites or other low molecular weight mediators (e.g., GPCR). When compared to traditional antibody drugs, peptides are significantly smaller: 2 kDa to 10 kDa for peptides versus 150 kDa for full-sized antibodies. Due to the decrease in size, the bio-distribution inside tumors and other non-vascularized tissues for peptide therapeutics, peptide-drug conjugates (examples of peptide-drug conjugates in clinical trials are TH1902, TH1904, BT5528, BT8009, BT1718, and MMP-14)

and peptide radionuclide delivery agents (e.g., Lurathera™) is significantly improved when compared to analogous antibody therapeutics, antibody-drug conjugates or antibody radionuclide conjugates.[320-322]

Unmodified peptides are cleared within minutes from plasma by renal filtration. Rapid clearance is beneficial in several modalities, such as imaging agents and radionuclide delivery agents.[323] For other classes of therapeutics based on peptides and small protein domains, rapid renal clearance is considered a poor pharmacokinetics trait because it mandates frequent administration of the therapeutics. In contrast, antibody drugs remain in circulation for 1-3 weeks due to the association of the Fc domain of antibodies with the neonatal Fc-receptor (FcRn) on the surface of immune cells.[324] This predictable prolonged circulation time is one of the most advantageous built-in properties of antibody therapeutic and possibly the most important reason for exponential growth in the development and approval of antibody therapeutics over the last 3 decades.

Few unmodified peptides exhibit a long circulation lifetime; however, a therapeutically relevant example is the 39-residue peptide 'exendin 4' (53% identical to GLP1(7–37aa)) isolated from the venom of the Gila monster that has low renal clearance in humans (5–7 h).[325] This peptide was developed into the FDA-approved drug exenatide administered twice daily by subcutaneous injection for the treatment of type 2 diabetes.[326-327] Most peptides that do not have a naturally long circulation time; thus, they mandate even more frequent administration and high dosages. Even the aforementioned, exendin 4 has been subject to modifications that improve its pharmacokinetics resulting in several

modified derivatives such as liraglutide, albiglutide, dulaglutide, lixisenatide and semaglutide.[236]

Size-dependent renal clearance is a well-known problem. Over the decades, these strategies have evolved into standalone research areas that aim to enhance the pharmacokinetic properties of peptides and small proteins. They could be conceptually divided into two chemical classes: i) covalent linkage either via chemical bonds or genetic-fusion to macromolecules such as a long-living serum protein,[328-330] polyethylene glycol (PEG) derivatives,[331-332] and polyglycerol[333] ; or ii) incorporation of moieties that lead to non-covalent binding to proteins with long circulation, such as albumin,[334-337] immunoglobulin,[338-339] FcRn,[340] transthyretin,[341] and transferrin.[342-343] One example of i) is conjugation to PEG, which is used in multiple FDA-approved therapeutics (e.g., PEG–bovine adenosine deaminase and PEG–α-interferon) and the pegylated form of exenatide (phase II trials), or the pegylated analog of the gut hormone oxyntomodulin (phase I trials). Interestingly, steric hindrance by these size-increasing moieties also protects against proteolytic degradation.[344-346] Another strategy to increase the size was developed by Trimeris Inc. and is based on a well-designed mechanism of oligomerization of helical peptides into triple-helical bundles or higher-order oligomers.[347] Again, such oligomers have 8-20 hours of circulation life in primates and humans.[347] Examples of ii) are the FDA-approved drugs albiglutide and dulaglutide, exanatide that conjugated to albumin and the IfG4 Fc domain, which binds to Fc-receptor and prolongs circulation.

Albumin can improve the half-life of therapeutic peptides and proteins by employing either of two strategies i) fusing the molecule of interest to albumin's N- or C- terminal end,[336] or ii) conjugating the molecule of interest to albumin binding moieties such as fatty acids. Albumin is the most abundant protein in plasma with an average concentration of 600 μM and has an average half-life of 19 days.[348] It mainly acts as a versatile carrier of essential fatty acids and increases the solubility of small organic molecules.[348] Among all the long-circulating serum proteins, albumin is considered to be one of the most important targets in the pharmaceutical industry because of its ability to interact with hydrophobic small molecule drugs and enhance the pharmacokinetic properties of many small molecule drugs.

The size of albumin is above the renal filtration threshold, but the main mechanism leading to the long half-life of albumin is similar to that of an antibody: both proteins interact with FcRn on the surface of immune cells. This binding results in transient endocytosis of these proteins, and as a result, they are frequently sequestered from circulation and protected from clearance. At physiological pH, the binding affinity between albumin and FcRn is low; however, the interaction under acidic conditions in the endosome is strong to avoid lysosomal degradations and recycling of albumin to the extracellular space.[324]

There are four FDA approved drugs: insulin degludec (Tresiba™), insulin detemir (Levemir™) and Liraglutide (Victozoa™) and semaglutide that contain albumin binding fatty acids to prolong their circulation time and efficacy *in*

vivo.[349] Building on this success, albumins binding peptides have been identified in addition to fatty acids. Such "lipidation" not only increases the size but also reduces renal clearance of these drugs due to binding to serum albumin.[350-352] Lipidation can also delay the release from the subcutaneous injection site due to local aggregation of peptides into an insoluble nanoparticle refer as "depo," and subsequent gradual release of soluble peptides from such "depo." A Both mechanisms can overcome the problem of renal clearance and increase plasma circulation times.[353]

3.1.1 Albumin as a drug carrier

The goal of using albumin as a drug carrier is to produce a tandem sequence of an albumin binding domain and a therapeutic peptide or protein with predictably enhanced pharmacokinetic properties. Examples include DX-236 (Ac-AEGTGDFWFCDRIAWYPQHLCEFLDPEGGGK-NH_2), identified by researcher from Dyax Corp., with a binding affinity of 1.9 μM at pH 6.1 to HSA, which used it to purifying albumin (Figure 3-1A).[79] Researchers at Genentech identified an 18 amino acids macrocyclic peptide, SA-21 (Ac-RLIEDICLPRWGCLWEDD-NH_2), with a binding affinity of 467 nM to HSA (Figure 3-1B).[93]

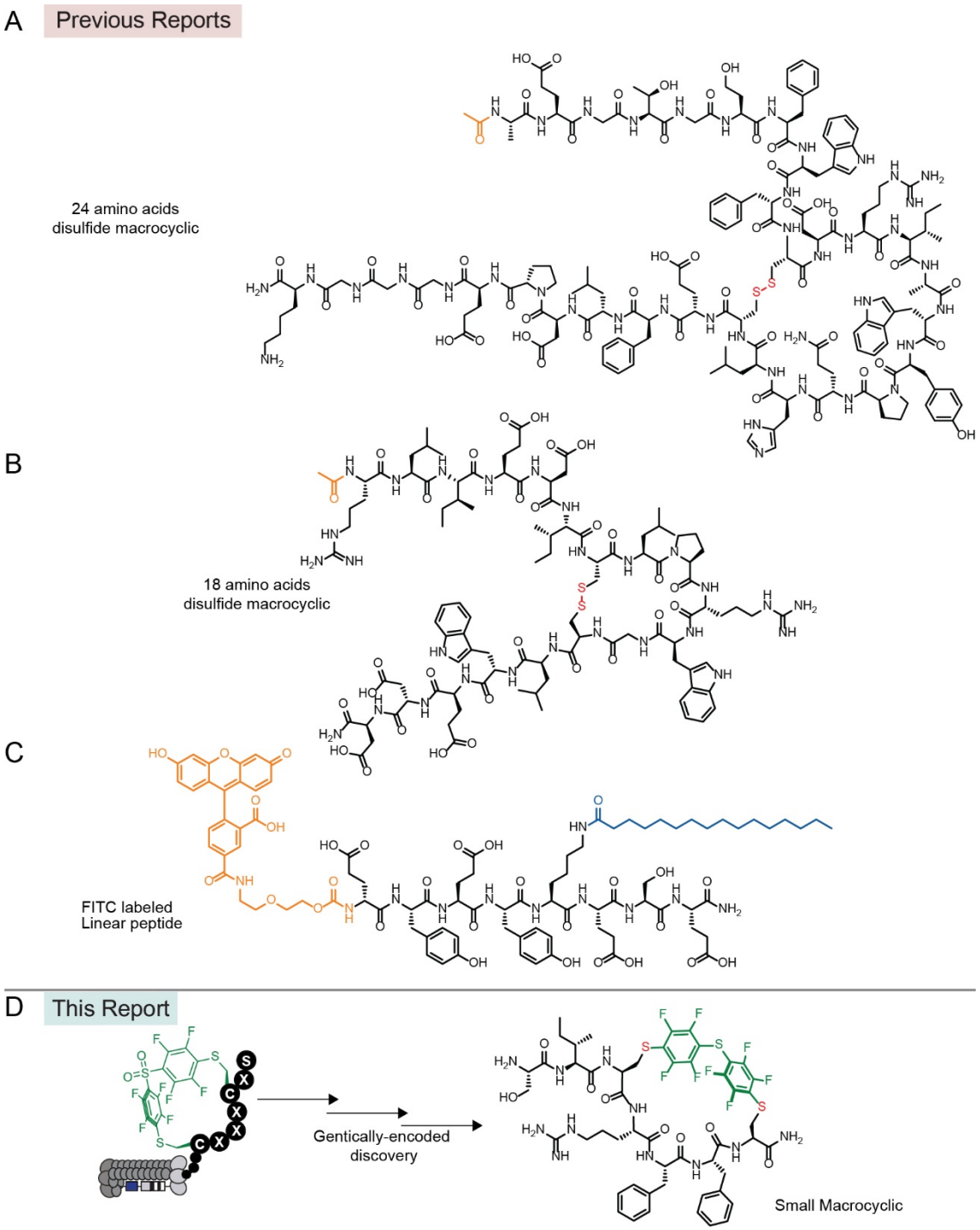

Figure 3-1. Overview of known albumin binding peptides. Previous reports of (A) macrocyclic peptide: DX-263, (B) macrocyclic peptide: SA-21 and (C) a linear peptide: FITC-EYEYK$_{palm}$ESE-NH$_2$. (D) This report describes a genetically modified library for discovering a small label-free macrocycle albumin binder.

Conjugation of SA-21 to bicyclic peptide ligands for urokinase-type plasminogen activator,[334, 354] Fab antibody fragments[355-356] and small proteins[357] significantly prolonged their circulation half-life. Heinis and co-workers developed a short palmitoylated, fluorescently labeled heptapeptide (FITC-EYEYK$_{palm}$ESE-NH$_2$) determined to have a K_d = 39 nM to HSA (Figure 3-1C).[335] The linear heptapeptide was fused to two different bicyclic peptides to boost the half-life from minutes to hours.[335] Interestingly, the authors found that the presence of fluorescein was critical for the binding of this peptide. An unlabeled palmitoylated heptapeptide EYEYK$_{palm}$ESE-NH$_2$ has a significantly lower albumin binding and circulation time. Both SA-21 and the acylated heptapeptide successfully demonstrated the possibility of using HSA binding peptides for extending circulation half-life in peptides and proteins; however, SA-21 suffered from low solubility due to a high percentage of hydrophobic amino acid residues and a relatively high molecular weight.[93, 335] While the acylated heptapeptide required a fluorescein molecule for efficient binding towards albumin.[335]

Many FDA-approved small molecule drugs have intrinsic affinity to albumin in addition to binding their therapeutic target. The development of small molecules with a specific, high affinity for albumin has been a topic of research over the last 15 years. Additionally, anti-albumin antibodies, nanobodies, [358] DARPins,[359] and other protein domains have been developed to conjugate with proteins and extend their circulation *in vivo*. A recent review by Angelini and co-workers summarized development in this area.[337] Examples of small peptides or small macrocycles with intrinsic binding to albumin are still scarce. The goal of

this manuscript is to employ genetically encoded libraries chemically modified macrocycles to develop new classes of albumin binding mini-scaffolds.

To discover a low molecular weight, label-free, a macrocyclic peptide that binds to albumin with low micro-molar affinity, we employed a phage-displayed library SX_nCX_mC, modified with decafluoro diphenylsulfone (**DFS**) where X is any amino acid with the exception of cysteine, n = 1 and m = 3-5 amino acids (Figure 3-1C).[219] We hypothesized cyclization with a perfluorinated aromatic linchpin would provide an amphiphilic scaffold (hydrophobic in one region and hydrophilic or charged in another) that would be recognized by one of the binding sites of HSA[219, 360] Perfluorinated linchpins have been shown to reduce the proteolytic degradation of peptides[360], and the hydrophobicity of this linchpin could aid the peptide binding to HSA similarly to the binding of a fatty acid in lipidated peptides.

3.2 Results and discussion:

3.2.1 Selection of albumin binders

We devised and conducted three discovery campaigns that used different library architecture and selection strategies. In the first discovery campaign, we modified the phage libraries of structure $SXCX_{4\text{-}5}C$ (where X = any amino acid but cysteine) with **DFS** following a previously published protocol and confirmed that 85% of the phage library had been modified with **DFS** (Figure 3-2, Figure 3-3A).[219] We performed three rounds of phage selection using HSA coated to the surface of 96 well polystyrene plates as bait. In parallel, we also panned the same

library on polystyrene wells coated with Protein A (negative control) to make it possible to distinguish specific HSA-binding sequences from poly-specific protein binding sequences (Figure 3-3A). In round 3, the phage recovery of the **DFS** modified library selection against HSA exhibited a minor increase compared to selection against Protein A and at least a two-fold increase compared to round 1 and round 2 (Figure 3-3D).

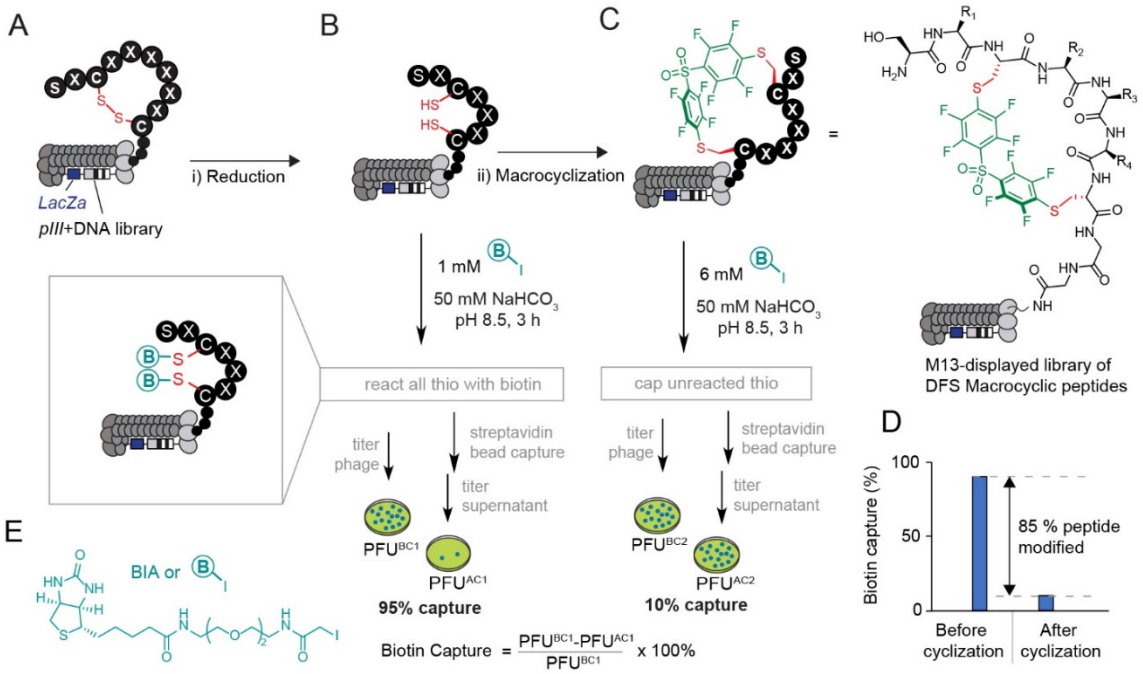

Figure 3-2. Modification of the library with a diversity of 10^{10} displayed on phage by **DFS**. A-C) M13 phage-displayed disulfide library was reduced and macro-cyclized with **DFS**. D) Quantification of the phage with the thiol-reactive group before and after macrocyclization. E) Chemical structure of the biotin-iodoacetamide probe (BIA).

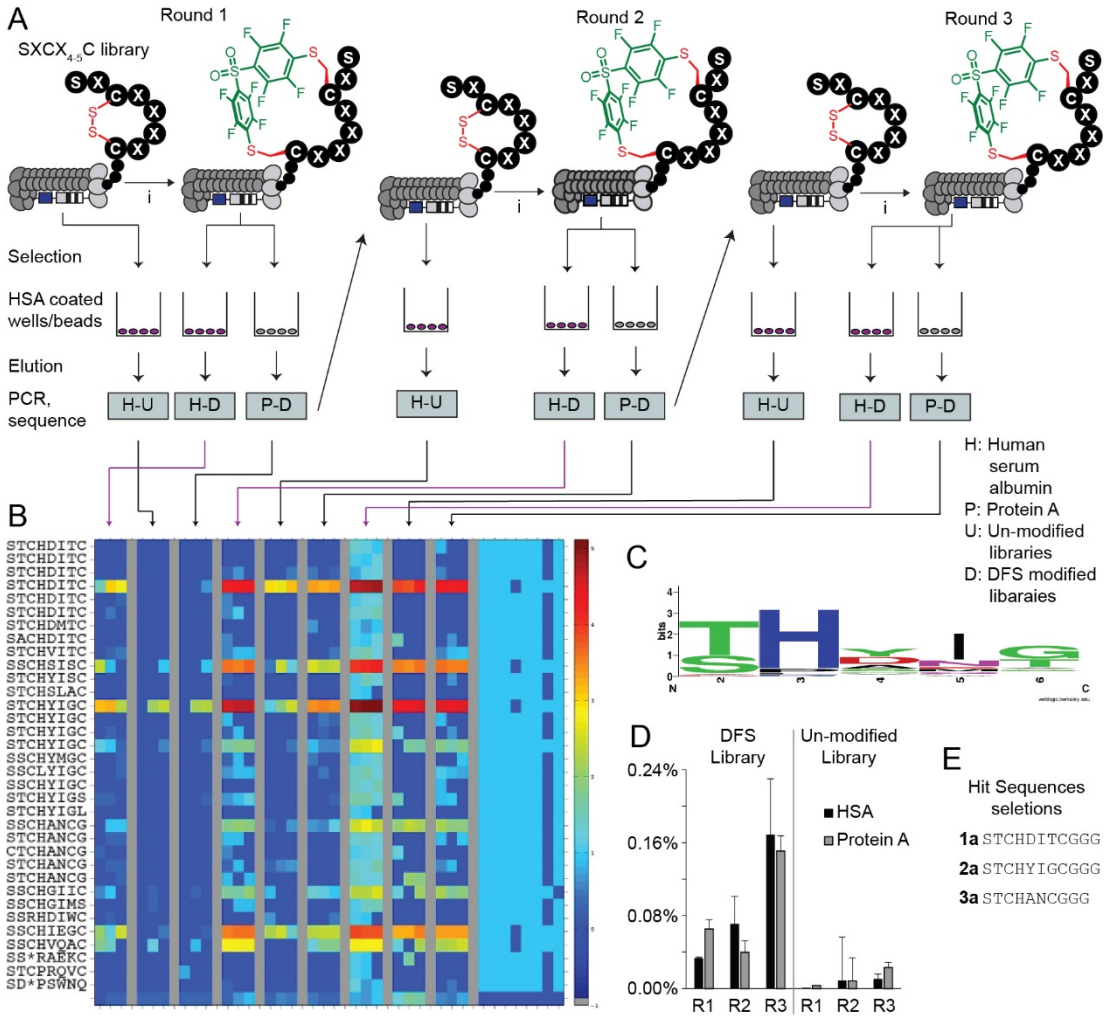

Figure 3-3. Bio-panning of **DFS**-modified phage-displayed library of peptides against the HSA proteins. (A) A scheme of three-rounds panning against HSA and negative controls. (B) The top 39 sequences from differential enrichment results. (C) LOGO analysis plot of the enriched sequences. (D) Percentage of the phage recovery after each round of bio-panning. (E) Selected sequences for chemical synthesis of the macrocycles.

The recovery of unmodified round 3-library panned against HSA was 17-fold lower than the recovery of the **DFS**-modified library, indicating the importance of the **DFS**-modification for protein binding (Figure 3-3D). Bioinformatic analysis of the deep sequencing the output of the campaign and the control experiments identified several families of peptide macrocycles that had statistically significantly higher ($p < 0.05$) enrichment in binding to HSA when compared to binding to Protein A (Figure 3-3 B-C). The analysis yielded three consensus motifs: STCHYIGC (**1a**), STCHTIYC (**2a**) and STCHANC (**3a**) (Figure 3-3E).

Since the degree of phage recovery of panning against HSA and Protein A was similar, we devised an improved selection strategy in the second discovery campaign which involved changing the presentation of the protein between the rounds. In rounds 1 and 3, the proteins were immobilized on a 96 well plate, and in round 2, biotinylated HSA was immobilized onto streptavidin beads. The negative control, Protein A, was handled similarly (Figure 3-4A). In round 3, the phage recovery of the **DFS** modified library selection against HSA was higher by a factor of two when compared to selection against Protein A and by a factor of 200 when compared to round 1 and round 2. The recovery of the unmodified library panned against HSA was insignificant (Figure 3-4D).

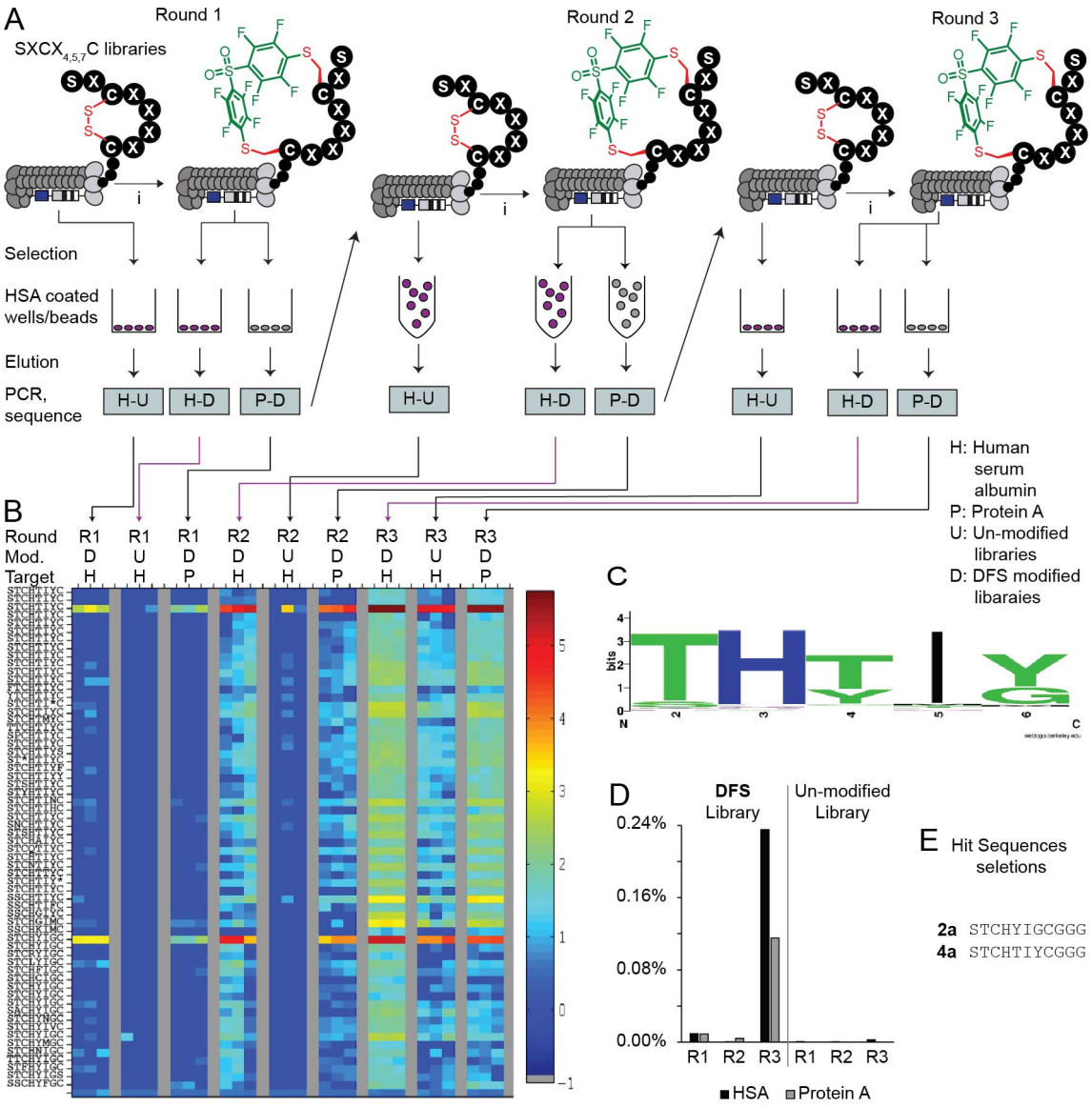

Figure 3-4. Second bio-panning campaign against the HSA protein. (A) Scheme of a three-rounds panning against HSA and the negative controls. (B) The top 65 sequences from differential enrichment results. (C) LOGO analysis plot of the enriched sequences. (D) Percentage of the phage recovery after each round of bio-panning. (E) Selected sequences for validation synthesized into macrocycles.

To confirm the specificity of the selection of the second campaign, we tested the binding of the **DFS**-modified phage library recovered from round 3 to Protein A, ConA and Casein. Under the same binding conditions, the recovery was two-fold lower in binding to Protein A, 14-fold lower in binding to ConA and 300-fold lower in binding to casein-coated wells when compared to recovery on HSA-coated wells. Recovery of the unmodified phage library from round 3 in binding to HSA decreased 400-fold (Figure 3-5). These observations suggested that (i) specific albumin-binding sequences had been selected, and (ii) the binding of these sequences to albumin required modification by **DFS** (Figure 3-5).

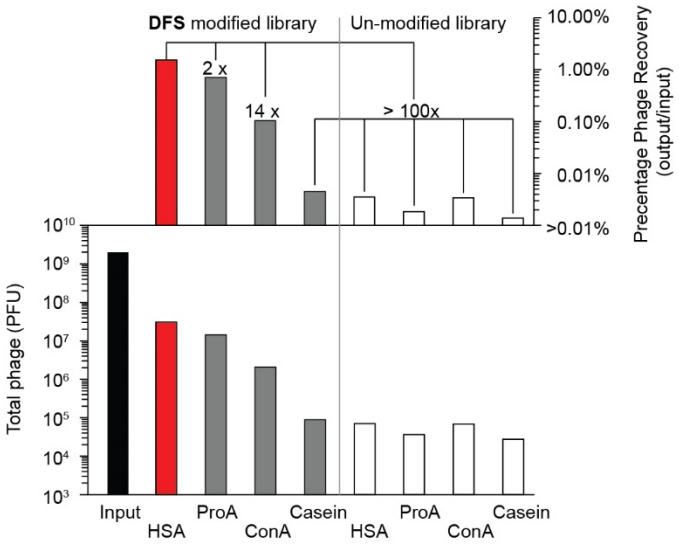

Figure 3-5. Phage recovered from the second selection campaign of round 3 were bound to different proteins on protein coated plates.

We deep sequenced the output of this second campaign and the control experiments. A differential enrichment analysis identified a new set of sequences that were significantly ($p < 0.05$) enriched by three-fold in the screen against

HSA but not against Protein A. The LOGO analysis yielded an overall consensus motif: STCHDITC (**4a**) (Figure 3-4E).

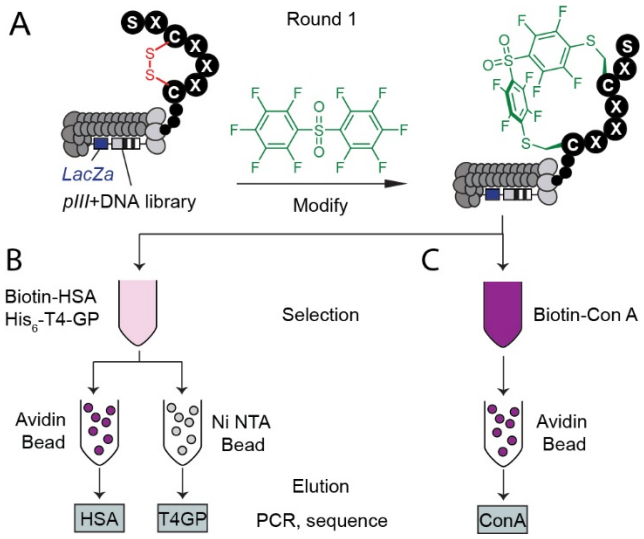

Figure 3-6. The third bio-panning campaign against the HSA proteins.(A) **DFS** modification of $SXCX_3C$ phage-displayed library (B) In tube 1, **DFS** modified phage-displayed library panned against two targets (biotinylated HSA and His-tag expressed T4-GP) parallel in solution and pull down with avidin beads and Ni-NTA beads affinity beads. (C) In the negative control, **DFS** modified phage-displayed library was panned against biotinylated ConA and pulled down with avidin beads.

We noted the selection of $SXCX_3C$ motifs in the first campaigns. Although the original libraries were designed as $SXCX_{4\text{-}5}C$, they contained a small fraction of $SXCX_3C$ libraries due to deletions during the synthesis of the DNA oligonucleotides used to generate these libraries.[305] To explore the apparent preference for smaller macrocycles, we devised a third selection campaign that employed only $SXCX_3C$ libraries modified with **DFS** (Figure 3-6A). The small diversity of the library made it possible to employ a single round panning and next-generation sequencing and to identify the binders. To mimic the complex serum environment, the panning environment was composed of a mixture of

biotinylated HSA (Bio-HSA), His-tag fusion T4-PG protein (His-T4-PG) and unlabeled milk proteins. In a control selection, we used the same mixture with biotinylated ConA (Bio-ConA) in place of Bio-HSA (Figure 3-6B). Proteins were captured with streptavidin or Ni-NTA affinity beads, respectively. The captured phage DNA was liberated from beads by treatment with hexane and the released DNA was amplified by PCR and sequenced with Illumina deep sequencing (Figure 3-6B).

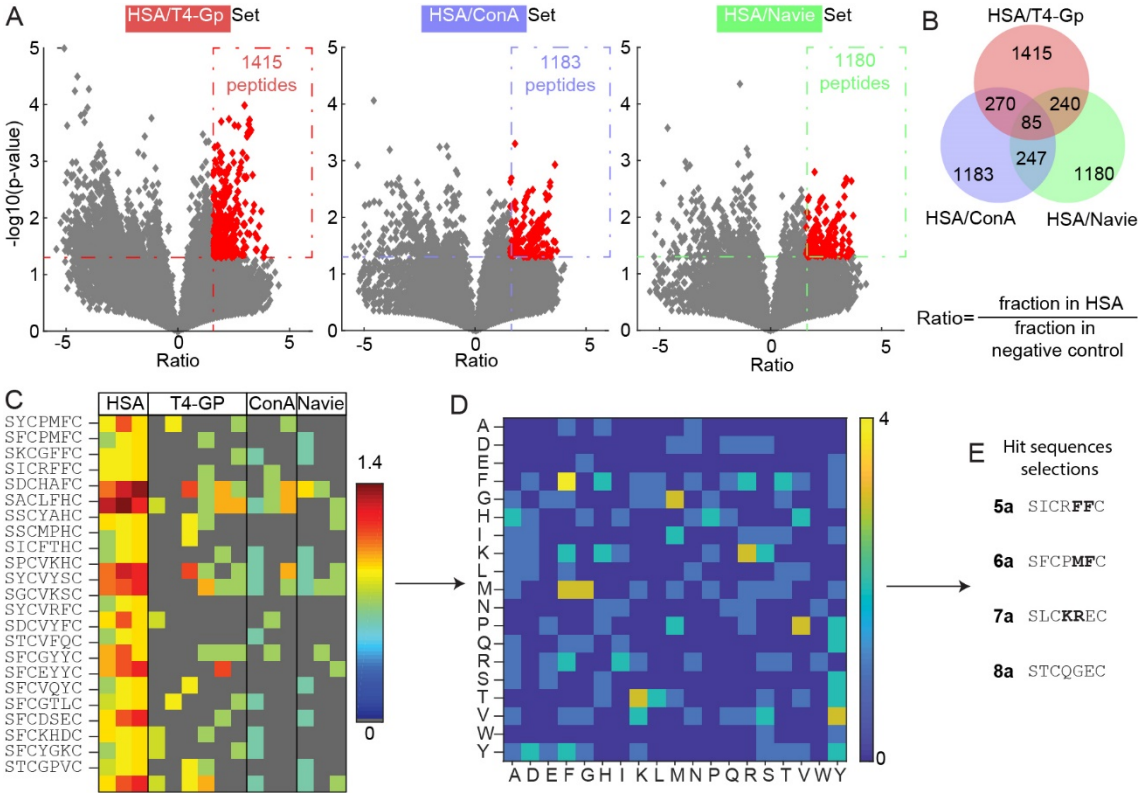

Figure 3-7. Student's *t*-test analysis of the third screening campaign: (A) A volcano plot visualizing the sequences from the **DFS**-SXCX$_3$C phage-displayed library that were significantly enriched in the HSA screen when compared to the naïve library or selection against the T4-GP, ConA. (B) A heat map display of the top 25 of 85 hits sequences from differential enrichment results. (D) Dipeptide motif analysis of all 85 hits. (B) Selected sequences for chemical synthesis of macrocycles for validation.

A differential enrichment analysis identified a set of 85 sequences that were significantly enriched ($p \leq 0.05$, >3-fold) in the screen against Bio-HSA when compared to the screen against His_6-T4-GP and Bio-ConA (Figure 3-7A-B). We applied a pairwise amino acid clustering to identify the 85 hit sequences (Figure 3-7C) and observed 8 motifs: FF, MF, MG, TK, GM, PV, VY and KR associated with these enriched sequences (Figure 3-7D). Based on this analysis, we nominated sequences SICRFFC (**5c**), STCQGEC (**6c**), SLCKREC (**7c**) and SFCPMFC (**8c**) for chemical synthesis (Figure 3-7E).

Campaign #	Sequences	DFS	Yield	PFS	Yield
1	**1a** STCHDITC	**1b**	5%	**1c**	30%
	2a STCHYIGC	**2b**	64%	**2c**	27%
	3a STCHANC	**3b**	24%	**3c**	40%
2	**4a** STCHTIYC	**4b**	36%	**4c**	11%
3	**5a** SICRFFC	**5b**	59%	**5c**	44%
	6a SFCPMFC	**6b**	16%	**6c**	37%
	7a SLCKREC	**7b**	39%	**7c**	28%
	8a STCQGEC	**8b**	67%	**8c**	38%

Figure 3-8. Summary of the selected peptide sequences nominated from three panning campaigns. The nominated peptides were chemically synthesized and modified with **DFS** and **PFS** for validation.

3.2.2 Validation of albumin binders

Synthesis of peptides identified in the three selection campaigns faced numerous solubility problems. Peptides **1a**-**8a** were poorly soluble in water, and evaluation of their binding to HSA was difficult. Peptides **1a**-**8a** were chemically synthesized with a Lys-Lys-Lys or Gly-Gly-Gly linker at the C-terminus to increase solubility. Once modified with **DFS** or pentafluorophenyl sulfide (**PFS**), **1b**-**8b** and **1c**-**8c** exhibited sufficient solubility for downstream analyses (Figure 3-8).

A second observation was the non-specific reactivity of **DFS**-modified peptides with thiol nucleophiles such as GSH over several hours in basic pH

(Figure 3-9). Replacing **DFS** with a less reactive **PFS** linchpin abolished the undesired reactivity. The **PFS**-macrocycles were unreactive to 2-mercaptoethanol over three weeks and unreactive towards free thiol on HSA (Figure 3-10). Molecular dynamics simulation suggested the **DFS** modified peptide and the **PFS** modified peptide exhibit identical ground state conformational landscape and maintained the overall conformation and binding to the peptide (Figure 3-11).

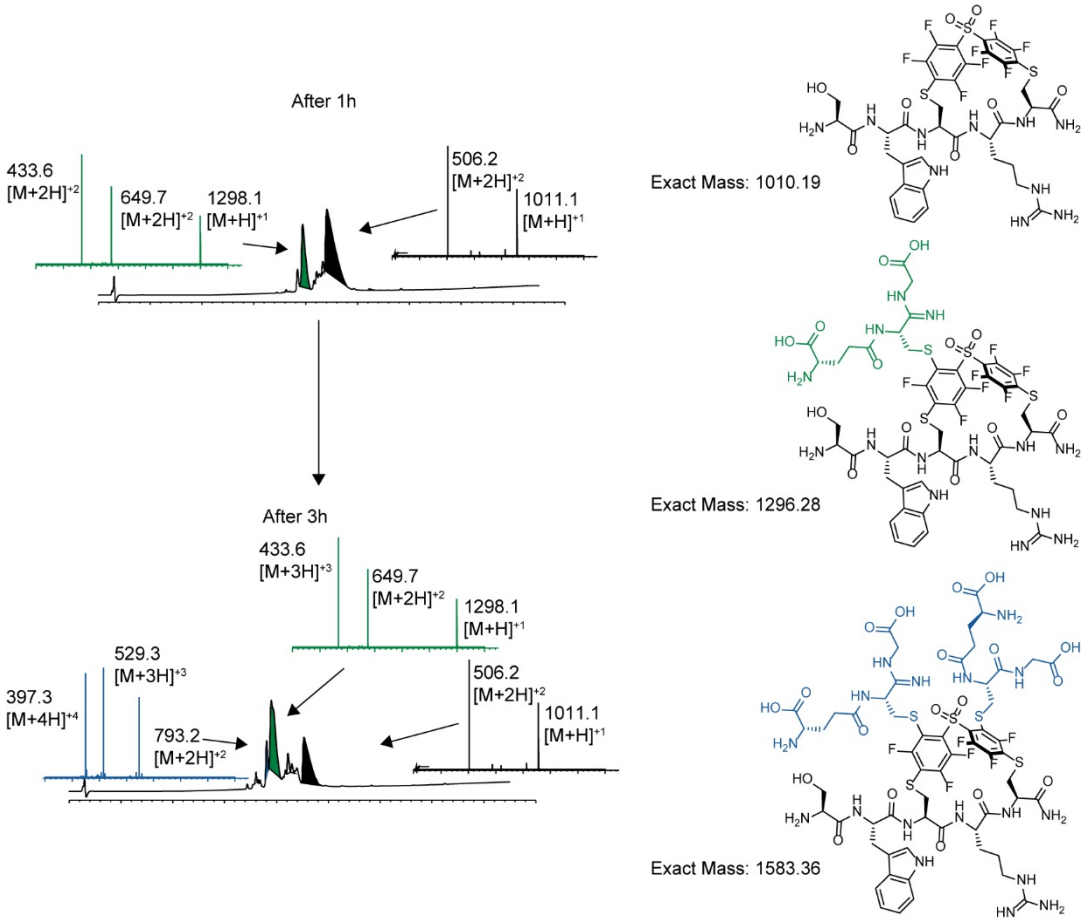

Figure 3-9. DFS stapled peptide reacted with GSH over 3 hours. The **DFS**-SWCRC peptide was added with one equivalent of GSH in 60% acetonitrile in 50 mM Tris-HCl at pH 8.5. The reaction was monitored by LC–MS.

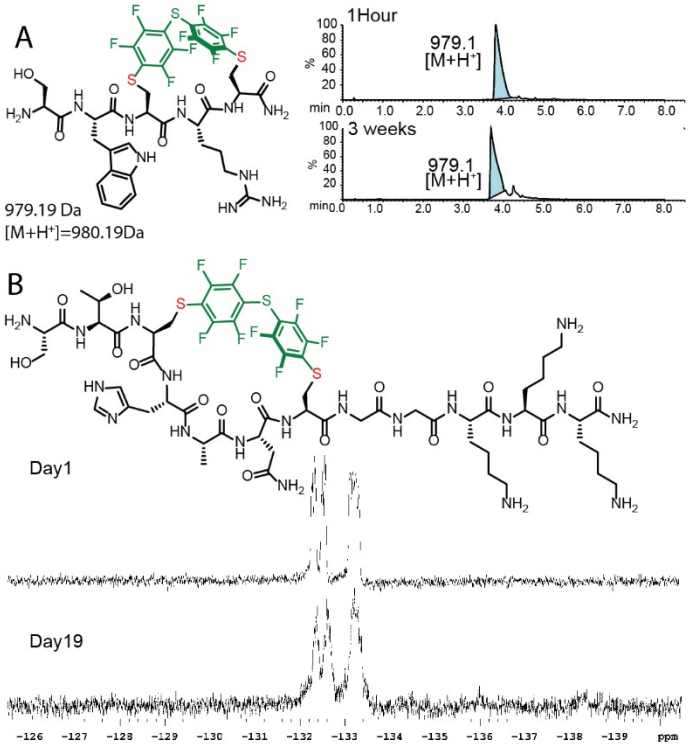

Figure 3-10. Stability of the **PFS** stapled peptides (A) Results of the **PFS**-SWCRC mixed with 2-mercaptoethanol and analyzed by LC–MS after 1 hour and 3 weeks. The **PFS**-SWCRC macrocycle was combined with 1 equivalent of 2-mercaptoethanol in 60% acetonitrile and 50 mM Tris-HCl at pH 8.5. The mixture was monitored by LC–MS. (B) A spectrum of 1 mg of **PFS**-STCHANCGGKKK mixed with 1 mg of HSA over 19 days in 1×PBS. The mixture was monitored by ^{19}F NMR in 1×PBS, 10% D_2O.

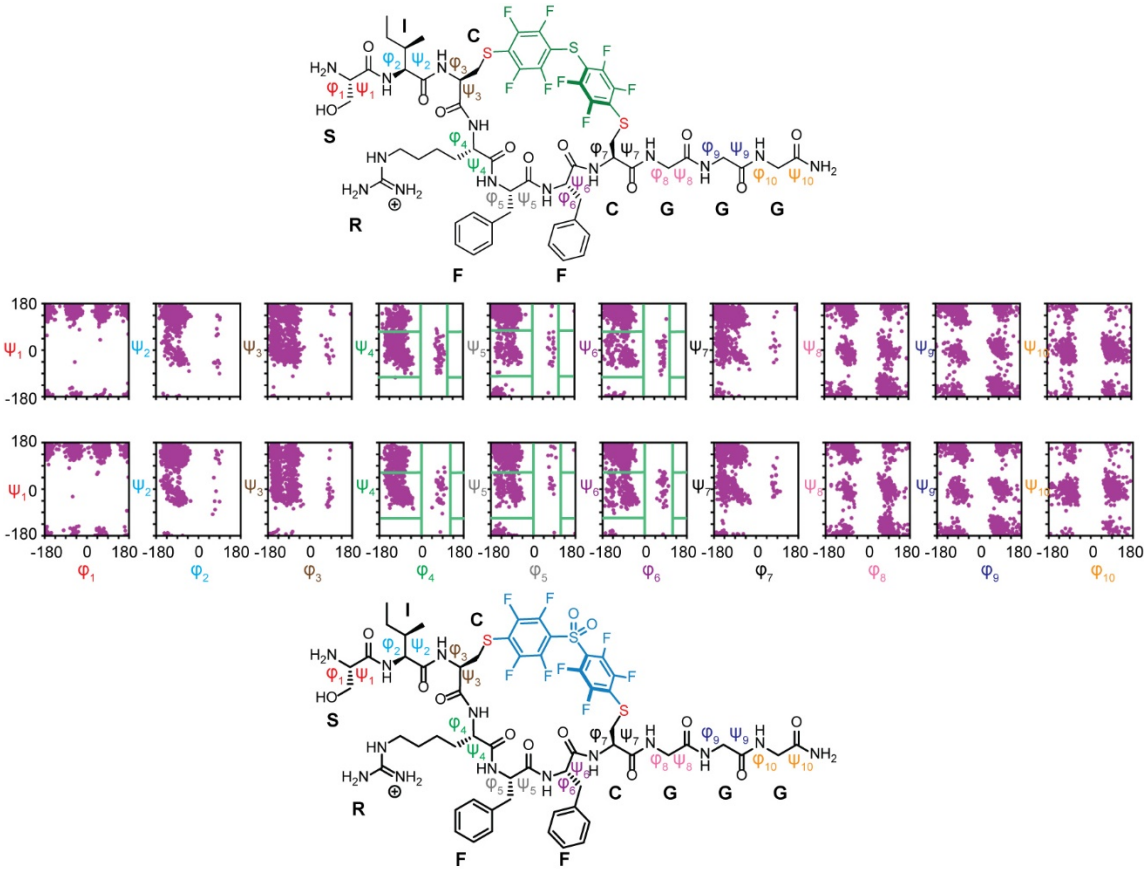

Figure 3-11. Ramachandran plot of the cyclic peptide backbone for **5b** and **5c**: Green lines indicate the binning boundaries used in the cluster analysis. The molecular dynamic simulation was performed by Dr. Jiayuan Miao and Dr. Yu-Shan Lin at Tufts University.

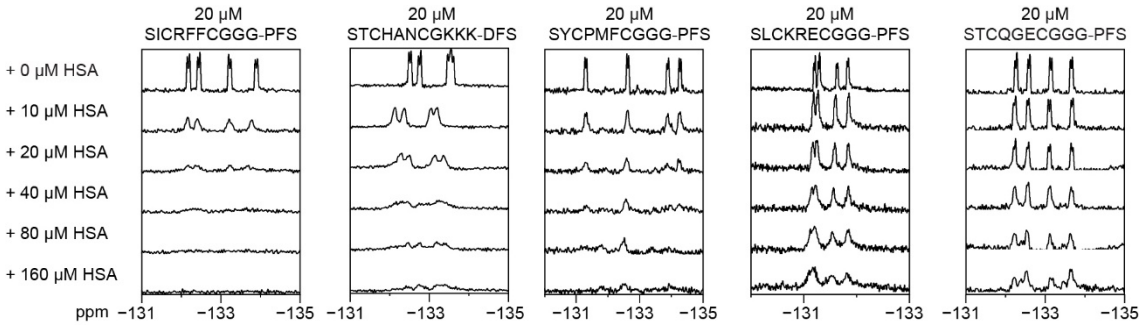

Figure 3-12. ^{19}F NMR binding assay **3b** and **5c**-**8c** held at 20 μM and titrated against various concentrations of HSA. The ^{19}F NMR binding assay was performed by Dr. Steven Kirberger at the University of Minnesota.

The unique fluorine handle in **PFS**-modified peptides made it possible to determine their binding to HSA using ^{19}F NMR (Figure 3-12). In a typical experiment, we maintained peptide concentration at 20 μM, added HSA at several different concentrations (10 μM, 20 μM, 80 μM, and 160 μM). Upon increasing the concentration of HSA, we observed broadening of and disappearance of ^{19}F signals that correspond to **PFS**, which indicated the slow tumbling resulting from the binding of the peptide to HSA. We could not fit a definitive K_d value to the binding response due to the complex binding behavior and quality of the NMR signal. However, in an albumin titration series, one can use qualitative estimates such as the concentration of albumin necessary to suppress 50% of the initial fluorine signal. Based on these qualitative analyses, it was apparent that some peptides (e.g., **5c**) have stronger binding to HSA, whereas other macrocycles (e.g., **8c**) have weaker binding towards HSA (Figure 3-12).

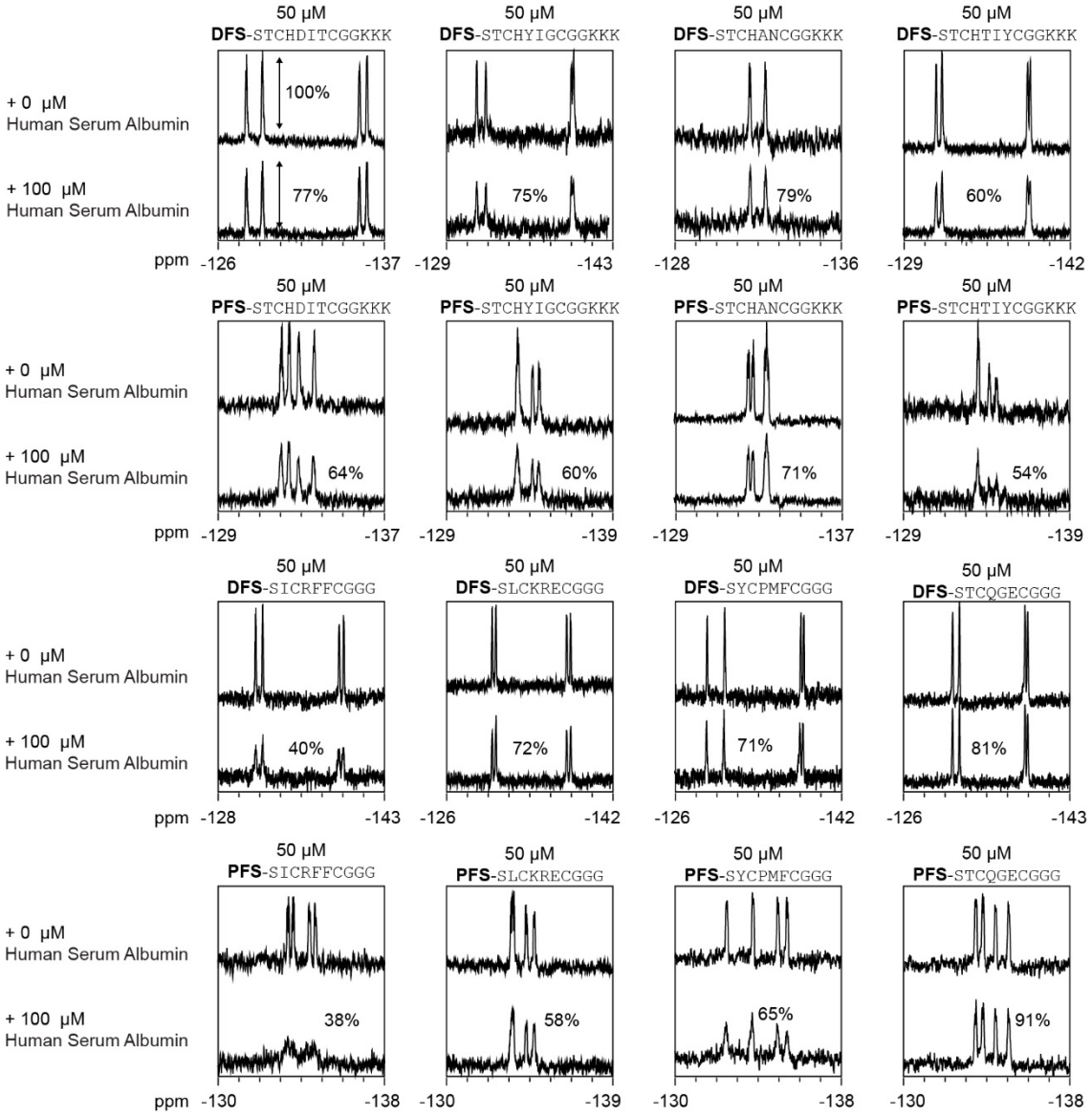

Figure 3-13. Summary of the ^{19}F NMR binding measurement of the HSA titration spectra of 50 μM of **1b**-**8b** and **1c**-**8c** against 100 μM of HSA. The percentage represents the peak intensity remaining after the addition of HSA.

Another estimate can be performed, for example, by measuring the decrease in the signal at a fixed concentration of peptide and HSA. Using this single-concentration scan, we evaluated all 16 peptides found in all discovery campaigns (Figure 3-13, Appendix B-Figure 3).

As a result of the ^{19}F profiling, we nominated SICRFFCGGG (**5a**) as the lead sequence and SICQGECGG (**8a**) as the control sequence for further investigation. The ^{19}F NMR assay is conveniently agnostic in its targeting, and it can be used with any protein or even a complex mixture of proteins. We titrated **PFS**-SICRFFCGGG against rat serum albumin in the ^{19}F binding assay and observed identical peak decay as in binding to HSA (Figure 3-14).

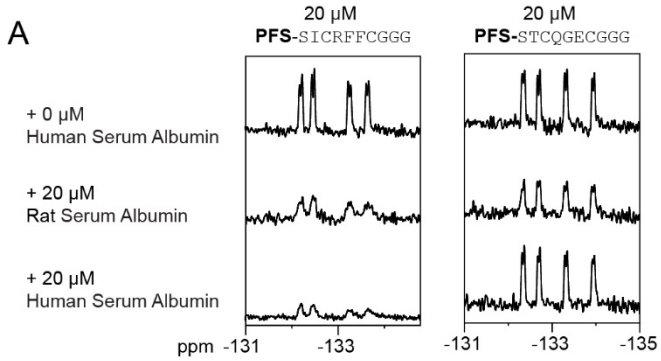

Figure 3-14. The ^{19}F NMR titration spectra of **5c** and **8C** against rat serum albumin.

We also evaluated whether binding pockets of **PFS**-SICRFFCGGG are similar to known albumin binders: carbamazepine, diclofenac and ibuprofen (Figure 3-15). We observed that the binding of the **PFS**-macrocycle did not decrease in the presence of any of these drugs; thus, **PFS**-SICRFFCGGG did not share the same binding pocket as carbamazepine, diclofenac, or ibuprofen (Figure 3-15B).

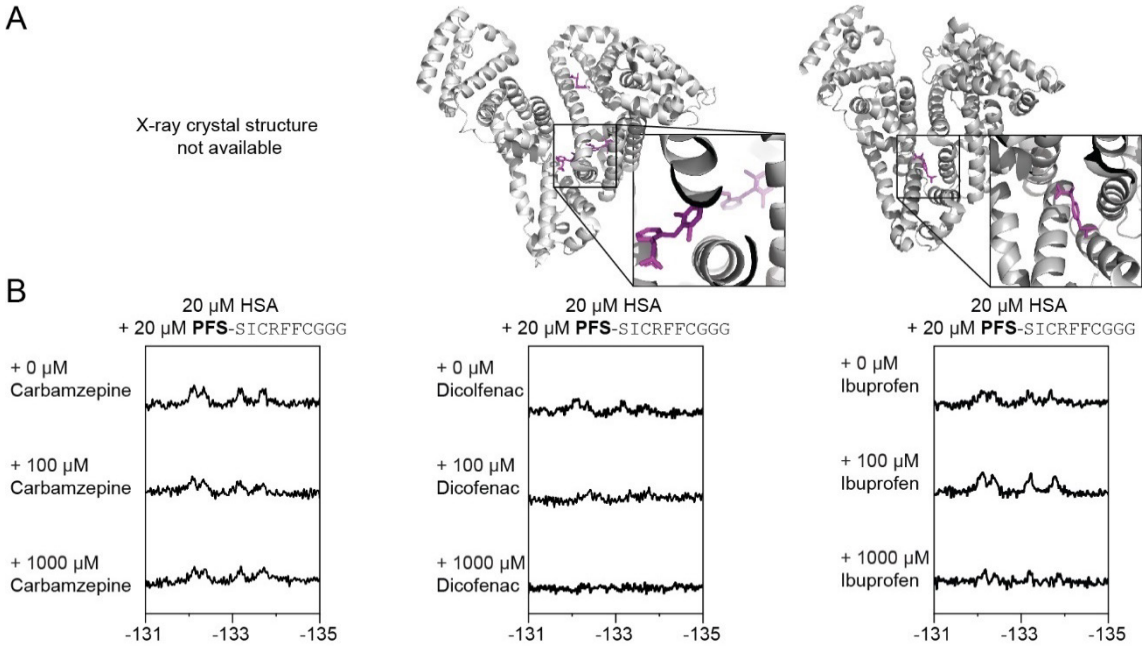

Figure 3-15. The ^{19}F NMR HSA binding and competitive binding assay comparison. (A) X-ray crystal structure of diclofenac bound HSA (pbd: 4Z69) and ibuprofen bound HSA (pbd: 2BXG). (B) ^{19}F NMR competitive inhibition assay with **5c** against carbamazepine, diclofenac and ibuprofen. The ^{19}F NMR HSA binding and competitive binding assay comparison was performed by Dr. Steven Kirberger at the University of Minnesota.

We attempted to quantify the binding affinity of **1b**-**5b** by ITC using the known albumin binder SA-21 as a control.[93] Analysis of the binding affinities of the **DFS**-modified peptides by ITC on HSA was optimized using peptide concentration at 400 μM and 40 μM for HSA. We found complex multi-location binding behavior for all peptides, which obscured the accurate evaluation of binding affinity by ITC (Figure 3-16A, Appendix B-Figure 4-5).

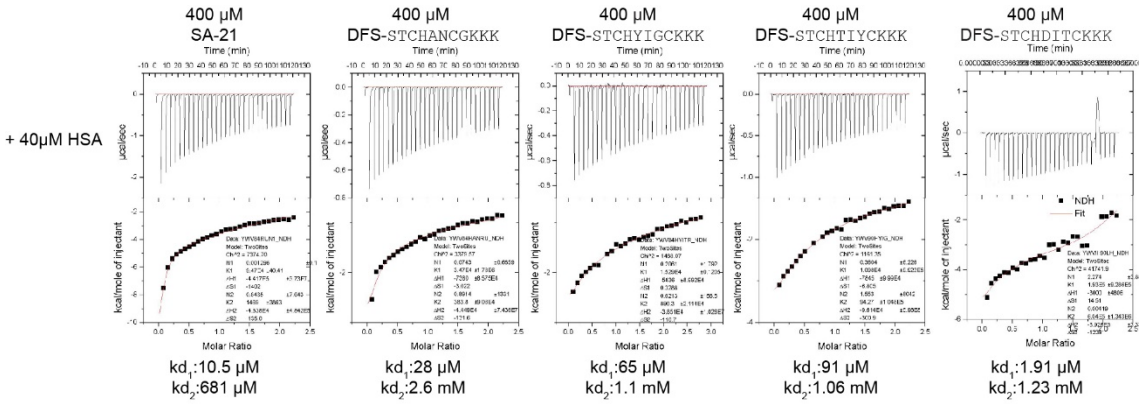

Figure 3-16. Summary of ITC binding assay SA-21 and **1b**-**5b** titrated against HSA.

We employed a fluorescence polarization binding assay (FP) to measure the binding affinities of the macrocycles with the fluorophore BODIPY at the C- or N-terminus. In a typical experiment, we used **5c** or **6c** at 1 µM concentration and titrated HSA from 0.1 µM to 100 µM. The dose-response curve could be fit to a single-state binding model with binding affinity of K_d = 4-6 µM for **5c** and at least 100 times weaker affinity for **6c**. (Figure 3-18A). BODIPY alone bound weakly to HSA with > 300 µM binding affinity (Figure 3-18A). The FP-assay made it possible to measure binding to other proteins or even complex mixtures (serum). A titration of the serum yielded a similar binding profile to that observed in binding to pure albumin (Figure 3-18A). Replacing HSA with lysozyme and RNAase A detected no binding response, confirming that **5c** binding was specific to HSA (Figure 3-18B).

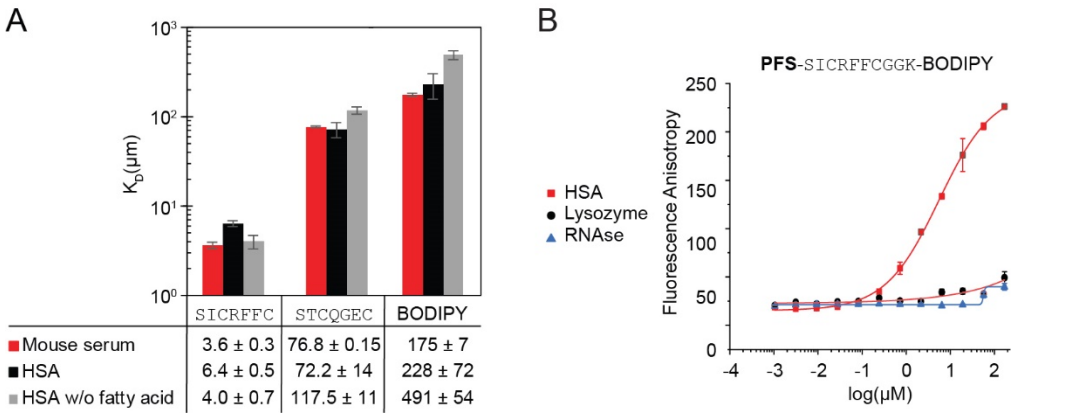

Figure 3-18. Binding assay data other than HSA: (A) FP assay measured the K_d of the **5c** and **8c** against various albumins. (B) The FP assay for BODIPY labelled **5c** titrated against HSA (black), lysozyme (red), and RNAse A (blue).

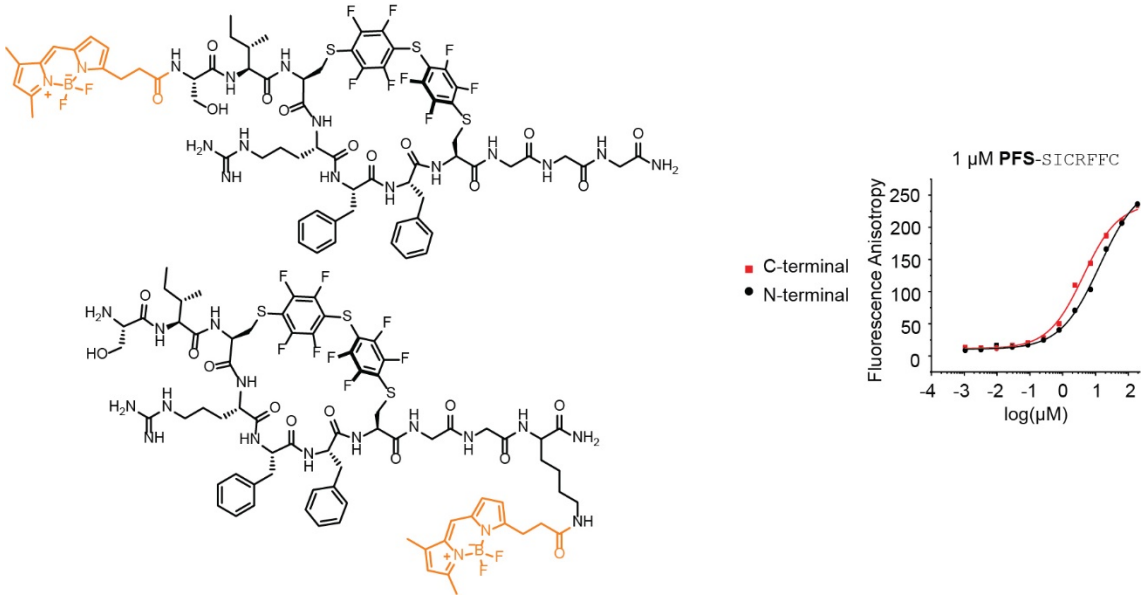

Figure 3-19. The FP binding assaying of conjugate **5c** with BODIPY installed at N-terminus and C-terminus

Switching location of the fluorescent probe from the N-terminus to C-terminus did not significantly change the affinity of **5c** (K_d = 4-6 μM, Figure 3-19). The switching from **DFS** to **PFS** also exhibited a minimal binding effect on the peptide between **5b** and **5c**. (Figure 3-20A) The results were in the same order of magnitude as semi-qualitative estimates acquired for BODIPY-free peptides by

the ^{19}F NMR binding assay, indicating that the presence of a fluorophore did not significantly increase the binding.

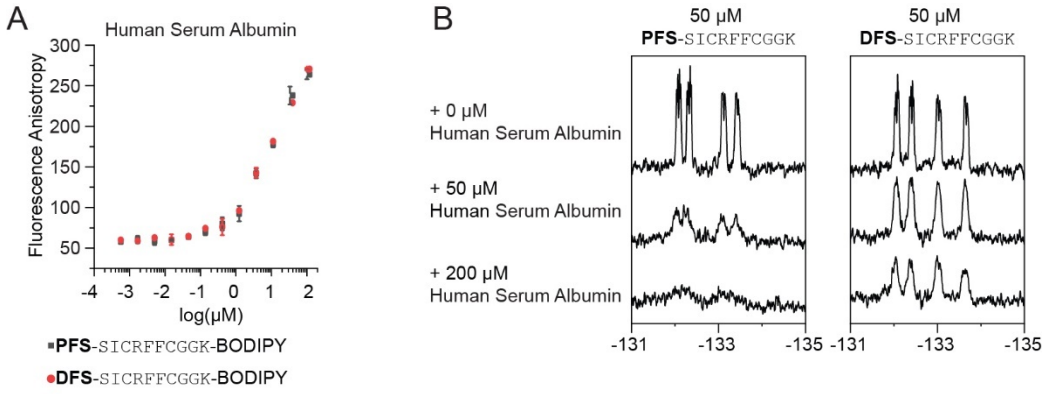

Figure 3-20. HSA binding between **5b** and **5c** (A) FP binding assay of **5b** and **5c**. (B) ^{19}F NMR binding assay of **5b** and **5c**

Heinis and co-workers recently observed that fluorophores could dramatically increase binding affinity to albumin, and removing the fluorophore is detrimental to the binding of the albumin binder. To exclude this possibility, we conducted an NMR-binding assay of N-terminally-labelled **PFS**-SICRFFCGG and BODIPY-free peptides. We observed that the binding affinity was similar (Figure 3-21A). In addition, we observed that binding peptide modified with either KKK or GGG have similar binding affinities (Figure 3-21B).

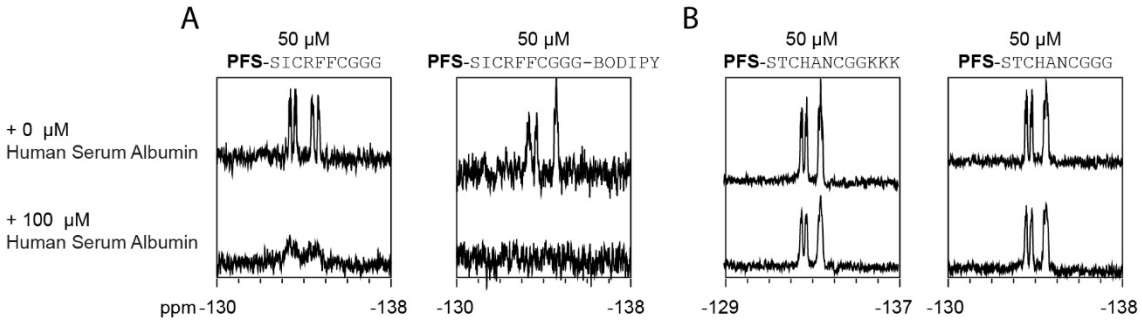

Figure 3-21. ^{19}F NMR assay of different labels. (A) comparison of BODIPY labeled **5c**. (B) Comparison of **3c** with the KKK and GGG solubility tag.

3.2.3 Stability of albumin peptides in mice

We compared **5c** with a bicycle **P5** that binds to Siglec-7 (Unpublished results) with SA-21 as control. We injected the peptide mixture into mice and monitored the remaining peptide level by LC–MS (Figure 3-22A). We observed **5c** had decreased 10-fold and SA-21 had decreased 5-fold after 2 hours. On the contrary, **P5** was undetectable after 5 min (Figure 3-22B).

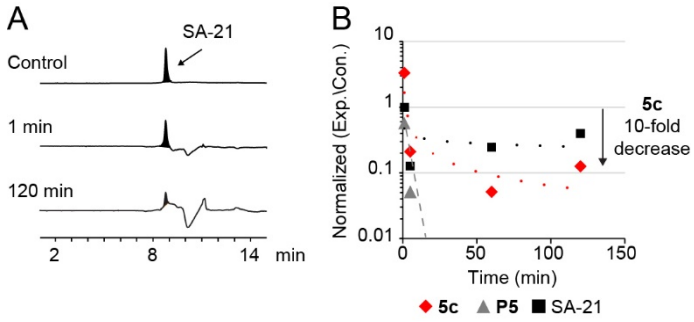

Figure 3-22. Pharmacokinetic studies for **5c**, **P5** and SA-21.(A) Chromatography of selected ion monitoring (SIM) for SA-21 ($[M+2H]^{+2}$ = 1136.4) to monitor *in vivo* stability in mice. (B) Blood samples were collected at time points 1, 5, 60 and 120 mins and analyzed by LC–MS. (n = 1).

3.3 Conclusion

In conclusion, we devised three different selection campaigns for discovering small perfluoro-stapled macrocyclic peptides that bind to human albumin. Macrocycle **5c** was the best among the selected candidates. We showed the linchpin **DFS** and **PFS** did not play an important role in binding and could be used interchangeably. We demonstrated the ability to discover macrocycles with a more reactive linchpin **DFS** and validate with a more stable linchpin **PFS**.

3.4 Materials and methods

3.4.1 General biochemistry information

HSA was purchased from Sigma-Aldrich (cat# A4327-1G), as were Protein A from Sigma-Aldrich (cat# P6031-1MG), and Concanavalin A (cat# C2010-100MG). The proteins were immobilized on a high binding plate (Corning, ref# 3369) with 100 µL of HSA or Protein A (100 µg/mL). The wells were washed 6 times with 200 µL of 1×PBS-T+0.1% tween 20, at pH 7.4 prior to phage incubation. The proteins were biotinylated in section **3.4.6**. Prior to capture proteins, the magnetic streptavidin beads (Promega, cat# Z5482) were washed with 1 × PBS. All proteins were captures with 20 µL magnetic streptavidin beads.

3.4.2 Preparation of SXCX$_3$C phage-displayed library

The procedures have been adopted and modified as previously described in two publications that produced the M13-displayed SXCXXXC library[305] and M13-SDB vector[42]. In short, the vector SB4 QFT*LHQ was digested with Kpn I HF (NEB cat# R3142S) and Eag I HF (NEB cat# R3505S). A primer/template

pair consisting of primer 5'-AT GGC GCC CGG CCG AAC CTC CAC C-3' and template 5'-CC CGG GTA CCT TTC TAT TCT CAC TCT TCT X TGT XXX TGT GGT GGA GGT TCG GCC GGG CGC TTG ATT-3' with 'X' representing a trinucleotide formed by annealing. The primer/template was then extended using Klenow DNA polymerase (NEB) according to the manufacturer's instructions. The insert fragment was then digested with Kpn1 HF and Eag1 HF, gel purified and ligated into the cut vector. The ligation products were then transformed into electrocompetent *E. coli* cells and the transformants were grown overnight on *E. coli* TG1 to allow for phage production. Phage cultures were then centrifuged to remove cells and debris and then the phage was precipitated by PEG precipitation (5% PEG 0.5 M NaCl). Other SD vectors have been processed identically. We sequenced the naïve libraries by Illumina sequencing and the naïve library of $SXCX_nC$ (n=3-5) composition are publicly available at the following links: https://48hd.cloud/file/1470

3.4.3 Panning strategy 1: panning on plate

$SXCX_4C$ and $SXCX_5C$ libraries were prepared as the described previous reports protocol.[278]

Round 1-3: The following protocol was repeated 3 times.

In Protein A coated wells, 100 μL of 2×10^9 PFU/mL **DFS** modified library or unmodified library was incubated for O/N at 4 ºC to remove unspecific bindings. The **DFS** modified library supernatant was then transferred to wells with HSA and incubated for 1.5 h at RT. In parallel, **DFS** modified library supernatants were also incubated with Protein A, and unmodified libraries were

incubated with HSA and protein as a negative control. After panning, all wells were washed 10 times with 1×PBST. The phage remaining in the wells were eluted with 200 µL of glycine elution buffer (Glycine-HCl pH 2.2, 0.1% BSA) for 9 min. The elution buffer was transferred into a new 1.7 mL microcentrifuge tube and neutralized with 20 µL of 1 M Tris-HCl (pH 9.1). The recovered phage solution was amplified for the next round of bio panning and for deep sequencing.

3.4.4 Panning strategy 2: panning on plate and in solution

Round 1:

In Protein A coated wells, 100 µL of 2×10^9 PFU/mL **DFS** modified library or unmodified library was incubated for O/N h at 4 ^{o}C to remove unspecific bindings. The **DFS** modified library supernatant was then transferred to wells with HSA and incubated for 1.5 h at RT. In parallel, **DFS** modified library supernatants were also incubated with Protein A, and unmodified libraries were incubated with HSA and protein A as a negative control. After panning, all wells were washed 10 times with 1×PBST. The phage remaining in the wells were eluted with 200 µL of glycine elution buffer (Glycine-HCl pH 2.2, 0.1% BSA) for 9 min. The elution buffer was transferred into a new 1.7 mL microcentrifuge tube and neutralized with 20 µL of 1 M Tris-HCl (pH 9.1). The recovered phage solution was amplified for the next round of bio-panning and for deep sequencing.

Round 2:

50 µL of magnetic streptavidin beads transferred to a 1.7 mL centrifuge tube. 1 mL of PBS+0.1% Tween was added to wash the beads. The beads then responded in 1 mL of blocking buffer (PBS+2% milk) for 1 hour at 4 ºC. In parallel, 200 µL (2×10^9 PFU/mL) of **DFS** modified phage and unmodified phage library were incubated for 1 hour at RT with pre-block beads to delete beads binders. The beads were captured with a magnetic rack and the supernatant was transferred to a new 1.7 mL centrifuge tube for panning. 100 µL of depleted **DFS** modified phage was combined with 10 µg of biotinylated HSA, increased the volume to 200 µL with 1×PBS and incubated for 1 hour at RT. In parallel, 100 µL of the depleted **DFS** modified phage was combined with 10 µg of biotinylated protein A, increased the volume to 200 µL with 1×PBS and incubated for 1 hour at RT, and 100 µL of depleted bead binder unmodified phage was combined with 10 µg of biotinylated protein A and HSA, increased the volume to 200 µL with 1×PBS and incubated for 1 hour at RT. After incubation, 50 µL of blocked streptavidin beads were added to the samples. Then, the beads were captured with a magnetic rack and washed 10 times with 1 mL of 1×PBST. The phage remaining on the beads were eluted with 200 µL of glycine elution buffer (Glycine-HCl pH 2.2, 0.1% BSA) for 9 min. The elution buffer was transferred into a new 1.7 mL microcentrifuge tube and neutralized with 20 µL of 1 M Tris-HCl (pH 9.1). The recovered phage solution was amplified for the next round of biopanning and for deep sequencing.

Round 3:

In Protein A coated wells, 100 µL of 2×10^9 PFU/mL **DFS** modified library or unmodified library was incubated for 1 h at 4 ºC to remove unspecific bindings. The **DFS** modified library supernatant was then transferred to wells with HSA and incubated for 1.5 h at RT. In parallel, **DFS** modified library supernatants were also incubated with Protein A, and unmodified libraries were incubated with HSA and protein as a negative control. After panning, all wells were washed 10 times with 1×PBST. The phage remaining in the wells were eluted with 200 µL of glycine elution buffer (Glycine-HCl pH 2.2, 0.1% BSA) for 9 min. The elution buffer was transferred into a new 1.7 mL microcentrifuge tube and neutralized with 20 µL of 1 M Tris-HCl (pH 9.1). The recovered phage solution was amplified for the next round of biopanning and for deep sequencing.

3.4.5 Panning strategy 3: panning in solution

Round 1: This strategy is 1 round of panning.

Magnetic streptavidin beads were blocked with blocking phage (phage were not able to PCR) overnight and washed 3 times with 1 mL of 1×PBS. **DFS** modified phage library (2×10^{11} pfu/mL) and blocking phage (2×10^{12} pfu/mL) were mixed in a 1:10 ratio and incubated with blocked streptavidin beads for 30 mins to depleted beads binders. The depleted **DFS** modified phages were incubated with 5 mg of biotinylated HSA and T4GP-His_6 in a total volume 100 µL in 1×PBS with 2% milk for 30 min at RT. In parallel, the depleted **DFS** modified phages were incubated with 5 mg of ConA-Bio in a total volume 100 µL in 1×PBS with 2% milk for 30 min at RT. After incubation, 25 µL of blocked

magnetic streptavidin beads were added to each mixture and incubated for 20 mins at RT. Pelleted by magnetic and remove supernatant. The beads were captured with a magnetic rack and were washed 9 times with 1 mL of 1×PBS. At last, the beads were resuspended in 1 mL 1×PBS and incubated for 30 mins. The beads were captured with a magnetic rack, discarded the supernatant, and resuspended with 30 µl of hexane and 30 µl of water (DNAase free water) and shaken for 15 mins (1500 rmp). The samples were heated to 55 °C for 10 mins or until hexane completely evaporated. The reminding water was collected, further converted to Illumina compatible DNA for deep sequencing by Illumina Next seq by PCR.

3.4.6 General protocol for proteins biotinylation

Protein was dissolved to 1 mg/mL in 1×PBS at pH 7.4. 5 molar fold excess of EZ-Link Sulfo-NHS-Biotin (Thermofisher, cat# 21217) were added to the protein solution. The reaction mixture was incubated O/N at 4 ºC. The next day, the protein was dialysis 3 times in 4 L of 1×PBS at pH 7.4. The biotinylated protein was captured with magnetic streptavidin beads to confirm biotinylation. The final concentration was determined with Nano-drop.

3.4.7 PCR amplification protocol for Illumina deep sequencing

Take 25 µL of eluted or amplified phage solution was used as a template for PCR with a total volume of 50 µL.

A Typical 50 µL PCR mixture contained:

8.	5× Phusion buffer	10 µL
9.	10 mM dNTPs	10 µL
10.	Phusion® High-Fidelity DNA Polymerase (NEB, cat# M0530S)	0.5 µL
11.	Forward primer (3'-CAAGCAGAAGACGGCATACGAGATCGGTCTCGGCATTCCTGCTGAACCGCTCTTCCGATCTXXXXXCCTTTCTATTCTCACTCT-5', 10 µM)	2.5 µL
12.	Reverse primer (3'-AATGATACGGCGACCACCGAGATCTACACTCTTTCCCTACACGACGCTCTTCCGATCTXXXXACAGTTTCGGCCGA-5', 10 µM)	2.5 µL
13.	Template solution	25 µL
14.	Nuclease free water	8.5 µL

Thermocycler was preformed using the following setting:

h) 95 °C for 30 sec

i) 95 °C for 30 sec

j) 60.5 °C for 15 sec

k) 72 °C for 30 sec

l) Repeat step b) to d) 25 times

m) 72 °C for 5 min

n) hold at 4°C

3.4.8 Illumina sequencing of samples before and after panning.

The PCR products were produced by PCR as described in general PCR amplification protocol for Illumina deep sequencing with one exception: in amplification of libraries before panning (input), the volume of the template (phage solution) was 2 μL. All products were quantified by 2% (w/v) agarose gel in Tris-Borate-EDTA buffer at 100 volts for ~35 min using a low molecular weight DNA ladder as standard (NEB, cat# N3233S). PCR products that contain different indexing barcodes were pooled, allowing 10 ng of each product in the mixture. The mixture was purified by eGel, quantified by quBit and sequenced using the Illumina NextSeq paired-end 500/550 High Output Kit v2.5 (2×75 Cycles). Data were automatically uploaded to BaseSpace™ Sequence Hub. Processing of the data is described in section processing of Illumina data.

3.4.9 Processing of Illumina data

The Gzip compressed FASTQ files were downloaded from BaseSpace™ Sequence Hub. The files were converted into tables of DNA sequences and their counts per experiment. Briefly, FASTQ files were parsed based on unique multiplexing barcodes within the reads discarding any reads that contained a low-quality score. Mapping the forward (F) and reverse (R) barcoding regions, mapping of F and R priming regions allowing no more than one base substitution each and F-R read alignment allowing no mismatches between F and R reads yielded DNA sequences located between the priming regions. The files with DNA reads, raw counts, and mapped peptide modifications were uploaded to

http://48hd.cloud/ server. Each experiment has a unique alphanumeric name and unique static URL in Table 3-1–3-3

Table 3-1. URL for 1st panning campaign deep sequencing results

	Modification	HSA	Protein A
R1	**DFS**	https://48hd.cloud/file/213	https://48hd.cloud/file/214
	none	https://48hd.cloud/file/217	https://48hd.cloud/file/218
R2	**DFS**	https://48hd.cloud/file/213	https://48hd.cloud/file/214
	none	https://48hd.cloud/file/217	https://48hd.cloud/file/218
R3	**DFS**	https://48hd.cloud/file/213	https://48hd.cloud/file/214
	none	https://48hd.cloud/file/217	https://48hd.cloud/file/218

Table 3-2. URL for 2nd panning campaign deep sequencing results

	Modification	HSA	Protein A
R1	**DFS**	https://48hd.cloud/file/236	https://48hd.cloud/file/237
	none	https://48hd.cloud/file/421	N/A
R2	**DFS**	https://48hd.cloud/file/236	https://48hd.cloud/file/237
	none	https://48hd.cloud/file/421	N/A
R3	**DFS**	https://48hd.cloud/file/236	https://48hd.cloud/file/237
	none	https://48hd.cloud/file/421	N/A

Table 3-3. URL for 3rd panning campaign deep sequencing results

		HSA	T4-GP	ConA
R1	Input + Modification	https://48hd.cloud/file/799	https://48hd.cloud/file/799	https://48hd.cloud/file/799
	Elution	https://48hd.cloud/file/798	https://48hd.cloud/file/797	https://48hd.cloud/file/796

3.4.10 General chemistry method

LC–MS analysis of peptide modifications was obtained on Agilent Technologies 6130 LC–MS. A gradient of solvent A (MQ water) and solvent B (MeCN/H_2O 95/5) was run at a flow rate of 0.5 mL/min (0-4.0 min 5% B; 4.0-5.0 min 5%→60% B; 5.0-5.5 min 60%→100% B; 5.5-7.5 100% B, 7.5-11 min 100%→5% B).

3.4.11 Peptide synthesis:

Peptides were synthesized on a PreludeX peptide synthesizer (Gyros Protein Technolgoes) by standard Fmoc solid chemistry using Rink Amide AM resin. Fmoc-protected amino acids, HBTU, Rink Amide AM resin were purchased from ChemPrep, Wellington FL USA. Peptides were cleaved from the resin by using a TFA/EDT/TIPS/Water (89.9/2.28/4.54/2.28 v/v) then precipitated and washed with ice-cold diethyl ether, and further purified by HPLC and lyophilized into the product.

3.4.12 General protocol for cyclization with decafluorodiphenylsulfone

Linear peptide (10 mM) was dissolved in 50% acetonitrile and Tris buffer (50 mM Tris-HCl, pH 8.5), then 2 equivalents of **DFS** in 50% acetonitrile and Tris buffer (50 mM Tris-HCl, pH 8.5) was added to the mixture. The mixture was vortex for 30 sec and let to proceed for 2 hours at room temperature. Then, the reaction mixture was purified by HPLC and further lyophilized into the product.

3.4.13 General protocol for cyclization with pentaflurophenyl-sulfide

Linear peptide (10 mM) was dissolved in 50mM Tris in DMF, then 2 equivalents of **PFS** was added to the mixture. The mixture was vortex for 30 sec and allow to react for 1 hour at RT. The reaction mixture was purified by HPLC and further lyophilized into the product.

3.4.14 BODIPY fluorescence C-terminus labeling of 5c and 8c

N-terminal Fmoc-protected **PFS** stapled peptides were dissolved in 1×PBS, 50% acetonitrile, then 1.5 equivalents of BODIPY-NHS ester (100 mg/mL DMSO, Anaspec) was added to the solution. The mixture was incubated for O/N at room temperature. Peperdine were add to a final concentration of 20% v/v for 30 mins to deportect the N-terminus Fmoc protecting group. The reaction mixture was purified by HPLC and further lyophilized into the product.

3.4.15 ^{19}F NMR binding experiment

This entire section was developed by Dr. Steven Kirberger at the University of Minnesota.

All NMR experiments were performed on a Bruker Avance III HD with a Prodigy TCI cryoprobe (2100:1 S/N for ^{19}F). **PFS**-peptides were tested as 20 μM solutions in experiments were performed with a fluorinated peptide concentration of 20 μM in 50 mM phosphate, 100 mM NaCl and 26.5 μM 2,2,2-trifluoroethanol, pH 7.4 with varying concentrations of rat or human serum albumin (from 0-160 μM). Parameters used for each experiment are as follows: 750 scans, acquisition time of 0.05 s, relaxation delay of 0.7 s, spectrum centered at -135 ppm with a sweep width of 20 ppm. A reference spectrum observing

2,2,2-trifluoroethanol was acquired for each sample with the following parameters: 16 scans, acquisition time of 0.5 s, relaxation delay of 1 s, spectrum centered at -75 with a sweep width of 10 ppm. The observed chemical shift of the reference was deducted from -77.75 ppm, and this difference was applied to the peptide spectrum.

Table 3-4. A typical experiment involving titration of HSA was setup as displayed in the table below

Component	HSA	**PFS**-peptide	TFE	D_2O	PBS
Stock (μM)	2000	200	26.5	n.a	n.a
	0	20	2	25	423
	2.5	20	2	25	420.5
	5	20	2	25	418
	10	20	2	25	413
	20	20	2	25	403
	40	20	2	25	383

n.a: Not applicable

This series would produce a titration with 20 μM **PFS**-peptide held constant and the HSA varying in a two-fold fashion: 0, 10, 20, 40, 80,160 μM. TFE refers to 2,2,2-trifluoroethanol as a 1/1000 dilution (approx. 26.5 μM), and PBS components were 50 mM phosphate, 100 mM NaCl, pH 7.4.

3.4.16 Fluorescence polarization binding assay

384 black well plates (PerkinElmer, cat# 6007270) were used to measure all binding assays. The fluorescent-labeled peptides were dissolved to 10 mM in DMSO and diluted to 20 μM in DMSO for use. Each well added with 19 μL of

HSA in 1×PBS with the range of final concentration from 190 μM to 15 nM. 1 μL of 20 μM of fluorescence landed peptide added to the wells to a final concentration of 1 μM. Each measuring point was made in duplicate. Before measuring, the plate was spun down with 500×g for 5 mins at RT, incubated for 10 mins, and shake for 5 mins in the dark. The measurement was performed in Cytation5 Cell Imaging Multi-Mode Reader from BioTek. The data were analyzed and processed in OrginLab.

3.4.17 Isothermal titration calorimetry (ITC) binding assay

Titration experiments were performed using a Microcal VP-ITC instrument. Pepties were discoved in 1×PBS at pH 7.4 to a final concentration of 400 μM . In the case, where ligands have poor solubility in the prepared buffer, up to 5% (v/v) DMF was used. The HAS solution was prepared with the identical buffer as the peptides to a final concentration of 40 μM. All solutions were degassed with MicroCal ThermoVac. All the titration in this studiy carried out at 37 ºC and stirring at 300 rpm. An initial injection of 2 μL follwed by a total of 41 injection of 10 μL peptide solution were added at the interal of 4 mins into the HSA solution. The data were evaluated using the MicroCal™ Origin™ Version 5.0, and the heat signals were fitted to “one set of sites” or “two sets of sites” models to obtain the binding enthalpy, affinity, and stoichiometry estimates.

3.4.18 *In vivo* pharmacokinetic experiment

All the procedures and experiments involving animals were carried out using a protocol approved by the Health Sciences Laboratory Animal Services (HSLAS), University of Alberta. The protocol was approved as per the Canadian Council on

Animal Care (CCAC) guidelines. All mice were maintained in pathogen-free conditions at the University of Alberta breeding facility. 50-100 μM of peptides mixture were dissolved in 1×PBS. Mice were administered 200 μL of the peptide mixture solution with tail veil injection. 6 blood samples were collected at serial time points from 1 min to 240 mins. Samples were collected in tubes that contained sodium citrate as an anticoagulant and then centrifuged at 5 min at 2,000×g to collect the blood plasma. 10 μL of plasma portion were transferred into a tube containing 40 μL of 8:2 acetonitrile/water to precipitate proteins. The sample was centrifuged at max speed for 10 min at 4 ºC. Supernatant then transferred to a clean tube and stored at -20 ºC for further LC–MS analysis.

3.4.19 LC–MS analysis for pharmacokinetics

LC–MS studies of the stability of peptides in mice were performed in Hewlett Packard 1100 series instrument using a Phenomenex Jupiter C4 protein column (300 Å, 2×50 mm, 0.3 mL/min, A: 0.1% formic acid in water, B: 0.1% formic acid in acetonitrile (0 min 2% B, 0→10 min 2%→70% B, 10→15 min 70% B, 15→20 min 70%→2% B). The amount of peptide remaining was calculated with the area under the curve of SIM (Selected Ion Monitoring) peak in LC–MS.

Chapter 4: Conclusion and future directions

4.1 Conclusion

This thesis presented a novel post-translational modification of macrocyclic disulfide peptide phage-displayed libraries. These libraries were used to discover bioactive ligands against the NODAL signaling pathway and the human serum albumin protein. Macrocyclization of peptides with a linchpin provides two advantages compared to their linear counterparts: i) linchpin diversification of the peptide library's chemical space, and ii) improvement of pharmacokinetic properties of the peptides, including increased binding affinity, penetration of cell membrane, penetration of the blood-brain barrier, and the resistance against enzymatic hydrolysis.[203-209] Hence, developing a linchpin compatible with phage display libraries is an attractive strategy to enhance readily available disulfide peptide phage-displayed libraries.

In chapter 2, I developed **TSL**s that convert a readily available disulfide phage-displayed library made of natural amino acid to bicycles. The **TSL**s were functionalized with an aminooxy group to react with the N-terminal aldehyde group derived from the N-terminal serine and two chloro-reactive groups to react with the disulfhydryl side chain. The **TSL**s successfully modified a series of peptides with the SX_nCX_mC motif. The modification enabled successful conversion of 50% of the library into bicycles. The **TLS-6** modified bicycles phage-displayed library was used to discover an antagonist against the NODAL signaling pathway with a potency of IC_{50} = 1-10 μM. We then demonstrated that

TSL-constrained peptides were more stable in mouse serum and a mixture of proteases than linear and **DBMB** modified macrocyclic peptides. In chapter 3, I employed **DFS** modified phage-displayed libraries to discover an HSA binder. After screening, I replaced **DFS** with **PFS** modification to abolish the undesired reactivity from the **DFS** modification. Based on MD simulations, the **PFS** modified peptide retained the same ground-state conformation as the **DFS** modified peptide. Using the ^{19}F NMR binding assay, I determined that the sequences, **PFS**-SICRFFCGGG, had the highest affinity binding towards HSA out of the validated peptides. Following up the results of the ^{19}F NMR binding assay, the **PFS**-SICRFFCGGG binding affinity of K_d = 4-6 μM was determined using fluorescence polarization assay.

4.2 Future direction

Chemical post-translational modification of a phage display library with a linchpin is a powerful method for unearthing proteolytically stable macrocyclic peptides. It is essential that the linchpin is able to modify a broad range of phage displaying peptide sequences. The linchpin should not be limited to thiol-specific bioconjugate chemistry but should combine with other methodologies that are already used to modify peptides of proteins.

In Chapter 2, the **TLS** modification relied on the phage display library with a serine N-terminus to generate aldehydes (Figure 4-1A). I envision the next generation linchpin for converting the disulfide macrocycle to a bicycle is accessible to the majority of phage displaying architectures, especially for

commercially available phage display libraries such as ACX_7C from New England Biolabs. As a proof of concept, the aminooxy group on the **TSL**s can be replaced with a benzaldehyde group (Figure 4-1B). The condensation at neutral pH between the benzaldehyde group and the proximity of N-terminal amine would lead to iminium ion formation, which $NaBH_3CN$ can chemoselectively reduce to an amine linkage.[201] The benzaldehyde group would bypass the need to aldehydes that oxidize from the N-terminal serine and allow the linchpin to modify a broader range of phage display libraries.

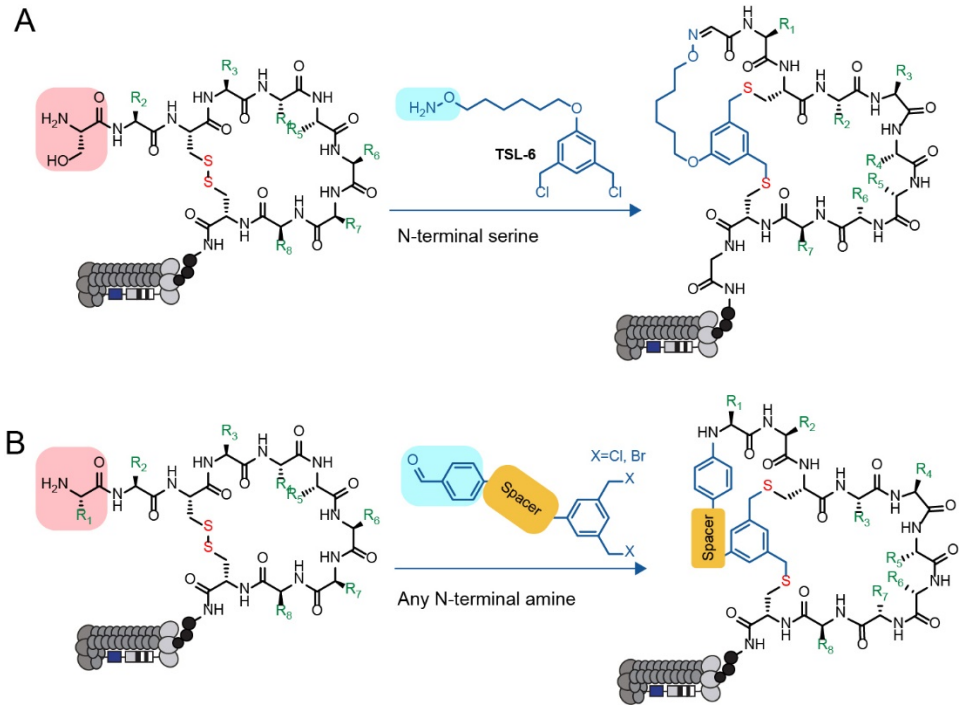

Figure 4-1. Next generation bicyclic linchpin. (A) Current **TSL**s linchpin design. (B) Future bicycle linchpin design.

The **TSL**s and **PFS** modified peptides have proven to be more proteolytic resistant than their linear counterpart; however, those modifications do not address a known drawback: poor *in vivo* circulation time. I hypothesized that

creating a bifunctional molecule, Small Molecular Antibody Like Scaffold (SMALS), will address the poor pharmacokinetics of those peptides. SMALS will contain two domains: i) a warhead for targeting therapeutic targets and ii) a albumin-binding domain for elongation. As a proof of concept, the first generation of SMALS will conjugate the HSA binding peptide from chapter 3 with the NODAL inhibiting bicycles from Chapter 2 (Figure 4-2). I envision that SMALS will not be limited to inhibiting the NODAL signaling pathway but will pave a universal elongation strategy, improving macrocycles' pharmacokinetic properties.

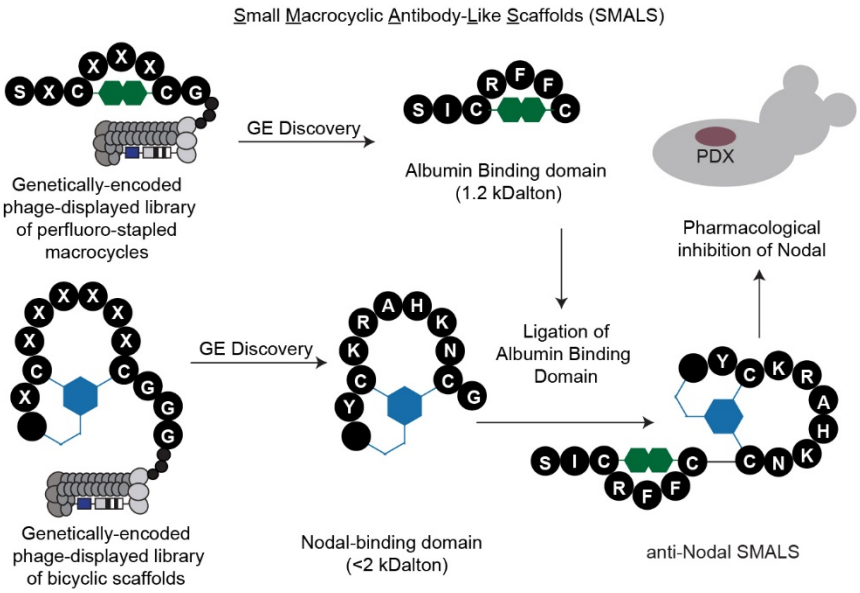

Figure 4-2. Overview of Small Macrocyclic Antibody-Like Scaffold (SMALS).

References

1. Dsouza, R. N.; Pischel, U.; Nau, W. M., Fluorescent Dyes and Their Supramolecular Host/Guest Complexes with Macrocycles in Aqueous Solution. *Chem. Rev.* **2011,** *111* (12), 7941-7980.
2. Villar, E. A.; Beglov, D.; Chennamadhavuni, S.; Porco, J. A.; Kozakov, D.; Vajda, S.; Whitty, A., How proteins bind macrocycles. *Nat. Chem. Biol.* **2014,** *10* (9), 723-731.
3. Neylon, C., Chemical and biochemical strategies for the randomization of protein encoding DNA sequences: library construction methods for directed evolution. *Nucleic Acids Res.* **2004,** *32* (4), 1448-59.
4. Tam, E. M.; Runyon, S. T.; Santell, L.; Quan, C.; Yao, X.; Kirchhofer, D.; Skelton, N. J.; Lazarus, R. A., Noncompetitive Inhibition of Hepatocyte Growth Factor-dependent Met Signaling by a Phage-derived Peptide. *J. Mol. Biol.* **2008,** *385* (1), 79-90.
5. Lowman, H. B.; Chen, Y. M.; Skelton, N. J.; Mortensen, D. L.; Tomlinson, E. E.; Sadick, M. D.; Robinson, I. C.; Clark, R. G., Molecular mimics of insulin-like growth factor 1 (IGF-1) for inhibiting IGF-1: IGF-binding protein interactions. *Biochemistry* **1998,** *37* (25), 8870-8.
6. Gordon, N. C.; Lien, S.; Johnson, J.; Wallweber, H. J.; Tran, T.; Currell, B.; Mathieu, M.; Quan, C.; Starovasnik, M. A.; Hymowitz, S. G.; Kelley, R. F., Multiple novel classes of APRIL-specific receptor-blocking peptides isolated by phage display. *J. Mol. Biol.* **2009,** *396* (1), 166-77.
7. Sidhu, S. S.; Lowman, H. B.; Cunningham, B. C.; Wells, J. A., Phage display for selection of novel binding peptides. *Methods Enzymol.* **2000,** *328*, 333-63.
8. Virnekas, B.; Ge, L. M.; Pluckthun, A.; Schneider, K. C.; Wellnhofer, G.; Moroney, S. E., Trinucleotide Phosphoramidites - Ideal Reagents for the Synthesis of Mixed Oligonucleotides for Random Mutagenesis. *Nucleic Acids Res.* **1994,** *22* (25), 5600-5607.
9. Sieber, T.; Hare, E.; Hofmann, H.; Trepel, M., Biomathematical Description of Synthetic Peptide Libraries. *PLoS One* **2015,** *10* (6), e0129200.
10. Knappik, A.; Ge, L.; Honegger, A.; Pack, P.; Fischer, M.; Wellnhofer, G.; Hoess, A.; Wölle, J.; Plückthun, A.; Virnekäs, B., Fully synthetic human combinatorial antibody libraries (HuCAL) based on modular consensus frameworks and CDRs randomized with trinucleotides11Edited by I. A. Wilson. *J. Mol. Biol.* **2000,** *296* (1), 57-86.
11. Kunkel, T. A., Rapid and efficient site-specific mutagenesis without phenotypic selection. *Proc. Natl. Acad. Sci. U.S.A* **1985,** *82* (2), 488-492.
12. Smith, G. P., Filamentous Fusion Phage: Novel Expression Vectors That Display Cloned Antigens on the Virion Surface. *Science* **1985,** *228* (4705), 1315-1317.
13. Young, R. A.; Davis, R. W., Efficient isolation of genes by using antibody probes. *Proc. Natl. Acad. Sci. U.S.A* **1983,** *80* (5), 1194-1198.

14. Dower, W. J.; Miller, J. F.; Ragsdale, C. W., High efficiency transformation of E.coli by high voltage electroporation. *Nucleic Acids Res.* **1988,** *16* (13), 6127-6145.
15. Tjhung, K. F.; Deiss, F.; Tran, J.; Chou, Y.; Derda, R., Intra-domain phage display (ID-PhD) of peptides and protein mini-domains censored from canonical pIII phage display. *Front. Microbiol.* **2015,** *6*, 340.
16. Smietana, K.; Kasztura, M.; Paduch, M.; Derewenda, U.; Derewenda, Z. S.; Otlewski, J., Degenerate specificity of PDZ domains from RhoA-specific nucleotide exchange factors PDZRhoGEF and LARG. *Acta Biochim. Pol.* **2008,** *55* (2), 269-80.
17. Fuh, G.; Pisabarro, M. T.; Li, Y.; Quan, C.; Lasky, L. A.; Sidhu, S. S., Analysis of PDZ domain-ligand interactions using carboxyl-terminal phage display. *J. Biol. Chem.* **2000,** *275* (28), 21486-91.
18. Fuh, G.; Sidhu, S. S., Efficient phage display of polypeptides fused to the carboxy-terminus of the M13 gene-3 minor coat protein. *FEBS Lett.* **2000,** *480* (2-3), 231-4.
19. Gao, C.; Mao, S.; Ditzel, H. J.; Farnaes, L.; Wirsching, P.; Lerner, R. A.; Janda, K. D., A cell-penetrating peptide from a novel pVII-pIX phage-displayed random peptide library. *Bioorg. Med. Chem.* **2002,** *10* (12), 4057-65.
20. Shi, L.; Wheeler, J. C.; Sweet, R. W.; Lu, J.; Luo, J. Q.; Tornetta, M.; Whitaker, B.; Reddy, R.; Brittingham, R.; Borozdina, L.; Chen, Q.; Amegadzie, B.; Knight, D. M.; Almagro, J. C.; Tsui, P., De Novo Selection of High-Affinity Antibodies from Synthetic Fab Libraries Displayed on Phage as pIX Fusion Proteins. *J. Mol. Biol.* **2010,** *397* (2), 385-396.
21. Loset, G. A.; Roos, N.; Bogen, B.; Sandlie, I., Expanding the Versatility of Phage Display II: Improved Affinity Selection of Folded Domains on Protein VII and IX of the Filamentous Phage. *PLoS One* **2011,** *6* (2), e17433.
22. Ma, H.; Zhou, B.; Kim, Y.; Janda, K. D., A cyclic peptide-polymer probe for the detection of Clostridium botulinum neurotoxin serotype A. *Toxicon* **2006,** *47* (8), 901-8.
23. Kim, Y.; Lillo, A. M.; Steiniger, S. C.; Liu, Y.; Ballatore, C.; Anichini, A.; Mortarini, R.; Kaufmann, G. F.; Zhou, B.; Felding-Habermann, B.; Janda, K. D., Targeting heat shock proteins on cancer cells: selection, characterization, and cell-penetrating properties of a peptidic GRP78 ligand. *Biochemistry* **2006,** *45* (31), 9434-44.
24. Malys, N.; Chang, D. Y.; Baumann, R. G.; Xie, D.; Black, L. W., A bipartite bacteriophage T4 SOC and HOC randomized peptide display library: detection and analysis of phage T4 terminase (gp17) and late sigma factor (gp55) interaction. *J. Mol. Biol.* **2002,** *319* (2), 289-304.
25. Overstreet, C. M.; Yuan, T. Z.; Levin, A. M.; Kong, C.; Coroneus, J. G.; Weiss, G. A., Self-made phage libraries with heterologous inserts in the Mtd of Bordetella bronchiseptica. *Protein Eng. Des. Sel.* **2012,** *25* (4), 145-51.
26. Ludtke, J. J.; Sololoff, A. V.; Wong, S. C.; Zhang, G.; Wolff, J. A., In vivo selection and validation of liver-specific ligands using a new T7 phage peptide display system. *Drug Deliv.* **2007,** *14* (6), 357-69.

27. van den Berk, L. C.; Landi, E.; Walma, T.; Vuister, G. W.; Dente, L.; Hendriks, W. J., An allosteric intramolecular PDZ-PDZ interaction modulates PTP-BL PDZ2 binding specificity. *Biochemistry* **2007,** *46* (47), 13629-37.
28. van den Berk, L. C.; Landi, E.; Harmsen, E.; Dente, L.; Hendriks, W. J., Redox-regulated affinity of the third PDZ domain in the phosphotyrosine phosphatase PTP-BL for cysteine-containing target peptides. *FEBS J.* **2005,** *272* (13), 3306-16.
29. Sternberg, N.; Hoess, R. H., Display of peptides and proteins on the surface of bacteriophage lambda. *Proc. Natl. Acad. Sci. U. S. A.* **1995,** *92* (5), 1609-13.
30. Kuwabara, I.; Maruyama, H.; Mikawa, Y. G.; Zuberi, R. I.; Liu, F. T.; Maruyama, I. N., Efficient epitope mapping by bacteriophage lambda surface display. *Nat. Biotechnol.* **1997,** *15* (1), 74-8.
31. Khuebachova, M.; Verzillo, V.; Skrabana, R.; Ovecka, M.; Vaccaro, P.; Panni, S.; Bradbury, A.; Novak, M., Mapping the C terminal epitope of the Alzheimer's disease specific antibody MN423. *J. Immunol. Methods* **2002,** *262* (1-2), 205-15.
32. Gupta, A.; Onda, M.; Pastan, I.; Adhya, S.; Chaudhary, V. K., High-density functional display of proteins on bacteriophage lambda. *J. Mol. Biol.* **2003,** *334* (2), 241-54.
33. Kang, S.; Lander, G. C.; Johnson, J. E.; Prevelige, P. E., Development of bacteriophage p22 as a platform for molecular display: genetic and chemical modifications of the procapsid exterior surface. *ChemBioChem* **2008,** *9* (4), 514-8.
34. Carbonell, X.; Villaverde, A., Insertional mutagenesis in the tailspike protein of bacteriophage P22. *Biochem. Biophys. Res. Commun.* **1998,** *244* (2), 428-33.
35. Carbonell, X.; Villaverde, A., Peptide display on functional tailspike protein of bacteriophage P22. *Gene* **1996,** *176* (1-2), 225-9.
36. O'Rourke, J. P.; Daly, S. M.; Triplett, K. D.; Peabody, D.; Chackerian, B.; Hall, P. R., Development of a Mimotope Vaccine Targeting the Staphylococcus aureus Quorum Sensing Pathway. *PLoS One* **2014,** *9* (11), e111198.
37. Chackerian, B.; Caldeira, J. D.; Peabody, J.; Peabody, D. S., Peptide Epitope Identification by Affinity Selection on Bacteriophage MS2 Virus-Like Particles. *J. Mol. Biol.* **2011,** *409* (2), 225-37.
38. Du, C.; Chan, W. C.; McKeithan, T. W.; Nickerson, K. W., Surface display of recombinant proteins on Bacillus thuringiensis spores. *Appl. Environ. Microbiol.* **2005,** *71* (6), 3337-41.
39. Lu, Z.; Murray, K. S.; Cleave, V. V.; LaVallie, E. R.; Stahl, M. L.; McCoy, J. M., Expression of Thioredoxin Random Peptide Libraries on the Escherichia coli Cell Surface as Functional Fusions to Flagellin: A System Designed for Exploring Protein-Protein Interactions. *Biotechnology. (N. Y.)* **1995,** *13* (4), 366-372.
40. Shukla, G. S.; Krag, D. N., Phage-displayed combinatorial peptide libraries in fusion to beta-lactamase as reporter for an accelerated clone

screening: Potential uses of selected enzyme-linked affinity reagents in downstream applications. *Comb. Chem. High Throughput Screen.* **2010,** *13* (1), 75-87.
41. van Houten, N. E.; Zwick, M. B.; Menendez, A.; Scott, J. K., Filamentous phage as an immunogenic carrier to elicit focused antibody responses against a synthetic peptide. *Vaccine* **2006,** *24* (19), 4188-200.
42. Sojitra, M.; Sarkar, S.; Maghera, J.; Rodrigues, E.; Carpenter, E. J.; Seth, S.; Ferrer Vinals, D.; Bennett, N. J.; Reddy, R.; Khalil, A.; Xue, X.; Bell, M. R.; Zheng, R. B.; Zhang, P.; Nycholat, C.; Bailey, J. J.; Ling, C.-C.; Lowary, T. L.; Paulson, J. C.; Macauley, M. S.; Derda, R., Genetically encoded multivalent liquid glycan array displayed on M13 bacteriophage. *Nat. Chem. Biol.* **2021,** *17* (7), 806-816.
43. Lima, G. M.; Atrazhev, A.; Sarkar, S.; Sojitra, M.; Reddy, R.; Macauley, M. S.; Monteiro, G.; Derda, R., DNA-Encoded Multivalent Display of Protein Tetramers on Phage: Synthesis and In Vivo Aplications. *bioRxiv* **2021**, 2021.02.20.432100.
44. Velappan, N.; Fisher, H. E.; Pesavento, E.; Chasteen, L.; D'Angelo, S.; Kiss, C.; Longmire, M.; Pavlik, P.; Bradbury, A. R., A comprehensive analysis of filamentous phage display vectors for cytoplasmic proteins: an analysis with different fluorescent proteins. *Nucleic Acids Res.* **2010,** *38* (4), e22.
45. Kalnina, Z.; Silina, K.; Meistere, I.; Zayakin, P.; Rivosh, A.; Abols, A.; Leja, M.; Minenkova, O.; Schadendorf, D.; Line, A., Evaluation of T7 and lambda phage display systems for survey of autoantibody profiles in cancer patients. *J. Immunol. Methods* **2008,** *334* (1-2), 37-50.
46. Santini, C.; Brennan, D.; Mennuni, C.; Hoess, R. H.; Nicosia, A.; Cortese, R.; Luzzago, A., Efficient display of an HCV cDNA expression library as C-terminal fusion to the capsid protein D of bacteriophage lambda. *J. Mol. Biol.* **1998,** *282* (1), 125-35.
47. Krumpe, L. R.; Atkinson, A. J.; Smythers, G. W.; Kandel, A.; Schumacher, K. M.; McMahon, J. B.; Makowski, L.; Mori, T., T7 lytic phage-displayed peptide libraries exhibit less sequence bias than M13 filamentous phage-displayed peptide libraries. *Proteomics* **2006,** *6* (15), 4210-22.
48. Smith, G. P.; Petrenko, V. A., Phage Display. *Chem. Rev.* **1997,** *97* (2), 391-410.
49. Hoydahl, L. S.; Nilssen, N. R.; Gunnarsen, K. S.; Pre, M. F.; Iversen, R.; Roos, N.; Chen, X.; Michaelsen, T. E.; Sollid, L. M.; Sandlie, I.; Loset, G. A., Multivalent pIX phage display selects for distinct and improved antibody properties. *Sci. Rep.* **2016,** *6*, 39066.
50. Burritt, J. B.; Bond, C. W.; Doss, K. W.; Jesaitis, A. J., Filamentous phage display of oligopeptide libraries. *Anal. Biochem.* **1996,** *238* (1), 1-13.
51. Derda, R.; Jafari, R. M., Synthetic Cross-linking of Peptides: Molecular Linchpins for Peptide Cyclization. *Protein Peptide Lett.* **2018,** *25* (12), 1051-1075.

52. Koivunen, E.; Gay, D. A.; Ruoslahti, E., Selection of peptides binding to the alpha 5 beta 1 integrin from phage display library. *J. Biol. Chem.* **1993,** *268* (27), 20205-20210.
53. Trexler, M.; Briknarová, K.; Gehrmann, M.; Llinás, M.; Patthy, L., Peptide Ligands for the Fibronectin Type II Modules of Matrix Metalloproteinase 2 (MMP-2)*. *J. Biol. Chem.* **2003,** *278* (14), 12241-12246.
54. Yu, M.; Than, K.; Colegate, S.; Shiell, B.; Michalski, W. P.; Prowse, S.; Wang, L.-F., Peptide mimotopes of phomopsins: Identification, characterization and application in an immunoassay. *Mol. Divers.* **2005,** *9* (1), 233-240.
55. Ding, H.; Prodinger, W. M.; Kopeček, J., Identification of CD21-Binding Peptides with Phage Display and Investigation of Binding Properties of HPMA Copolymer−Peptide Conjugates. *Bioconjugate Chem.* **2006,** *17* (2), 514-523.
56. Bonnycastle, L. L.; Mehroke, J. S.; Rashed, M.; Gong, X.; Scott, J. K., Probing the basis of antibody reactivity with a panel of constrained peptide libraries displayed by filamentous phage. *J. Mol. Biol.* **1996,** *258* (5), 747-62.
57. Bublil, E. M.; Yeger-Azuz, S.; Gershoni, J. M., Computational prediction of the cross-reactive neutralizing epitope corresponding to the [corrected] monclonal [corrected] antibody b12 specific for HIV-1 gp120. *FASEB J.* **2006,** *20* (11), 1762-74.
58. Adda, C. G.; Tilley, L.; Anders, R. F.; Foley, M., Isolation of peptides that mimic epitopes on a malarial antigen from random peptide libraries displayed on phage. *Infect. Immun.* **1999,** *67* (9), 4679-4688.
59. Zhan, J.; Xia, Z.; Xu, L.; Yan, Z.; Wang, K., A peptide mimetic of Gal-alpha 1,3-Gal is able to block human natural antibodies. *Biochem. Biophys. Res. Commun.* **2003,** *308* (1), 19-22.
60. Harris, S. L.; Craig, L.; Mehroke, J. S.; Rashed, M.; Zwick, M. B.; Kenar, K.; Toone, E. J.; Greenspan, N.; Auzanneau, F. I.; Marino-Albernas, J. R.; Pinto, B. M.; Scott, J. K., Exploring the basis of peptide-carbohydrate crossreactivity: evidence for discrimination by peptides between closely related anti-carbohydrate antibodies. *Proc. Natl. Acad. Sci. U. S. A.* **1997,** *94* (6), 2454-9.
61. Fogaça, R. L.; Capelli-Peixoto, J.; Yamanaka, I. B.; de Almeida, R. P. M.; Muzzi, J. C. D.; Borges, M.; Costa, A. J.; Chávez-Olortegui, C.; Thomaz-Soccol, V.; Alvarenga, L. M.; de Moura, J., Phage-displayed peptides as capture antigens in an innovative assay for Taenia saginata-infected cattle. *Appl. Microbiol. Biotechnol.* **2014,** *98* (21), 8887-8894.
62. Bentley, L.; Fehrsen, J.; Jordaan, F.; Huismans, H.; du Plessis, D. H., Identification of antigenic regions on VP2 of African horsesickness virus serotype 3 by using phage-displayed epitope libraries. *J. Gen. Virol.* **2000,** *81* (4), 993-1000.
63. Guo, Y.; Zhang, J.; Wang, J. C.; Yan, F. X.; Zhu, B. Y.; Huang, H. L.; Liao, D. F., Identification of peptides inhibiting adhesion of monocytes to the injured vascular endothelial cells through phage-displaying screening. *Acta biochimica et biophysica Sinica* **2005,** *37* (4), 227-33.

64. Michael, D. S.; John, W. K.; Brian, K. K., Efficient Construction of a Large Collection of Phage-Displayed Combinatorial Peptide Libraries. *Combinatorial Chem. High Throughput Screening* **2005,** *8* (6), 545-551.
65. Wu, Y.-Q.; Qu, H.; Sfyroera, G.; Tzekou, A.; Kay, B. K.; Nilsson, B.; Nilsson Ekdahl, K.; Ricklin, D.; Lambris, J. D., Protection of nonself surfaces from complement attack by factor H-binding peptides: implications for therapeutic medicine. *Journal of immunology (Baltimore, Md. : 1950)* **2011,** *186* (7), 4269-4277.
66. Falk, S. P.; Weisblum, B., Phosphorylation of the Streptococcus pneumoniae cell wall biosynthesis enzyme MurC by a eukaryotic-like Ser/Thr kinase. *FEMS Microbiol. Lett.* **2013,** *340* (1), 19-23.
67. Tarnovitski, N.; Matthews, L. J.; Sui, J.; Gershoni, J. M.; Marasco, W. A., Mapping a neutralizing epitope on the SARS coronavirus spike protein: computational prediction based on affinity-selected peptides. *J. Mol. Biol.* **2006,** *359* (1), 190-201.
68. Liu, Y.; Higgins, C. D.; Overstreet, C. M.; Rai, K. R.; Chiorazzi, N.; Lai, J. R., Peptides that bind specifically to an antibody from a chronic lymphocytic leukemia clone expressing unmutated immunoglobulin variable region genes. *Molecular medicine (Cambridge, Mass.)* **2013,** *19* (1), 245-252.
69. Shanmugam, A.; Suriano, R.; Chaudhuri, D.; Rajoria, S.; George, A.; Mittelman, A.; Tiwari, R. K., Identification of PSA peptide mimotopes using phage display peptide library. *Peptides* **2011,** *32* (6), 1097-102.
70. Kouzmitcheva, G. A.; Petrenko, V. A.; Smith, G. P., Identifying diagnostic peptides for lyme disease through epitope discovery. *Clin. Diagn. Lab. Immunol.* **2001,** *8* (1), 150-60.
71. Sidhu, S. S.; Lowman, H. B.; Cunningham, B. C.; Wells, J. A., [21] Phage display for selection of novel binding peptides. In *Methods Enzymol.*, Thorner, J.; Emr, S. D.; Abelson, J. N., Eds. Academic Press: 2000; Vol. 328, pp 333-IN5.
72. Holig, P.; Bach, M.; Volkel, T.; Nahde, T.; Hoffmann, S.; Muller, R.; Kontermann, R. E., Novel RGD lipopeptides for the targeting of liposomes to integrin-expressing endothelial and melanoma cells. *Protein Eng. Des. Sel.* **2004,** *17* (5), 433-41.
73. Tamm, I.; Trepel, M.; Cardo-Vila, M.; Sun, Y.; Welsh, K.; Cabezas, E.; Swatterthwait, A.; Arap, W.; Reed, J. C.; Pasqualini, R., Peptides targeting caspase inhibitors. *J. Biol. Chem.* **2003,** *278* (16), 14401-5.
74. Giebel, L. B.; Cass, R. T.; Milligan, D. L.; Young, D. C.; Arze, R.; Johnson, C. R., Screening of cyclic peptide phage libraries identifies ligands that bind streptavidin with high affinities. *Biochemistry* **1995,** *34* (47), 15430-5.
75. Scott, J. K.; Huang, S. F.; Gangadhar, B. P.; Samoriski, G. M.; Clapp, P.; Gross, R. A.; Taussig, R.; Smrcka, A. V., Evidence that a protein-protein interaction 'hot spot' on heterotrimeric G protein betagamma subunits is used for recognition of a subclass of effectors. *EMBO J.* **2001,** *20* (4), 767-76.
76. Lederer, F. L.; Curtis, S. B.; Bachmann, S.; Dunbar, W. S.; MacGillivray, R. T., Identification of lanthanum-specific peptides for future recycling of rare

earth elements from compact fluorescent lamps. *Biotechnol. Bioeng.* **2017,** *114* (5), 1016-1024.
77. Rajotte, D.; Arap, W.; Hagedorn, M.; Koivunen, E.; Pasqualini, R.; Ruoslahti, E., Molecular heterogeneity of the vascular endothelium revealed by in vivo phage display. *J. Clin. Invest.* **1998,** *102* (2), 430-7.
78. Gho, Y. S.; Lee, J. E.; Oh, K. S.; Bae, D. G.; Chae, C. B., Development of antiangiogenin peptide using a phage-displayed peptide library. *Cancer Res.* **1997,** *57* (17), 3733-40.
79. Sato, A. K.; Sexton, D. J.; Morganelli, L. A.; Cohen, E. H.; Wu, Q. L.; Conley, G. P.; Streltsova, Z.; Lee, S. W.; Devlin, M.; DeOliveira, D. B.; Enright, J.; Kent, R. B.; Wescott, C. R.; Ransohoff, T. C.; Ley, A. C.; Ladner, R. C., Development of Mammalian Serum Albumin Affinity Purification Media by Peptide Phage Display. *Biotechnol. Progr.* **2002,** *18* (2), 182-192.
80. Dromey, J. A.; Weenink, S. M.; Peters, G. H.; Endl, J.; Tighe, P. J.; Todd, I.; Christie, M. R., Mapping of epitopes for autoantibodies to the type 1 diabetes autoantigen IA-2 by peptide phage display and molecular modeling: overlap of antibody and T cell determinants. *J. Immunol.* **2004,** *172* (7), 4084-90.
81. Curtis, S.; Lederer, F. L.; Dunbar, W. S.; MacGillivray, R. T., Identification of mineral-binding peptides that discriminate between chalcopyrite and enargite. *Biotechnol. Bioeng.* **2017,** *114* (5), 998-1005.
82. Al-bukhari, T. A.; Tighe, P.; Todd, I., An immuno-precipitation assay for determining specific interactions between antibodies and phage selected from random peptide expression libraries. *J. Immunol. Methods* **2002,** *264* (1-2), 163-71.
83. Pulli, T.; Koivunen, E.; Hyypia, T., Cell-surface interactions of echovirus 22. *J. Biol. Chem.* **1997,** *272* (34), 21176-80.
84. Koivunen, E.; Wang, B.; Ruoslahti, E., Phage libraries displaying cyclic peptides with different ring sizes: ligand specificities of the RGD-directed integrins. *Biotechnology. (N. Y.)* **1995,** *13* (3), 265-70.
85. Pasqualini, R.; Koivunen, E.; Ruoslahti, E., A peptide isolated from phage display libraries is a structural and functional mimic of an RGD-binding site on integrins. *J. Cell Biol.* **1995,** *130* (5), 1189-96.
86. Pasqualini, R.; Ruoslahti, E., Organ targeting in vivo using phage display peptide libraries. *Nature* **1996,** *380* (6572), 364-6.
87. Koivunen, E.; Arap, W.; Valtanen, H.; Rainisalo, A.; Medina, O. P.; Heikkila, P.; Kantor, C.; Gahmberg, C. G.; Salo, T.; Konttinen, Y. T.; Sorsa, T.; Ruoslahti, E.; Pasqualini, R., Tumor targeting with a selective gelatinase inhibitor. *Nat. Biotechnol.* **1999,** *17* (8), 768-74.
88. De Ciechi, P. A.; Devine, C. S.; Lee, S. C.; Howard, S. C.; Olins, P. O.; Caparon, M. H., Utilization of multiple phage display libraries for the identification of dissimilar peptide motifs that bind to a B7-1 monoclonal antibody. *Mol. Divers.* **1996,** *1* (2), 79-86.
89. Bellotto, S.; Chen, S.; Rentero Rebollo, I.; Wegner, H. A.; Heinis, C., Phage selection of photoswitchable peptide ligands. *J. Am. Chem. Soc.* **2014,** *136* (16), 5880-3.

90. Arap, W.; Pasqualini, R.; Ruoslahti, E., Cancer treatment by targeted drug delivery to tumor vasculature in a mouse model. *Science* **1998,** *279* (5349), 377-80.
91. Tuccillo, F. M.; Palmieri, C.; Fiume, G.; de Laurentiis, A.; Schiavone, M.; Falcone, C.; Iaccino, E.; Galandrini, R.; Capuano, C.; Santoni, A.; D'Armiento, F. P.; Arra, C.; Barbieri, A.; Dal Piaz, F.; Venzon, D.; Bonelli, P.; Buonaguro, F. M.; Scala, I.; Mallardo, M.; Quinto, I.; Scala, G., Cancer-associated CD43 glycoforms as target of immunotherapy. *Mol. Cancer Ther.* **2014,** *13* (3), 752-62.
92. De Bolle, X.; Laurent, T.; Tibor, A.; Godfroid, F.; Weynants, V.; Letesson, J. J.; Mertens, P., Antigenic properties of peptidic mimics for epitopes of the lipopolysaccharide from Brucella. *J. Mol. Biol.* **1999,** *294* (1), 181-91.
93. Dennis, M. S.; Zhang, M.; Meng, Y. G.; Kadkhodayan, M.; Kirchhofer, D.; Combs, D.; Damico, L. A., Albumin binding as a general strategy for improving the pharmacokinetics of proteins. *J. Biol. Chem.* **2002,** *277* (38), 35035-43.
94. Houimel, M.; Dellagi, K., Peptide mimotopes of rabies virus glycoprotein with immunogenic activity. *Vaccine* **2009,** *27* (34), 4648-55.
95. Galili, N.; Devemy, E.; Raza, A., Isolation of specific and biologically active peptides that bind cells from patients with acute myeloid leukemia (AML). *J. Hematol. Oncol.* **2008,** *1*, 8.
96. Lauvrak, V.; Berntzen, G.; Heggelund, U.; Herstad, T. K.; Sandin, R. H.; Dalseg, R.; Rosenqvist, E.; Sandlie, I.; Michaelsen, T. E., Selection and characterization of cyclic peptides that bind to a monoclonal antibody against meningococcal L3,7,9 lipopolysaccharides. *Scand. J. Immunol.* **2004,** *59* (4), 373-84.
97. Braathen, R.; Sandvik, A.; Berntzen, G.; Hammerschmidt, S.; Fleckenstein, B.; Sandlie, I.; Brandtzaeg, P.; Johansen, F. E.; Lauvrak, V., Identification of a polymeric Ig receptor binding phage-displayed peptide that exploits epithelial transcytosis without dimeric IgA competition. *J. Biol. Chem.* **2006,** *281* (11), 7075-81.
98. Vanhoorelbeke, K.; Depraetere, H.; Romijn, R. A.; Huizinga, E. G.; De Maeyer, M.; Deckmyn, H., A consensus tetrapeptide selected by phage display adopts the conformation of a dominant discontinuous epitope of a monoclonal anti-VWF antibody that inhibits the von Willebrand factor-collagen interaction. *J. Biol. Chem.* **2003,** *278* (39), 37815-21.
99. Mintz, P. J.; Rietz, A. C.; Cardo-Vila, M.; Ozawa, M. G.; Dondossola, E.; Do, K. A.; Kim, J.; Troncoso, P.; Logothetis, C. J.; Sidman, R. L.; Pasqualini, R.; Arap, W., Discovery and horizontal follow-up of an autoantibody signature in human prostate cancer. *Proc. Natl. Acad. Sci. U. S. A.* **2015,** *112* (8), 2515-20.
100. Mintz, P. J.; Kim, J.; Do, K. A.; Wang, X.; Zinner, R. G.; Cristofanilli, M.; Arap, M. A.; Hong, W. K.; Troncoso, P.; Logothetis, C. J.; Pasqualini, R.; Arap, W., Fingerprinting the circulating repertoire of antibodies from cancer patients. *Nat. Biotechnol.* **2003,** *21* (1), 57-63.

101. Meyer, S. C.; Gaj, T.; Ghosh, I., Highly selective cyclic peptide ligands for NeutrAvidin and avidin identified by phage display. *Chem. Biol. Drug Des.* **2006,** *68* (1), 3-10.
102. Houimel, M.; Mazzucchelli, L., Random phage-epitope library based identification of a peptide antagonist of Mac-1 beta2 integrin ligand binding. *Matrix Biol.* **2012,** *31* (1), 66-77.
103. Houimel, M.; Mazzucchelli, L., hCXCR1 and hCXCR2 antagonists derived from combinatorial peptide libraries. *Cytokine* **2012,** *57* (3), 322-31.
104. Houimel, M.; Mach, J. P.; Corthesy-Theulaz, I.; Corthesy, B.; Fisch, I., New inhibitors of Helicobacter pylori urease holoenzyme selected from phage-displayed peptide libraries. *Eur. J. Biochem.* **1999,** *262* (3), 774-80.
105. Houimel, M.; Loetscher, P.; Baggiolini, M.; Mazzucchelli, L., Functional inhibition of CCR3-dependent responses by peptides derived from phage libraries. *Eur. J. Immunol.* **2001,** *31* (12), 3535-45.
106. Giordano, R. J.; Cardo-Vila, M.; Lahdenranta, J.; Pasqualini, R.; Arap, W., Biopanning and rapid analysis of selective interactive ligands. *Nat. Med.* **2001,** *7* (11), 1249-53.
107. Ferguson, M. R.; Fan, X.; Mukherjee, M.; Luo, J.; Khan, R.; Ferreon, J. C.; Hilser, V. J.; Shope, R. E.; Fox, R. O., Directed discovery of bivalent peptide ligands to an SH3 domain. *Protein Sci.* **2004,** *13* (3), 626-32.
108. Depraetere, H.; Viaene, A.; Deroo, S.; Vauterin, S.; Deckmyn, H., Identification of peptides, selected by phage display technology, that inhibit von Willebrand factor binding to collagen. *Blood* **1998,** *92* (11), 4207-11.
109. Demangel, C.; Lafaye, P.; Mazie, J. C., Reproducing the immune response against the Plasmodium vivax merozoite surface protein 1 with mimotopes selected from a phage-displayed peptide library. *Mol. Immunol.* **1996,** *33* (11-12), 909-16.
110. Liu, Y.; O'Connor, M. B.; Mandell, K. J.; Zen, K.; Ullrich, A.; Bühring, H. J.; Parkos, C. A., Peptide-mediated inhibition of neutrophil transmigration by blocking CD47 interactions with signal regulatory protein alpha. *J. Immunol.* **2004,** *172* (4), 2578-85.
111. Houimel, M.; Mazzucchelli, L., hCXCR1 and hCXCR2 antagonists derived from combinatorial peptide libraries. *Cytokine* **2011,** *57* (3), 322-31.
112. Houimel, M.; Mazzucchelli, L., Random phage-epitope library based identification of a peptide antagonist of Mac-1 ?2 integrin ligand binding. *Matrix Biol.* **2011,** *31* (1), 66-77.
113. Nielsen, K. M.; Kyneb, M. H.; Alstrup, A. K.; Jensen, J. J.; Bender, D.; Schonheyder, H. C.; Afzelius, P.; Nielsen, O. L.; Jensen, S. B., (68)Ga-labeled phage-display selected peptides as tracers for positron emission tomography imaging of Staphylococcus aureus biofilm-associated infections: Selection, radiolabelling and preliminary biological evaluation. *Nucl. Med. Biol.* **2016,** *43* (10), 593-605.
114. Thirumala-Devi, K.; Miller, J. S.; Reddy, G.; Reddy, D. V.; Mayo, M. A., Phage-displayed peptides that mimic aflatoxin B1 in serological reactivity. *J. Appl. Microbiol.* **2001,** *90* (3), 330-6.

115. Chen, L.; Wang, Y.; Liu, X.; Dou, S.; Liu, G.; Hnatowich, D. J.; Rusckowski, M., A new TAG-72 cancer marker peptide identified by phage display. *Cancer Lett.* **2008,** *272* (1), 122-32.
116. Newton-Northup, J. R.; Figueroa, S. D.; Deutscher, S. L., Streamlined In Vivo Selection and Screening of Human Prostate Carcinoma Avid Phage Particles for Development of Peptide Based In Vivo Tumor Imaging Agents. *Comb. Chem. High Throughput Screen.* **2010,** *14* (1), 9-21.
117. Sibille, P.; Ternynck, T.; Nato, F.; Buttin, G.; Strosberg, D.; Avrameas, A., Mimotopes of polyreactive anti-DNA antibodies identified using phage-display peptide libraries. *Eur. J. Immunol.* **1997,** *27* (5), 1221-8.
118. Rusckowski, M.; Gupta, S.; Liu, G.; Dou, S.; Hnatowich, D. J., Evidence of specificity of radiolabeled phage display peptides for the TAG-72 antigen. *Cancer Biother. Radiopharm.* **2007,** *22* (4), 564-72.
119. Zou, J.; Glinsky, V. V.; Landon, L. A.; Matthews, L.; Deutscher, S. L., Peptides specific to the galectin-3 carbohydrate recognition domain inhibit metastasis-associated cancer cell adhesion. *Carcinogenesis* **2005,** *26* (2), 309-18.
120. Graham, W. D.; Barley-Maloney, L.; Stark, C. J.; Kaur, A.; Stolyarchuk, K.; Sproat, B.; Leszczynska, G.; Malkiewicz, A.; Safwat, N.; Mucha, P.; Guenther, R.; Agris, P. F., Functional Recognition of the Modified Human tRNA(Lys3)(UUU) Anticodon Domain by HIV's Nucleocapsid Protein and a Peptide Mimic. *J. Mol. Biol.* **2011,** *410* (4), 698-715.
121. Eshete, M.; Marchbank, M. T.; Deutscher, S. L.; Sproat, B.; Leszczynska, G.; Malkiewicz, A.; Agris, P. F., Specificity of phage display selected peptides for modified anticodon stem and loop domains of tRNA. *Protein J.* **2007,** *26* (1), 61-73.
122. Seker, U. O.; Wilson, B.; Dincer, S.; Kim, I. W.; Oren, E. E.; Evans, J. S.; Tamerler, C.; Sarikaya, M., Adsorption behavior of linear and cyclic genetically engineered platinum binding peptides. *Langmuir* **2007,** *23* (15), 7895-900.
123. Umair, S.; Deng, Q.; Roberts, J. M.; Shaw, R. J.; Sutherland, I. A.; Pernthaner, A., Identification of Peptide Mimics of a Glycan Epitope on the Surface of Parasitic Nematode Larvae. *PLoS One* **2016,** *11* (8), e0162016.
124. Li, Y.; Cao, B.; Yang, M.; Zhu, Y.; Suh, J.; Mao, C., Identification of Novel Short BaTiO3-Binding/Nucleating Peptides for Phage-Templated in Situ Synthesis of BaTiO3 Polycrystalline Nanowires at Room Temperature. *ACS Appl. Mater. Interfaces* **2016,** *8* (45), 30714-30721.
125. Lunder, M.; Bratkovic, T.; Urleb, U.; Kreft, S.; Strukelj, B., Ultrasound in phage display: a new approach to nonspecific elution. *BioTechniques* **2008,** *44* (7), 893-900.
126. Paduano, F.; Ortuso, F.; Campiglia, P.; Raso, C.; Iaccino, E.; Gaspari, M.; Gaudio, E.; Mangone, G.; Carotenuto, A.; Bilotta, A.; Narciso, D.; Palmieri, C.; Agosti, V.; Artese, A.; Gomez-Monterrey, I.; Sala, M.; Cuda, G.; Iuliano, R.; Perrotti, N.; Scala, G.; Viglietto, G.; Alcaro, S.; Croce, C. M.; Novellino, E.; Fusco, A.; Trapasso, F., Isolation and functional characterization of peptide agonists of PTPRJ, a tyrosine phosphatase receptor endowed with tumor suppressor activity. *ACS Chem. Biol.* **2012,** *7* (10), 1666-76.

127. Arap, W.; Kolonin, M. G.; Trepel, M.; Lahdenranta, J.; Cardo-Vila, M.; Giordano, R. J.; Mintz, P. J.; Ardelt, P. U.; Yao, V. J.; Vidal, C. I.; Chen, L.; Flamm, A.; Valtanen, H.; Weavind, L. M.; Hicks, M. E.; Pollock, R. E.; Botz, G. H.; Bucana, C. D.; Koivunen, E.; Cahill, D.; Troncoso, P.; Baggerly, K. A.; Pentz, R. D.; Do, K. A.; Logothetis, C. J.; Pasqualini, R., Steps toward mapping the human vasculature by phage display. *Nat. Med.* **2002,** *8* (2), 121-7.
128. Li, J.; Zhang, Q.; Pang, Z.; Wang, Y.; Liu, Q.; Guo, L.; Jiang, X., Identification of peptide sequences that target to the brain using in vivo phage display. *Amino Acids* **2012,** *42* (6), 2373-81.
129. Prudencio, C. R.; Perez de la Lastra, J. M.; Canales, M.; Villar, M.; de la Fuente, J., Mapping protective epitopes in the tick and mosquito subolesin ortholog proteins. *Vaccine* **2010,** *28* (33), 5398-406.
130. Chen, Y.; Shen, Y.; Guo, X.; Zhang, C.; Yang, W.; Ma, M.; Liu, S.; Zhang, M.; Wen, L. P., Transdermal protein delivery by a coadministered peptide identified via phage display. *Nat. Biotechnol.* **2006,** *24* (4), 455-60.
131. Gunay, K. A.; Berthier, D. L.; Jerri, H. A.; Benczedi, D.; Klok, H. A.; Herrmann, A., Selective Peptide-Mediated Enhanced Deposition of Polymer Fragrance Delivery Systems on Human Hair. *ACS Appl. Mater. Interfaces* **2017,** *9* (28), 24238-24249.
132. Rice, J. J.; Schohn, A.; Bessette, P. H.; Boulware, K. T.; Daugherty, P. S., Bacterial display using circularly permuted outer membrane protein OmpX yields high affinity peptide ligands. *Protein Sci.* **2006,** *15* (4), 825-36.
133. Dane, K. Y.; Chan, L. A.; Rice, J. J.; Daugherty, P. S., Isolation of cell specific peptide ligands using fluorescent bacterial display libraries. *J. Immunol. Methods* **2006,** *309* (1-2), 120-9.
134. Deng, Q.; Zhuang, M.; Kong, Y. Y.; Xie, Y. H.; Wang, Y., Screening for PreS specific binding ligands with a phage displayed peptides library. *World J. Gastroenterol.* **2005,** *11* (26), 4018-23.
135. Hoess, R.; Brinkmann, U.; Handel, T.; Pastan, I., Identification of a peptide which binds to the carbohydrate-specific monoclonal antibody B3. *Gene* **1993,** *128* (1), 43-9.
136. Fairlie, W. D.; Spurck, T. P.; McCoubrie, J. E.; Gilson, P. R.; Miller, S. K.; McFadden, G. I.; Malby, R.; Crabb, B. S.; Hodder, A. N., Inhibition of malaria parasite development by a cyclic peptide that targets the vital parasite protein SERA5. *Infect. Immun.* **2008,** *76* (9), 4332-44.
137. Wrighton, N. C.; Farrell, F. X.; Chang, R.; Kashyap, A. K.; Barbone, F. P.; Mulcahy, L. S.; Johnson, D. L.; Barrett, R. W.; Jolliffe, L. K.; Dower, W. J., Small peptides as potent mimetics of the protein hormone erythropoietin. *Science* **1996,** *273* (5274), 458-64.
138. Pilch, J.; Brown, D. M.; Komatsu, M.; Järvinen, T. A.; Yang, M.; Peters, D.; Hoffman, R. M.; Ruoslahti, E., Peptides selected for binding to clotted plasma accumulate in tumor stroma and wounds. *Proc. Natl. Acad. Sci. U. S. A.* **2006,** *103* (8), 2800-4.

139. Wang, Y.; Wang, H.; Li, P.; Zhang, Q.; Kim, H. J.; Gee, S. J.; Hammock, B. D., Phage-displayed peptide that mimics aflatoxins and its application in immunoassay. *J. Agric. Food Chem.* **2013,** *61* (10), 2426-33.
140. Ding, Y.; Hua, X.; Sun, N.; Yang, J.; Deng, J.; Shi, H.; Wang, M., Development of a phage chemiluminescent enzyme immunoassay with high sensitivity for the determination of imidaclothiz in agricultural and environmental samples. *Sci. Total Environ.* **2017,** *609*, 854-860.
141. Yin, W.; Hua, X.; Liu, X.; Shi, H.; Gee, S. J.; Wang, M.; Hammock, B. D., Development of an enzyme-linked immunosorbent assay for thiacloprid in soil and agro-products with phage-displayed peptide. *Anal. Biochem.* **2015,** *481*, 27-32.
142. Heikkila, O.; Merilahti, P.; Hakanen, M.; Karelehto, E.; Alanko, J.; Sukki, M.; Kiljunen, S.; Susi, P., Integrins are not essential for entry of coxsackievirus A9 into SW480 human colon adenocarcinoma cells. *Virol J.* **2016,** *13* (1), 171.
143. Aalto, K.; Autio, A.; Kiss, E. A.; Elima, K.; Nymalm, Y.; Veres, T. Z.; Marttila-Ichihara, F.; Elovaara, H.; Saanijoki, T.; Crocker, P. R.; Maksimow, M.; Bligt, E.; Salminen, T. A.; Salmi, M.; Roivainen, A.; Jalkanen, S., Siglec-9 is a novel leukocyte ligand for vascular adhesion protein-1 and can be utilized in PET-imaging of inflammation and cancer. *Blood* **2011,** *118* (13), 3725-33.
144. Tilgmann, C.; Pollesello, P.; Ovaska, M.; Kaivola, J.; Pystynen, J.; Tiainen, E.; Yliperttula, M.; Annila, A.; Levijoki, J., Discovery and Structural Characterization of a Phospholamban-Binding Cyclic Peptide and Design of Novel Inhibitors of Phospholamban. *Chem. Biol. Drug Des.* **2012,** *81* (4), 463-73.
145. Beppler, J.; Mkaddem, S. B.; Michaloski, J.; Honorato, R. V.; Velasco, I. T.; de Oliveira, P. S.; Giordano, R. J.; Monteiro, R. C.; da Silva, F. P., Negative regulation of bacterial killing and inflammation by two novel CD16 ligands. *Eur. J. Immunol.* **2016,** *46* (8), 1926-35.
146. Daquinag, A. C.; Zhang, Y.; Amaya-Manzanares, F.; Simmons, P. J.; Kolonin, M. G., An Isoform of Decorin Is a Resistin Receptor on the Surface of Adipose Progenitor Cells. *Cell Stem Cell* **2011,** *9* (1), 74-86.
147. Leinonen, J.; Wu, P.; Stenman, U. H., Epitope mapping of antibodies against prostate-specific antigen with use of peptide libraries. *Clin. Chem.* **2002,** *48* (12), 2208-16.
148. Villard, S.; Lacroix-Desmazes, S.; Kieber-Emmons, T.; Piquer, D.; Grailly, S.; Benhida, A.; Kaveri, S. V.; Saint-Remy, J. M.; Granier, C., Peptide decoys selected by phage display block in vitro and in vivo activity of a human anti-FVIII inhibitor. *Blood* **2003,** *102* (3), 949-52.
149. Vega-Rodriguez, J.; Perez-Barreto, D.; Ruiz-Reyes, A.; Jacobs-Lorena, M., Targeting molecular interactions essential for Plasmodium sexual reproduction. *Cell. Microbiol.* **2015,** *17* (11), 1594-604.
150. Toledo-Machado, C. M.; de Avila, R. A.; C, N. G.; Granier, C.; Bueno, L. L.; Carneiro, C. M.; Menezes-Souza, D.; Carneiro, R. A.; Chavez-Olortegui, C.; Fujiwara, R. T., Immunodiagnosis of canine visceral leishmaniasis using mimotope peptides selected from phage displayed combinatorial libraries. *Biomed Res Int* **2015,** *2015*, 401509.

151. Ruiz, A.; Perez, D.; Munoz, M. C.; Molina, J. M.; Taubert, A.; Jacobs-Lorena, M.; Vega-Rodriguez, J.; Lopez, A. M.; Hermosilla, C., Targeting essential Eimeria ninakohlyakimovae sporozoite ligands for caprine host endothelial cell invasion with a phage display peptide library. *Parasitol. Res.* **2015,** *114* (11), 4327-31.
152. Luo, W.; Hsu, J. C.; Tsao, C. Y.; Ko, E.; Wang, X.; Ferrone, S., Differential immunogenicity of two peptides isolated by high molecular weight-melanoma-associated antigen-specific monoclonal antibodies with different affinities. *J. Immunol.* **2005,** *174* (11), 7104-10.
153. Liu, S.; Sivakumar, S.; Sparks, W. O.; Miller, W. A.; Bonning, B. C., A peptide that binds the pea aphid gut impedes entry of Pea enation mosaic virus into the aphid hemocoel. *Virology* **2010,** *401* (1), 107-16.
154. Ghosh, A. K.; Ribolla, P. E.; Jacobs-Lorena, M., Targeting Plasmodium ligands on mosquito salivary glands and midgut with a phage display peptide library. *Proc. Natl. Acad. Sci. U. S. A.* **2001,** *98* (23), 13278-81.
155. Desai, S. A.; Wang, X.; Noronha, E. J.; Zhou, Q.; Rebmann, V.; Grosse-Wilde, H.; Moy, F. J.; Powers, R.; Ferrone, S., Structural relatedness of distinct determinants recognized by monoclonal antibody TP25.99 on beta 2-microglobulin-associated and beta 2-microglobulin-free HLA class I heavy chains. *J. Immunol.* **2000,** *165* (6), 3275-83.
156. Cha, S. J.; Park, K.; Srinivasan, P.; Schindler, C. W.; van Rooijen, N.; Stins, M.; Jacobs-Lorena, M., CD68 acts as a major gateway for malaria sporozoite liver infection. *J. Exp. Med.* **2015,** *212* (9), 1391-403.
157. Welply, J. K.; Steininger, C. N.; Caparon, M.; Michener, M. L.; Howard, S. C.; Pegg, L. E.; Meyer, D. M.; De Ciechi, P. A.; Devine, C. S.; Casperson, G. F., A peptide isolated by phage display binds to ICAM-1 and inhibits binding to LFA-1. *Proteins* **1996,** *26* (3), 262-70.
158. Bonetto, S.; Spadola, L.; Buchanan, A. G.; Jermutus, L.; Lund, J., Identification of cyclic peptides able to mimic the functional epitope of IgG1-Fc for human Fc{gamma}RI. *FASEB J.* **2008,** *23* (2), 575-85.
159. Hatanaka, T.; Ohzono, S.; Park, M.; Tsukamoto, S.; Sugita, R.; Sakamoto, K.; Ishitobi, H.; Mori, T.; Ito, O.; Sorajo, K.; Sugimura, K.; Ham, S.; Ito, Y., Human IgA-binding peptides selected from random peptide libraries: affinity maturation and application in IgA purification. *J. Biol. Chem.* **2012,** *287* (51), 43126-36.
160. Torregrossa, P.; Buhl, L.; Bancila, M.; Durbec, P.; Schafer, C.; Schachner, M.; Rougon, G., Selection of poly-alpha 2,8-sialic acid mimotopes from a random phage peptide library and analysis of their bioactivity. *J. Biol. Chem.* **2004,** *279* (29), 30707-14.
161. Luzzago, A.; Felici, F.; Tramontano, A.; Pessi, A.; Cortese, R., Mimicking of discontinuous epitopes by phage-displayed peptides, I. Epitope mapping of human H ferritin using a phage library of constrained peptides. *Gene* **1993,** *128* (1), 51-7.
162. Felici, F.; Luzzago, A.; Folgori, A.; Cortese, R., Mimicking of discontinuous epitopes by phage-displayed peptides, II. Selection of clones

recognized by a protective monoclonal antibody against the Bordetella pertussis toxin from phage peptide libraries. *Gene* **1993,** *128* (1), 21-7.
163. Oligino, L.; Lung, F. D.; Sastry, L.; Bigelow, J.; Cao, T.; Curran, M.; Burke, T. R., Jr.; Wang, S.; Krag, D.; Roller, P. P.; King, C. R., Nonphosphorylated peptide ligands for the Grb2 Src homology 2 domain. *J. Biol. Chem.* **1997,** *272* (46), 29046-52.
164. Koivunen, E.; Wang, B.; Ruoslahti, E., Isolation of a highly specific ligand for the alpha 5 beta 1 integrin from a phage display library. *J. Cell Biol.* **1994,** *124* (3), 373-80.
165. Jensen, J. K.; Malmendal, A.; Schiott, B.; Skeldal, S.; Pedersen, K. E.; Celik, L.; Nielsen, N. C.; Andreasen, P. A.; Wind, T., Inhibition of plasminogen activator inhibitor-1 binding to endocytosis receptors of the low-density-lipoprotein receptor family by a peptide isolated from a phage display library. *Biochem. J* **2006,** *399* (3), 387-96.
166. Wu, P.; Leinonen, J.; Koivunen, E.; Lankinen, H.; Stenman, U. H., Identification of novel prostate-specific antigen-binding peptides modulating its enzyme activity. *Eur. J. Biochem.* **2000,** *267* (20), 6212-20.
167. Gesteira, T. F.; Coulson-Thomas, V. J.; Taunay-Rodrigues, A.; Oliveira, V.; Thacker, B. E.; Juliano, M. A.; Pasqualini, R.; Arap, W.; Tersariol, I. L.; Nader, H. B.; Esko, J. D.; Pinhal, M. A., Inhibitory peptides of the sulfotransferase domain of the heparan sulfate enzyme, N-deacetylase-N-sulfotransferase-1. *J. Biol. Chem.* **2011,** *286* (7), 5338-46.
168. Fan, X.; Venegas, R.; Fey, R.; van der Heyde, H.; Bernard, M. A.; Lazarides, E.; Woods, C. M., An in vivo approach to structure activity relationship analysis of peptide ligands. *Pharm. Res.* **2007,** *24* (5), 868-79.
169. Wilkinson, R. A.; Evans, J. R.; Jacobs, J. M.; Slunaker, D.; Pincus, S. H.; Pinter, A.; Parkos, C. A.; Burritt, J. B.; Teintze, M., Peptides selected from a phage display library with an HIV-neutralizing antibody elicit antibodies to HIV gp120 in rabbits, but not to the same epitope. *AIDS Res. Hum. Retroviruses* **2007,** *23* (11), 1416-27.
170. Untersmayr, E.; Szalai, K.; Riemer, A. B.; Hemmer, W.; Swoboda, I.; Hantusch, B.; Scholl, I.; Spitzauer, S.; Scheiner, O.; Jarisch, R.; Boltz-Nitulescu, G.; Jensen-Jarolim, E., Mimotopes identify conformational epitopes on parvalbumin, the major fish allergen. *Mol. Immunol.* **2006,** *43* (9), 1454-61.
171. Riemer, A. B.; Kurz, H.; Klinger, M.; Scheiner, O.; Zielinski, C. C.; Jensen-Jarolim, E., Vaccination with cetuximab mimotopes and biological properties of induced anti-epidermal growth factor receptor antibodies. *J. Natl. Cancer Inst.* **2005,** *97* (22), 1663-70.
172. Riemer, A. B.; Klinger, M.; Wagner, S.; Bernhaus, A.; Mazzucchelli, L.; Pehamberger, H.; Scheiner, O.; Zielinski, C. C.; Jensen-Jarolim, E., Generation of Peptide mimics of the epitope recognized by trastuzumab on the oncogenic protein Her-2/neu. *J. Immunol.* **2004,** *173* (1), 394-401.
173. Mazzucchelli, L.; Burritt, J. B.; Jesaitis, A. J.; Nusrat, A.; Liang, T. W.; Gewirtz, A. T.; Schnell, F. J.; Parkos, C. A., Cell-specific peptide binding by human neutrophils. *Blood* **1999,** *93* (5), 1738-48.

174. Hantusch, B.; Krieger, S.; Untersmayr, E.; Scholl, I.; Knittelfelder, R.; Flicker, S.; Spitzauer, S.; Valenta, R.; Boltz-Nitulescu, G.; Scheiner, O.; Jensen-Jarolim, E., Mapping of conformational IgE epitopes on Phl p 5a by using mimotopes from a phage display library. *J. Allergy Clin. Immunol.* **2004,** *114* (6), 1294-300.
175. Hafner, C.; Wagner, S.; Allwardt, D.; Riemer, A. B.; Scheiner, O.; Pehamberger, H.; Breiteneder, H., Cross-reactivity of mimotopes with a monoclonal antibody against the high molecular weight melanoma-associated antigen (HMW-MAA) does not predict cross-reactive immunogenicity. *Melanoma Res.* **2005,** *15* (2), 111-7.
176. Frick, C.; Odermatt, A.; Zen, K.; Mandell, K. J.; Edens, H.; Portmann, R.; Mazzucchelli, L.; Jaye, D. L.; Parkos, C. A., Interaction of ICAM-1 with beta 2-integrin CD11c/CD18: characterization of a peptide ligand that mimics a putative binding site on domain D4 of ICAM-1. *Eur. J. Immunol.* **2005,** *35* (12), 3610-21.
177. Förster-Waldl, E.; Riemer, A. B.; Dehof, A. K.; Neumann, D.; Brämswig, K.; Boltz-Nitulescu, G.; Pehamberger, H.; Zielinski, C. C.; Scheiner, O.; Pollak, A.; Lode, H.; Jensen-Jarolim, E., Isolation and structural analysis of peptide mimotopes for the disialoganglioside GD2, a neuroblastoma tumor antigen. *Mol. Immunol.* **2005,** *42* (3), 319-25.
178. Fagerlund, A.; Myrset, A. H.; Kulseth, M. A., Construction and characterization of a 9-mer phage display pVIII-library with regulated peptide density. *Appl. Microbiol. Biotechnol.* **2008,** *80* (5), 925-36.
179. Bramswig, K. H.; Knittelfelder, R.; Gruber, S.; Untersmayr, E.; Riemer, A. B.; Szalai, K.; Horvat, R.; Kammerer, R.; Zimmermann, W.; Zielinski, C. C.; Scheiner, O.; Jensen-Jarolim, E., Immunization with mimotopes prevents growth of carcinoembryonic antigen positive tumors in BALB/c mice. *Clin. Cancer. Res.* **2007,** *13* (21), 6501-8.
180. Audige, A.; Frick, C.; Frey, F. J.; Mazzucchelli, L.; Odermatt, A., Selection of peptide ligands binding to the basolateral cell surface of proximal convoluted tubules. *Kidney Int.* **2002,** *61* (1), 342-8.
181. Pero, S. C.; Shukla, G. S.; Armstrong, A. L.; Peterson, D.; Fuller, S. P.; Godin, K.; Kingsley-Richards, S. L.; Weaver, D. L.; Bond, J.; Krag, D. N., Identification of a small peptide that inhibits the phosphorylation of ErbB2 and proliferation of ErbB2 overexpressing breast cancer cells. *Int. J. Cancer* **2004,** *111* (6), 951-60.
182. Krag, D. N.; Shukla, G. S.; Shen, G. P.; Pero, S.; Ashikaga, T.; Fuller, S.; Weaver, D. L.; Burdette-Radoux, S.; Thomas, C., Selection of tumor-binding ligands in cancer patients with phage display libraries. *Cancer Res.* **2006,** *66* (15), 7724-33.
183. Roitburd-Berman, A.; Dela, G.; Kaplan, G.; Lewis, G. K.; Gershoni, J. M., Allosteric induction of the CD4-bound conformation of HIV-1 Gp120. *Retrovirology* **2013,** *10*, 147.
184. Enshell-Seijffers, D.; Denisov, D.; Groisman, B.; Smelyanski, L.; Meyuhas, R.; Gross, G.; Denisova, G.; Gershoni, J. M., The mapping and

reconstitution of a conformational discontinuous B-cell epitope of HIV-1. *J. Mol. Biol.* **2003,** *334* (1), 87-101.
185. Choi, S. J.; Ahn, M.; Lee, J. S.; Jung, W. J., Selection of a high affinity angiogenin-binding peptide from a peptide library displayed on phage coat protein. *Mol. Cells* **1997,** *7* (5), 575-81.
186. Ting, J. P.; Tung, F.; Antonysamy, S.; Wasserman, S.; Jones, S. B.; Zhang, F. F.; Espada, A.; Broughton, H.; Chalmers, M. J.; Woodman, M. E.; Bina, H. A.; Dodge, J. A.; Benach, J.; Zhang, A.; Groshong, C.; Manglicmot, D.; Russell, M.; Afshar, S., Utilization of peptide phage display to investigate hotspots on IL-17A and what it means for drug discovery. *PLoS One* **2018,** *13* (1), e0190850.
187. Heiskanen, T.; Lundkvist, A.; Soliymani, R.; Koivunen, E.; Vaheri, A.; Lankinen, H., Phage-displayed peptides mimicking the discontinuous neutralization sites of puumala Hantavirus envelope glycoproteins. *Virology* **1999,** *262* (2), 321-32.
188. Wang, B.; Yang, H.; Liu, Y. C.; Jelinek, T.; Zhang, L.; Ruoslahti, E.; Fu, H., Isolation of high-affinity peptide antagonists of 14-3-3 proteins by phage display. *Biochemistry* **1999,** *38* (38), 12499-504.
189. Michon, I. N.; Hauer, A. D.; von der Thusen, J. H.; Molenaar, T. J.; van Berkel, T. J.; Biessen, E. A.; Kuiper, J., Targeting of peptides to restenotic vascular smooth muscle cells using phage display in vitro and in vivo. *Biochim. Biophys. Acta* **2002,** *1591* (1-3), 87-97.
190. Florea, B. I.; Molenaar, T. J.; Bot, I.; Michon, I. N.; Kuiper, J.; Van Berkel, T. J.; Junginger, H. E.; Biessen, E. A.; Borchard, G., Identification of an internalising peptide in differentiated Calu-3 cells by phage display technology; application to gene delivery to the airways. *J. Drug Target.* **2003,** *11* (7), 383-90.
191. Edalat, M.; Pettersson, S.; Persson, M. A.; Mannervik, B., Probing biomolecular interactions of glutathione transferase M2-2 by using peptide phage display. *ChemBioChem* **2002,** *3* (9), 823-8.
192. Heinis, C.; Rutherford, T.; Freund, S.; Winter, G., Phage-encoded combinatorial chemical libraries based on bicyclic peptides. *Nat. Chem. Biol.* **2009,** *5* (7), 502-7.
193. Stevens, C. A.; Bachtiger, F.; Kong, X.-D.; Abriata, L. A.; Sosso, G. C.; Gibson, M. I.; Klok, H.-A., A minimalistic cyclic ice-binding peptide from phage display. *Nat. Commun.* **2021,** *12* (1), 2675.
194. Zha, M.; Lin, P.; Yao, H.; Zhao, Y.; Wu, C., A phage display-based strategy for the de novo creation of disulfide-constrained and isomer-free bicyclic peptide affinity reagents. *Chem. Commun.* **2018,** *54* (32), 4029-4032.
195. Lu, S.; Wu, Y.; Li, J.; Meng, X.; Hu, C.; Zhao, Y.; Wu, C., Directed Disulfide Pairing and Folding of Peptides for the De Novo Development of Multicyclic Peptide Libraries. *J. Am. Chem. Soc.* **2020,** *142* (38), 16285-16291.
196. Wang, C. K.; Craik, D. J., Designing macrocyclic disulfide-rich peptides for biotechnological applications. *Nat. Chem. Biol.* **2018,** *14* (5), 417-427.

197. Souriau, C.; Chiche, L.; Irving, R.; Hudson, P., New Binding Specificities Derived from Min-23, a Small Cystine-Stabilized Peptidic Scaffold. *Biochemistry* **2005,** *44* (19), 7143-7155.
198. Zoller, F.; Markert, A.; Barthe, P.; Zhao, W.; Weichert, W.; Askoxylakis, V.; Altmann, A.; Mier, W.; Haberkorn, U., Combination of phage display and molecular grafting generates highly specific tumor-targeting miniproteins. *Angew. Chem. Int. Ed. Engl.* **2012,** *51* (52), 13136-9.
199. Wang, X. S.; Chen, P. C.; Hampton, J. T.; Tharp, J. M.; Reed, C. A.; Das, S. K.; Wang, D. S.; Hayatshahi, H. S.; Shen, Y.; Liu, J.; Liu, W. R., A Genetically Encoded, Phage-Displayed Cyclic-Peptide Library. *Angew. Chem. Int. Ed. Engl.* **2019,** *58* (44), 15904-15909.
200. Owens, A. E.; Iannuzzelli, J. A.; Gu, Y.; Fasan, R., MOrPH-PhD: An Integrated Phage Display Platform for the Discovery of Functional Genetically Encoded Peptide Macrocycles. *ACS Cent. Sci.* **2020,** *6* (3), 368-381.
201. Oppewal, T. R.; Hekelaar, J.; Mayer, C., A phage-compatible strategy to access macrocyclic peptides featuring asymmetric molecular scaffolds as cyclization units. *Chemrxiv.***2021**, 10.26434/chemrxiv.13705618.v1 (accessed 2021-08-31).
202. Boutureira, O.; Bernardes, G. J. L., Advances in Chemical Protein Modification. *Chem. Rev.* **2015,** *115* (5), 2174-2195.
203. Tran, H. L.; Lexa, K. W.; Julien, O.; Young, T. S.; Walsh, C. T.; Jacobson, M. P.; Wells, J. A., Structure–Activity Relationship and Molecular Mechanics Reveal the Importance of Ring Entropy in the Biosynthesis and Activity of a Natural Product. *J. Am. Chem. Soc.* **2017,** *139* (7), 2541-2544.
204. Craik, D. J.; Fairlie, D. P.; Liras, S.; Price, D., The future of peptide-based drugs. *Chem. Biol. Drug Des.* **2013,** *81* (1), 136-47.
205. Nielsen, D. S.; Shepherd, N. E.; Xu, W.; Lucke, A. J.; Stoermer, M. J.; Fairlie, D. P., Orally Absorbed Cyclic Peptides. *Chem. Rev.* **2017,** *117* (12), 8094-8128.
206. Gao, Y.; Kodadek, T., Direct Comparison of Linear and Macrocyclic Compound Libraries as a Source of Protein Ligands. *ACS Comb. Sci.* **2015,** *17* (3), 190-195.
207. Vinogradov, A. A.; Yin, Y.; Suga, H., Macrocyclic Peptides as Drug Candidates: Recent Progress and Remaining Challenges. *J. Am. Chem. Soc.* **2019,** *141* (10), 4167-4181.
208. Fadzen, C. M.; Wolfe, J. M.; Cho, C.-F.; Chiocca, E. A.; Lawler, S. E.; Pentelute, B. L., Perfluoroarene–Based Peptide Macrocycles to Enhance Penetration Across the Blood–Brain Barrier. *J. Am. Chem. Soc.* **2017,** *139* (44), 15628-15631.
209. Rhodes, C. A.; Dougherty, P. G.; Cooper, J. K.; Qian, Z.; Lindert, S.; Wang, Q.-E.; Pei, D., Cell-Permeable Bicyclic Peptidyl Inhibitors against NEMO-IκB Kinase Interaction Directly from a Combinatorial Library. *J. Am. Chem. Soc.* **2018,** *140* (38), 12102-12110.

210. Timmerman, P.; Beld, J.; Puijk, W. C.; Meloen, R. H., Rapid and quantitative cyclization of multiple peptide loops onto synthetic scaffolds for structural mimicry of protein surfaces. *ChemBioChem* **2005,** *6* (5), 821-4.
211. Diderich, P.; Bertoldo, D.; Dessen, P.; Khan, M. M.; Pizzitola, I.; Held, W.; Huelsken, J.; Heinis, C., Phage Selection of Chemically Stabilized α-Helical Peptide Ligands. *ACS Chem. Biol.* **2016,** *11* (5), 1422-1427.
212. Jafari, M. R.; Deng, L.; Kitov, P. I.; Ng, S.; Matochko, W. L.; Tjhung, K. F.; Zeberoff, A.; Elias, A.; Klassen, J. S.; Derda, R., Discovery of Light-Responsive Ligands through Screening of a Light-Responsive Genetically Encoded Library. *ACS Chem. Biol.* **2014,** *9* (2), 443-450.
213. Wong, J. Y. K.; Mukherjee, R.; Miao, J.; Bilyk, O.; Triana, V.; Miskolzie, M.; Henninot, A.; Dwyer, J. J.; Kharchenko, S.; Iampolska, A.; Volochnyuk, D. M.; Lin, Y.-S.; Postovit, L.-M.; Derda, R., Genetically-encoded discovery of proteolytically stable bicyclic inhibitors for morphogen NODAL. *Chem. Sci.* **2021,** *12* (28), 9694-9703.
214. Assem, N.; Ferreira, D. J.; Wolan, D. W.; Dawson, P. E., Acetone-Linked Peptides: A Convergent Approach for Peptide Macrocyclization and Labeling. *Angew. Chem. Int. Ed. Engl.* **2015,** *54* (30), 8665-8.
215. Ng, S.; Derda, R., Phage-displayed macrocyclic glycopeptide libraries. *Org. Biomol. Chem.* **2016,** *14* (24), 5539-5545.
216. Knorr, L., Einwirkung von Acetessigester auf Phenylhydrazin. *Berichte der deutschen chemischen Gesellschaft* **1883,** *16* (2), 2597-2599.
217. Ekanayake, A. I.; Sobze, L.; Kelich, P.; Youk, J.; Bennett, N. J.; Mukherjee, R.; Bhardwaj, A.; Wuest, F.; Vukovic, L.; Derda, R., Genetically Encoded Fragment-Based Discovery from Phage-Displayed Macrocyclic Libraries with Genetically Encoded Unnatural Pharmacophores. *J. Am. Chem. Soc.* **2021,** *143* (14), 5497-5507.
218. Dhanjee, H. H.; Saebi, A.; Buslov, I.; Loftis, A. R.; Buchwald, S. L.; Pentelute, B. L., Protein–Protein Cross-Coupling via Palladium–Protein Oxidative Addition Complexes from Cysteine Residues. *J. Am. Chem. Soc.* **2020,** *142* (20), 9124-9129.
219. Kalhor-Monfared, S.; Jafari, M. R.; Patterson, J. T.; Kitov, P. I.; Dwyer, J. J.; Nuss, J. M.; Derda, R., Rapid biocompatible macrocyclization of peptides with decafluoro-diphenylsulfone. *Chem. Sci.* **2016,** *7* (6), 3785-3790.
220. Zheng, X.; Liu, W.; Liu, Z.; Zhao, Y.; Wu, C., Biocompatible and Rapid Cyclization of Peptides with 2,4-Difluoro-6-hydroxy-1,3,5-benzenetricarbonitrile for the Development of Cyclic Peptide Libraries. *Bioconjugate Chem.* **2020,** *31* (9), 2085-2091.
221. Jafari, M. R.; Lakusta, J.; Lundgren, R. J.; Derda, R., Allene Functionalized Azobenzene Linker Enables Rapid and Light-Responsive Peptide Macrocyclization. *Bioconjugate Chem.* **2016,** *27* (3), 509-514.
222. Baeriswyl, V.; Rapley, H.; Pollaro, L.; Stace, C.; Teufel, D.; Walker, E.; Chen, S.; Winter, G.; Tite, J.; Heinis, C., Bicyclic Peptides with Optimized Ring Size Inhibit Human Plasma Kallikrein and its Orthologues While Sparing Paralogous Proteases. *ChemMedChem* **2012,** *7* (7), 1173-1176.

223. Teufel, D. P.; Bennett, G.; Harrison, H.; van Rietschoten, K.; Pavan, S.; Stace, C.; Le Floch, F.; Van Bergen, T.; Vermassen, E.; Barbeaux, P.; Hu, T. T.; Feyen, J. H. M.; Vanhove, M., Stable and Long-Lasting, Novel Bicyclic Peptide Plasma Kallikrein Inhibitors for the Treatment of Diabetic Macular Edema. *J. Med. Chem.* **2018,** *61* (7), 2823-2836.
224. Urech-Varenne, C.; Radtke, F.; Heinis, C., Phage Selection of Bicyclic Peptide Ligands of the Notch1 Receptor. *ChemMedChem* **2015,** *10* (10), 1754-1761.
225. Luo, Y.; Schofield, J. A.; Na, Z.; Hann, T.; Simon, M. D.; Slavoff, S. A., Discovery of cellular substrates of human RNA-decapping enzyme DCP2 using a stapled bicyclic peptide inhibitor. *Cell Chem. Biol.* **2020,** *28* (4), 463-474 e7.
226. Liu, K. C.; Röder, K.; Mayer, C.; Adhikari, S.; Wales, D. J.; Balasubramanian, S., Affinity-Selected Bicyclic Peptide G-Quadruplex Ligands Mimic a Protein-like Binding Mechanism. *J. Am. Chem. Soc.* **2020,** *142* (18), 8367-8373.
227. Chen, S.; Bertoldo, D.; Angelini, A.; Pojer, F.; Heinis, C., Peptide Ligands Stabilized by Small Molecules. *Angew. Chem. Int. Ed.* **2014,** *53* (6), 1602-1606.
228. Angelini, A.; Cendron, L.; Chen, S.; Touati, J.; Winter, G.; Zanotti, G.; Heinis, C., Bicyclic Peptide Inhibitor Reveals Large Contact Interface with a Protease Target. *ACS Chem. Biol.* **2012,** *7* (5), 817-821.
229. Deyle, K.; Kong, X.-D.; Heinis, C., Phage Selection of Cyclic Peptides for Application in Research and Drug Development. *Acc. Chem. Res.* **2017,** *50* (8), 1866-1874.
230. van de Langemheen, H.; Korotkovs, V.; Bijl, J.; Wilson, C.; Kale, S. S.; Heinis, C.; Liskamp, R. M. J., Polar Hinges as Functionalized Conformational Constraints in (Bi)cyclic Peptides. *ChemBioChem* **2017,** *18* (4), 387-395.
231. Middendorp, S. J.; Wilbs, J.; Quarroz, C.; Calzavarini, S.; Angelillo-Scherrer, A.; Heinis, C., Peptide Macrocycle Inhibitor of Coagulation Factor XII with Subnanomolar Affinity and High Target Selectivity. *J. Med. Chem.* **2017,** *60* (3), 1151-1158.
232. Mudd, G. E.; Brown, A.; Chen, L.; van Rietschoten, K.; Watcham, S.; Teufel, D. P.; Pavan, S.; Lani, R.; Huxley, P.; Bennett, G. S., Identification and Optimization of EphA2-Selective Bicycles for the Delivery of Cytotoxic Payloads. *J. Med. Chem.* **2020,** *63* (8), 4107-4116.
233. Kong, X. D.; Moriya, J.; Carle, V.; Pojer, F.; Abriata, L. A.; Deyle, K.; Heinis, C., De novo development of proteolytically resistant therapeutic peptides for oral administration. *Nature Biomedical Engineering* **2020,** *4* (5), 560-571.
234. Tian, F.; Tsao, M. L.; Schultz, P. G., A phage display system with unnatural amino acids. *J. Am. Chem. Soc.* **2004,** *126* (49), 15962-3.
235. Oller-Salvia, B.; Chin, J. W., Efficient Phage Display with Multiple Distinct Non-Canonical Amino Acids Using Orthogonal Ribosome-Mediated Genetic Code Expansion. *Angew. Chem. Int. Ed. Engl.* **2019,** *58* (32), 10844-10848.
236. Muttenthaler, M.; King, G. F.; Adams, D. J.; Alewood, P. F., Trends in peptide drug discovery. *Nat. Rev. Drug Discov.* **2021,** *20* (4), 309-325.

237. Lau, J. L.; Dunn, M. K., Therapeutic peptides: Historical perspectives, current development trends, and future directions. *Biorg. Med. Chem.* **2018,** *26* (10), 2700-2707.
238. Giordanetto, F.; Kihlberg, J., Macrocyclic Drugs and Clinical Candidates: What Can Medicinal Chemists Learn from Their Properties? *J. Med. Chem.* **2014,** *57* (2), 278-295.
239. Zorzi, A.; Deyle, K.; Heinis, C., Cyclic peptide therapeutics: past, present and future. *Curr. Opin. Chem. Biol.* **2017,** *38*, 24-29.
240. Hacker, D. E.; Abrigo, N. A.; Hoinka, J.; Richardson, S. L.; Przytycka, T. M.; Hartman, M. C. T., Direct, Competitive Comparison of Linear, Monocyclic, and Bicyclic Libraries Using mRNA Display. *ACS Comb. Sci.* **2020,** *22* (6), 306-310.
241. Matinkhoo, K.; Pryyma, A.; Todorovic, M.; Patrick, B. O.; Perrin, D. M., Synthesis of the Death-Cap Mushroom Toxin alpha-Amanitin. *J. Am. Chem. Soc.* **2018,** *140* (21), 6513-6517.
242. Hosseinzadeh, P.; Bhardwaj, G.; Mulligan, V. K.; Shortridge, M. D.; Craven, T. W.; Pardo-Avila, F.; Rettie, S. A.; Kim, D. E.; Silva, D. A.; Ibrahim, Y. M.; Webb, I. K.; Cort, J. R.; Adkins, J. N.; Varani, G.; Baker, D., Comprehensive computational design of ordered peptide macrocycles. *Science* **2017,** *358* (6369), 1461-1466.
243. Iaccarino, E.; Calvanese, L.; Untiveros, G.; Falcigno, L.; D'Auria, G.; Latino, D.; Sivaccumar, J. P.; Strizzi, L.; Ruvo, M.; Sandomenico, A., Structure-based design of small bicyclic peptide inhibitors of Cripto-1 activity. *Biochem. J* **2020,** *477* (8), 1391-1407.
244. Sindhikara, D.; Wagner, M.; Gkeka, P.; Güssregen, S.; Tiwari, G.; Hessler, G.; Yapici, E.; Li, Z.; Evers, A., Automated Design of Macrocycles for Therapeutic Applications: From Small Molecules to Peptides and Proteins. *J. Med. Chem.* **2020,** *63* (20), 12100-12115.
245. Richelle, G. J. J.; Schmidt, M.; Ippel, H.; Hackeng, T. M.; van Maarseveen, J. H.; Nuijens, T.; Timmerman, P., A One-Pot "Triple-C" Multicyclization Methodology for the Synthesis of Highly Constrained Isomerically Pure Tetracyclic Peptides. *ChemBioChem* **2018,** *19* (18), 1934-1938.
246. Wolfe, J. M.; Fadzen, C. M.; Holden, R. L.; Yao, M.; Hanson, G. J.; Pentelute, B. L., Perfluoroaryl Bicyclic Cell-Penetrating Peptides for Delivery of Antisense Oligonucleotides. *Angew. Chem. Int. Ed. Engl.* **2018,** *57* (17), 4756-4759.
247. Liu, W.; Zheng, Y.; Kong, X.; Heinis, C.; Zhao, Y.; Wu, C., Precisely Regulated and Efficient Locking of Linear Peptides into Stable Multicyclic Topologies through a One-Pot Reaction. *Angew. Chem. Int. Ed. Engl.* **2017,** *56* (16), 4458-4463.
248. Trinh, T. B.; Upadhyaya, P.; Qian, Z.; Pei, D., Discovery of a Direct Ras Inhibitor by Screening a Combinatorial Library of Cell-Permeable Bicyclic Peptides. *ACS Comb. Sci.* **2016,** *18* (1), 75-85.

249. Robinson, J. A.; Demarco, S.; Gombert, F.; Moehle, K.; Obrecht, D., The design, structures and therapeutic potential of protein epitope mimetics. *Drug Discov Today* **2008,** *13* (21-22), 944-51.
250. Lian, W.; Upadhyaya, P.; Rhodes, C. A.; Liu, Y.; Pei, D., Screening Bicyclic Peptide Libraries for Protein–Protein Interaction Inhibitors: Discovery of a Tumor Necrosis Factor-α Antagonist. *J. Am. Chem. Soc.* **2013,** *135* (32), 11990-11995.
251. Huang, Y.; Wiedmann, M. M.; Suga, H., RNA Display Methods for the Discovery of Bioactive Macrocycles. *Chem. Rev.* **2019,** *119* (17), 10360-10391.
252. Bashiruddin, N. K.; Nagano, M.; Suga, H., Synthesis of fused tricyclic peptides using a reprogrammed translation system and chemical modification. *Bioorg. Chem.* **2015,** *61*, 45-50.
253. Hacker, D. E.; Hoinka, J.; Iqbal, E. S.; Przytycka, T. M.; Hartman, M. C., Highly Constrained Bicyclic Scaffolds for the Discovery of Protease-Stable Peptides via mRNA Display. *ACS Chem. Biol.* **2017,** *12* (3), 795-804.
254. Kale, S. S.; Villequey, C.; Kong, X. D.; Zorzi, A.; Deyle, K.; Heinis, C., Cyclization of peptides with two chemical bridges affords large scaffold diversities. *Nat. Chem.* **2018,** *10* (7), 715-723.
255. Li, Y.; De Luca, R.; Cazzamalli, S.; Pretto, F.; Bajic, D.; Scheuermann, J.; Neri, D., Versatile protein recognition by the encoded display of multiple chemical elements on a constant macrocyclic scaffold. *Nat. Chem.* **2018,** *10* (4), 441-448.
256. Tse, B. N.; Snyder, T. M.; Shen, Y.; Liu, D. R., Translation of DNA into a Library of 13 000 Synthetic Small-Molecule Macrocycles Suitable for in Vitro Selection. *J. Am. Chem. Soc.* **2008,** *130* (46), 15611-15626.
257. Lu, X.; Fan, L.; Phelps, C. B.; Davie, C. P.; Donahue, C. P., Ruthenium Promoted On-DNA Ring-Closing Metathesis and Cross-Metathesis. *Bioconjugate Chem.* **2017,** *28* (6), 1625-1629.
258. Stress, C. J.; Sauter, B.; Schneider, L. A.; Sharpe, T.; Gillingham, D., A DNA-Encoded Chemical Library Incorporating Elements of Natural Macrocycles. *Angew. Chem. Int. Ed.* **2019,** *58* (28), 9570-9574.
259. Zhu, Z.; Shaginian, A.; Grady, L. C.; O'Keeffe, T.; Shi, X. E.; Davie, C. P.; Simpson, G. L.; Messer, J. A.; Evindar, G.; Bream, R. N.; Thansandote, P. P.; Prentice, N. R.; Mason, A. M.; Pal, S., Design and Application of a DNA-Encoded Macrocyclic Peptide Library. *ACS Chem. Biol.* **2018,** *13* (1), 53-59.
260. Pham, M. V.; Bergeron-Brlek, M.; Heinis, C., Synthesis of DNA-Encoded Disulfide- and Thioether-Cyclized Peptides. *ChemBioChem* **2020,** *21* (4), 543-549.
261. Iskandar, S. E.; Haberman, V. A.; Bowers, A. A., Expanding the Chemical Diversity of Genetically Encoded Libraries. *ACS Comb. Sci.* **2020,** *22* (12), 712-733.
262. Derda, R.; Ng, S., Genetically encoded fragment-based discovery. *Curr. Opin. Chem. Biol.* **2019,** *50*, 128-137.
263. Angelini, A.; Heinis, C., Post-translational modification of genetically encoded polypeptide libraries. *Curr. Opin. Chem. Biol.* **2011,** *15* (3), 355-361.

264. Yin, Y.; Fei, Q.; Liu, W.; Li, Z.; Suga, H.; Wu, C., Chemical and Ribosomal Synthesis of Topologically Controlled Bicyclic and Tricyclic Peptide Scaffolds Primed by Selenoether Formation. *Angew. Chem. Int. Ed.* **2019,** *58* (15), 4880-4885.
265. Yao, A.; Reed, S. A.; Koh, M.; Yu, C.; Luo, X.; Mehta, A. P.; Schultz, P. G., Progress toward a reduced phage genetic code. *Bioorg. Med. Chem.* **2018,** *26* (19), 5247-5252.
266. Nicolet, B. H.; Shinn, L. A., The Action of Periodic Acid on α-Amino Alcohols. *J. Am. Chem. Soc.* **1939,** *61* (6), 1615-1615.
267. Geoghegan, K. F.; Stroh, J. G., Site-directed conjugation of nonpeptide groups to peptides and proteins via periodate oxidation of a 2-amino alcohol. Application to modification at N-terminal serine. *Bioconjugate Chem.* **1992,** *3* (2), 138-46.
268. Gaertner, H. F.; Offord, R. E., Site-specific attachment of functionalized poly(ethylene glycol) to the amino terminus of proteins. *Bioconjugate Chem.* **1996,** *7* (1), 38-44.
269. Nie, Y.; Zhang, X.; Wang, X.; Chen, J., Preparation and stability of N-terminal mono-PEGylated recombinant human endostatin. *Bioconjugate Chem.* **2006,** *17* (4), 995-9.
270. Bai, C.; Reid, E. E.; Wilhelm, A.; Shizuka, M.; Maloney, E. K.; Laleau, R.; Harvey, L.; Archer, K. E.; Vitharana, D.; Adams, S.; Kovtun, Y.; Miller, M. L.; Chari, R.; Keating, T. A.; Yoder, N. C., Site-Specific Conjugation of the Indolinobenzodiazepine DGN549 to Antibodies Affords Antibody-Drug Conjugates with an Improved Therapeutic Index as Compared with Lysine Conjugation. *Bioconjug. Chem.* **2020,** *31* (1), 93-103.
271. Ng, S.; Jafari, M. R.; Matochko, W. L.; Derda, R., Quantitative synthesis of genetically encoded glycopeptide libraries displayed on M13 phage. *ACS Chem. Biol.* **2012,** *7* (9), 1482-1487.
272. Kitov, P. I.; Vinals, D. F.; Ng, S.; Tjhung, K. F.; Derda, R., Rapid, hydrolytically stable modification of aldehyde-terminated proteins and phage libraries. *J. Am. Chem. Soc.* **2014,** *136* (23), 8149-52.
273. Triana, V.; Derda, R., Tandem Wittig/Diels-Alder diversification of genetically encoded peptide libraries. *Org. Biomol. Chem.* **2017,** *15* (37), 7869-7877.
274. Ng, S.; Lin, E.; Kitov, P. I.; Tjhung, K. F.; Gerlits, O. O.; Deng, L.; Kasper, B.; Sood, A.; Paschal, B. M.; Zhang, P.; Ling, C.-C.; Klassen, J. S.; Noren, C. J.; Mahal, L. K.; Woods, R. J.; Coates, L.; Derda, R., Genetically Encoded Fragment-Based Discovery of Glycopeptide Ligands for Carbohydrate-Binding Proteins. *J. Am. Chem. Soc.* **2015,** *137* (16), 5248-5251.
275. Chou, Y.; Kitova, E. N.; Joe, M.; Brunton, R.; Lowary, T. L.; Klassen, J. S.; Derda, R., Genetically-encoded fragment-based discovery (GE-FBD) of glycopeptide ligands with differential selectivity for antibodies related to mycobacterial infections. *Org. Biomol. Chem.* **2018,** *16* (2), 223-227.

276. Vinals, D. F.; Kitov, P. I.; Tu, Z.; Zou, C.; Cairo, C. W.; Lin, H. C.-H.; Derda, R., Selection of galectin-3 ligands derived from genetically encoded glycopeptide libraries. *Peptide Science* **2019,** *111* (1), e24097.
277. Ng, S.; Bennett, N. J.; Schulze, J.; Gao, N.; Rademacher, C.; Derda, R., Genetically-encoded fragment-based discovery of glycopeptide ligands for DC-SIGN. *Bioorg. Med. Chem.* **2018,** *26* (19), 5368-5377.
278. Tjhung, K. F.; Kitov, P. I.; Ng, S.; Kitova, E. N.; Deng, L.; Klassen, J. S.; Derda, R., Silent Encoding of Chemical Post-Translational Modifications in Phage-Displayed Libraries. *J. Am. Chem. Soc.* **2016,** *138* (1), 32-35.
279. Jafari, M. R.; Yu, H.; Wickware, J. M.; Lin, Y. S.; Derda, R., Light-responsive bicyclic peptides. *Org. Biomol. Chem.* **2018,** *16* (41), 7588-7594.
280. Schier, A. F., Nodal Signaling in Vertebrate Development. *Annu. Rev. Cell Dev. Biol.* **2003,** *19* (1), 589-621.
281. Quail, D. F.; Zhang, G.; Findlay, S. D.; Hess, D. A.; Postovit, L. M., Nodal promotes invasive phenotypes via a mitogen-activated protein kinase-dependent pathway. *Oncogene* **2014,** *33* (4), 461-73.
282. Quail, D. F.; Siegers, G. M.; Jewer, M.; Postovit, L.-M., Nodal signalling in embryogenesis and tumourigenesis. *The International Journal of Biochemistry & Cell Biology* **2013,** *45* (4), 885-898.
283. Hooijkaas, A. I.; Gadiot, J.; van Boven, H.; Blank, C., Expression of the embryological morphogen Nodal in stage III/IV melanoma. *Melanoma Res.* **2011,** *21* (6), 491-501.
284. Lonardo, E.; Hermann, Patrick C.; Mueller, M.-T.; Huber, S.; Balic, A.; Miranda-Lorenzo, I.; Zagorac, S.; Alcala, S.; Rodriguez-Arabaolaza, I.; Ramirez, Juan C.; Torres-Ruíz, R.; Garcia, E.; Hidalgo, M.; Cebrián, David Á.; Heuchel, R.; Löhr, M.; Berger, F.; Bartenstein, P.; Aicher, A.; Heeschen, C., Nodal/Activin Signaling Drives Self-Renewal and Tumorigenicity of Pancreatic Cancer Stem Cells and Provides a Target for Combined Drug Therapy. *Cell Stem Cell* **2011,** *9* (5), 433-446.
285. Kirsammer, G.; Strizzi, L.; Margaryan, N. V.; Gilgur, A.; Hyser, M.; Atkinson, J.; Kirschmann, D. A.; Seftor, E. A.; Hendrix, M. J., Nodal signaling promotes a tumorigenic phenotype in human breast cancer. *Semin. Cancer Biol.* **2014,** *29*, 40-50.
286. Gong, Y.; Guo, Y.; Hai, Y.; Yang, H.; Liu, Y.; Yang, S.; Zhang, Z.; Ma, M.; Liu, L.; Li, Z.; He, Z., Nodal promotes the self-renewal of human colon cancer stem cells via an autocrine manner through Smad2/3 signaling pathway. *Biomed Res Int* **2014,** *2014*, 364134.
287. Strizzi, L.; Hardy, K. M.; Margaryan, N. V.; Hillman, D. W.; Seftor, E. A.; Chen, B.; Geiger, X. J.; Thompson, E. A.; Lingle, W. L.; Andorfer, C. A.; Perez, E. A.; Hendrix, M. J., Potential for the embryonic morphogen Nodal as a prognostic and predictive biomarker in breast cancer. *Breast Cancer Res.* **2012,** *14* (3), R75.
288. Topczewska, J. M.; Postovit, L. M.; Margaryan, N. V.; Sam, A.; Hess, A. R.; Wheaton, W. W.; Nickoloff, B. J.; Topczewski, J.; Hendrix, M. J., Embryonic

and tumorigenic pathways converge via Nodal signaling: role in melanoma aggressiveness. *Nat. Med.* **2006,** *12* (8), 925-32.
289. Lee, C. C.; Jan, H. J.; Lai, J. H.; Ma, H. I.; Hueng, D. Y.; Lee, Y. C.; Cheng, Y. Y.; Liu, L. W.; Wei, H. W.; Lee, H. M., Nodal promotes growth and invasion in human gliomas. *Oncogene* **2010,** *29* (21), 3110-23.
290. Lawrence, M. G.; Margaryan, N. V.; Loessner, D.; Collins, A.; Kerr, K. M.; Turner, M.; Seftor, E. A.; Stephens, C. R.; Lai, J.; Postovit, L. M.; Clements, J. A.; Hendrix, M. J., Reactivation of embryonic nodal signaling is associated with tumor progression and promotes the growth of prostate cancer cells. *Prostate* **2011,** *71* (11), 1198-209.
291. Cavallari, C.; Fonsato, V.; Herrera, M. B.; Bruno, S.; Tetta, C.; Camussi, G., Role of Lefty in the anti tumor activity of human adult liver stem cells. *Oncogene* **2013,** *32* (7), 819-26.
292. Chen, J.; Liu, W. B.; Jia, W. D.; Xu, G. L.; Ma, J. L.; Ren, Y.; Chen, H.; Sun, S. N.; Huang, M.; Li, J. S., Embryonic morphogen nodal is associated with progression and poor prognosis of hepatocellular carcinoma. *PLoS One* **2014,** *9* (1), e85840.
293. Law, J.; Zhang, G.; Dragan, M.; Postovit, L. M.; Bhattacharya, M., Nodal signals via beta-arrestins and RalGTPases to regulate trophoblast invasion. *Cell. Signal.* **2014,** *26* (9), 1935-42.
294. Kong, B.; Wang, W.; Esposito, I.; Friess, H.; Michalski, C. W.; Kleeff, J., Increased expression of Nodal correlates with reduced patient survival in pancreatic cancer. *Pancreatology* **2015,** *15* (2), 156-61.
295. Focà, A.; Sanguigno, L.; Focà, G.; Strizzi, L.; Iannitti, R.; Palumbo, R.; Hendrix, M.; Leonardi, A.; Ruvo, M.; Sandomenico, A., New Anti-Nodal Monoclonal Antibodies Targeting the Nodal Pre-Helix Loop Involved in Cripto-1 Binding. *Int. J. Mol. Sci.* **2015,** *16* (9), 21342.
296. Strizzi, L.; Sandomenico, A.; Margaryan, N. V.; Foca, A.; Sanguigno, L.; Bodenstine, T. M.; Chandler, G. S.; Reed, D. W.; Gilgur, A.; Seftor, E. A.; Seftor, R. E.; Khalkhali-Ellis, Z.; Leonardi, A.; Ruvo, M.; Hendrix, M. J., Effects of a novel Nodal-targeting monoclonal antibody in melanoma. *Oncotarget* **2015,** *6* (33), 34071-86.
297. Dirksen, A.; Dawson, P. E., Rapid Oxime and Hydrazone Ligations with Aromatic Aldehydes for Biomolecular Labeling. *Bioconjugate Chem.* **2008,** *19* (12), 2543-2548.
298. Kalhor-Monfared, S.; Jafari, M. R.; Patterson, J. T.; Kitov, P. I.; Dwyer, J. J.; Nuss, J. M.; Derda, R., Rapid biocompatible macrocyclization of peptides with decafluoro-diphenylsulfone. *Chem. Sci.* **2016,** *7* (6), 3785-3790.
299. Zou, Y.; Spokoyny, A. M.; Zhang, C.; Simon, M. D.; Yu, H.; Lin, Y. S.; Pentelute, B. L., Convergent diversity-oriented side-chain macrocyclization scan for unprotected polypeptides. *Org. Biomol. Chem.* **2014,** *12* (4), 566-73.
300. Kitov, P. I.; Vinals, D. F.; Ng, S.; Tjhung, K. F.; Derda, R., Rapid, hydrolytically stable modification of aldehyde-terminated proteins and phage libraries. *J. Am. Chem. Soc.* **2014,** *136* (23), 8149-52.

301. Coda, D. M.; Gaarenstroom, T.; East, P.; Patel, H.; Miller, D. S. J.; Lobley, A.; Matthews, N.; Stewart, A.; Hill, C. S., Distinct modes of SMAD2 chromatin binding and remodeling shape the transcriptional response to NODAL/Activin signaling. *eLife* **2017,** *6*, e22474.
302. Diderich, P.; Bertoldo, D.; Dessen, P.; Khan, M. M.; Pizzitola, I.; Held, W.; Huelsken, J.; Heinis, C., Phage Selection of Chemically Stabilized alpha-Helical Peptide Ligands. *ACS Chem. Biol.* **2016,** *11* (5), 1422-7.
303. Damas, J. o. M.; Filipe, L. C.; Campos, S. R.; Lousa, D.; Victor, B. L.; Baptista, A. n. M.; Soares, C. u. M., Predicting the thermodynamics and kinetics of helix formation in a cyclic peptide model. *J. Chem. Theory Comput.* **2013,** *9* (11), 5148-5157.
304. Li, K.; Wang, W.; Gao, J., Fast and Stable N-Terminal Cysteine Modification through Thiazolidino Boronate Mediated Acyl Transfer. *Angew. Chem. Int. Ed. Engl.* **2020,** *59* (34), 14246-14250.
305. He, B.; Tjhung, K. F.; Bennett, N. J.; Chou, Y.; Rau, A.; Huang, J.; Derda, R., Compositional Bias in Naive and Chemically-modified Phage-Displayed Libraries uncovered by Paired-end Deep Sequencing. *Sci. Rep.* **2018,** *8* (1), 1214.
306. Sojitra, M.; Sarkar, S.; Maghera, J.; Rodrigues, E.; Carpenter, E.; Seth, S.; Vinals, D. F.; Bennett, N.; Reddy, R.; Khalil, A.; Xue, X.; Bell, M.; Zheng, R. B.; Ling, C.-C.; Lowary, T. L.; Paulson, J. C.; Macauley, M. S.; Derda, R., Genetically Encoded, Multivalent Liquid Glycan Array (LiGA). *bioRxiv* **2020**, 2020.03.24.997536.
307. Maestro. 11.7 ed.; Schrödinger, LLC: New York, NY, 2018.
308. Frolov, A. I.; Kiselev, M. G., Prediction of Cosolvent Effect on Solvation Free Energies and Solubilities of Organic Compounds in Supercritical Carbon Dioxide Based on Fully Atomistic Molecular Simulations. *J. Phys. Chem. B* **2014,** *118* (40), 11769-11780.
309. Hess, B.; Kutzner, C.; van der Spoel, D.; Lindahl, E., GROMACS 4: Algorithms for Highly Efficient, Load-Balanced, and Scalable Molecular Simulation. *J. Chem. Theory Comput.* **2008,** *4* (3), 435-447.
310. Kaminski, G. A.; Friesner, R. A.; Tirado-Rives, J.; Jorgensen, W. L., Evaluation and Reparametrization of the OPLS-AA Force Field for Proteins via Comparison with Accurate Quantum Chemical Calculations on Peptides. *J. Phys. Chem. B* **2001,** *105* (28), 6474-6487.
311. Jorgensen, W. L.; Chandrasekhar, J.; Madura, J. D.; Impey, R. W.; Klein, M. L., Comparison of simple potential functions for simulating liquid water. *J. Chem. Phys.* **1983,** *79* (2), 926-935.
312. Bussi, G.; Donadio, D.; Parrinello, M., Canonical sampling through velocity rescaling. *J. Chem. Phys.* **2007,** *126* (1), 014101.
313. Cheng, A.; Merz, K. M., Application of the Nosé−Hoover Chain Algorithm to the Study of Protein Dynamics. *J. Phys. Chem.* **1996,** *100* (5), 1927-1937.
314. Lingenheil, M.; Denschlag, R.; Reichold, R.; Tavan, P., The "Hot-Solvent/Cold-Solute" Problem Revisited. *J. Chem. Theory Comput.* **2008,** *4* (8), 1293-1306.

315. Berendsen, H. J. C.; Postma, J. P. M.; Gunsteren, W. F. v.; DiNola, A.; Haak, J. R., Molecular dynamics with coupling to an external bath. *J. Chem. Phys.* **1984,** *81* (8), 3684-3690.
316. Hess, B.; Bekker, H.; Berendsen, H. J. C.; Fraaije, J. G. E. M., LINCS: A linear constraint solver for molecular simulations. *J. Comput. Chem.* **1997,** *18* (12), 1463-1472.
317. Hockney, R. W.; Eastwood, J. W., *Computer simulation using particles*. Taylor & Francis Group: New York, 1988.
318. Darden, T.; York, D.; Pedersen, L., Particle mesh Ewald: An N· log (N) method for Ewald sums in large systems. *J. Chem. Phys.* **1993,** *98* (12), 10089-10092.
319. Essmann, U.; Perera, L.; Berkowitz, M. L.; Darden, T.; Lee, H.; Pedersen, L. G., A smooth particle mesh Ewald method. *J. Chem. Phys.* **1995,** *103* (19), 8577-8593.
320. Jain, R. K.; Stylianopoulos, T., Delivering nanomedicine to solid tumors. *Nat. Rev. Clin. Oncol.* **2010,** *7* (11), 653-664.
321. Dreher, M. R.; Liu, W.; Michelich, C. R.; Dewhirst, M. W.; Yuan, F.; Chilkoti, A., Tumor Vascular Permeability, Accumulation, and Penetration of Macromolecular Drug Carriers. *J. Natl. Cancer Inst.* **2006,** *98* (5), 335-344.
322. Firer, M. A.; Gellerman, G., Targeted drug delivery for cancer therapy: the other side of antibodies. *J. Hematol. Oncol.* **2012,** *5* (1), 70.
323. Li, X.; Sun, Y.; Ma, L.; Liu, G.; Wang, Z., The Renal Clearable Magnetic Resonance Imaging Contrast Agents: State of the Art and Recent Advances. *Molecules* **2020,** *25* (21), 5072.
324. Andersen, J. T.; Dalhus, B.; Cameron, J.; Daba, M. B.; Plumridge, A.; Evans, L.; Brennan, S. O.; Gunnarsen, K. S.; Bjørås, M.; Sleep, D.; Sandlie, I., Structure-based mutagenesis reveals the albumin-binding site of the neonatal Fc receptor. *Nat. Commun.* **2012,** *3* (1), 610.
325. Eng, J.; Kleinman, W. A.; Singh, L.; Singh, G.; Raufman, J. P., Isolation and characterization of exendin-4, an exendin-3 analogue, from Heloderma suspectum venom. Further evidence for an exendin receptor on dispersed acini from guinea pig pancreas. *J. Biol. Chem.* **1992,** *267* (11), 7402-5.
326. Nielsen, L. L.; Young, A. A.; Parkes, D. G., Pharmacology of exenatide (synthetic exendin-4): a potential therapeutic for improved glycemic control of type 2 diabetes. *Regul. Pept.* **2004,** *117* (2), 77-88.
327. Drucker, D. J.; Nauck, M. A., The incretin system: glucagon-like peptide-1 receptor agonists and dipeptidyl peptidase-4 inhibitors in type 2 diabetes. *Lancet* **2006,** *368* (9548), 1696-1705.
328. Arslan, F. B.; Ozturk Atar, K.; Calis, S., Antibody-mediated drug delivery. *Int. J. Pharm.* **2021,** *596*, 120268.
329. Richards, D. A., Exploring alternative antibody scaffolds: Antibody fragments and antibody mimics for targeted drug delivery. *Drug Discovery Today: Technol.* **2018,** *30*, 35-46.

330. Duivelshof, B. L.; Murisier, A.; Camperi, J.; Fekete, S.; Beck, A.; Guillarme, D.; D'Atri, V., Therapeutic Fc-fusion proteins: Current analytical strategies. *J. Sep. Sci.* **2021,** *44* (1), 35-62.
331. Turecek, P. L.; Bossard, M. J.; Schoetens, F.; Ivens, I. A., PEGylation of Biopharmaceuticals: A Review of Chemistry and Nonclinical Safety Information of Approved Drugs. *J. Pharm. Sci.* **2016,** *105* (2), 460-475.
332. Wu, L.; Chen, J.; Wu, Y.; Zhang, B.; Cai, X.; Zhang, Z.; Wang, Y.; Si, L.; Xu, H.; Zheng, Y.; Zhang, C.; Liang, C.; Li, J.; Zhang, L.; Zhang, Q.; Zhou, D., Precise and combinatorial PEGylation generates a low-immunogenic and stable form of human growth hormone. *J. Control. Release* **2017,** *249*, 84-93.
333. Tully, M.; Dimde, M.; Weise, C.; Pouyan, P.; Licha, K.; Schirner, M.; Haag, R., Polyglycerol for Half-Life Extension of Proteins—Alternative to PEGylation? *Biomacromolecules* **2021,** *22* (4), 1406-1416.
334. Angelini, A.; Morales-Sanfrutos, J.; Diderich, P.; Chen, S.; Heinis, C., Bicyclization and Tethering to Albumin Yields Long-Acting Peptide Antagonists. *J. Med. Chem.* **2012,** *55* (22), 10187-10197.
335. Zorzi, A.; Middendorp, S. J.; Wilbs, J.; Deyle, K.; Heinis, C., Acylated heptapeptide binds albumin with high affinity and application as tag furnishes long-acting peptides. *Nat Commun* **2017,** *8*, 16092.
336. Bern, M.; Sand, K. M. K.; Nilsen, J.; Sandlie, I.; Andersen, J. T., The role of albumin receptors in regulation of albumin homeostasis: Implications for drug delivery. *J. Control. Release* **2015,** *211*, 144-162.
337. Zorzi, A.; Linciano, S.; Angelini, A., Non-covalent albumin-binding ligands for extending the circulating half-life of small biotherapeutics. *MedChemComm* **2019,** *10* (7), 1068-1081.
338. Menegatti, S.; Hussain, M.; Naik, A. D.; Carbonell, R. G.; Rao, B. M., mRNA display selection and solid-phase synthesis of Fc-binding cyclic peptide affinity ligands. *Biotechnol. Bioeng.* **2013,** *110* (3), 857-870.
339. Sockolosky, J. T.; Kivimäe, S.; Szoka, F. C., Fusion of a Short Peptide that Binds Immunoglobulin G to a Recombinant Protein Substantially Increases Its Plasma Half-Life in Mice. *PLoS One* **2014,** *9* (7), e102566.
340. Sockolosky, J. T.; Szoka, F. C., The neonatal Fc receptor, FcRn, as a target for drug delivery and therapy. *Adv. Drug Del. Rev.* **2015,** *91*, 109-124.
341. Penchala, S. C.; Miller, M. R.; Pal, A.; Dong, J.; Madadi, N. R.; Xie, J.; Joo, H.; Tsai, J.; Batoon, P.; Samoshin, V.; Franz, A.; Cox, T.; Miles, J.; Chan, W. K.; Park, M. S.; Alhamadsheh, M. M., A biomimetic approach for enhancing the in vivo half-life of peptides. *Nat. Chem. Biol.* **2015,** *11* (10), 793-798.
342. Wang, Z.; Zhao, Y.; Jiang, Y.; Lv, W.; Wu, L.; Wang, B.; Lv, L.; Xu, Q.; Xin, H., Enhanced anti-ischemic stroke of ZL006 by T7-conjugated PEGylated liposomes drug delivery system. *Sci. Rep.* **2015,** *5* (1), 12651.
343. Kuang, Y.; Jiang, X.; Zhang, Y.; Lu, Y.; Ma, H.; Guo, Y.; Zhang, Y.; An, S.; Li, J.; Liu, L.; Wu, Y.; Liang, J.; Jiang, C., Dual Functional Peptide-Driven Nanoparticles for Highly Efficient Glioma-Targeting and Drug Codelivery. *Mol. Pharm.* **2016,** *13* (5), 1599-1607.

344. Ilyas, H.; van der Plas, M. J. A.; Agnoletti, M.; Kumar, S.; Mandal, A. K.; Atreya, H. S.; Bhunia, A.; Malmsten, M., Effect of PEGylation on Host Defense Peptide Complexation with Bacterial Lipopolysaccharide. *Bioconjugate Chem.* **2021,** *32* (8), 1729-1741.
345. Lawrence, P. B.; Gavrilov, Y.; Matthews, S. S.; Langlois, M. I.; Shental-Bechor, D.; Greenblatt, H. M.; Pandey, B. K.; Smith, M. S.; Paxman, R.; Torgerson, C. D.; Merrell, J. P.; Ritz, C. C.; Prigozhin, M. B.; Levy, Y.; Price, J. L., Criteria for Selecting PEGylation Sites on Proteins for Higher Thermodynamic and Proteolytic Stability. *J. Am. Chem. Soc.* **2014,** *136* (50), 17547-17560.
346. Xiao, Q.; Ashton, D. S.; Jones, Z. B.; Thompson, K. P.; Price, J. L., Long-range PEG stapling: macrocyclization for increased protein conformational stability and resistance to proteolysis. *RSC Chem. Biol.* **2020,** *1* (4), 273-280.
347. Dwyer, J. J.; Wilson, K. L.; Davison, D. K.; Freel, S. A.; Seedorff, J. E.; Wring, S. A.; Tvermoes, N. A.; Matthews, T. J.; Greenberg, M. L.; Delmedico, M. K., Design of helical, oligomeric HIV-1 fusion inhibitor peptides with potent activity against enfuvirtide-resistant virus. *Proc. Natl. Acad. Sci. U.S.A* **2007,** *104* (31), 12772-12777.
348. Peters, T., *All About Albumin: Biochemistry, Genetics, and Medical Applications*. Elsevier Science: 1995.
349. Zaykov, A. N.; Mayer, J. P.; DiMarchi, R. D., Pursuit of a perfect insulin. *Nat. Rev. Drug Discov.* **2016,** *15* (6), 425-439.
350. Elbrønd, B.; Jakobsen, G.; Larsen, S.; Agersø, H.; Jensen, L. B.; Rolan, P.; Sturis, J.; Hatorp, V.; Zdravkovic, M., Pharmacokinetics, pharmacodynamics, safety, and tolerability of a single-dose of NN2211, a long-acting glucagon-like peptide 1 derivative, in healthy male subjects. *Diabetes Care* **2002,** *25* (8), 1398-404.
351. Kurtzhals, P.; Havelund, S.; Jonassen, I.; Kiehr, B.; Larsen, U. D.; Ribel, U.; Markussen, J., Albumin binding of insulins acylated with fatty acids: characterization of the ligand-protein interaction and correlation between binding affinity and timing of the insulin effect in vivo. *Biochem. J* **1995,** *312 (Pt 3)* (Pt 3), 725-31.
352. Pollaroa, L.; Heinis, C., Strategies to prolong the plasma residence time of peptide drugs. *Med. Chem. Commun.* **2010,** *1* (5), 319-324.
353. Havelund, S.; Plum, A.; Ribel, U.; Jonassen, I.; Vølund, A.; Markussen, J.; Kurtzhals, P., The Mechanism of Protraction of Insulin Detemir, a Long-Acting, Acylated Analog of Human Insulin. *Pharm. Res.* **2004,** *21* (8), 1498-1504.
354. Pollaro, L.; Raghunathan, S.; Morales-Sanfrutos, J.; Angelini, A.; Kontos, S.; Heinis, C., Bicyclic Peptides Conjugated to an Albumin-Binding Tag Diffuse Efficiently into Solid Tumors. *Mol. Cancer Ther.* **2015,** *14* (1), 151-161.
355. Nguyen, A.; Reyes, A. E., II; Zhang, M.; McDonald, P.; Wong, W. L. T.; Damico, L. A.; Dennis, M. S., The pharmacokinetics of an albumin-binding Fab (AB.Fab) can be modulated as a function of affinity for albumin. *Protein Eng. Des. Sel.* **2006,** *19* (7), 291-297.

356. Dennis, M. S.; Jin, H.; Dugger, D.; Yang, R.; McFarland, L.; Ogasawara, A.; Williams, S.; Cole, M. J.; Ross, S.; Schwall, R., Imaging Tumors with an Albumin-Binding Fab, a Novel Tumor-Targeting Agent. *Cancer Res.* **2007,** *67* (1), 254-261.
357. Langenheim, J. F.; Chen, W. Y., Improving the pharmacokinetics/pharmacodynamics of prolactin, GH, and their antagonists by fusion to a synthetic albumin-binding peptide. *J. Endocrinol.* **2009,** *203* (3), 375-387.
358. Tijink, B. M.; Laeremans, T.; Budde, M.; Walsum, M. S.-v.; Dreier, T.; de Haard, H. J.; Leemans, C. R.; van Dongen, G. A. M. S., Improved tumor targeting of anti–epidermal growth factor receptor Nanobodies through albumin binding: taking advantage of modular Nanobody technology. *Mol. Cancer Ther.* **2008,** *7* (8), 2288-2297.
359. Steiner, D.; Merz, F. W.; Sonderegger, I.; Gulotti-Georgieva, M.; Villemagne, D.; Phillips, D. J.; Forrer, P.; Stumpp, M. T.; Zitt, C.; Binz, H. K., Half-life extension using serum albumin-binding DARPin® domains. *Protein Eng. Des. Sel.* **2017,** *30* (9), 583-591.
360. Spokoyny, A. M.; Zou, Y.; Ling, J. J.; Yu, H.; Lin, Y.-S.; Pentelute, B. L., A Perfluoroaryl-Cysteine SNAr Chemistry Approach to Unprotected Peptide Stapling. *J. Am. Chem. Soc.* **2013,** *135* (16), 5946-5949.
361. Wang, G.; Li, X.; Wang, Z., APD3: the antimicrobial peptide database as a tool for research and education. *Nucleic Acids Res.* **2016,** *44* (D1), D1087-93.
362. Thevenet, P.; Shen, Y.; Maupetit, J.; Guyon, F.; Derreumaux, P.; Tuffery, P., PEP-FOLD: an updated de novo structure prediction server for both linear and disulfide bonded cyclic peptides. *Nucleic Acids Res.* **2012,** *40* (Web Server issue), W288-93.
363. Shen, Y.; Maupetit, J.; Derreumaux, P.; Tuffery, P., Improved PEP-FOLD Approach for Peptide and Miniprotein Structure Prediction. *J. Chem. Theory Comput.* **2014,** *10* (10), 4745-58.
364. Lamiable, A.; Thevenet, P.; Rey, J.; Vavrusa, M.; Derreumaux, P.; Tuffery, P., PEP-FOLD3: faster de novo structure prediction for linear peptides in solution and in complex. *Nucleic Acids Res.* **2016,** *44* (W1), W449-54.
365. Staquicini, F. I.; Ozawa, M. G.; Moya, C. A.; Driessen, W. H.; Barbu, E. M.; Nishimori, H.; Soghomonyan, S.; Flores, L. G., 2nd; Liang, X.; Paolillo, V.; Alauddin, M. M.; Basilion, J. P.; Furnari, F. B.; Bogler, O.; Lang, F. F.; Aldape, K. D.; Fuller, G. N.; Hook, M.; Gelovani, J. G.; Sidman, R. L.; Cavenee, W. K.; Pasqualini, R.; Arap, W., Systemic combinatorial peptide selection yields a non-canonical iron-mimicry mechanism for targeting tumors in a mouse model of human glioblastoma. *J. Clin. Invest.* **2011,** *121* (1), 161-73.

Appendix A: Supporting information for chapter 2

Appendix A-1: Chemistry data

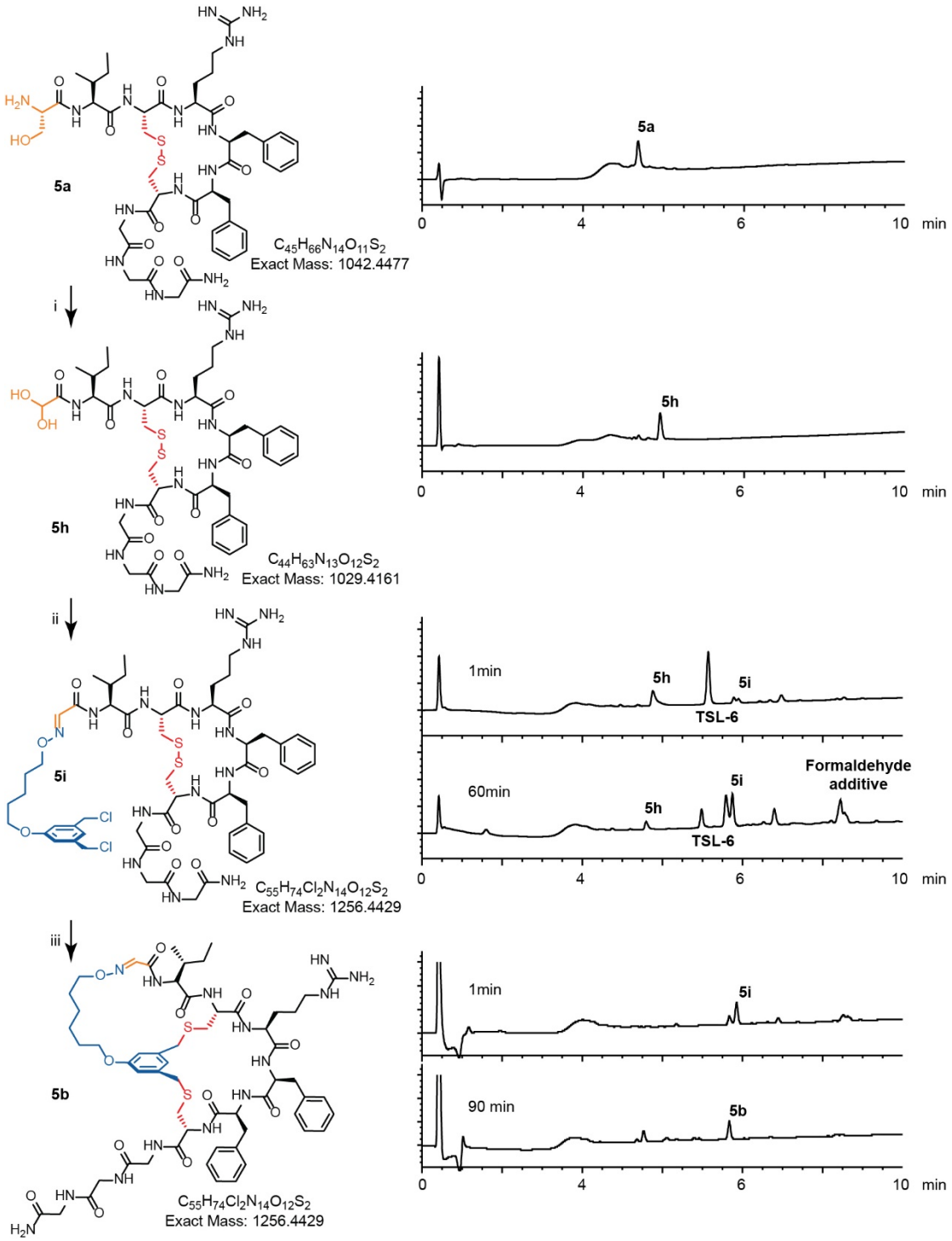

Appendix A-Scheme 1. One-pot bicyclization of **5a** (0.2 mmol) with **TSL-6**: Reagents and conditions: (i) 2.4 mM $NaIO_4$, PBS (pH 7.4), 5 min, 1 mM Met, 20 min (ii) 0.1% TFA, 1 mM TSL-6, 1 h; 1 mM TCEP, 30 min; (iii) 150 mM NaHCO3 (pH 10), 90 mins;

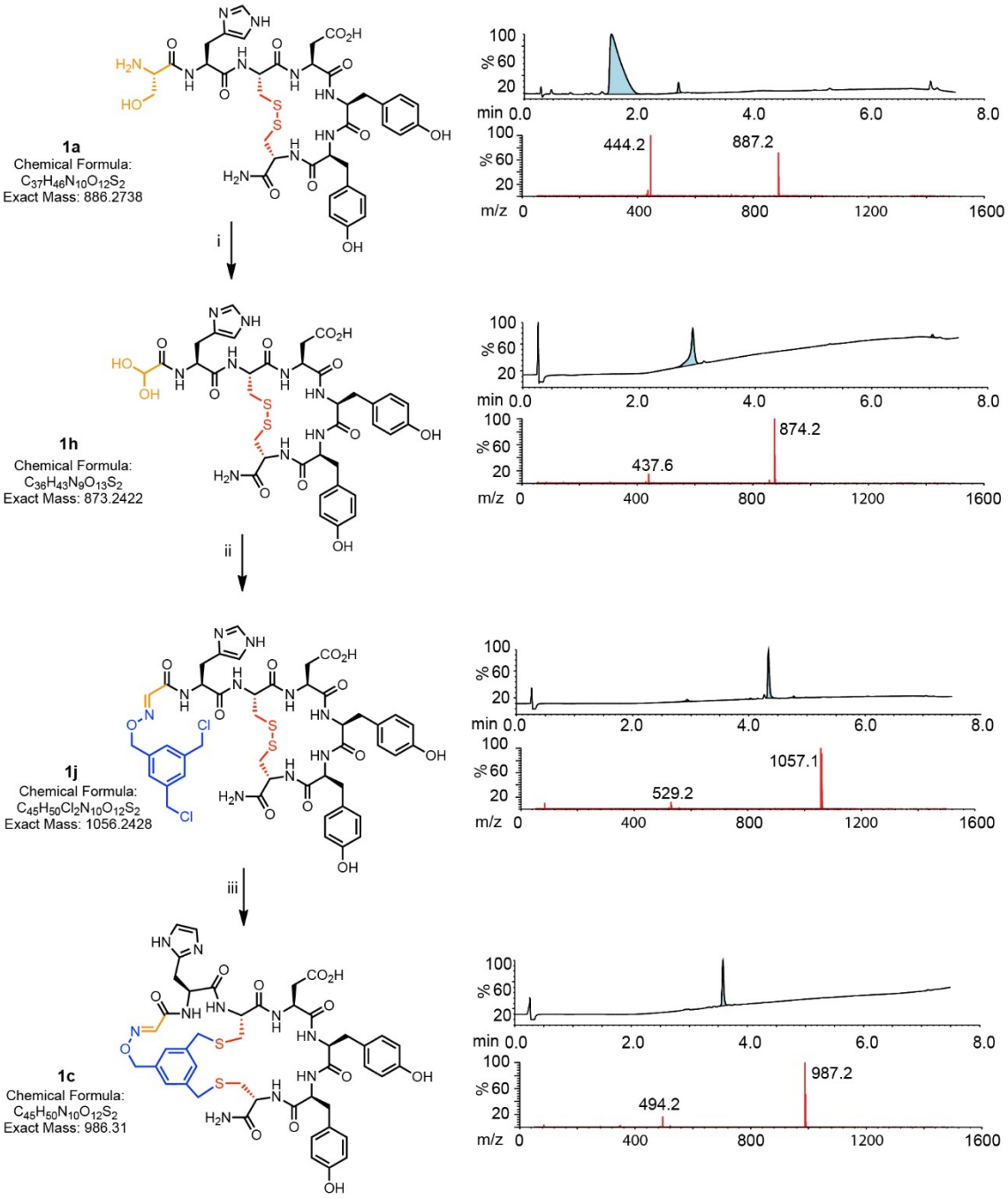

Appendix A-Scheme 2. One-pot bicyclization of **1a** (0.5 mM) with **TSL-1**. Reagents and conditions: (i) 0.6 mM $NaIO_4$, PBS (pH 7.4), 5 min. (ii) 0.1% TFA, 0.6 mM **TSL-1** (pH 4), 1 h; (iii) 2.5 mM TCEP, 30 min; 100 mM TRIS (pH 8.5), 1 h.

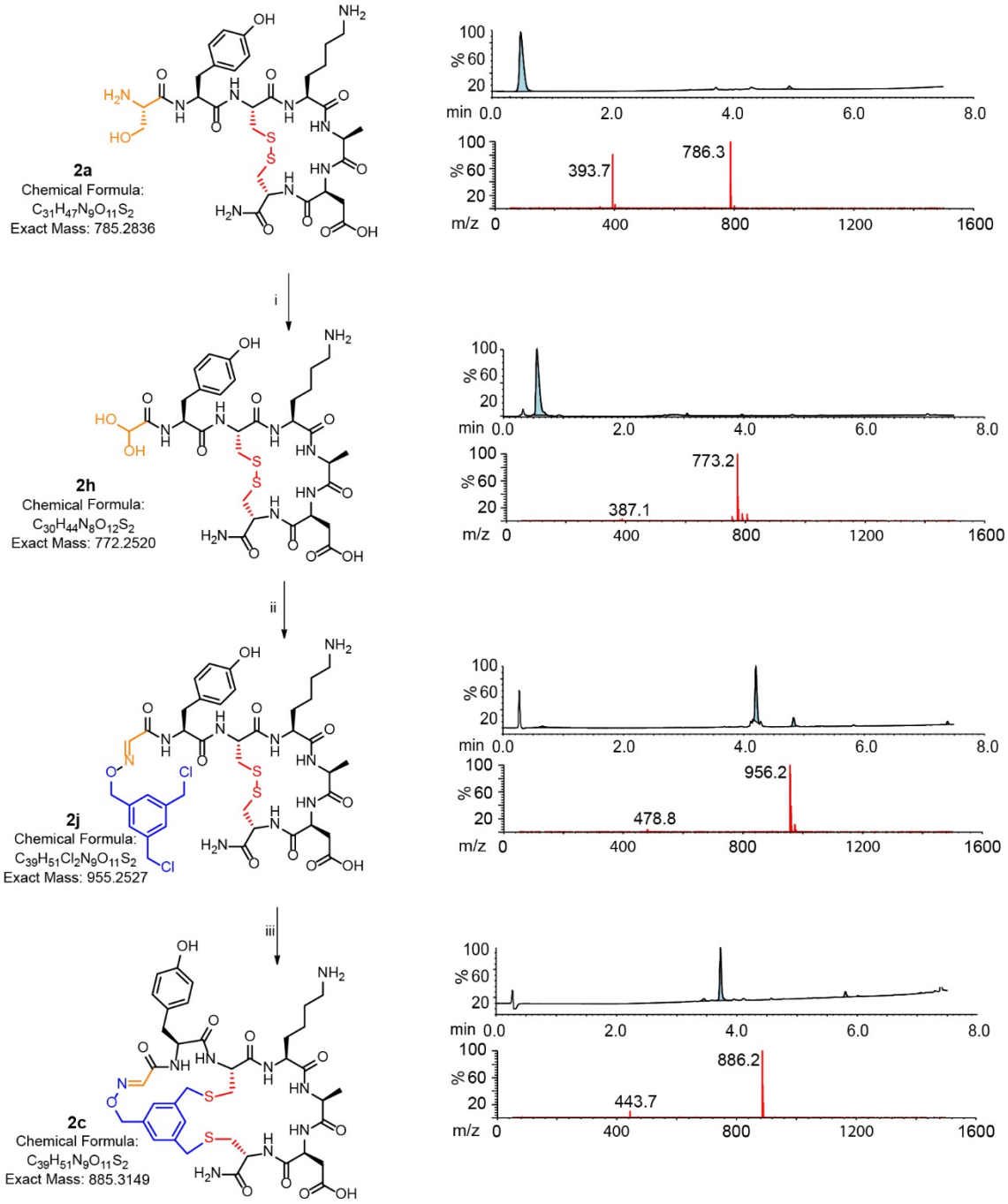

Appendix A-Scheme 3. One-pot bicyclization of **2a** (0.5 mM) with **TSL-1**. Reagents and conditions: (i) 0.6 mM $NaIO_4$, PBS (pH 7.4), 5 min. (ii) 0.1% TFA, 0.6 mM **TSL-1** (pH 4), 1 h; (iii) 2.5 mM TCEP, 30 min; 100 mM TRIS (pH 8.5), 1 h.

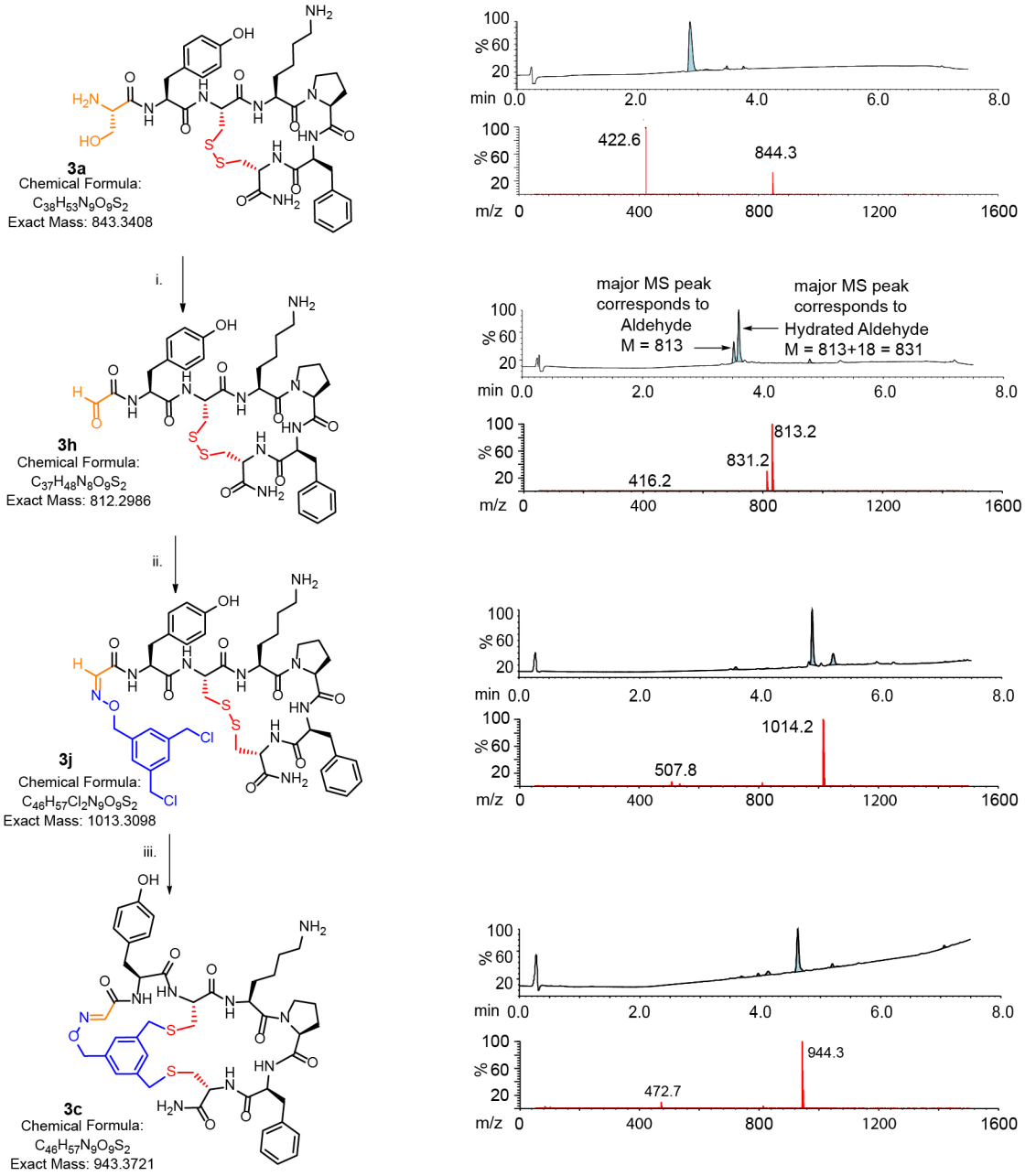

Appendix A-Scheme 4. One-pot bicyclization of **3a** (0.5 mM) with **TSL-1**. Reagents and conditions: (i) 0.6 mM $NaIO_4$, PBS (pH 7.4), 5 min, 1 mM Met, 15 min (ii) 0.1% TFA, 0.6 mM **TSL-1** (pH 4), 1 h; (iii) 2.5 mM TCEP, 30 min; 100 mM TRIS (pH 8.5), 1 h.

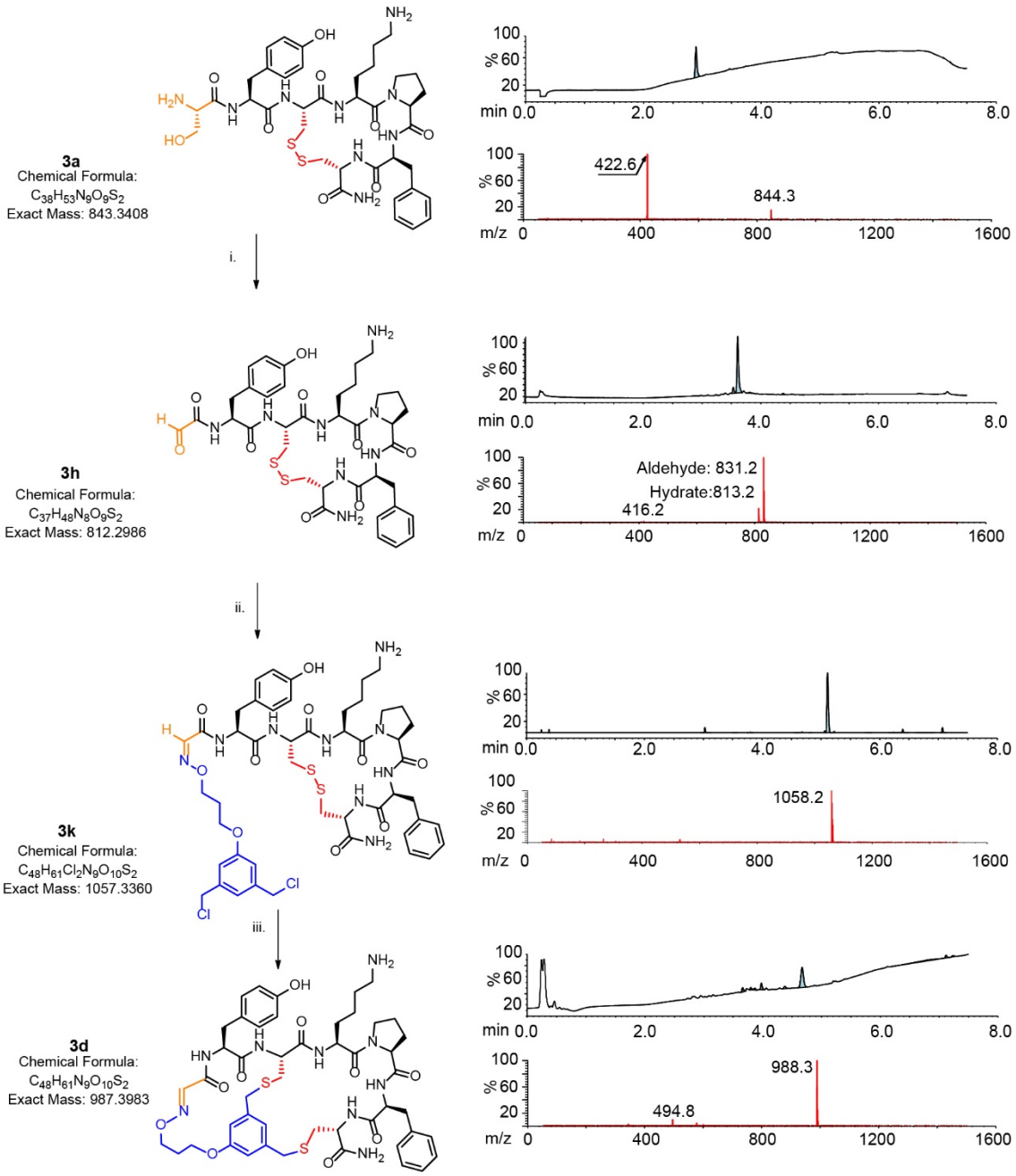

Appendix A-Scheme 5. One-pot bicyclization of **3a** (0.5 mM) with **TSL-3**. Reagents and conditions: (i) 0.6 mM $NaIO_4$, PBS (pH 7.4), 5 min, 1 mM Met, 15 min (ii) 0.1% TFA, 0.6 mM **TSL-3** (pH 4), 1 h; (iii) 2.5 mM TCEP, 30 min; 100 mM TRIS (pH 8.5), 1 h.

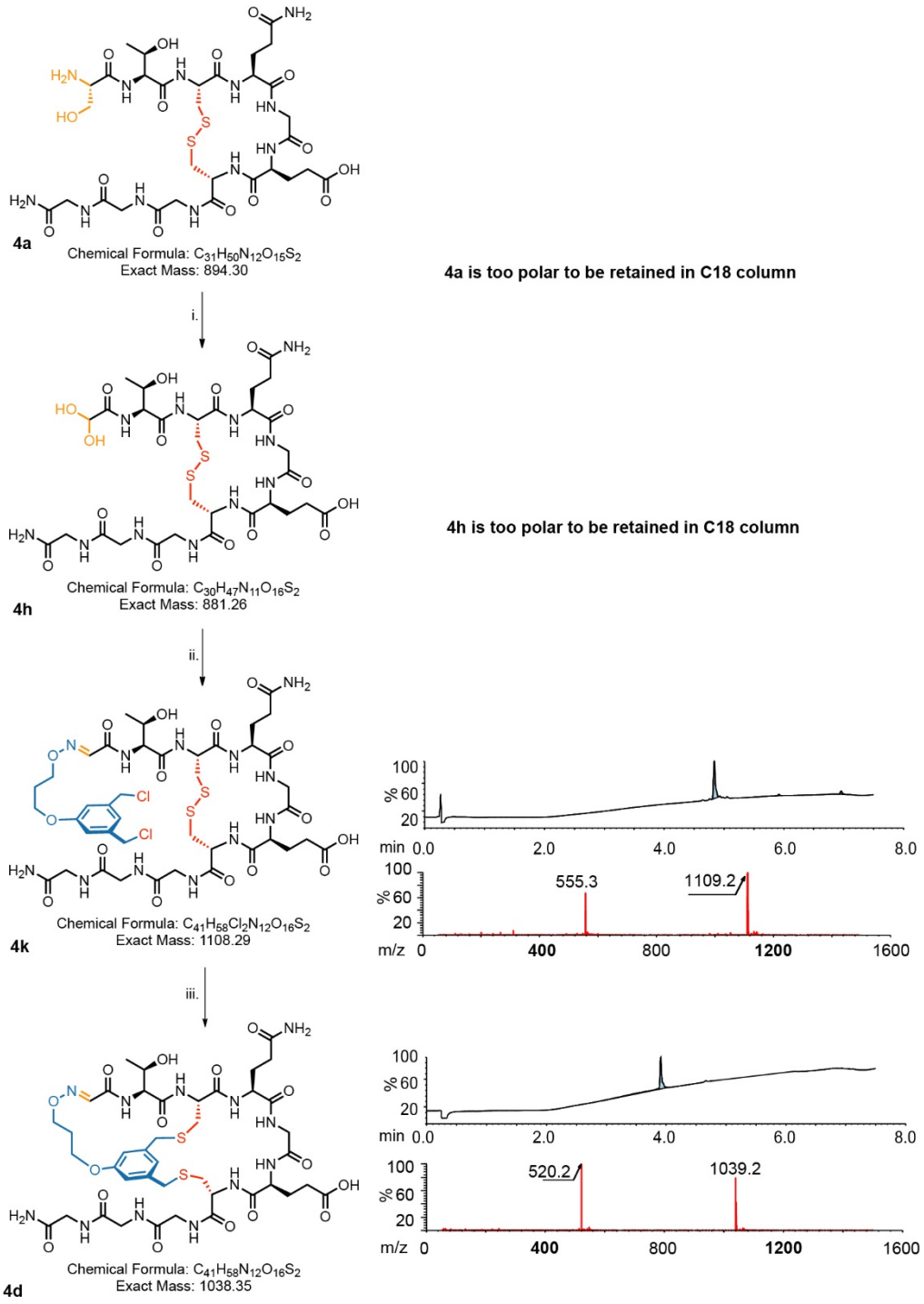

Appendix A-Scheme 6. One-pot bicyclization of **4a** with **TSL-3**: Reagents and conditions: (i) 0.6 mM $NaIO_4$, PBS (pH 7.4), 5 min, 1 mM Met, 15 min (ii) 0.1% TFA, 0.6 mM **TSL-3** (pH 4), 1 h; (iii) 2.5 mM TCEP, 30 min; 100 mM $NaHCO_3$ (pH 10), 30 min.

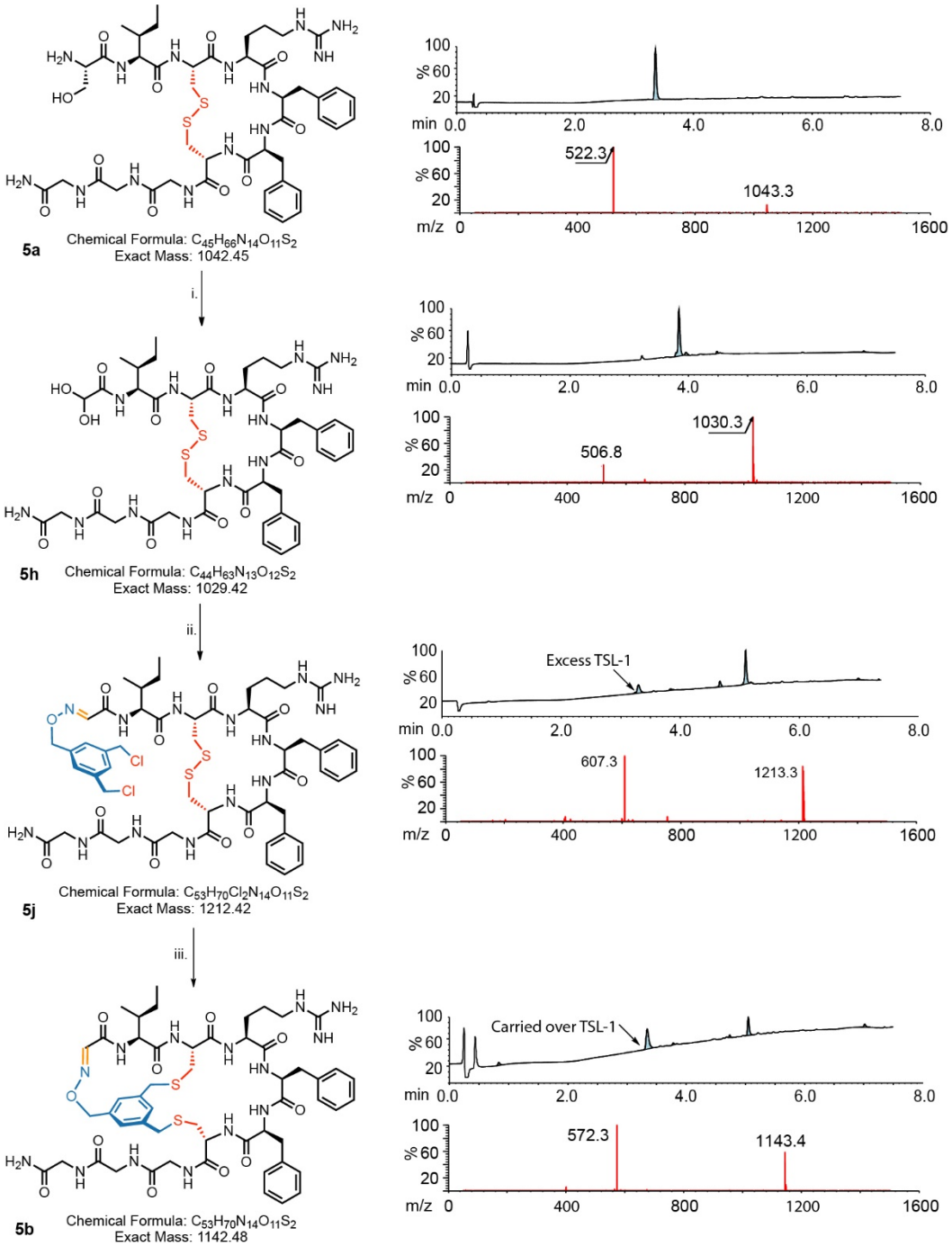

Appendix A-Scheme 7. One-pot bicyclization of **5a** with **TSL-1**: Reagents and conditions: (i) 0.6 mM $NaIO_4$, PBS (pH 7.4), 5 min, 1 mM Met, 15 min (ii) 0.1% TFA, 0.6 mM **TSL-1** (pH 4), 1 h; (iii) 2.5 mM TCEP, 30 min; 100 mM $NaHCO_3$ (pH 10), 30 min.

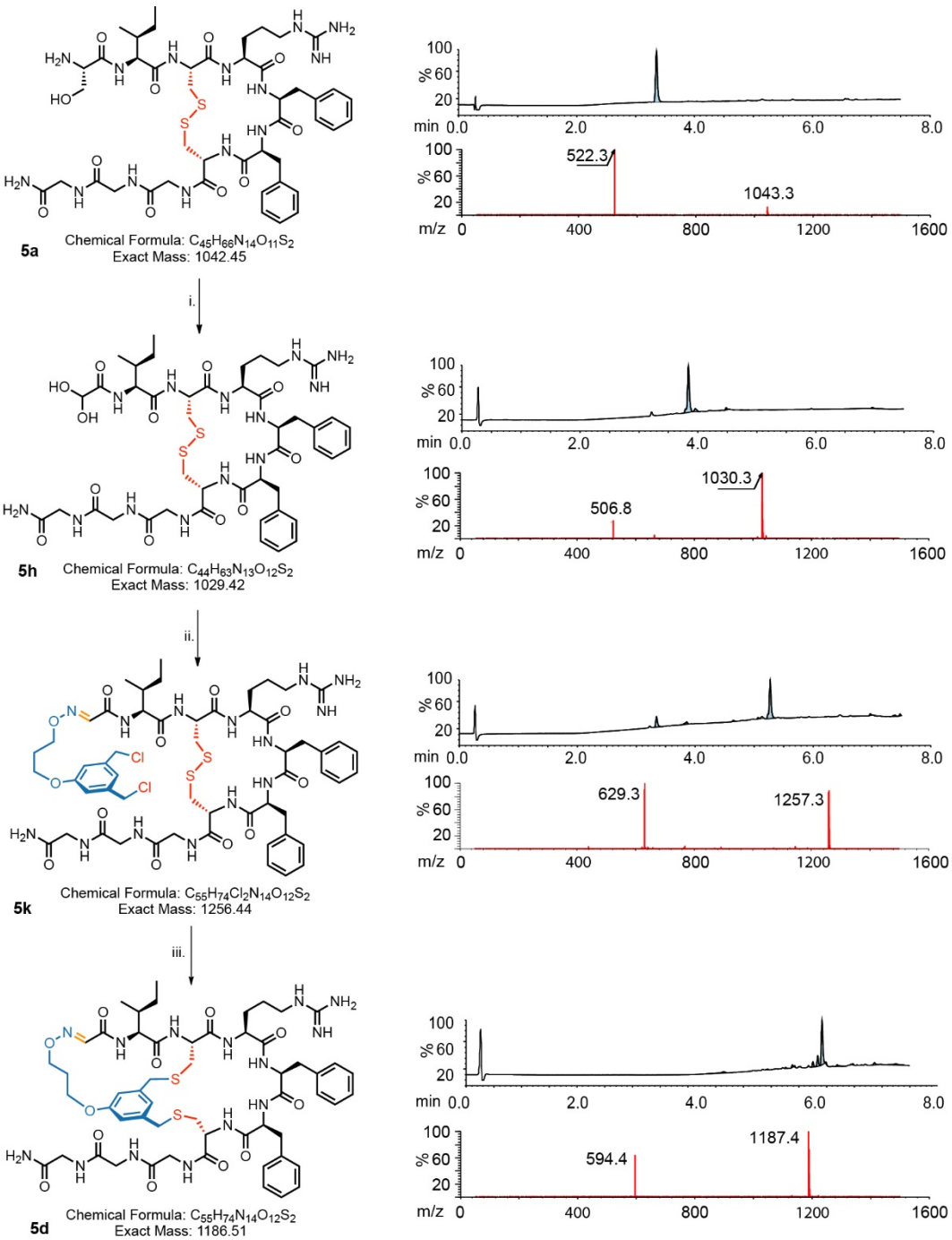

Appendix A-Scheme 8. One-pot bicyclization of **5a** with **TSL-3**: Reagents and conditions: (i) 0.6 mM $NaIO_4$, PBS (pH 7.4), 5 min, 1 mM Met, 15 min (ii) 0.1% TFA, 0.6 mM **TSL-3** (pH 4), 1 h; (iii) 2.5 mM TCEP, 30 min; 100 mM NaHCO3 (pH 10), 30 min.

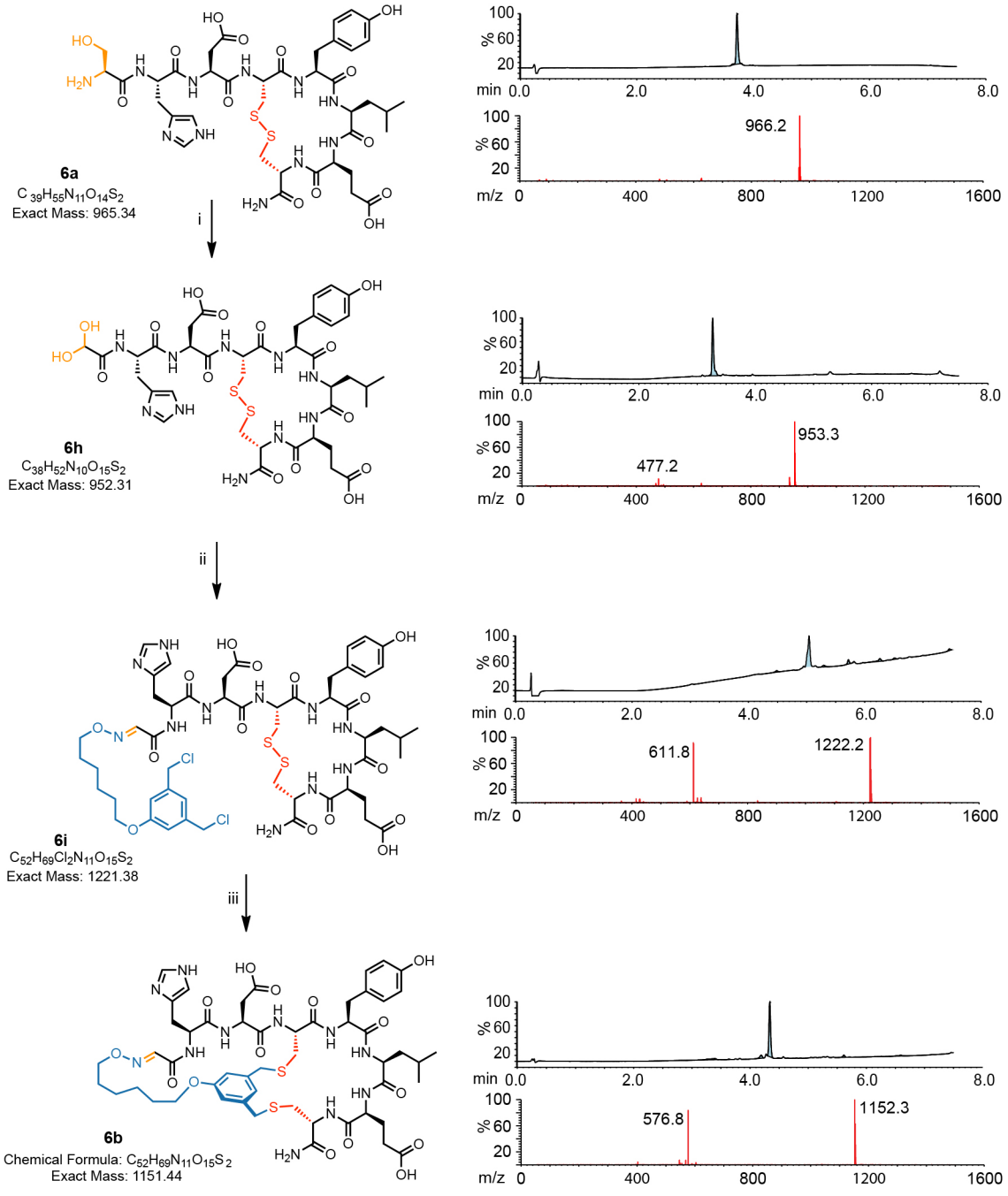

Appendix A-Scheme 9. One pot bicyclization of **6a** (0.5 mM) with **TSL-6**. Reagents and conditions: (i) 0.6 mM $NaIO_4$, PBS (pH 7.4), 5 min. (ii) 0.1% TFA, 0.6 mM **TSL-6** (pH 4), 1 h; (iii) 2.5 mM TCEP, 30 min; 100 mM TRIS (pH 8.5), 1 h.

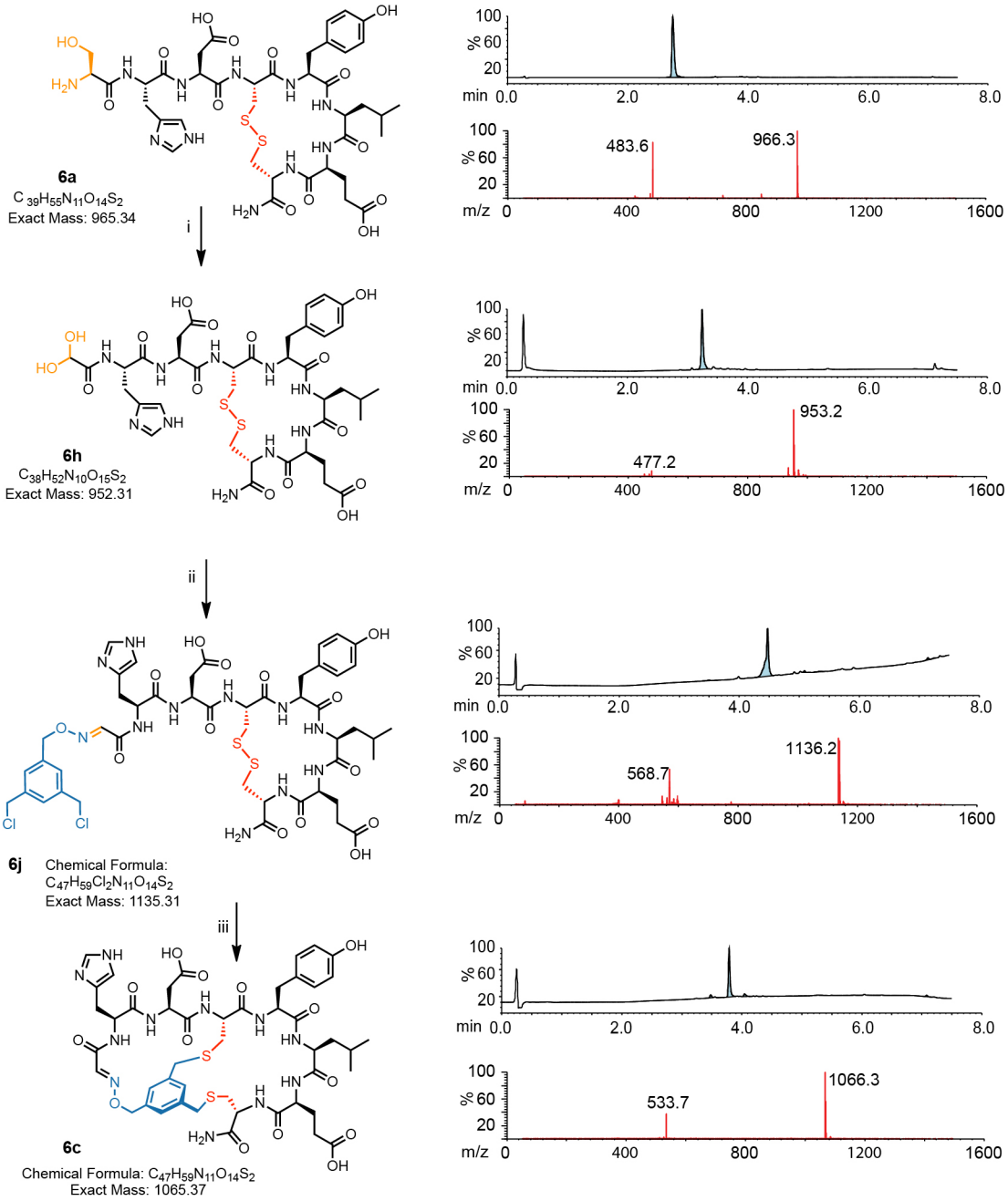

Appendix A-Scheme 10. One-pot bicyclization of **6a** (0.5 mM) with **TSL-1**. Reagents and conditions: (i) 0.6 mM NaIO4, PBS (pH 7.4), 5 min. (ii) 0.1% TFA, 0.6 mM **TSL-1** (pH 4), 1 h; (iii) 2.5 mM TCEP, 30 min; 100 mM TRIS (pH 8.5), 1 h.

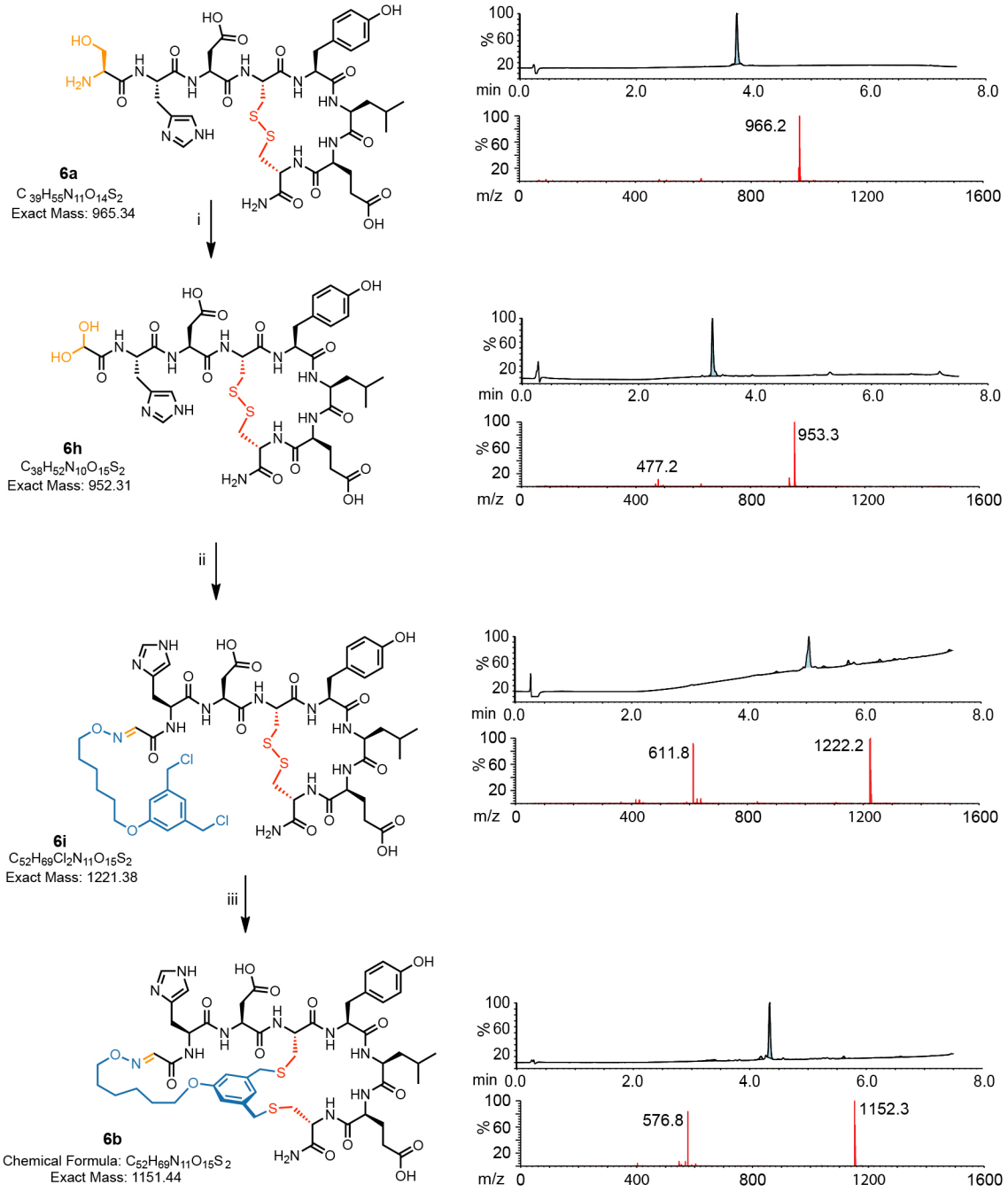

Appendix A-Scheme 11. One-pot bicyclization of **6a** (0.5 mM) with **TSL-6**. Reagents and conditions: (i) 0.6 mM $NaIO_4$, PBS (pH 7.4), 5 min, 1 mM Met, 15 min (ii) 0.1% TFA, 0.6 mM **TSL-6** (pH 4), 1 h; (iii) 2.5 mM TCEP, 30 min; 100 mM TRIS (pH 8.5), 1 h.

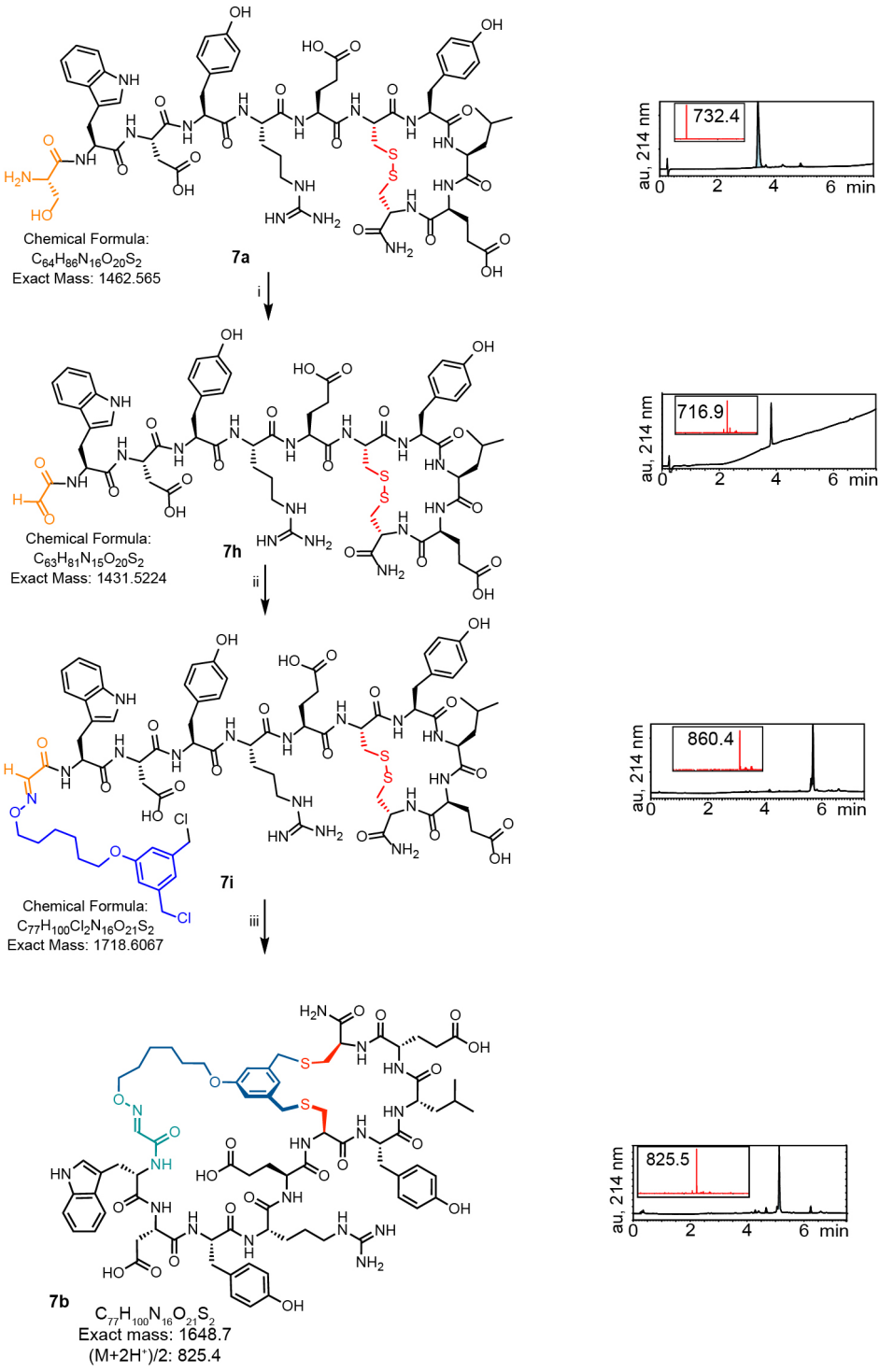

Appendix A-Scheme 12. One-pot bicyclization of **7a** (0.5 mM) with **TSL-1**.Reagents and conditions: (i) 0.6 mM $NaIO_4$, PBS (pH 7.4), 5 min. (ii) 0.1% TFA, 0.6 mM **TSL-1** (pH 4), 1 h; (iii) 2.5 mM TCEP, 30 min; 100 mM TRIS (pH 8.5), 1 h.

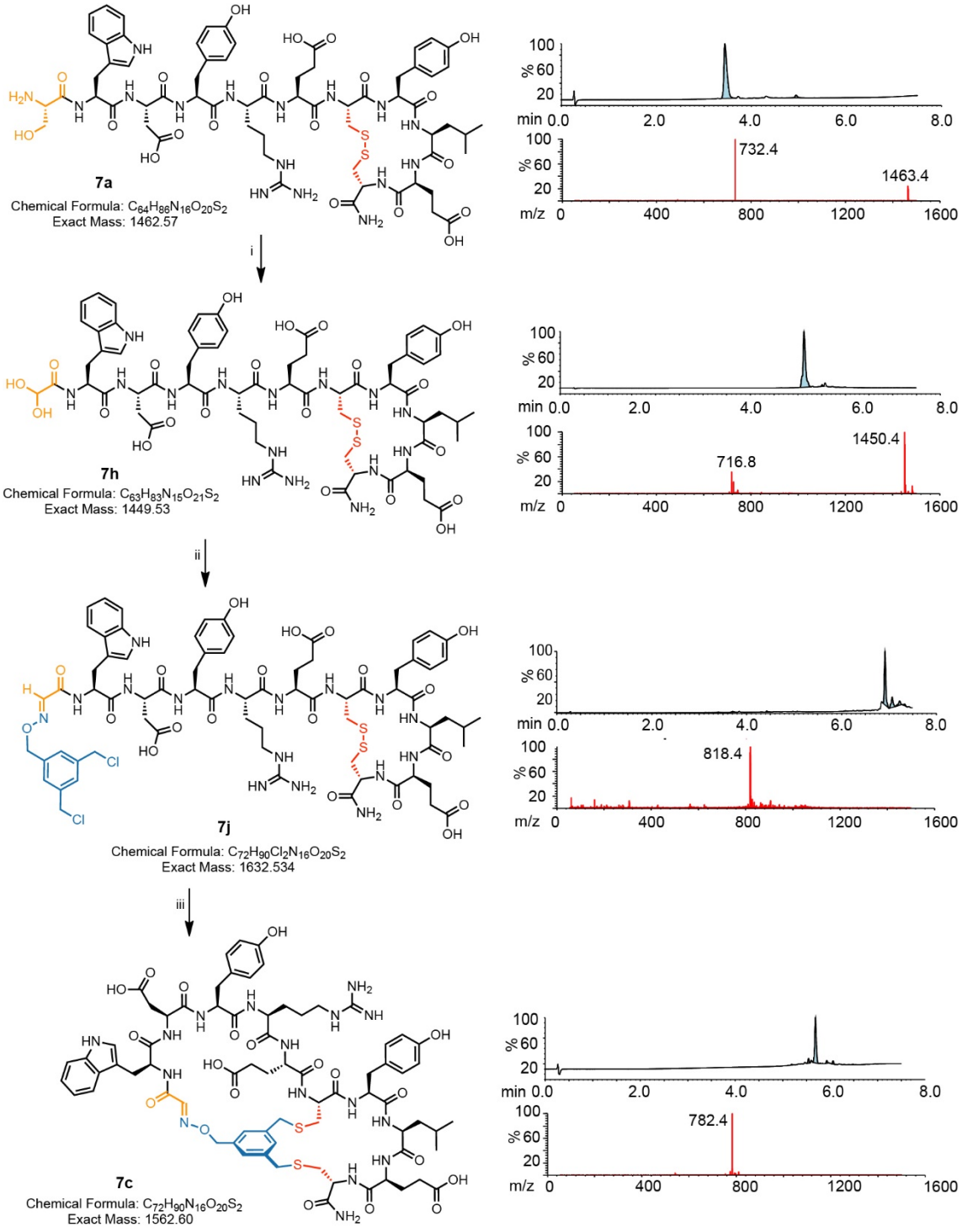

Appendix A-Scheme 13. One-pot bicyclization of **7a** (0.5 mM) with **TSL-1**.Reagents and conditions: (i) 0.6 mM $NaIO_4$, PBS (pH 7.4), 5 min. (ii) 0.1% TFA, 0.6 mM **TSL-1** (pH 4), 1 h; (iii) 2.5 mM TCEP, 30 min; 100 mM TRIS (pH 8.5), 1 h.

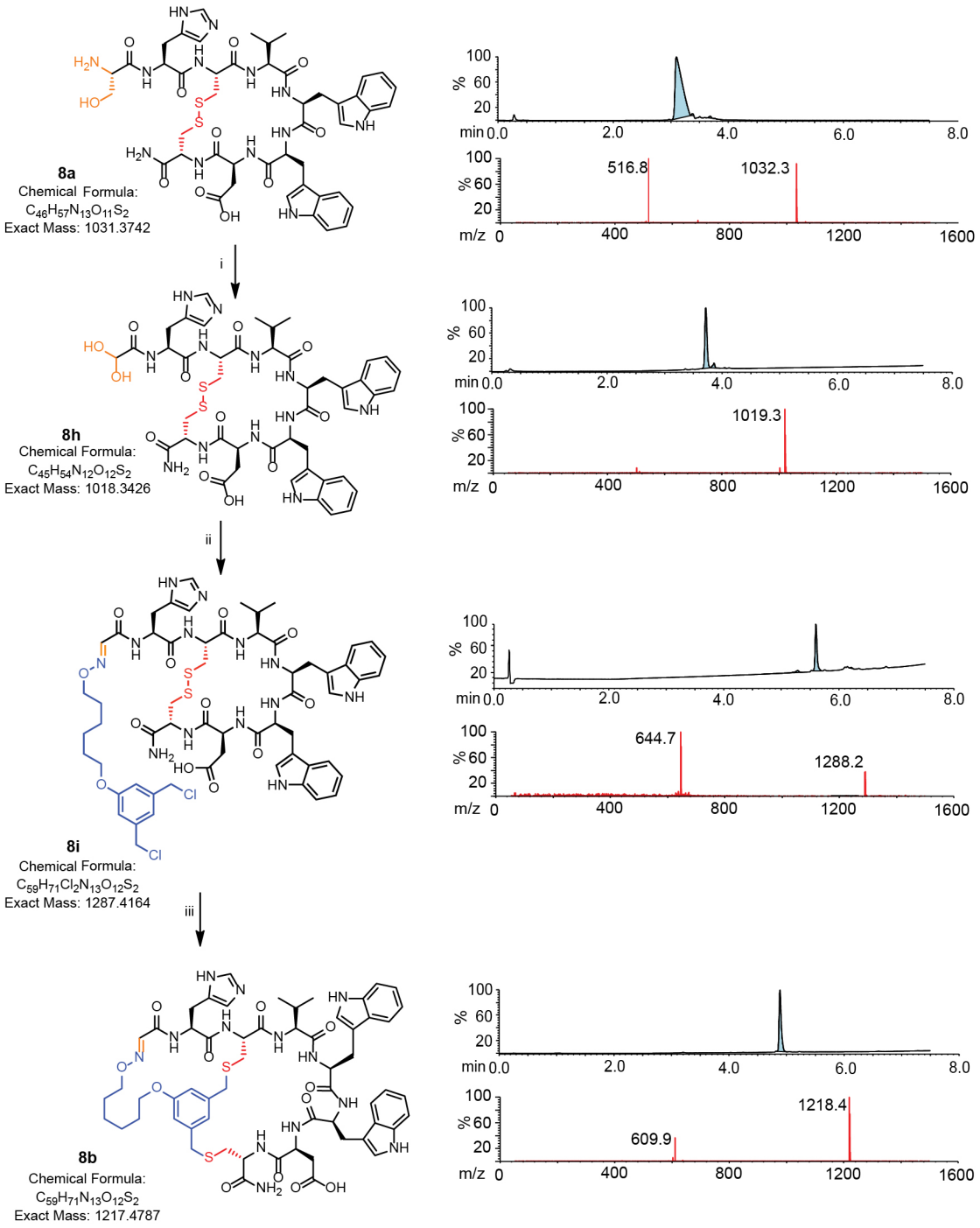

Appendix A-Scheme 14. One-pot bicyclization of **8a** (0.5 mM) with **TSL-6**.Reagents and conditions: (i) 0.6 mM $NaIO_4$, PBS (pH 7.4), 5 min. (ii) 0.1% TFA, 0.6 mM **TSL-6** (pH 4), 1 h; (iii) 2.5 mM TCEP, 30 min; 100 mM TRIS (pH 8.5), 1 h.

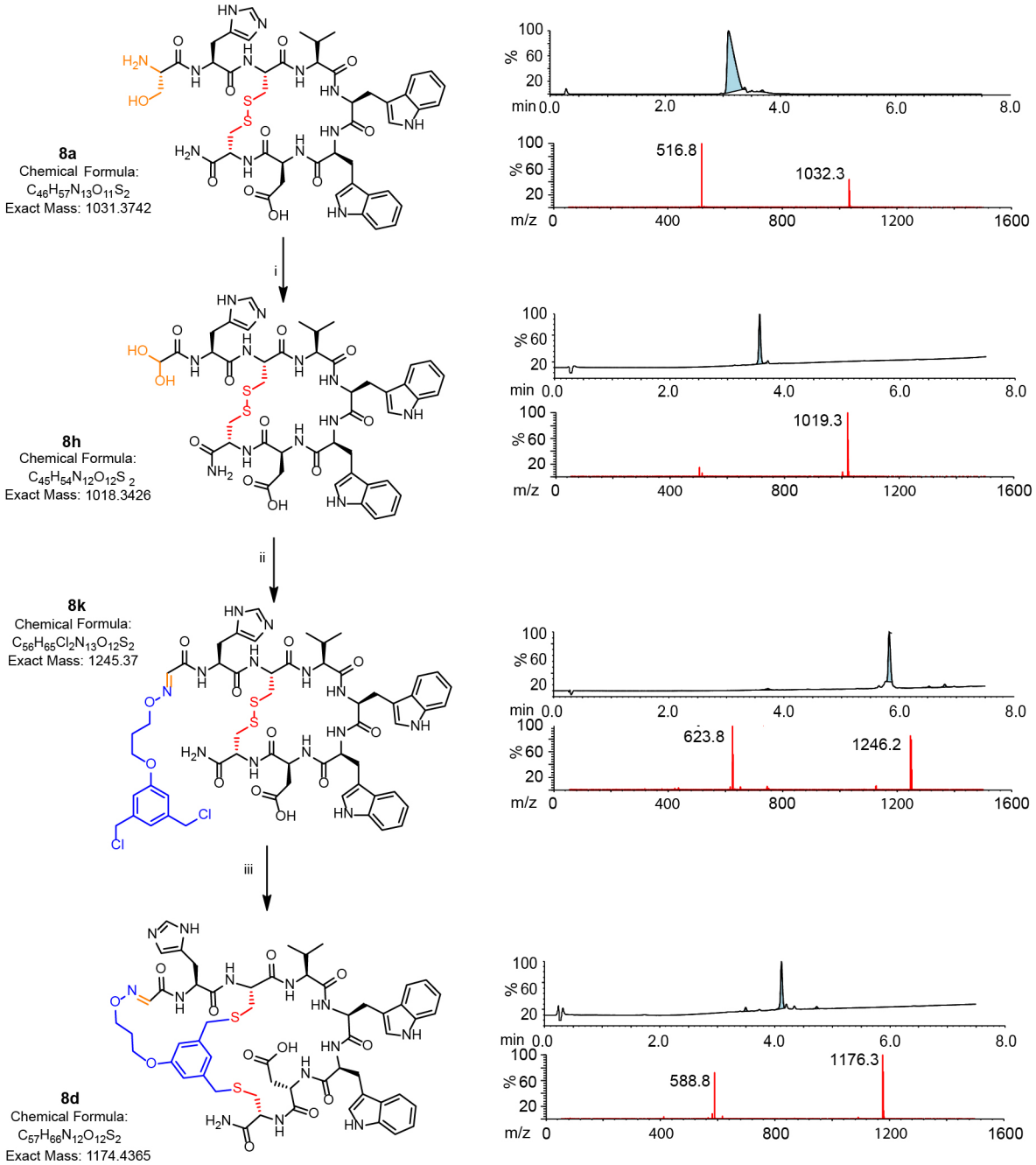

Appendix A-Scheme 15. One-pot bicyclization of **8a** (0.5 mM) with **TSL-3**. Reagents and conditions: (i) 0.6 mM $NaIO_4$, PBS (pH 7.4), 5 min. (ii) 0.1% TFA, 0.6 mM **TSL-3** (pH 4), 1 h; (iii) 2.5 mM TCEP, 30 min; 100 mM TRIS (pH 8.5), 1 h.

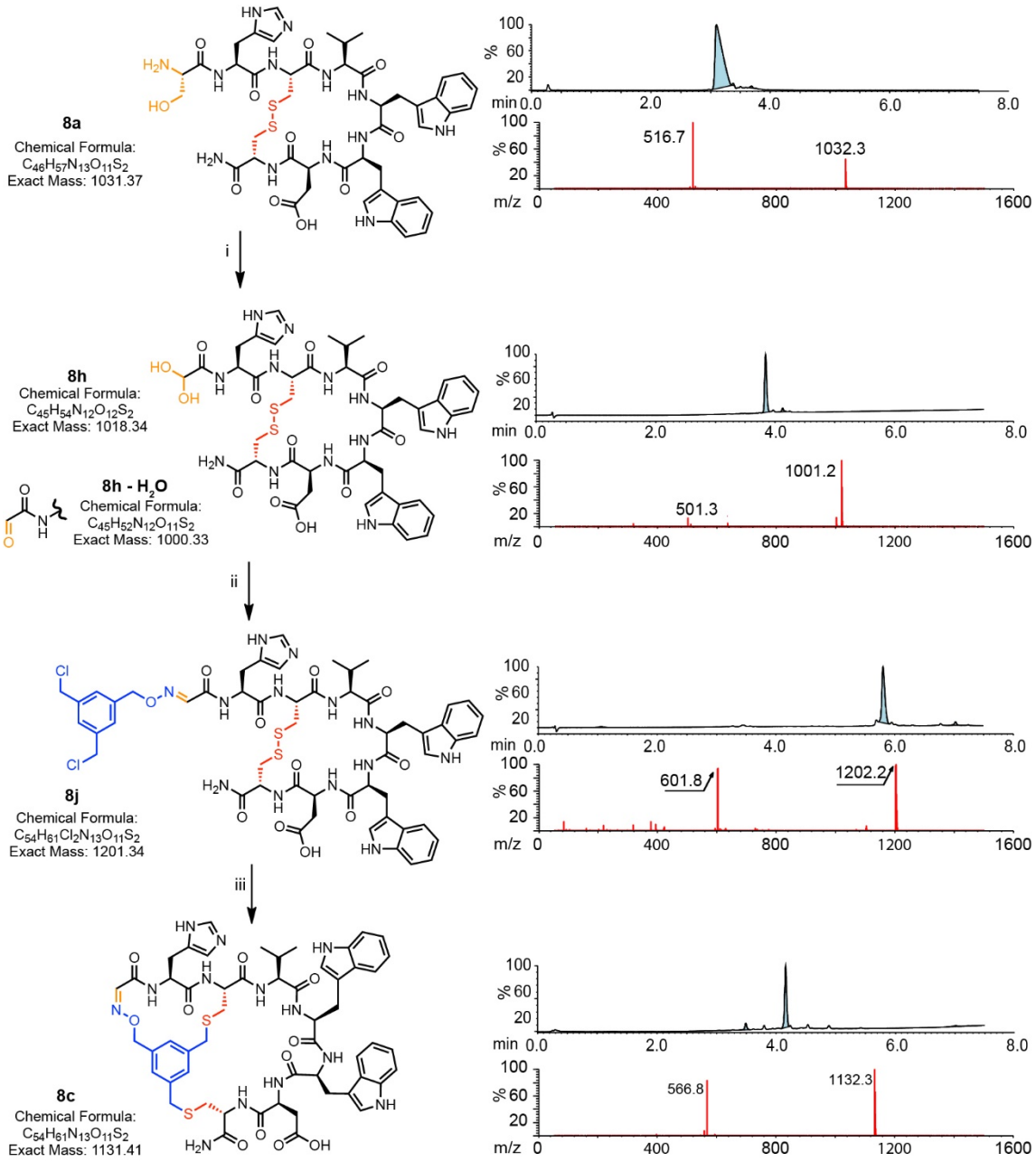

Appendix A-Scheme 16. One-pot bicyclization of **8a** (0.5 mM) with **TSL-1**. Reagents and conditions: (i) 0.6 mM $NaIO_4$, PBS (pH 7.4), 5 min. (ii) 0.1% TFA, 0.6 mM **TSL-1** (pH 4), 1 h; (iii) 2.5 mM TCEP, 30 min; 100 mM TRIS (pH 8.5), 1 h.

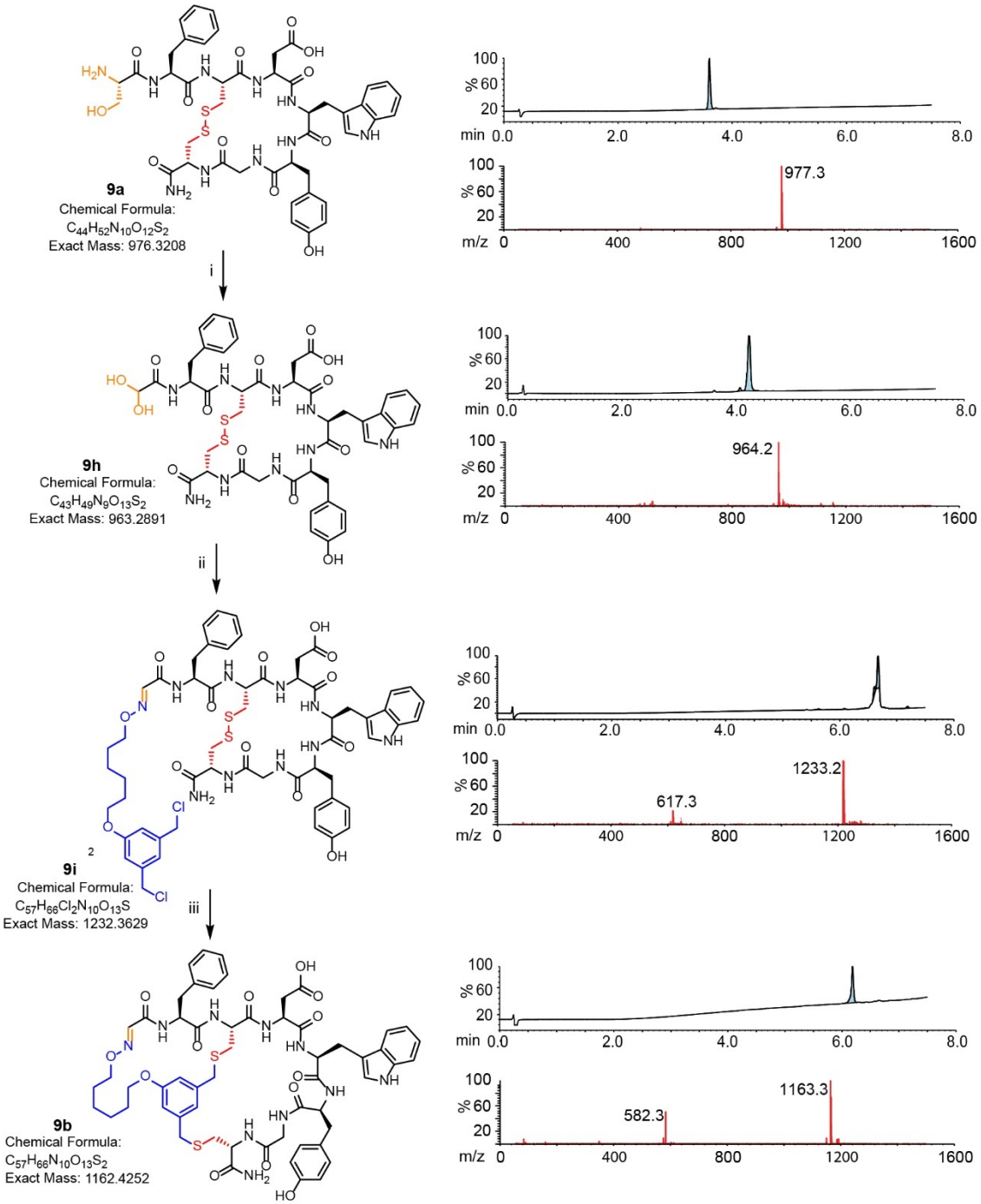

Appendix A-Scheme 17. One-pot bicyclization of **9a** (0.5 mM) with **TSL-1**. Reagents and conditions: (i) 0.6 mM $NaIO_4$, PBS (pH 7.4), 5 min. (ii) 0.1% TFA, 0.6 mM **TSL-1** (pH 4), 1 h; (iii) 2.5 mM TCEP, 30 min; 100 mM TRIS (pH 8.5), 1 h.

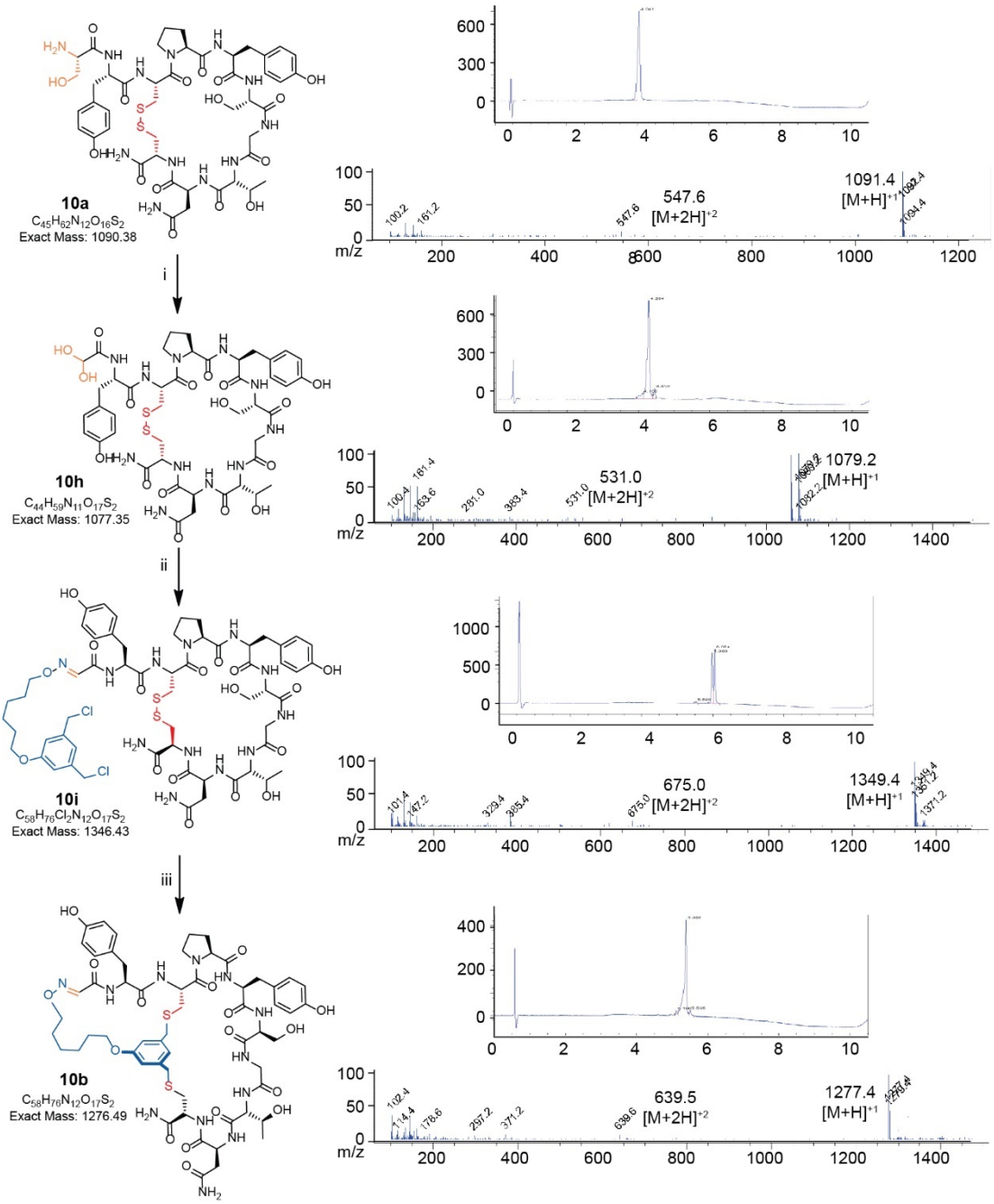

Appendix A-Scheme 18. Bicyclization of **10a** (10 mg, 84 nmol) with **TSL-6*:*** Reagents and conditions: (i) $NaIO_4$ (1.2 eq.), PBS (pH 7.4), 5 min. Met (12 eq.), 1 h. Desalting with C18 spin column (ii) 0.1% TFA, **TSL-6** (1.2 eq.), 2 h at 30 °C; (iii) TCEP (5 eq.), 1 h; 100 mM $KHCO_3$ buffer (pH 8.0), 3 h; purify w/ RP-HPLC.

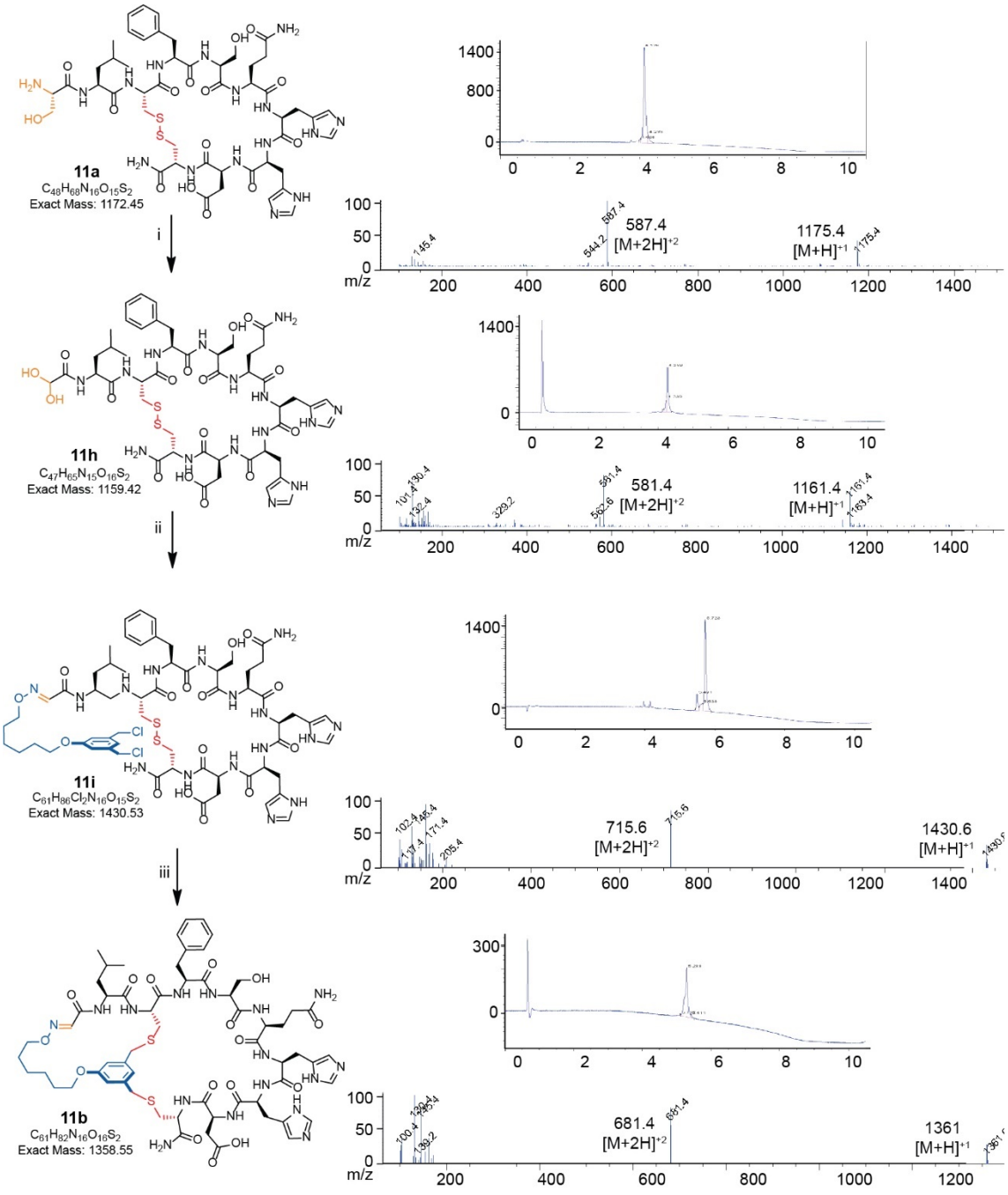

Appendix A-Scheme 19. Bicyclization of **11a** (10 mg, 66 nmol) with **TSL-6**: Reagents and conditions: (i) $NaIO_4$ (1.2 eq.), PBS (pH 7.4), 5 min, dark. Met (12 eq.), 1 h. Desalting with C18 spin column (ii) 0.1% TFA, **TSL-6** (1.2 eq.), 2 h at 30 °C; (iii) TCEP (5 eq.), 1 h; 100 mM $KHCO_3$ buffer (pH 8.0), 3 h; purify w/ RP-HPLC.

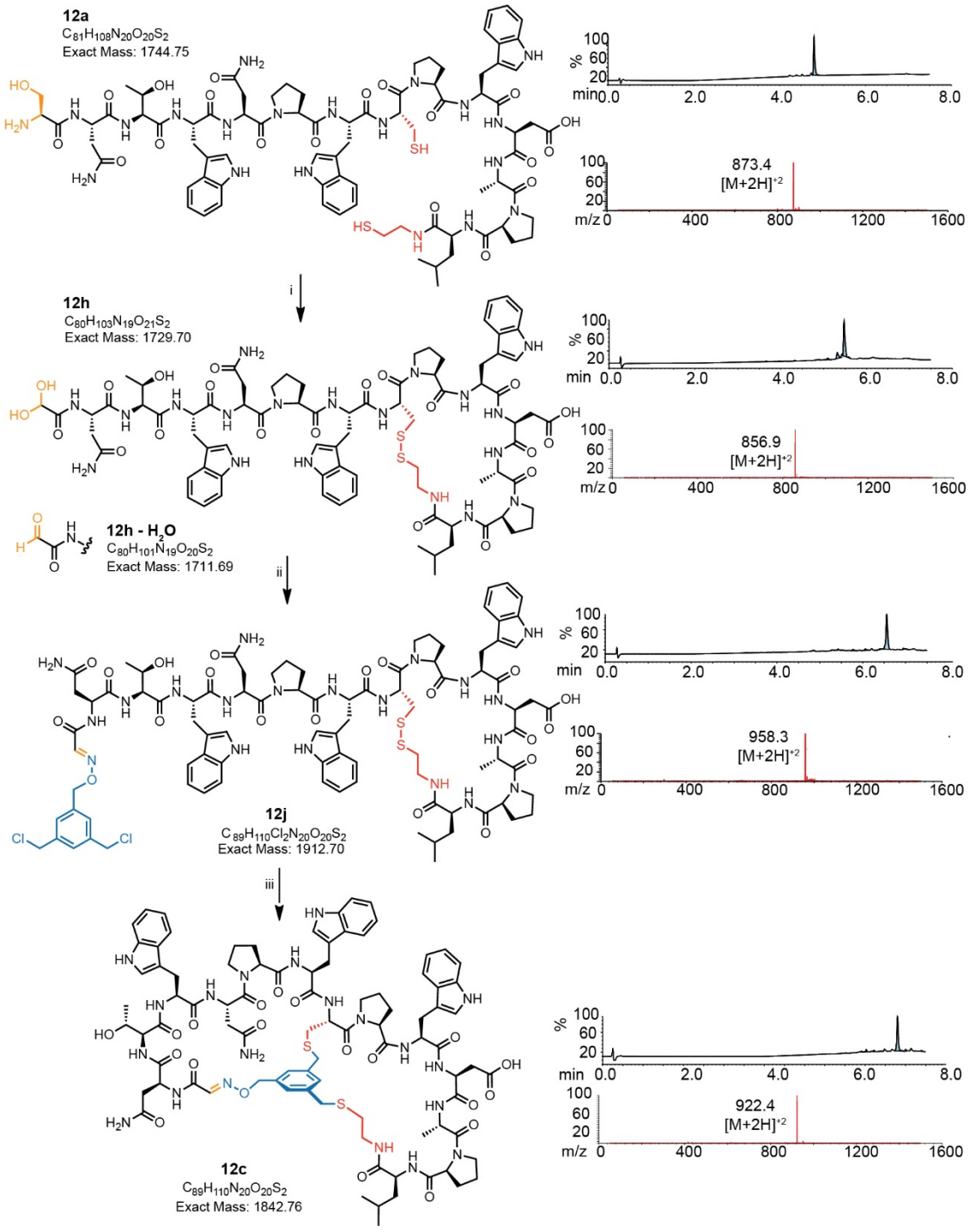

Appendix A-Scheme 20. One-pot bicyclization of **12a** with **TSL-1**: Reagents and conditions: (i) 0.6 mM $NaIO_4$, PBS (pH 7.4), 5 min, 1 mM Met, 15 min (ii) 0.1% TFA, 0.6 mM **TSL-1** (pH 4), 1 h; (iii) 2.5 mM TCEP, 30 min; 100 mM $NaHCO_3$ (pH 10), 30 min.

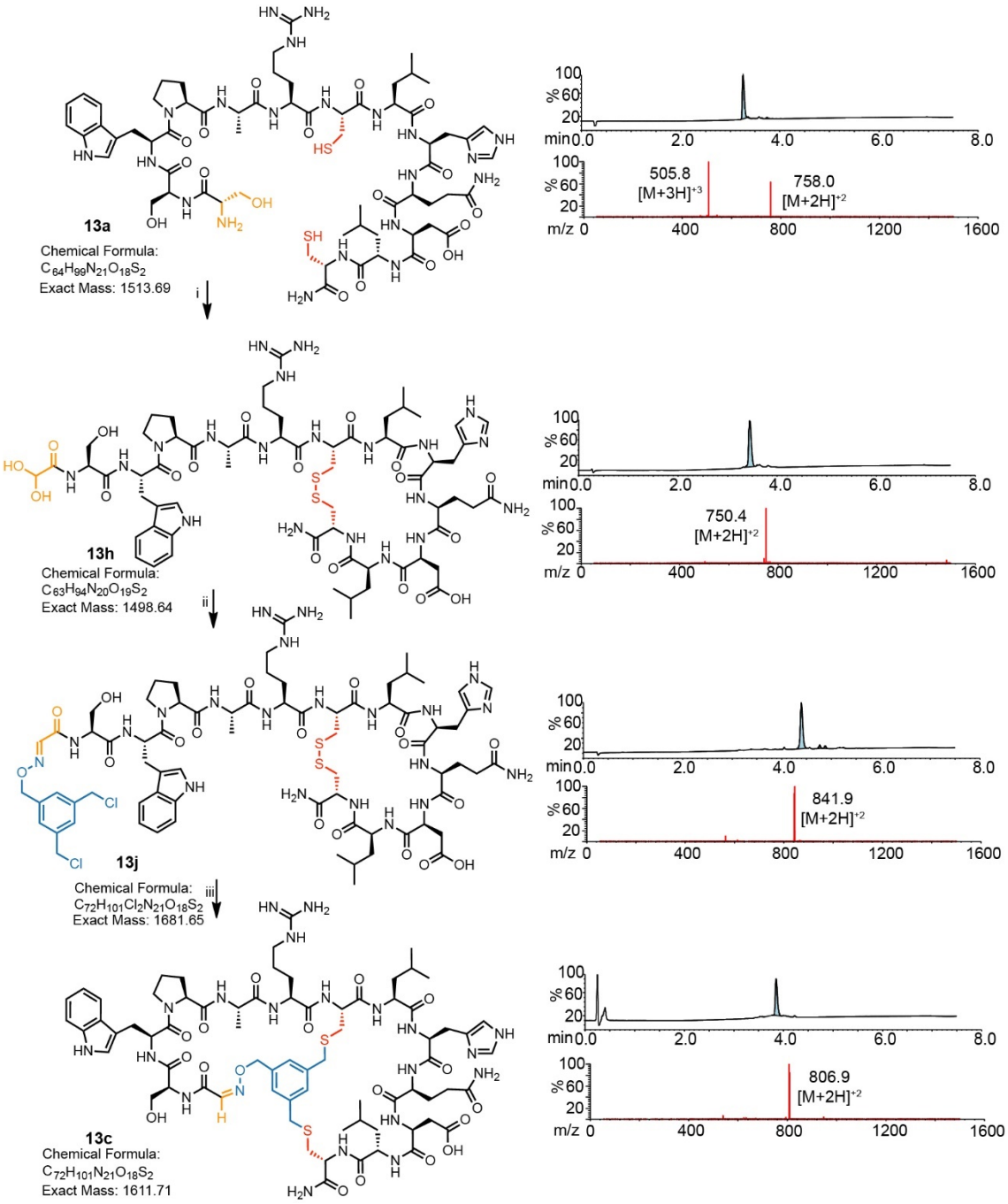

Appendix A-Scheme 21. One-pot bicyclization of **13a** with **TSL-1**: Reagents and conditions: (i) 0.6 mM $NaIO_4$, PBS (pH 7.4), 5 min, 1 mM Met, 15 min (ii) 0.1% TFA, 0.6 mM **TSL-1** (pH 4), 1 h; (iii) 2.5 mM TCEP, 30 min; 100 mM $NaHCO_3$ (pH 10), 1 h.

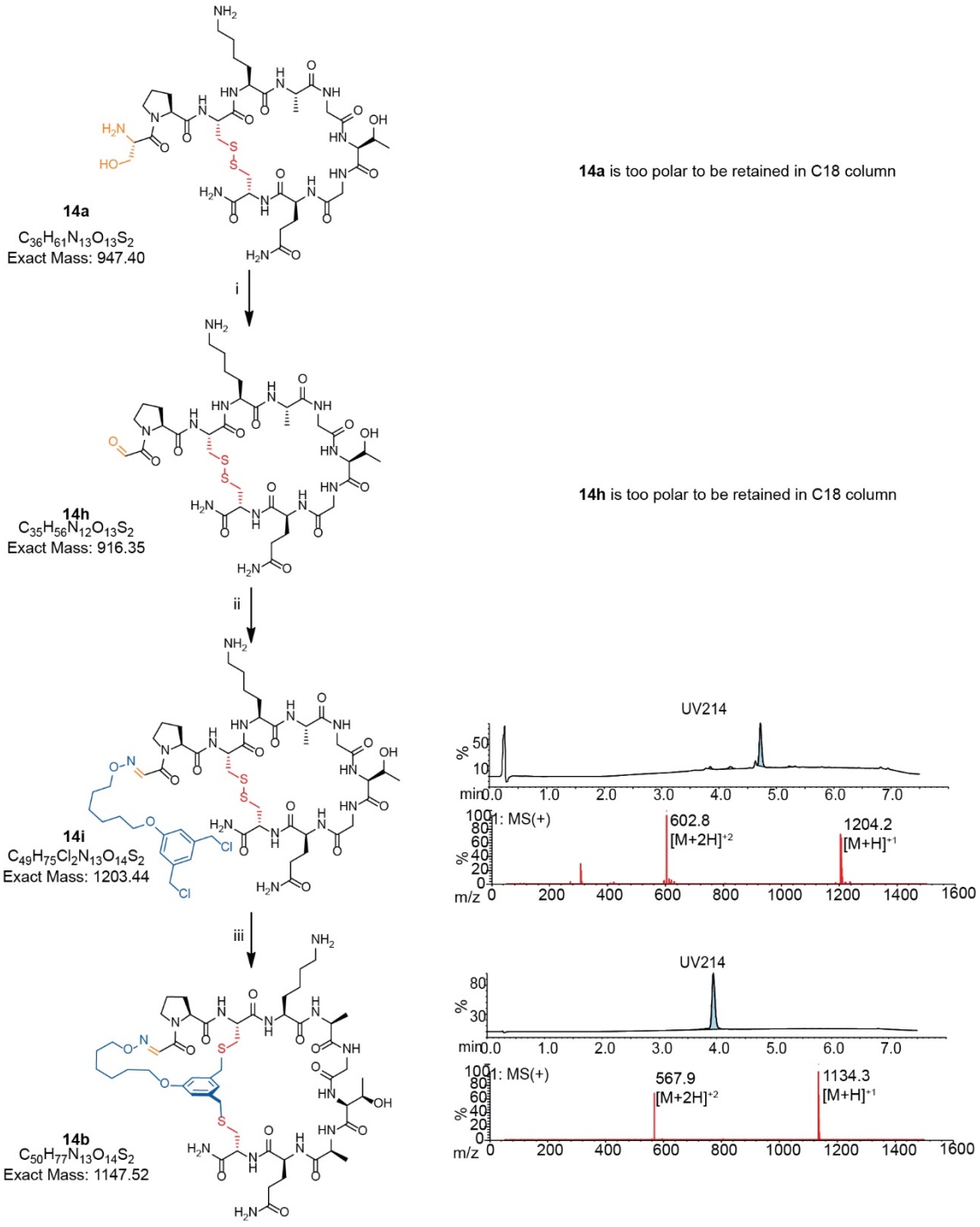

Appendix A-Scheme 22. Bicyclization of **14a** with **TSL-6** : Reagents and conditions: (i) 2.4 mM $NaIO_4$, PBS (pH 7.4), 5 min, 1 mM Met, 15 min (ii) 0.1% TFA, 2.4 mM **TSL-6**, 1 h; (iii) 2.5 mM TCEP, 30 min; 100 mM $NaHCO_3$ (pH 10), O/N; purify w/ RP-HPLC.

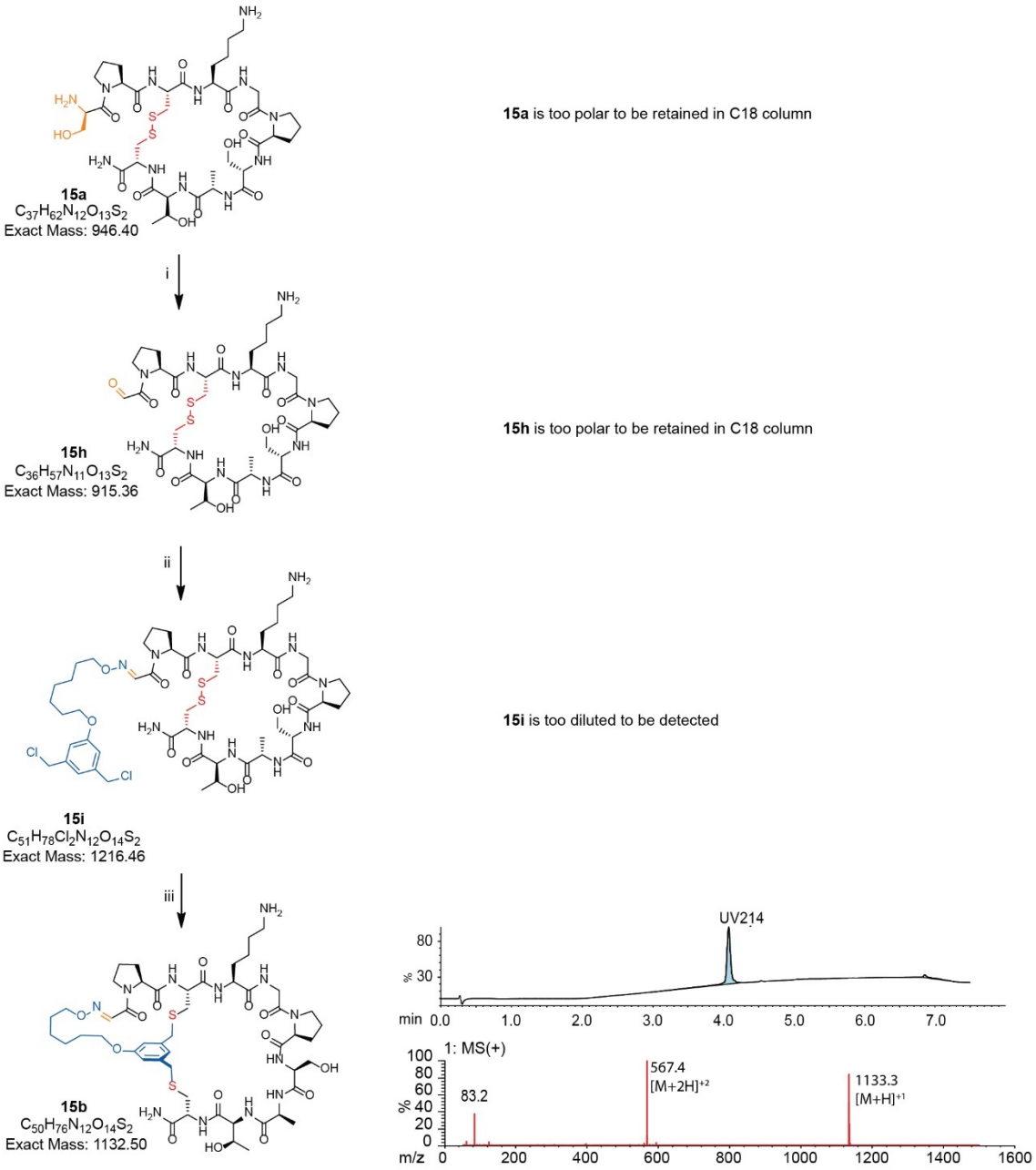

Appendix A-Scheme 23. Bicyclization of **15a** with **TSL-6**: Reagents and conditions: (i) 2.4 mM $NaIO_4$, PBS (pH 7.4), 5 min, 1 mM Met, 15 min, 15 min (ii) 0.1% TFA, 2.4 mM **TSL-6**, 1 h; (iii) 2.5 mM TCEP, 30 min; 100 mM NaHCO3 (pH 10), O/N; Purify w/ RP-HPLC.

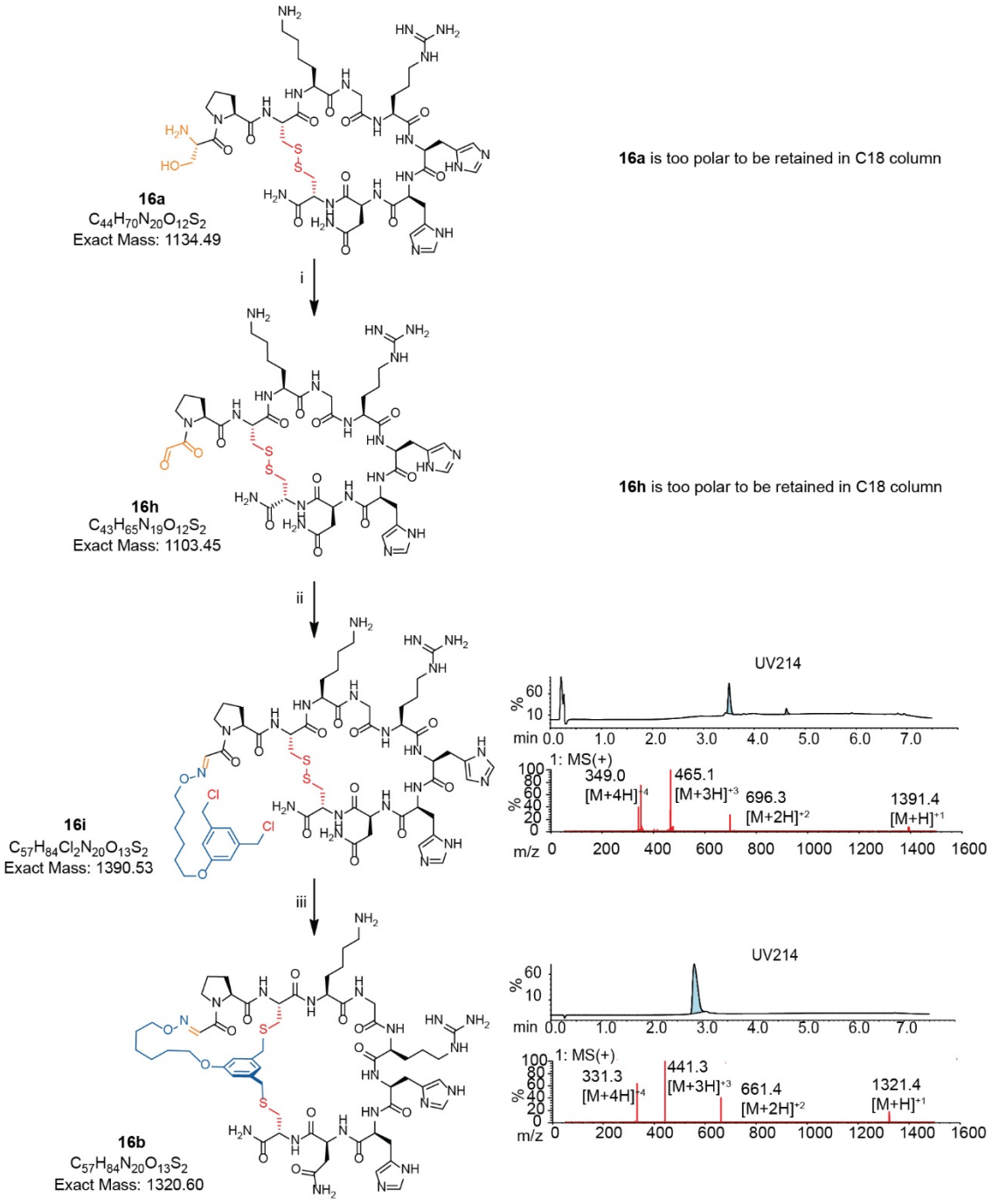

Appendix A-Scheme 24. Bicyclization of **16a** with **TSL-6** : Reagents and conditions: (i) 2.4 mM $NaIO_4$, PBS (pH 7.4), 5 min, 1 mM Met, 15 min (ii) 0.1% TFA, 2.4 mM **TSL-6**, 1 h; (iii) 2.5 mM TCEP, 30 min; 100 mM $NaHCO_3$ (pH 10), O/N; purify w/ RP-HPLC.

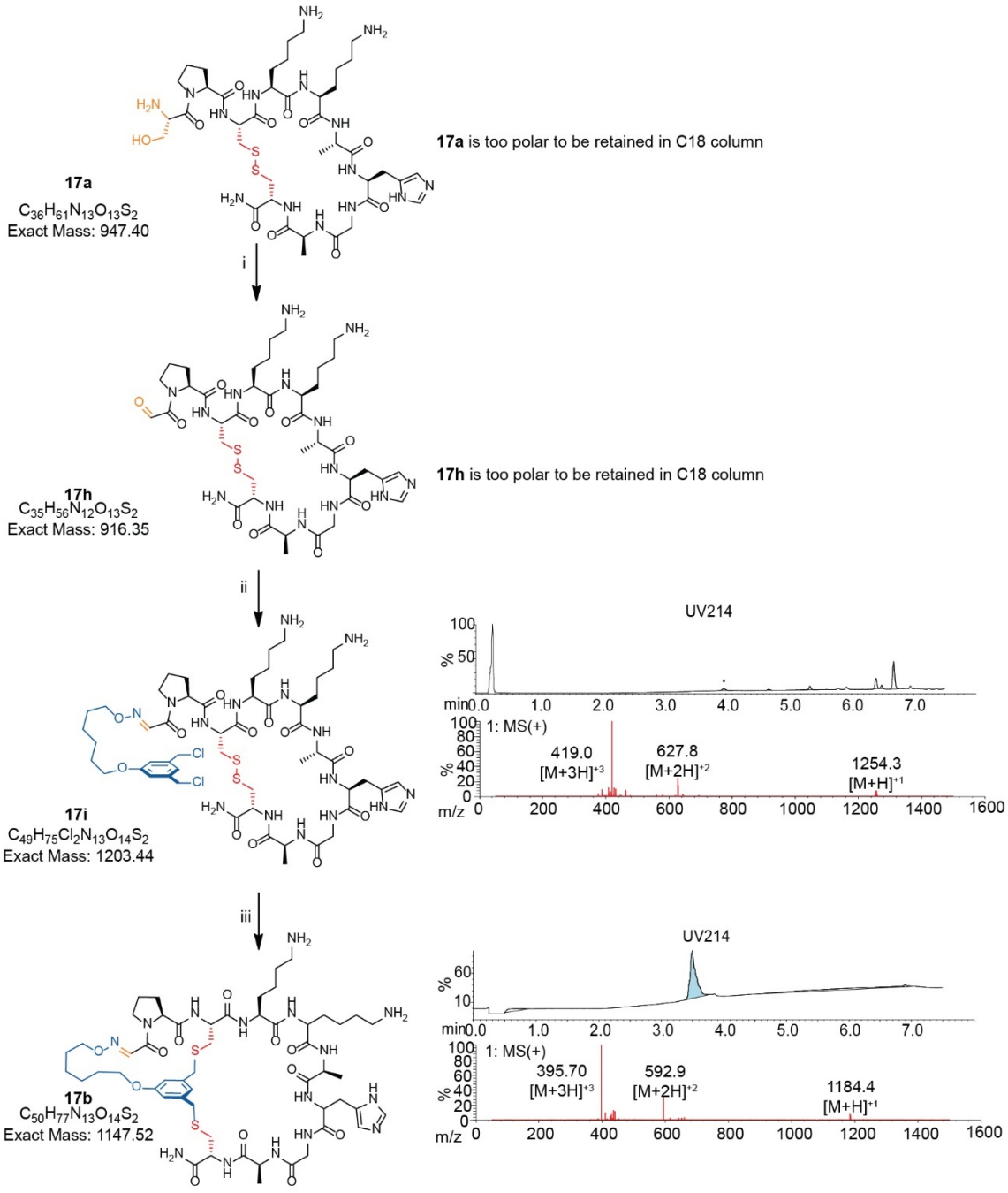

Appendix A-Scheme 25. Bicyclization of **17a** with **TSL-6** : Reagents and conditions: (i) 2.4 mM $NaIO_4$, PBS (pH 7.4), 5 min, 1 mM Met, 15 min (ii) 0.1% TFA, 2.4 mM **TSL-6**, 1 h; (iii) 2.5 mM TCEP, 30 min; 100 mM $NaHCO_3$ (pH 10), O/N.

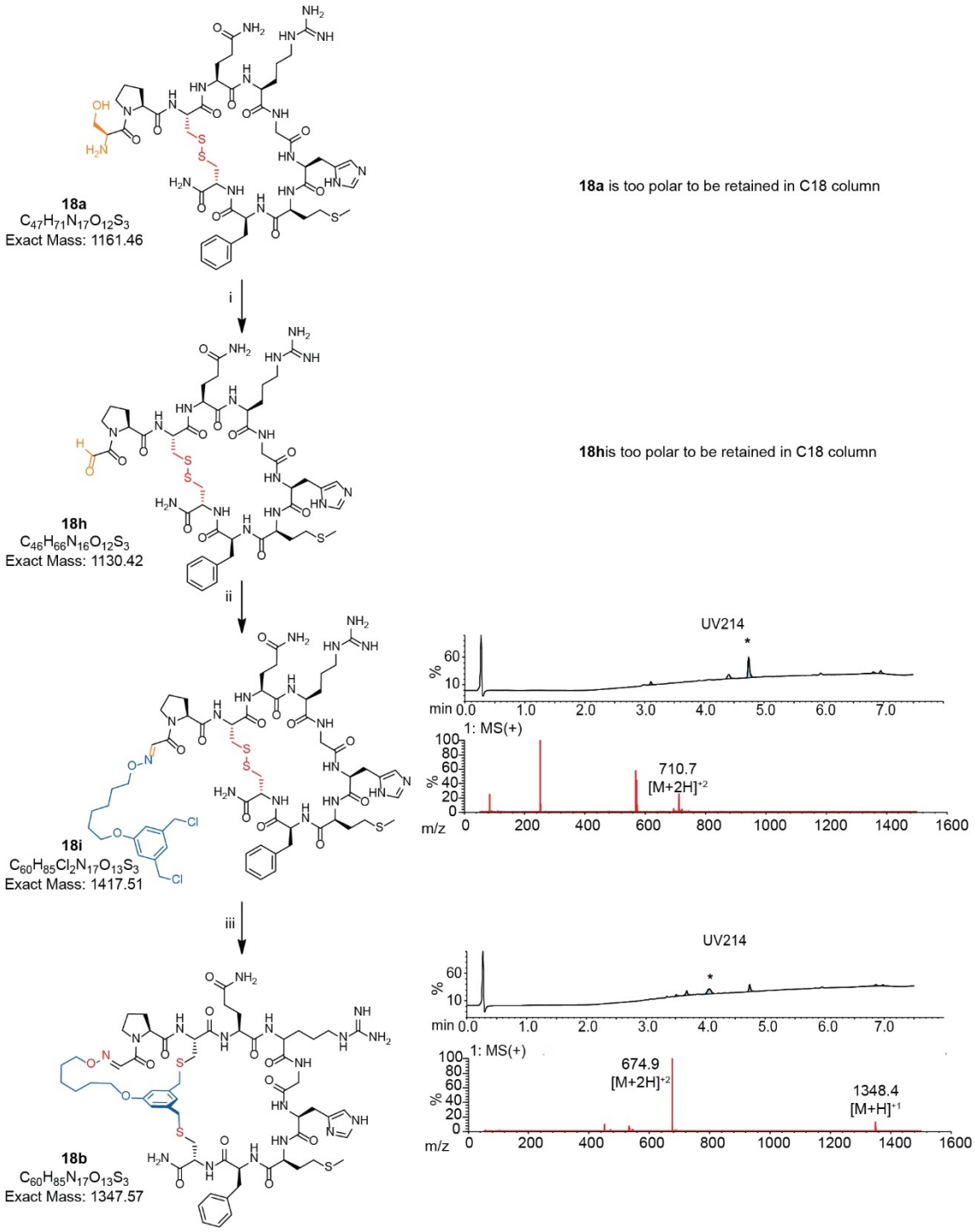

Appendix A-Scheme 26. Bicyclization of **18a** with **TSL-6**: Reagents and conditions: (i) 2.4 mM $NaIO_4$, PBS (pH 7.4), 10 sec on ice, 1 mM Met, 15 min (ii) 0.1% TFA, 2.4 mM **TSL-6**, 1 h; (iii) 2.5 mM TCEP, 30 min; 100 mM $NaHCO_3$ (pH 10), O/N; purify w/ RP-HPLC.

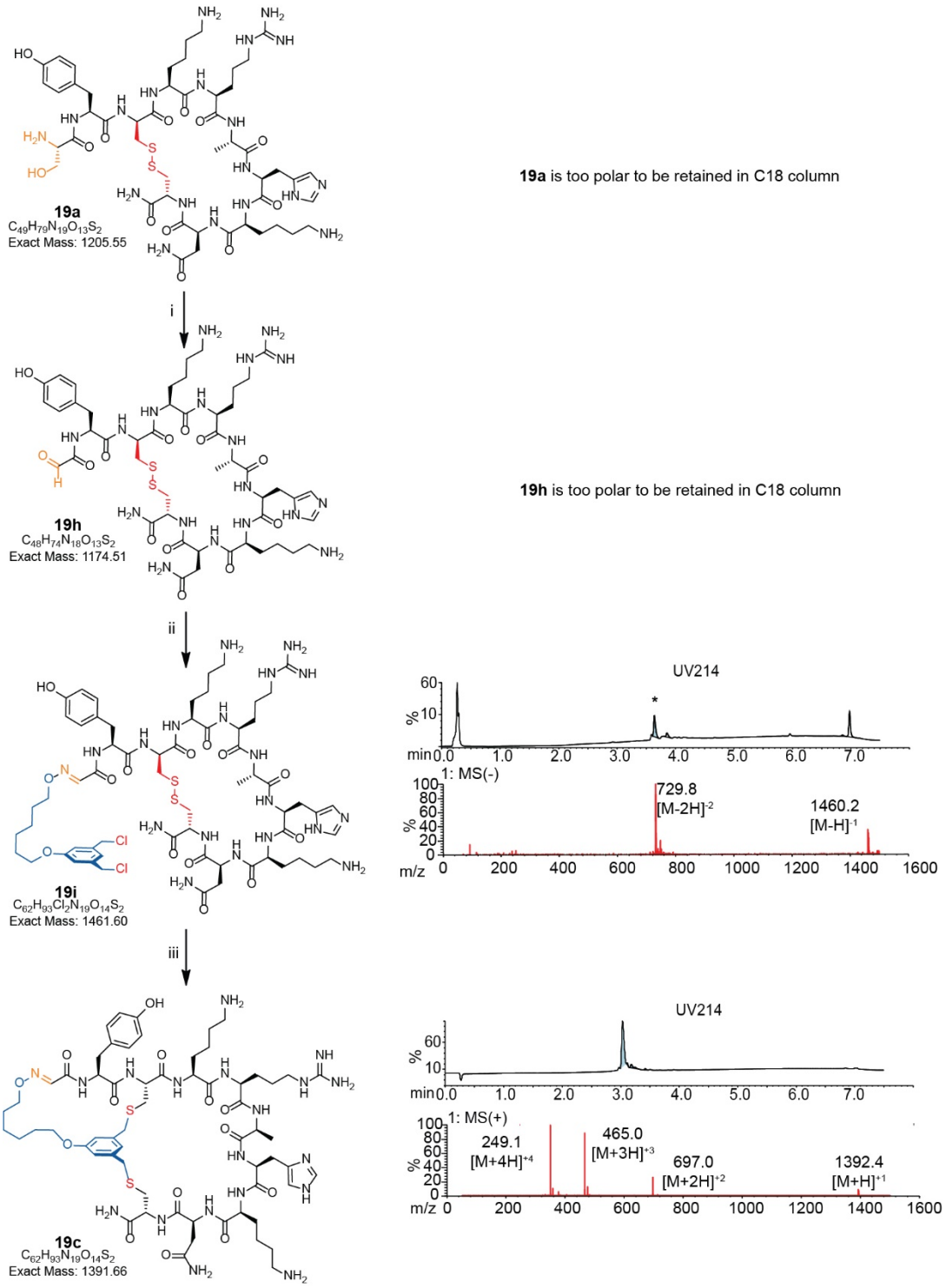

Appendix A-Scheme 27. Bicyclization of **19a** with **TSL-6**: Reagents and conditions: (i) 2.4 mM $NaIO_4$, PBS (pH 7.4), 5 min, 1 mM Met, 15 min (ii) 0.1% TFA, 2.4 mM **TSL-6**, 1 h; (iii) 2.5 mM TCEP, 30 min; 100 mM $NaHCO_3$ (pH 10), O/N; purify w/ RP-HPLC.

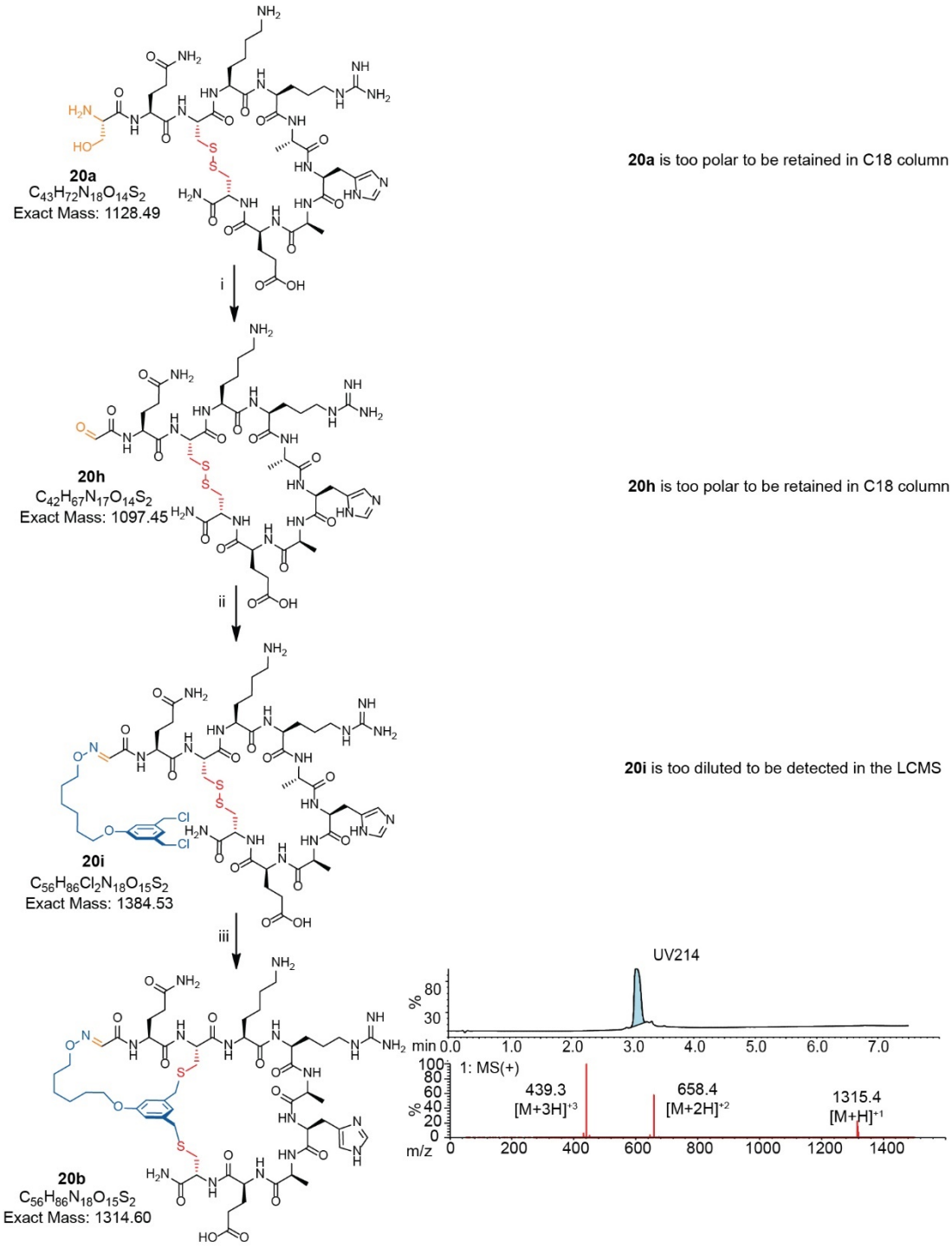

Appendix A-Scheme 28. Bicyclization of **20a** with **TSL-6**: Reagents and conditions: (i) 2.4 mM $NaIO_4$, PBS (pH 7.4), 5 min, 1 mM Met, 15 min (ii) 0.1% TFA, 2.4 mM **TSL-6**, 1 h; (iii) 2.5 mM TCEP, 30 min; 100 mM $NaHCO_3$ (pH 10), O/N; Purify w/ RP-HPLC.

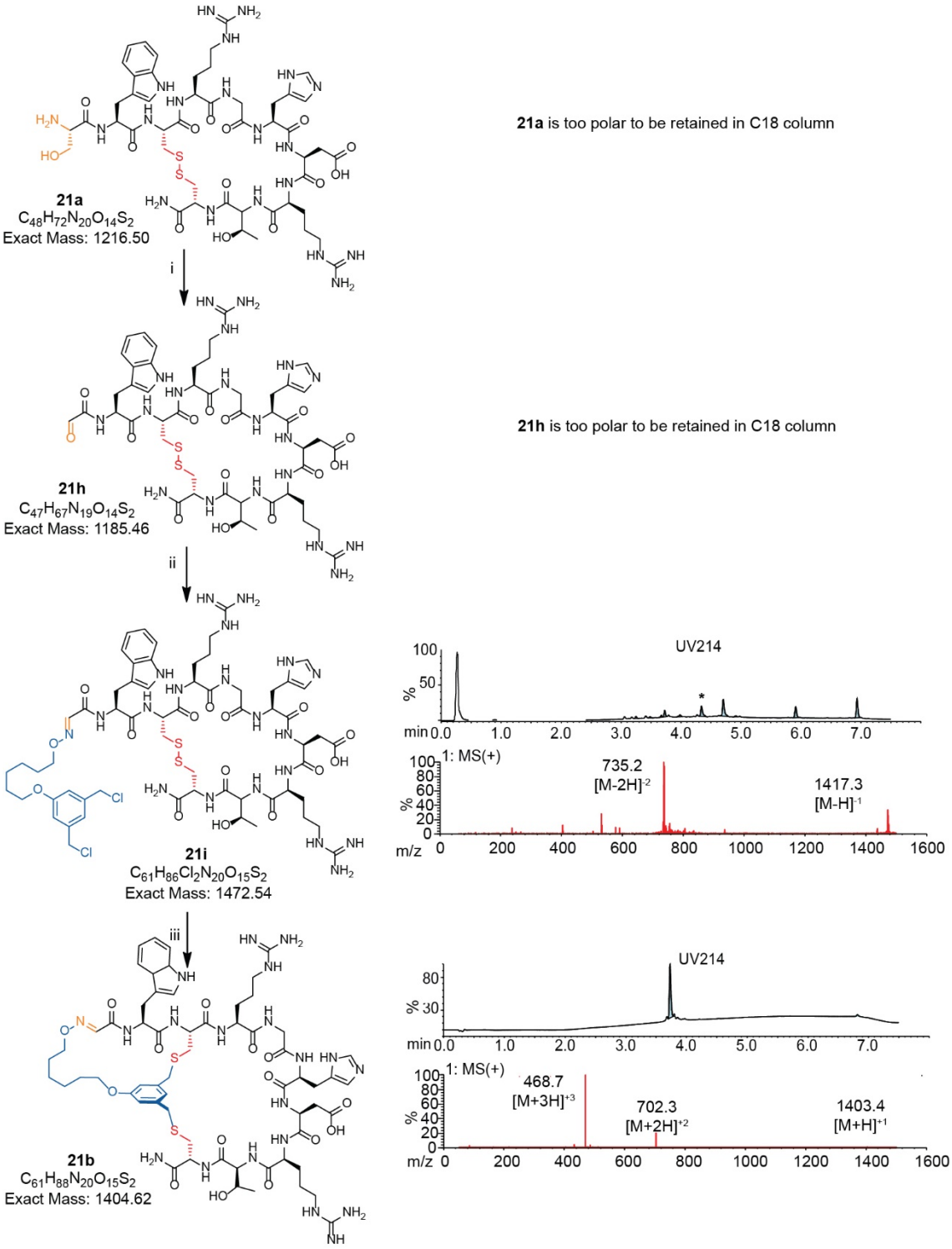

Appendix A-Scheme 29. Bicyclization of **21a** with **TSL-6**: Reagents and conditions: (i) 2.4 mM $NaIO_4$, PBS (pH 7.4), 5 min, 1 mM Met, 15 min (ii) 0.1% TFA, 2.4 mM **TSL-6**, 1 h; (iii) 2.5 mM TCEP, 30 min; 100 mM $NaHCO_3$ (pH 10), O/N.

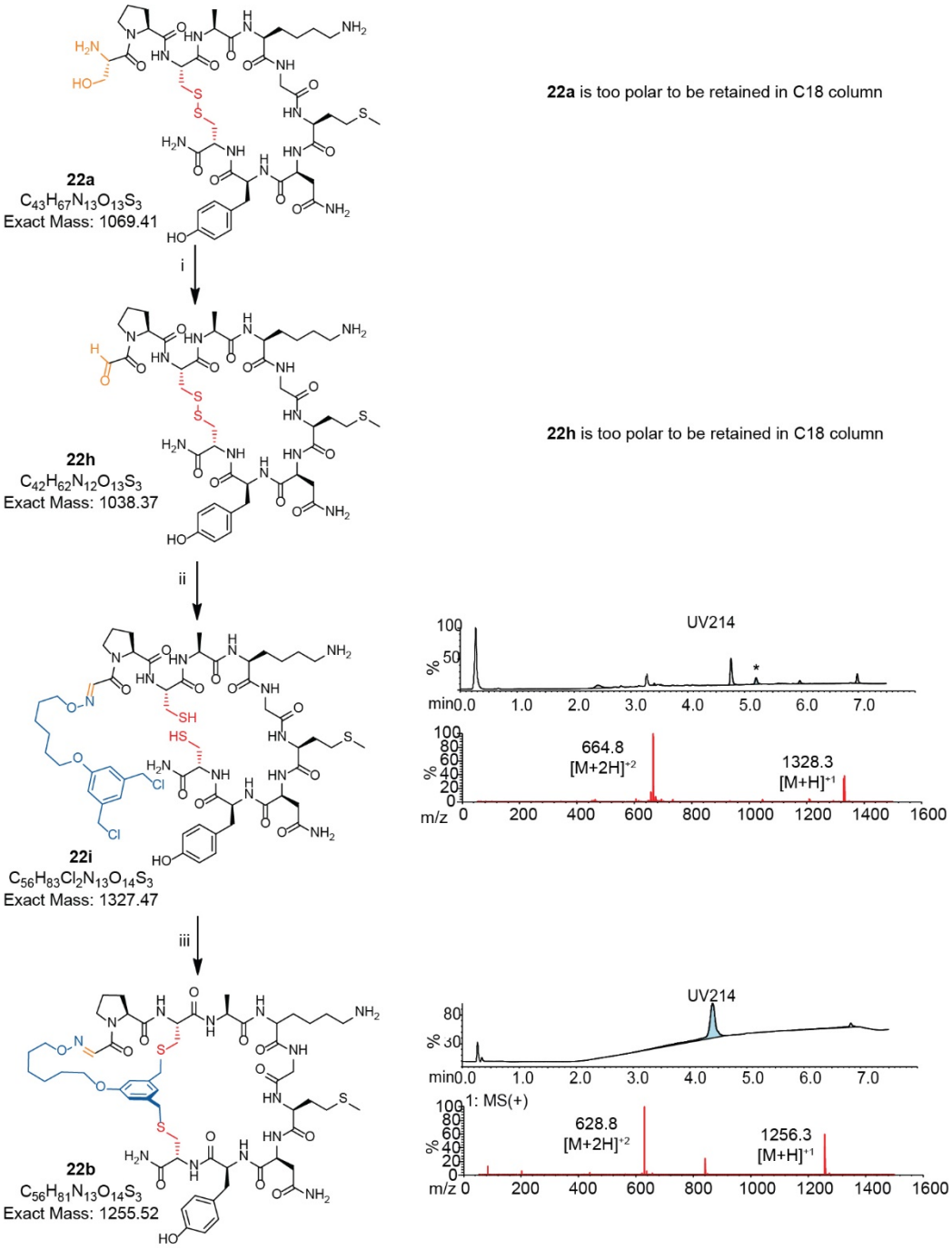

Appendix A-Scheme 30. Bicyclization of **22a** with **TSL-6**: Reagents and conditions: (i) 2.4 mM $NaIO_4$, PBS (pH 7.4), 5 min, 1 mM Met, 15 min (ii) 0.1% TFA, 2.4 mM **TSL-6**, 1 h; 2.5 mM TCEP, 30 min; (iii) 100 mM $NaHCO_3$ (pH 10), O/N.

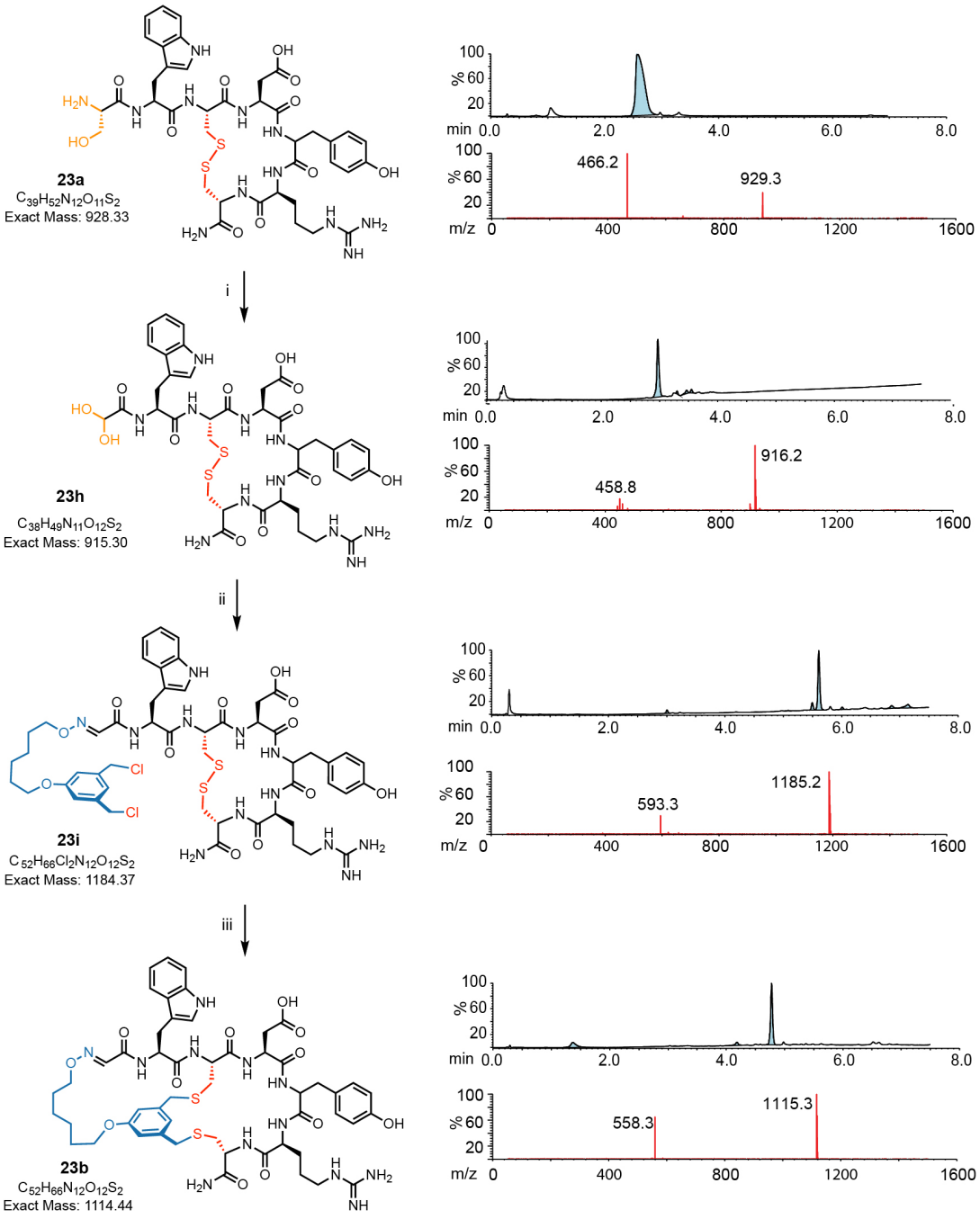

Appendix A-Scheme 31. One-pot bicyclization of **23a** (0.5 mM) with **TSL-6**. Reagents and conditions: (i) 0.6 mM $NaIO_4$, PBS (pH 7.4), 5 min. (ii) 0.1% TFA, 0.6 mM **TSL-6** (pH 4), 1 h; (iii) 2.5 mM TCEP, 30 min; 100 mM TRIS (pH 8.5), 1 h.

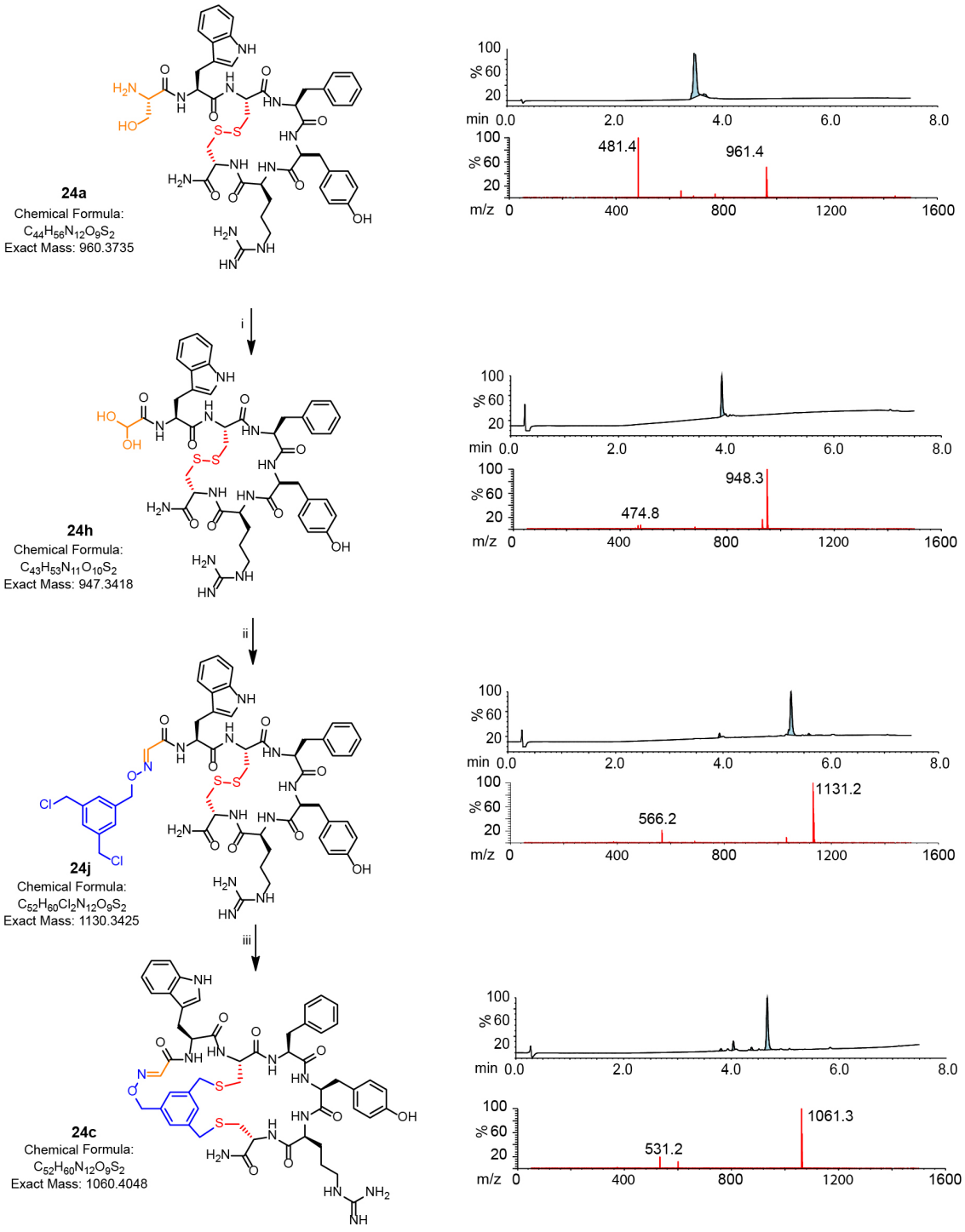

Appendix A-Scheme 32. One-pot bicyclization of **24a** (0.5 mM) with **TSL-6**. Reagents and conditions: (i) 0.6 mM $NaIO_4$, PBS (pH 7.4), 5 min. (ii) 0.1% TFA, 0.6 mM **TSL-6** (pH 4), 1 h; (iii) 2.5 mM TCEP, 30 min; 100 mM TRIS (pH 8.5), 1 h.

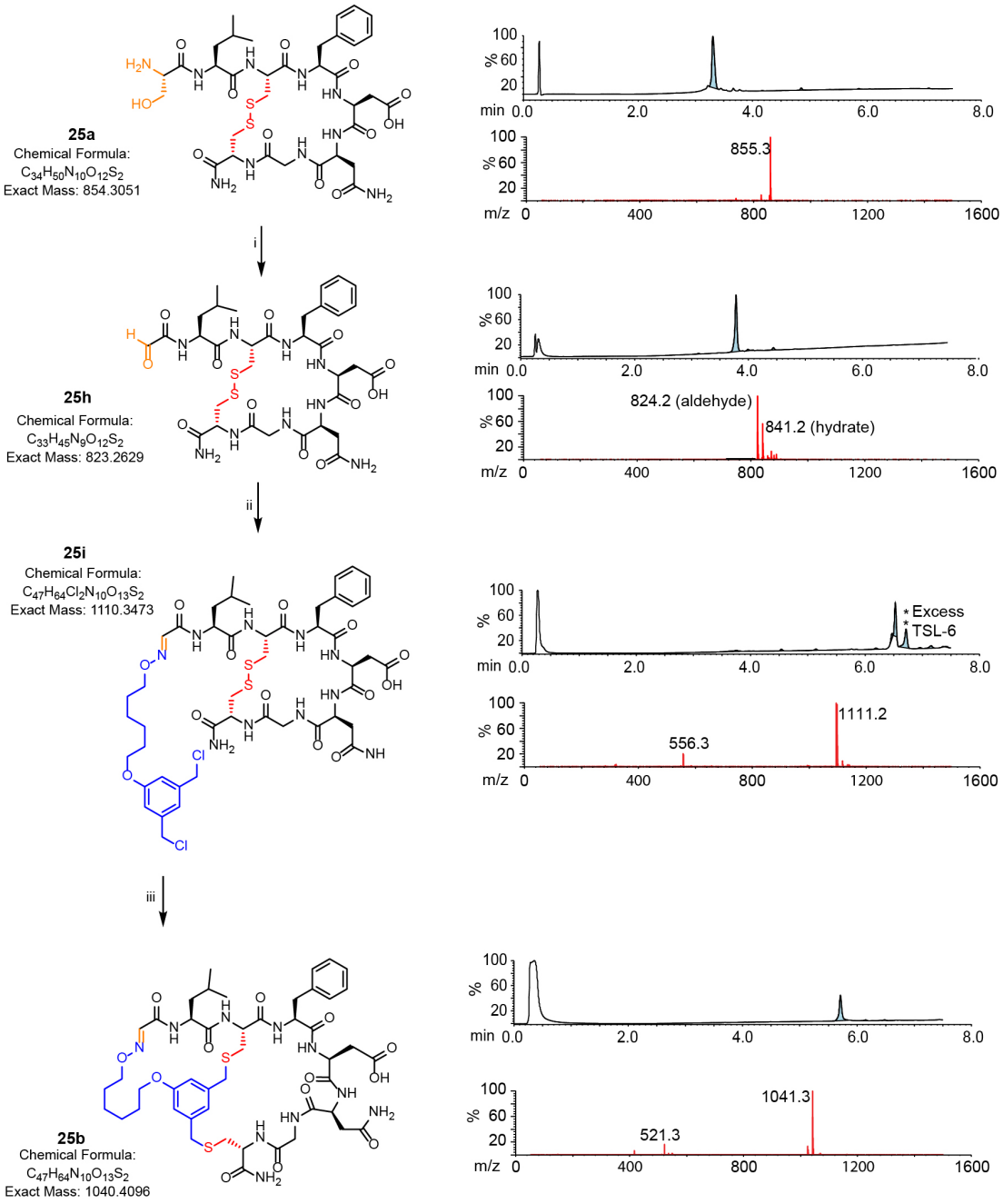

Appendix A-Scheme 33. One-pot bicyclization of **25a** (0.5 mM) with **TSL-6**. Reagents and conditions: (i) 0.6 mM $NaIO_4$, PBS (pH 7.4), 5 min. (ii) 0.1% TFA, 0.6 mM **TSL-6** (pH 4), 1 h; (iii) 2.5 mM TCEP, 30 min; 100 mM TRIS (pH 8.5), 1 h.

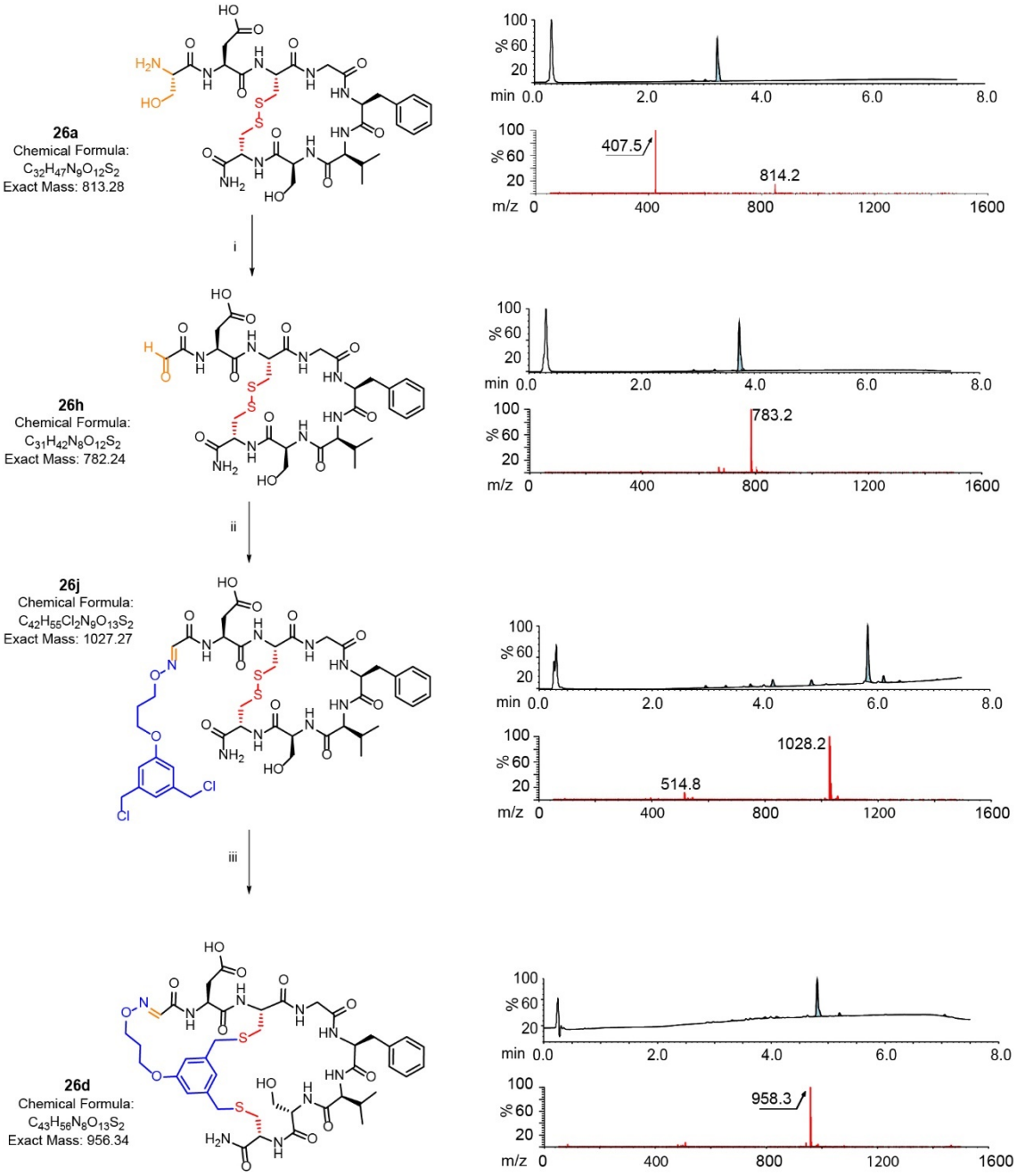

Appendix A-Scheme 34. One-pot bicyclization of **26a** (0.5 mM) with **TSL-3**. Reagents and conditions: (i) 0.6 mM $NaIO_4$, PBS (pH 7.4), 5 min. (ii) 0.1% TFA, 0.6 mM **TSL-3** (pH 4), 1 h; (iii) 2.5 mM TCEP, 30 min; 100 mM TRIS (pH 8.5), 1 h.

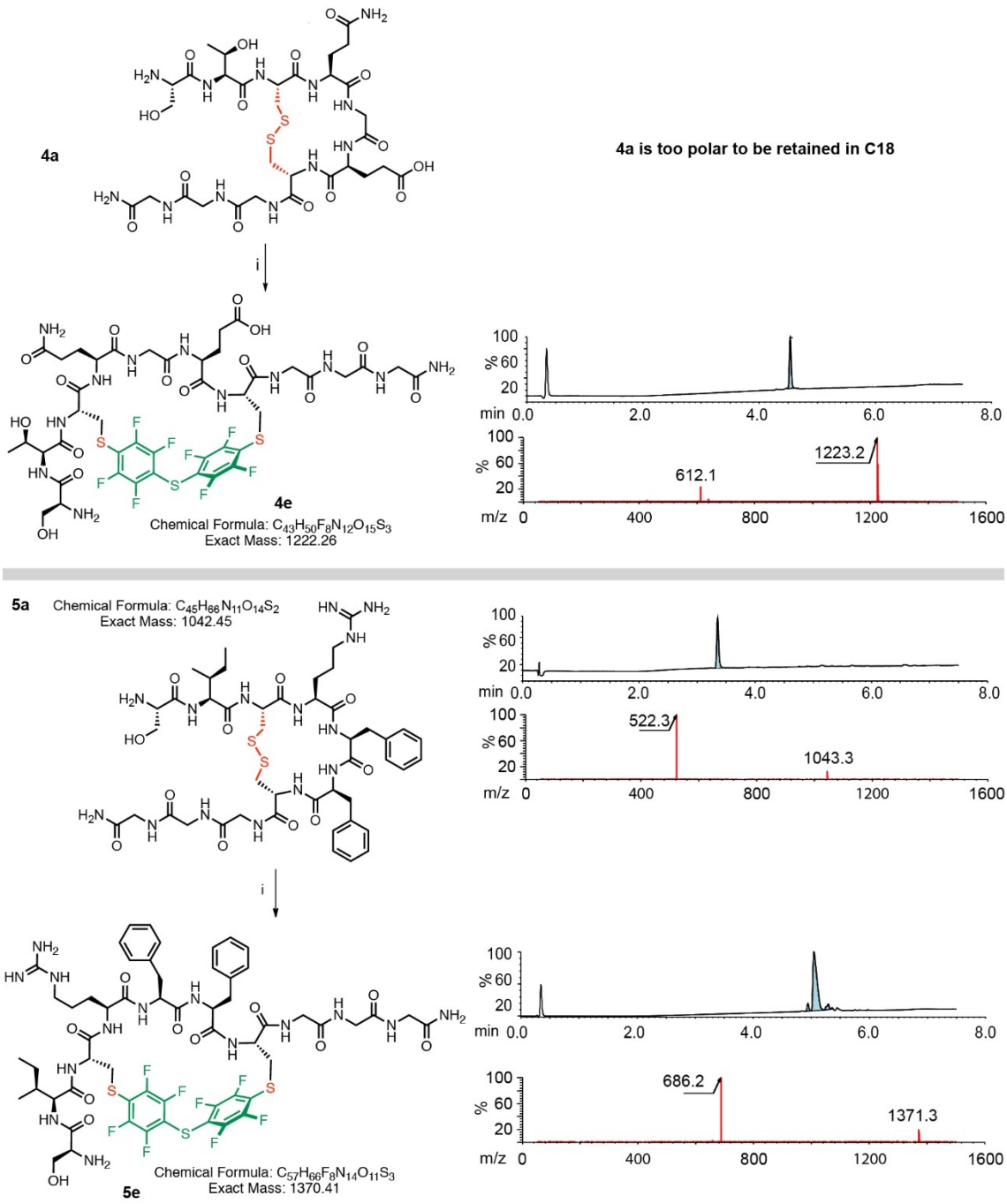

Appendix A-Scheme 35. Cyclization of **4a** and **5a** with **PFS** : For reagents and conditions see General Protocol for cyclization with pentaflurophenyl-sulfide (**PFS**).

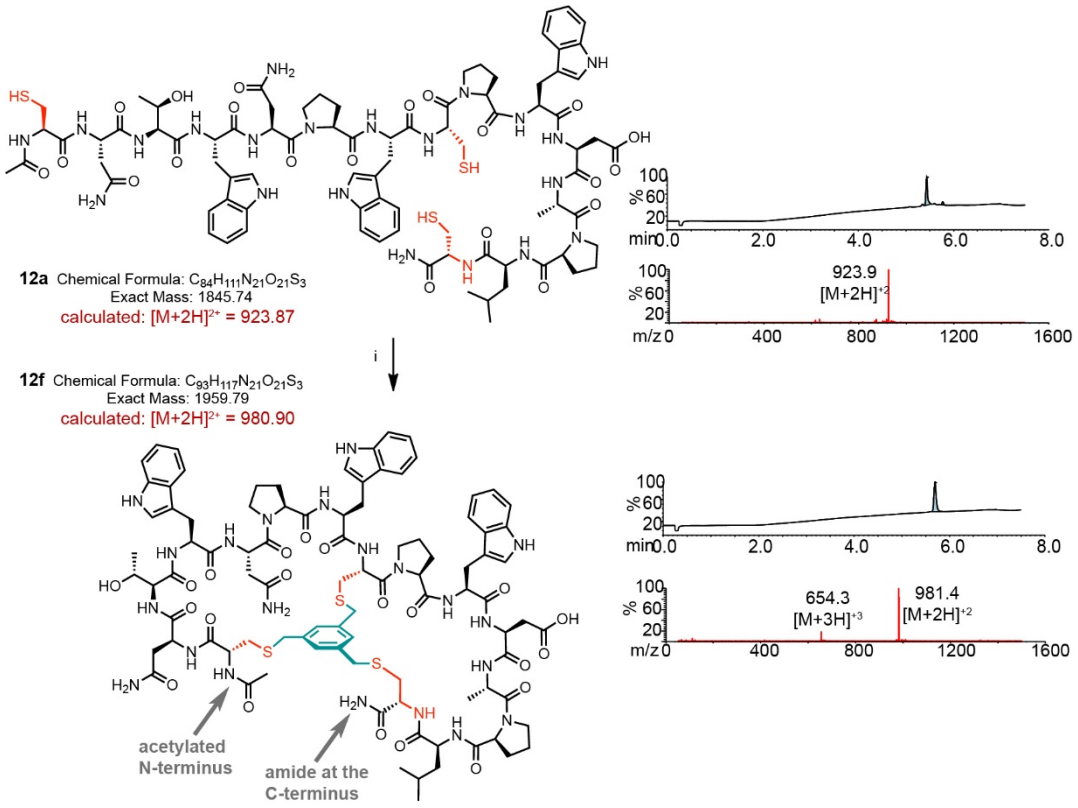

Appendix A-Scheme 36. Bicyclization of **23a** with **TBMB**: Reagents and conditions: 2.5 mM TCEP, 100 mM NaHCO3 (pH 10), 20 h. For details, see: General Protocol for bicyclization with **TBMB**

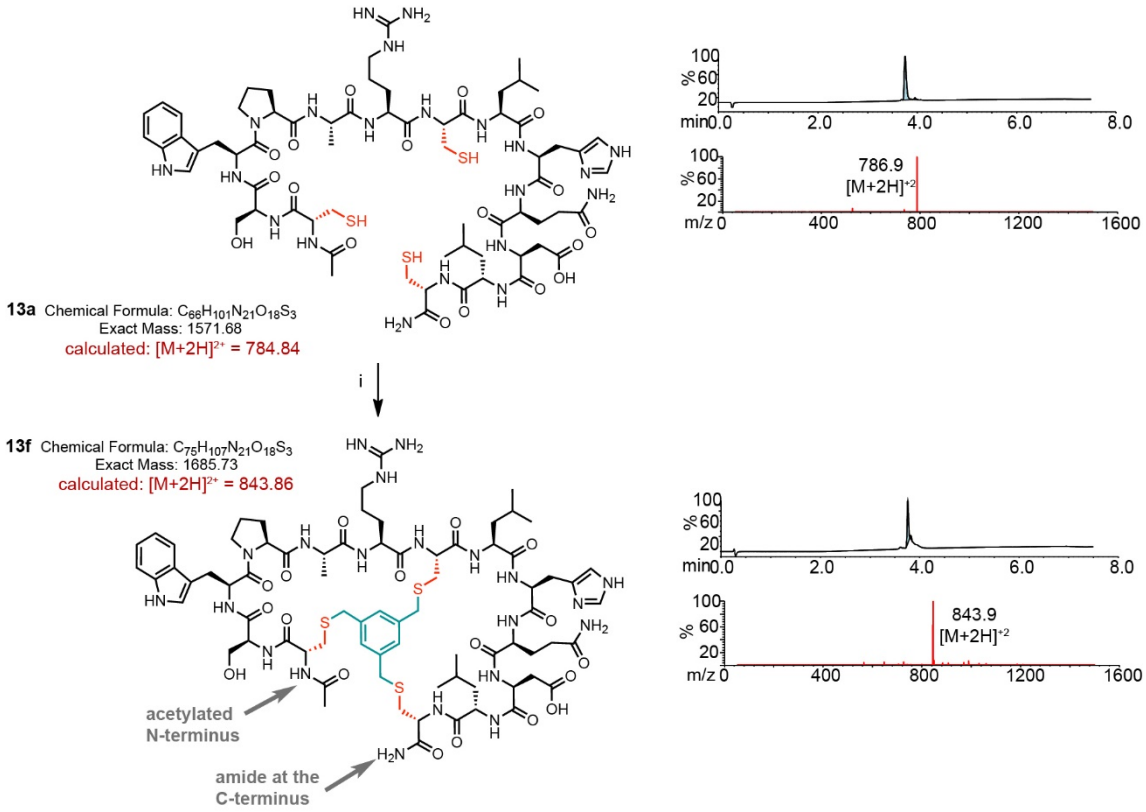

Appendix A-Scheme 37. Bicyclization of **24a** with **TBMB**: Reagents and conditions: 2.5 mM TCEP, 100 mM NaHCO3 (pH 10), 20 h. For details, see: General Protocol for bicyclization with **TBMB**

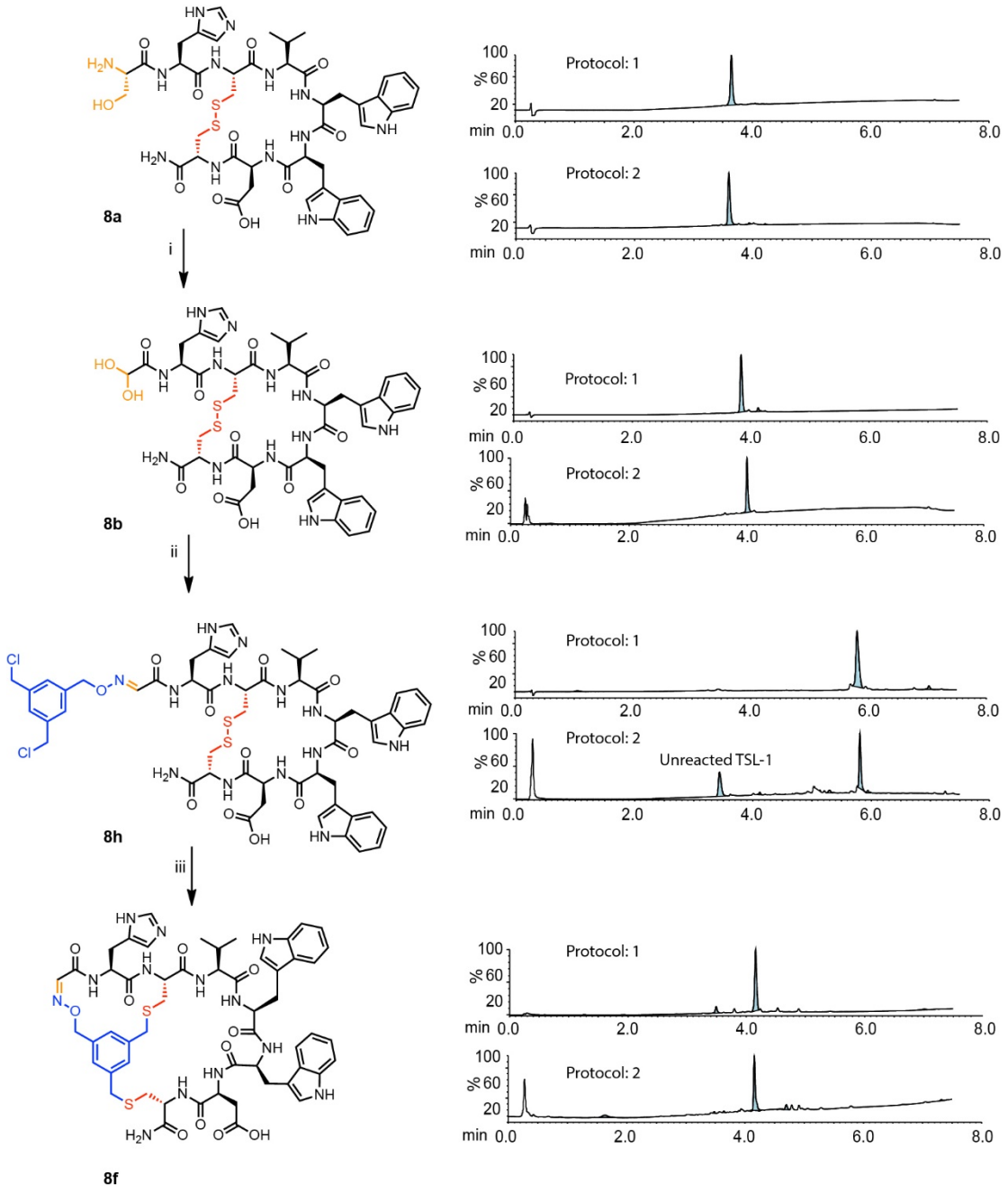

Appendix A-Scheme 38. Comparison between bicyclization of **8a** with **TSL-1** in two different protocols (Protocol 1: Bicyclization of Peptides SX_mCX_nC with **TSL** using C18 spin column and Protocol 2: Bicyclization of Peptides SX_mCX_nC with **TSL** using Met as quencher)

Appendix A-Table1. List of peptide sequences, **TSL**s and resulting bicyclic products.

S.M.	Pr	Sequence	% Y	TSL	# R	m,n	# S
1a	1c	SHCDYYC-NH_2	22%	TSL-1	7	1, 3	2
2a	2c	SYCKADC-NH_2	37%	TSL-1	7	1, 3	3
3a	3d	SYCKPFC-NH_2	N.D.	TSL-3	7	1, 3	4
3a	3c	SYCKPFC-NH_2	41%	TSL-1	7	1, 3	5
4a	4d	STCQGECGGG-NH_2	47%	TSL-3	10	1, 3	6
5a	5b	SICRFFCGGG-NH_2	N.D.	TSL-6	10	1, 3	1
5a	5c	SICRFFCGGG-NH_2	N.D.	TSL-1	10	1, 3	7
5a	5d	SICRFFCGGG-NH_2	55%	TSL-3	10	1, 3	8
6a	6b	SHDCYLEC-NH_2	N.D.	TSL-6	8	2, 3	9
6a	6c	SHDCYLEC-NH_2	43%	TSL-1	8	2, 3	10
6a	6d	SHDCYLEC-NH_2	N.D.	TSL-3	8	2, 3	11
7a	7b	SWDYRECYLEC-NH_2	42%	TSL-6	11	5, 3	12
7a	7c	SWDYRECYLEC-NH_2	54%	TSL-1	8	5, 3	13
8a	8b	SHCVWWDC-NH_2	N.D.	TSL-6	8	1, 4	14
8a	8d	SHCVWWDC-NH_2	N.D.	TSL-3	8	1, 4	15
8a	8c	SHCVWWDC-NH_2	48%	TSL-1	8	1, 4	16
9a	9b	SFCDWYGC-NH_2	20%	TSL-6	8	1, 4	17
10a	10b	SYCPYSGTNC-NH_2	32%	TSL-6	10	1, 6	18
11a	11b	SLCFSQHHDC-NH_2	28%	TSL-6	10	1, 6	19
12a	12c	SSWPARCLHQDLC-NH_2	29%	TSL-1	13	5, 5	20
13a	13c	SNTWNPWCPWDAPL-cam	41%	TSL-1	14	6, 5	21
14a	14b	SPCKAGTGQC-NH_2	30%	TSL-6	10	1, 6	22
15a	15b	SPCKGPSATC-NH_2	9%	TSL-6	10	1, 6	23
16a	16b	SPCKGRHHNC-NH_2	51%	TSL-6	10	1, 6	24
17a	17b	SPCKKAHGAC-NH_2	9%	TSL-6	10	1, 6	25
18a	18b	SPCQRGHMFC-NH_2	8.6%	TSL-6	10	1, 6	26
19a	19b	SYCKRAHKNC-NH_2	14%	TSL-6	10	1, 6	27
20a	20b	SQCKRAHAEC-NH_2	31%	TSL-6	10	1, 6	28
21a	21b	SWCRGHDRTC-NH_2	6%	TSL-6	10	1, 6	29
22a	22b	SPCAKGMNYC-NH_2	5.9%	TSL-6	10	1, 6	30
23a	23b	SWCDYRC-NH_2	N.D.	TSL-6	7	1, 3	31
24a	24c	SWCFYRC-NH_2	N.D.	TSL-1	7	1, 3	32
25a	25b	SLCFDNGC-NH_2	N.D.	TSL-6	8	1, 3	33
26a	26d	SDCGFVSC-NH_2	N.D.	TSL-3	8	1, 4	34

% Y = isolated % yield.

N.D = Not determined or reaction were carried out in analytical scale

#R = Number of residues

#S = Scheme number in appendix A

Appendix A-Table2. Peptide sequence used in the study and their properties.

	Sequence (SX_mCX_nC)	# R	m, n	Ch	GH	BI	2s
1a	SHCDYYC-NH_2	7	1, 3	-0.75	-0.72	2.07	L
2a	SYCKADC-NH_2	7	1, 3	0	-0.39	1.92	L
3a	SYCKPFC-NH_2	7	1, 3	1	0.03	0.5	L
4a	STCQGECGGG-NH_2	10	1, 3	-1	-0.51	2.11	L
5a	SICRFFCGGG-NH_2	10	1, 3	1	0.86	0.69	α
6a	SHDCYLEC-NH_2	8	2, 3	-1.75	-0.43	2.03	L
7a	SWDYRECYLEC-NH_2	11	5, 3	-2	-0.95	2.83	α
8a	SHCVWWDC-NH_2	8	1, 4	-0.75	-0.01	0.69	L
9a	SFCDWYGC-NH_2	8	1, 4	-1	0.11	0.43	L
10a	SYCPYSGTNC-NH_2	10	1,6	0	-0.54	1.27	β
11a	SLCFSQHHDC-NH_2	10	1,6	-0.5	-0.34	1.99	α
12a	SSWPARCLHQDLC-NH_2	13	5, 5	1	-0.34	1.85	α
13a	SNTWNPWCPWDAPL-*cam*	15	6, 5	-1	-0.81	0.92	L
14a	SPCKAGTGQC-NH_2	10	1, 6	1	-0.45	1.08	L
15a	SPCKGPSATC-NH_2	10	1, 6	1	-0.3	0.96	L
16a	SPCKGRHHNC-NH_2	10	1, 6	2.5	-1.61	3.63	L
17a	SPCKKAHGAC-NH_2	10	1, 6	2.25	-0.52	1.2	α
18a	SPCQRGHMFC-NH_2	10	1, 6	1.25	-0.43	1.96	L
19a	SYCKRAHKNC-NH_2	10	1, 6	3.25	-1.43	3.64	α
20a	SQCKRAHAEC-NH_2	10	1, 6	1.25	-1.08	3.47	α
21a	SWCRGHDRTC-NH_2	10	1, 6	1.25	-1.35	4.33	L
22a	SPCAKGMNYC-NH_2	10	1, 6	1	-0.28	0.8	α
23a	CNTWNPWCPWDAPLC-NH_2	15	6, 5	0.25	-0.37	0.46	L
24a	CSWPARCLHQDLC-NH_2	13	5, 5	0.25	-0.08	1.49	α
25a	SWCDYRC-NH_2	7	1, 3	0	-0.85	3.18	α
26a	SWCFYRC-NH_2	7	1, 3	1	0.04	1.51	α
27a	SLCFDNGC-NH_2	8	1, 4	-1	0.42	0.92	L
28a	SDCGFVSC-NH_2	8	1, 4	-1	0.81	0.62	L

Ch = Charge (pH 7)

GH = GRAVY Hydrophobicity[361]

BI = Boman Index[361]

2s = 2nd structure prediction[362-364]

L= loop, β = β-sheet, α = α-helix

Appendix A-Table3. Modifiers other than **TSL** and resulting bicyclic/monocyclic products.

S.M.	Pr	Sequence	% Y	Linker	#R	m,n	#S/#F
4a	4e	STCQGECGGG-NH_2	31	PFS	10	1, 3	S 35
5a	5e	SICRFFCGGG-NH_2	40	PFS	10	1, 3	S 35
23a	23f	Ac-CNTWNPWCPWDAPL*Cam*	38	TBMB	14	6, 5	S 36
24a	24f	Ac-CSWPARCLHQDLC-NH_2	33	TBMB	13	5, 5	S 37
1a	1g	SHCDYYC-NH_2	47	DBMB	7	1, 3	F 56
2a	2g	SYCKADC-NH_2	47	DBMB	7	1, 3	F 57
3a	3g	SYCKPFC-NH_2	62	DBMB	7	1, 3	F 58
4a	4g	STCQGECGGG-NH_2	19	DBMB	7	1, 3	F 59
5a	5g	SICRFFCGGG-NH_2	46	DBMB	7	1, 3	F 60
6a	6g	SHDCYLEC-NH_2	27	DBMB	8	2, 3	F 61
7a	7g	SWDYRECYLEC-NH_2	12	DBMB	11	5, 3	F 62
8a	8g	SHCVWWDC-NH_2	16	DBMB	8	1, 4	F 63
9a	9g	SFCDWYGC-NH_2	10	DBMB	8	1, 4	F 64
12a	12g	SSWPARCLHQDLC-NH_2	46	DBMB	14	6, 5	F 65
14a	14g	SPCKAGTGQC-NH_2	12	DBMB	10	1, 6	F 66
15a	15g	SPCKGPSATC-NH_2	10	DBMB	10	1, 6	F 67
16a	16g	SPCKGRHHNC-NH_2	63	DBMB	10	1, 6	F 68
19a	19g	SYCKRAHKNC-NH_2	32	DBMB	10	1, 6	F 69
20a	20g	SQCKRAHAEC-NH_2	10	DBMB	10	1, 6	F 70
22a	22g	SPCAKGMNYC-NH_2	25	DBMB	10	1, 6	F 71

% Y = isolated % yield.

N.D = Not determined or reaction were carried out in analytical scale

#R = Number of residues

#S = Scheme number in appendix A

#F = Figure number in appendix A

Appendix A-2: Phage modifications

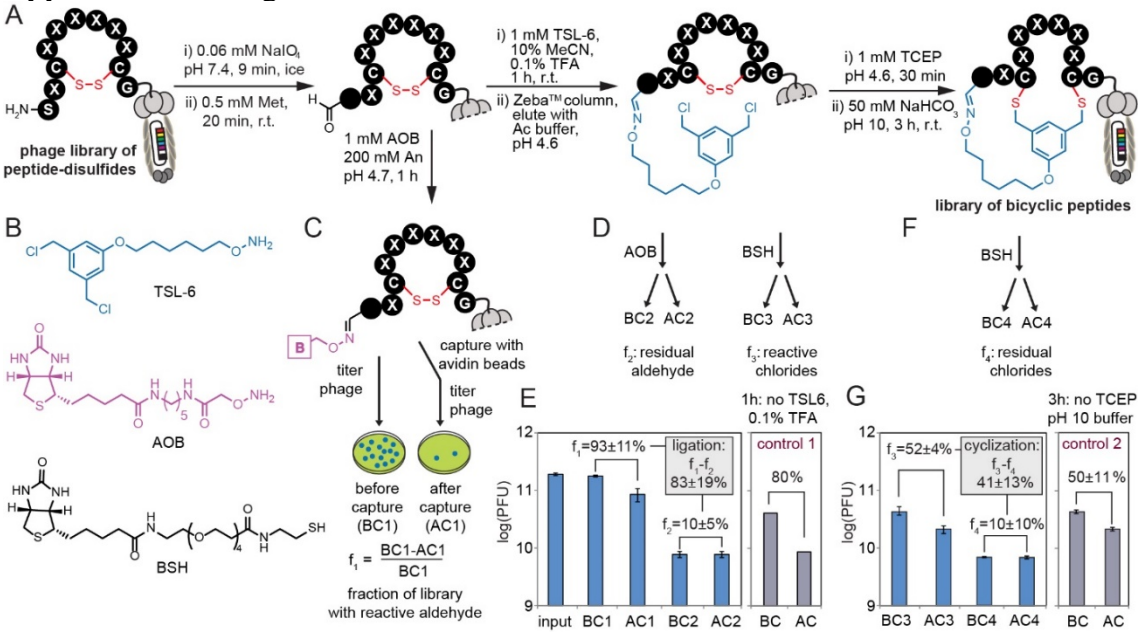

Appendix A-Figure 1. Modification of the library of 10^8 peptides displayed on phage by the **TSL-6. (**A) Scheme of the modification. (B) Reagents for synthesis or monitoring of the reactions. (C-D) Exposure of the aldehyde-peptide library to AOB and counting the number of phage particles before and after the capture with streptavidin-agarose measured the fraction of library with aldehyde. (E) Reaction of aldehyde-phage with **TSL-6** decreased the fraction of library with aldehyde from 73±11 to 10±5%. Control incubation in TFA in the absence of **TSL-6** did not decrease the fraction of aldehydes. (F) Ligation of **TSL-6** introduced thiol-reactive chlorobenzyl groups on phage that were detected by BSH. (G) Reduction with TCEP at pH 4.6 and increase of the pH to 10 induced bicyclization and decreased the fraction of library with thiol reactive groups from 52±4 to 10±10%. Control incubation of **TSL-6**-modified phage in pH 10 buffer for 3 h in the absence of TCEP did not lead to a significant decrease of thiol-reactive groups: phage remained reactive to BSH (E-F)

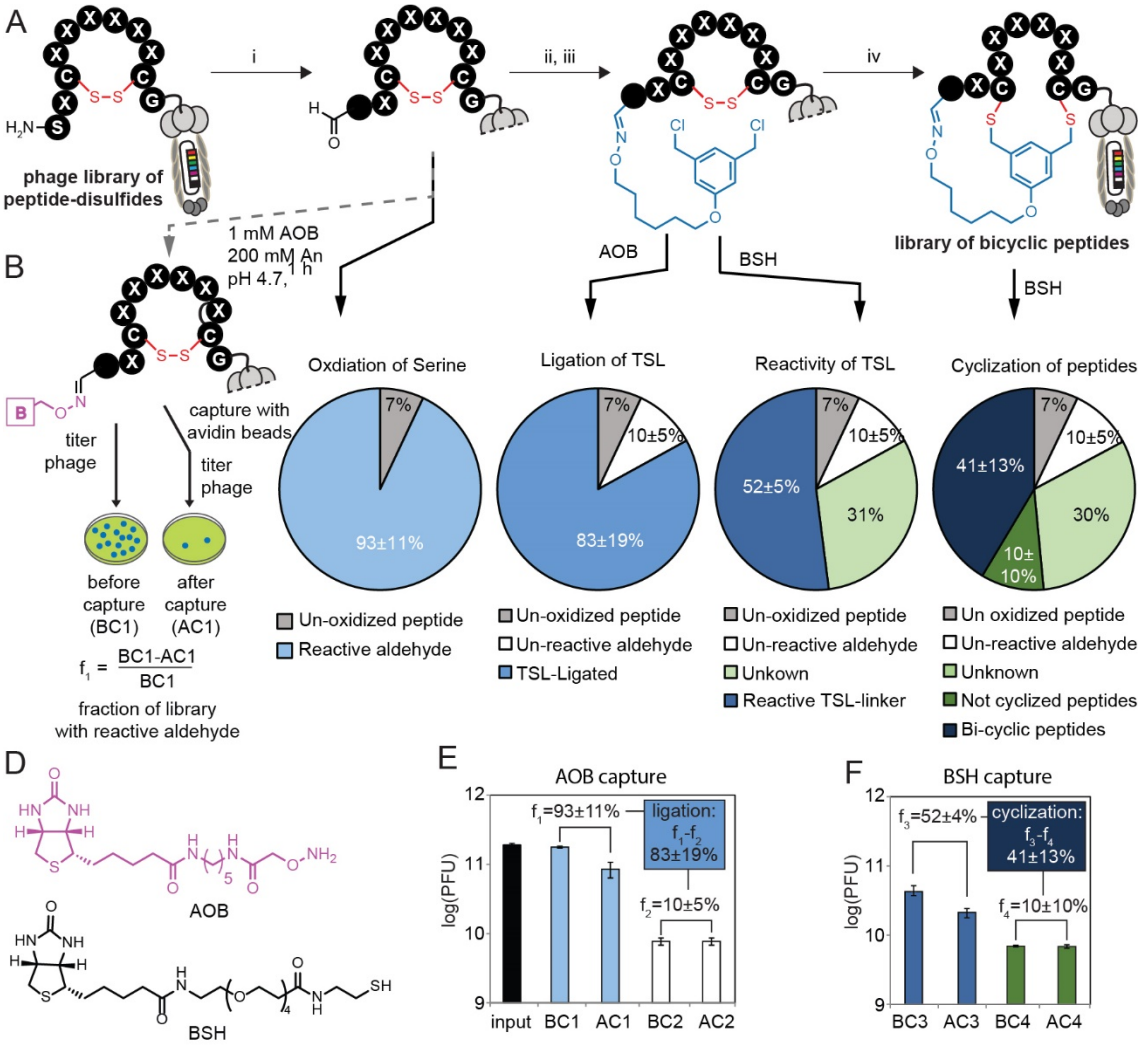

Appendix A-Figure 2. Composition of $SXCX_6C$ library during modification with **TSL-6 (**A) Overall step-by-step modification of $SXCX_6C$ displyed peptide library by **TSL-6**. (i) 0.06 mM $NaIO_4$, pH 7.9, 9 min, ice. 0.5 mM Met, 20 min, r.t.(ii) 1 mM **TSL-6**, 10% MeCN, 0.1% TFA, 1 h, r.t. (iii) Zeba^{TM} column, elute with 10 mM NaAc buffer, pH 4.6 (iv) 1 mM TCEP in 10 mM NaAc buffer, pH 4.6, 30 min. Increase the pH to 10 by adding 1 M $NaHCO_3$ and incubate for 3 h, r.t. (B) The efficiency of oxidation was measured by exposure of the phage to aminooxybiotin (AOB) and measuring the biotinylation by counting the number of phage particles before and after the capture of the modified phage with streptavidin paramagnetic particles. (C) The percentage of different chemical species in the different steps of the modification of $SXCX_6C$ displyed peptide library. (D) Thiol and aldehyde reactive compound for generating bicyclic phage (**TSL-6**). Biotinylating compounds to monitor reaction progress for oxime ligation (AOB) and cyclization (BSH). (E-F)

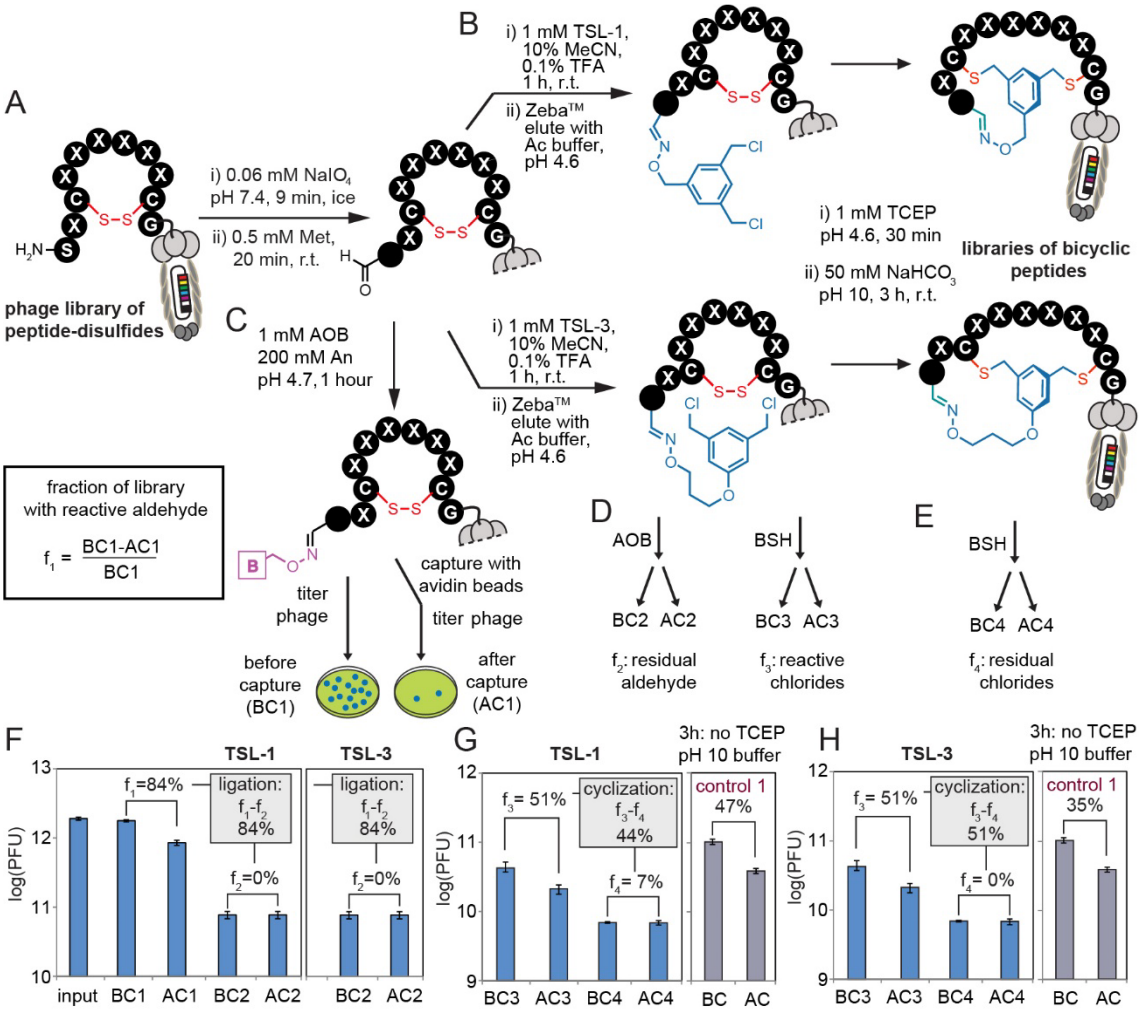

Appendix A-Figure 3. Modification of the $SXCX_6C$ library by the **TSL-1** and **TSL-3**. (A-B) Overall step-by-step modification of $SXCX_6C$ displyed peptide library by **TSL-1** and **TSL-6**. (C) The efficiency of oxidation was measured by exposure of the library to aminooxybiotin (AOB) and measuring the biotinylation by counting the number of phage particles before and after the capture of the library with streptavidin paramagnetic particles. (D) "AOB-capture" after ligation of **TSL** detects disappearance of aldehydes; similar "BSH-capture" detects concurrent appearance of thiol-reactive chlorobenzyl groups and (E) their disappearance after bicyclization. (F) "AOB capture" shows that 84% of library was oxidized, and **TSL-1** or **3** consumed all aldehyde groups. (G-H) BSH-capture confirms appearance thiol-reactive groups on phage and their disappearance after bicyclization. In control conditions, incubation of **TSL-1** or **3** ligated phage in pH 10 buffer for 3 h in the absence of TCEP did not lead to a significant decrease of chlorobenzyl groups: phage remained reactive to BSH.

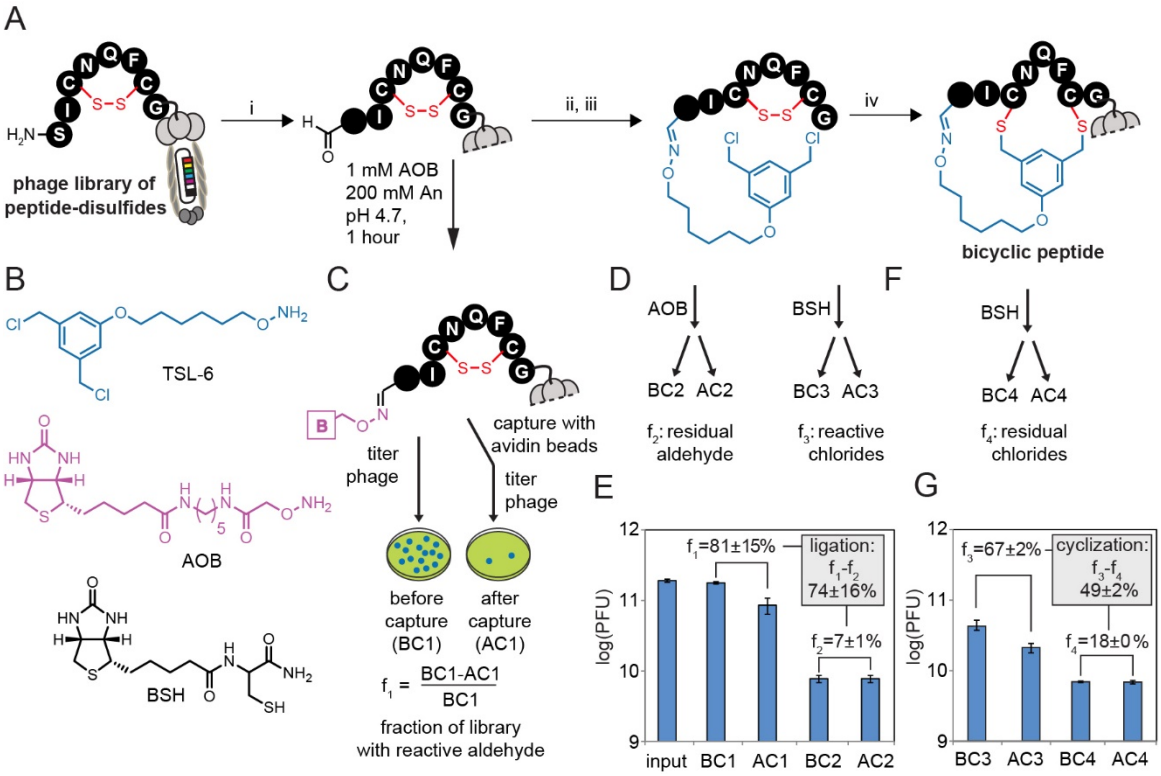

Appendix A-Figure 4. Modification of monoclonal phage displaying SICNQFC with **TSL-6**.(A) Overall step-by-step modification of the peptide, SICNQFC displayed on M13KE phage by the linchpin **TSL-6**. (B) Thiol and aldehyde reactive compound for generating bicyclic phage (**TSL-6**). Biotinylating compounds to monitor reaction progress for oxime ligation (AOB) and cyclization (BSH). (C) The efficiency of oxidation was measured by exposure of the phage to aminooxybiotin (AOB) and measuring the biotinylation by counting the number of phage particles before and after the capture of the modified phage with streptavidin paramagnetic particles. (D-E) Reaction with **TSL-6** in 0.1% TFA for 1 hour led to the disappearance of aldehyde functionality and loss of biotinylation after exposure to AOB and concurrent appearance of thiol-reactive chlorobenzyl groups: their presence was detected by exposure of phage to biotin-thiol (BSH). After purification by size-exclusion Zeba^{TM} column, to remove excess of the linchpin **TSL-6**, and elution with acetate buffer (pH 4.6), exposure to TCEP at pH 4.6 for 30 minutes for reducing the disulfides. The increase of the pH to 10 induced bicyclization. Exposure of the bicyclized product to BSH did not produce visible biotinylating, indicating the disappearance of reactive thiol groups.

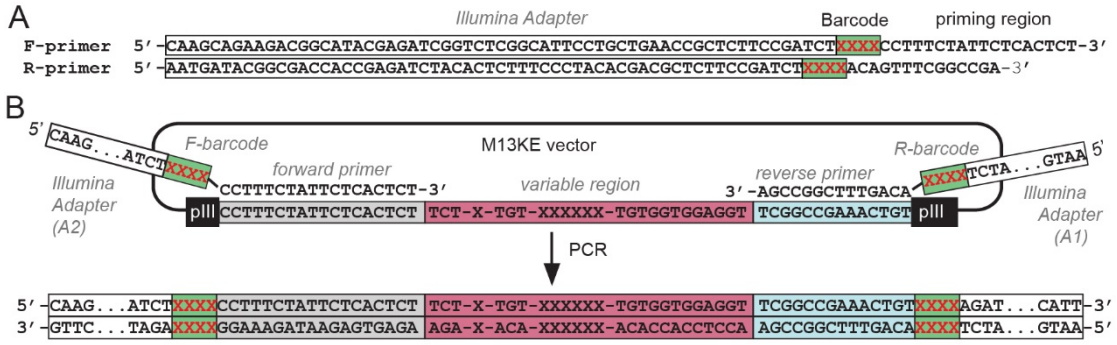

Appendix A-Figure 5. DNA sequences of PCR amplification protocol for Illumina deep sequencing (A) Primers used for amplifying ligated or naïve oligonucleotide DNA. XXXX denotes 4-nucleotide-long barcodes used to trace multiple samples in an Illumina sequencing experiment. (B) Generation of PCR product. Alignment of forward and reverse primers to 18-bp and 14-bp sequences flanking the variable region at the N-terminus of the pIII gene in M13KE vector, respectively.

Appendix A-3: General NODAL selection and validation

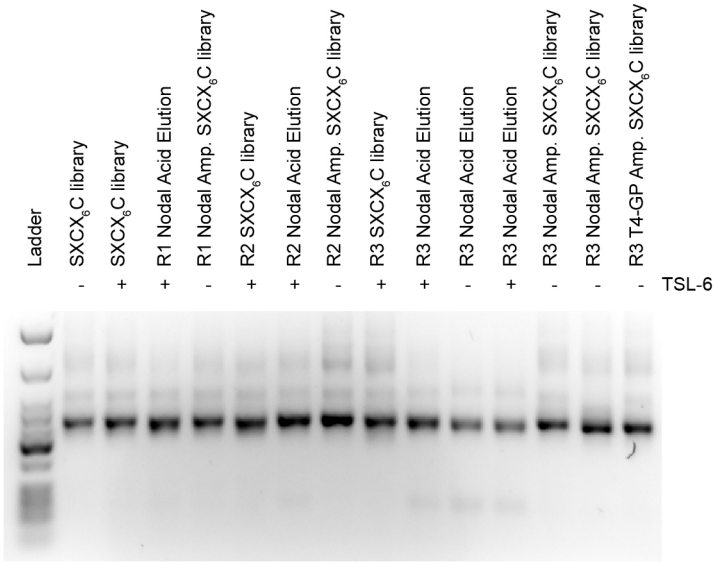

Appendix A-Figure 6. PCR product of **TSL-6** modification and 3 rounds of the NODAL panning.

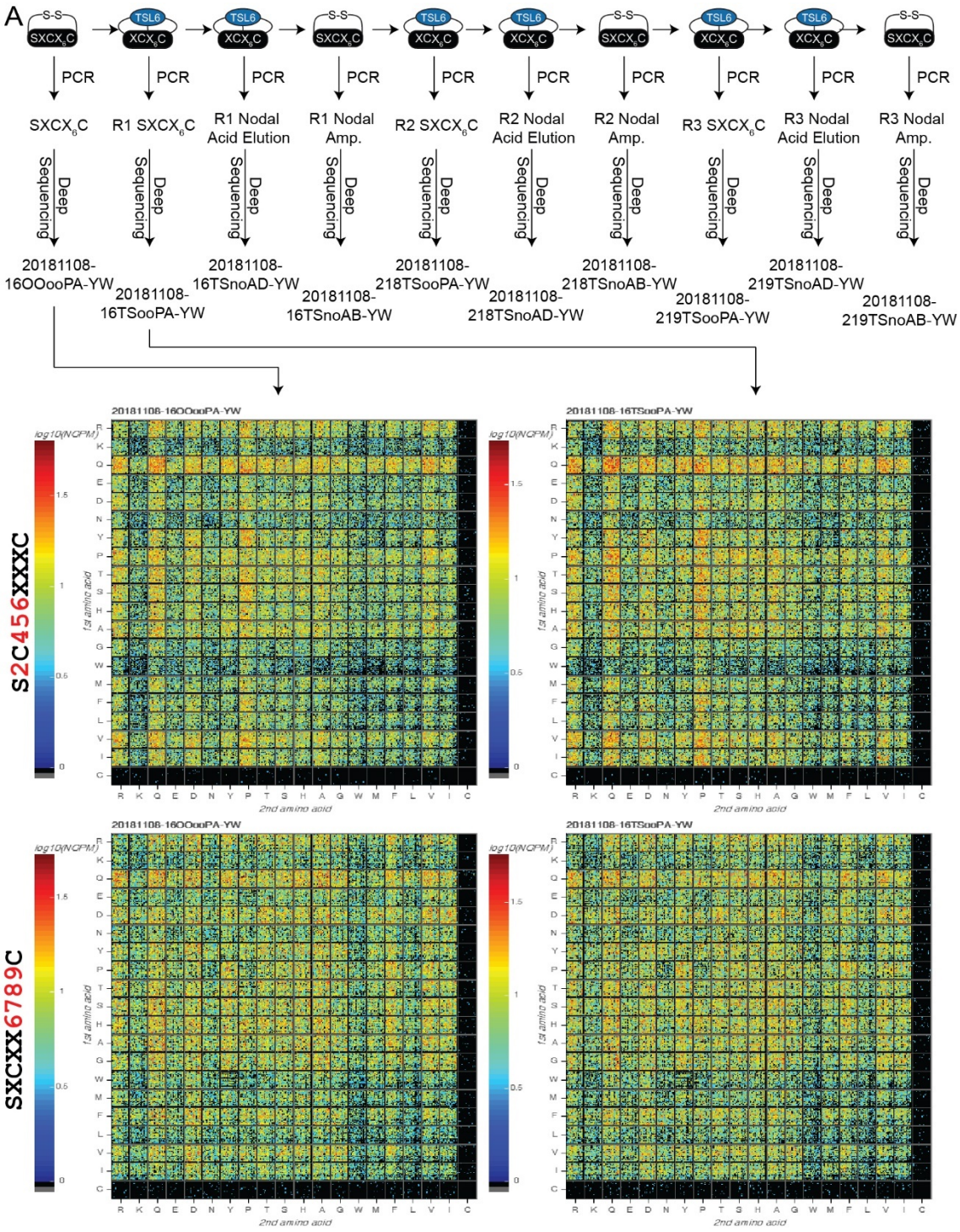

Appendix A-Figure 7. 20 × 20 plot comparison before and after **TSL-6** modification in input library. (20181108-16OO00PA-YW) example of names from deep sequencing files.) 20x20 plot are produce as previous publications.

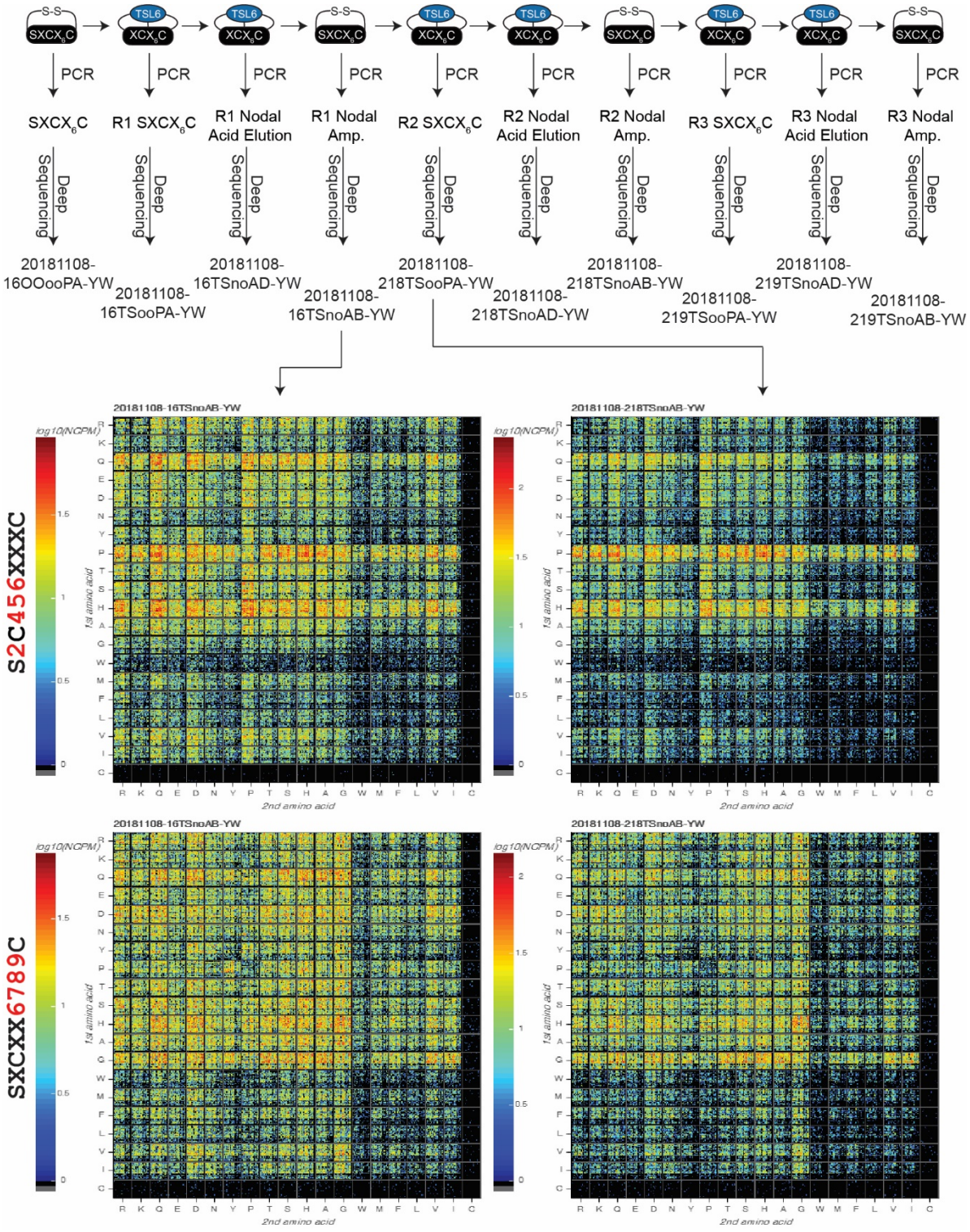

Appendix A-Figure 8. 20 × 20 plot comparison before and after **TSL-6** modification after R1 selection.

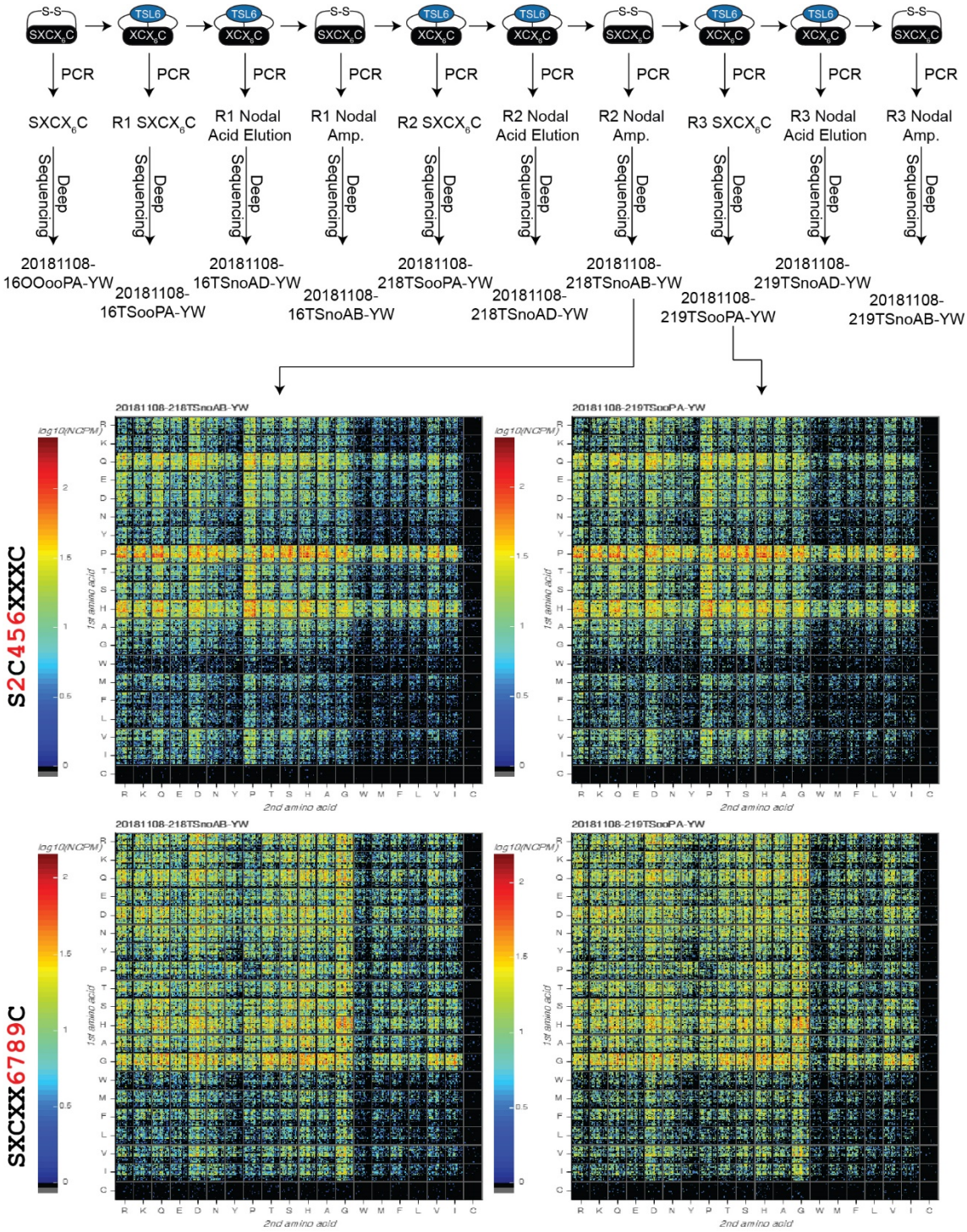

Appendix A-Figure 9. 20 × 20 plot comparison before and after **TSL-6** modification after R2 selection

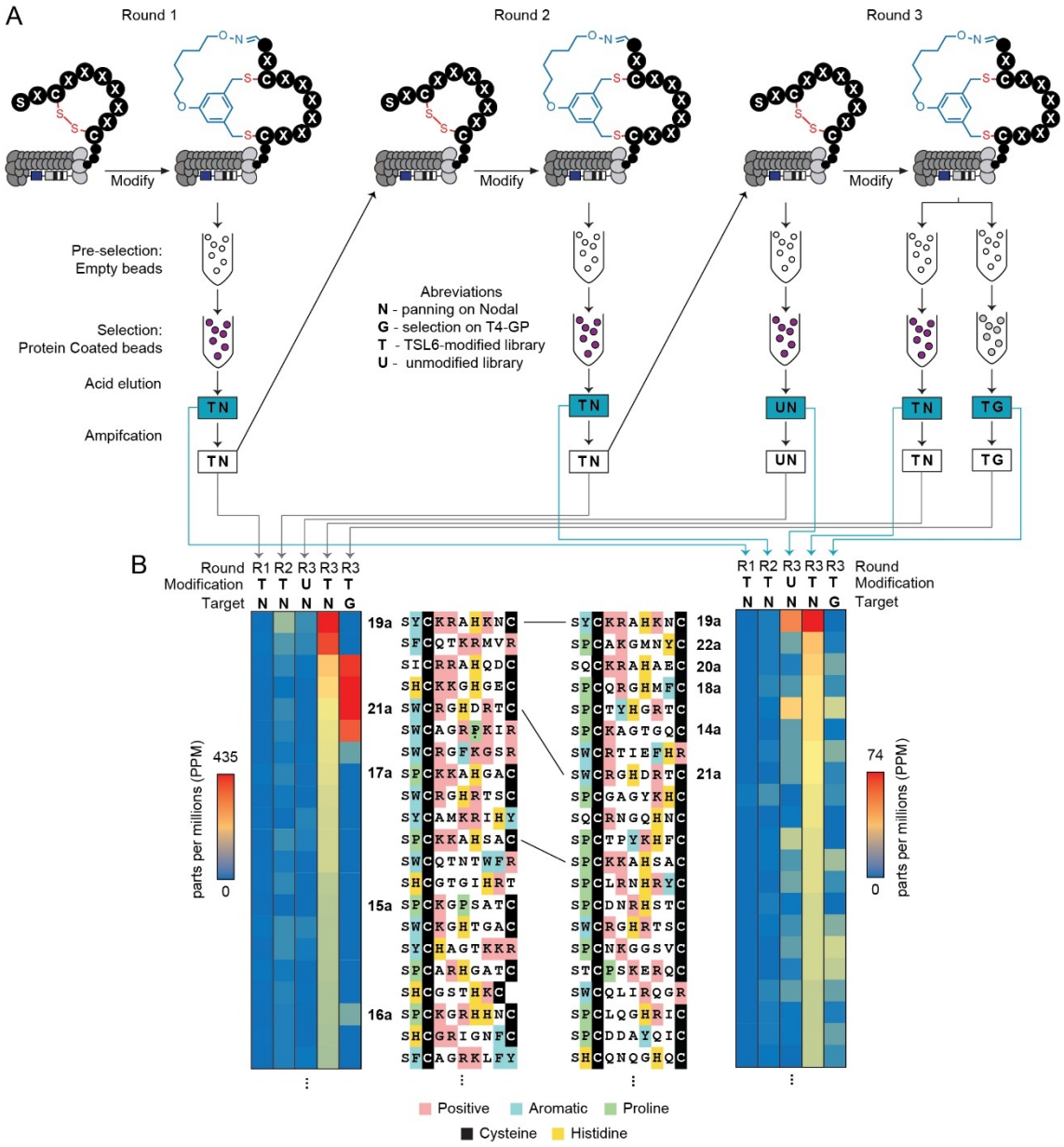

Appendix A-Figure 10. Scheme of selection of NODAL bicycles and post-selection analysis of selection samples . (A) A detail flow-chart of 3 rounds of panning against Nodal protein. (B) Heat map of top 22 sequences after amplification (right) and acid elution. (left) Sequences were rank from high to low in the TN.

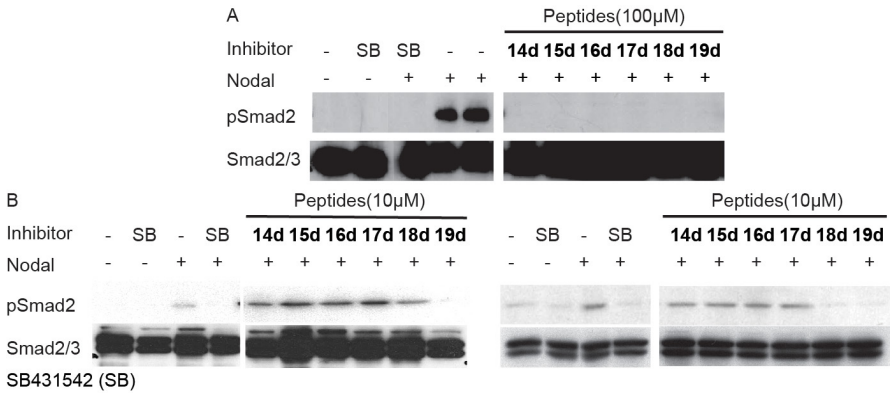

Appendix A-Figure 11. Western blot analysis of p-SMAD2 in response to treatment with rhNODAL and bicycles inhibitors at 100 μM (A) and 10 μM (B) in P19 cells. Total SMAD2/3 used as controls.

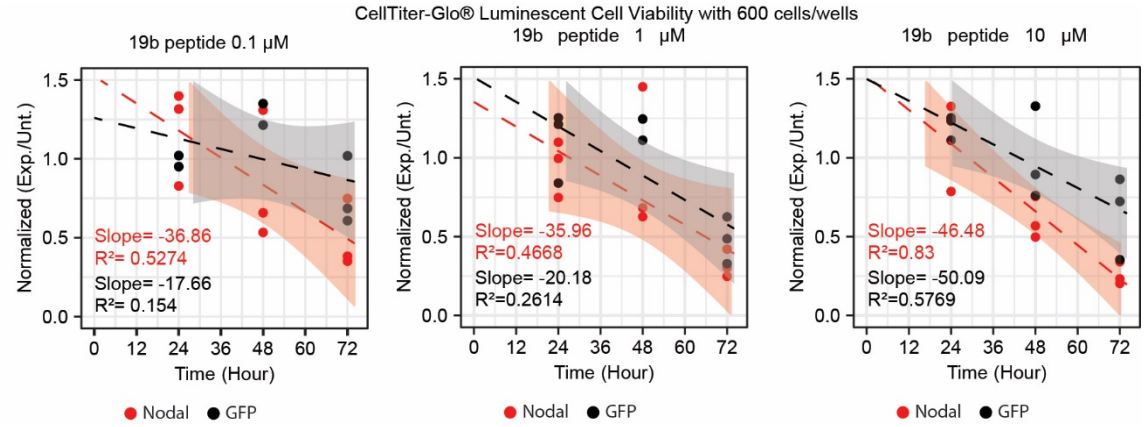

Appendix A-Figure 12. CellTiter-Glo® Luminescent Cell Viability 600 cells/wellAssay with TYK-nu-Nodal and TYK-nu-GFP treated with **19b** peptide inhibitor at 10 µM, 1 µM and 0.1 µM over 72 hours.

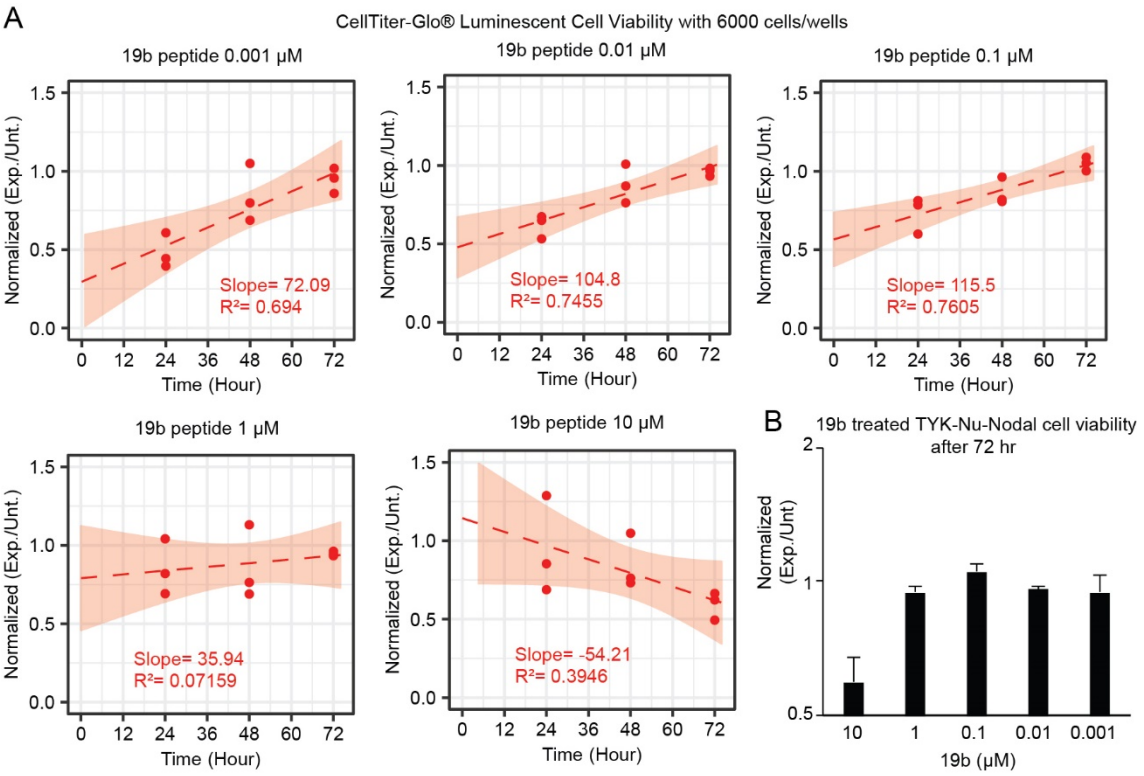

Appendix A-Figure 13. CellTiter-Glo® Luminescent Cell Viability 6000 cells/wellAssay with TYK-nu-Nodal treated with **19b** peptides inhibitors at 10 µM, 1 µM, 0.1 µM, 0.01 µM and 0.001 µM over 72 hours.

Appendix A-4: Peptide stability data

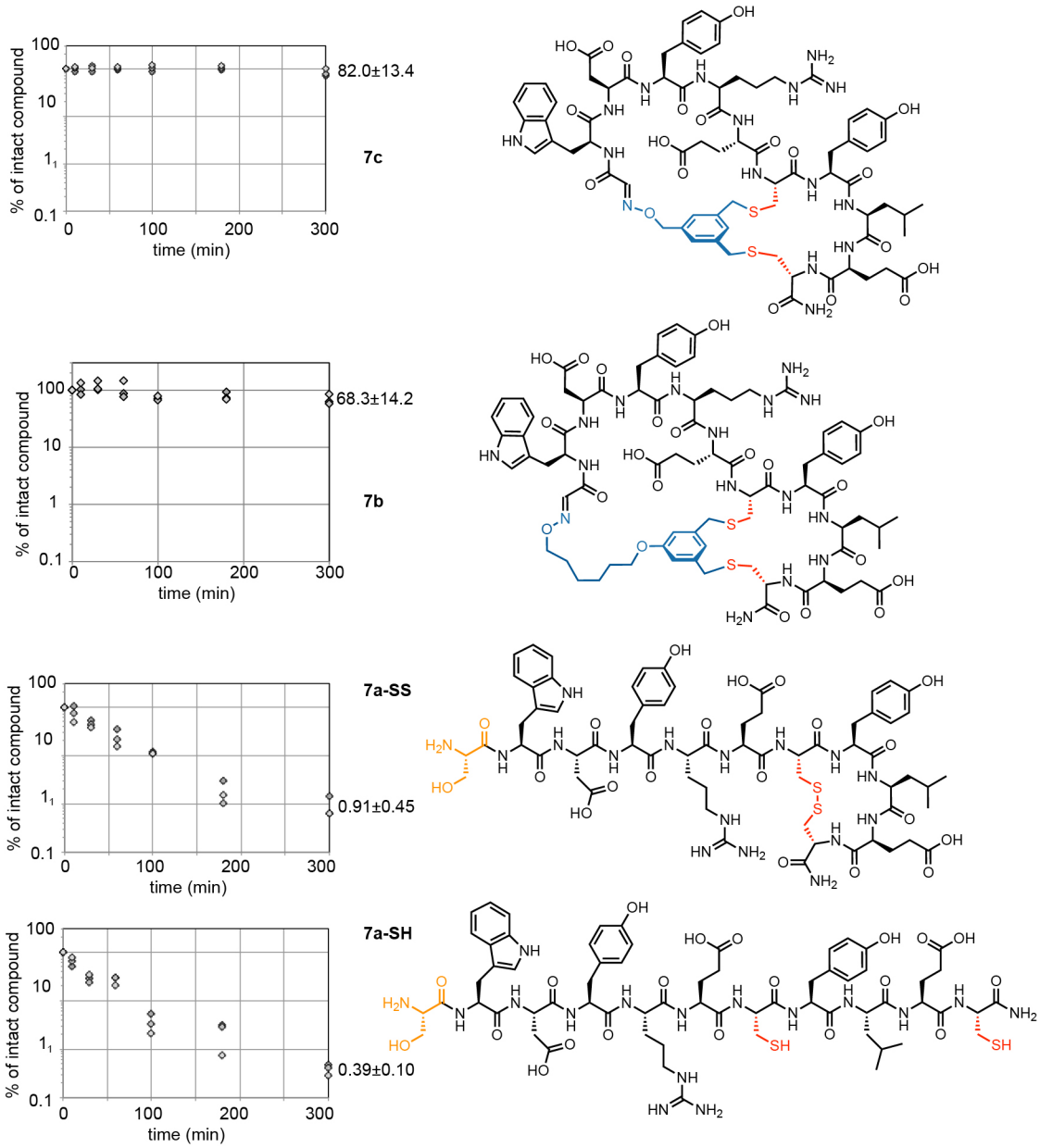

Appendix A-Figure 14. Proteolytic stability of **7a**, **7b** and **7c** in Pronase^{TM}: **7a** disulfide-peptide and **7a** linear peptide.

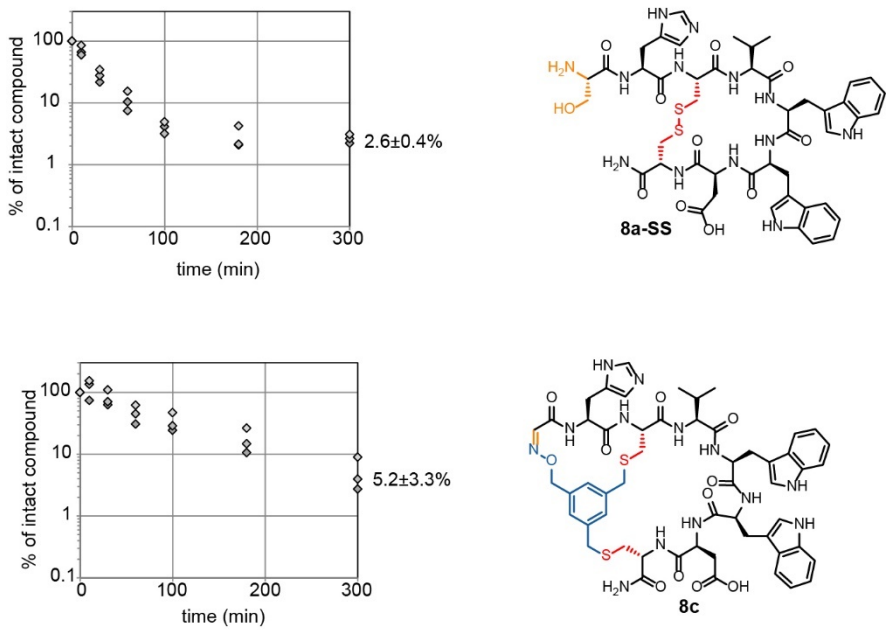

Appendix A-Figure 15. Proteolytic stability of **8a**, and **8c** in Pronase^{TM}

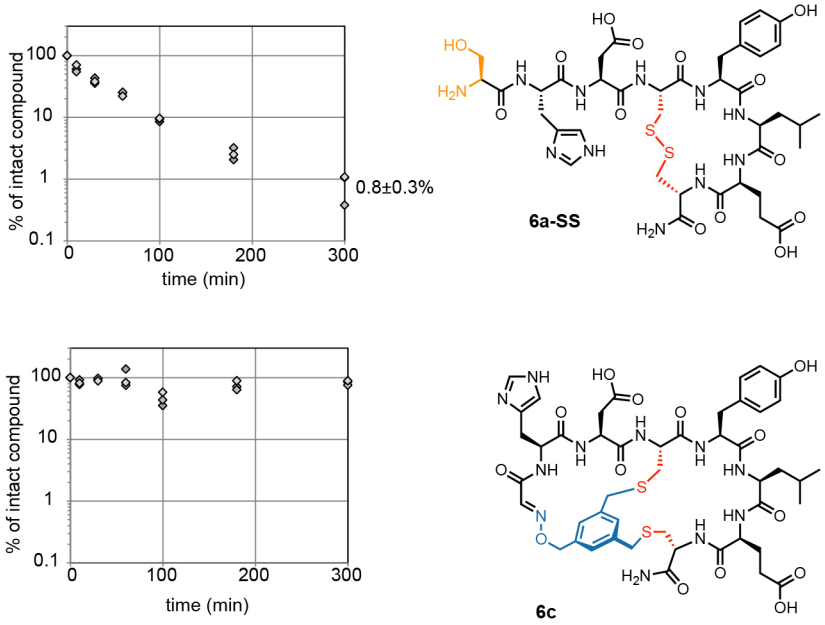

Appendix A-Figure 16. Proteolytic stability of **6a** and **6c** in Pronase^{TM}.

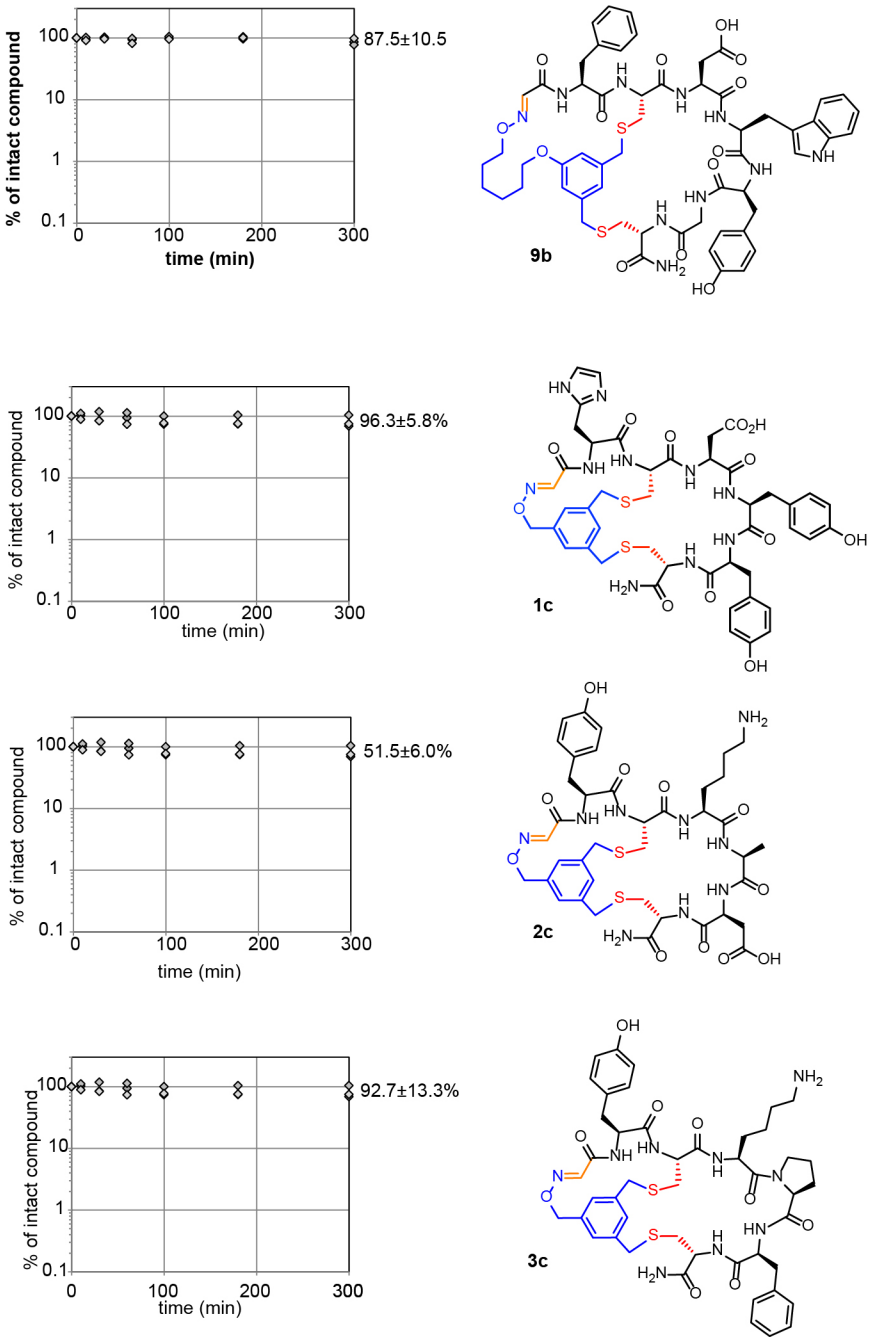

Appendix A-Figure 17. Proteolytic stability of **9b**, **1c**, **2c** and **3c** in Pronase™.

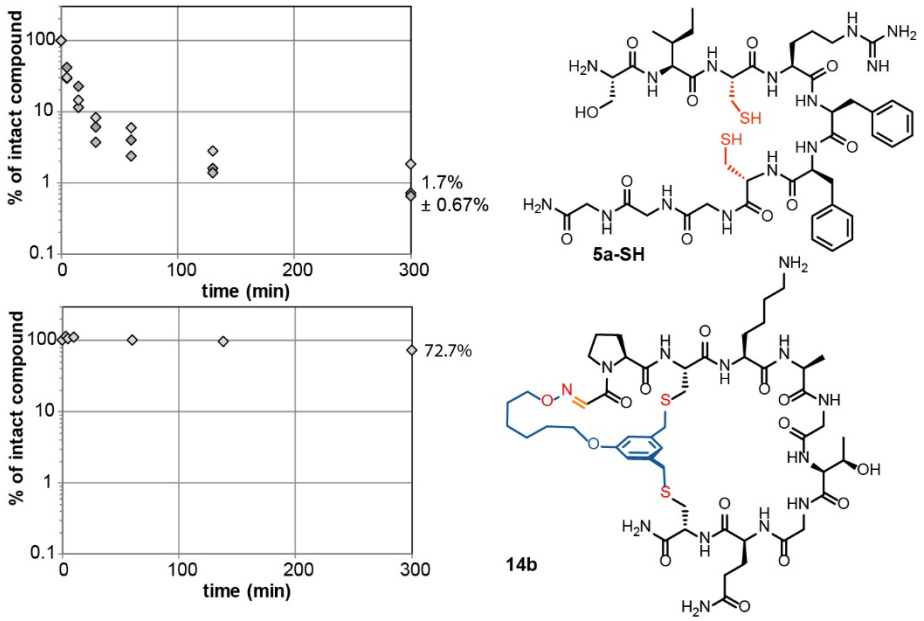

Appendix A-Figure 18. Proteolytic stability of **5a-SH**, and **14b15b**, and **16b** in Pronase^{TM}.

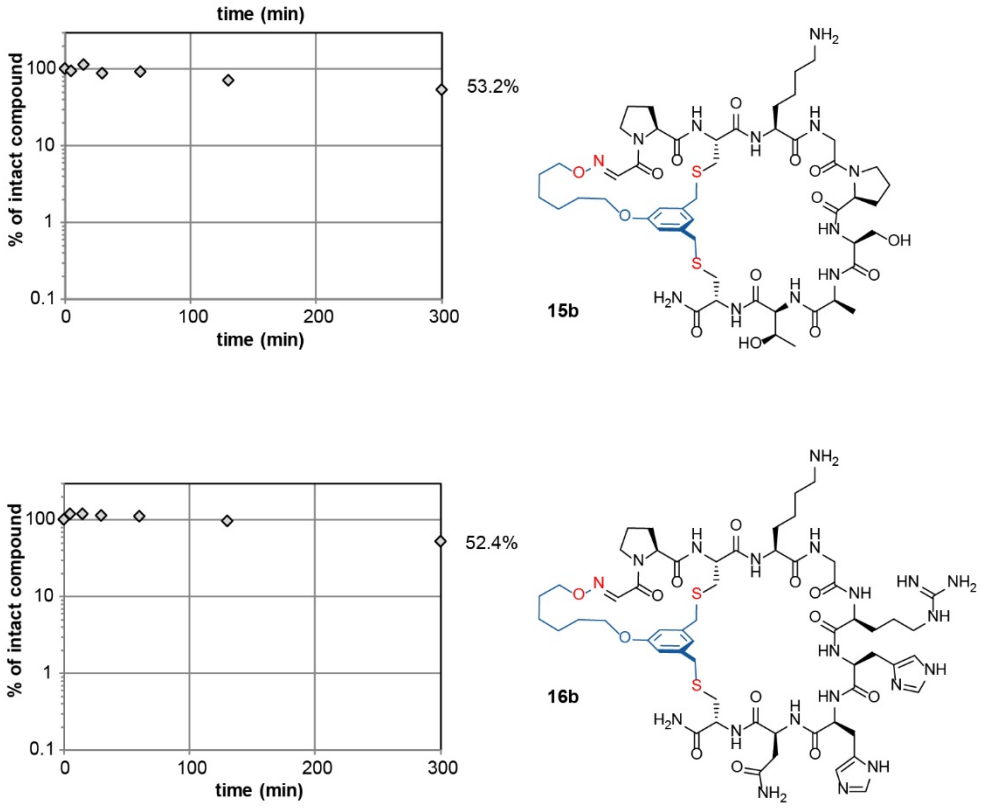

Appendix A-Figure 19. Proteolytic stability of **15b**, and **16b** in Pronase^{TM}.

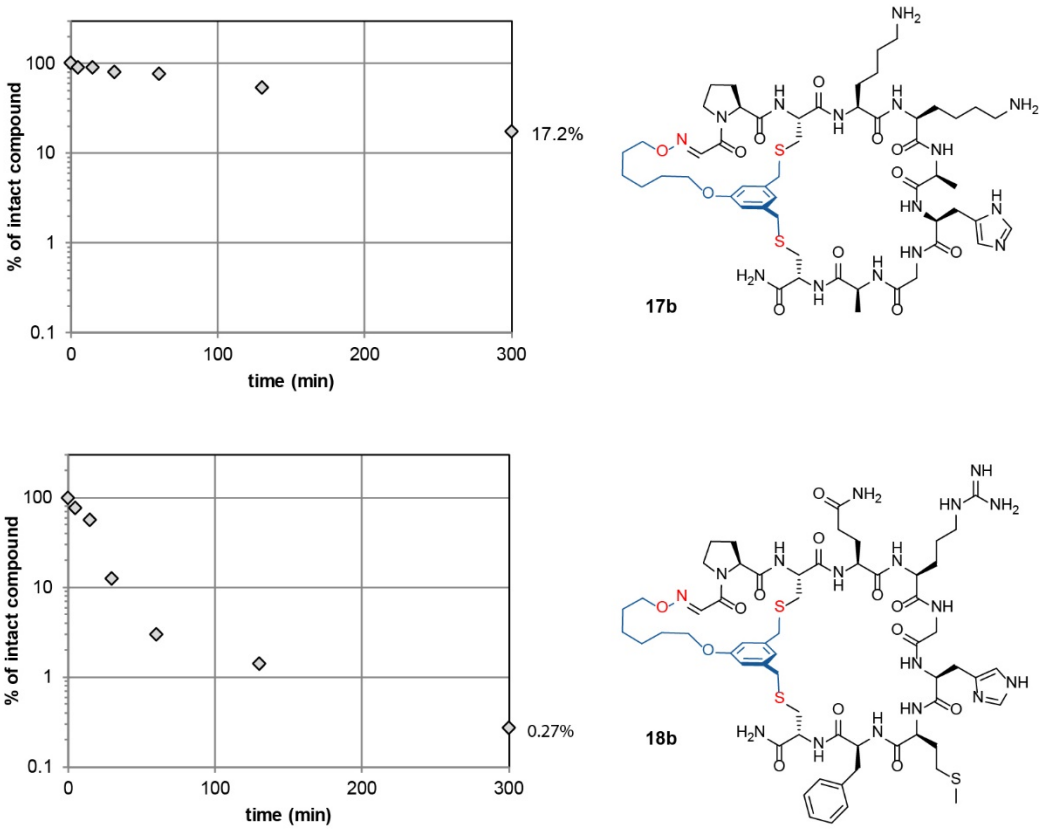

Appendix A-Figure 20. Proteolytic stability of **17b** and **18b** in Pronase^{TM}.

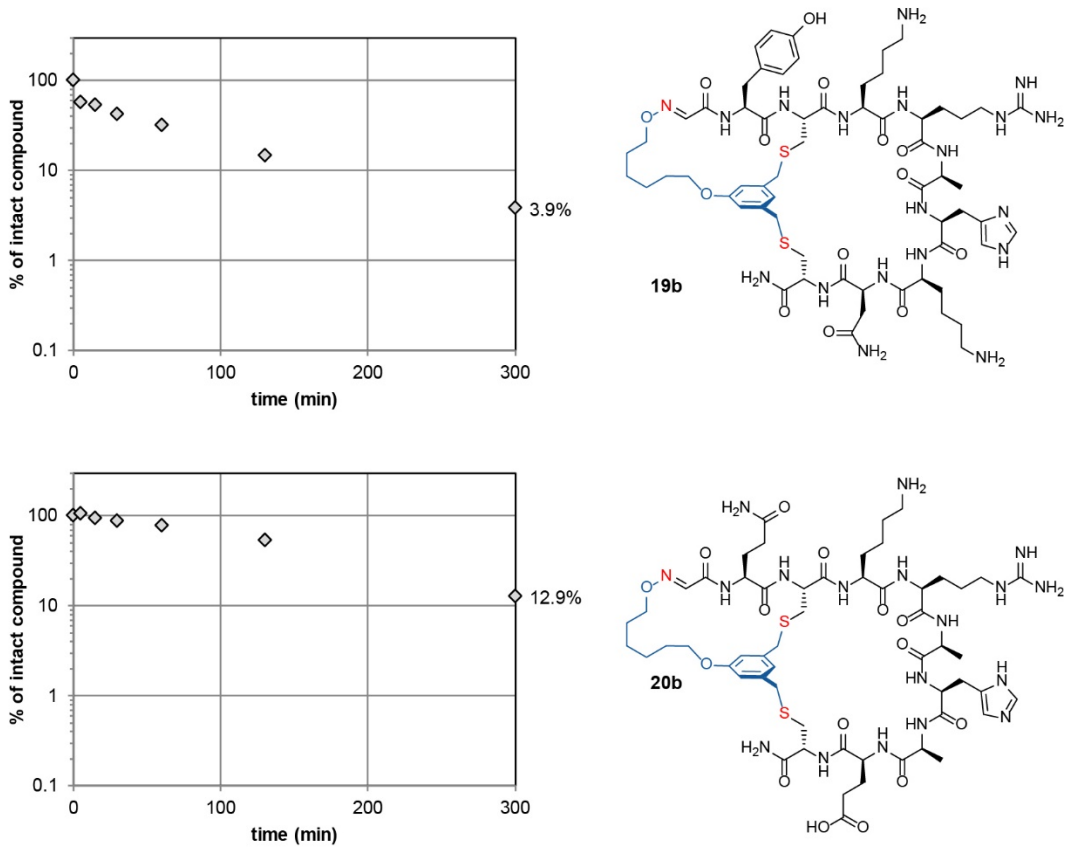

Appendix A-Figure 21. Proteolytic stability of **19b**, and **20b** in Pronase^{TM}.

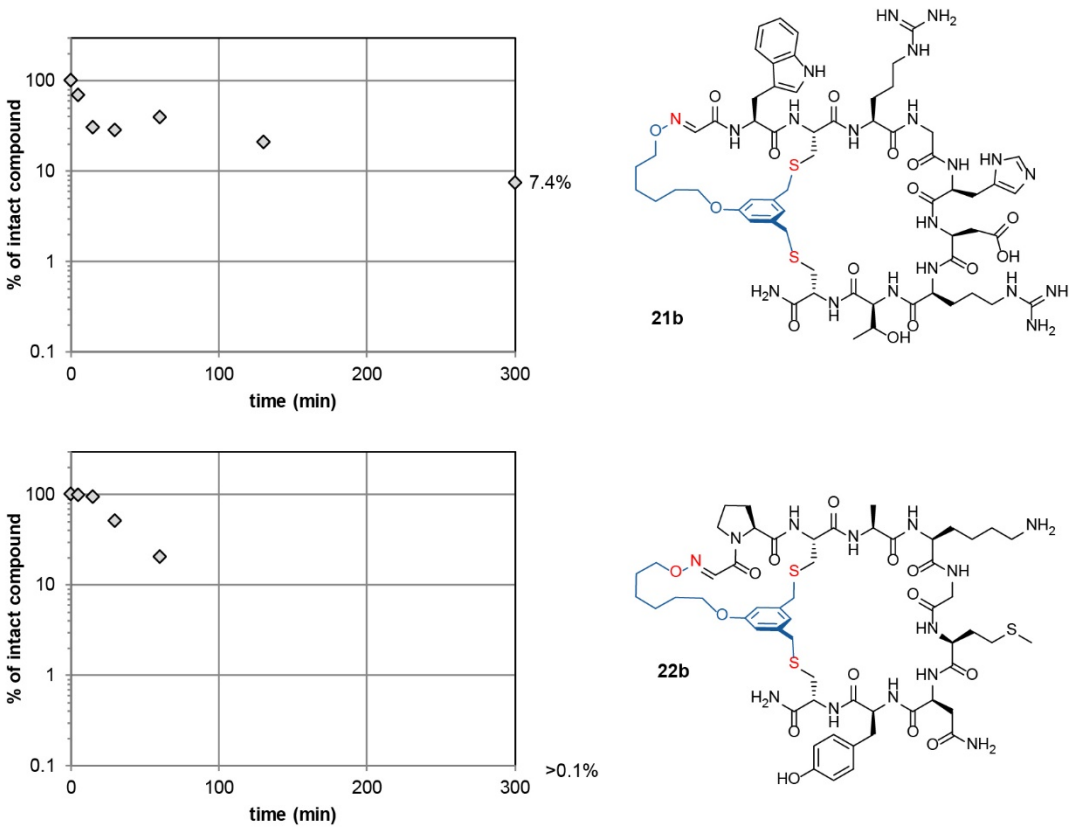

Appendix A-Figure 22. Proteolytic stability of **21b** and **22b** in Pronase^{TM}.

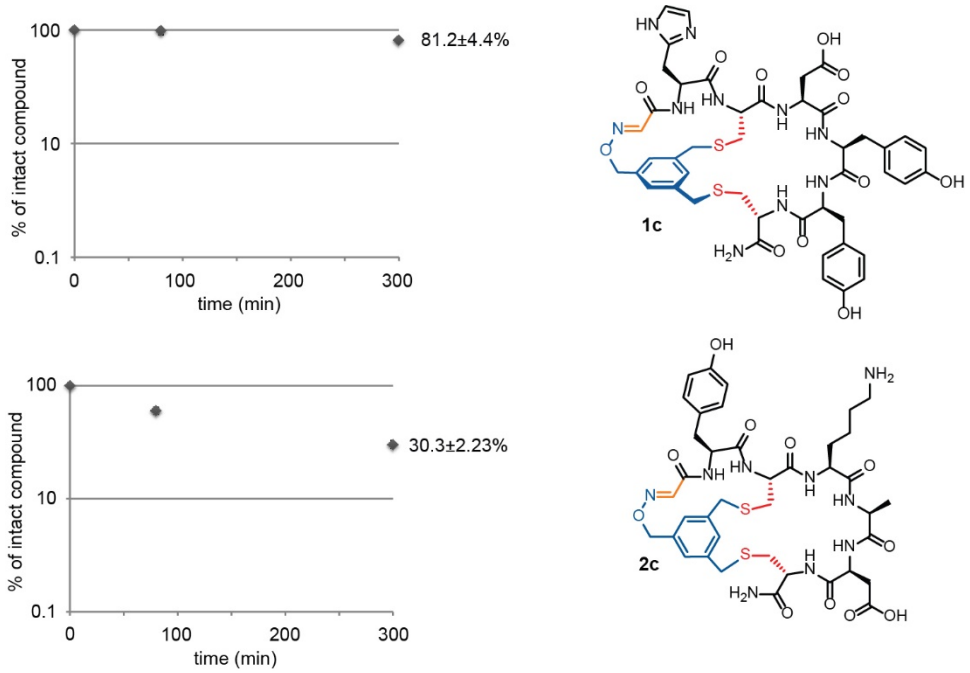

Appendix A-Figure 23. Proteolytic stability of **1c,** and **2c** in fresh mouse serum.

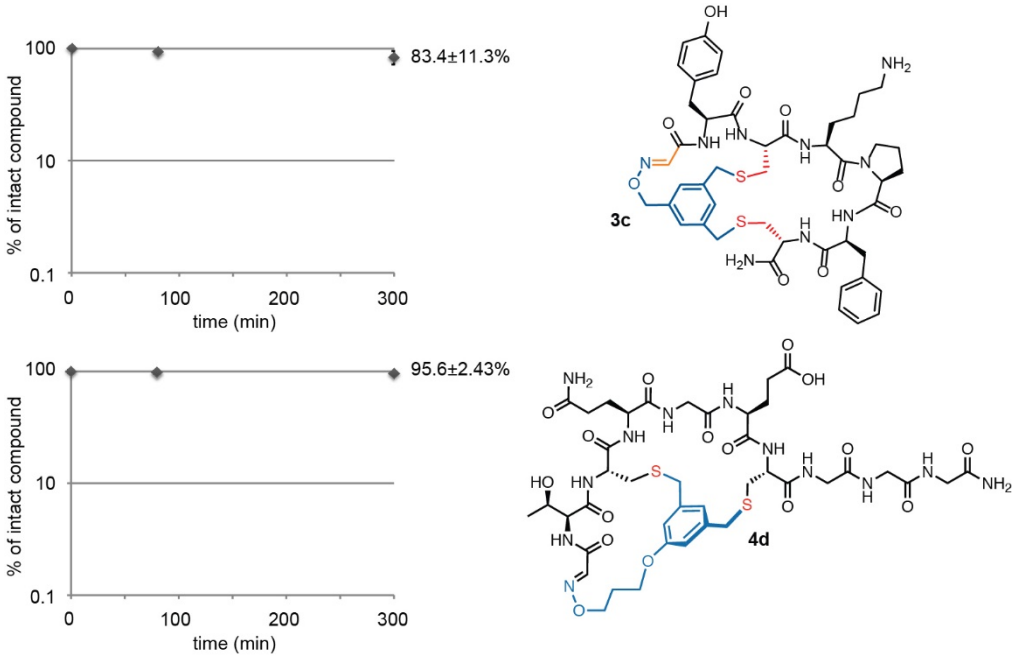

Appendix A-Figure 24. Proteolytic stability of **3c** and **4d** in fresh mouse serum.

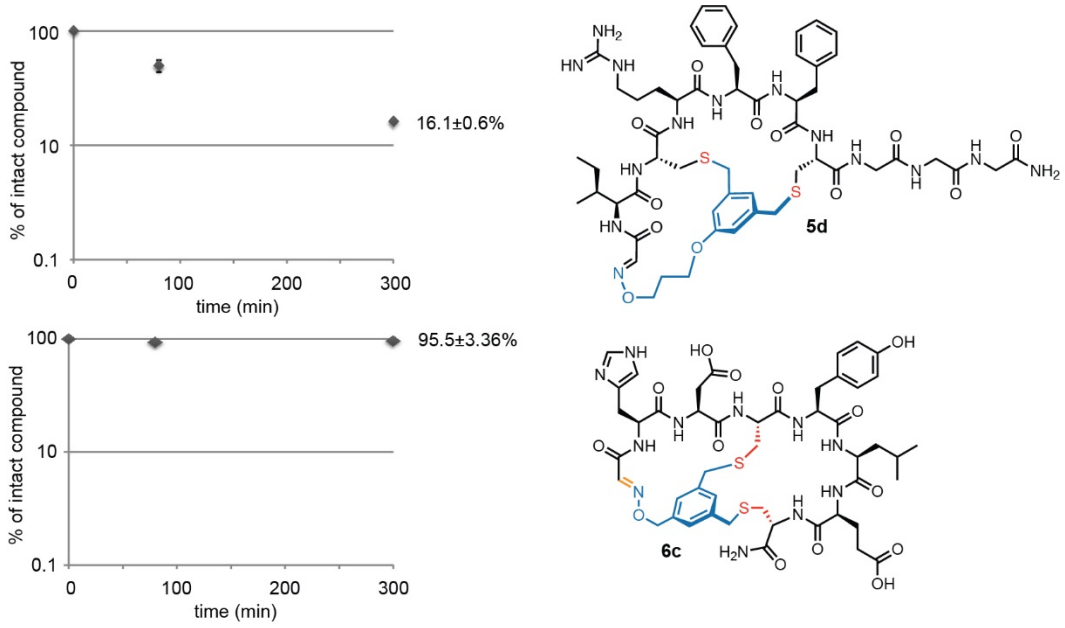

Appendix A-Figure 25. Proteolytic stability of **5d** and **6c** in fresh mouse serum.

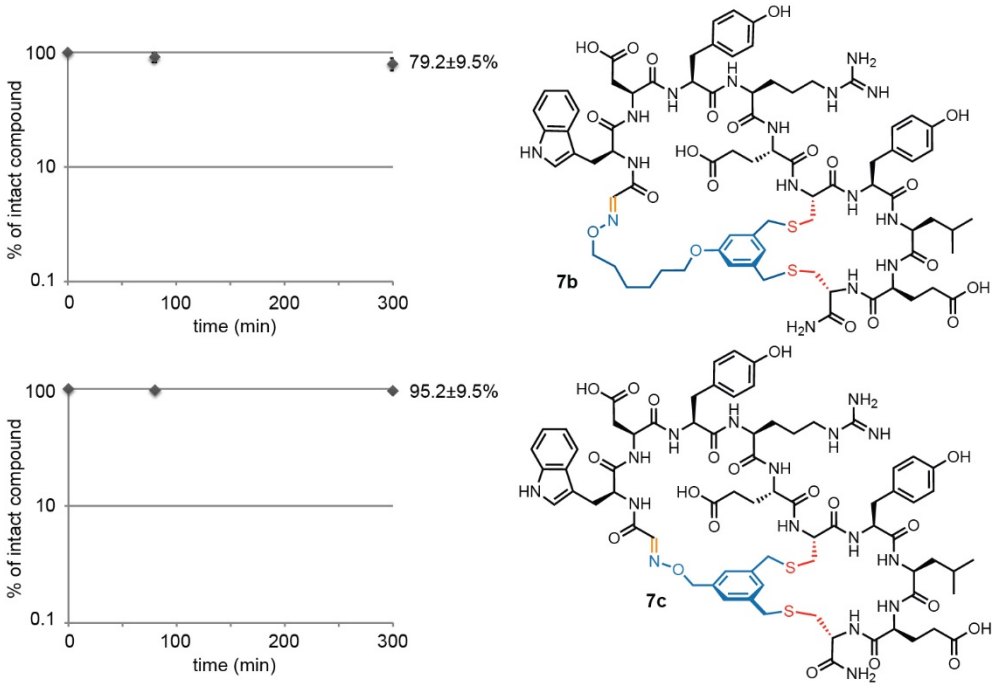

Appendix A-Figure 26. Proteolytic stability of **7b** and **7c** in fresh mouse serum.

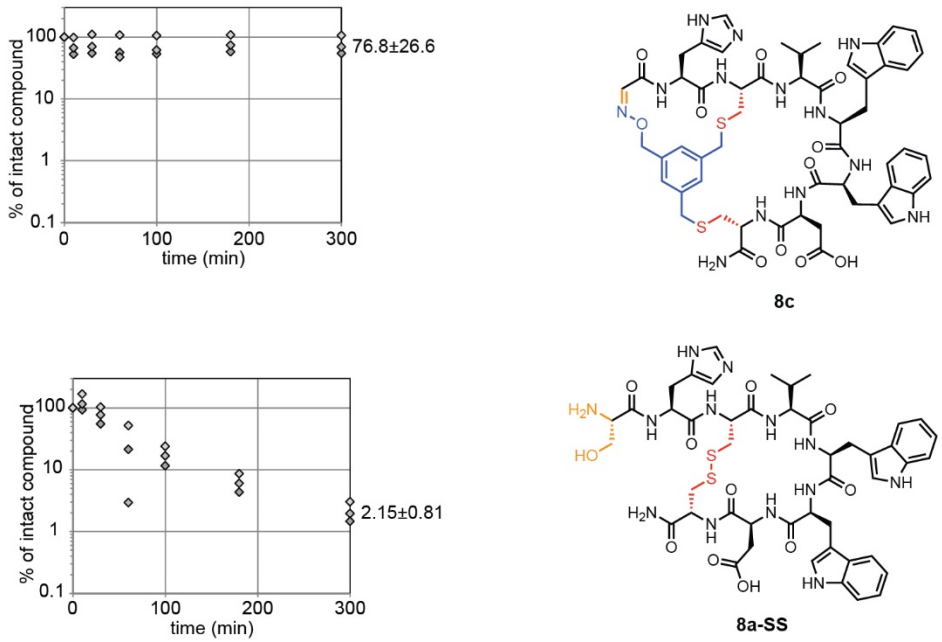

Appendix A-Figure 27. Proteolytic stability of **8c** and **8a-SS** in fresh mouse serum.

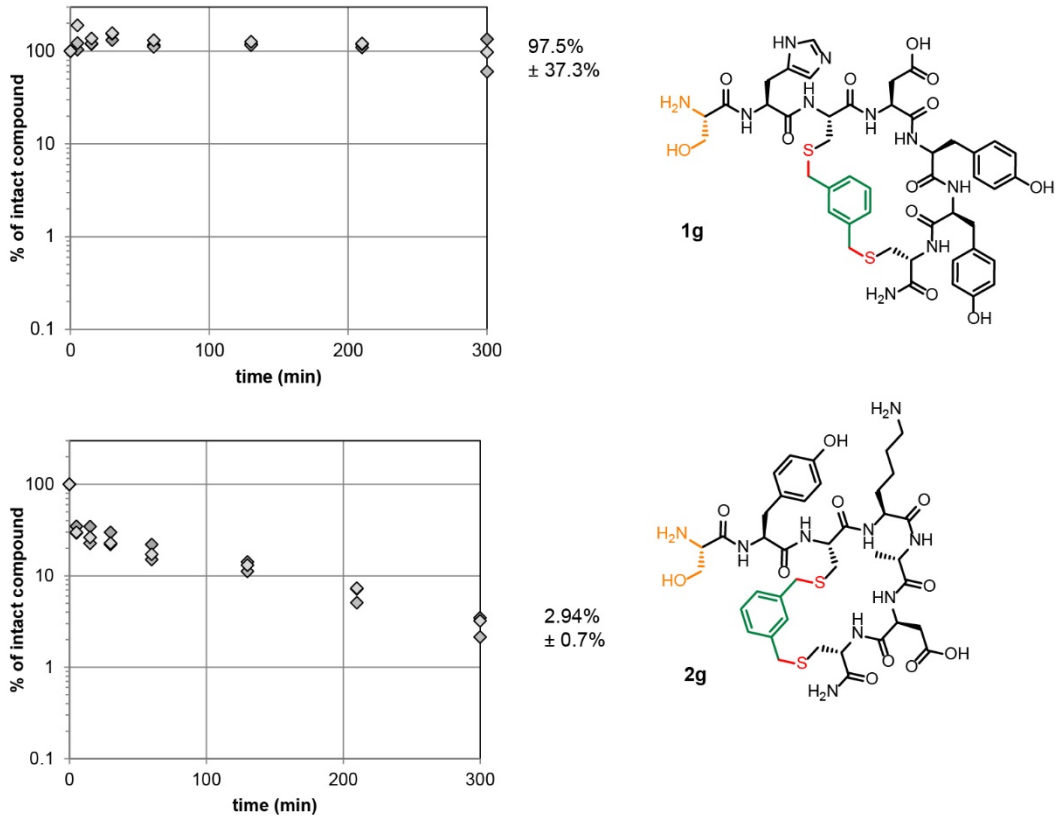

Appendix A-Figure 28. Proteolytic stability of **1g** and **2g** in Pronase^{TM}.

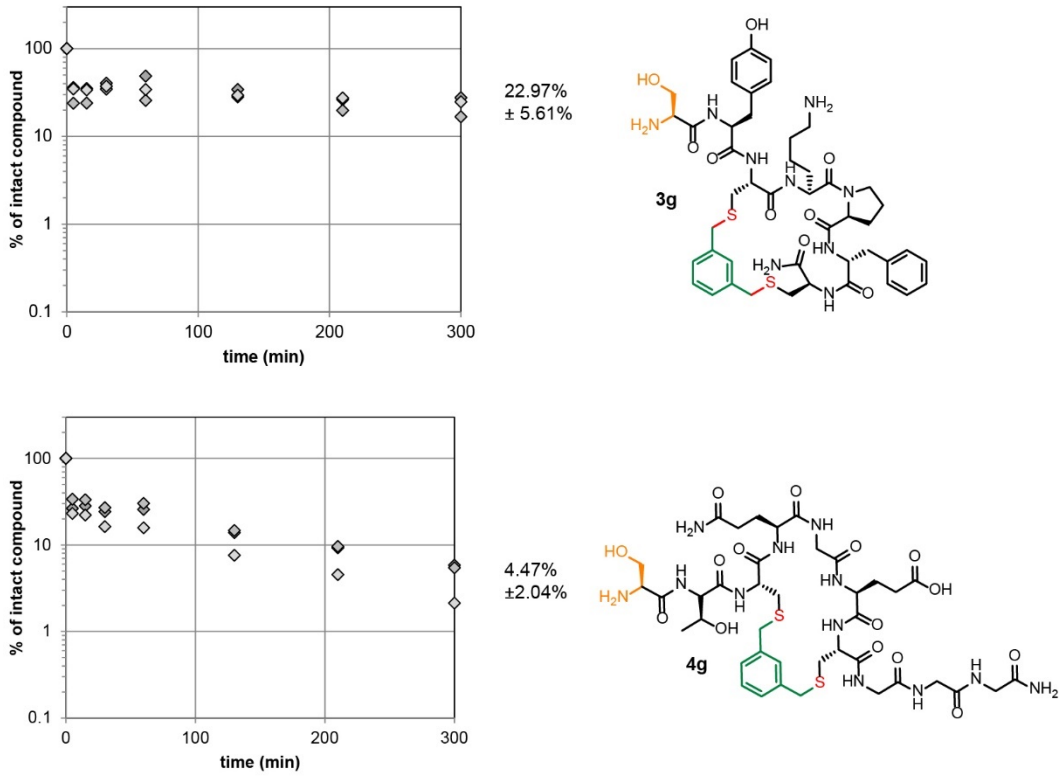

Appendix A-Figure 29. Proteolytic stability of **3g** and **4g** in Pronase^{TM}.

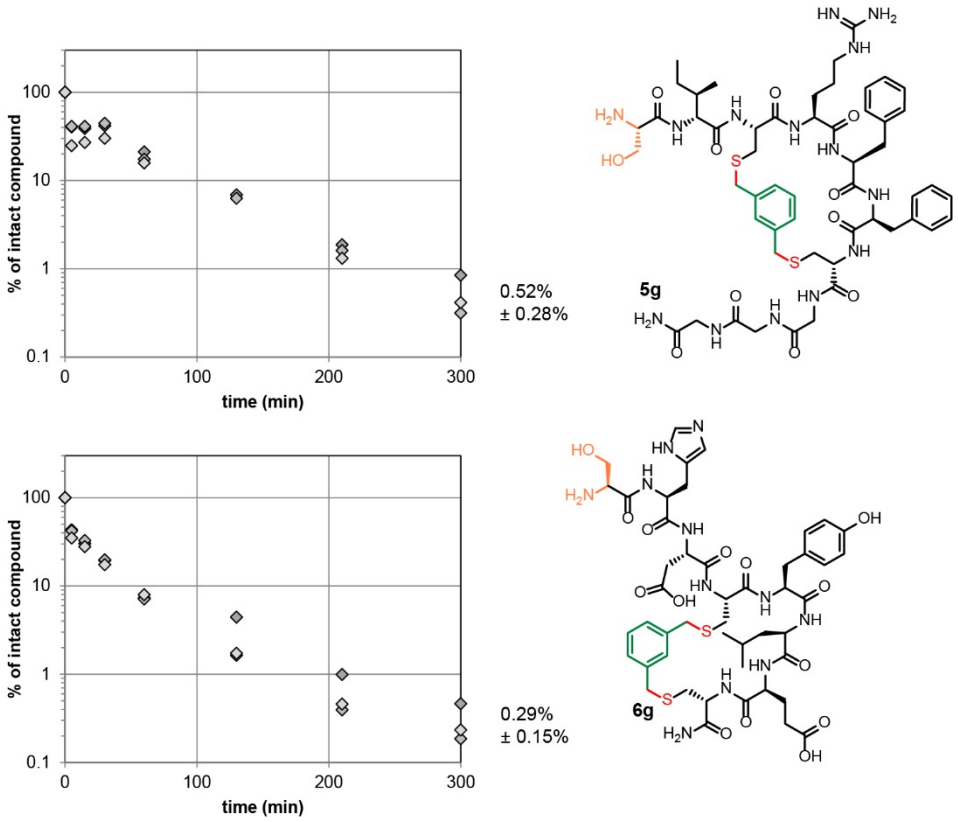

Appendix A-Figure 30. Proteolytic stability of **5g** and **6g** in Pronase^{TM}.

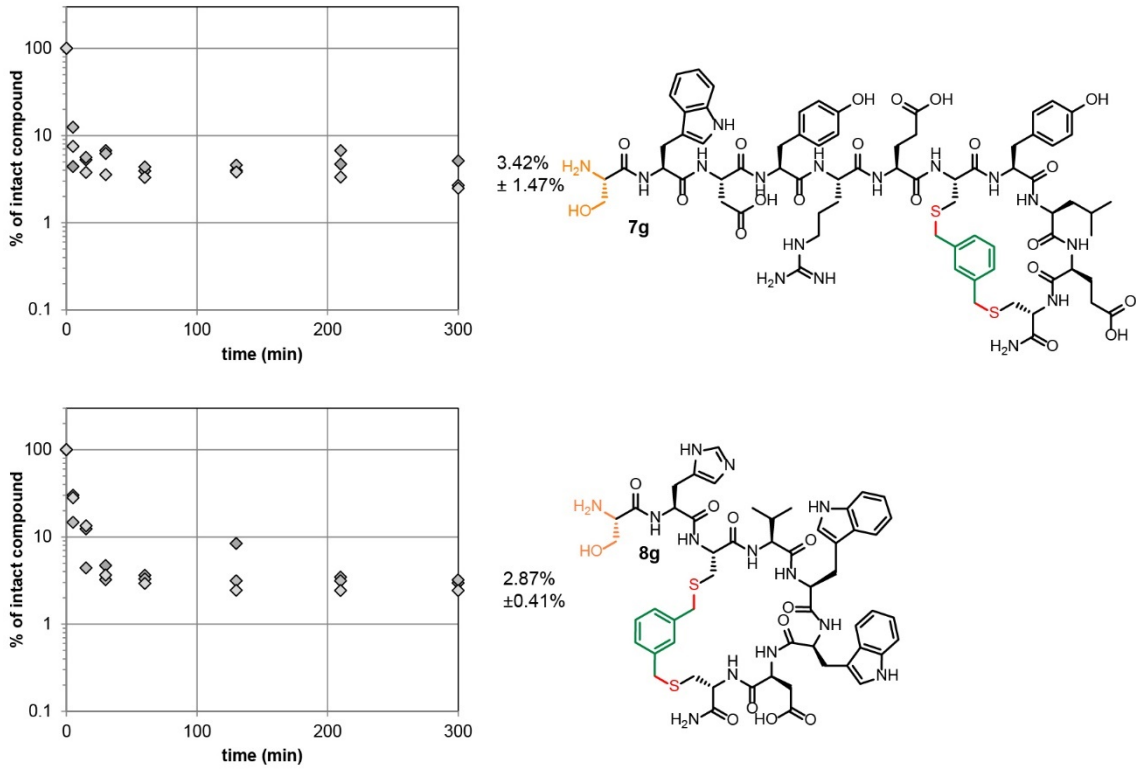

Appendix A-Figure 31. Proteolytic stability of **7g** and **8g** in Pronase^{TM}.

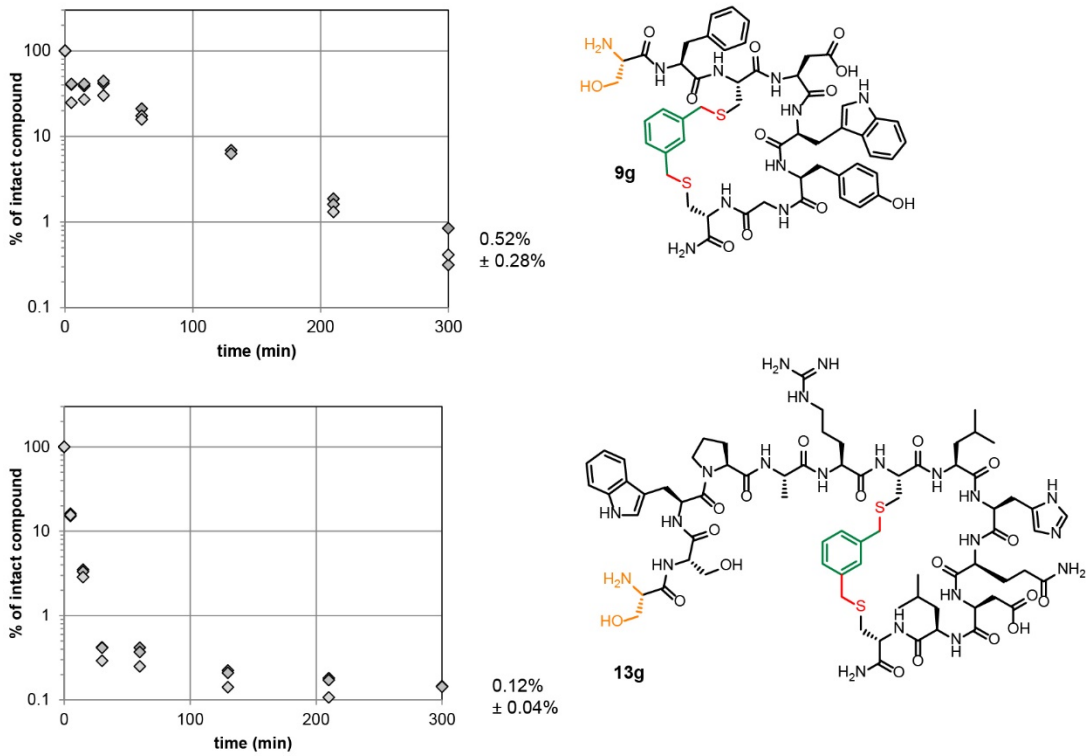

Appendix A-Figure 32. Proteolytic stability of **9g** and **13g** in Pronase^{TM}.

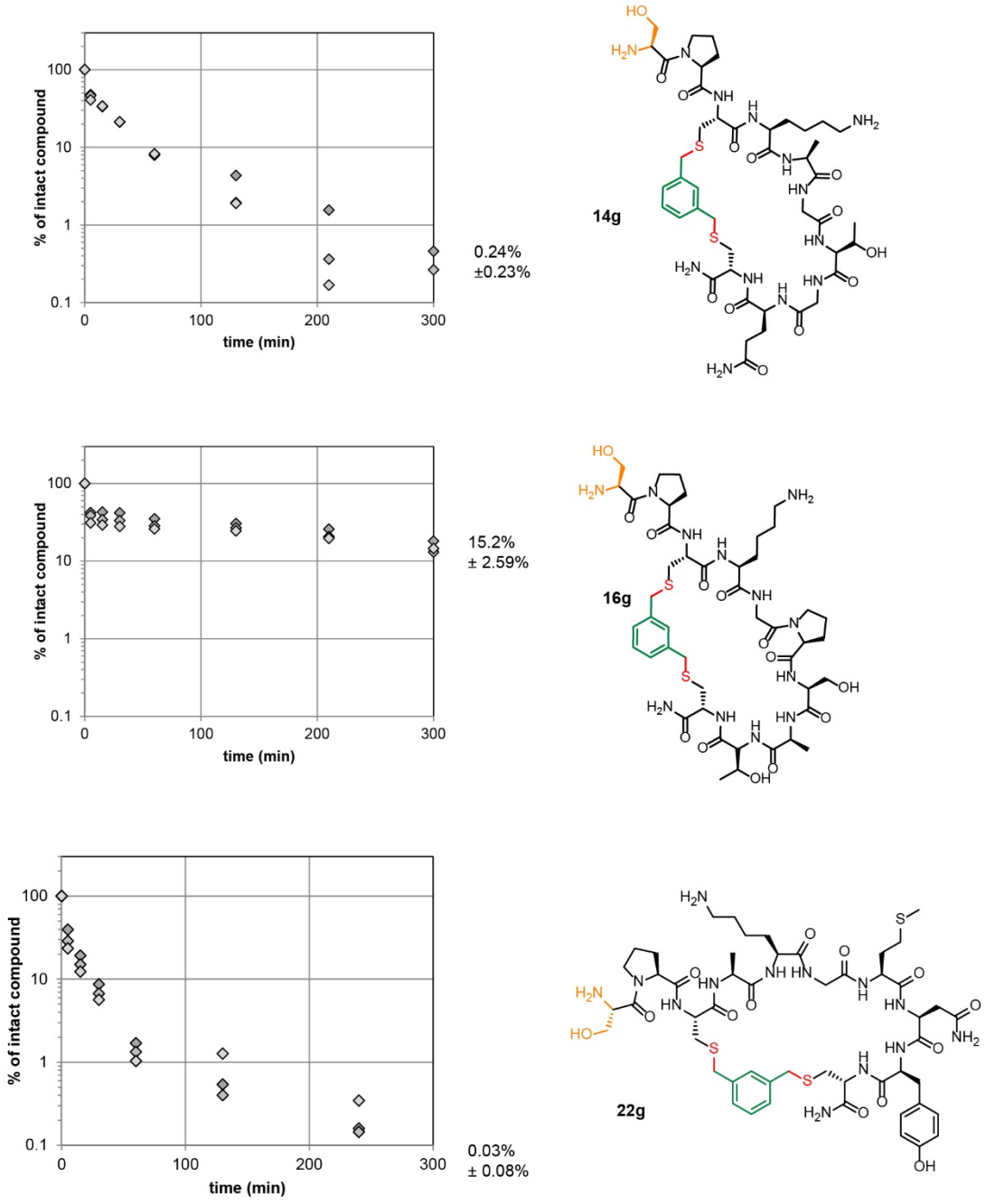

Appendix A-Figure 33. Proteolytic stability of **14g**, **16g** and **22g** in Pronase^{TM}.

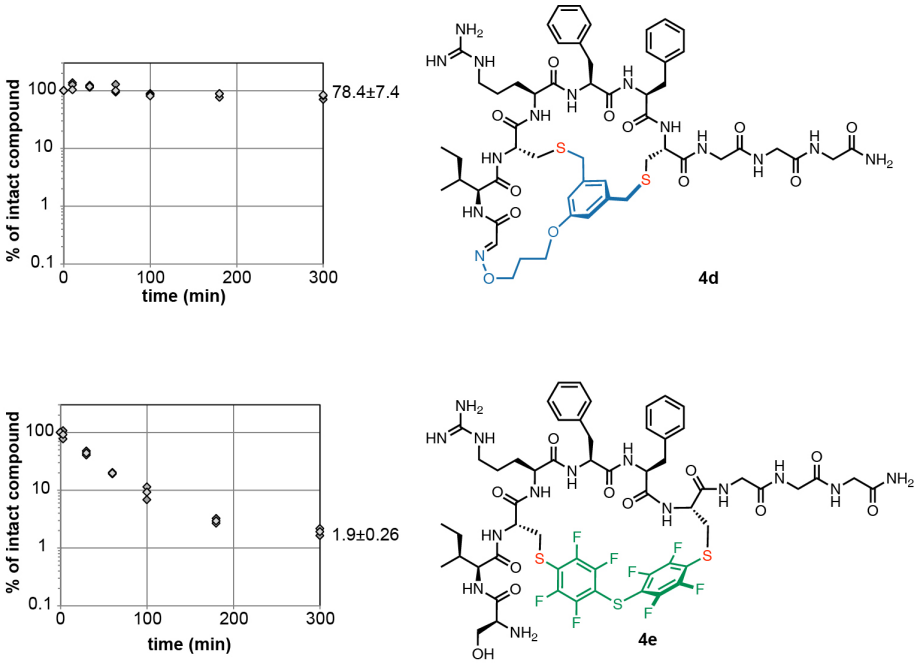

Appendix A-Figure 34. Proteolytic stability of **4d** and **4e** in Pronase^{TM}.

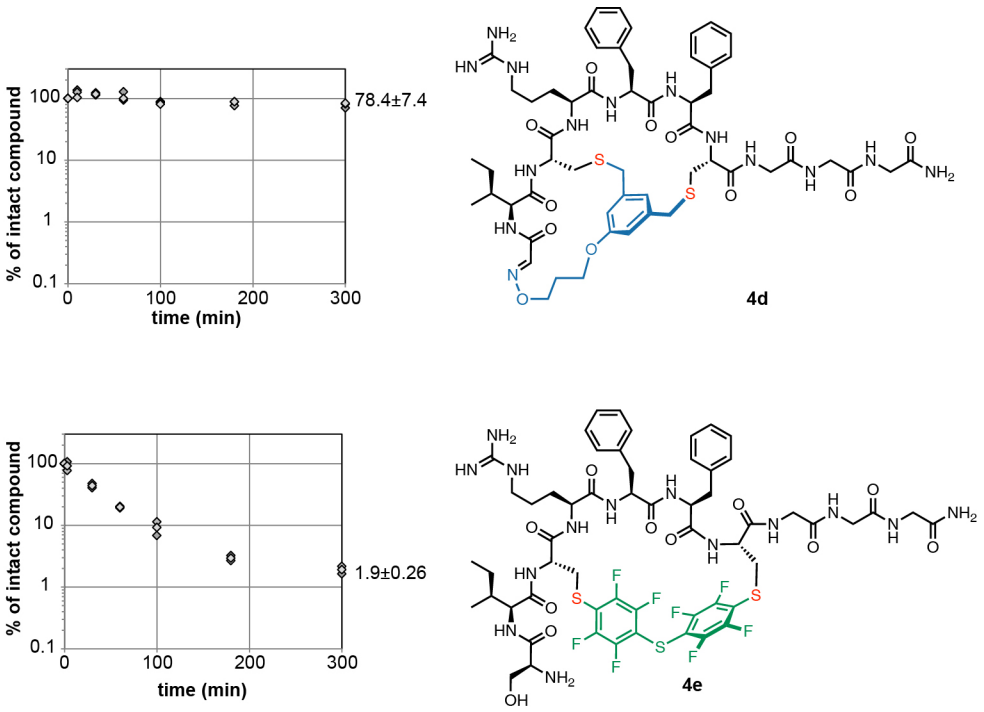

Appendix A-Figure 35. Proteolytic stability of **5d** and **5e** in Pronase^{TM}.

Appendix A-5: Summary of synthesis

SHCDYYC-TSL1

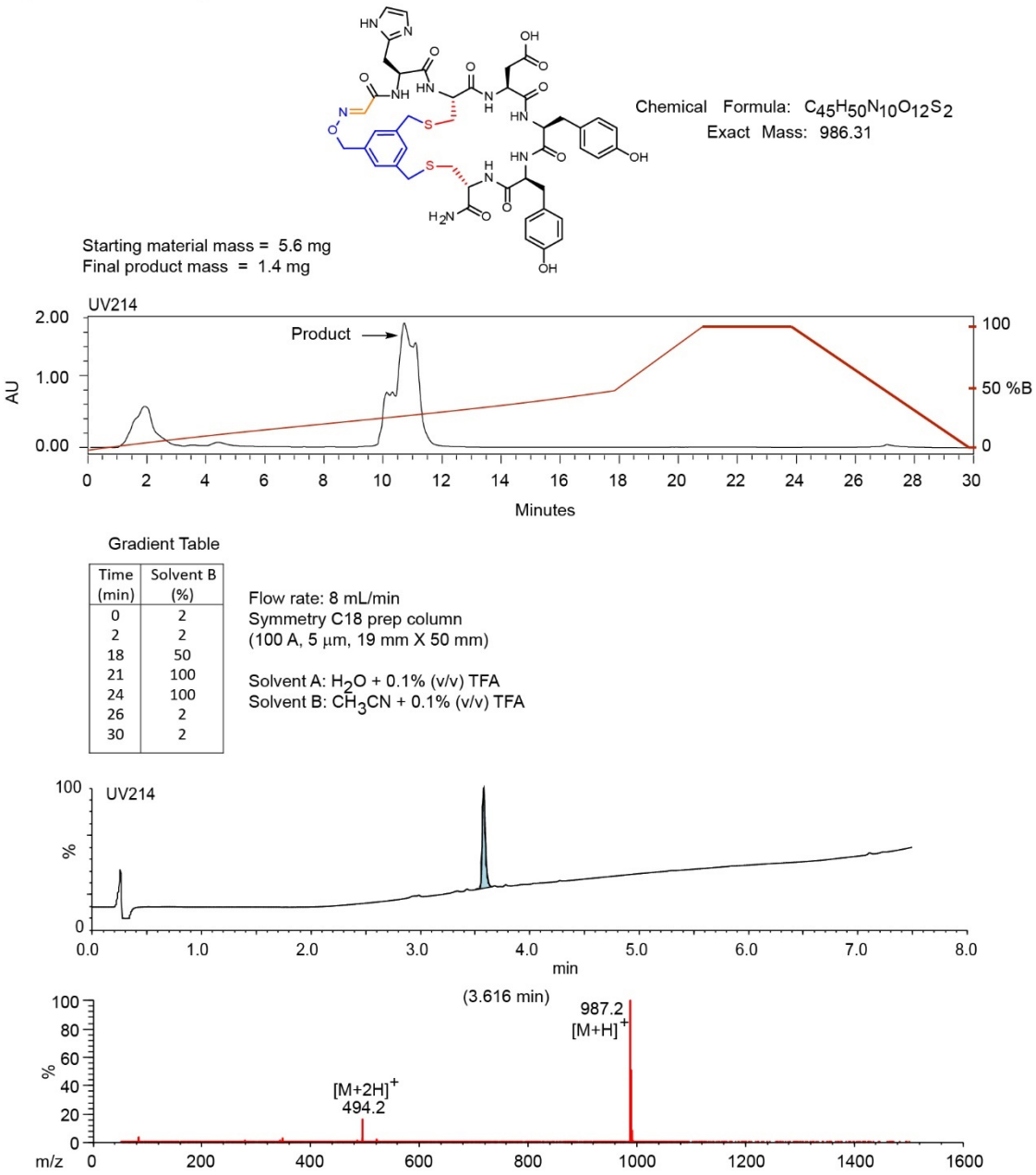

Appendix A-Figure 36. Synthesis summary of **1c**.

SYCKADC-TSL1

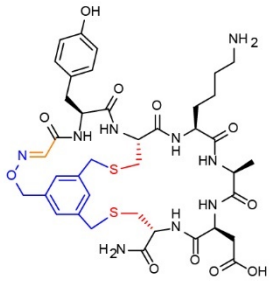

Chemical Formula: $C_{39}H_{51}N_9O_{11}S_2$
Exact Mass: 885.3149

Starting material mass = 9.0 mg
Final product mass = 3.7mg

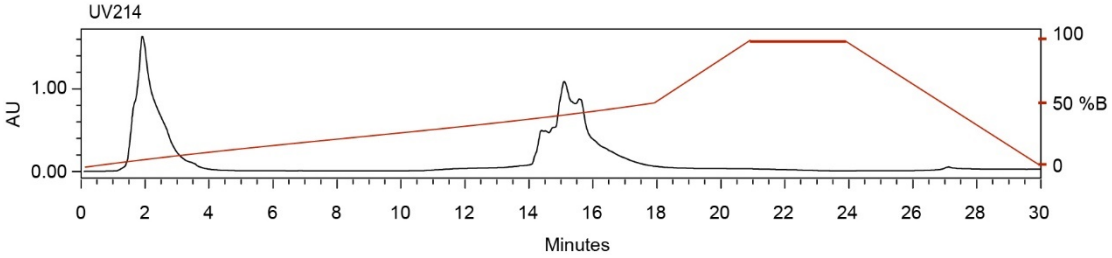

Gradient Table

Time (min)	Solvent B (%)
0	2
2	2
18	50
21	100
24	100
26	2
30	2

Flow rate: 8 mL/min
Symmetry C18 prep column
(100 A, 5 μm, 19 mm X 50 mm)

Solvent A: H_2O + 0.1% (v/v) TFA
Solvent B: CH_3CN + 0.1% (v/v) TFA

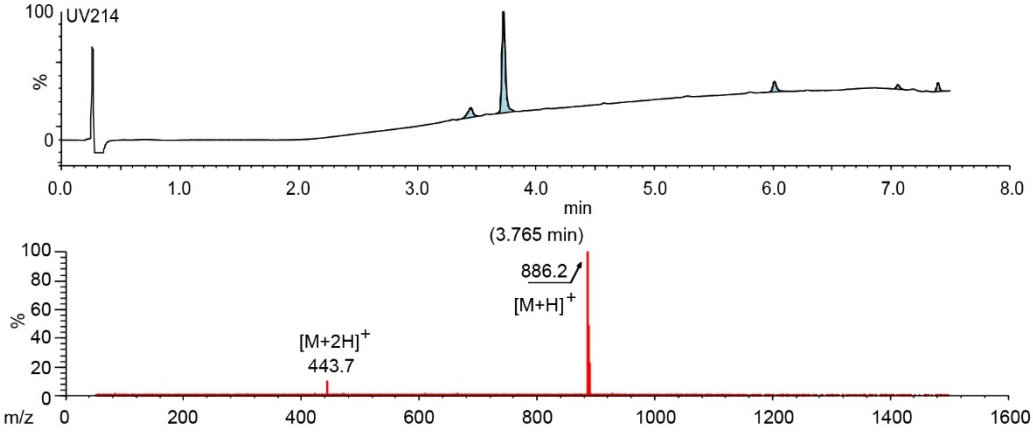

Appendix A-Figure 37. Synthesis summary of **2c**.

SYCKPFC-TSL1

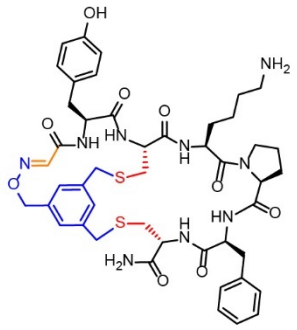

Chemical Formula: $C_{46}H_{57}N_9O_9S_2$
Exact Mass: 943.3721

Starting material mass = 10 mg
Final product mass = 4.6 mg

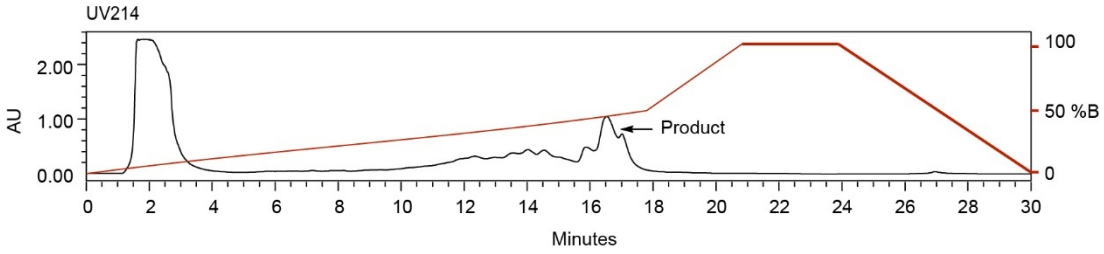

Gradient Table

Time (min)	Solvent B (%)
0	2
2	2
18	50
21	100
24	100
26	2
30	2

Flow rate: 8 mL/min
Symmetry C18 prep column
(100 A, 5 μm, 19 mm X 50 mm)

Solvent A: H_2O + 0.1% (v/v) TFA
Solvent B: CH_3CN + 0.1% (v/v) TFA

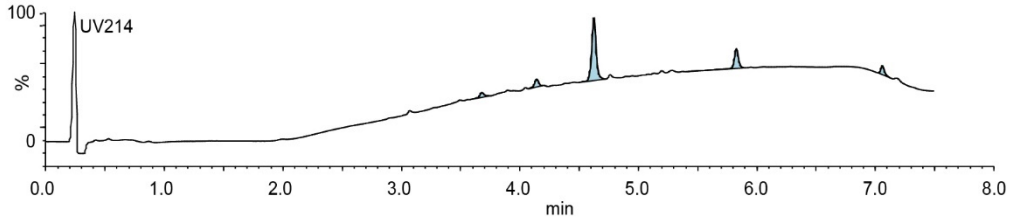

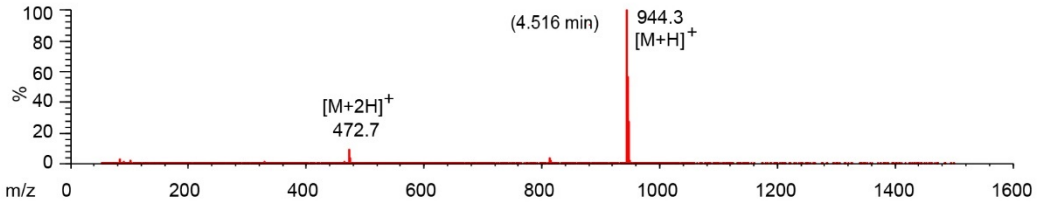

Appendix A-Figure 38. Synthesis summary of **3c**.

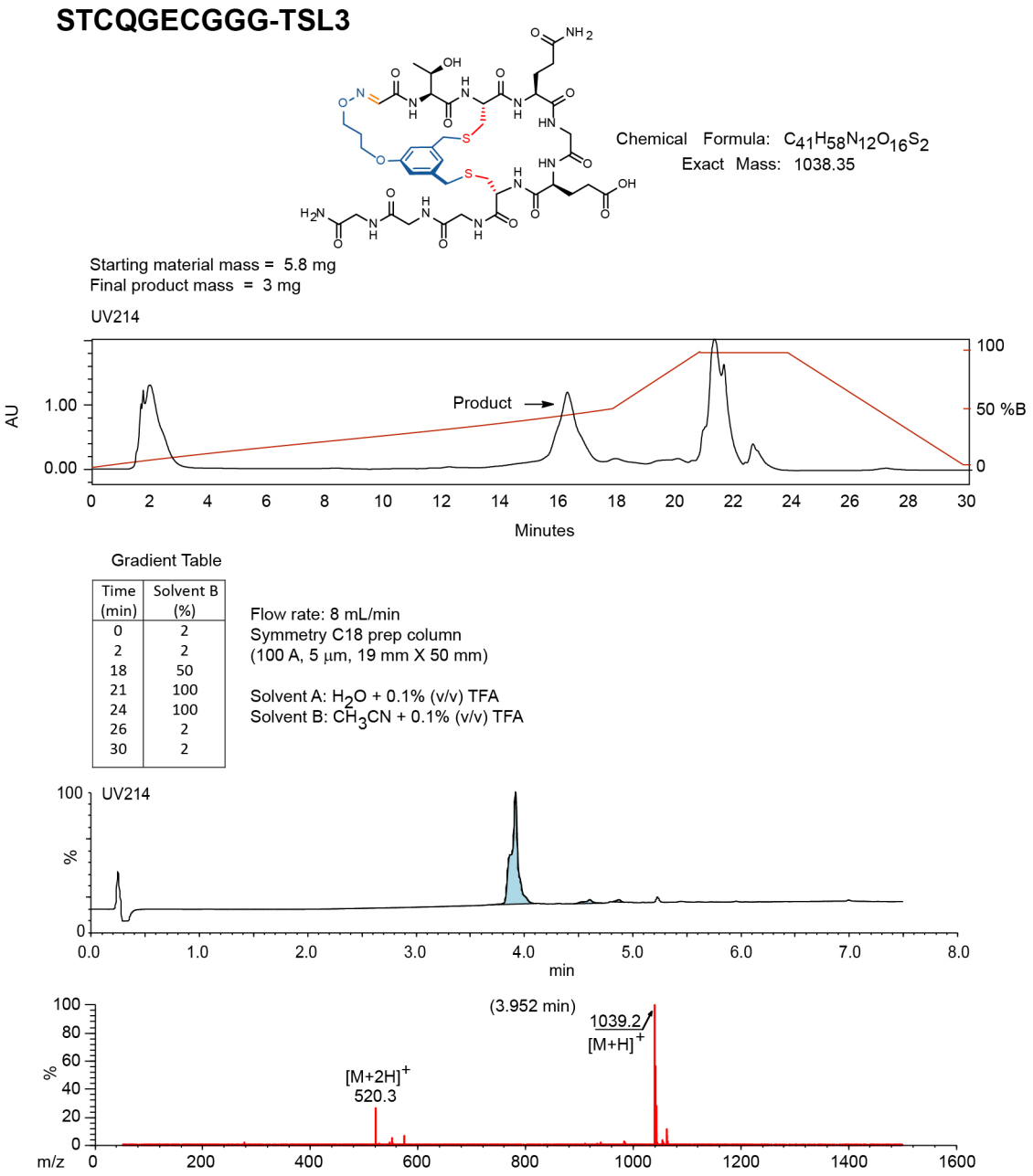

Appendix A-Figure 39. Synthesis summary of **4d**.

SICRFFCGGG-TSL3

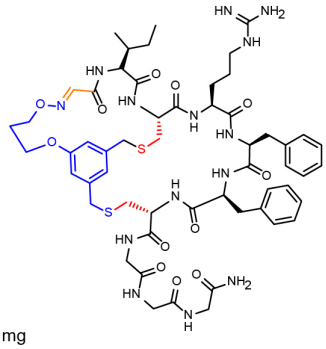

Chemical Formula: $C_{55}H_{74}N_{14}O_{12}S_2$
Exact Mass: 1186.5052

Starting material mass = 5.9 mg
Final product mass = 3.7 mg

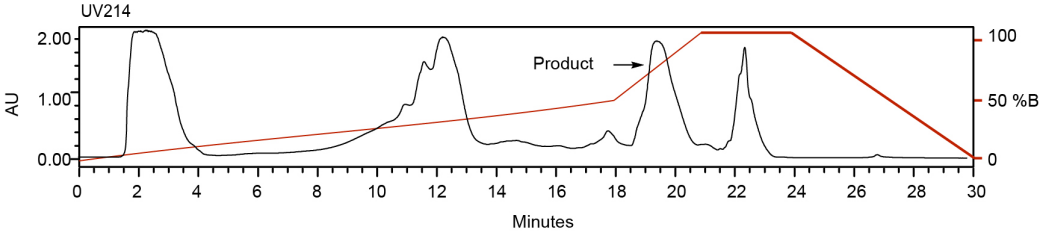

Gradient Table

Time (min)	Solvent B (%)
0	2
2	2
18	50
21	100
24	100
26	2
30	2

Flow rate: 8 mL/min
Symmetry C18 prep column
(100 A, 5 μm, 19 mm X 50 mm)

Solvent A: H_2O + 0.1% (v/v) TFA
Solvent B: CH_3CN + 0.1% (v/v) TFA

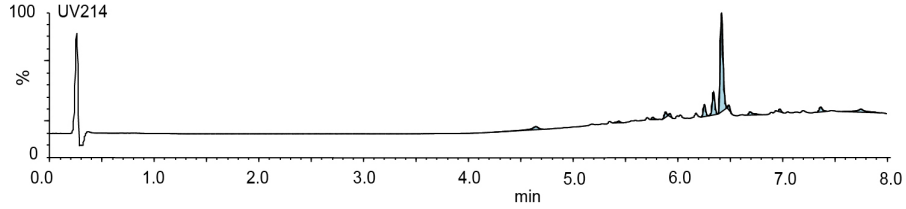

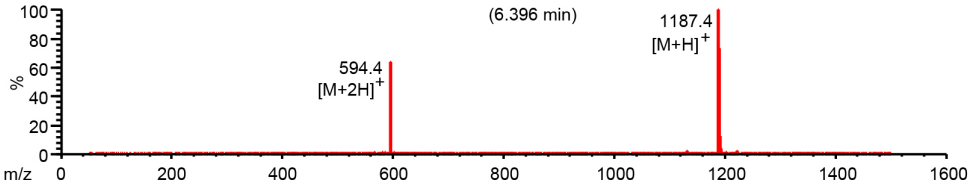

Appendix A-Figure 40. Synthesis summary of **5d**.

SWDYRECYLEC-TSL1

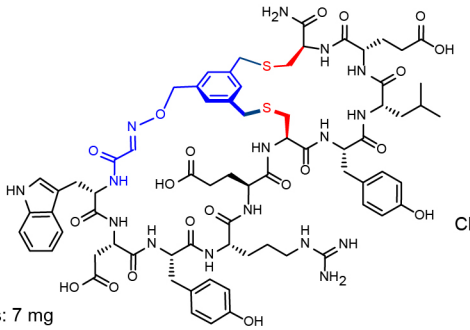

Chemical Formula: $C_{72}H_{90}N_{16}O_{20}S_2$
Exact Mass: 1562.60

Starting material mass: 7 mg
Final product mass: 3 mg

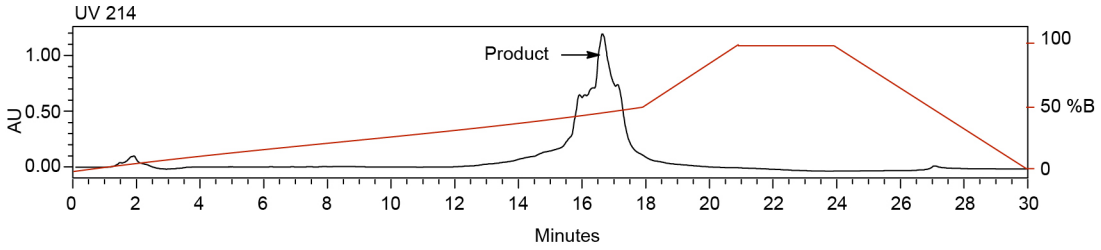

Gradient Table

Time (min)	Solvent B (%)
0	2
2	2
18	50
21	100
24	100
26	2
30	2

Flow rate: 8 mL/min
Symmetry C18 prep column
(100 A, 5 μm, 19 mm X 50 mm)

Solvent A: H_2O + 0.1% (v/v) TFA
Solvent B: CH_3CN + 0.1% (v/v) TFA

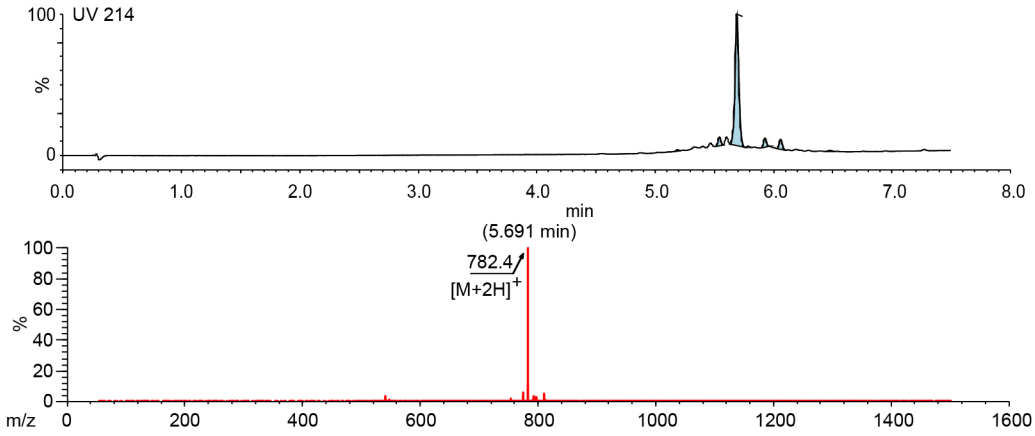

Appendix A-Figure 41. Synthesis summary of **7c**.

SWDYRECYLEC-TSL6

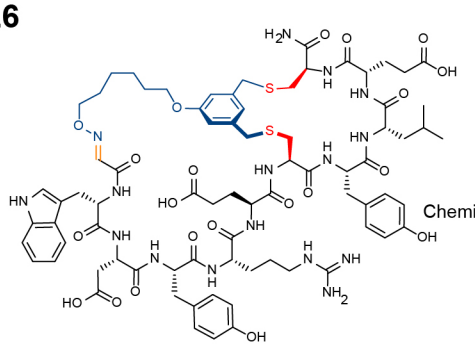

Chemical Formula: $C_{77}H_{100}N_{16}O_{21}S_2$
Exact Mass: 1648.6690

Starting material mass: 19 mg
Final product mass: 8 mg

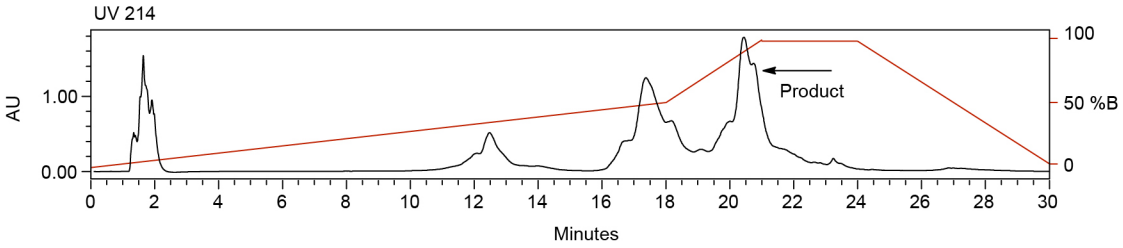

Gradient Table

Time (min)	Solvent B (%)
0	2
2	2
18	50
21	100
24	100
26	2
30	2

Flow rate: 8 mL/min
Symmetry C18 prep column
(100 A, 5 μm, 19 mm X 50 mm)

Solvent A: H_2O + 0.1% (v/v) TFA
Solvent B: CH_3CN + 0.1% (v/v) TFA

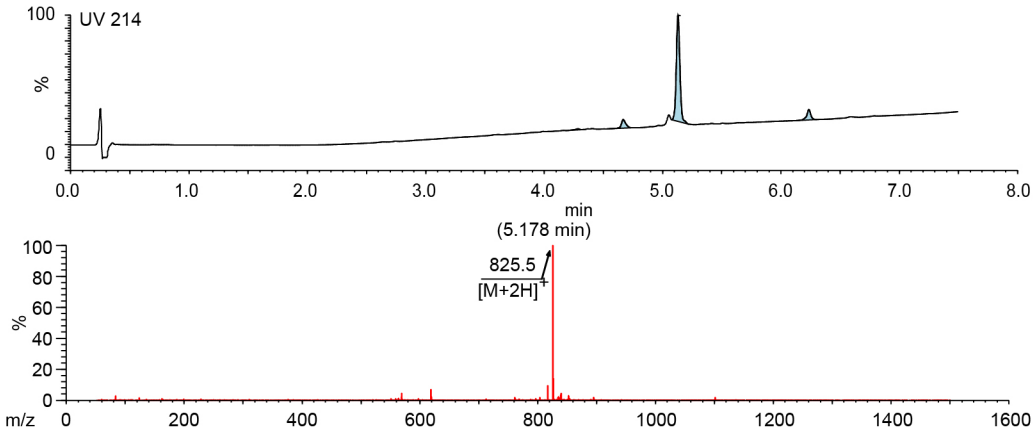

Appendix A-Figure 42. Synthesis summary of **7b**.

SHCVWWDC-TSL1

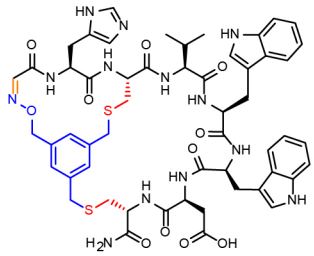

Chemical Formula: $C_{54}H_{61}N_{13}O_{11}S_2$
Exact Mass: 1131.41

Starting material mass = 9.1 mg
Final product mass = 4.2 mg

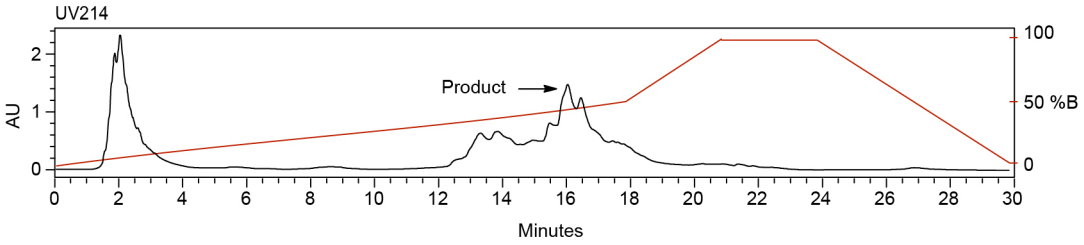

Gradient Table

Time (min)	Solvent B (%)
0	2
2	2
18	50
21	100
24	100
26	2
30	2

Flow rate: 8 mL/min
Symmetry C18 prep column
(100 A, 5 μm, 19 mm X 50 mm)

Solvent A: H_2O + 0.1% (v/v) TFA
Solvent B: CH_3CN + 0.1% (v/v) TFA

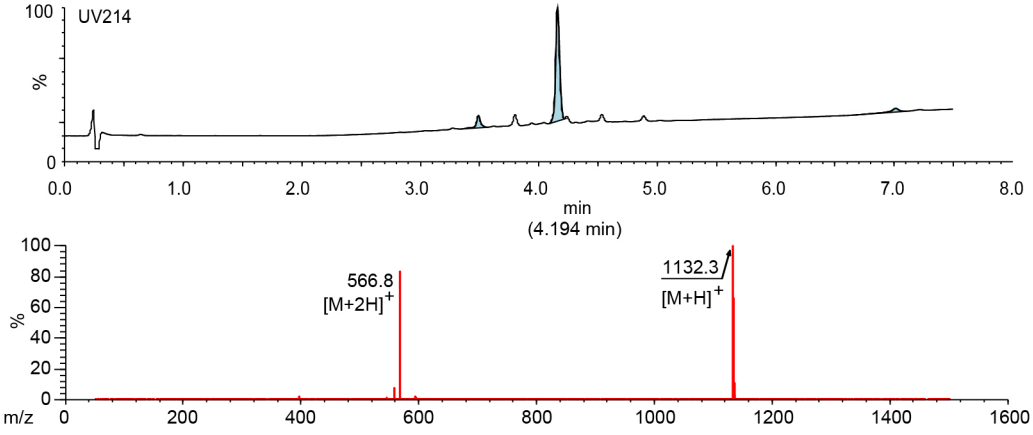

Appendix A-Figure 43. Synthesis summary of **8c**.

SFCDWYGC-TSL6

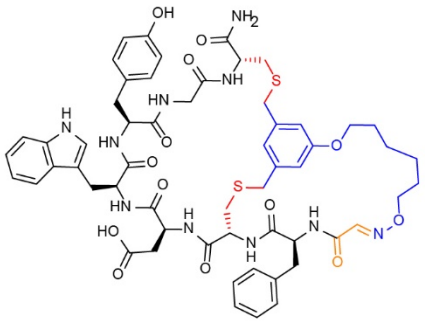

Chemical Formula: $C_{57}H_{66}N_{10}O_{13}S_2$
Exact Mass: 1162.4252

Starting material mass = 20 mg
Final product mass = 5 mg

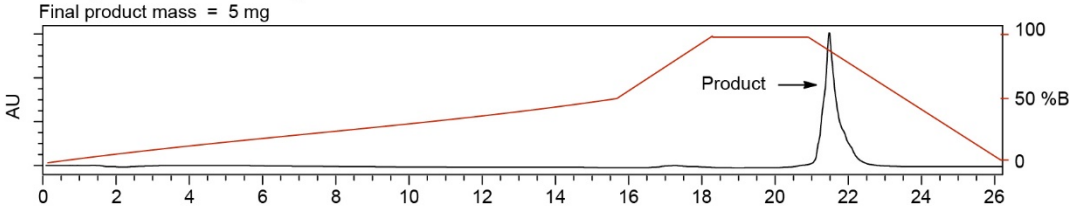

Gradient Table

Time (min)	Solvent B (%)
0	2
2	2
18	50
21	100
24	100
26	2
30	2

Flow rate: 8 mL/min
Symmetry C18 prep column
(100 A, 5 μm, 19 mm X 50 mm)

Solvent A: H_2O + 0.1% (v/v) TFA
Solvent B: CH_3CN + 0.1% (v/v) TFA

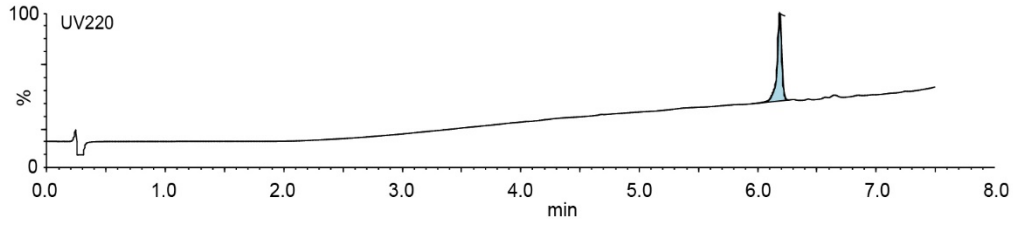

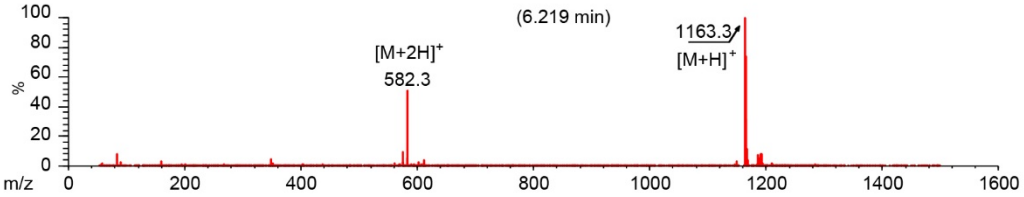

Appendix A-Figure 44. Synthesis summary of **9b**.

SSWPARCLHQDLC-TSL1

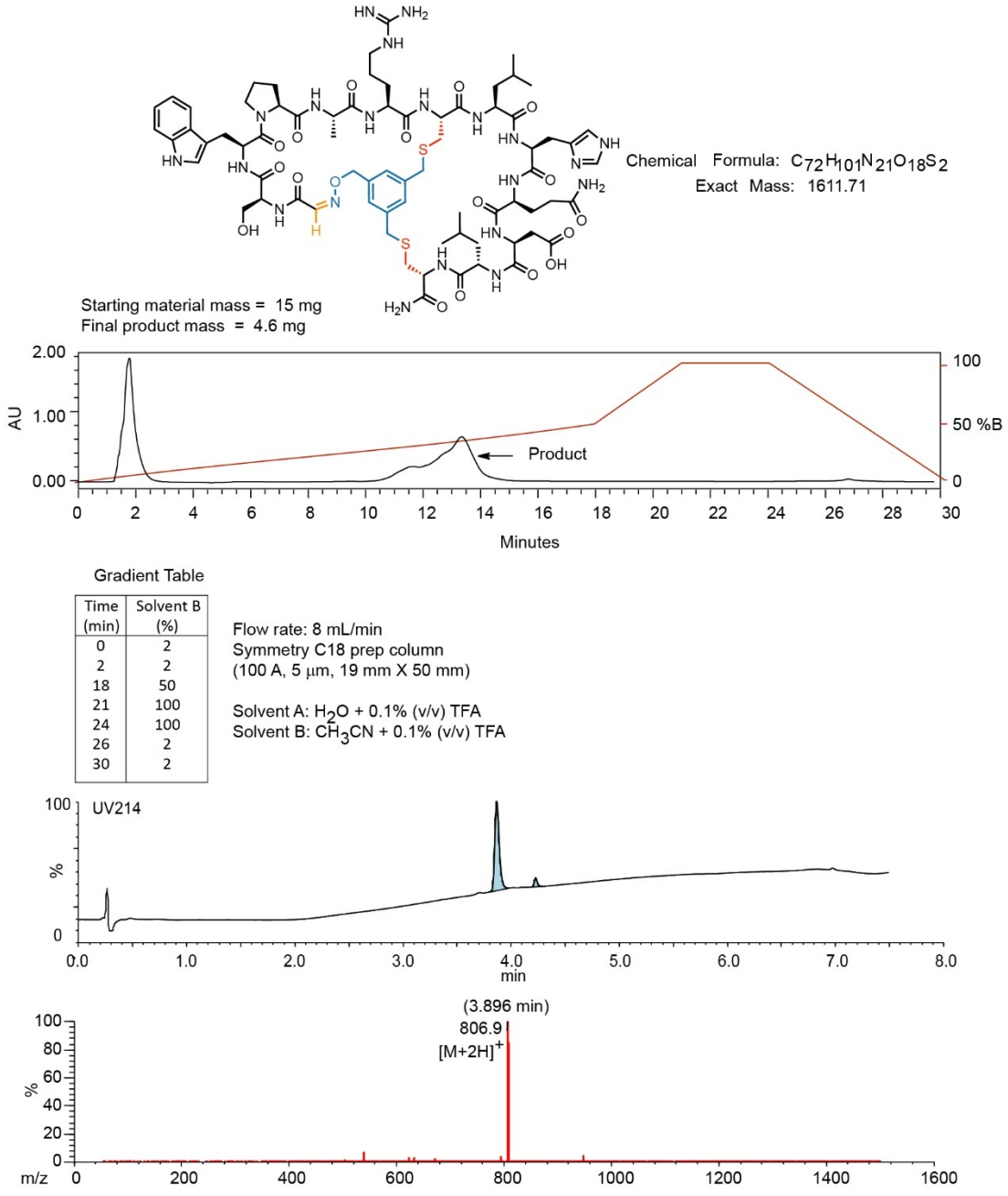

Appendix A-Figure 45. Synthesis summary of **13c**.

SNTWNPWCPWDAPLCam-TSL1

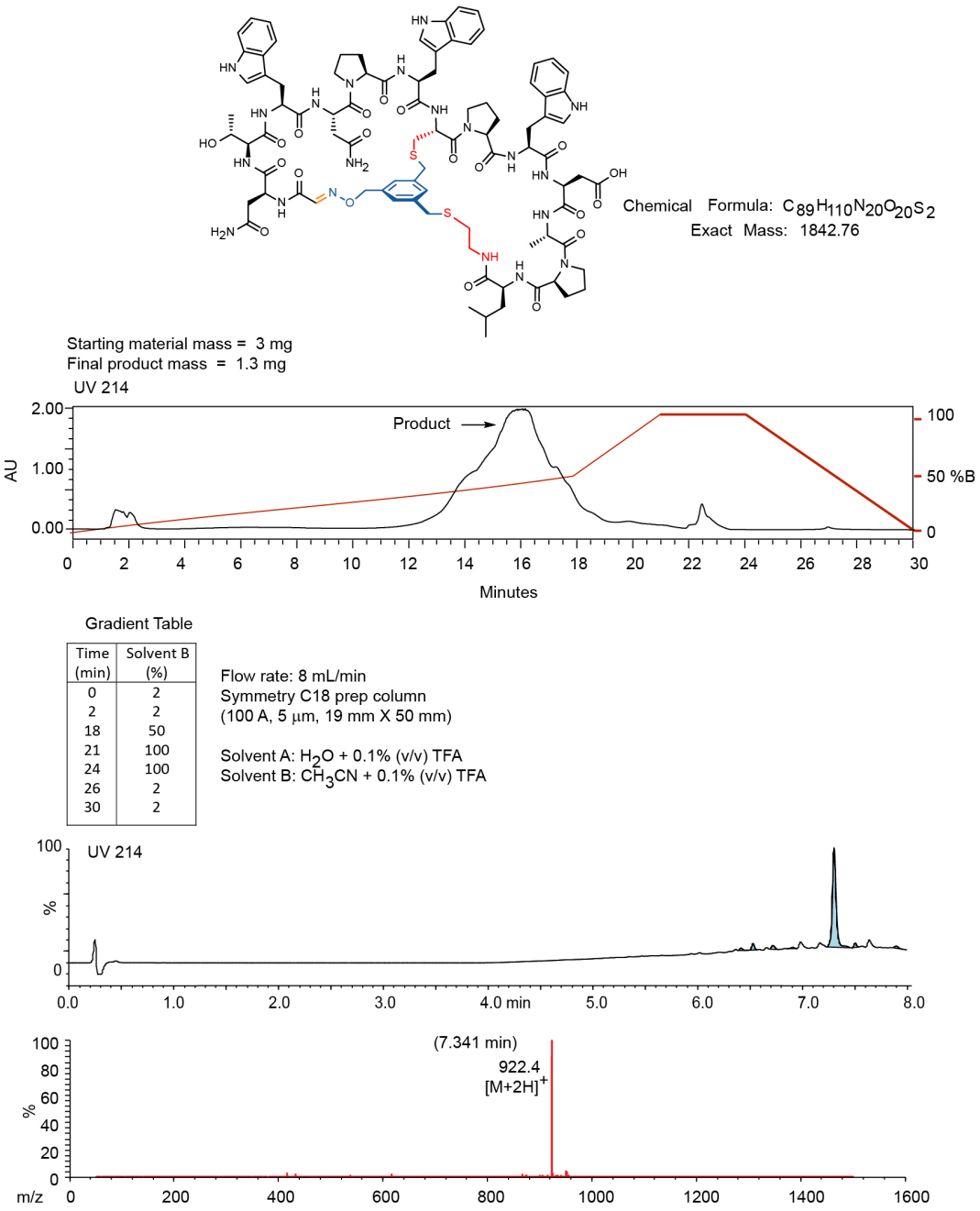

Appendix A-Figure 46. Synthesis summary of **12c**.

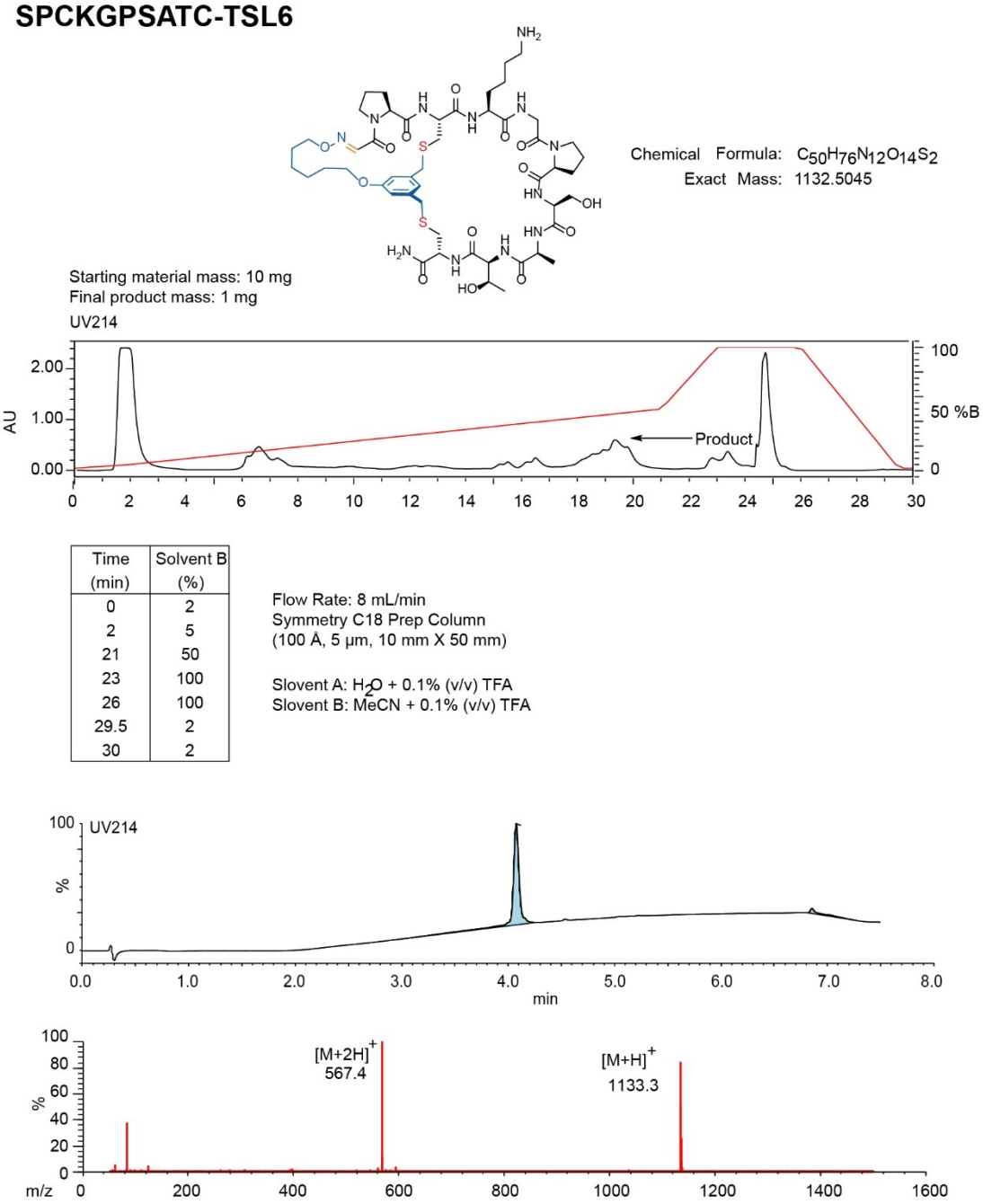

Appendix A-Figure 47. Synthesis summary of **15b**.

SPCKGRHHNC-TSL6

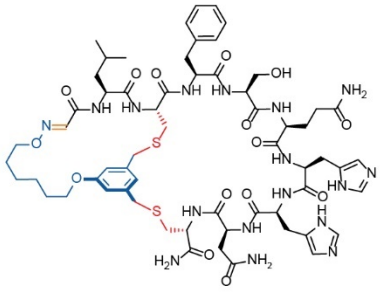

Chemical Formula: $C_{57}H_{84}N_{20}O_{13}S_2$
Exact Mass: 1320.5968

Starting material mass: 6.0 mg
Final product mass: 10.0 mg

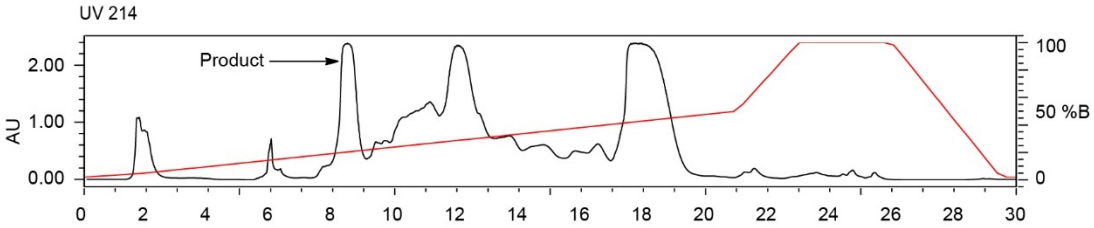

Time (min)	Solvent B (%)
0	2
2	5
21	50
23	100
26	100
29.5	2
30	2

Flow Rate: 8 mL/min
Symmetry C18 Prep Column
(100 Å, 5 µm, 10 mm X 50 mm)

Slovent A: H_2O + 0.1% (v/v) TFA
Slovent B: MeCN + 0.1% (v/v) TFA

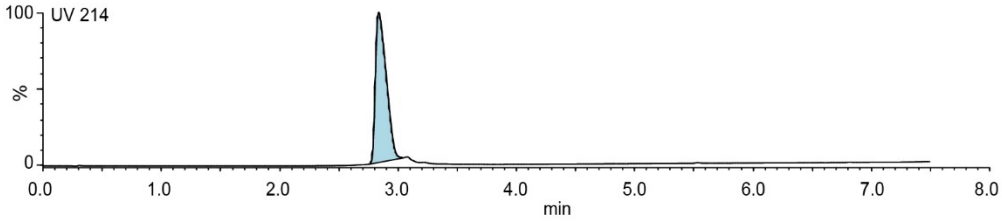

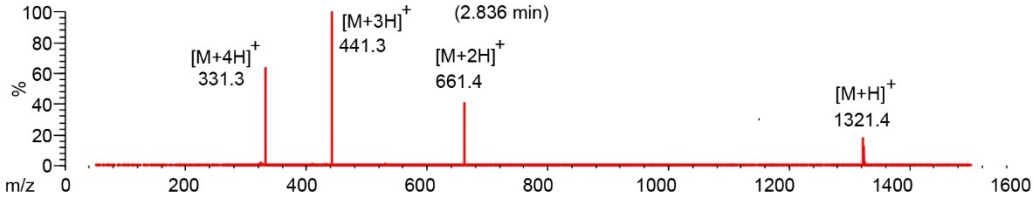

Appendix A-Figure 48. Synthesis summary of **16b**.

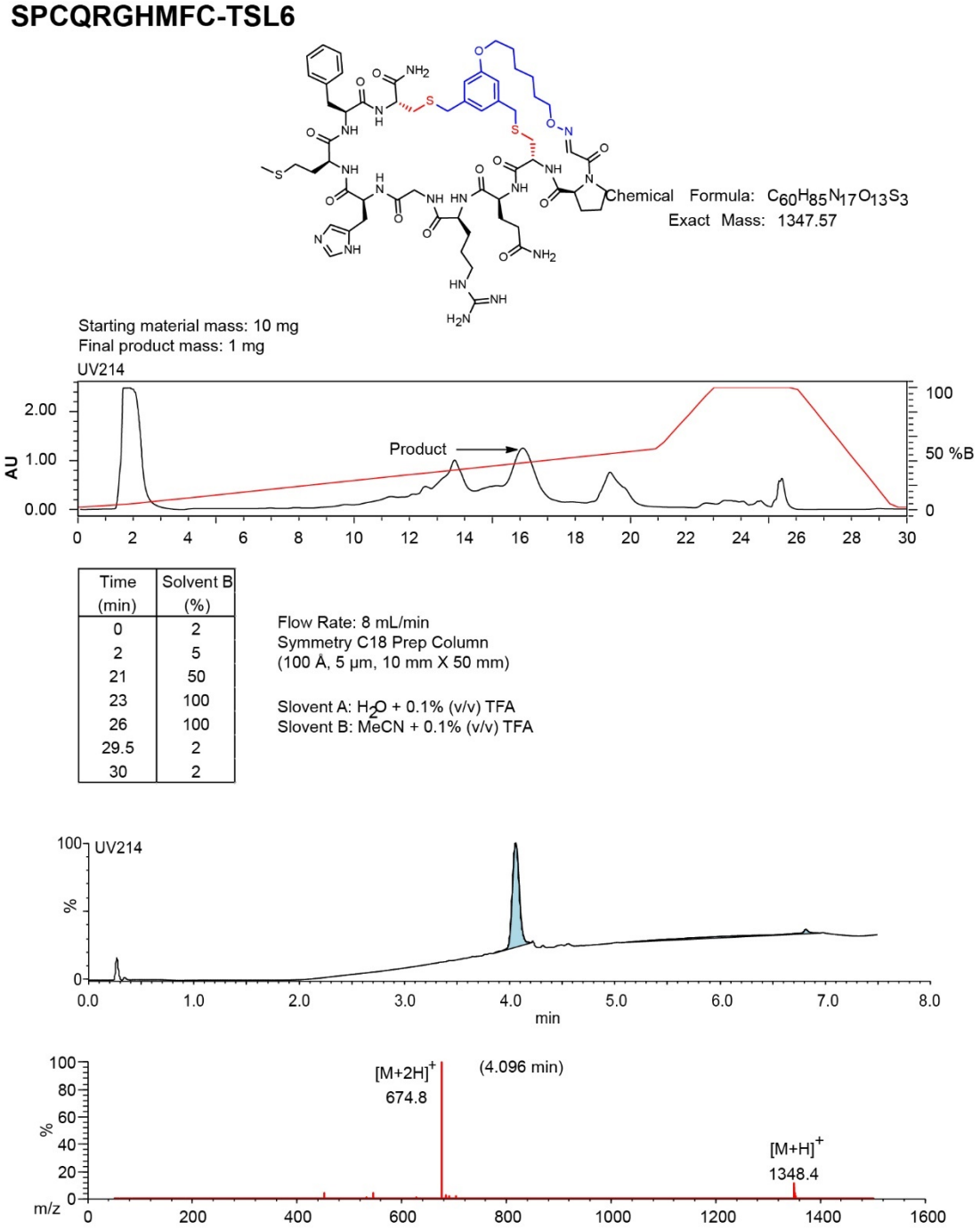

Appendix A-Figure 49. Synthesis summary of **18b**.

SYCKRAHKNC-TSL6

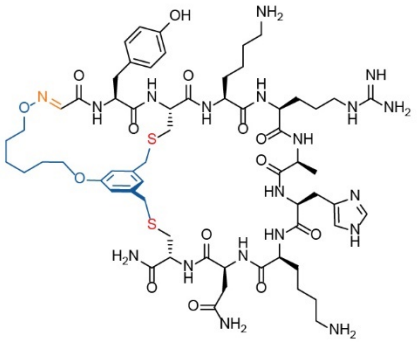

Chemical Formula: $C_{62}H_{93}N_{19}O_{14}S_2$
Exact Mass: 1391.66
Molecular Weight: 1392.67

Starting material mass :10 mg
Final product mass: 1.6 mg

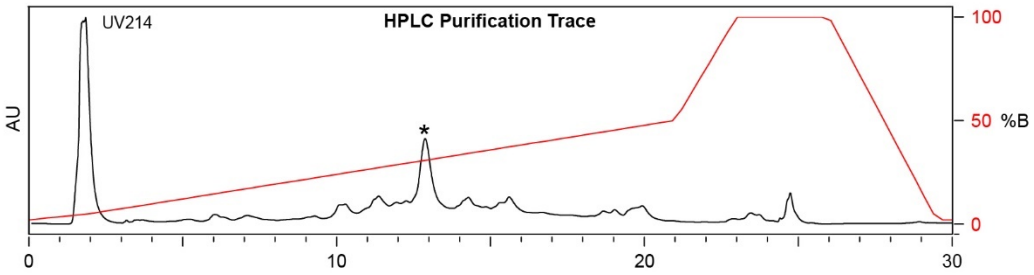

Time (min)	Solvent B (%)
0	2
2	5
21	50
23	100
26	100
29.5	2
30	2

Flow Rate: 8 mL/min
Symmetry C18 Prep Column
(100 Å, 5 µm, 10 mm X 50 mm)

Slovent A: H_2O + 0.1% (v/v) TFA
Slovent B: MeCN + 0.1% (v/v) TFA

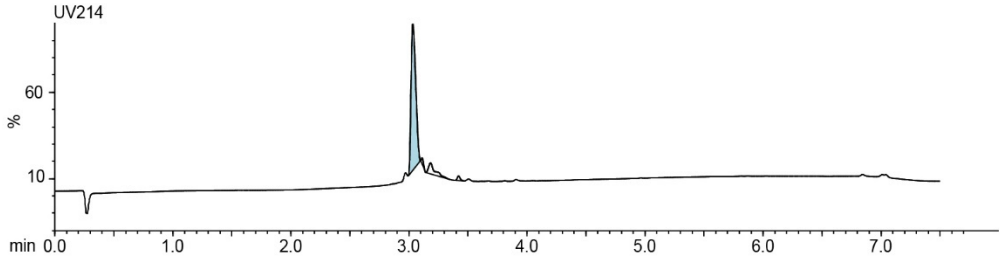

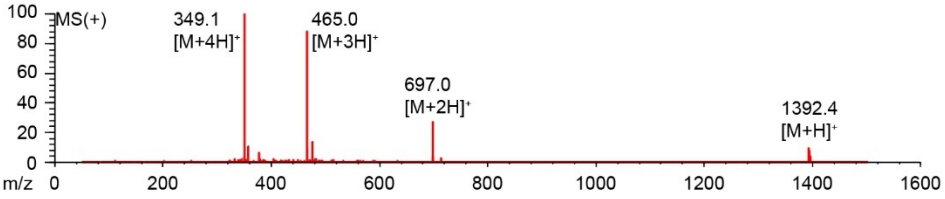

Appendix A-Figure 50. Synthesis summary of **19b**.

SWCRGHDRTC-TSL6

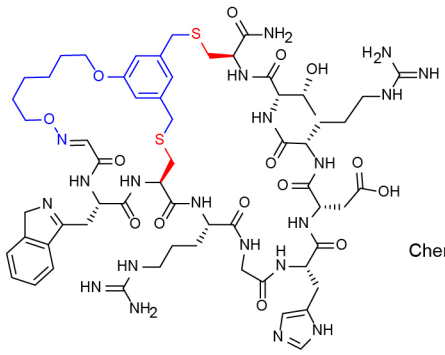

Chemical Formula: $C_{61}H_{86}N_{20}O_{15}S_2$
Exact Mass: 1402.6023

Starting material mass: 10 mg
Final product mass: 0.7 mg

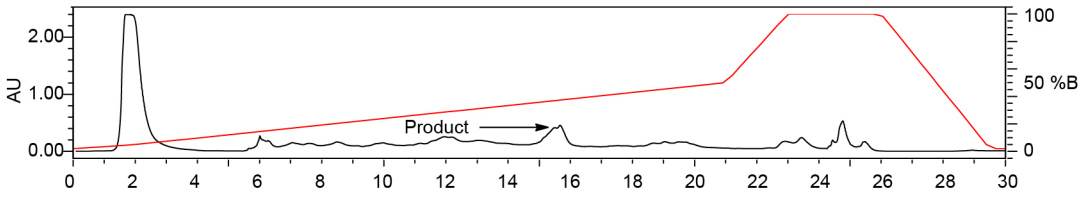

Time (min)	Solvent B (%)
0	2
2	5
21	50
23	100
26	100
29.5	2
30	2

Flow Rate: 8 mL/min
Symmetry C18 Prep Column
(100 Å, 5 µm, 10 mm X 50 mm)

Slovent A: H_2O + 0.1% (v/v) TFA
Slovent B: MeCN + 0.1% (v/v) TFA

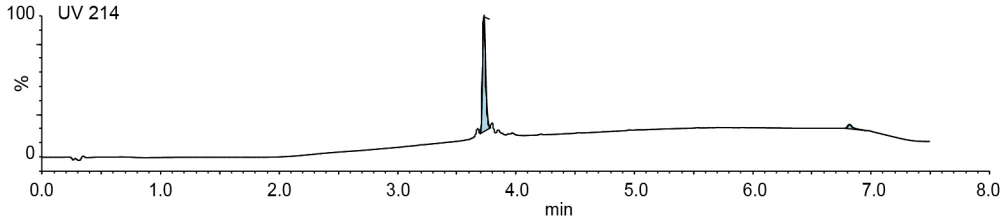

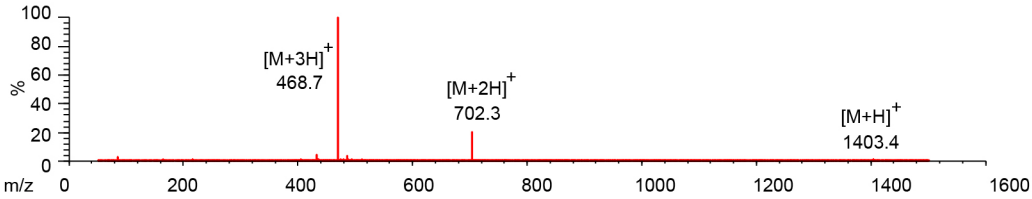

Appendix A-Figure 51. Synthesis summary of **21b**.

SPCAKGMNYC-TSL6

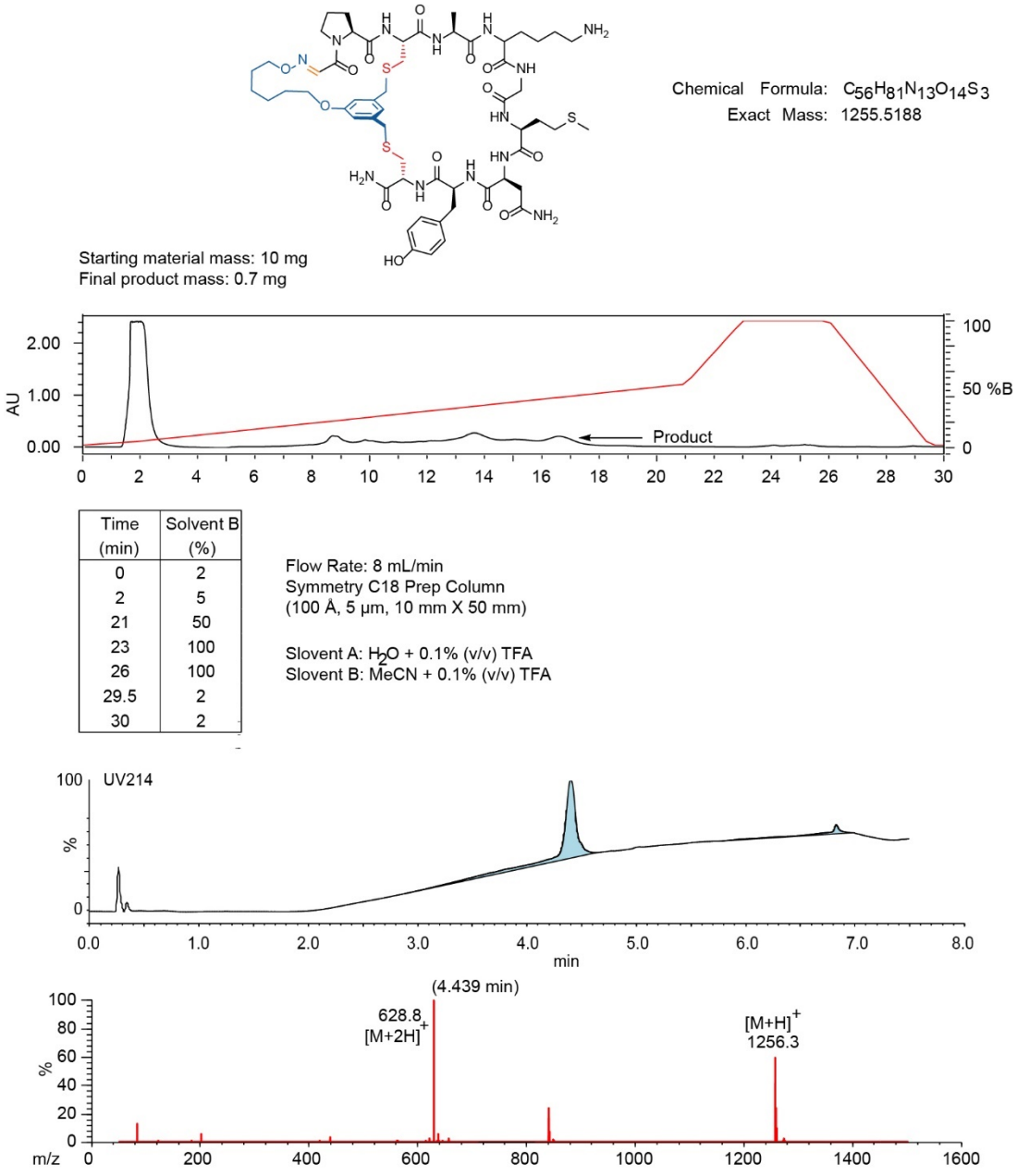

Appendix A-Figure 52. Synthesis summary of **22b**.

STCQGECGGG-PFS

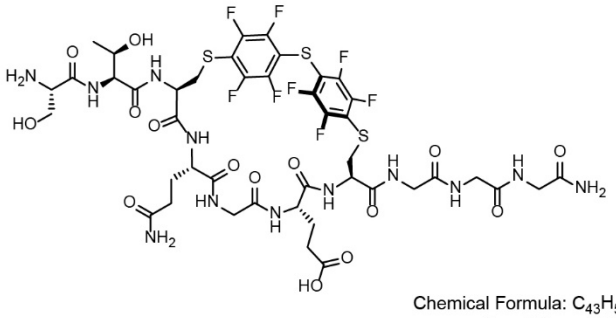

Chemical Formula: $C_{43}H_{50}F_8N_{12}O_{15}S_3$
Exact Mass: 1222.26
Molecular Weight: 1223.11

Starting material mass : 9.7 mg
Final product mass: 5.0 mg

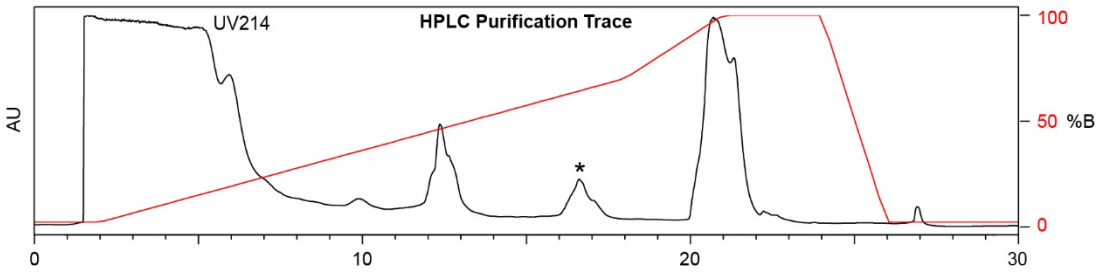

Time (min)	Solvent B %
0	2
2	2
18	70
21	100
24	100
26	0
30	0

Flow Rate: 8 mL/min
Symmetry C18 Prep Column
(100 Å, 5 µm, 10 mm X 50 mm)

Slovent A: H_2O + 0.1% (v/v) TFA
Slovent B: MeCN + 0.1% (v/v) TFA

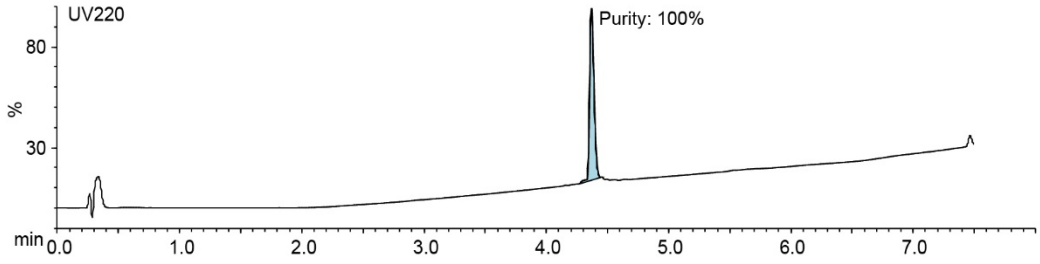

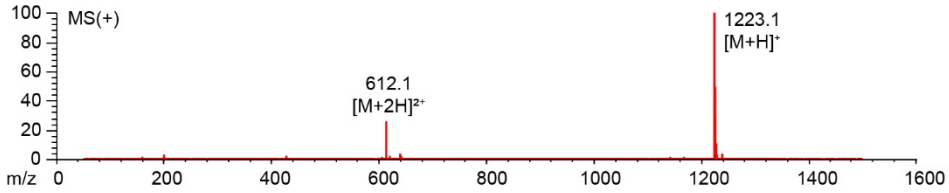

Appendix A-Figure 53. Synthesis summary of **4e**.

SICRFFCGGG-PFS

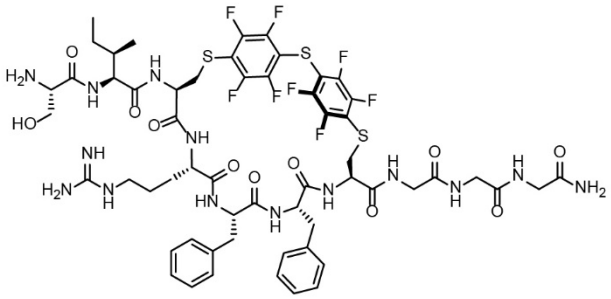

Chemical Formula: $C_{57}H_{66}F_8N_{14}O_{11}S_3$
Exact Mass: 1370.41
Molecular Weight: 1371.41

Starting material mass : 5.5 mg
Final product mass: 3.2 mg

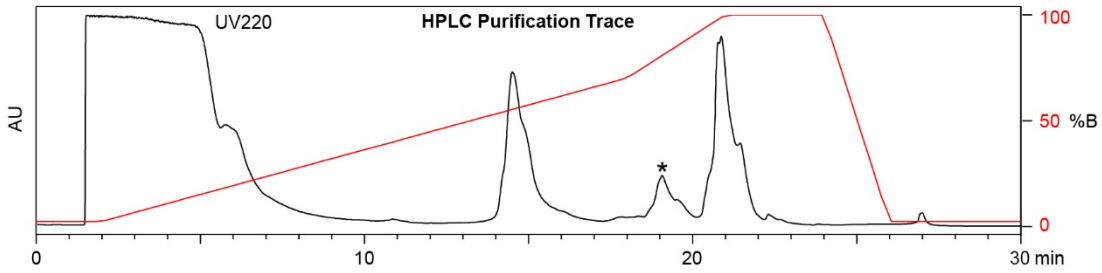

Time (min)	Solvent B (%)
0	2
2	2
18	70
21	100
24	100
26	0
30	0

Flow Rate: 8 mL/min
Symmetry C18 Prep Column
(100 Å, 5 µm, 10 mm X 50 mm)

Slovent A: H_2O + 0.1% (v/v) TFA
Slovent B: MeCN + 0.1% (v/v) TFA

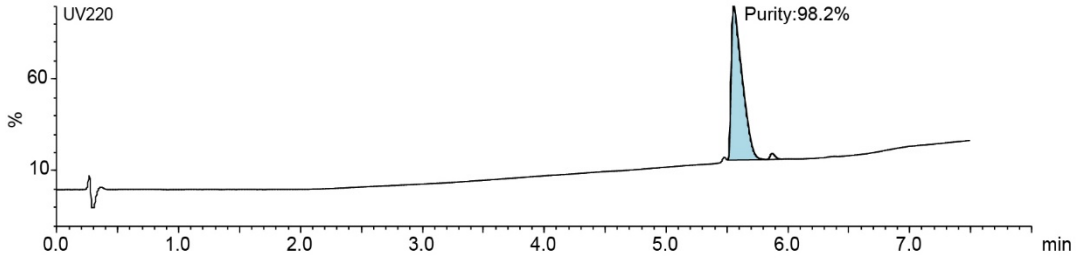

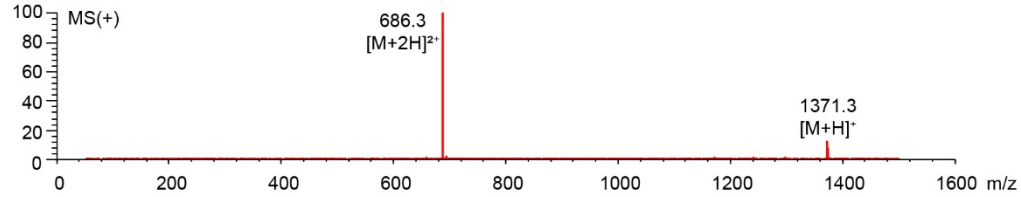

Appendix A-Figure 54. Synthesis summary of **5e**.

SHCDYYC-DBMB

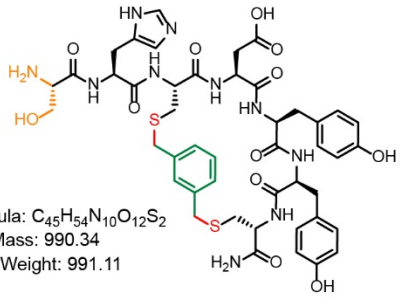

Chemical Formula: $C_{45}H_{54}N_{10}O_{12}S_2$
Exact Mass: 990.34
Molecular Weight: 991.11

Starting material mass :10 mg
Final product mass: 5.2 mg

HPLC Purification Trace

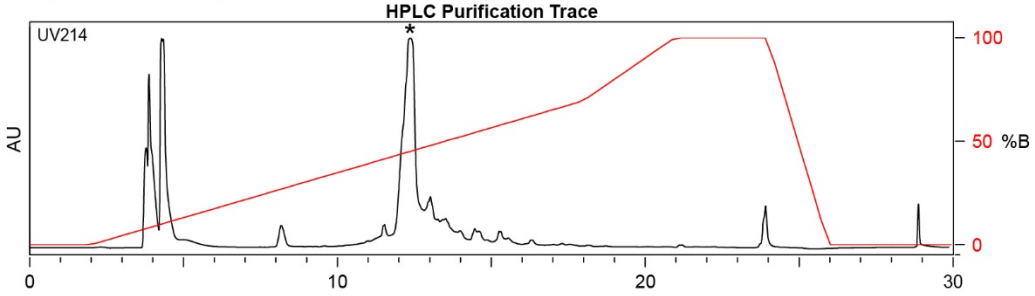

Time (min)	Solvent B (%)
0	2
2	2
18	70
21	100
24	100
26	2
29.5	2
30	2

Flow Rate: 13 mL/min
Phenomenex Kinetex EVO C18 Prep Column
(100 Å, 5 µm, 21.5 mm X 250 mm)

Slovent A: H_2O + 0.1% (v/v) TFA
Slovent B: MeCN + 0.1% (v/v) TFA

LC-MS Trace

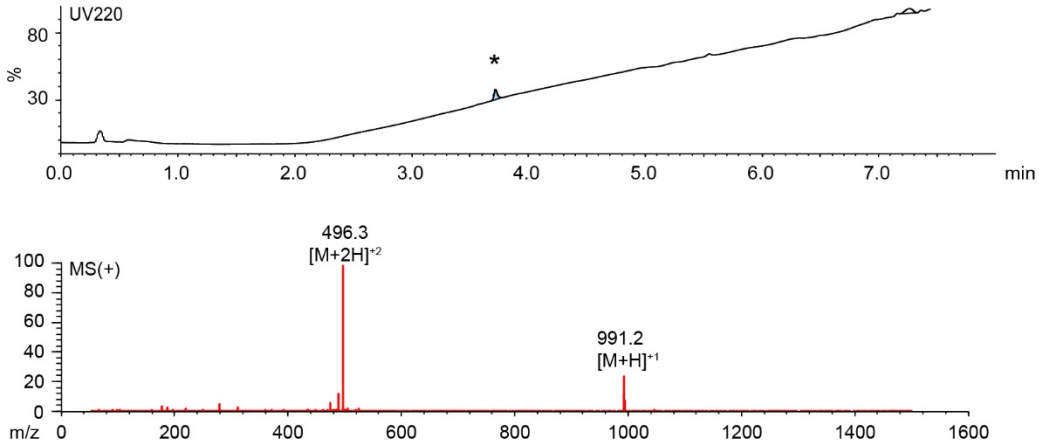

Appendix A-Figure 55. Synthesis summary of **1g**.

SYCKADC-DBMB

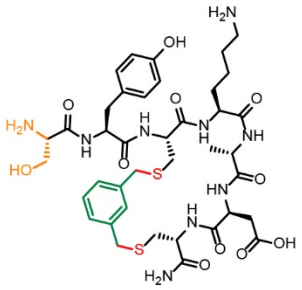

Chemical Formula: $C_{39}H_{55}N_9O_{11}S_2$
Exact Mass: 889.35
Molecular Weight: 890.04

Starting material mass: 10 mg
Final product mass: 5.3 mg

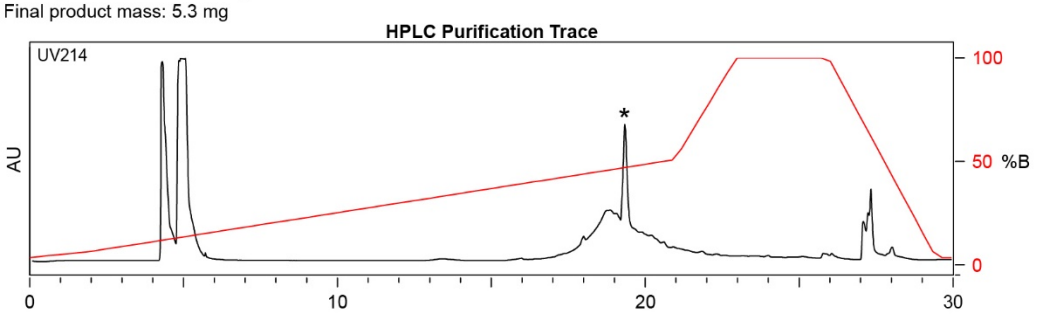

Time (min)	Solvent B (%)
0	2
2	2
21	50
23	100
26	100
29.5	2
30	2

Flow Rate: 13 mL / min
Phenomenex Kinetex EVO C18 Prep Column
(100 Å, 5 µm, 21.5 mm X 250 mm)

Slovent A: H_2O + 0.1% (v/v) TFA
Slovent B: MeCN + 0.1% (v/v) TFA

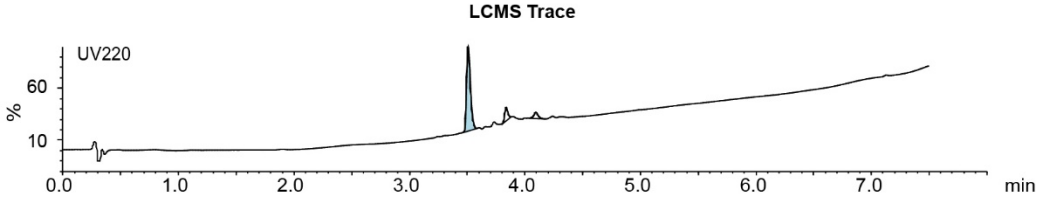

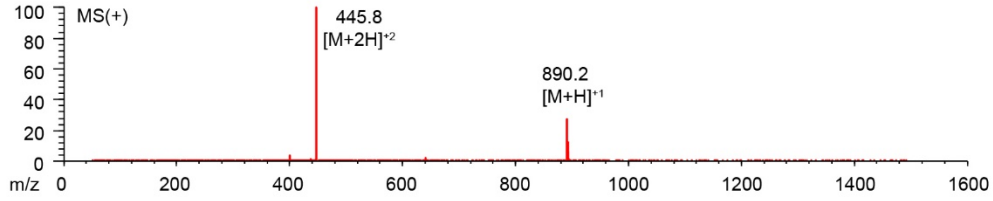

Appendix A-Figure 56. Synthesis summary of **2g**.

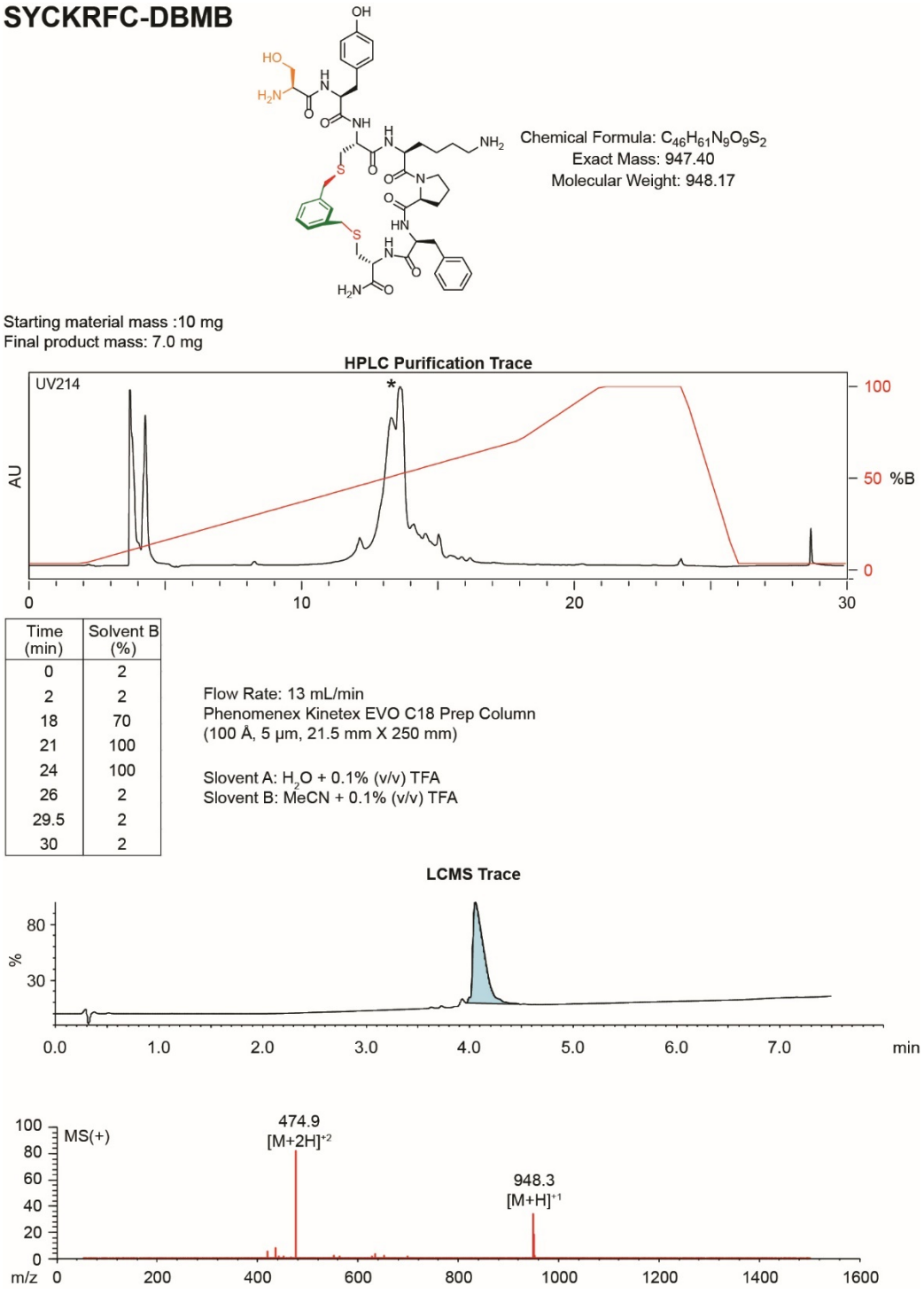

Appendix A-Figure 57. Synthesis summary of **3g**.

STCQGECGGG-DBMB

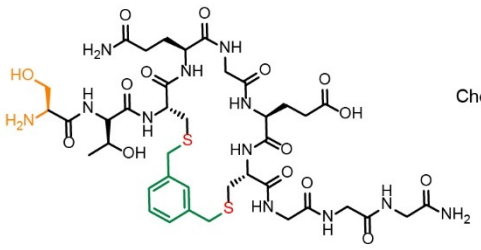

Chemical Formula: $C_{39}H_{58}N_{12}O_{15}S_2$
Exact Mass: 998.36
Molecular Weight: 999.08

Starting material mass :10 mg
Final product mass: 1.7 mg

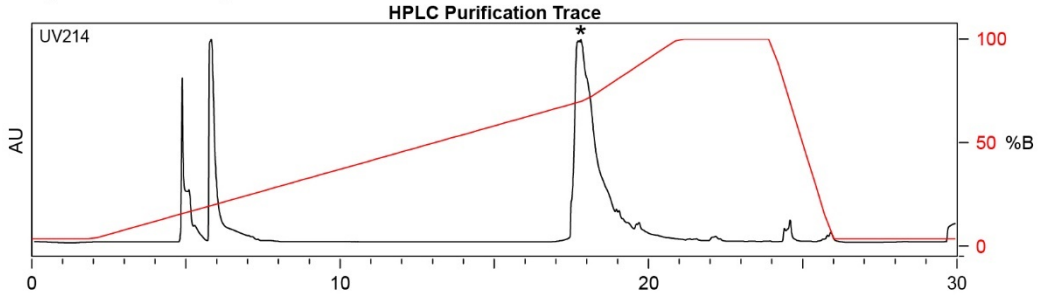

Time (min)	Solvent B (%)
0	2
2	2
18	70
21	100
24	100
26	2
29.5	2
30	2

Flow Rate: 13 mL / min
Phenomenex Kinetex EVO C18 Prep Column
(100 Å, 5 µm, 21.5 mm X 250 mm)

Slovent A: H_2O + 0.1% (v/v) TFA
Slovent B: MeCN + 0.1% (v/v) TFA

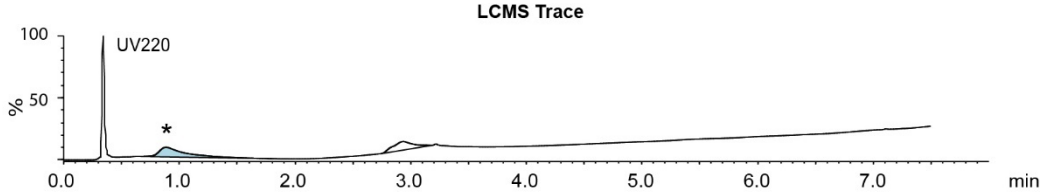

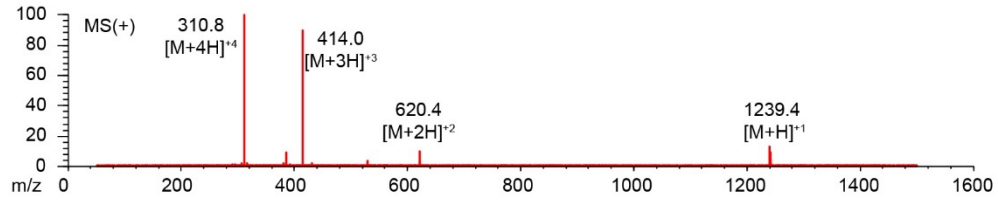

Appendix A-Figure 58. Synthesis summary of **4g**.

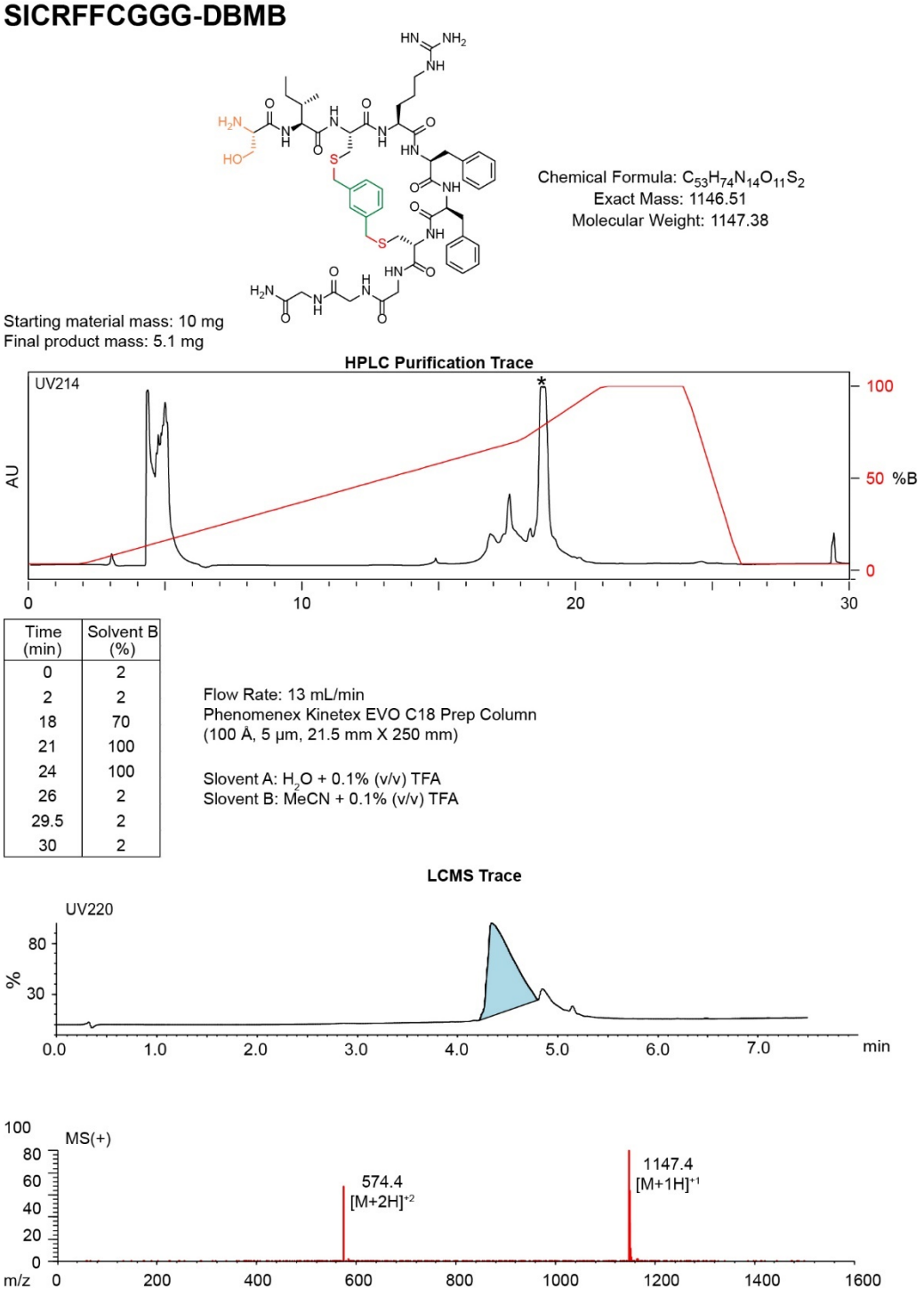

Appendix A-Figure 59. Synthesis summary of **5g**.

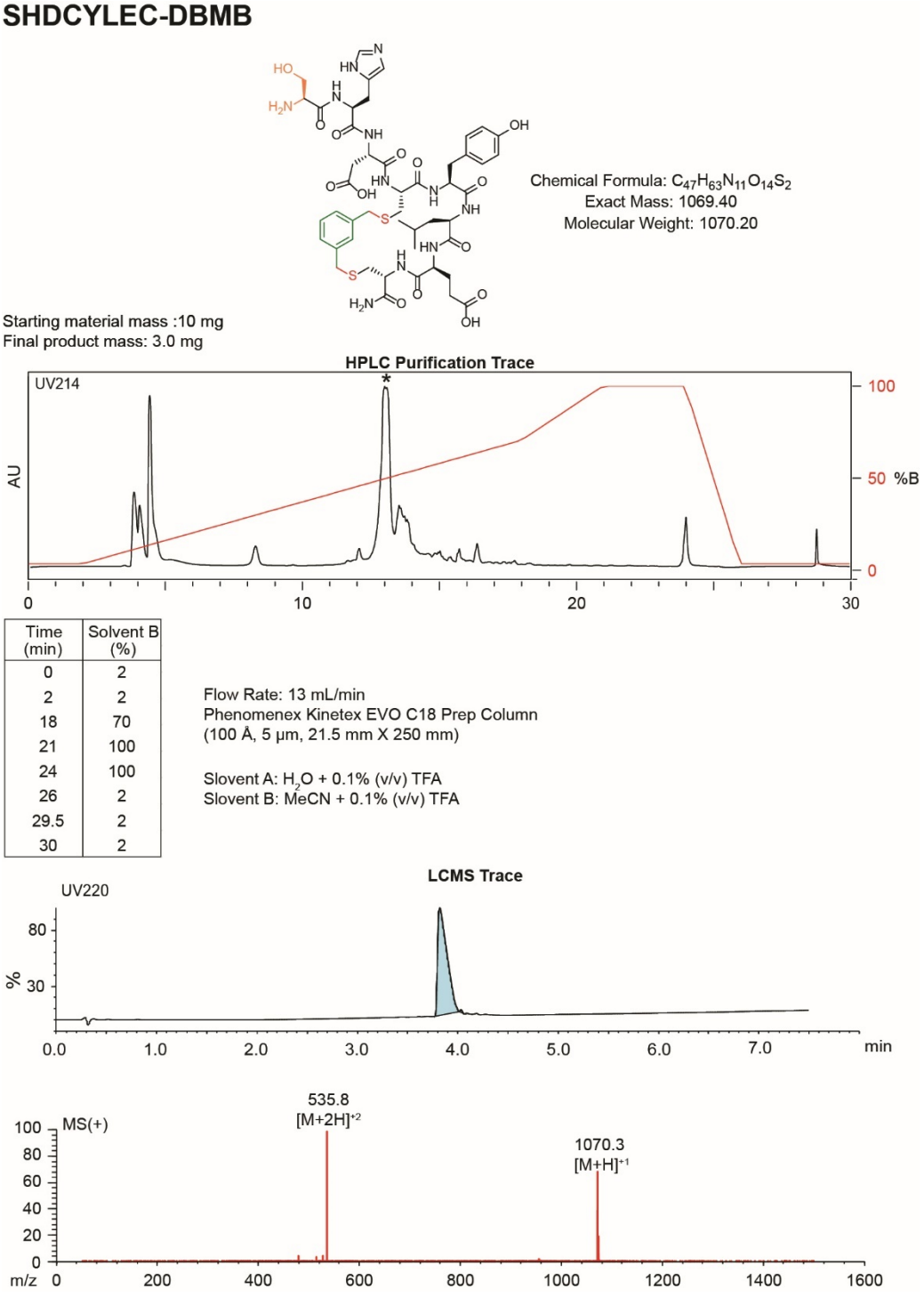

Appendix A-Figure 60. Synthesis summary of **6g**.

SWDYRECYLEC-DBMB

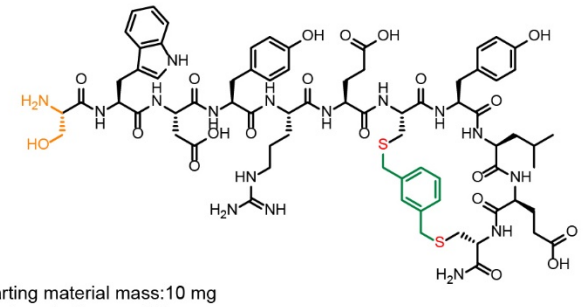

Chemical Formula: $C_{72}H_{94}N_{16}O_{20}S_2$
Exact Mass: 1566.63
Molecular Weight: 1567.76

Starting material mass:10 mg
Final product mass: 1.3 mg

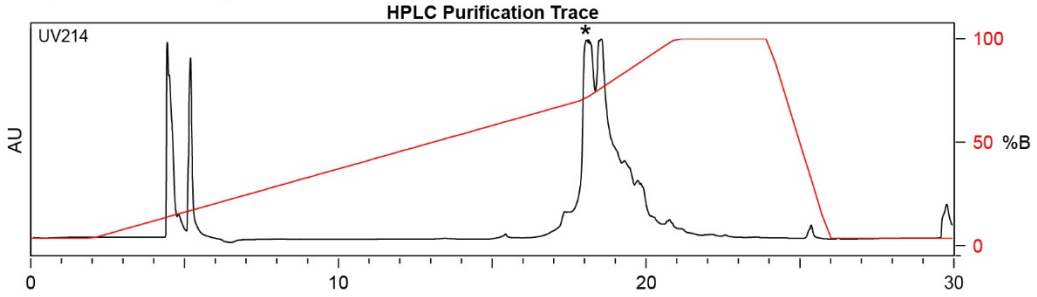

Time (min)	Solvent B (%)
0	2
2	2
18	70
21	100
24	100
26	2
29.5	2
30	2

Flow Rate: 13 mL/min
Phenomenex Kinetex EVO C18 Prep Column
(100 Å, 5 µm, 21.5 mm X 250 mm)

Slovent A: H_2O + 0.1% (v/v) TFA
Slovent B: MeCN + 0.1% (v/v) TFA

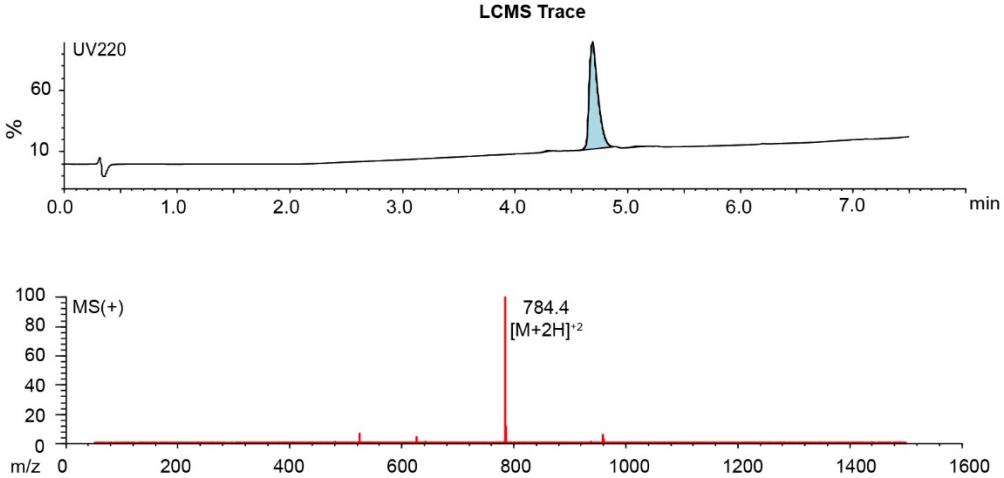

Appendix A-Figure 61. Synthesis summary of **7g**.

SHCVWWDC-DBMB

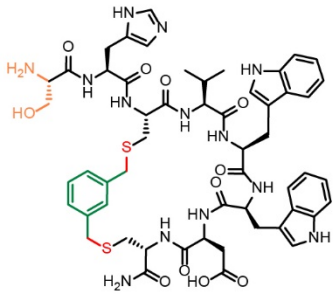

Chemical Formula: $C_{54}H_{65}N_{13}O_{11}S_2$
Exact Mass: 1135.44
Molecular Weight: 1136.31

Starting material mass: 20.0 mg
Final product mass: 3.6 mg

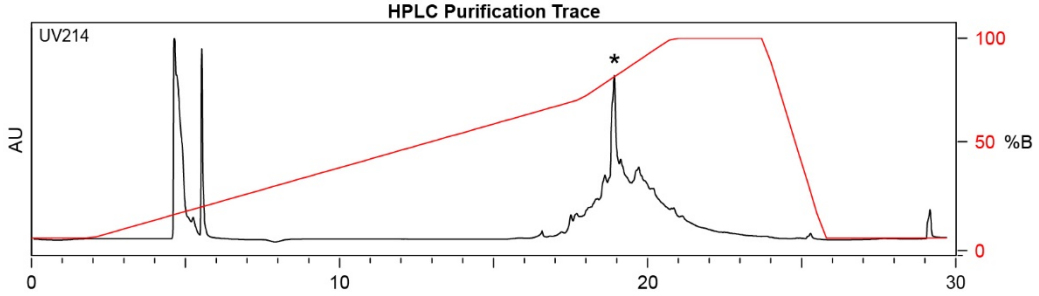

Time (min)	Solvent B (%)
0	2
2	2
18	70
21	100
24	100
26	2
29.5	2
30	2

Flow Rate: 13 mL/min
Phenomenex Kinetex EVO C18 Prep Column
(100 Å, 5 µm, 21.5 mm X 250 mm)

Slovent A: H_2O + 0.1% (v/v) TFA
Slovent B: MeCN + 0.1% (v/v) TFA

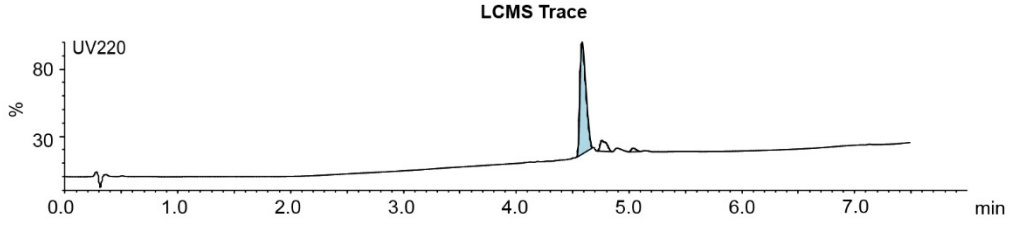

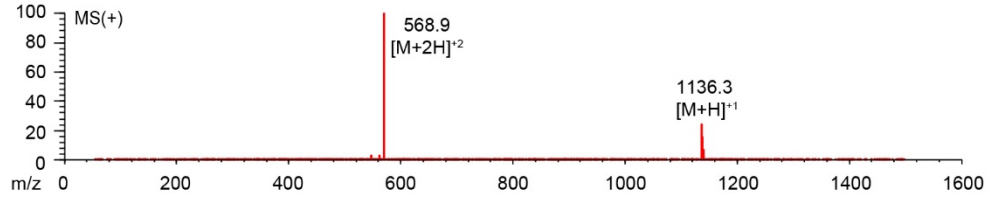

Appendix A-Figure 62. Synthesis summary of **8g**.

SFCDWYGC-DBMB

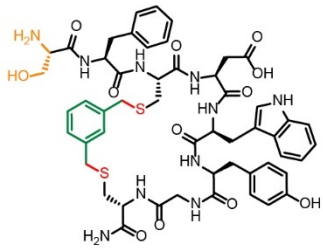

Chemical Formula: $C_{52}H_{60}N_{10}O_{12}S_2$
Exact Mass: 1080.38
Molecular Weight: 1081.23

Starting material mass :10 mg
Final product mass: 1.1 mg

HPLC Purification Trace

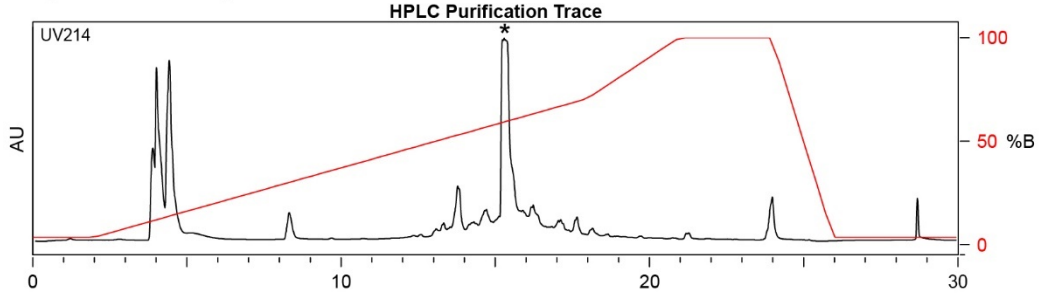

Time (min)	Solvent B (%)
0	2
2	2
18	70
21	100
24	100
26	2
29.5	2
30	2

Flow Rate: 13 mL/min
Phenomenex Kinetex EVO C18 Prep Column
(100 Å, 5 µm, 21.5 mm X 250 mm)

Slovent A: H_2O + 0.1% (v/v) TFA
Slovent B: MeCN + 0.1% (v/v) TFA

LCMS Trace

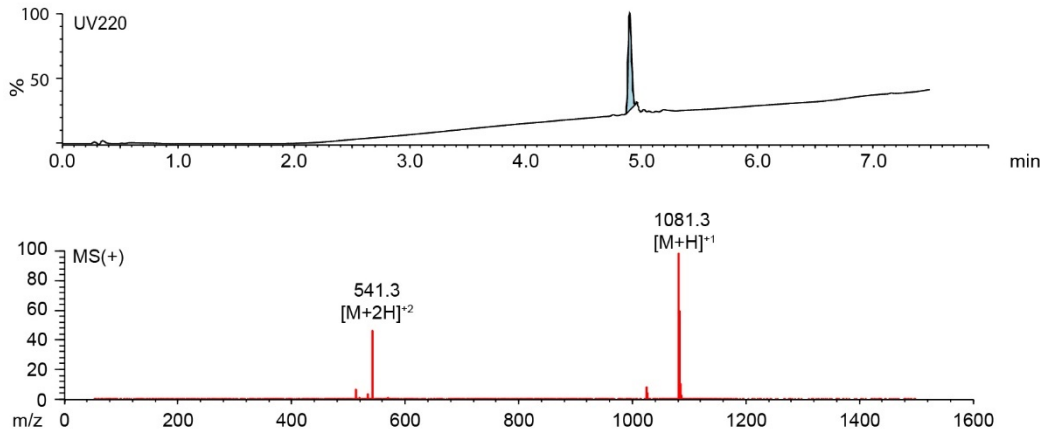

Appendix A-Figure 63. Synthesis summary of **9g**.

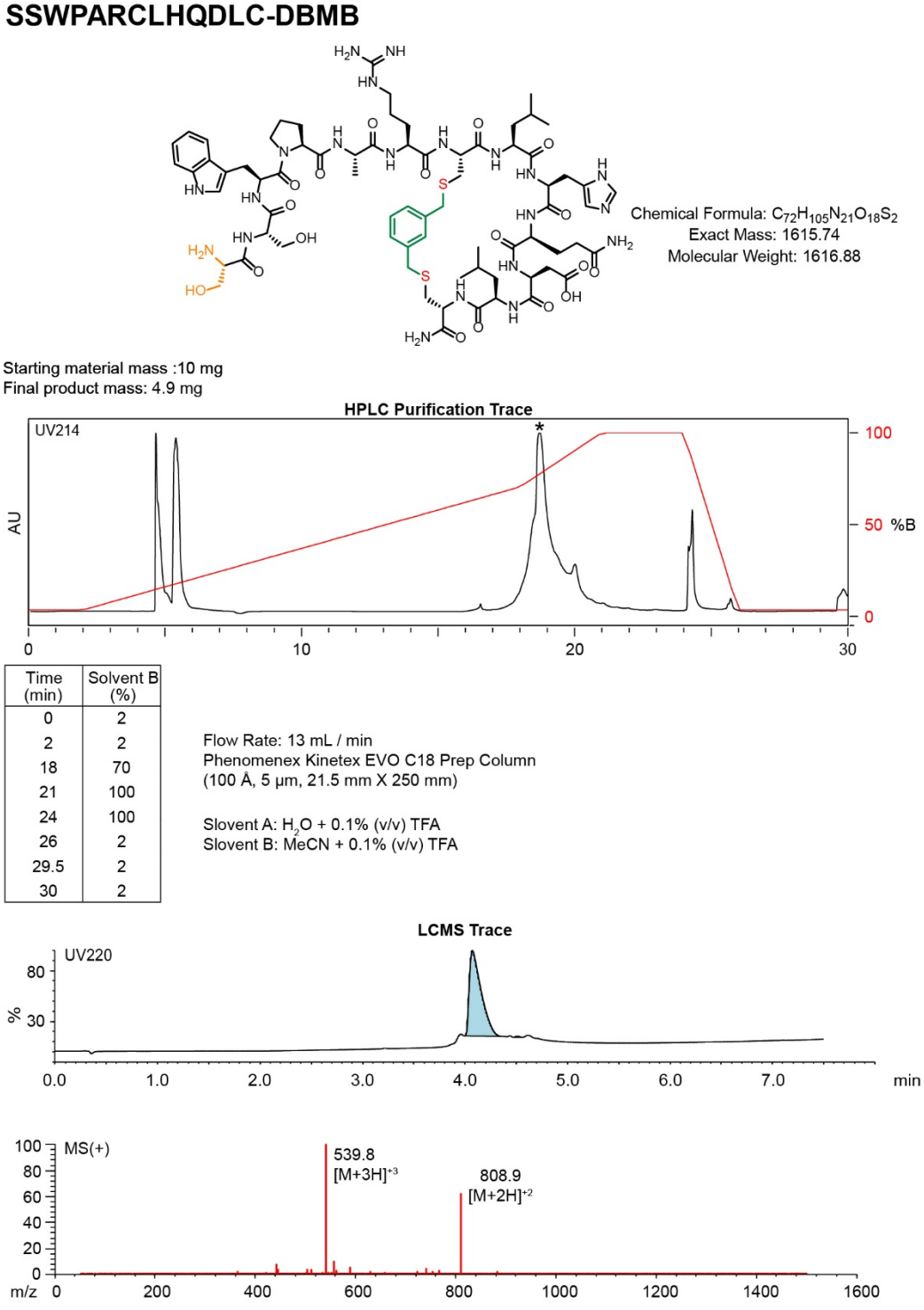

Appendix A-Figure 64. Synthesis summary of **12g**.

SPCKAGTGQC-DBMB

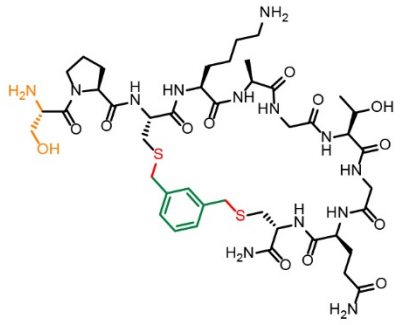

Chemical Formula: $C_{44}H_{69}N_{13}O_{13}S_2$
Exact Mass: 1051.46
Molecular Weight: 1052.23

Starting material mass: 10.0 mg
Final product mass: 1.3 mg

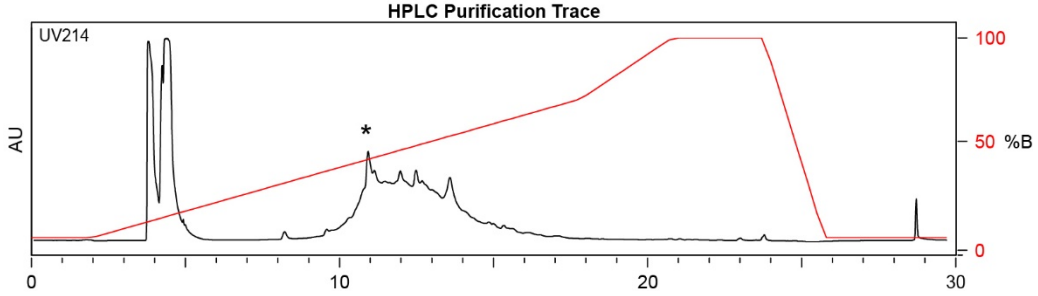

Time (min)	Solvent B (%)
0	2
2	2
18	70
21	100
24	100
26	2
29.5	2
30	2

Flow Rate: 13 mL/min
Phenomenex Kinetex EVO C18 Prep Column
(100 Å, 5 µm, 21.5 mm X 250 mm)

Slovent A: H_2O + 0.1% (v/v) TFA
Slovent B: MeCN + 0.1% (v/v) TFA

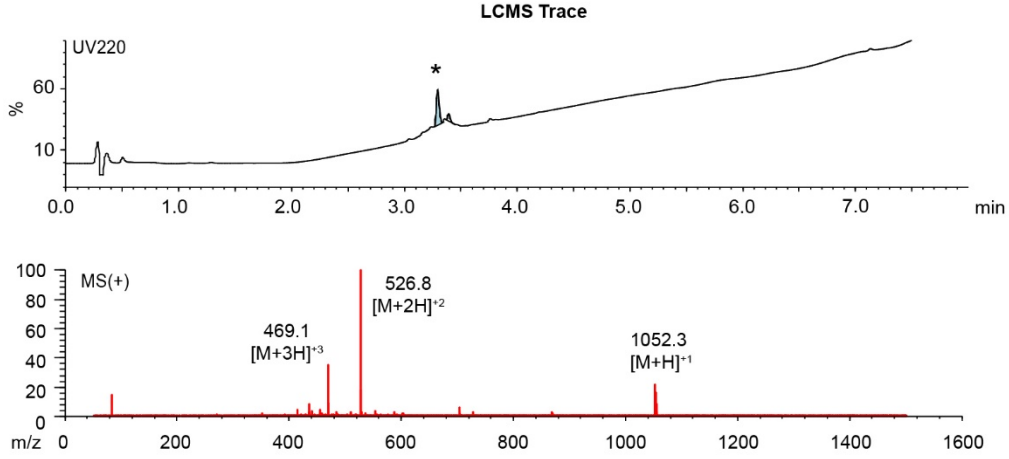

Appendix A-Figure 65. Synthesis summary of **14g**.

SPCKGPSATC-DBMB

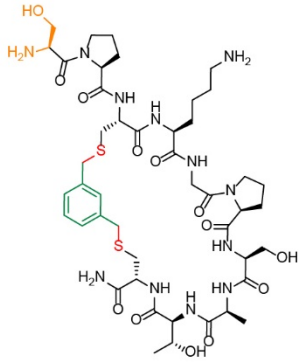

Chemical Formula: $C_{45}H_{70}N_{12}O_{13}S_2$
Exact Mass: 1050.46
Molecular Weight: 1051.25

Starting material mass: 5 mg
Final product mass: 0.5 mg

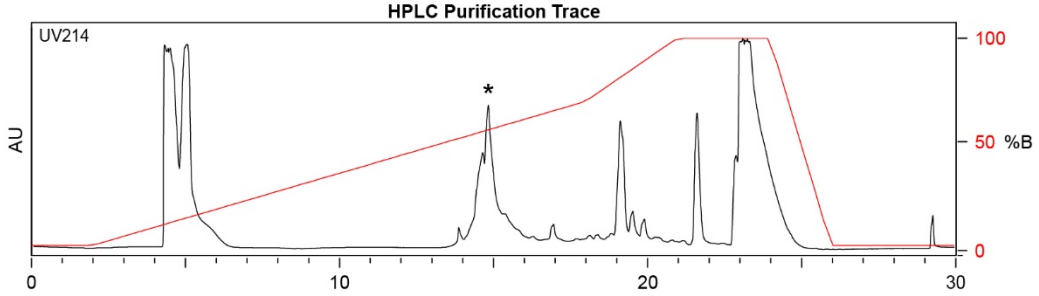

Time (min)	Solvent B (%)
0	2
2	2
18	70
21	100
24	100
26	2
29.5	2
30	2

Flow Rate: 13 mL/min
Phenomenex Kinetex EVO C18 Prep Column
(100 Å, 5 µm, 21.5 mm X 250 mm)

Slovent A: H_2O + 0.1% (v/v) TFA
Slovent B: MeCN + 0.1% (v/v) TFA

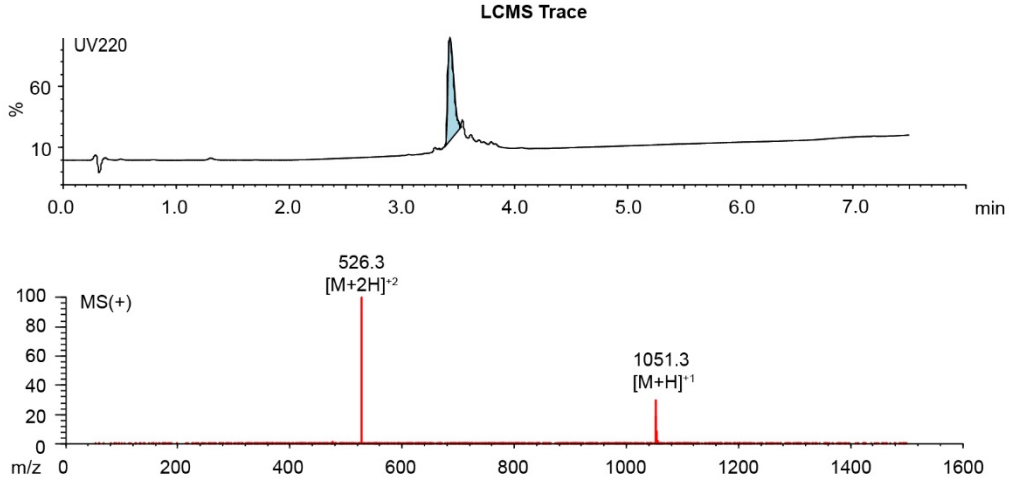

Appendix A-Figure 66. Synthesis summary of **15g**.

SPCKGRHHNC-DBMB

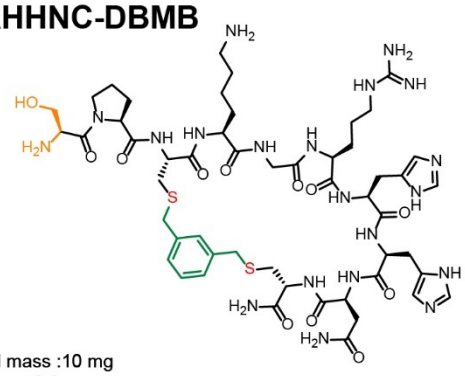

Chemical Formula: $C_{52}H_{78}N_{20}O_{12}S_2$
Exact Mass: 1238.55
Molecular Weight: 1239.44

Starting material mass :10 mg
Final product mass: 6.8 mg

HPLC Purification Trace

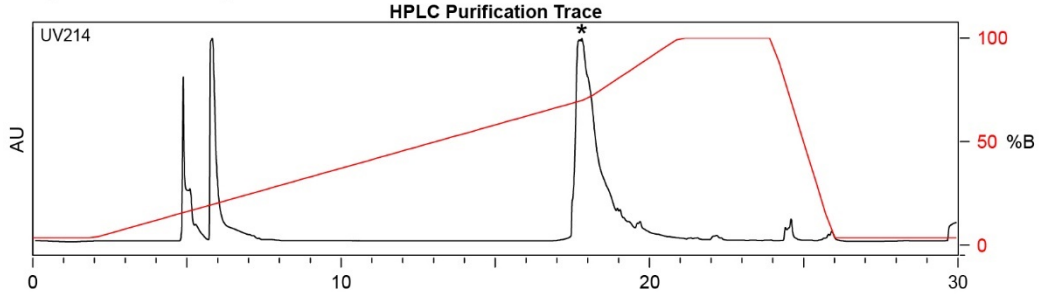

Time (min)	Solvent B (%)
0	2
2	2
18	70
21	100
24	100
26	2
29.5	2
30	2

Flow Rate: 13 mL / min
Phenomenex Kinetex EVO C18 Prep Column
(100 Å, 5 µm, 21.5 mm X 250 mm)

Slovent A: H_2O + 0.1% (v/v) TFA
Slovent B: MeCN + 0.1% (v/v) TFA

LCMS Trace

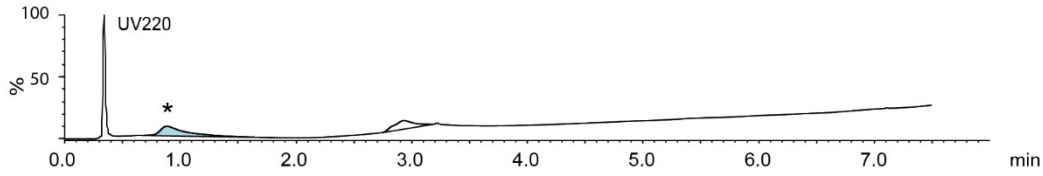

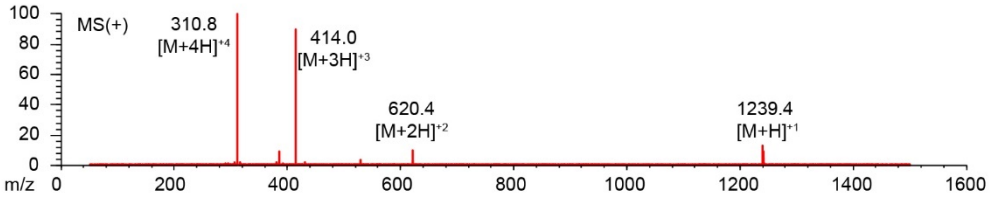

Appendix A-Figure 67. Synthesis summary of **16g**.

SYCKRAHKNC-DBMB

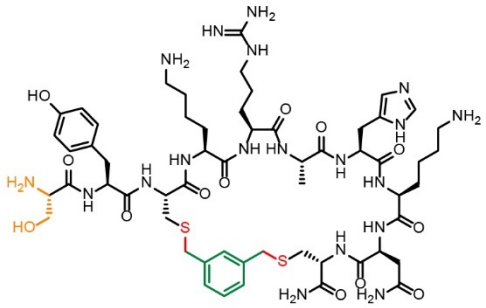

Chemical Formula: $C_{57}H_{87}N_{19}O_{13}S_2$
Exact Mass: 1309.62
Molecular Weight: 1310.56

Starting material mass : 4 mg
Final product mass: 2.3 mg

HPLC Purification Trace

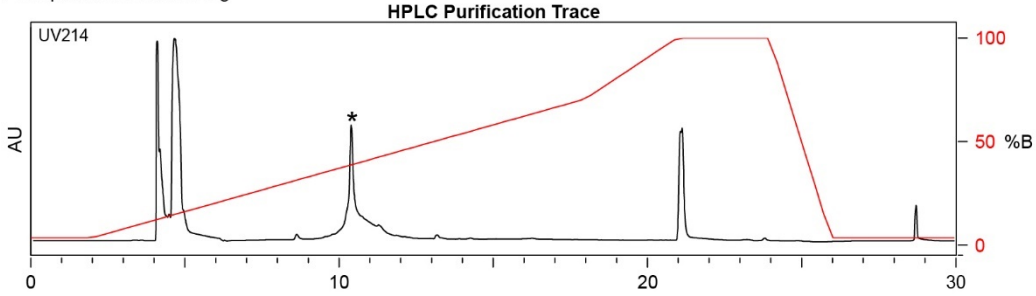

Time (min)	Solvent B (%)
0	2
2	2
18	70
21	100
24	100
26	2
29.5	2
30	2

Flow Rate: 13 mL / min
Phenomenex Kinetex EVO C18 Prep Column
(100 Å, 5 µm, 21.5 mm X 250 mm)

Slovent A: H_2O + 0.1% (v/v) TFA
Slovent B: MeCN + 0.1% (v/v) TFA

LCMS Trace

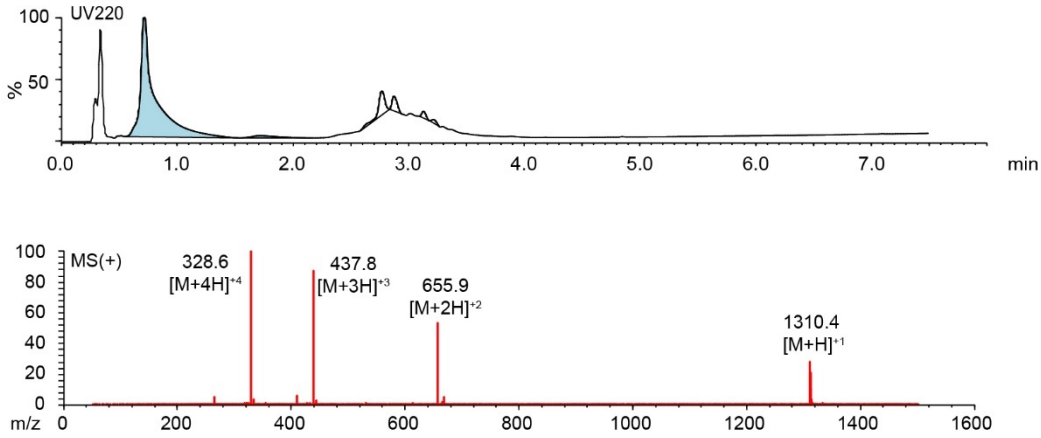

Appendix A-Figure 68. Synthesis summary of **19g**.

SQCKRAHAEC-DBMB

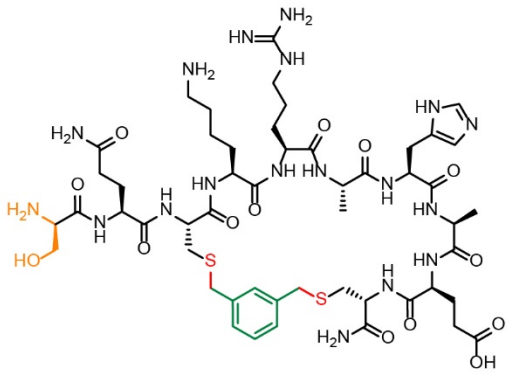

Chemical Formula: $C_{51}H_{80}N_{18}O_{14}S_2$
Exact Mass: 1232.55
Molecular Weight: 1233.43

Starting material mass: 5.0 mg
Final product mass: 0.5 mg

HPLC Purification Trace

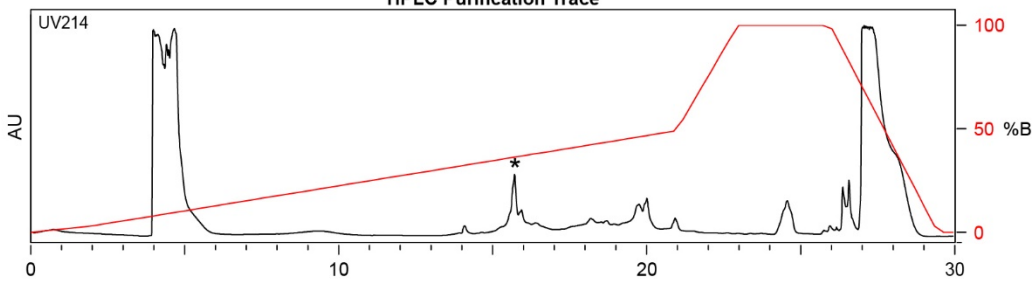

Time (min)	Solvent B (%)
0	2
2	2
18	50
21	100
24	100
26	2
29.5	2
30	2

Flow Rate: 13 mL/min
Phenomenex Kinetex EVO C18 Prep Column
(100 Å, 5 µm, 21.5 mm X 250 mm)

Slovent A: H_2O + 0.1% (v/v) TFA
Slovent B: MeCN + 0.1% (v/v) TFA

LCMS Trace

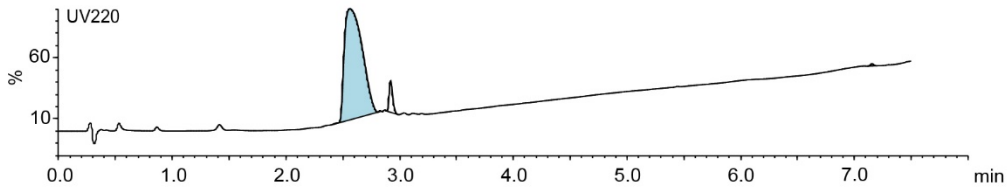

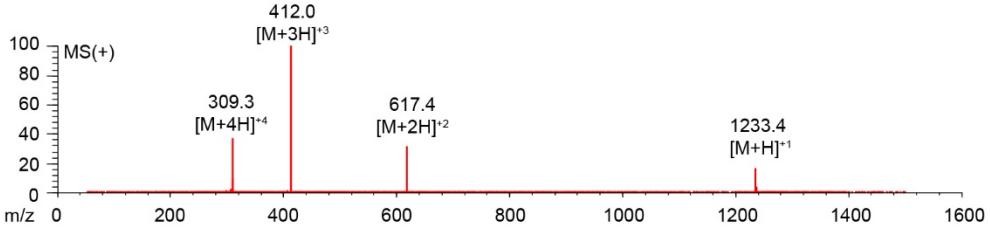

Appendix A-Figure 69. Synthesis summary of **20g**.

SPCAKGMNYC-DBMB

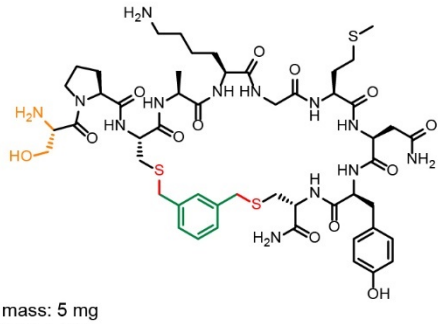

Chemical Formula: $C_{51}H_{75}N_{13}O_{13}S_3$
Exact Mass: 1173.48
Molecular Weight: 1174.42

Starting material mass: 5 mg
Final product mass: 1.4 mg

HPLC Purification Trace

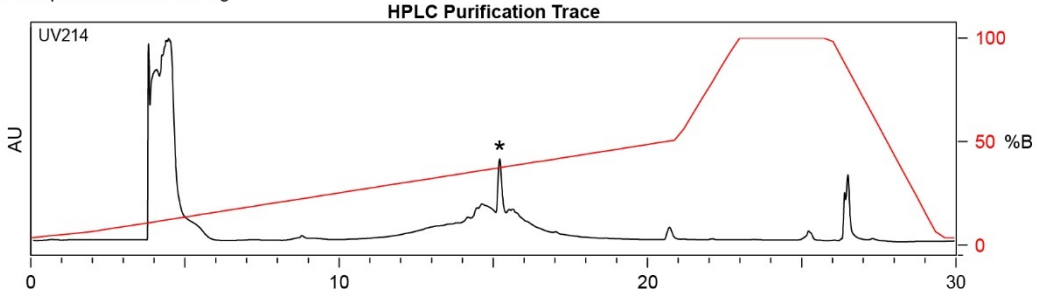

Time (min)	Solvent B (%)
0	2
2	2
21	50
23	100
26	100
29.5	2
30	2

Flow Rate: 13 mL / min
Phenomenex Kinetex EVO C18 Prep Column
(100 Å, 5 µm, 21.5 mm X 250 mm)

Slovent A: H_2O + 0.1% (v/v) TFA
Slovent B: MeCN + 0.1% (v/v) TFA

LCMS Trace

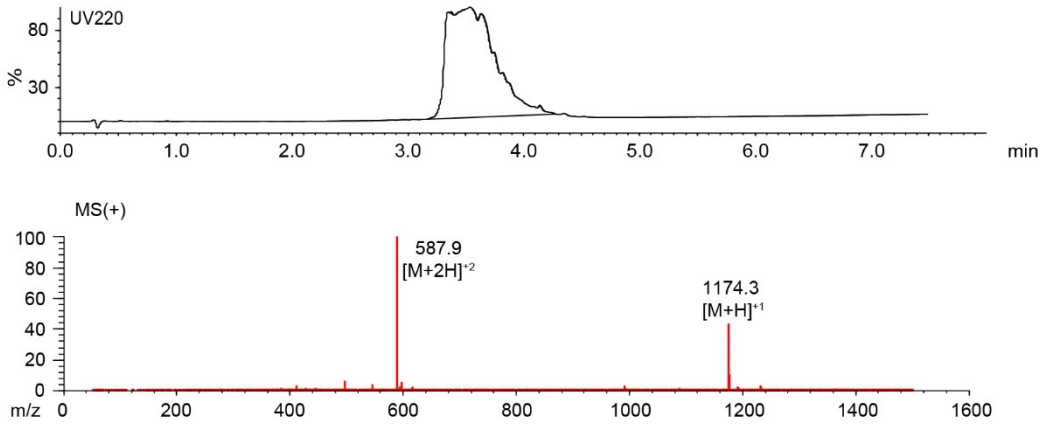

Appendix A-Figure 70. Synthesis summary of **22g**.

Appendix A-6: NMR spectra

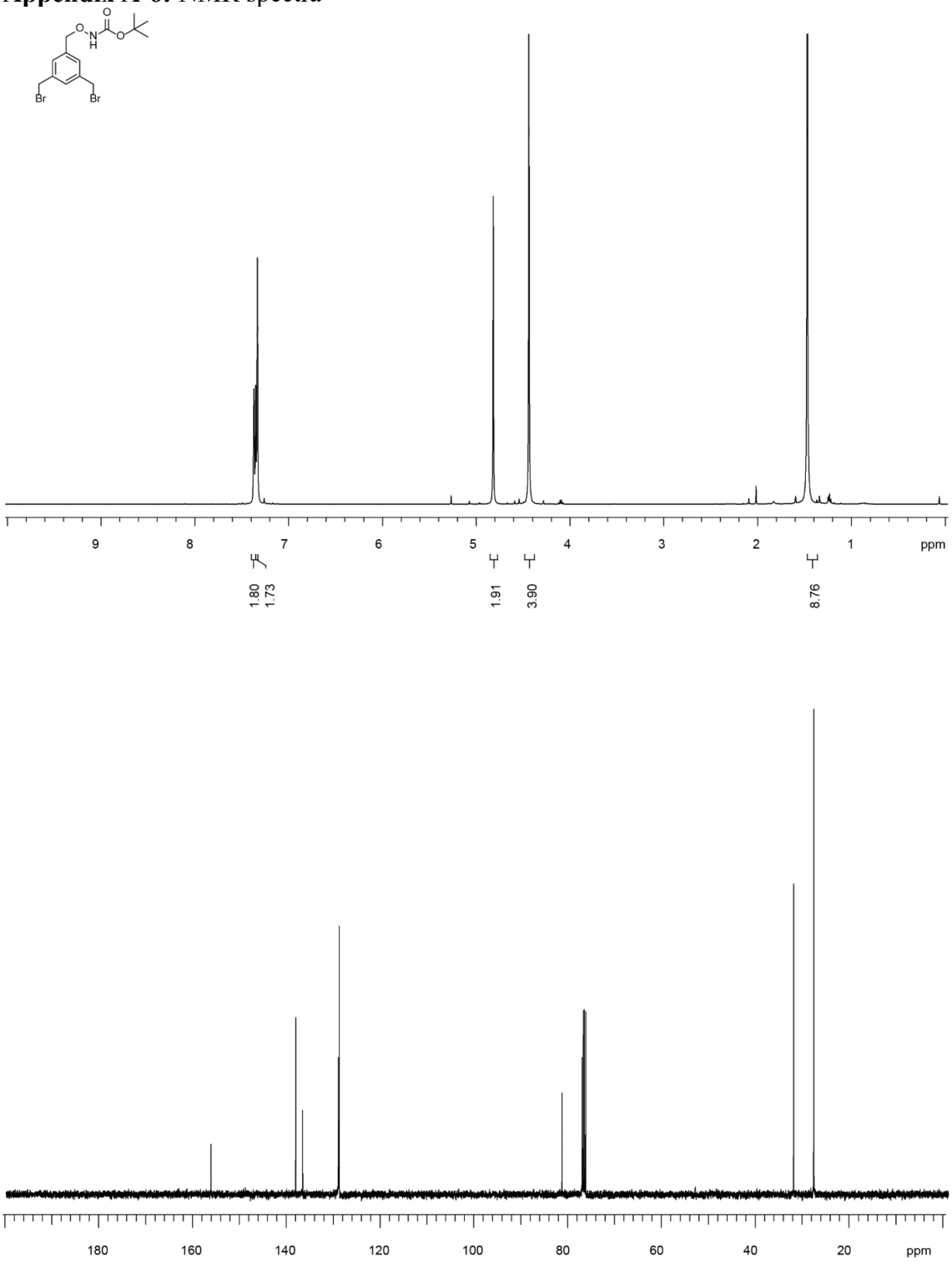

Appendix A-Figure 71. ^{1}H and ^{13}C NMR spectra of **S1**

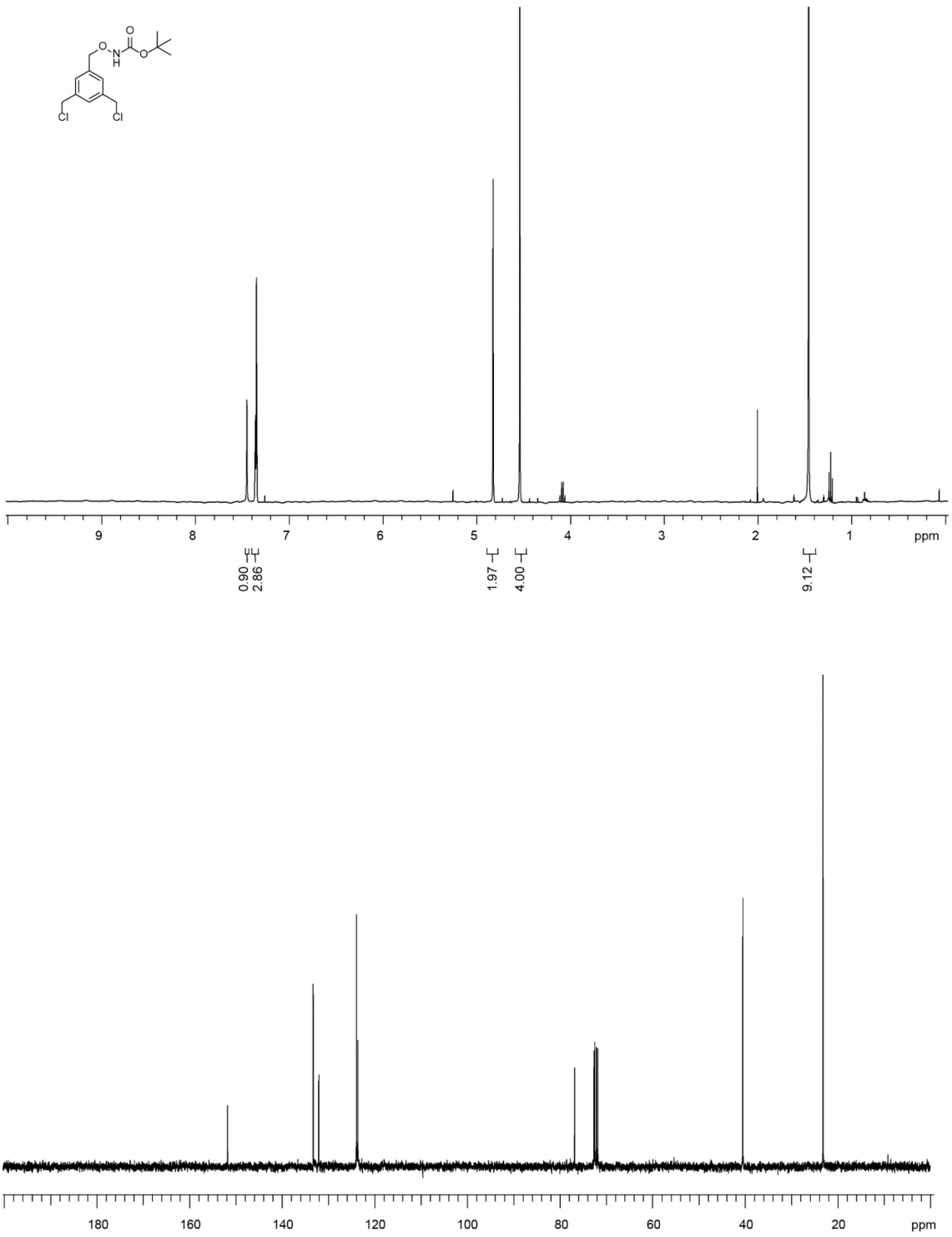

Appendix A-Figure 72. ^{1}H and ^{13}C NMR spectra of **S2**

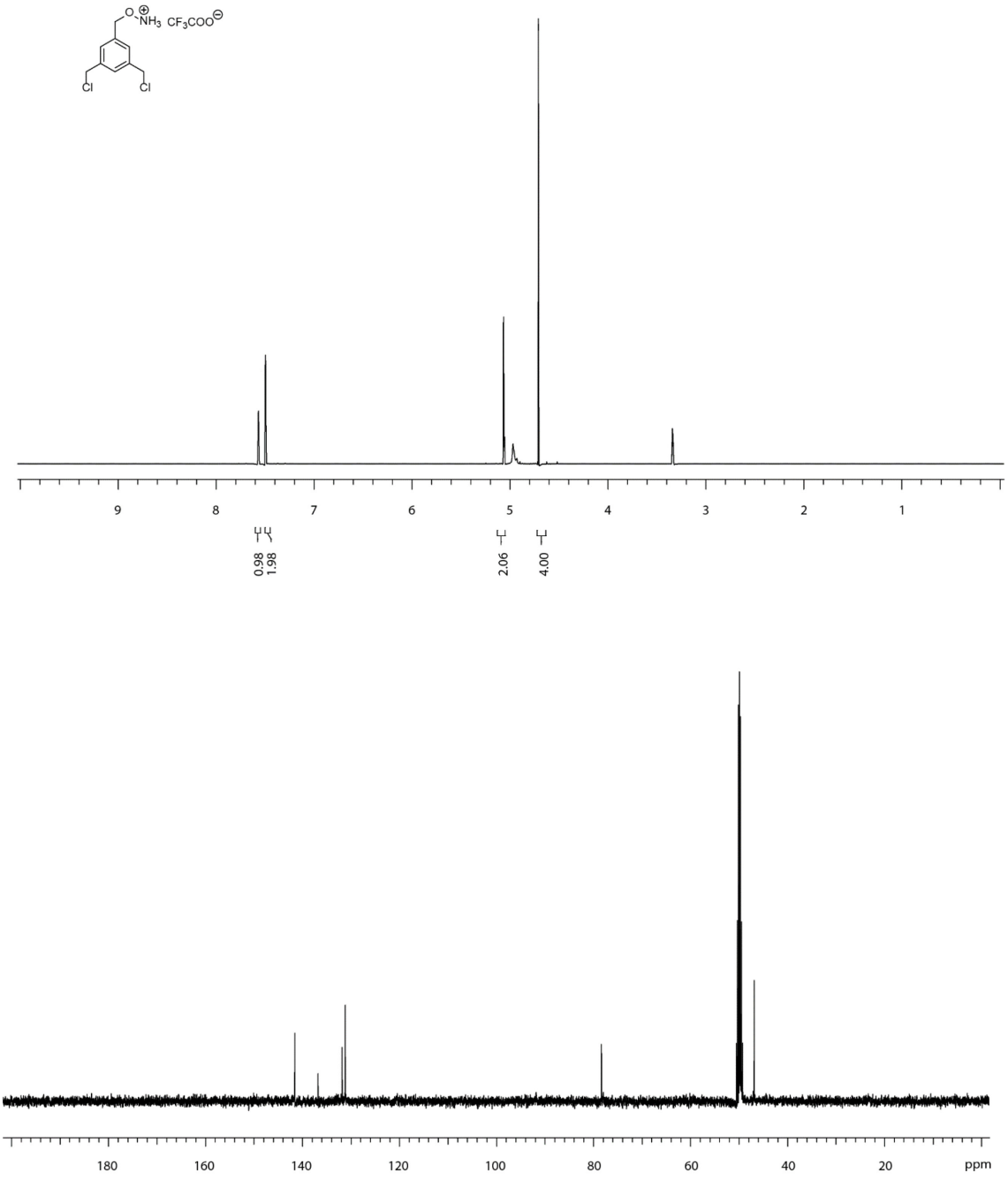

Appendix A-Figure 73. ^{1}H and ^{13}C NMR spectra of **TSL-1**

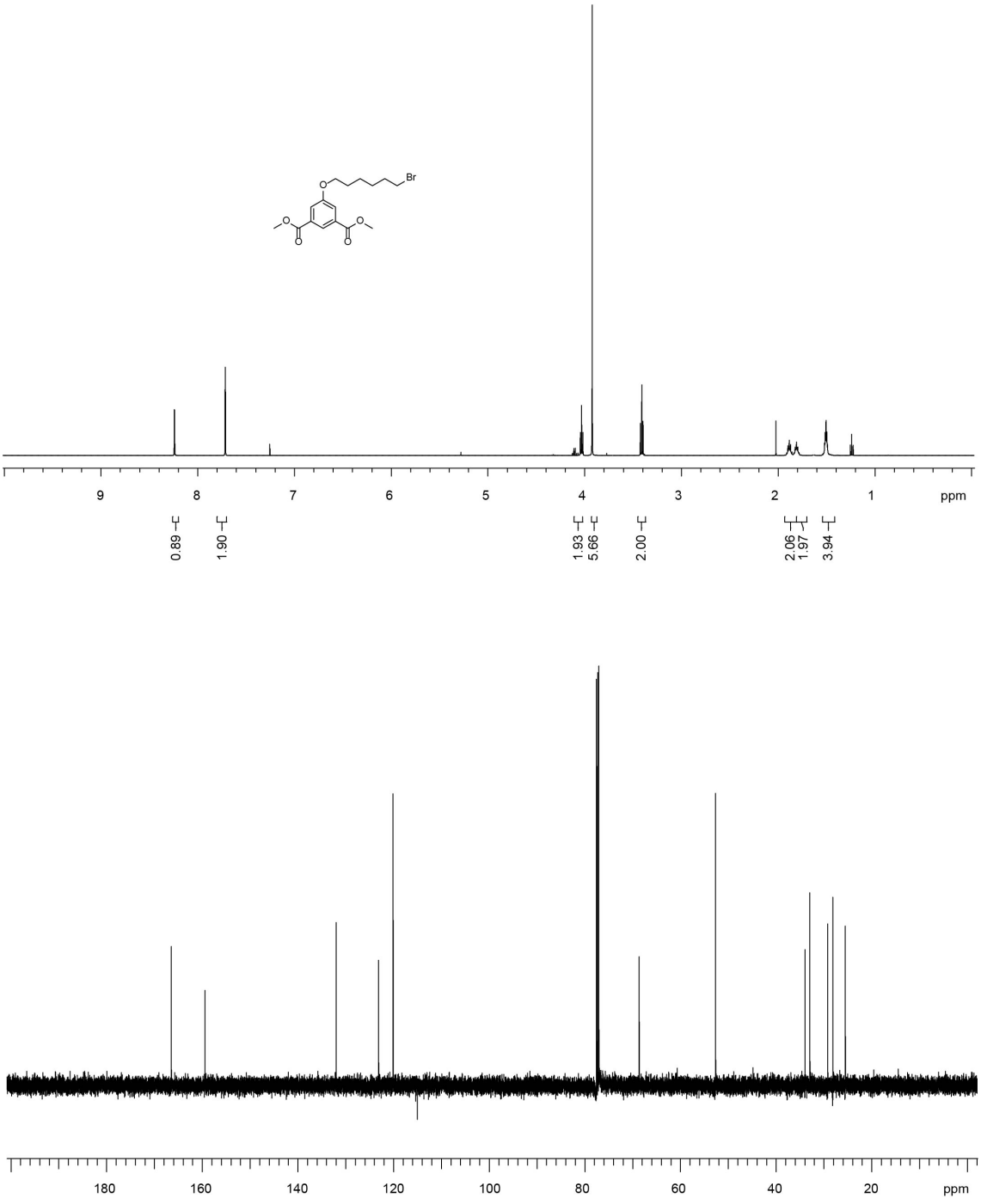

Appendix A-Figure 74. ^{1}H and ^{13}C NMR spectra of **S4**

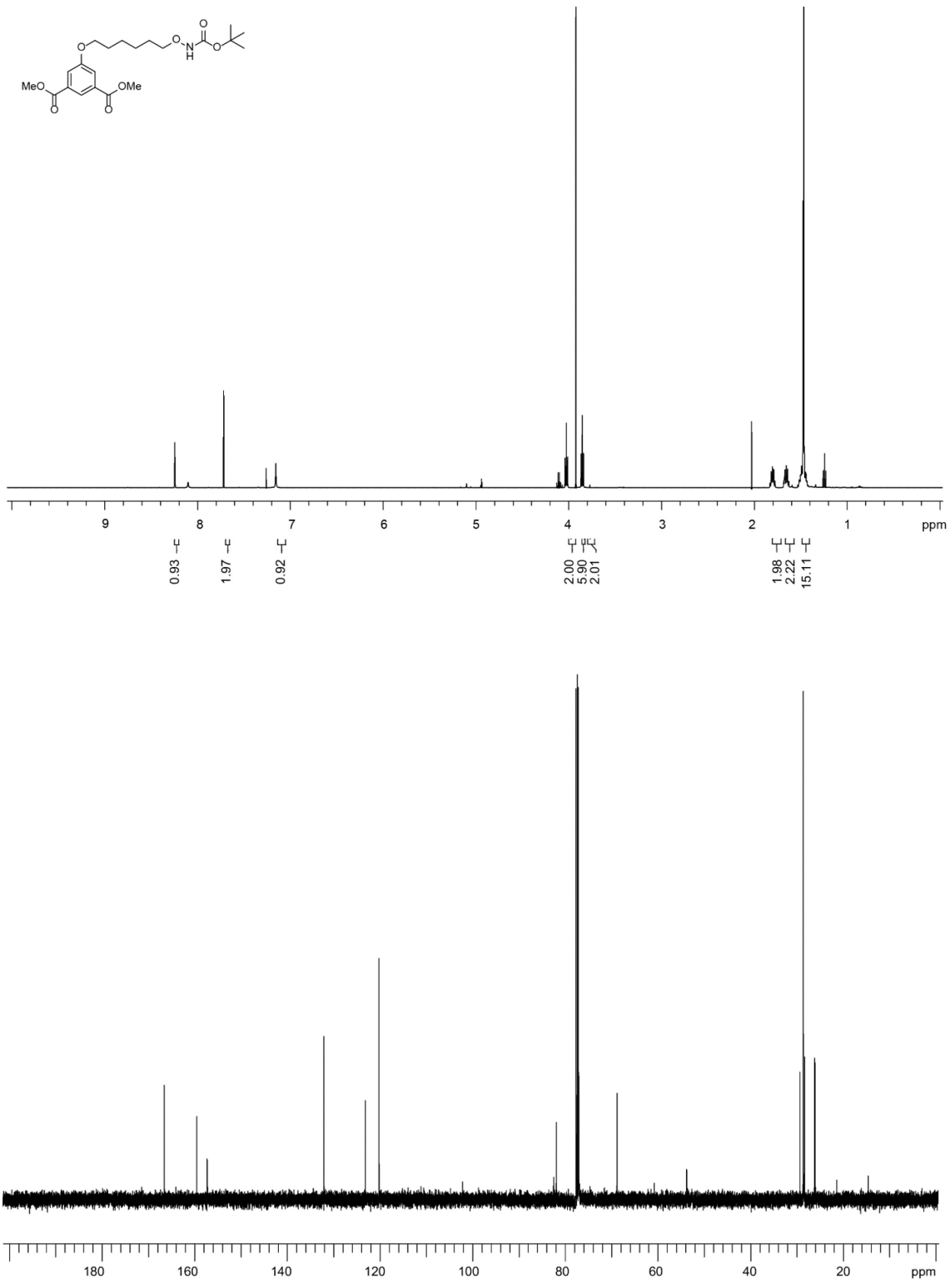

Appendix A-Figure 75. ^{1}H and ^{13}C NMR spectra of **S5**

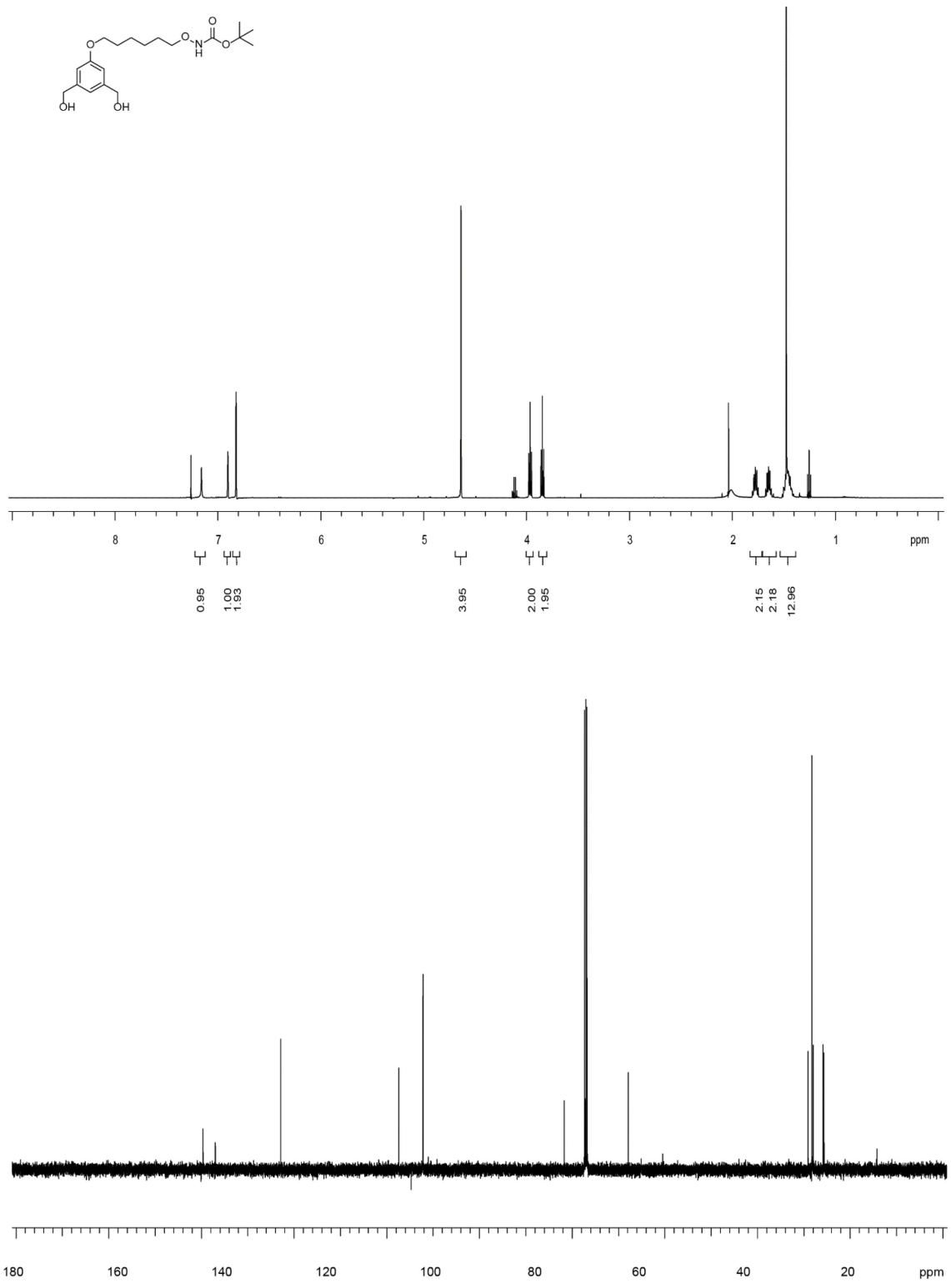

Appendix A-Figure 76. ^{1}H and ^{13}C NMR spectra of **S6**

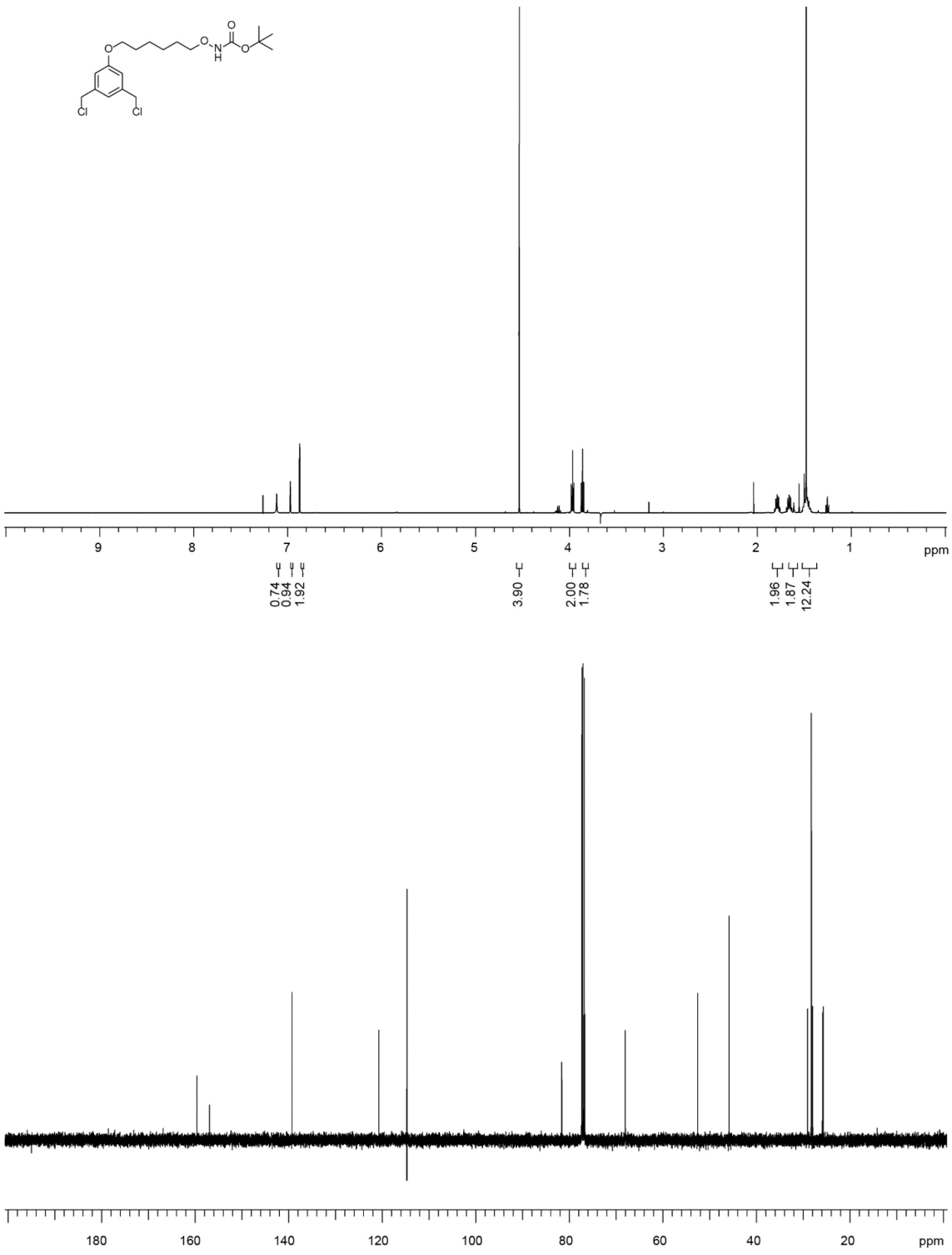

Appendix A-Figure 77. ^{1}H and ^{13}C NMR spectra of **S7**

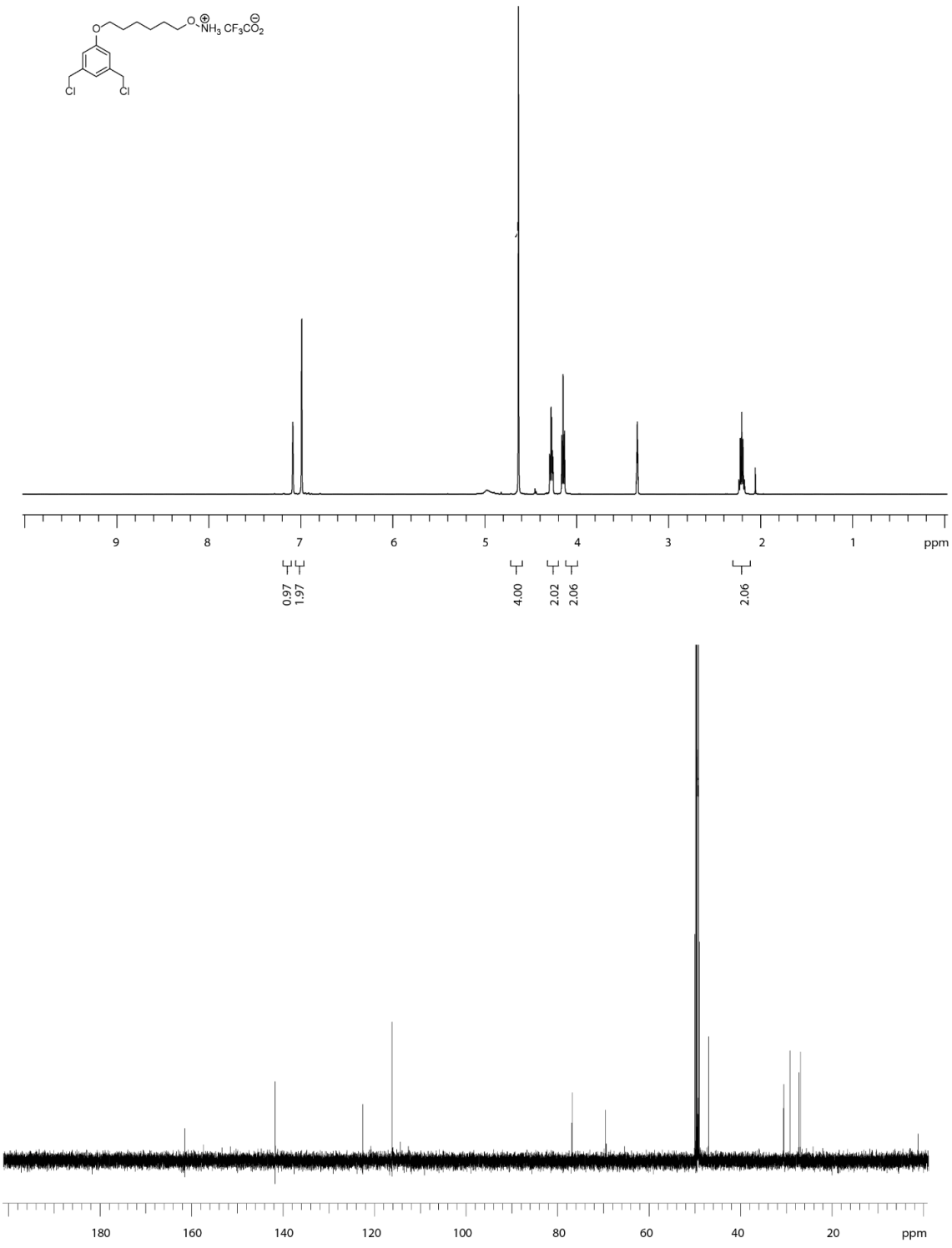

Appendix A-Figure 78. ^{1}H and ^{13}C NMR spectra of **TSL-6**

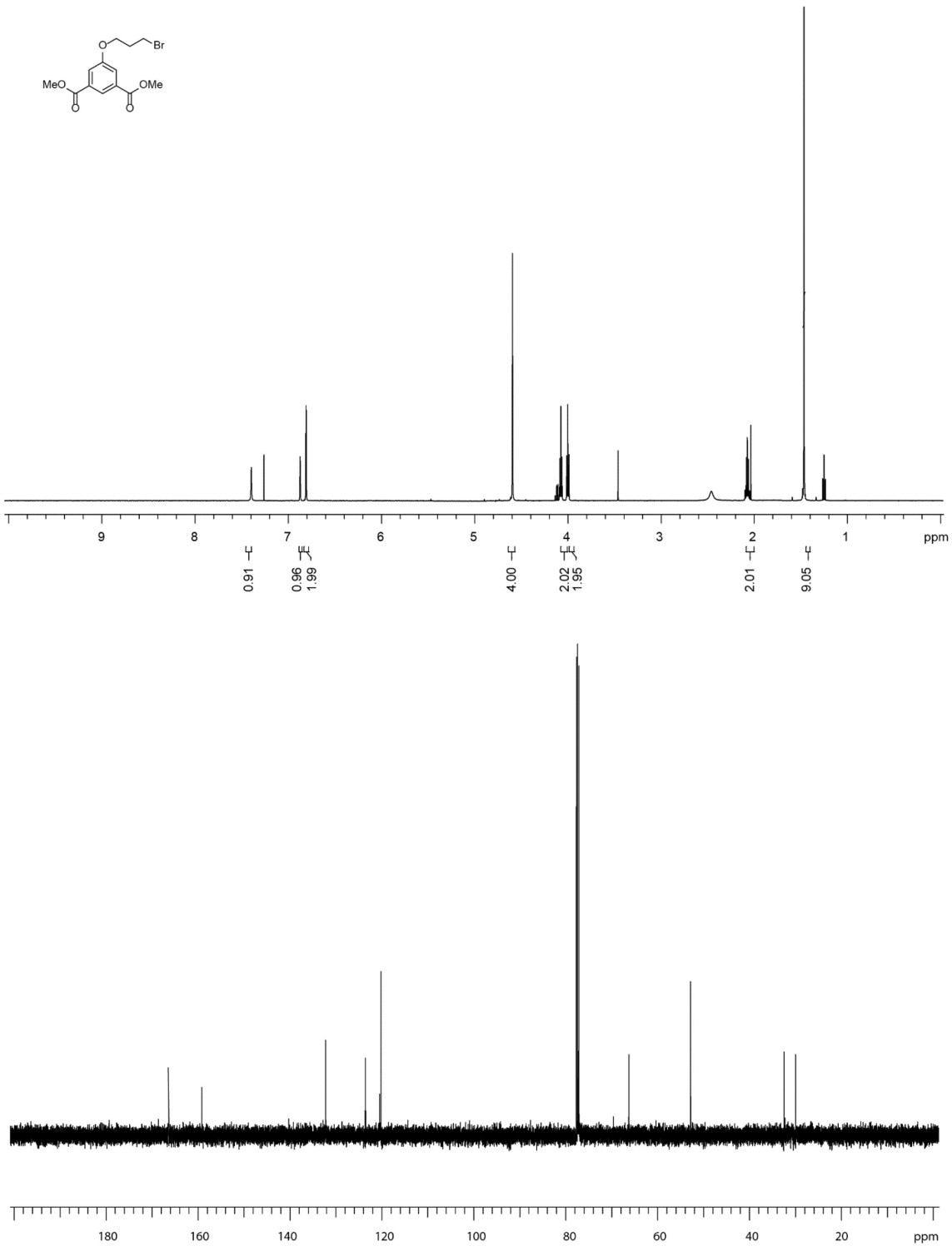

Appendix A-Figure 79. ^{1}H and ^{13}C NMR spectra of **S8**

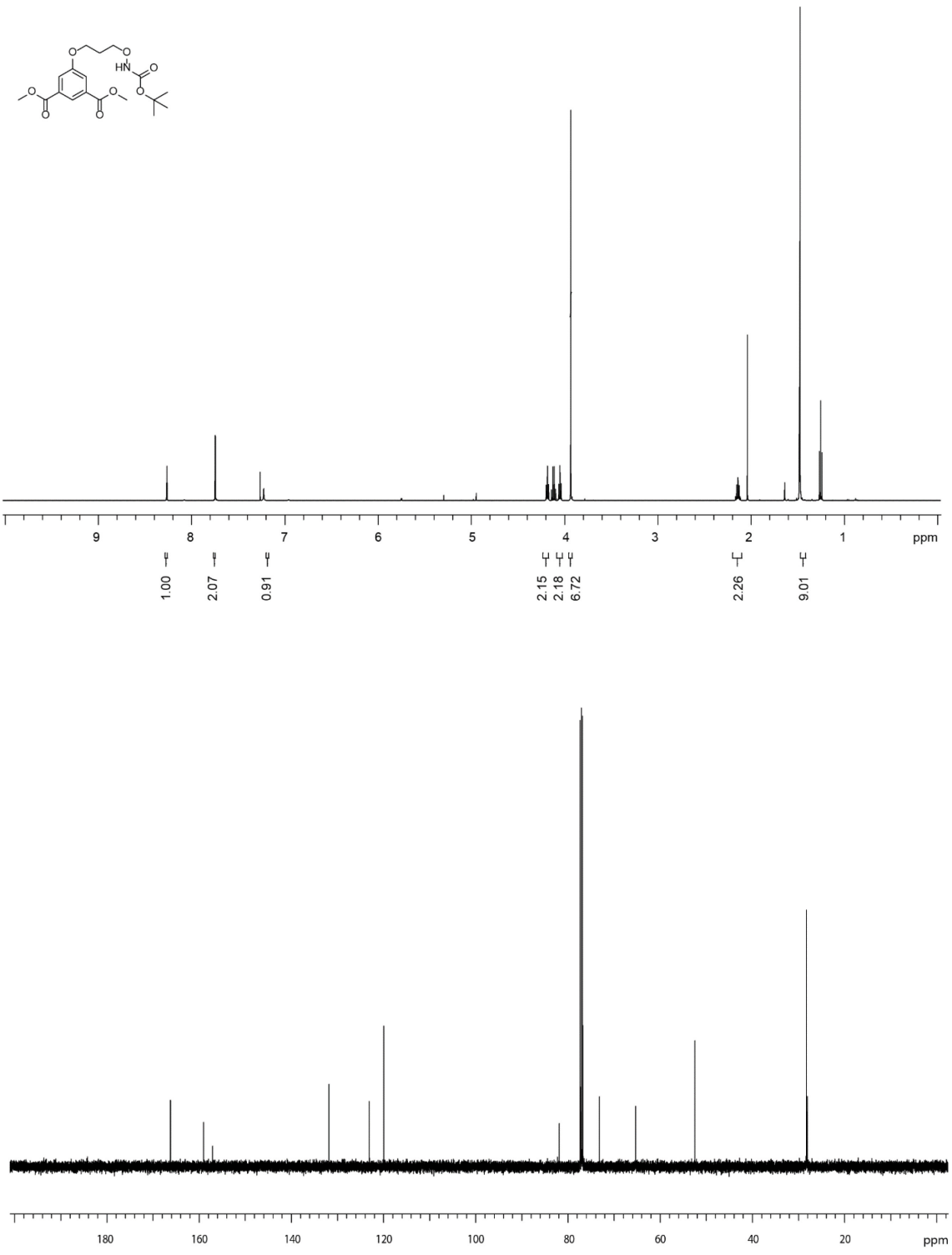

Appendix A-Figure 80. ^{1}H and ^{13}C NMR spectra of **S9**

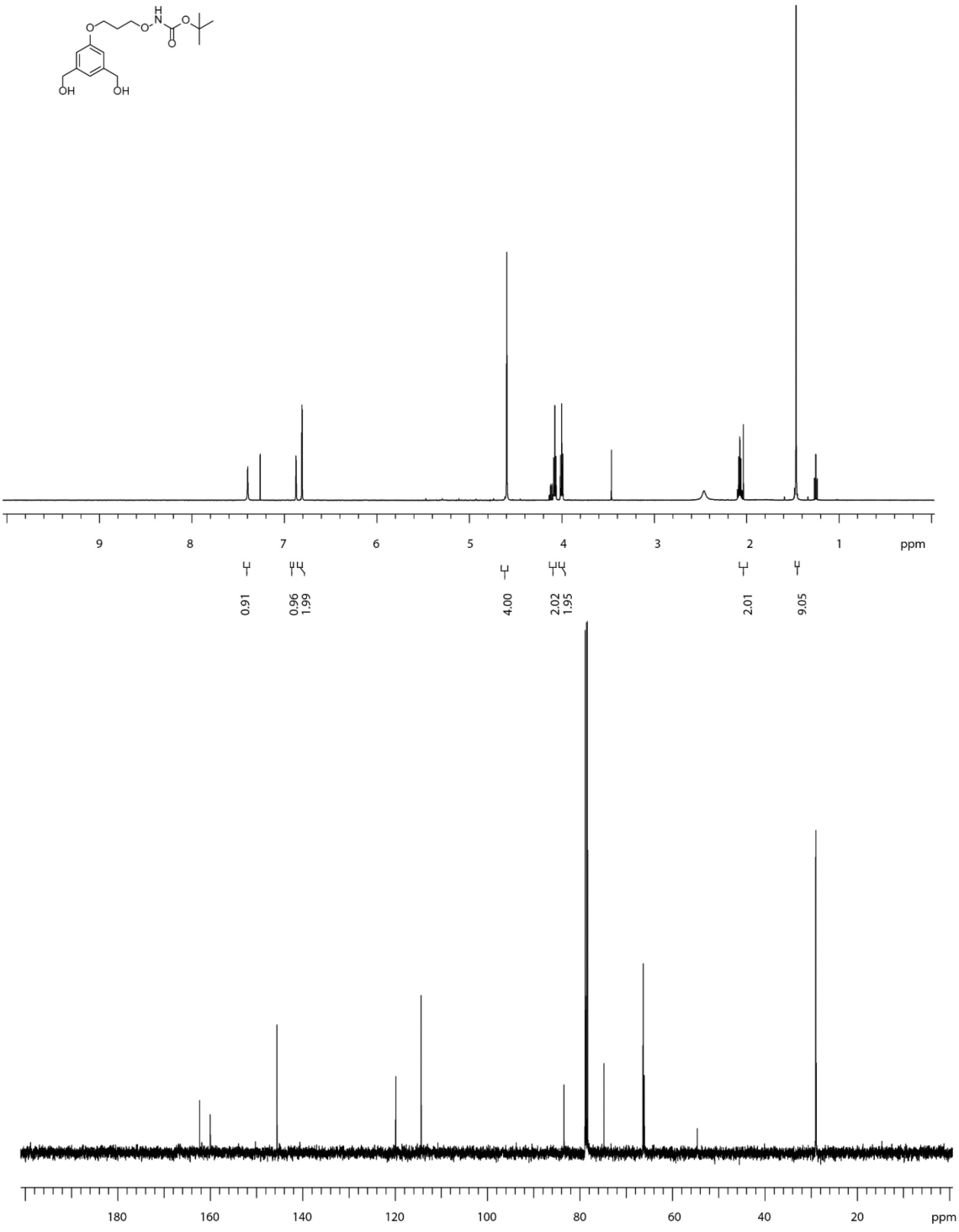

Appendix A-Figure 81. ^{1}H and ^{13}C NMR spectra of **S10**

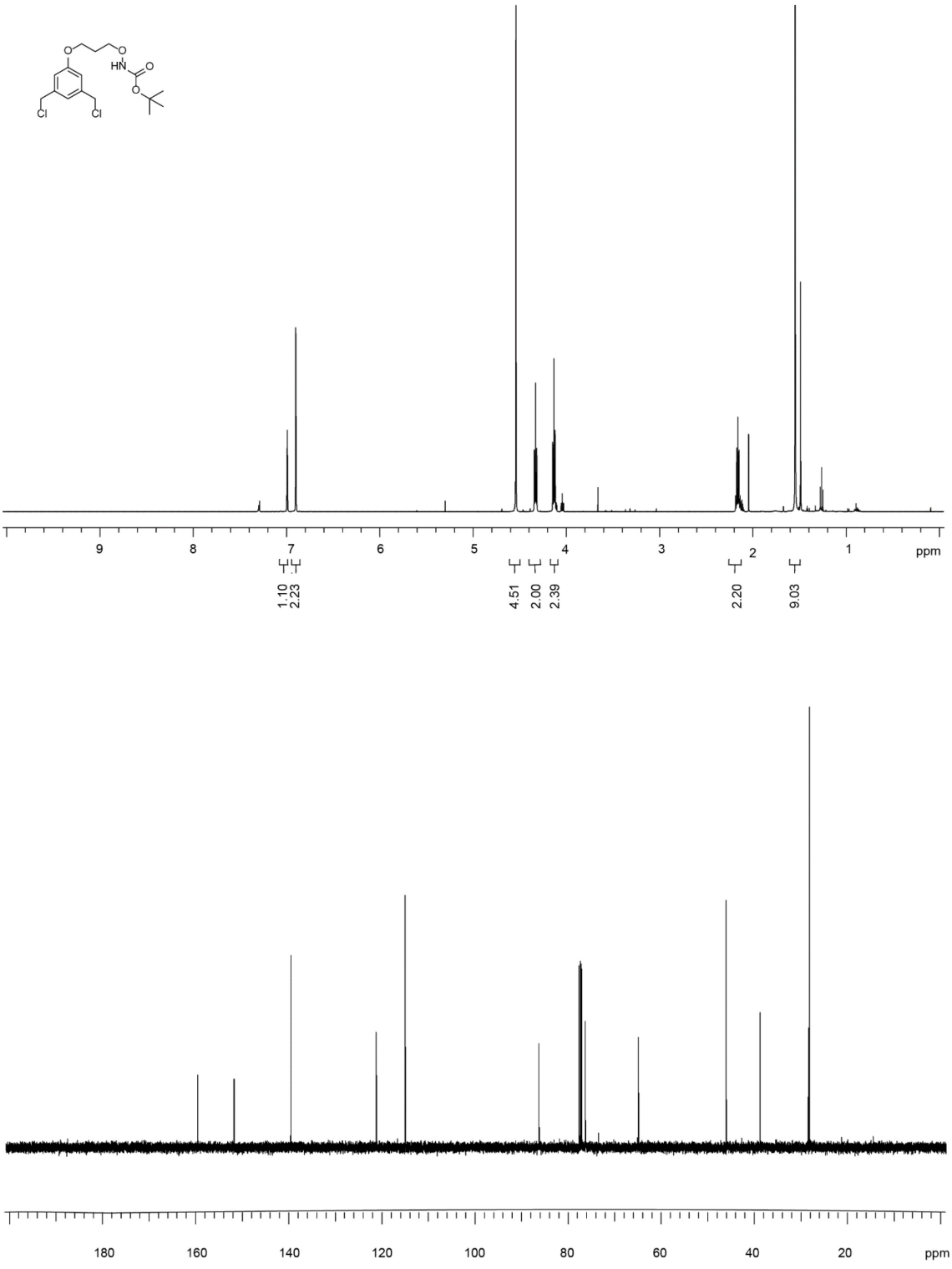

Appendix A-Figure 82. ^{1}H and ^{13}C NMR spectra of **S11**

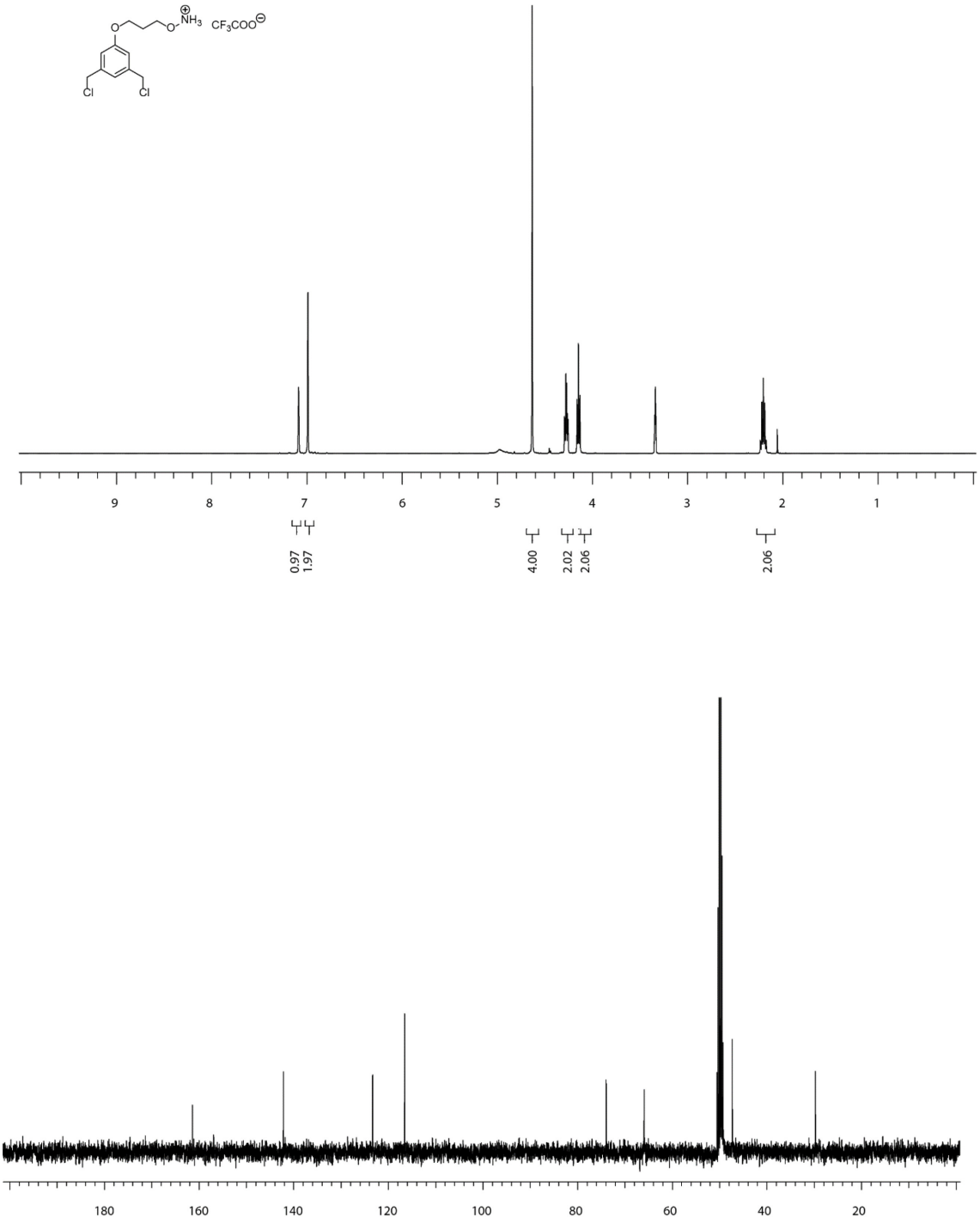

Appendix A-Figure 83. ^{1}H and ^{13}C NMR spectra of **TSL-3**

Appendix A-6.2. Proton NMR assignment and corresponding NMR spectra of 7c (1H, COSY, TOCSY, NOESY and ROESY)

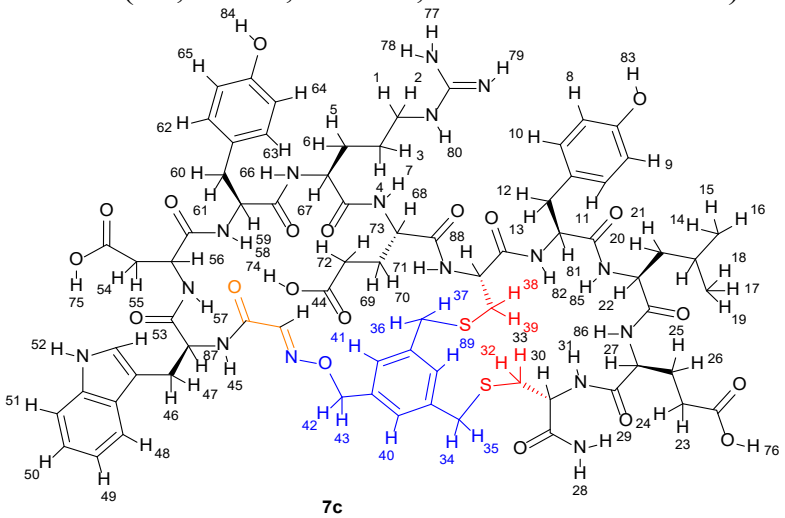

7c

Res.	NH	ppm	H_α	ppm	H_β,	ppm	H_γ,	ppm	H_δ,	ppm	H_ε,	ppm
Trp	45	7.54	87	4.52	46, 47	3.16						
Asp	57	7.50	56	4.54	54, 55	2.66, 2.48						
Tyr	58	7.79	59	4.32	60, 61	2.90						
Arg	66	8.12	67	3.83	5, 6	1.69	1, 2	1.47	80	3.05	77-80	7.15
Glu	7	7.58	68	4.12	69, 70	2.00, 1.87	72, 73	2.36	-			
Cys	71	7.53	88	4.06	38, 39	2.64, 2.40						
Tyr	82	7.59	81	4.02	12, 13	2.77						
Leu	85	7.36	22	3.96	20, 21	1.55, 1.39	90	1.34				
Glu	86	7.63	27	4.19	25, 26	2.09, 1.99	23, 24	2.43, 2.38	-			
Cys	31	7.63	30	4.46	32, 33	3.00, 2.72		-	-			
Other signals												
Cys	28	7.04	29	6.71								
Trp (Ar)	52	9.96	53	7.02	50	7.13	51	7.56	48	7.36	49	7.05
Tyr (Ar)	62, 63	6.92	64, 65	6.60								

Tyr (Ar)	11, 10	6.92	8, 9	6.64								
TSL-1	89	7.12	40	7.04	41	6.95	42, 43	4.95	34, 35	3.66	36, 37	3.51

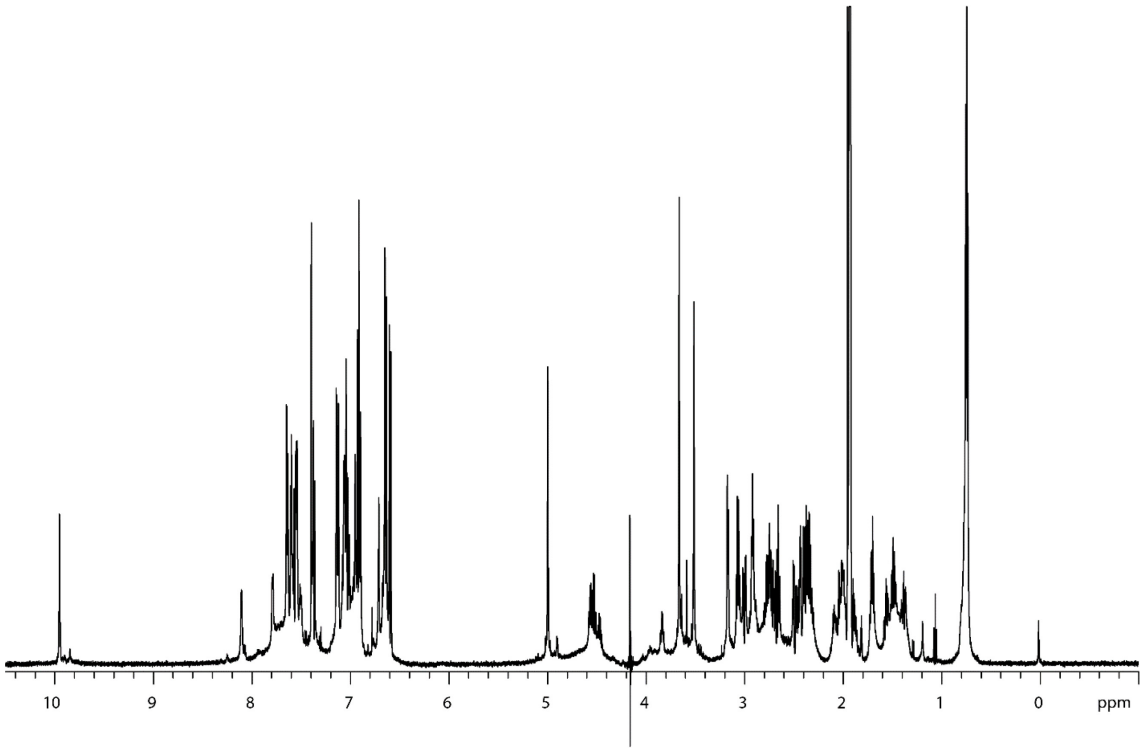

Appendix A-Figure 84. ^{1}H NMR of **7c**

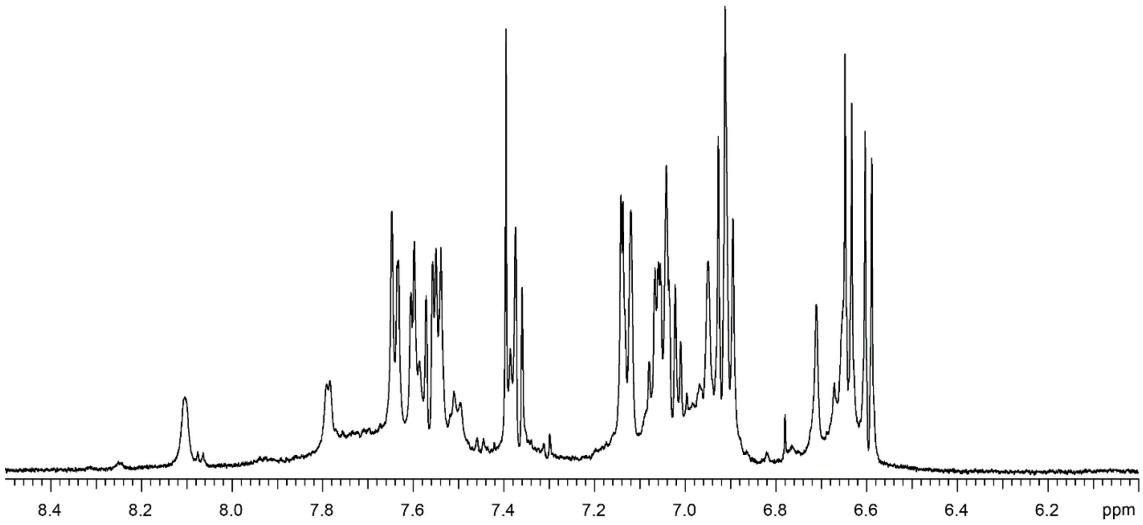

Appendix A-Figure 85. 1H NMR of **7c** (expanded)

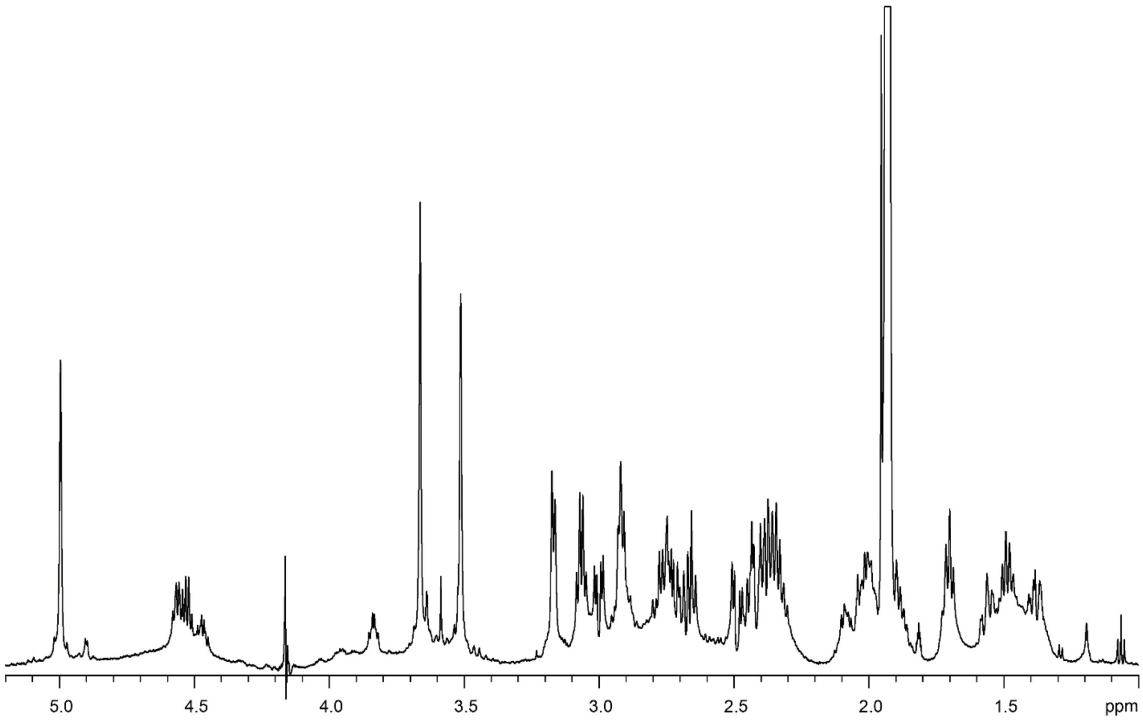

Appendix A-Figure 86. 1H NMR of **7c** (expanded)

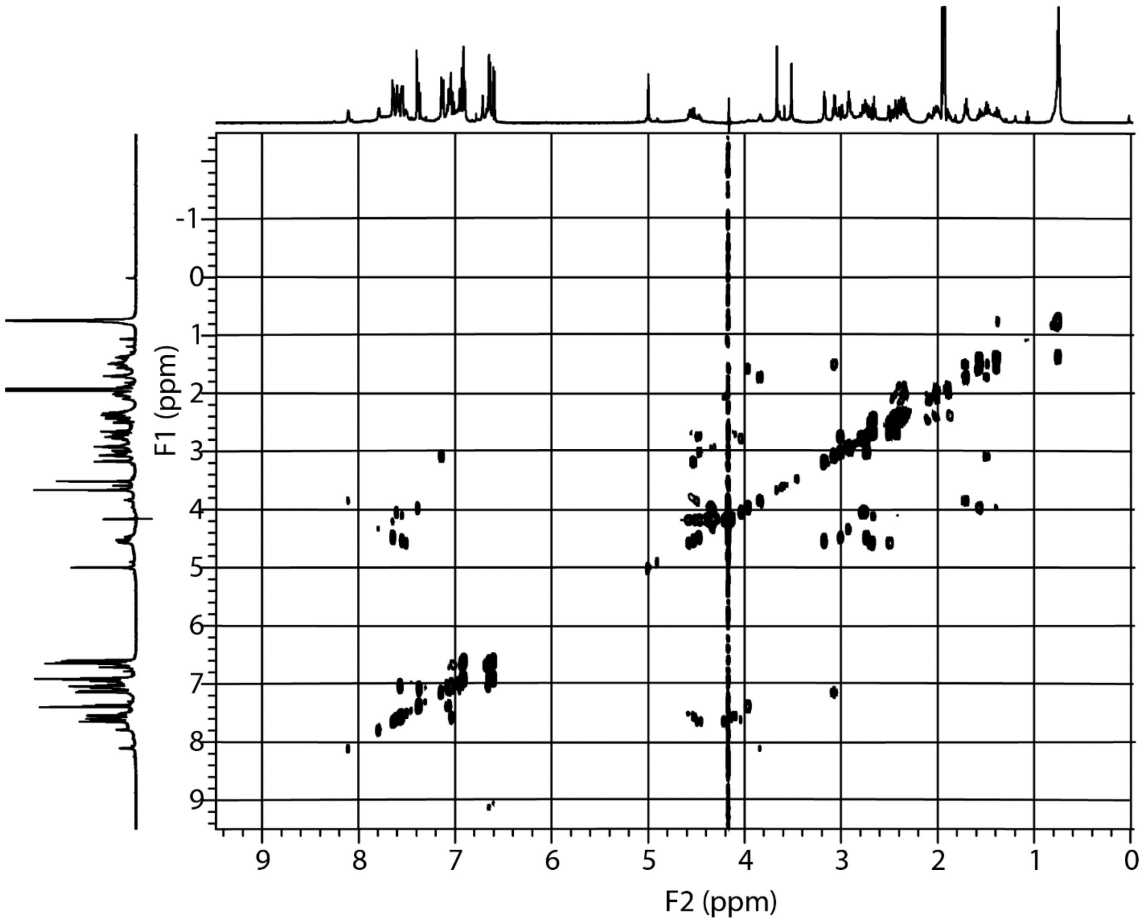

Appendix A-Figure 87. COSY NMR of **7c**

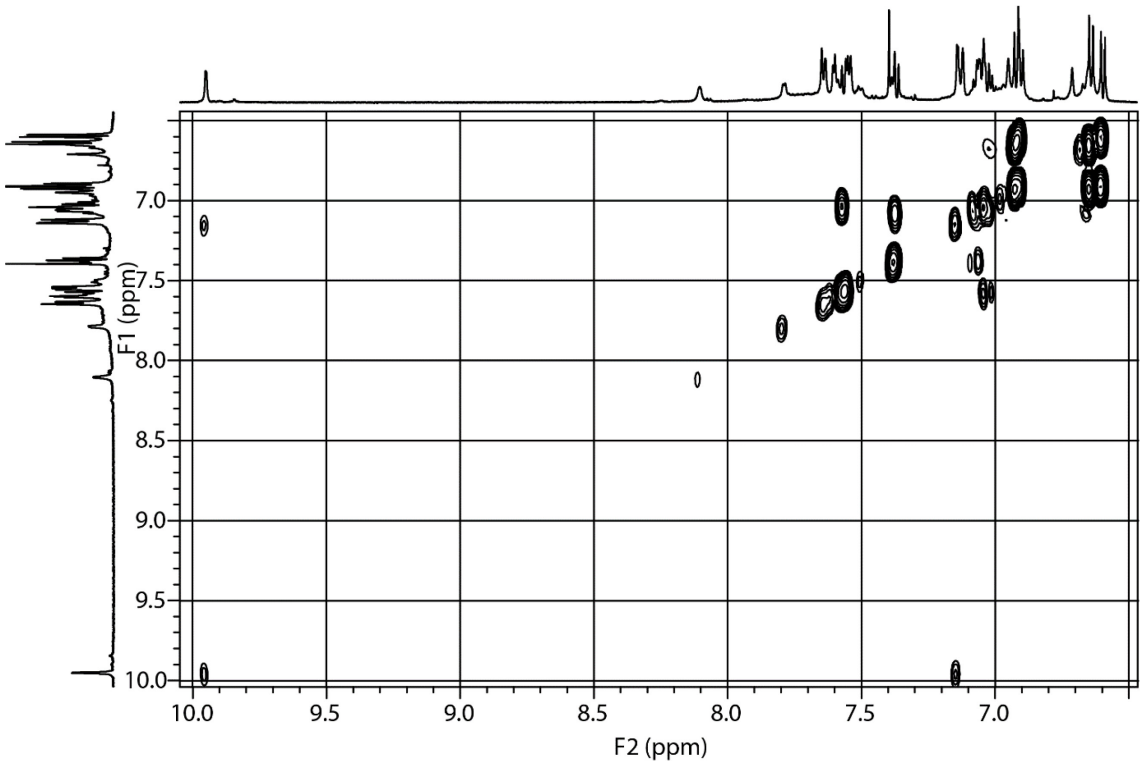

Appendix A-Figure 88. COSY NMR (expanded) of **7c**

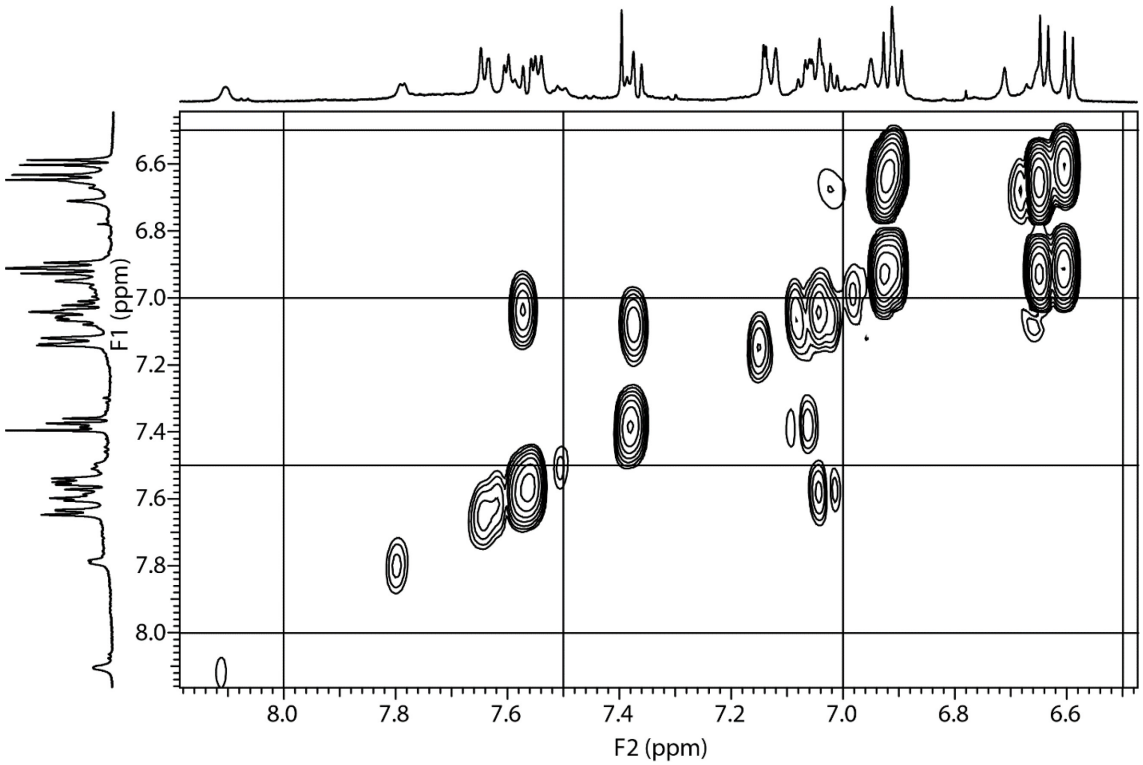

Appendix A-Figure 89. COSY NMR (expanded) of **7c**

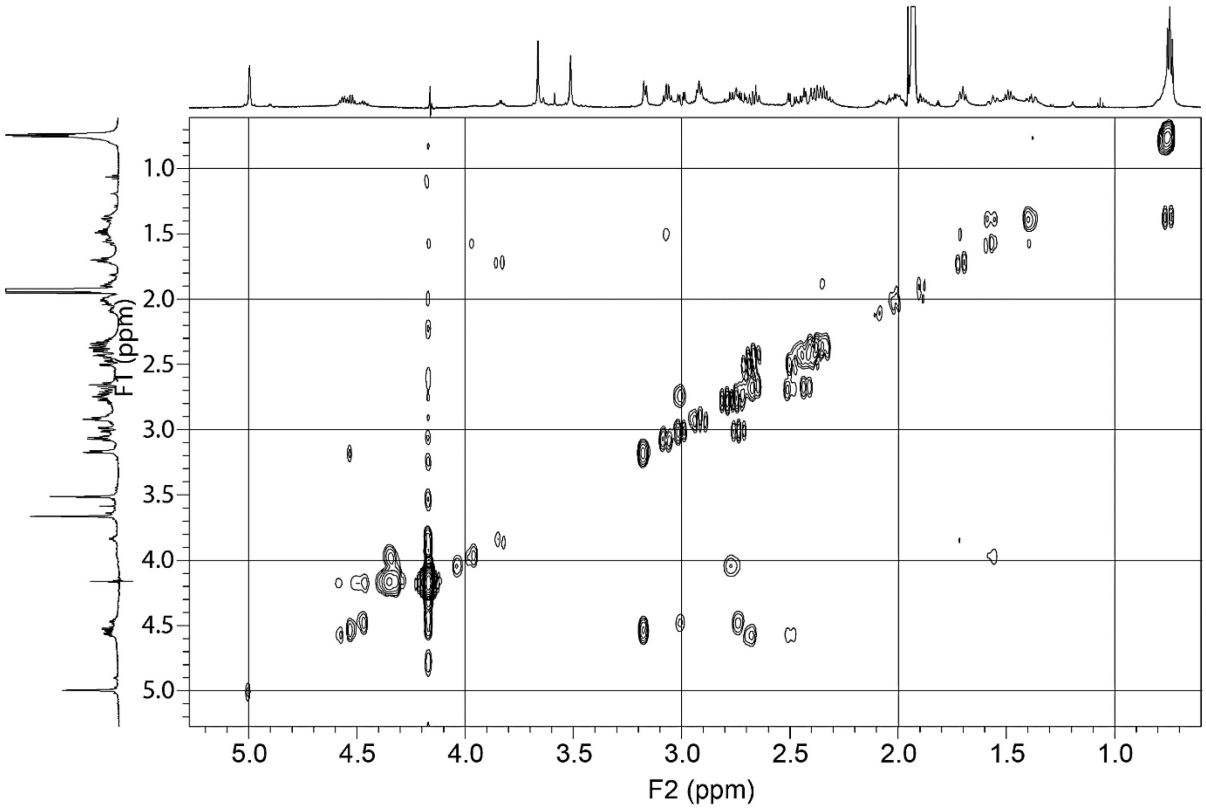

Appendix A-Figure 90. COSY NMR (expanded) of **7c**

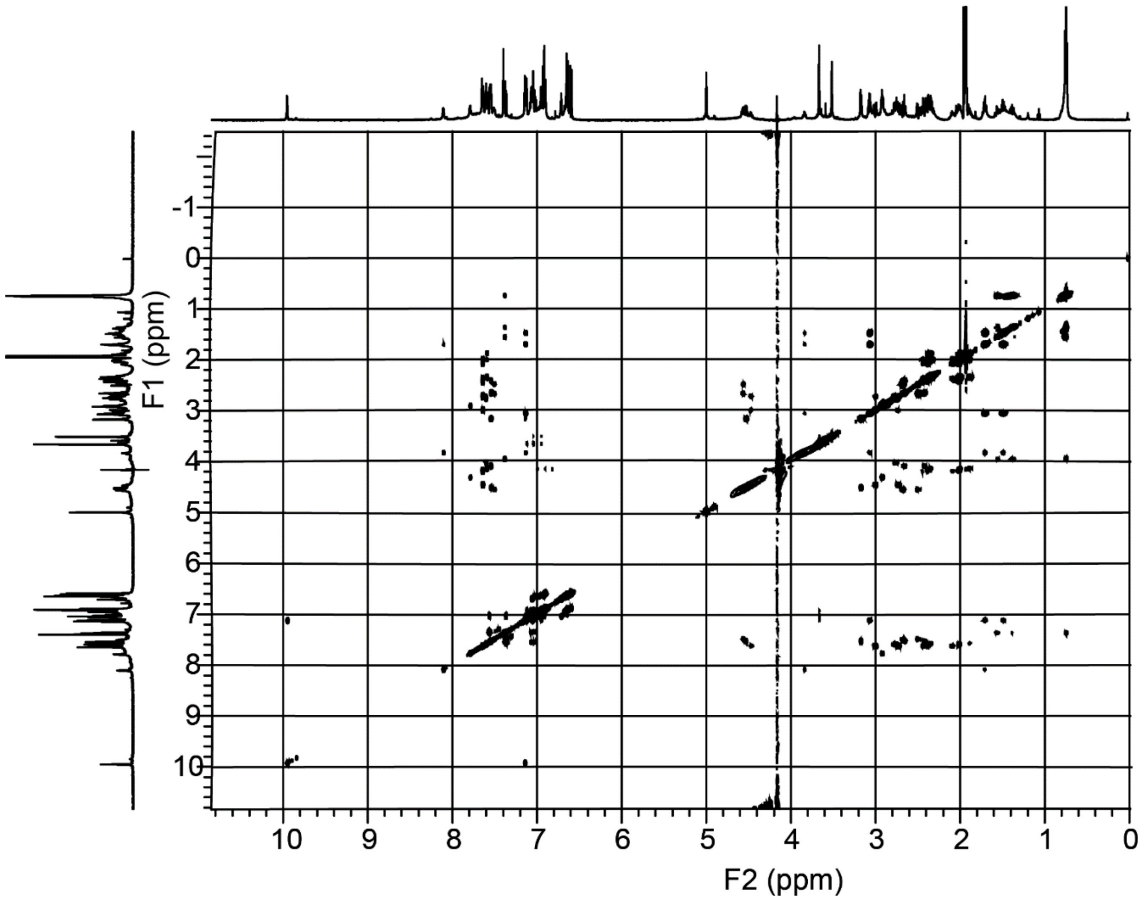

Appendix A-Figure 91. TOCSY NMR of **7c**

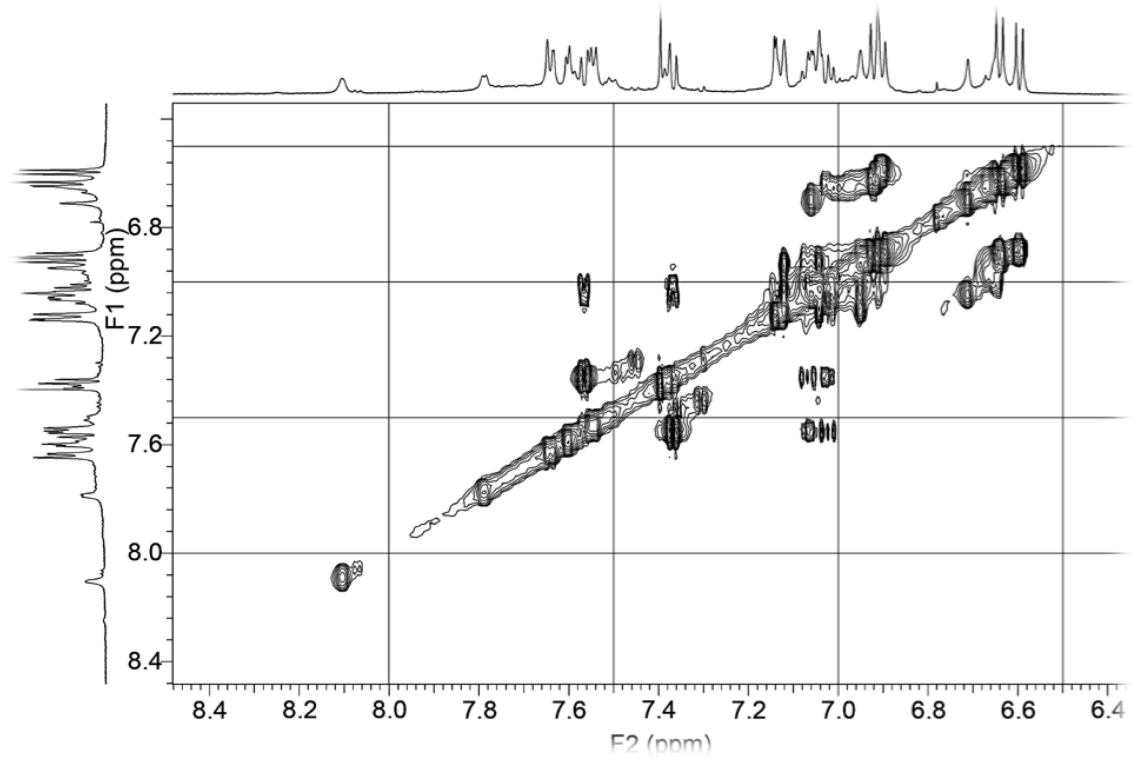

Appendix A-Figure 92. TOCSY NMR (expanded) of **7c**

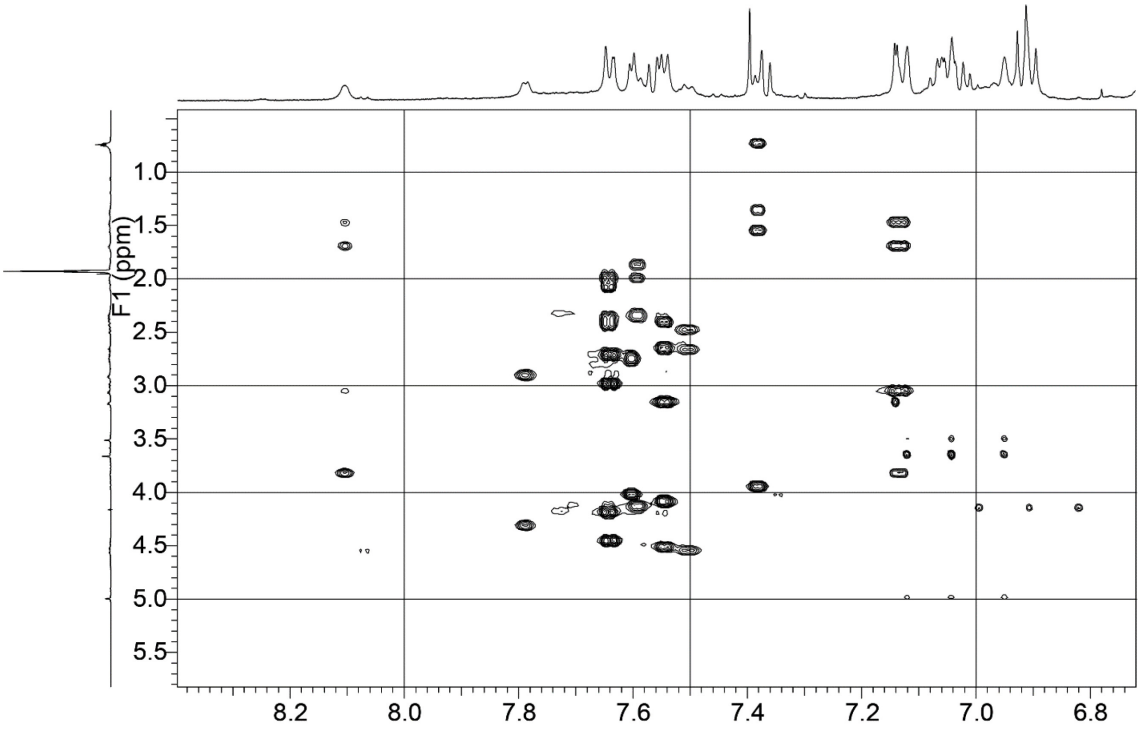

Appendix A-Figure 93. TOCSY NMR (expanded) of **7c**

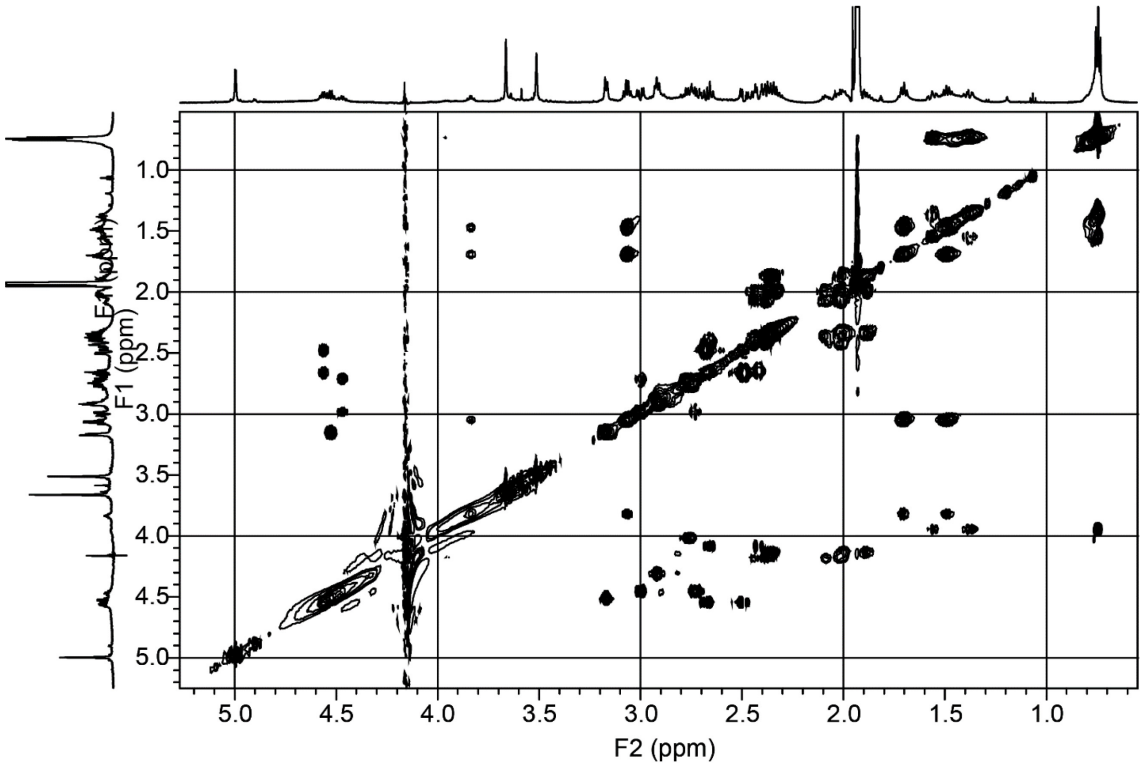

Appendix A-Figure 94. TOCSY NMR (expanded) of **7c**

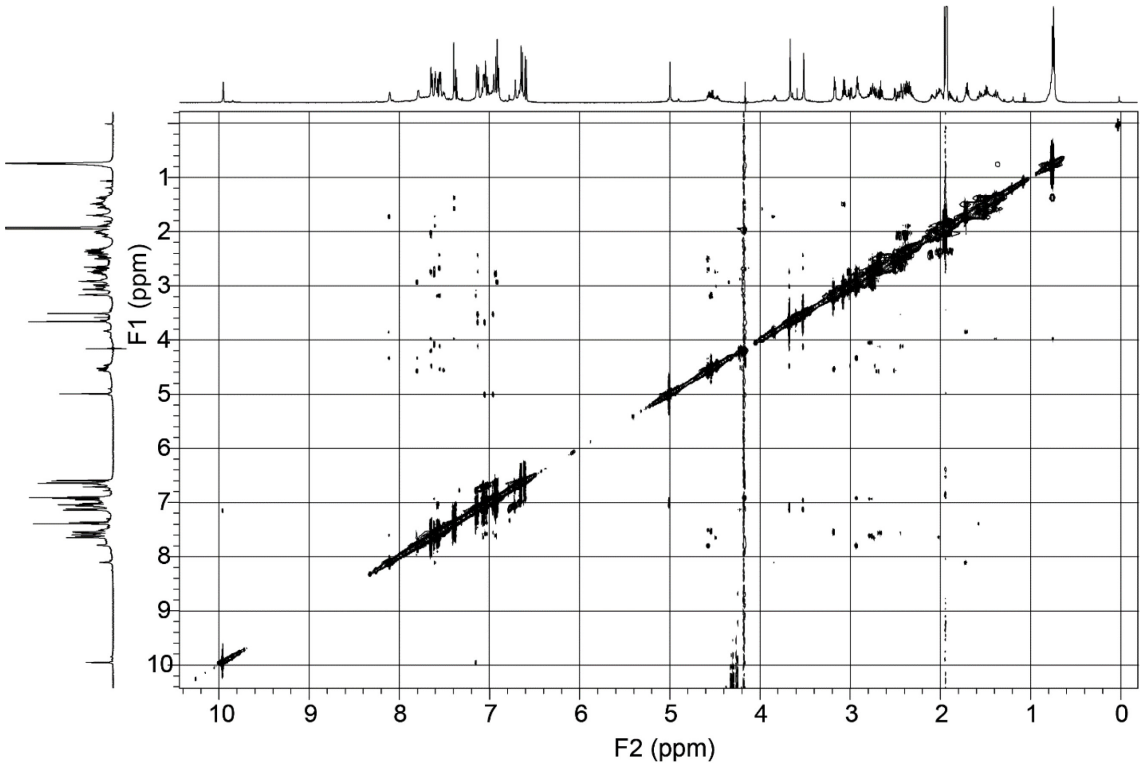

Appendix A-Figure 95. NOESY NMR of **7c**

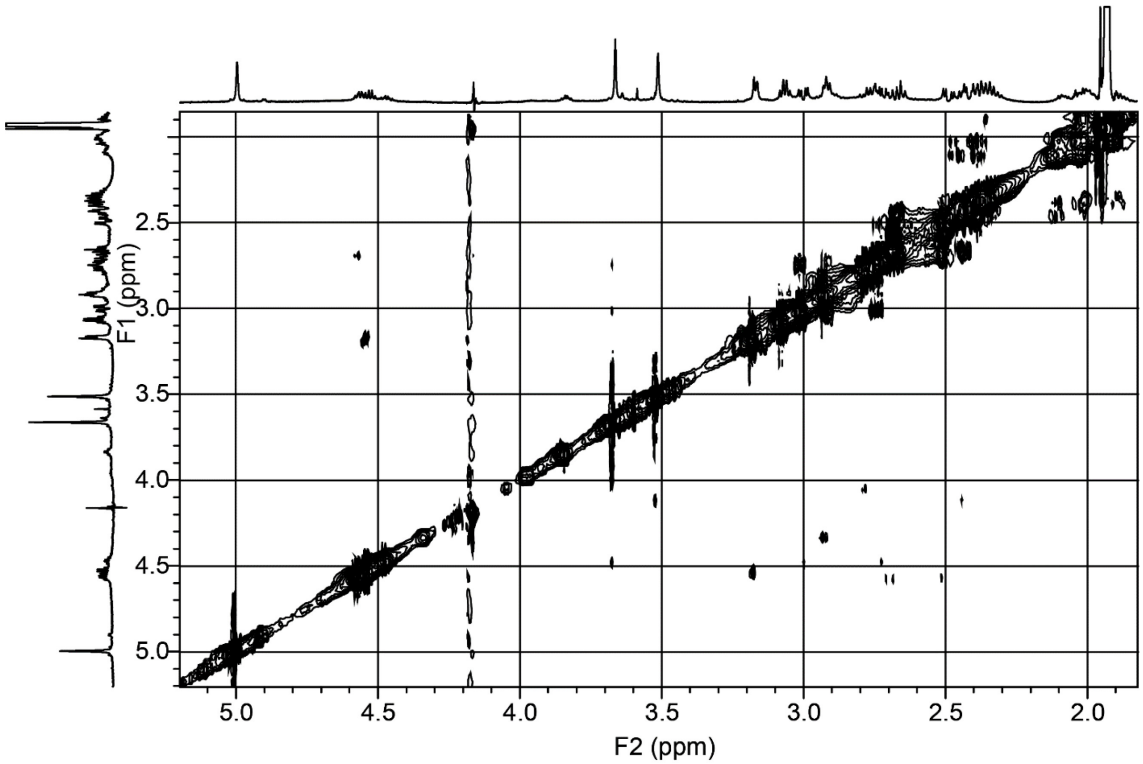

Appendix A-Figure 96. NOESY NMR (expanded) of 7c

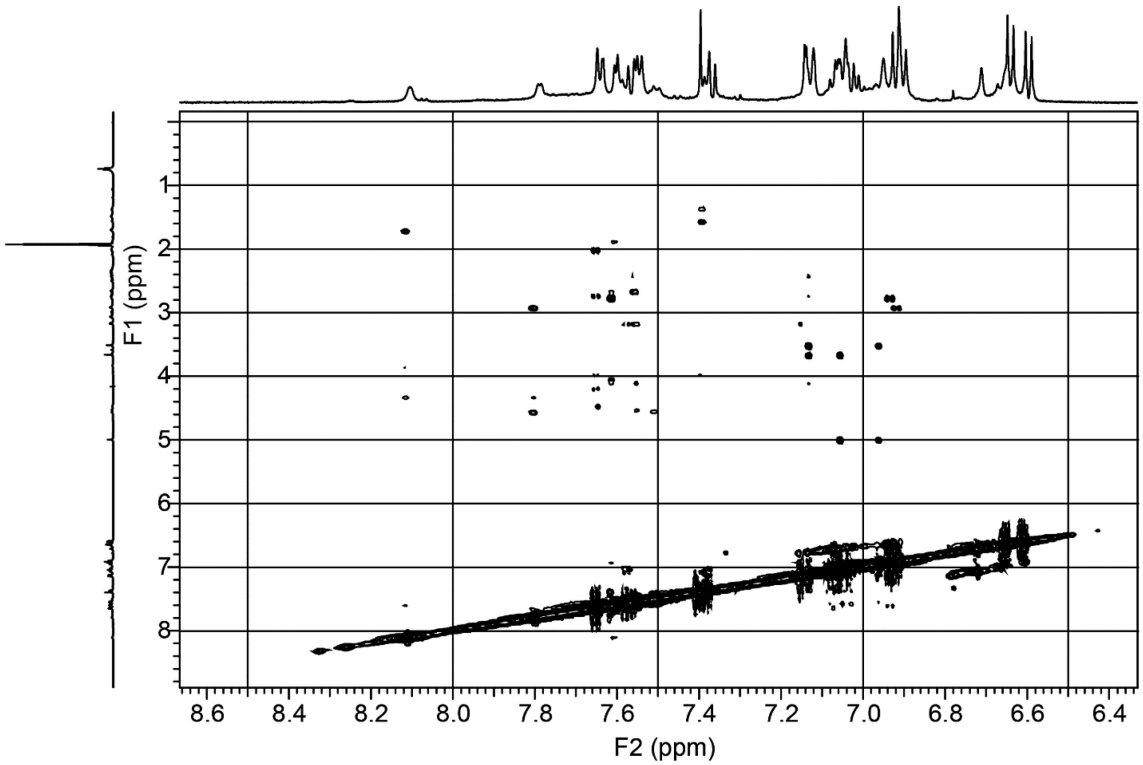

Appendix A-Figure 97. NOESY NMR (expanded) of **7c**

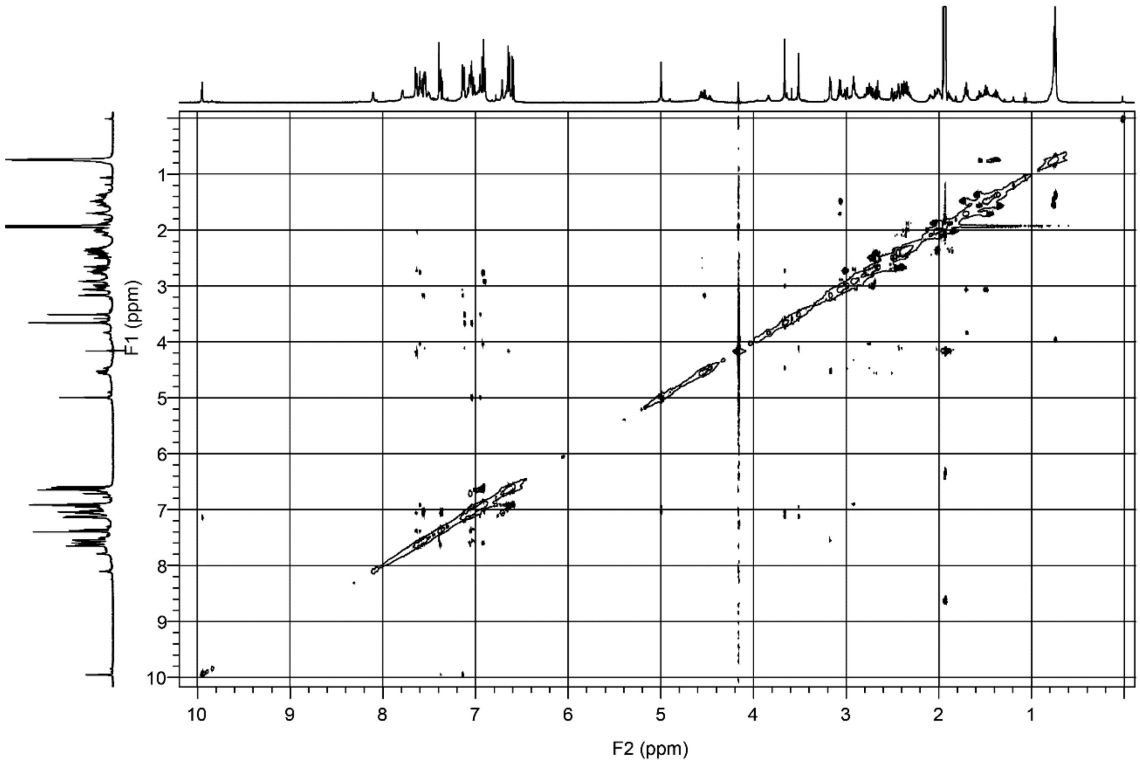

Appendix A-Figure 98. ROESY NMR of **7c**

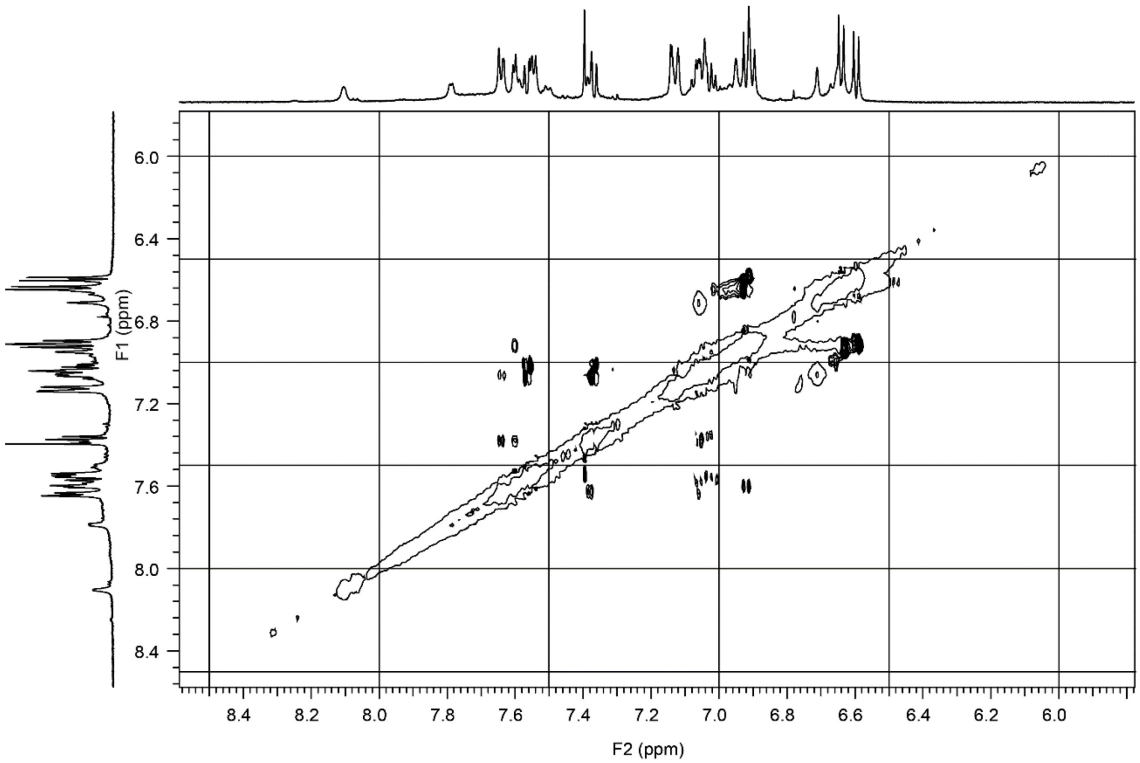

Appendix A-Figure 99. ROESY NMR (expanded) of **7c**

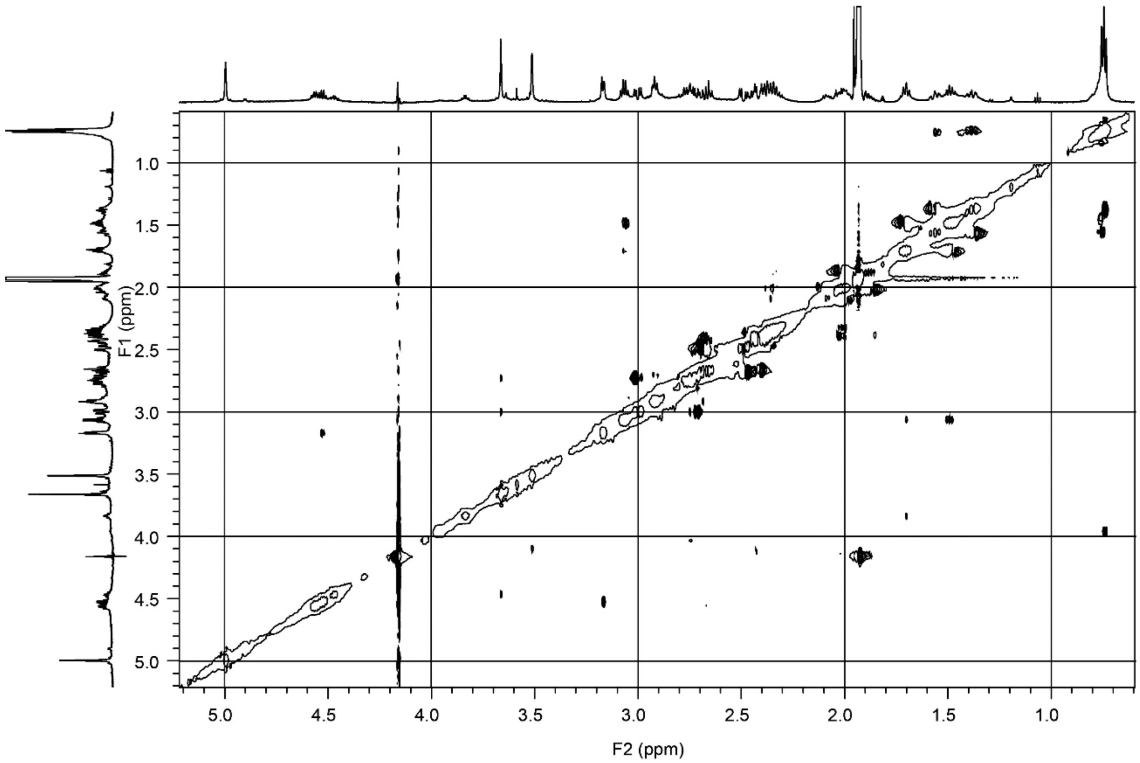

Appendix A-Figure 100. ROESY NMR (expanded) of **7c**

Appendix A-6.3. Proton NMR assignment and corresponding NMR spectra of 3c (1H, COSY, TOCSY, NOESY and ROESY)

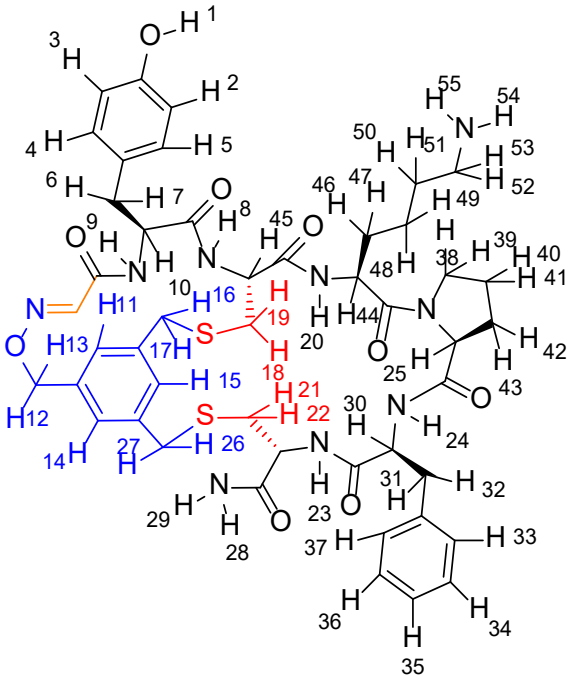

Res	NH	ppm	Hα	ppm	Hβ,	ppm	Hγ	ppm	Hδ,	ppm	Hε,	ppm
Tyr	9	7.27	10	4.86	6, 7	3.05						
Cys	8	7.07	45	4.50	18, 19	3.14 2.02						
Lys	20	7.47	44	3.88	46, 47	1.54 1.49	48 49	1.28 1.16	50 51	1.45	52 53	2.75
Pro			25	4.26	42, 43	2.03 1.84	40 41	1.53 0.70	18 39	3.12 2.84		
Phe	24	7.95	30	4.25	31, 32	3.20 3.00						
Cys	23	7.36	66	4.44	21, 22	2.29						
Other signals												
Cys	28	7.32	29	6.64								
Lys	54, 55	7.29										
Phe (Ar)	33 37	7.28	34-36	7.21 1								
Tyr (Ar)	2 3	7.04	4 5	6.77								
TSL-1	11	7.18	14	7.17	15	6.92	12 13	5.08 4.97	21 22	3.64	18 19	3.55

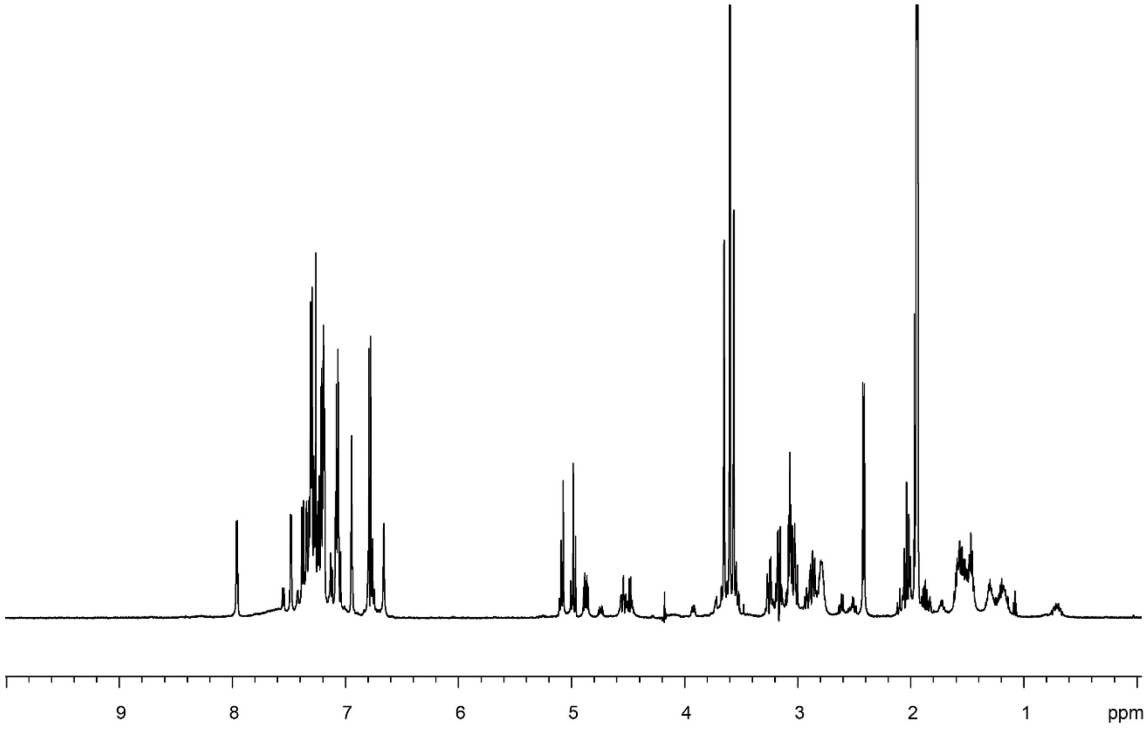

Appendix A-Figure 101. ^{1}H NMR of **3c**

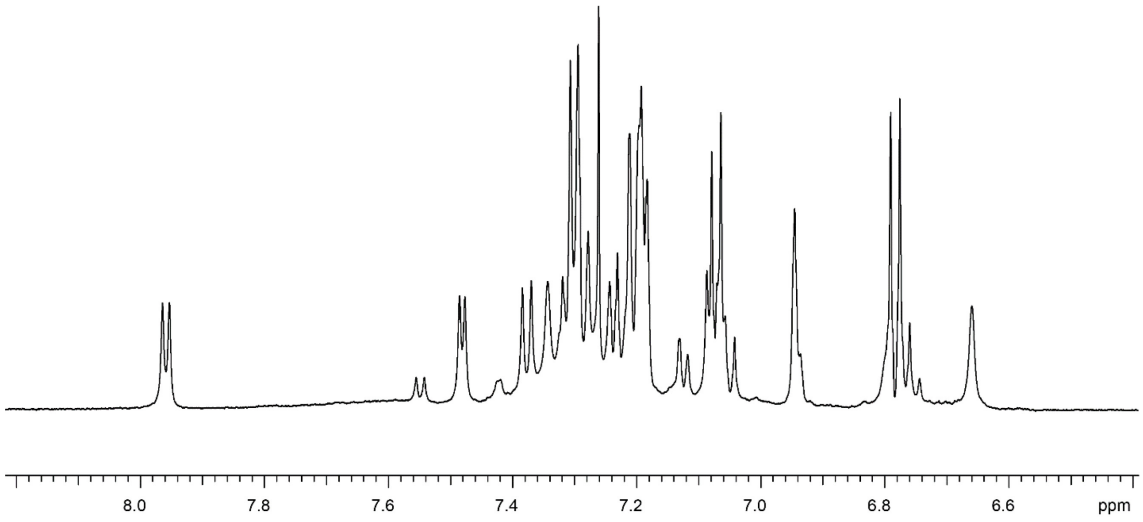

Appendix A-Figure 102. ^{1}H NMR (expended) of **3c**

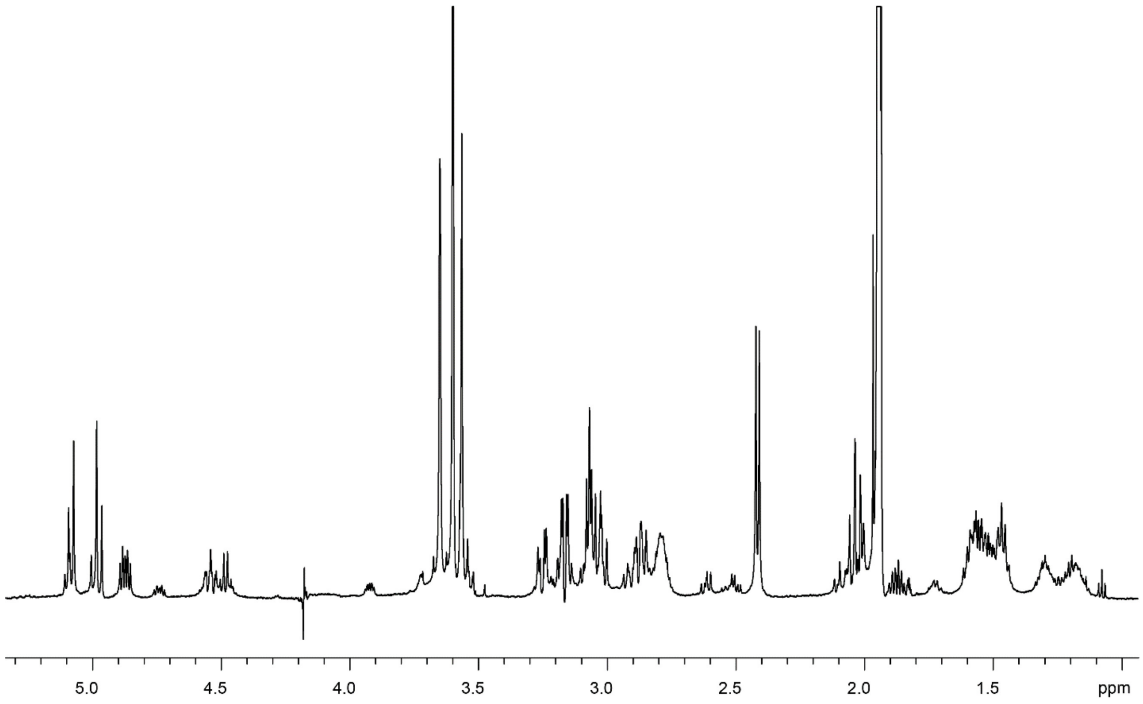

Appendix A-Figure 103. ^{1}H NMR (expended) of **3c**

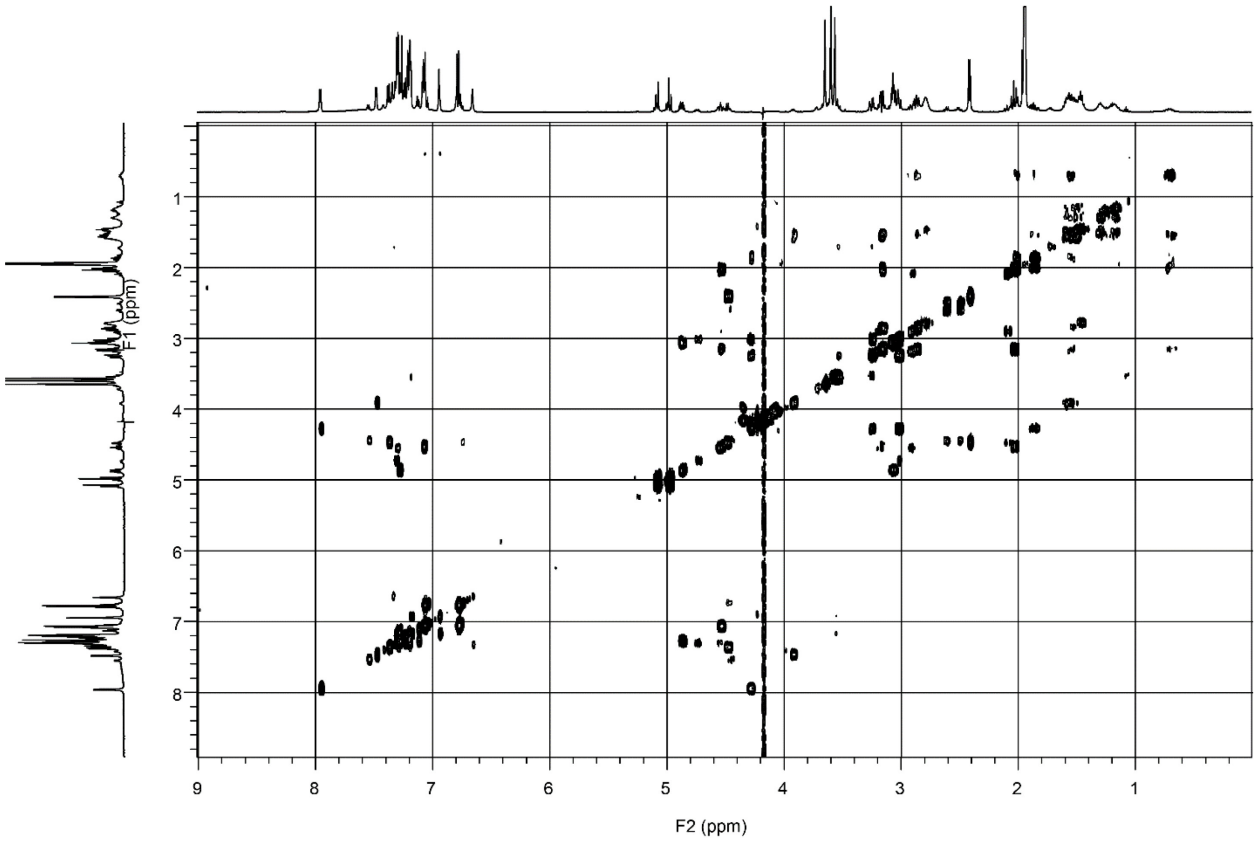

Appendix A-Figure 104. COSY NMR of **3c**

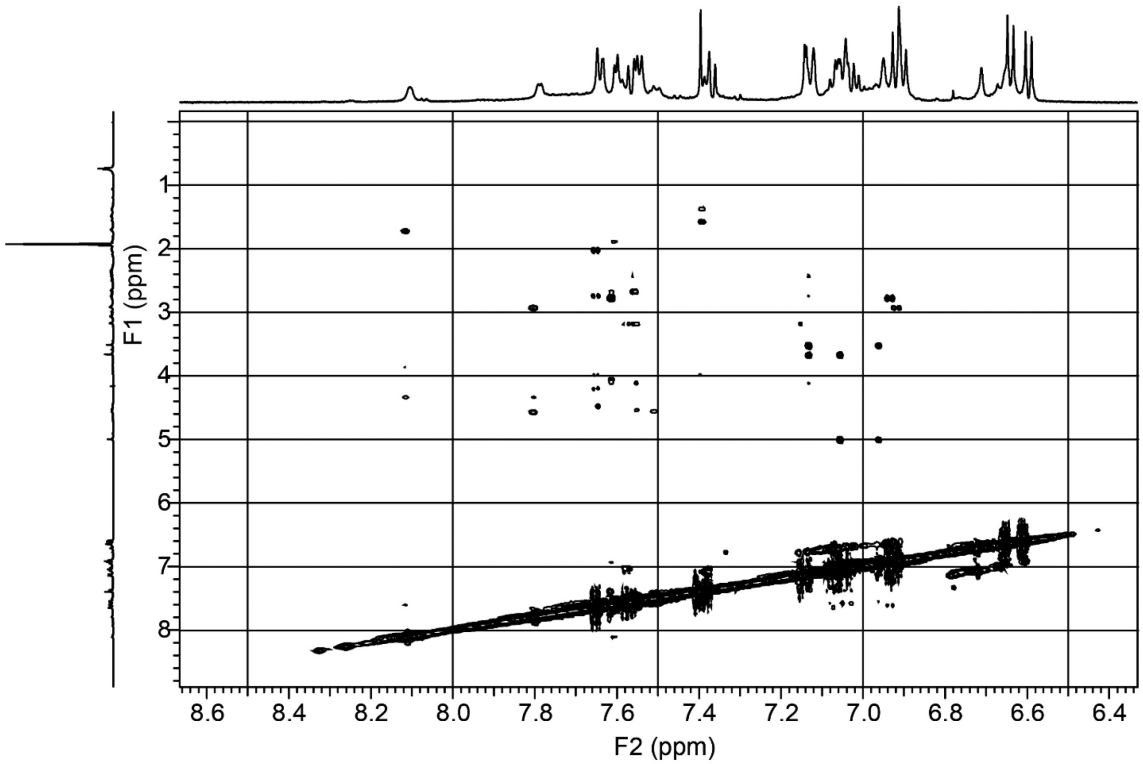

Appendix A-Figure 105. COSY NMR (expended) of **3c**

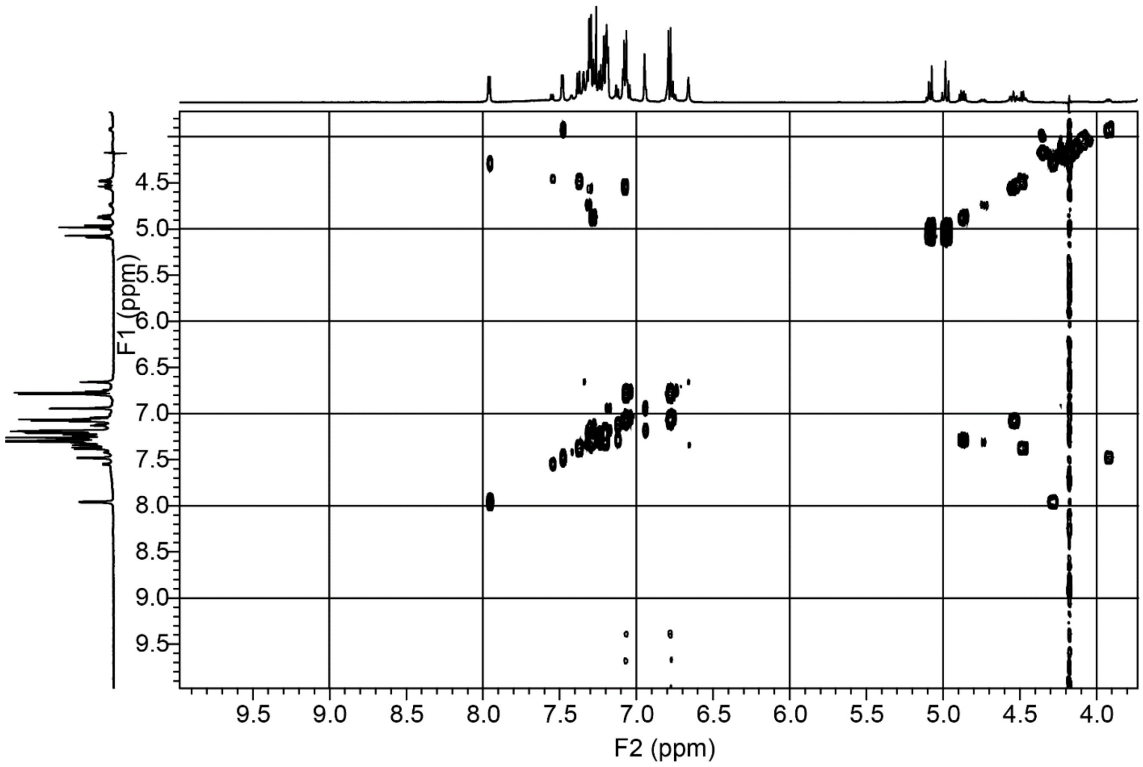

Appendix A-Figure 106. COSY NMR (expanded) of **3c**

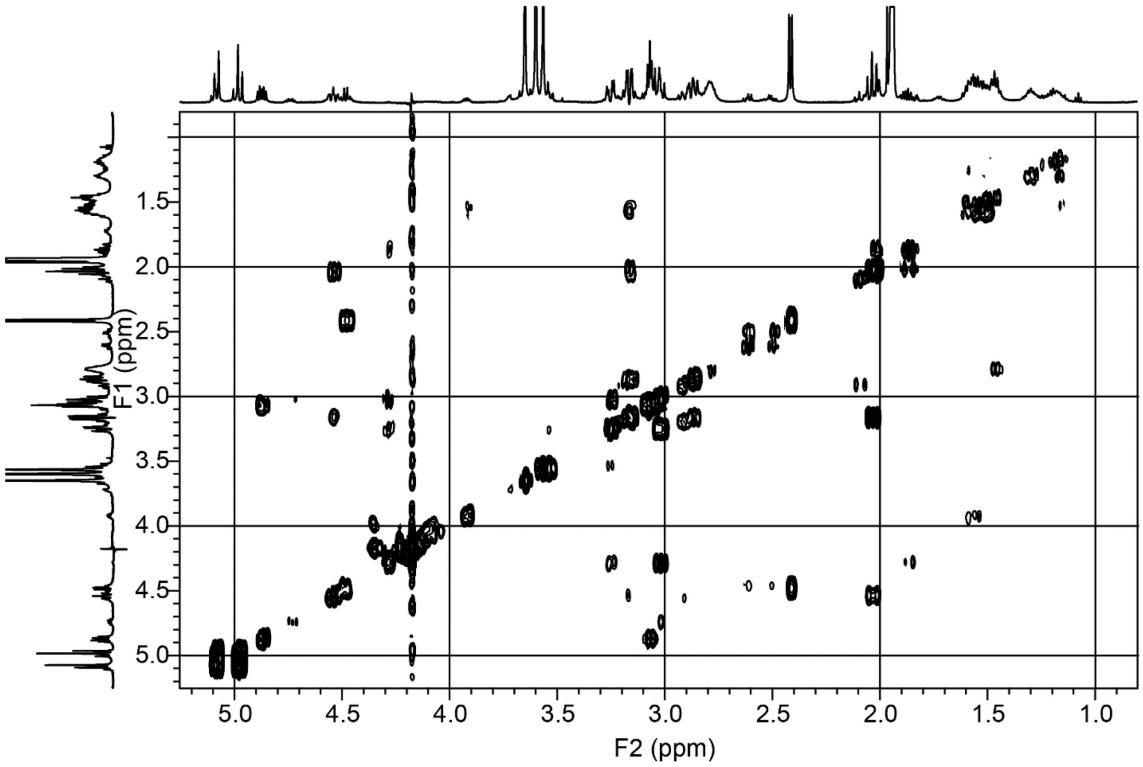

Appendix A-Figure 107. COSY NMR (expanded) of **3c**

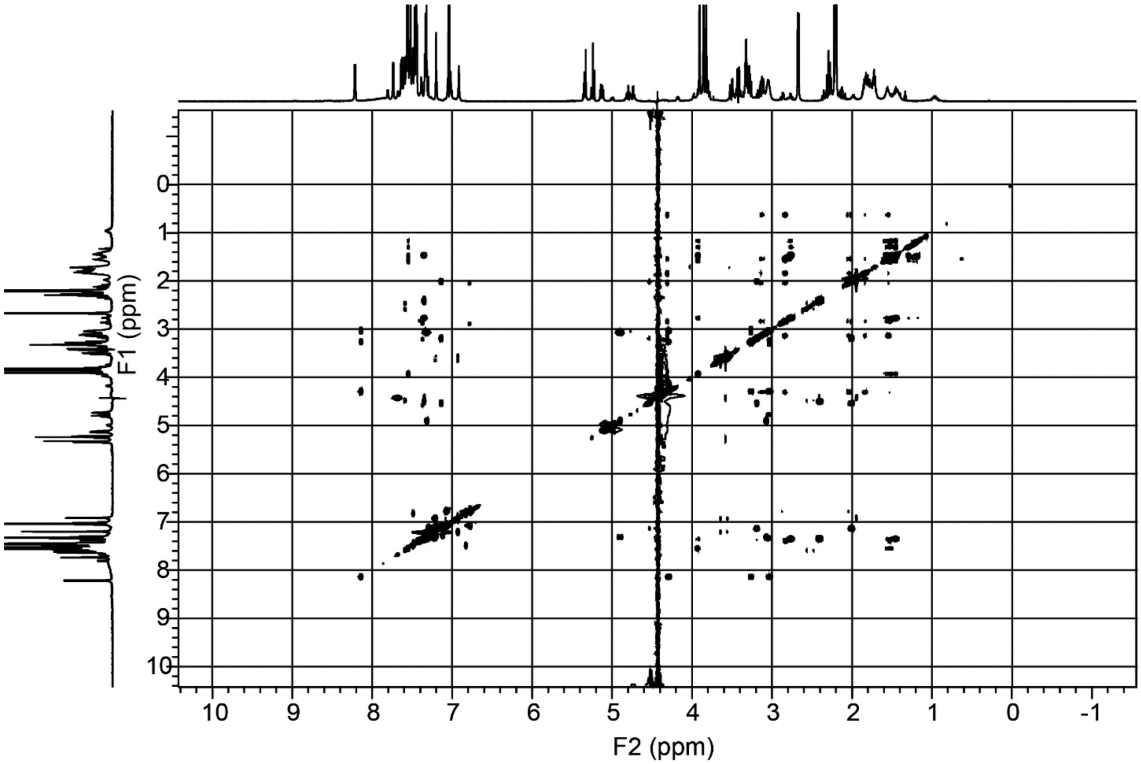

Appendix A-Figure 108. TOCSY NMR of **3c**

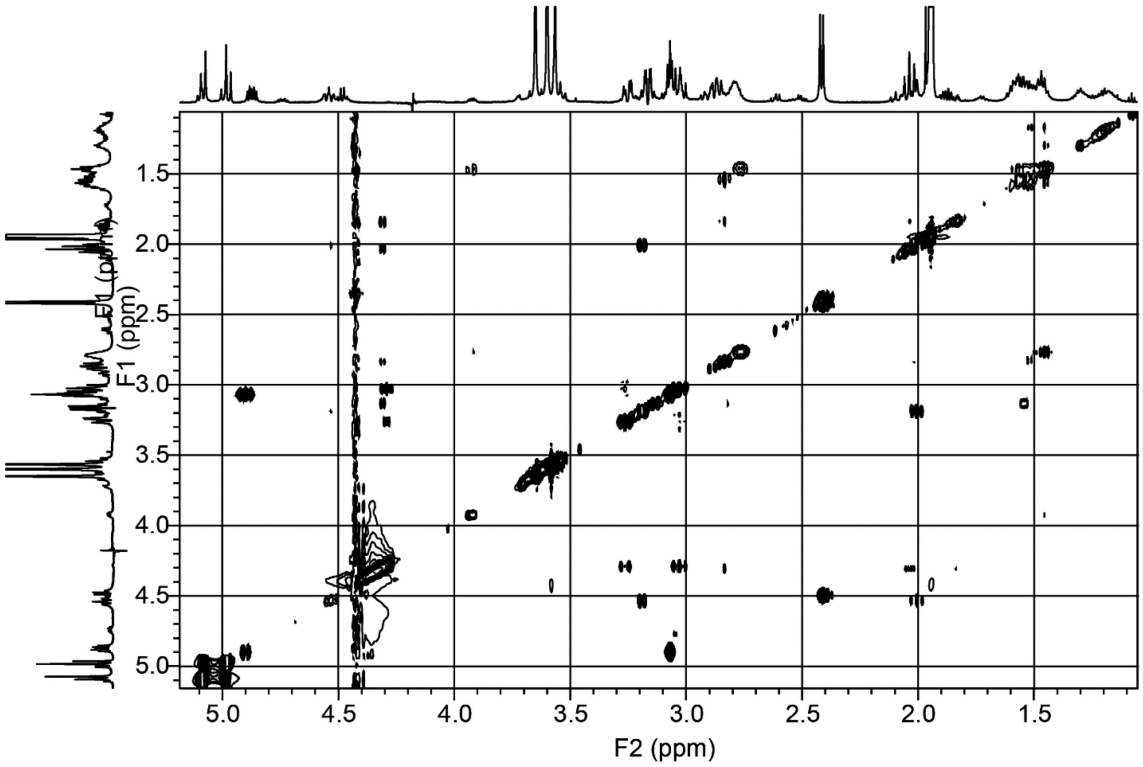

Appendix A-Figure 109. TOCSY NMR (expanded) of **3c**

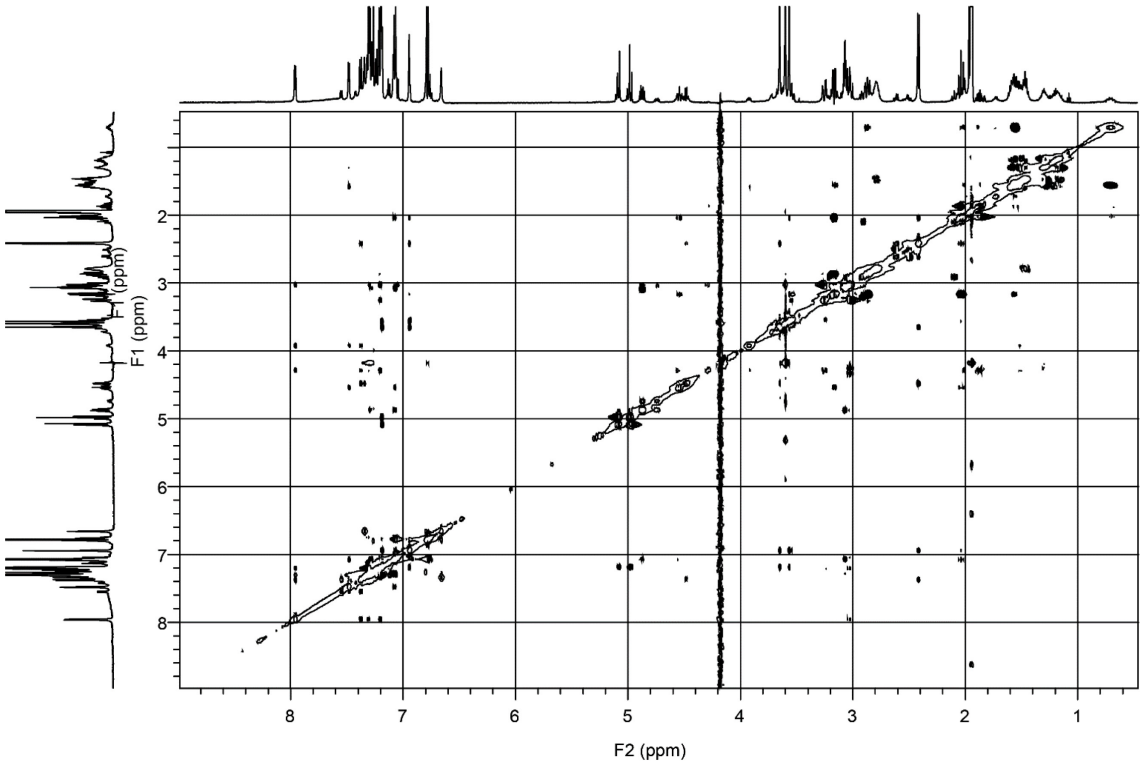

Appendix A-Figure 110. ROESY NMR of **3c**

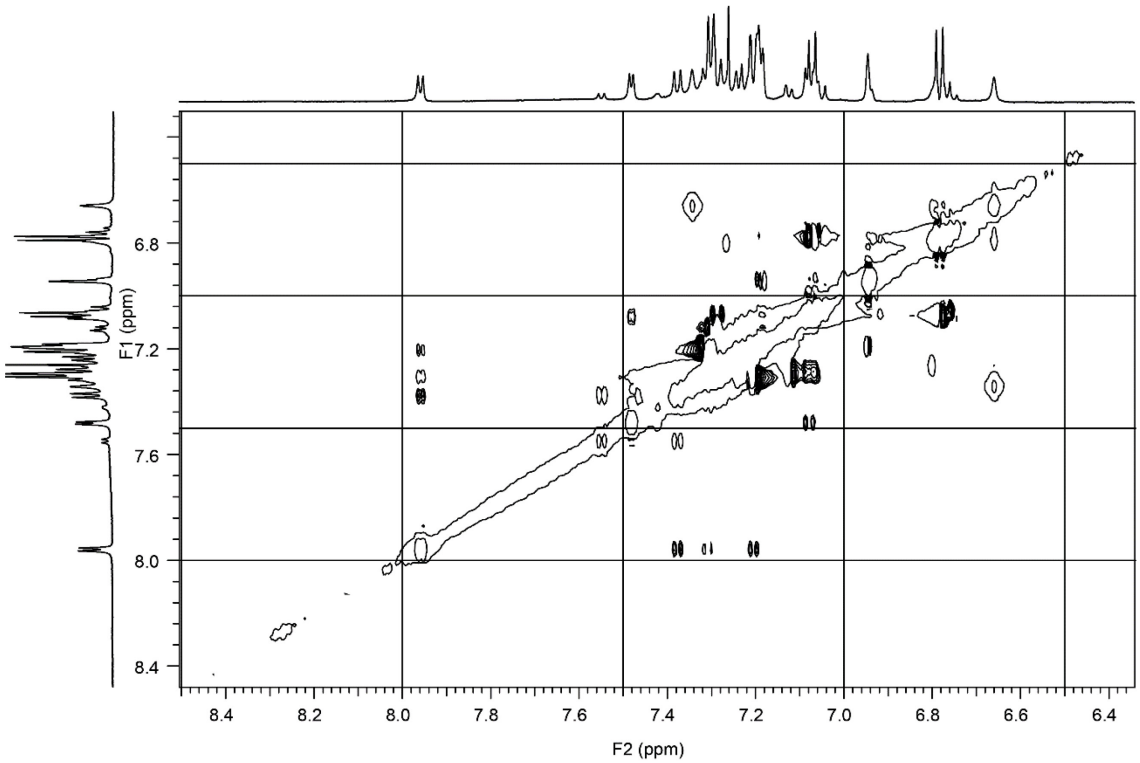

Appendix A-Figure 111. TOCSY NMR (expanded) of **3c**

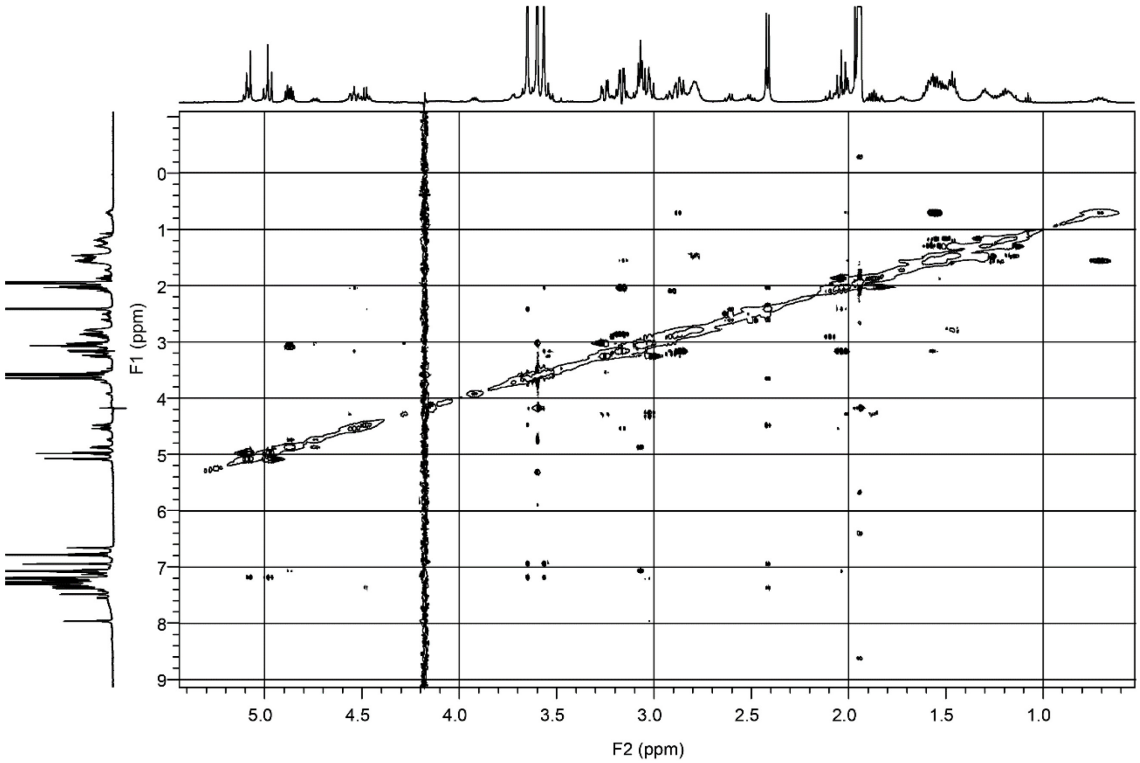

Appendix A-Figure 112. ROESY NMR (expanded) of **3c**

Appendix B: Supporting information for chapter 3

Appendix B-1: General screening and validation

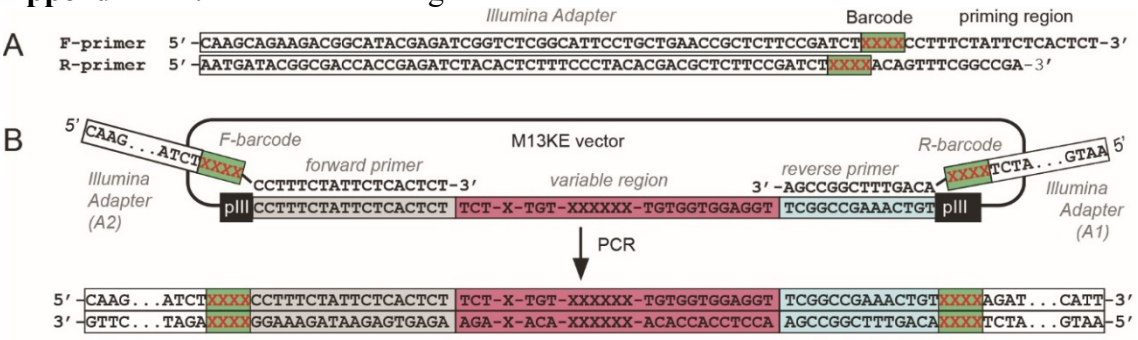

Appendix B-Figure 1. DNA sequences of PCR amplification protocol for Illumina deep sequencing (A) Primers used for amplifying ligated or naïve oligonucleotide DNA. XXXX denotes 4-nucleotide-long barcodes used to trace multiple samples in an Illumina sequencing experiment. (B) Generation of PCR product. Alignment of forward and reverse primers to 18-bp and 14-bp sequences flanking the variable region at the N-terminus of the pIII gene in M13KE vector, respectively.

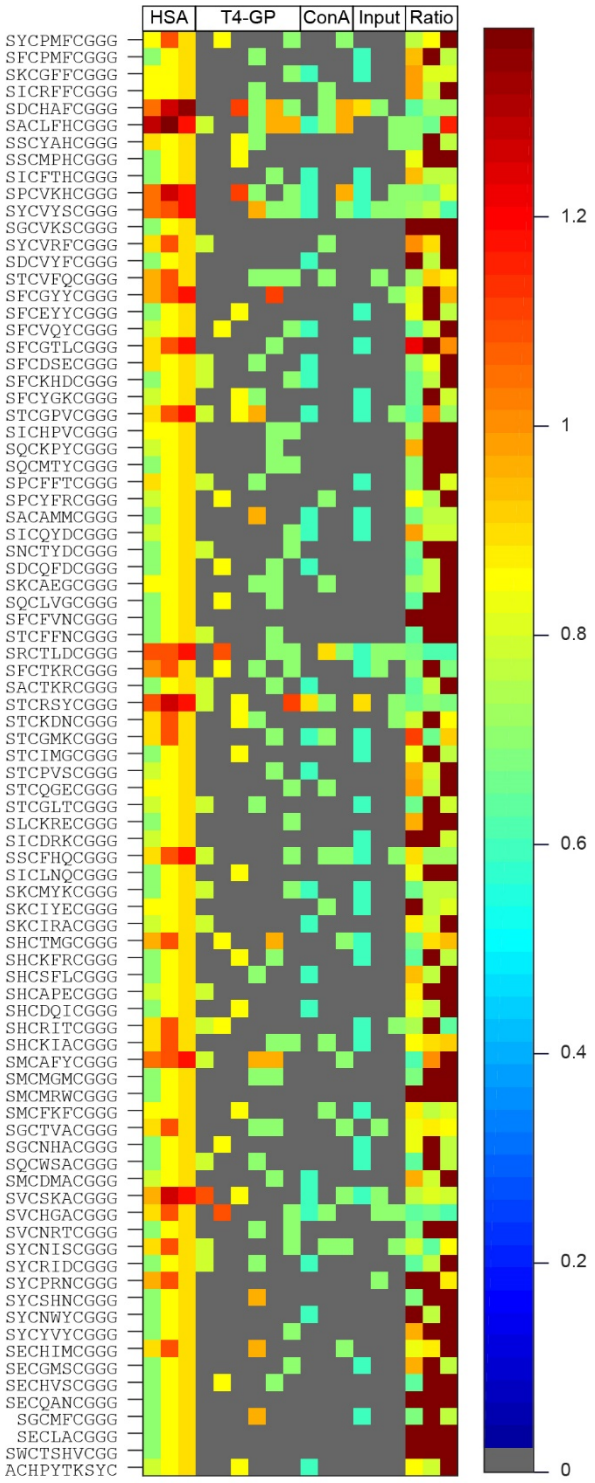

Appendix B-Figure 2. A heat map is showing of 85 putative hits discovered from the third campaign panning. The sequences were enriched greater or equal to 4-fold (R>3, p=0.05) when compared to T4-GP and ConA.

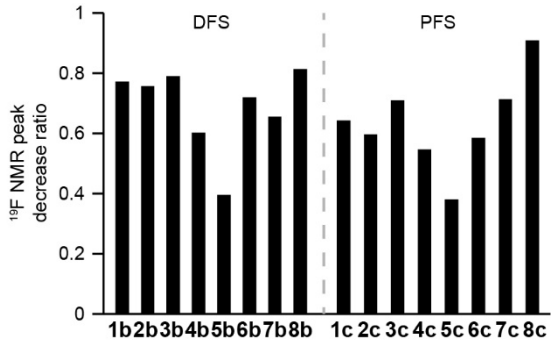

Appendix B-Figure 3. Summary all 16 peptides of ^{19}F NMR binding assay peaks decrease ratios. Ratios were calculated by peptide peak intensity after addition of HSA / original peptide peak intensity.

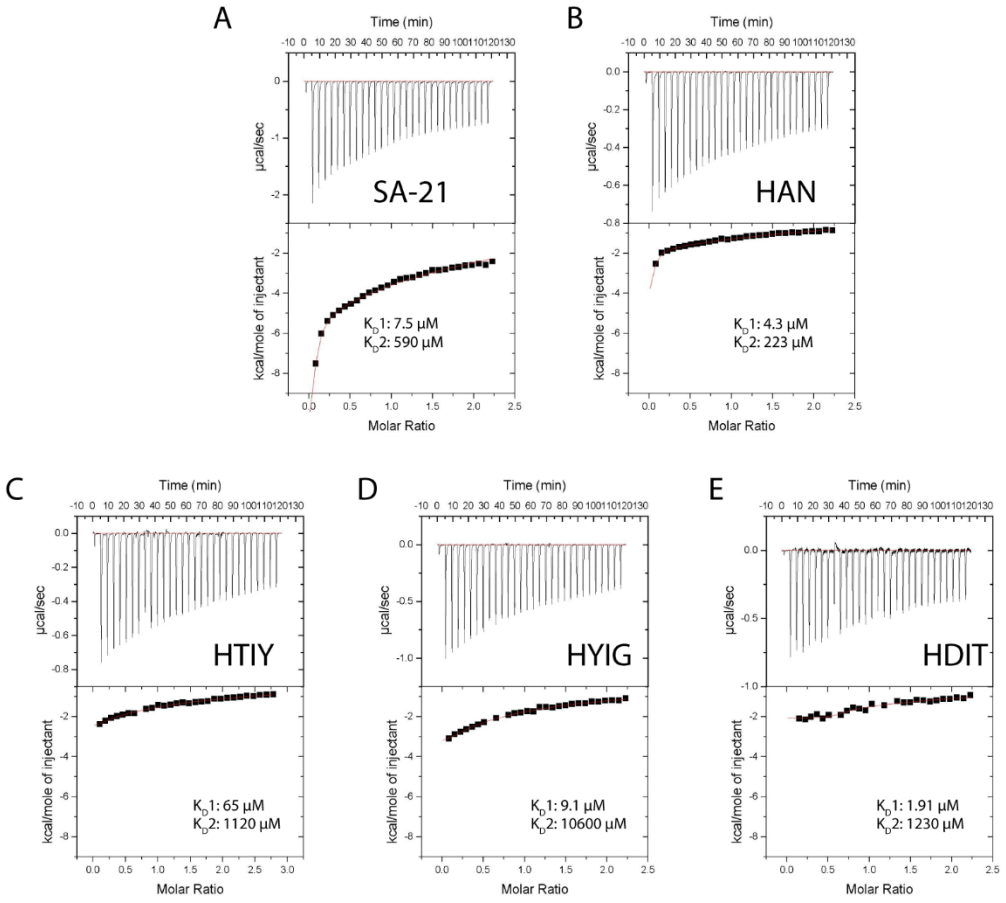

Appendix B-Figure 4. The first round of equilibrium dissociation constants of the selected peptides on HSA determined by ITC. The ITC traces and binding isotherms for peptides (A) SA-21 (4 mM), HSA (0.4 mM), (B) **DFS**-STCHANCGGKKK (4 mM), and HSA (0.4 mM), (C) **DFS**-STCHTIYCGGKKK (4 mM), HSA (0.4 mM), (D) **DFS**-STCHYIGCGGKKK (4mM), HSA (0.4 mM) and **DFS**-STCHDITCGGKKK (4 mM), HSA (0.4 mM) in 1×PBS.

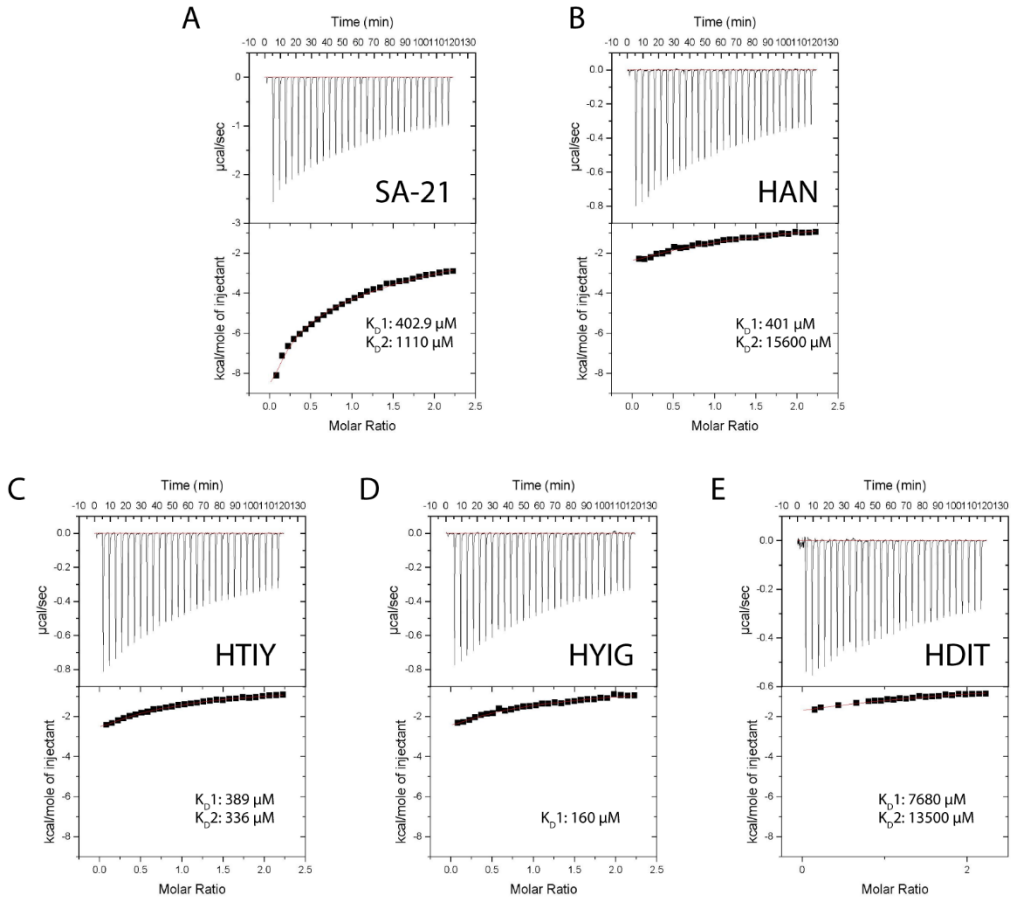

Appendix B-Figure 5. Second round of equilibrium dissociation constants of the selected peptides on HSA determined by ITC. The ITC traces and binding isotherms for peptides (A) SA-21 (1 mM), HSA (0.1 mM), (B) **DFS**-STCHANCGGKKK (1 mM), and HSA (0.1 mM), (C) **DFS**-STCHTIYCGGKKK (1 mM), HSA (0.1 mM), (D) **DFS**-STCHYIGCGGKKK (1mM), HSA (0.1 mM) and **DFS**-STCHDITCGGKKK (1mM), HSA (0.1 mM) in 1×PBS.

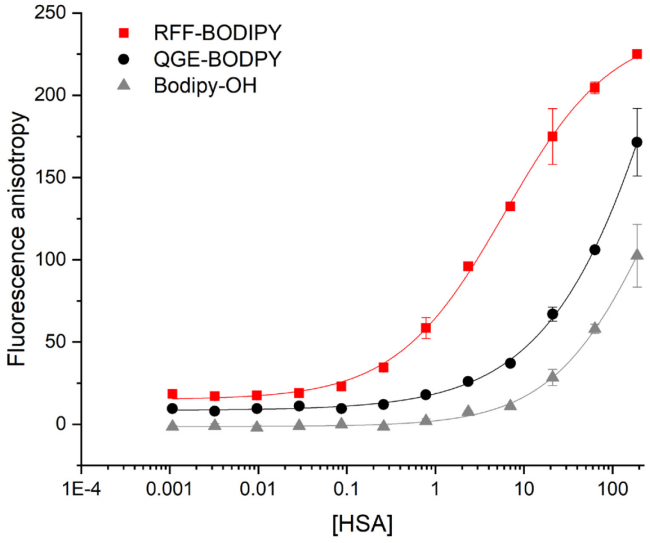

Appendix B-Figure 6. FP assay for BODIPY labeled **5d** titrated against **HSA 5d** found to have 6 μM binding affinity, **8d** (Black) found to have >82 μM and BODIPY-OH (grey) found to have >320 μM binding affinity.

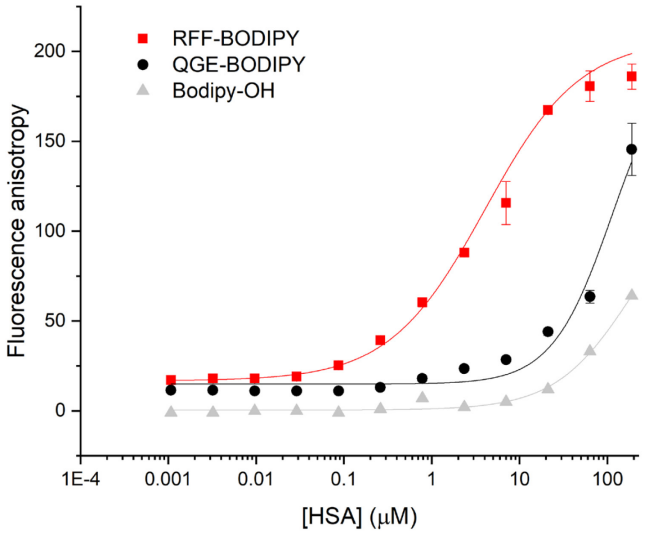

Appendix B-Figure 7. FP assay for BODIPY labeled **5d** (red) titrated against fatty acid free HAS. **5d** found to have 4 μM binding affinity, **8d** (Black) found to have >112 μM and BODIPY-OH (grey) found to have >196 μM binding affinity.

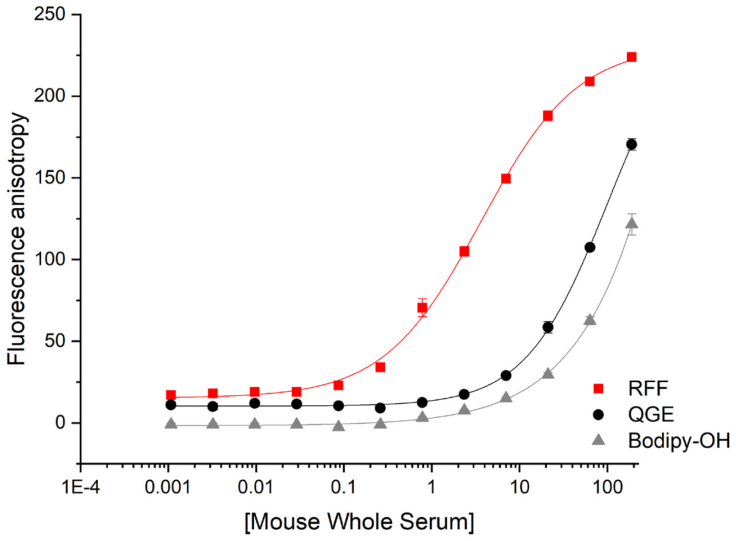

Appendix B-Figure 8. FP assay for Bodipy labeled RFF-**PFS**(red) titrated against whole mouse serum found to have 4 µM binding affinity, QGE-PGS(Black) found to have >100 µM and Bodipy -OH (grey) found to have >80 µM binding affinity.

Appendix B-2: MATLAB script for DE analysis

```
clear;

Dir='';
File = 'YW_unfiltered_20170829_ed.txt';


SET{1}  = 1:3;        % HSA
SET^365 = 4:9;        % T4-GP1
SET{3}  = 10:12;      % ConA
SET{4}  = 13:15;      % Input


TEST_SET = 1;
TARGET = 'HSA';
CONTROL_SETS = [2 3 4];

REREAD=1;   % change to zero if you don't want to wait for -re-reading of data

close all

OUTPUT='normalized';   % other output_type: 'normalized' 'normalized+1' 'raw'

if REREAD
    disp('reading...');
    [Nuc, AA, Fr] = readMulticolumn('Dir', Dir, 'File', File, ...
                                    'column', 1:max(cell2mat(SET)),...
                                    'skip', 2, 'output', OUTPUT);
end
%%% To plot Figure S1D chage the variables above to the variables below
% TEST_SET = 9;
% CONTROL_SETS = [10 11];

HITS2DISPLAY = 50; % maximum numer of hits to display
SHOWaminoACIDS = [18 19 20 21 22 23 24 25 26 27];

CLUSTERbyH = 1;          % 1 if you want your hits to be clustered by Hamming dist.
PLOT_VOLCANO = 1;       % set to 1 if you want to see the actual volcano plot
Sort_CXC_file = 1;       % set to 1 if you want to sort the reslt into different
CXC files
AA_AXA_Analysis = 1;    % set to 1 if you want to see the actual AA_AXA_Analysis

%%%%%%% volcano plot parameters here %%%%%%%%%%%%%%%%%%%%%%%%%%%%%%%%%%%%%%%%
p_cutoff = 0.05;             % p-value cutoff
R_cutoff = 3;               % ratio cutoff
MaxX=6;                     % maximum on the X-scale (if plotting volcano)
vert_cutoff = 0.00001;      % maximum on the Y-scale (if plotting volcano)
%%%%%%%%%%%%%%%%%%%%%%%%%%%%%%%%%%%%%%%%%%%%%%%%%%%%%%%%%%%%%%%%%%%%%%%%%%%



%%%%%%%%%%%%%%%%%%%%%%% do not change things beyond this point %%%%%%%%%%%%%%
%%%%%%%%%%%%%%%%%%%%%%% unless you know what you are doing %%%%%%%%%%%%%%%%%

if CLUSTERbyH == 1
    disp('Culster on')
else
    disp('Culster off')
end

if PLOT_VOLCANO == 1
    disp('Volcano Plot on')
else
    disp('Volcano plot off')
end
```

```
if Sort_CXC_file == 1
    disp('Sort CXC on')
else
    disp('Sort CXC off')
end


if AA_AXA_Analysis == 1
    disp('AA AXA Analysis on')
else
    disp('AA AXA Analysis off')
end

SAVEto = [File(1:end-4) TARGET '_'...
                        OUTPUT...
                        'CONTR_' num2str(CONTROL_SETS) '_'...
                        '_P' num2str(p_cutoff)...
                        '_R' num2str(R_cutoff)...
                        '.CSV'];  % keep blank if don't want to save


% select only the aminoacids you want to see
cAA = char(AA);
sAA=cellstr(cAA(:,SHOWaminoACIDS));
SQUARE=zeros(size(Fr,1),1);


i=0;
disp('calculating p and R...');
IX=zeros(size(Fr,1),numel(CONTROL_SETS));


disp('calculating p and R...');
i=0;
for j=CONTROL_SETS
    i=i+1;
    ratio(:,i) = mean(Fr(:,SET{TEST_SET}), 2) ./ mean(Fr(:,SET{j}), 2);


    [~,confi(:,i)] = ttest2(Fr(:,SET{TEST_SET})',Fr(:,SET{j})',....
                            p_cutoff,'both','unequal');

    IX(:,i) = (confi(:,i) <= p_cutoff) & (ratio(:,i) >= R_cutoff);

    SQUARE = SQUARE + ratio(:,i).^2;


    if PLOT_VOLCANO
        subplot(1,numel(CONTROL_SETS),i);

        plot(log2 (ratio(:,i)),...
            -log10(confi(:,i)),'d',...
            'MarkerSize',4,...
            'MarkerFaceColor',0.5*[1 1 1],...
            'MarkerEdgeColor',0.5*[1 1 1]); hold on;

        plot( log2 (ratio(find(IX(:,i)),i)),...
             -log10(confi(find(IX(:,i)),i)),'d',...
                    'MarkerSize',4,...
                    'MarkerFaceColor','r',...
                    'MarkerEdgeColor','r'); hold on;

        line([log2(R_cutoff) MaxX],[-log10(p_cutoff) -log10(p_cutoff)]);
        line([log2(R_cutoff)   log2(R_cutoff)],...
             [-log10(p_cutoff) -log10(vert_cutoff)]);

        xlim([-MaxX MaxX]);
```

```
    end
end

    R2 = sqrt(SQUARE);

    IXall = find( (sum(IX,2)==size(IX,2)) ); % hits that satisfy all criteria


   % you can loosen the stringency if necessary
   % IXall = find( (sum(IX,2)>=2) ); %hits that satisfy two or more criteria


    hits    = char(sAA(IXall,:));
    Rhits   = ratio(IXall,:);
    R2hits  = R2(IXall);

%%%%%%%%%%%% this is part where hits are clustered by H-dist %%%%%%%%%%%%%%%

if CLUSTERbyH
    disp('clustering...');
    if numel(hits)>3
        figure(2)
        Y = pdist(hits,'hamming');
        Z = linkage(Y,'complete');
        [H,T,perm] = dendrogram(Z,0,'colorthreshold',20);
        set(H,'LineWidth',2)

        for i =1:size(hits,1)
            label{i} = i;
        end
        set(gca,'XTick', 1:1:size(hits,1), 'XTickLabel',label);

        hits    = hits(perm,:);
        Rhits   = Rhits(perm,:);
        R2hits  = R2(perm);
        IXall   = IXall(perm);
    end
end

%%%%%%%%%%%%%%%%%%%display all results as heat map%%%%%%%%%%%%%%%%%%%%%%%%%

figure(3)

if size(IXall,1)>=HITS2DISPLAY
    N=HITS2DISPLAY;  % display only the first or defined number of hits
else
    N=size(IXall,1); %display all
end

FrPPM = round(10^6*Fr);   % convert normalized fraction frequency to PPM

imagesc( log10([FrPPM(IXall(1:N),:) ratio(IXall(1:N),:) ]+1) );

set(gca,'YTick', 1:1:N, 'YTickLabel',cellstr(hits(1:N,:)),'TickDir','out',...
    'FontName','Courier New','FontSize',14);
set(gca,'XTick', 1:1:size(Fr,2)+4, 'TickDir','out');
jet1=jet;
jet1(1,:)=[0.4 0.4 0.4];
colormap(jet1);
colorbar;

% generate a plain text table for saving or copy from command line
S = char(32*ones(size(hits,1),2));
COM = char(','*ones(size(hits,1),1));

L = [ S(:,1) char(124*ones(size(hits,1),1)) S(:,1)];
if strcmp(OUTPUT,'raw')
    F  = Fr(IXall,:);   % display frequency raw
```

```
else
    F  = FrPPM(IXall,:);    % display frequency in ppm
end

toDisp = [hits     S  ];
toSave = [hits     COM  ];


for i=1:numel(SET)
    for j=1:numel(SET{i})
        toDisp = [toDisp num2str(F(:,SET{i}(j))) S];
        toSave = [toSave num2str(F(:,SET{i}(j))) COM];
    end
    toDisp = [toDisp L];
end
toDisp = [toDisp S  num2str(round(Rhits)) L];
for i=1:size(Rhits,2)
    toSave = [toSave  num2str(round(Rhits(:,i))) COM ];
end

disp(toSave);
disp(toDisp);

if ~isempty(SAVEto)

    fs = fopen(fullfile(Dir,SAVEto),'w');
    RET = char(10*ones(size(toSave,1),1));
    fprintf( fs, '%s\r\n', [toSave(:,1:end-1) RET]');
    fclose all;
    disp('file saved');
end

%%%%%%%%%%%%%%%%%%%%%%%%%%%%%%%%C3C Sorting%%%%%%%%%%%%%%%%%%%%%%%%%%%%%%%%

if Sort_CXC_file

    disp('sorting...') ;


    %Sorting conditions
    C2X = ['S' '\w' 'C' '\w' '\w' 'C' '\w' '\w' '\w'] ;
    C3X = ['S' '\w' 'C' '\w' '\w' '\w' 'C' '\w' '\w' '\w'] ;
    C4X = ['S' '\w' 'C' '\w' '\w' '\w' '\w' 'C' '\w' '\w'] ;
    C5X = ['S' '\w' 'C' '\w' '\w' '\w' '\w' '\w' 'C' '\w'] ;
    C7X = ['A' 'C' '\w' '\w' '\w' '\w' '\w' '\w' '\w' 'C'] ;
    % Creat sorting array
    C2XHits = [];
    C3XHits = [];
    C4XHits = [];
    C5XHits = [];
    C7XHits = [];
    indexs=[];              %for data puposes not really useful for now
    j=0;

    % sort C2C
    disp('Sorting C2C...')
    C2s = regexp(cellstr(hits),C2X);
    for i=1:numel(C2s)
        if ~isempty(C2s{i})
            j=j+1;
            C2XHits = [C2XHits; hits(i,:)];
            indexs(j) = i;
        end
    end
    %C2Cfound(s) = numel(indexs);


    %Sort C3C
```

```
    disp('Sorting C3C...')
    indexs=[];
    j=0;
    C3s = regexp(cellstr(hits),C3X);
    for i=1:numel(C3s)
        if ~isempty(C3s{i})
            j=j+1;
            C3XHits = [C3XHits; hits(i,:)];
            indexs(j) = i;
        end
    end
    %C3Cfound(s) = numel(indexs);

    %Sort C4C
    disp('Sorting C4C...')
    indexs=[];
    j=0;
    C4s = regexp(cellstr(hits),C4X);
    for i=1:numel(C4s)
        if ~isempty(C4s{i})
            j=j+1;
            C4XHits = [C4XHits; hits(i,:)];
            indexs(j) = i;
        end
    end
    %C4Cfound(s) = numel(indexs);

    %Sort C5C
    disp('Sorting C5C...')
    indexs=[];
    j=0;
    C5s = regexp(cellstr(hits),C5X);
    for i=1:numel(C5s)
        if ~isempty(C5s{i})
            j=j+1;
            C5XHits = [C5XHits; hits(i,:)];
            indexs(j) = i;
        end
    end
    %C5Cfound(s) = numel(indexs);

    % Sort C7C
    disp('Sorting C7C...')
    indexs=[];
    j=0;
    C7s = regexp(cellstr(hits),C7X);
    for i=1:numel(C7s)
        if ~isempty(C7s{i})
            j=j+1;
            C7XHits = [C7XHits; hits(i,:)];
            indexs(j) = i;
        end
    end
    %C7Cfound(s) = numel(indexs);

end
if ~isempty(C2XHits)
    C2 = fopen(fullfile(Dir,['C2C',SAVEto]),'w');
    RET = char(10*ones(size(C2XHits,1),1));
    fprintf(C2, '%s\r\n',[C2XHits(:,1:end-1) RET]');
    fclose all;
    disp('C2C saved');
end

if ~isempty(C3XHits)
    C3 = fopen(fullfile(Dir,['C3C',SAVEto]),'w');
    RET = char(10*ones(size(C3XHits,1),1));
    fprintf(C2, '%s\r\n',[C3XHits(:,1:end-1) RET]');
```

```
    fclose all;
    disp('C3C saved');
end

if ~isempty(C4XHits)
    C4 = fopen(fullfile(Dir,['C4C',SAVEto]),'w');
    RET = char(10*ones(size(C4XHits,1),1));
    fprintf(C2, '%s\r\n',[C4XHits(:,1:end-1) RET]');
    fclose all;
    disp('C4C saved');
end

if ~isempty(C5XHits)
    C5 = fopen(fullfile(Dir,['C5C',SAVEto]),'w');
    RET = char(10*ones(size(C5XHits,1),1));
    fprintf(C2, '%s\r\n',[C5XHits(:,1:end-1) RET]');
    fclose all;
    disp('C5C saved');
end

if ~isempty(C7XHits)
    C7 = fopen(fullfile(Dir,['C7C',SAVEto]),'w');
    RET = char(10*ones(size(C7XHits,1),1));
    fprintf(C2, '%s\r\n',[C7XHits(:,1:end-1) RET]');
    fclose all;
    disp('C7C saved');

end


%%%%%%%%%%%%%%%%%AA & AxA analysis%%%%%%%%%%%%%%%%%%%%%%%%%%%%%%%%%%%%%%%%%%%%%%%%%

if AA_AXA_Analysis
    disp('Start AA AXA Analysis...')
    figure(100);
    AAA = 'ADEFHIKLMNPQRSTVWY';
    Y = [];

    for i=1:numel(AAA)
        Y(i) = numel(find(hits==AAA(i)));
        xlabel{i} = AAA(i);
    end

    plot(1:numel(AAA), Y, 'ok');
    set(gca, 'xTick', 1:numel(AAA), 'xTickLabel', xlabel, 'TickDir','out');


    %%

    Nfound =  [];
    NfoundS = [];
    toSaveIX = [];
    toSaveIXS = [];



    M = 9;

    fs = fopen(fullfile(Dir,['AA' SAVEto]),'w');
    fsS = fopen(fullfile(Dir,['AxA' SAVEto]),'w');
    fclose all;

    fs = fopen(fullfile(Dir,['AA' SAVEto]),'a+');
    fsS = fopen(fullfile(Dir,['AxA' SAVEto]),'a+');


    for ii = 1:numel(AAA)
        %disp(num2str(ii));
```

```
for jj= 1:numel(AAA)


    phrase = [ AAA(ii) AAA(jj) ] ;
    phraseS = [ AAA(ii) '\w' AAA(jj) ] ;

    phraseHits = [];
    spacedHits = [];
    index=[];
    j=0;


    IX = regexp(cellstr(hits),phrase);
    for i=1:numel(IX)
        if ~isempty(IX{i})
            %check whether his is S**** or A****; if it is, discard
            if (phrase(1) =='S' || phrase(1) =='A')
                if (numel(IX{i})==1 && IX{i}==1)
                    continue
                end
            end

            j=j+1;
            phraseHits = [phraseHits; hits(i,:)];
            index(j) = i;

            S1 = char (32*ones(1, M-IX{i}(1)));
            S2 = char (32*ones(1, IX{i}(1)  ));
            spacedHits = [spacedHits; S1 hits(i,:) S2];
        end
    end
    Nfound(ii,jj) = numel(index);

    % lets save this with offsets
    RET = char(10*ones(size(index,2),1));
    fprintf( fs, '%s\r\n', [spacedHits toSave(index,:) RET]');

    phraseHits = [];
    index=[];
    spacedHits = [];
    j=0;
    clear IX

    IX = regexp(cellstr(hits),phraseS);
    for i=1:numel(IX)
        if ~isempty(IX{i})
            %check whether his is S**** or A****; if it is, discard
            if (phraseS(1) =='S' || phraseS(1) =='A')
                if (numel(IX{i})==1 && IX{i}==1)
                    continue
                end
            end

            j=j+1;
            phraseHits = [phraseHits; hits(i,:)];
            index(j) = i;

            S1 = char (32*ones(1, M-IX{i}(1)));
            S2 = char (32*ones(1, IX{i}(1)  ));
            spacedHits = [spacedHits; S1 hits(i,:) S2];
        end
    end
    NfoundS(ii,jj) = numel(index);
    toSaveIXS = [toSaveIXS index];

    % lets save this with offsets
    RET = char(10*ones(size(index,2),1));
    fprintf( fsS, '%s\r\n', [spacedHits toSave(index,:) RET]');
```

```
        end
    end

    figure(200);
    subplot(1,2,1);
    imagesc(Nfound); colorbar;
    set(gca, 'xTick', 1:numel(AAA), 'xTickLabel', xlabel, 'TickDir','out',...
        'yTick', 1:numel(AAA), 'yTickLabel', xlabel);

    subplot(1,2,2);
    imagesc(NfoundS); colorbar;
    set(gca, 'xTick', 1:numel(AAA), 'xTickLabel', xlabel, 'TickDir','out',...
        'yTick', 1:numel(AAA), 'yTickLabel', xlabel);


    fclose all;
    fs = fopen(fullfile(Dir,['AA' SAVEto]),'w');
    fsS = fopen(fullfile(Dir,['AxA' SAVEto]),'w');
    RET = char(10*ones(size(toSaveIX,2),1));
    fprintf( fs, '%s\r\n', [toSave(toSaveIX,:) RET]');
    disp('AA Saved')

    RET = char(10*ones(size(toSaveIXS,2),1));
    fprintf( fsS, '%s\r\n', [toSave(toSaveIXS,:) RET]');
    disp('AxA Saved')
end
```

Appendix B-3: Summary of synthesis
STCHDITCGGKKK-DFS

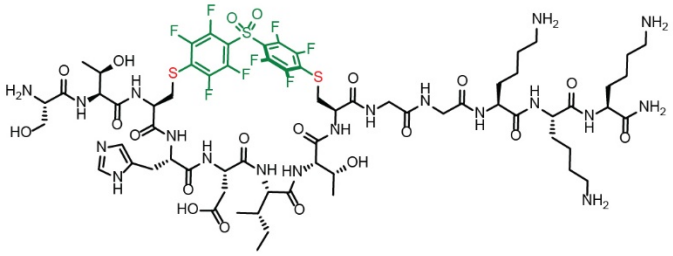

Chemical Formula: $C_{67}H_{95}F_8N_{19}O_{20}S_3$
Exact Mass: 1733.60
Molecular Weight: 1734.78

Starting material mass: 8.8 mg
Final product mass: 0.5 mg

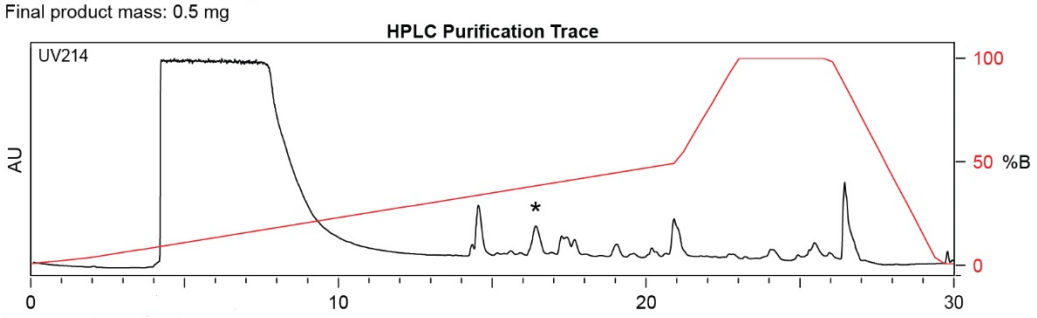

Time (min)	Solvent B (%)
0	2
5	30
24	95
25	100
27	100
28	2
30	2

Flow Rate: 13 mL / min
Phenomenex Kinetex EVO C18 Prep Column
(100 Å, 5 µm, 21.5 mm X 250 mm)

Slovent A: H_2O + 0.1% (v/v) TFA
Slovent B: MeCN + 0.1% (v/v) TFA

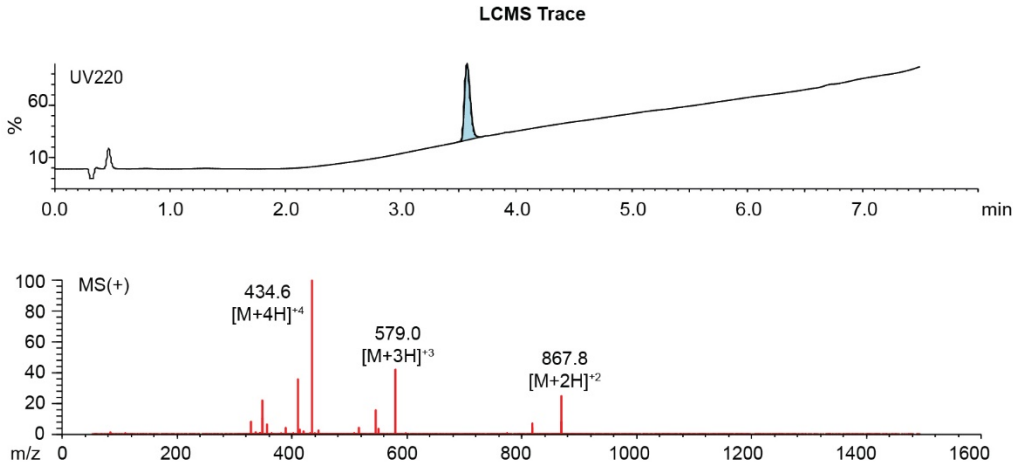

Appendix B-Figure 9. Synthesis summary of **1b**

STCHDITCGGKKK-PFS

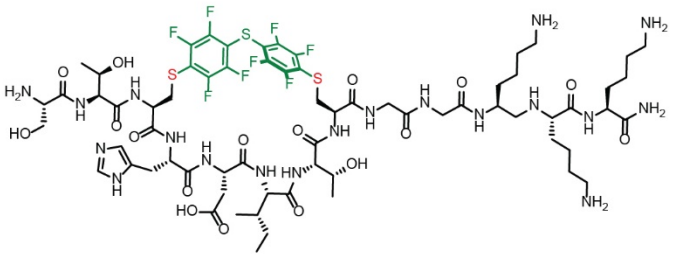

Chemical Formula: $C_{67}H_{97}F_8N_{19}O_{17}S_3$
Exact Mass: 1687.63
Molecular Weight: 1688.80

Starting material mass: 9.2 mg
Final product mass: 3.3 mg

HPLC Purification Trace

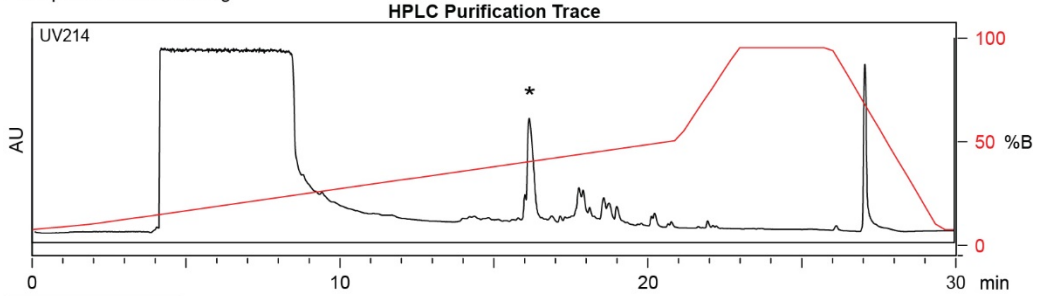

Time (min)	Solvent B (%)
0	2
2	5
21	50
23	100
26	100
29.5	2
30	2

Flow Rate: 13 mL / min
Phenomenex Kinetex EVO C18 Prep Column
(100 Å, 5 µm, 21.5 mm X 250 mm)

Solvent A: H_2O + 0.1% (v/v) TFA
Solvent B: MeCN + 0.1% (v/v) TFA

LCMS Trace

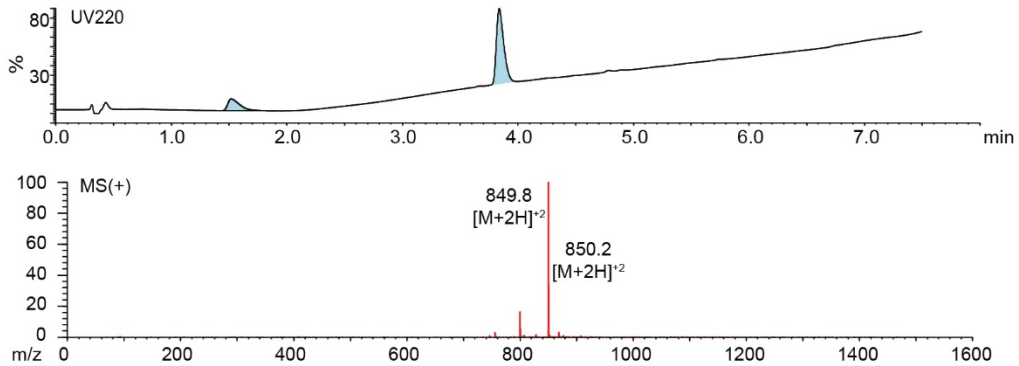

Appendix B-Figure 10. Synthesis summary of **1c.**

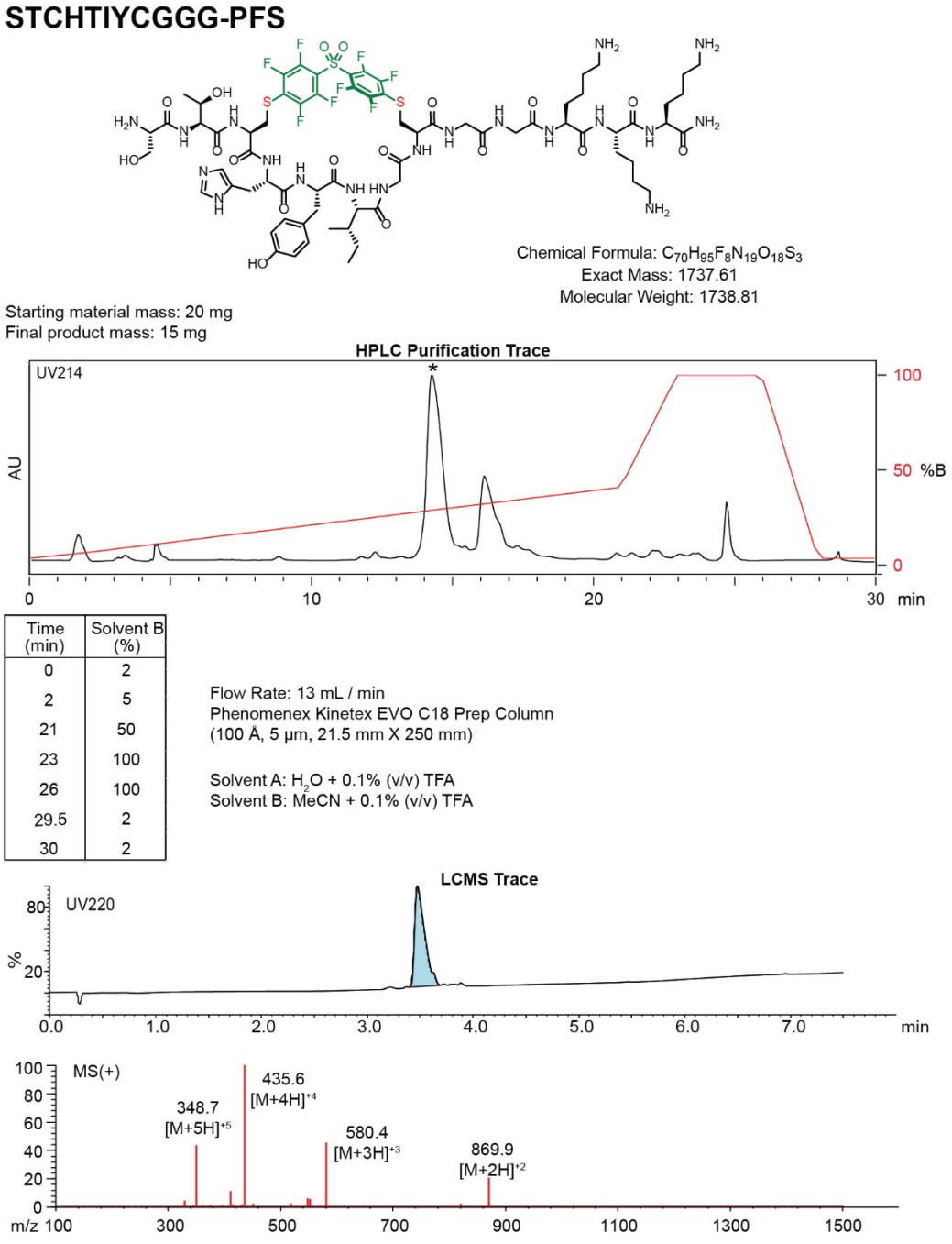

Appendix B-Figure 11. Synthesis summary of **2b**.

STCHYIGCGGKKK-PFS

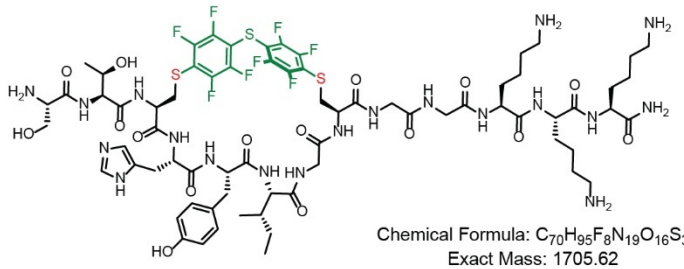

Chemical Formula: $C_{70}H_{95}F_8N_{19}O_{16}S_3$
Exact Mass: 1705.62
Molecular Weight: 1706.81

Starting material mass: 10 mg
Final product mass: 3.4 mg

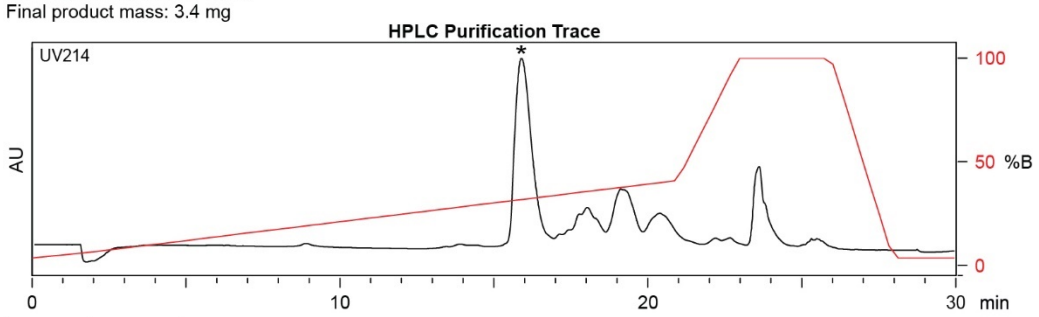

Time (min)	Solvent B (%)
0	2
2	5
21	50
23	100
26	100
29.5	2
30	2

Flow Rate: 13 mL / min
Phenomenex Kinetex EVO C18 Prep Column
(100 Å, 5 µm, 21.5 mm X 250 mm)

Solvent A: H_2O + 0.1% (v/v) TFA
Solvent B: MeCN + 0.1% (v/v) TFA

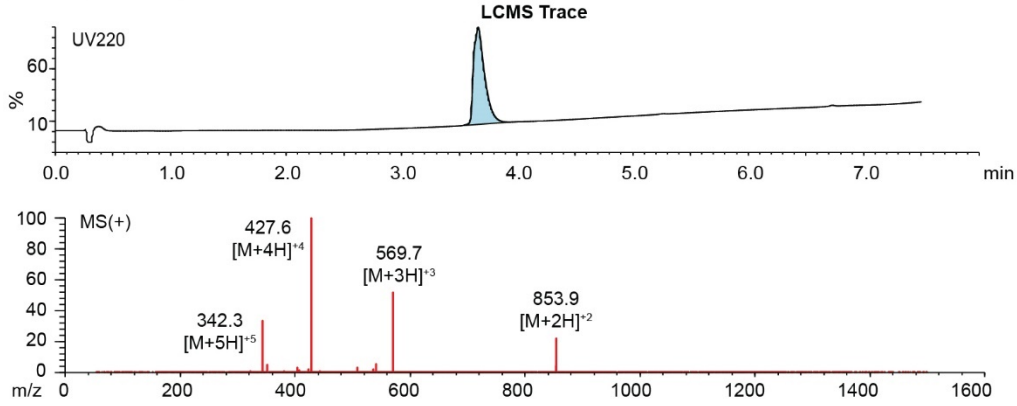

Appendix B-Figure 12. Synthesis summary of **2c**.

STCHANCGGKKK-DFS

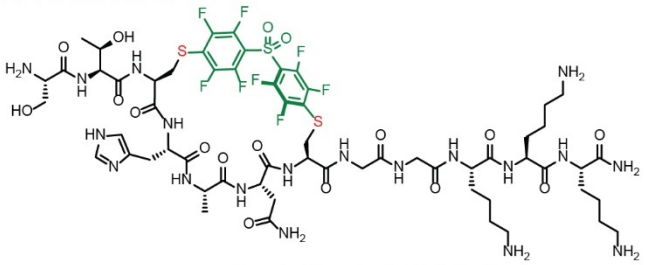

Chemical Formula: $C_{60}H_{83}F_8N_{19}O_{17}S_3$
Exact Mass: 1589.52
Molecular Weight: 1590.61

Starting material mass: 10.5 mg
Final product mass: 3.3 mg

HPLC Purification Trace

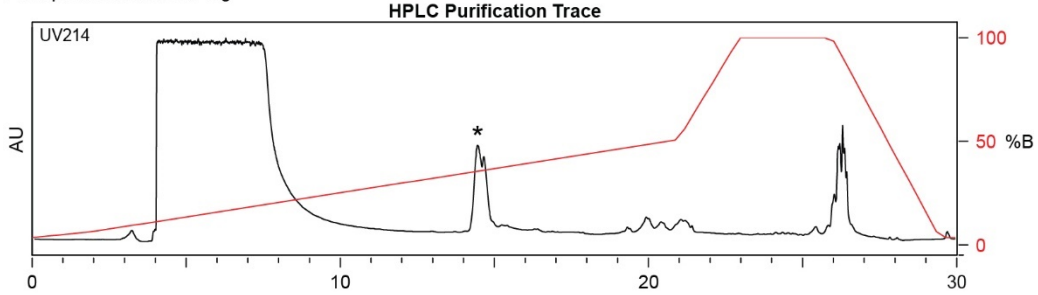

Time (min)	Solvent B (%)
0	2
2	5
21	50
23	100
26	100
29.5	2
30	2

Flow Rate: 13 mL / min
Phenomenex Kinetex EVO C18 Prep Column
(100 Å, 5 µm, 21.5 mm X 250 mm)

Slovent A: H_2O + 0.1% (v/v) TFA
Slovent B: MeCN + 0.1% (v/v) TFA

LCMS Trace

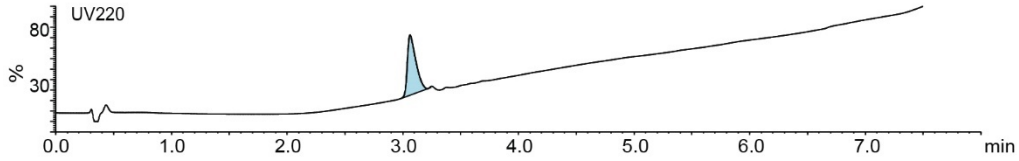

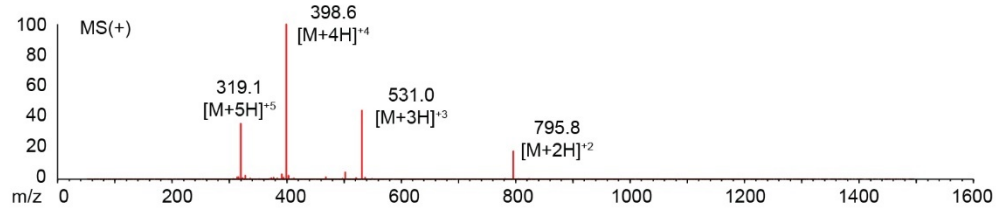

Appendix B-Figure 13. Synthesis summary of **3b**.

STCHANCGGKKK-PFS

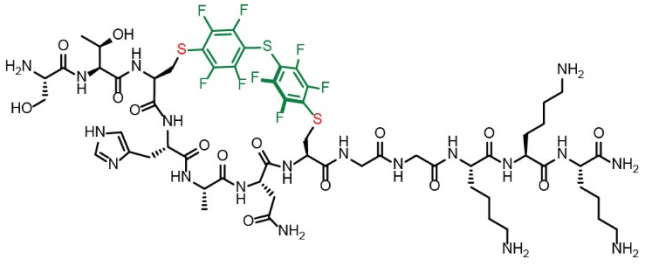

Chemical Formula: $C_{60}H_{83}F_8N_{19}O_{15}S_3$
Exact Mass: 1557.54
Molecular Weight: 1558.61

Starting material mass: 11.4 mg
Final product mass: 2.0 mg

HPLC Purification Trace

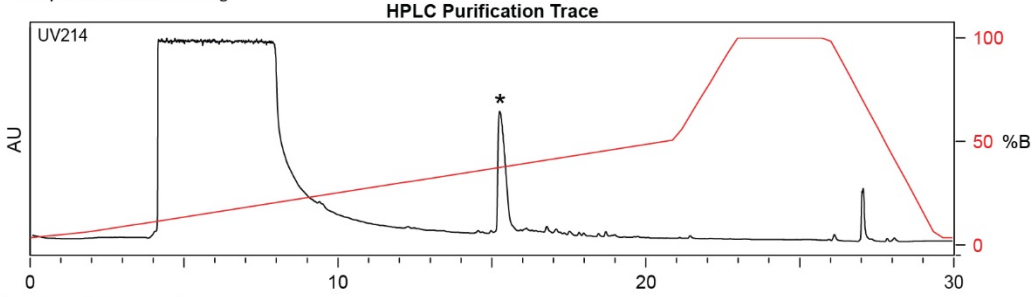

Time (min)	Solvent B (%)
0	2
2	5
21	50
23	100
26	100
29.5	2
30	2

Flow Rate: 13 mL / min
Phenomenex Kinetex EVO C18 Prep Column
(100 Å, 5 µm, 21.5 mm X 250 mm)

Solvent A: H_2O + 0.1% (v/v) TFA
Solvent B: MeCN + 0.1% (v/v) TFA

LCMS Trace

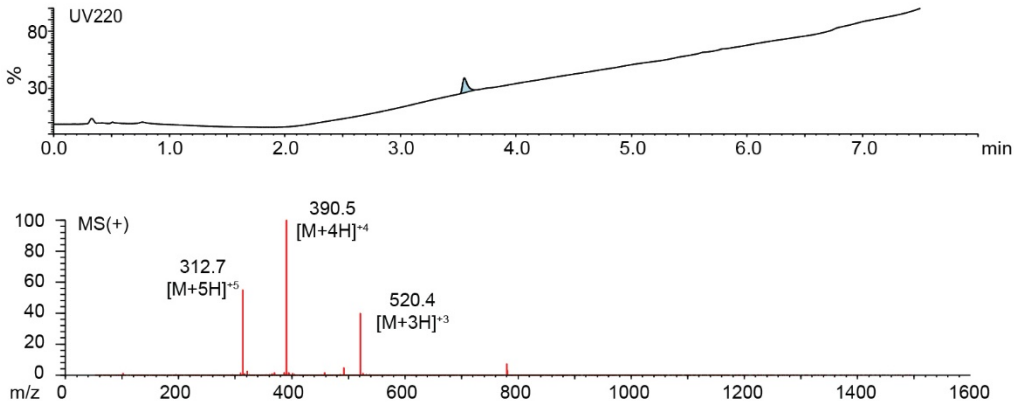

Appendix B-Figure 14. Synthesis summary of **3c**.

STCHANCGGG-PFS

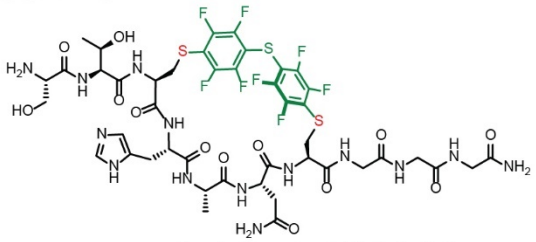

Chemical Formula: $C_{44}H_{50}F_8N_{14}O_{13}S_3$
Exact Mass: 1230.27
Molecular Weight: 1231.14

Starting material mass: 8.8mg
Final product mass: 3.3 mg

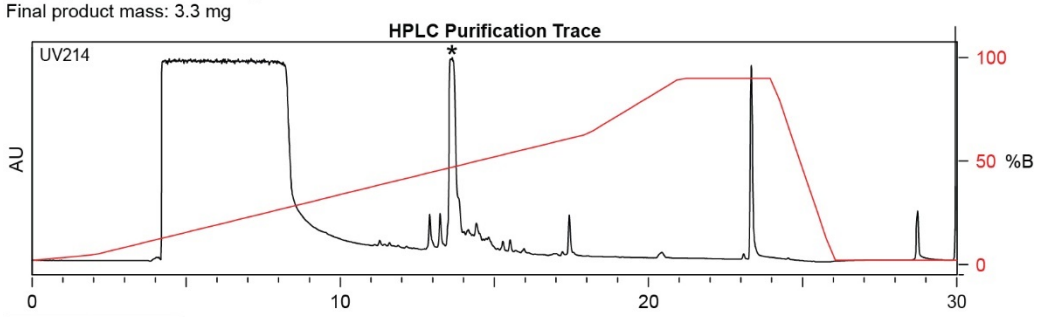

Time (min)	Solvent B (%)
0	2
2	5
18	70
21	100
24	100
26	2
30	2

Flow Rate: 13 mL / min
Phenomenex Kinetex EVO C18 Prep Column
(100 Å, 5 µm, 21.5 mm X 250 mm)

Solvent A: H_2O + 0.1% (v/v) TFA
Solvent B: MeCN + 0.1% (v/v) TFA

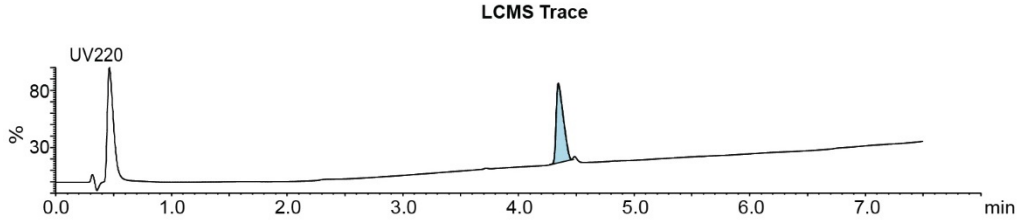

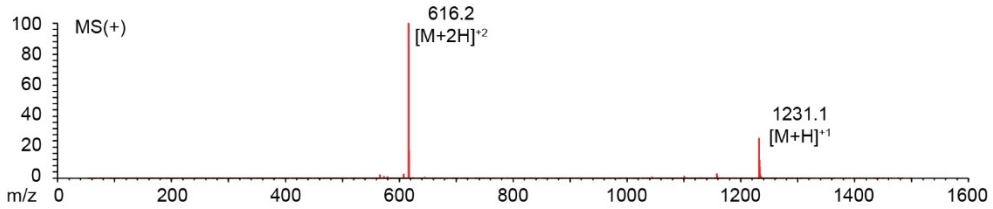

Appendix B-Figure 15. Synthesis summary of **3c**.

STCHTIYGGKKK-DFS

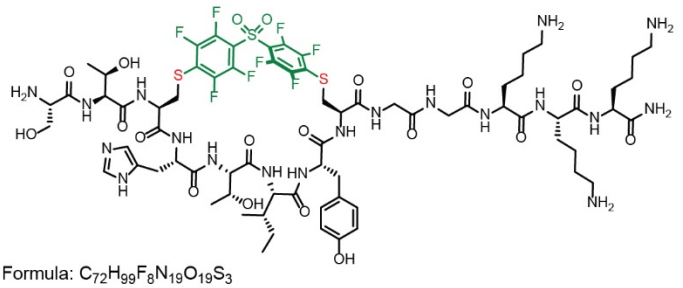

Chemical Formula: $C_{72}H_{99}F_8N_{19}O_{19}S_3$
Exact Mass: 1781.64
Molecular Weight: 1782.87

Starting material mass: 9.0 mg
Final product mass: 1.0 mg

HPLC Purification Trace

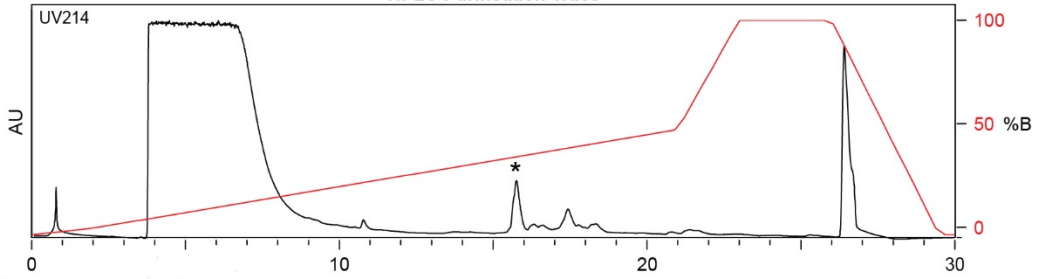

Time (min)	Solvent B (%)
0	2
2	5
21	50
25	100
27	100
28	2
30	2

Flow Rate: 13 mL / min
Phenomenex Kinetex EVO C18 Prep Column
(100 Å, 5 µm, 21.5 mm X 250 mm)

Slovent A: H_2O + 0.1% (v/v) TFA
Slovent B: MeCN + 0.1% (v/v) TFA

LCMS Trace

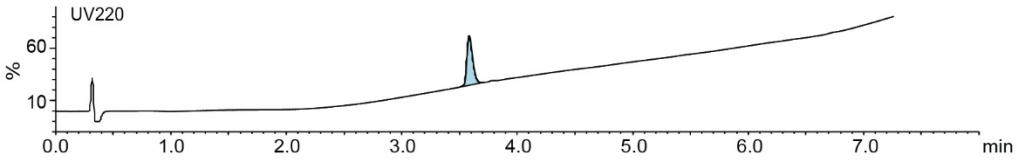

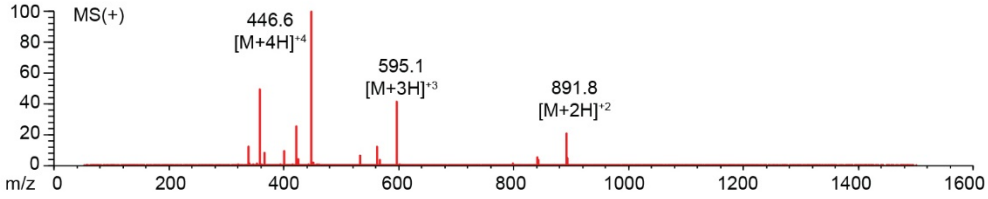

Appendix B-Figure 16. Synthesis summary of **4b**.

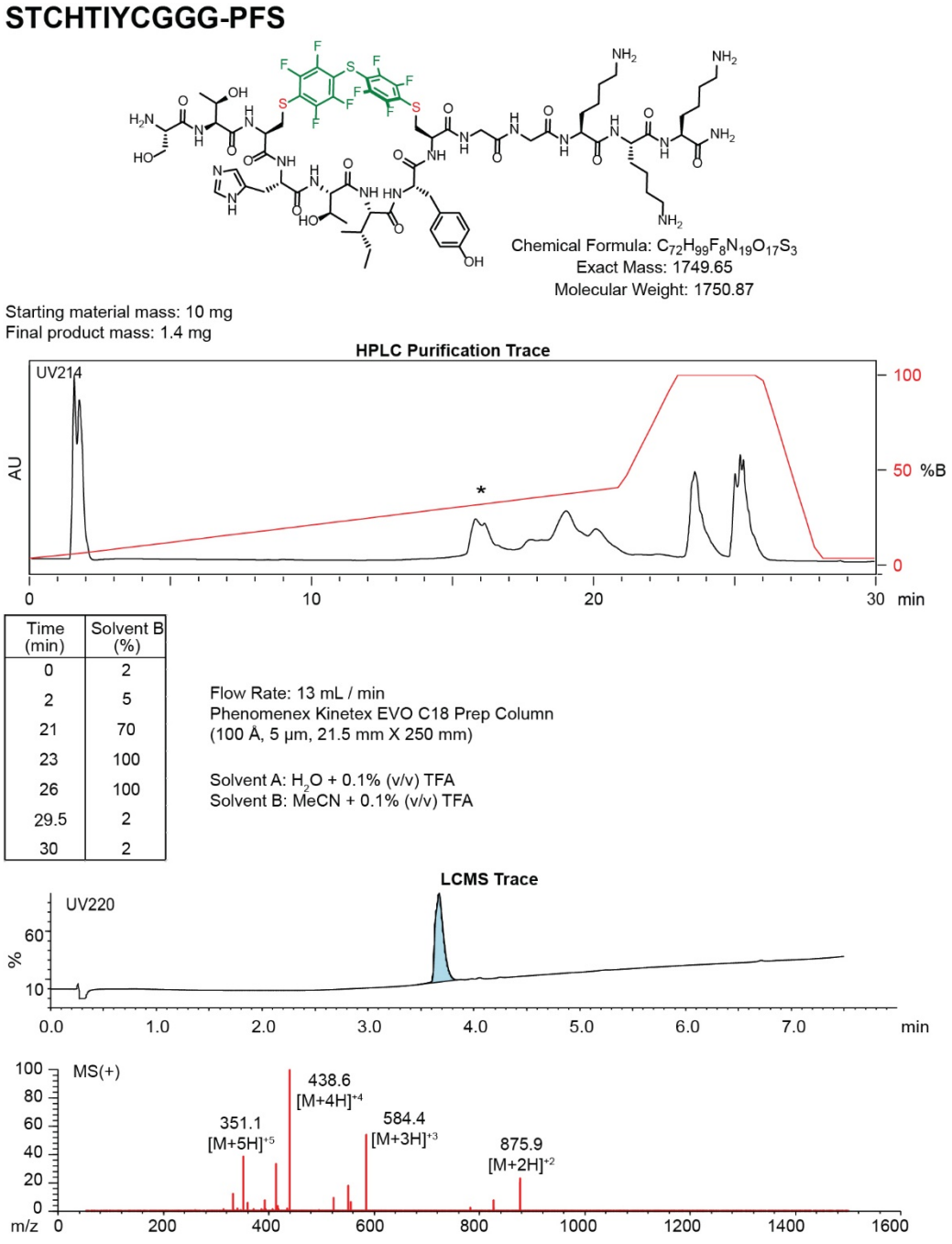

Appendix B-Figure 17. Synthesis summary of **4c**.

SICRFFCGGG-DFS

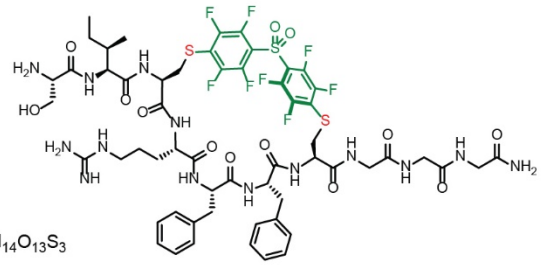

Chemical Formula: $C_{57}H_{66}F_8N_{14}O_{13}S_3$
Exact Mass: 1402.40
Molecular Weight: 1403.41

Starting material mass: 10 mg
Final product mass: 7.9 mg

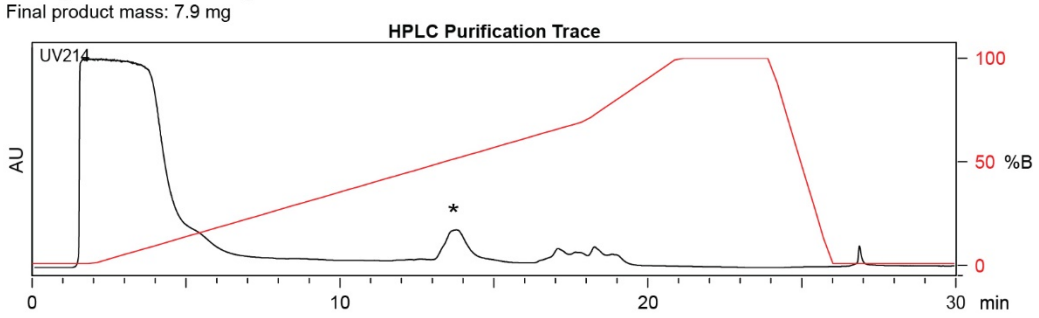

Time (min)	Solvent B (%)
0	2
2	5
21	50
23	100
26	100
29.5	2
30	2

Flow Rate: 13 mL / min
Phenomenex Kinetex EVO C18 Prep Column
(100 Å, 5 µm, 21.5 mm X 250 mm)

Solvent A: H_2O + 0.1% (v/v) TFA
Solvent B: MeCN + 0.1% (v/v) TFA

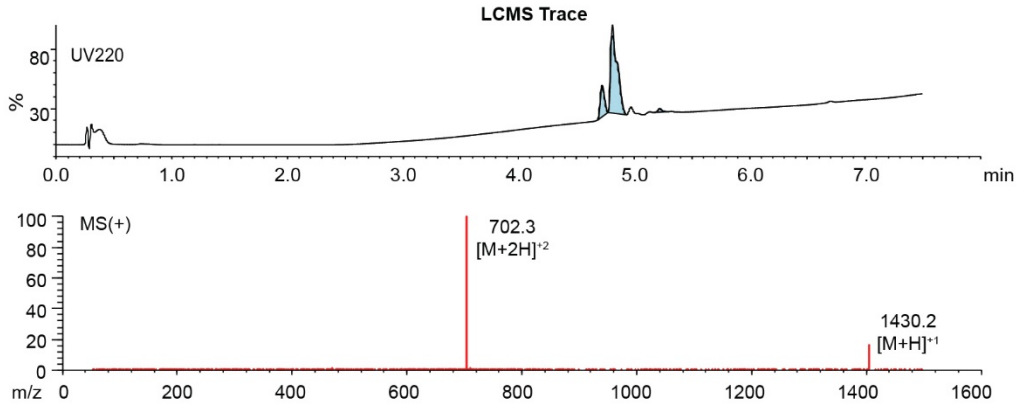

Appendix B-Figure 18. Synthesis summary of **5b**.

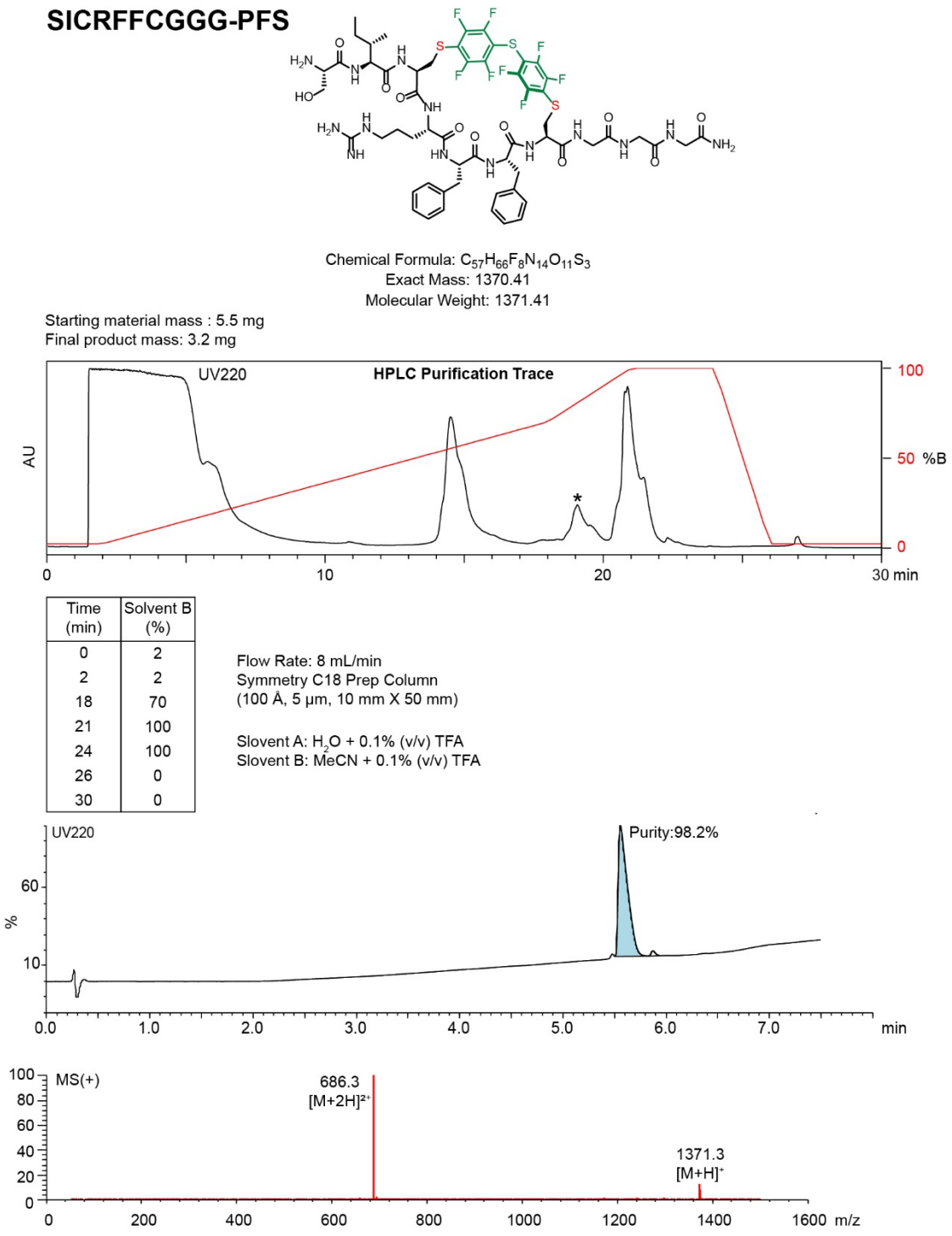

Appendix B-Figure 19. Synthesis summary of **5c**.

SFCPMFGGG-DFS

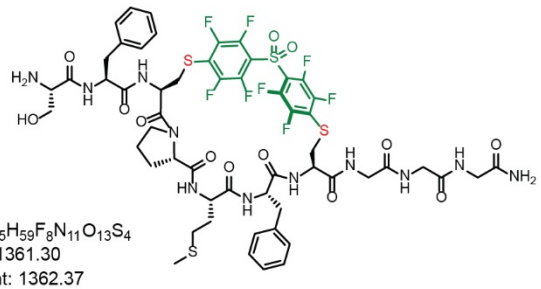

Chemical Formula: $C_{55}H_{59}F_8N_{11}O_{13}S_4$
Exact Mass: 1361.30
Molecular Weight: 1362.37

Starting material mass: 4.7 mg
Final product mass: 2.1 mg

HPLC Purification Trace

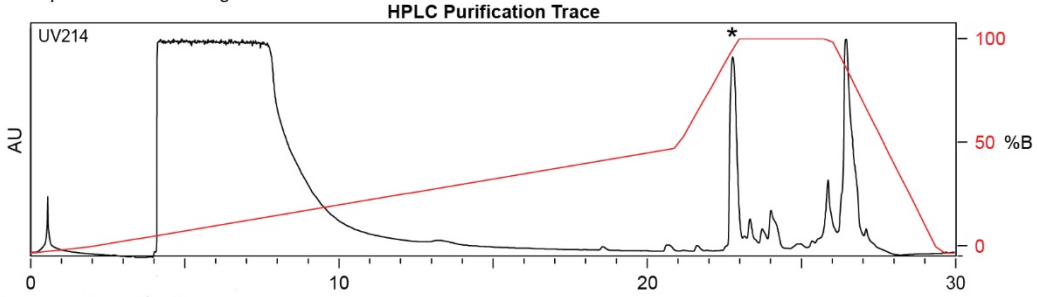

Time (min)	Solvent B (%)
0	2
2	5
21	50
25	100
27	100
28	2
30	2

Flow Rate: 13 mL / min
Phenomenex Kinetex EVO C18 Prep Column
(100 Å, 5 µm, 21.5 mm X 250 mm)

Slovent A: H_2O + 0.1% (v/v) TFA
Slovent B: MeCN + 0.1% (v/v) TFA

LCMS Trace

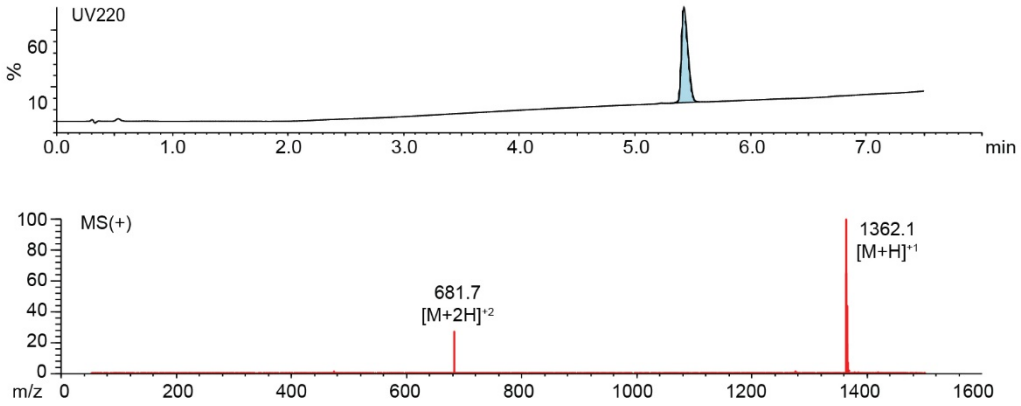

Appendix B-Figure 20. Synthesis summary of **6b**.

SFCPMFCGGG-PFS

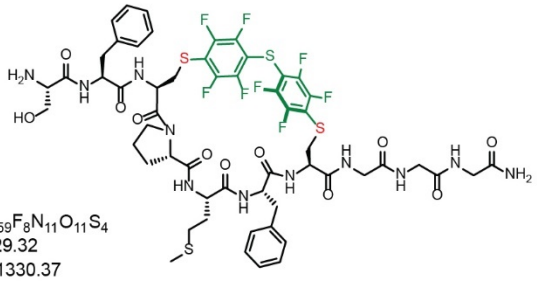

Chemical Formula: $C_{55}H_{59}F_8N_{11}O_{11}S_4$
Exact Mass: 1329.32
Molecular Weight: 1330.37

Starting material mass: 10 mg
Final product mass: 5.1 mg

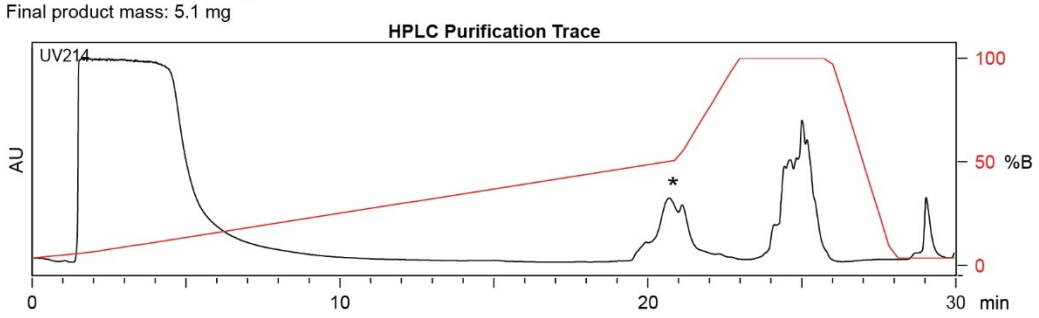

Time (min)	Solvent B (%)
0	2
2	5
21	50
23	100
26	100
29.5	2
30	2

Flow Rate: 13 mL / min
Phenomenex Kinetex EVO C18 Prep Column
(100 Å, 5 µm, 21.5 mm X 250 mm)

Solvent A: H_2O + 0.1% (v/v) TFA
Solvent B: MeCN + 0.1% (v/v) TFA

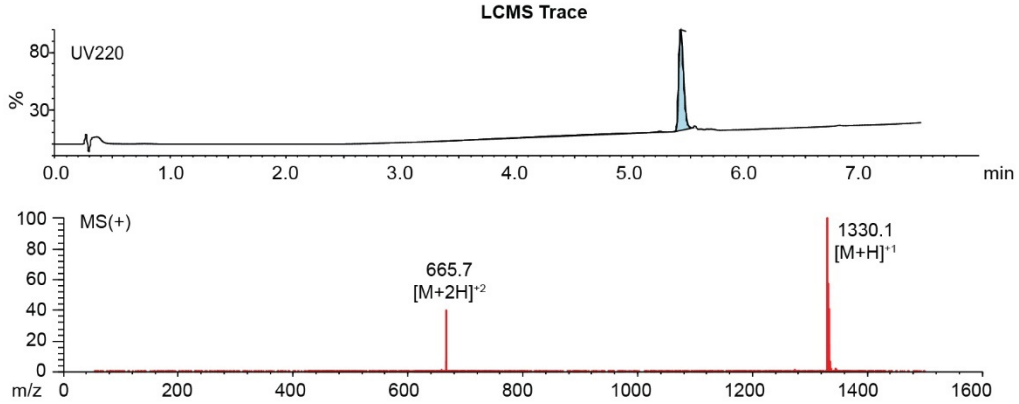

Appendix B-Figure 21. Synthesis summary of **6c**.

SLCKRECGGG-DFS

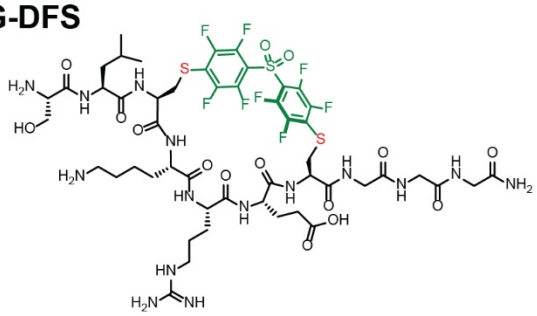

Chemical Formula: $C_{51}H_{68}F_8N_{14}O_{15}S_3$
Exact Mass: 1364.40
Molecular Weight: 1365.36

Starting material mass: 10.6 mg
Final product mass: 5.6 mg

HPLC Purification Trace

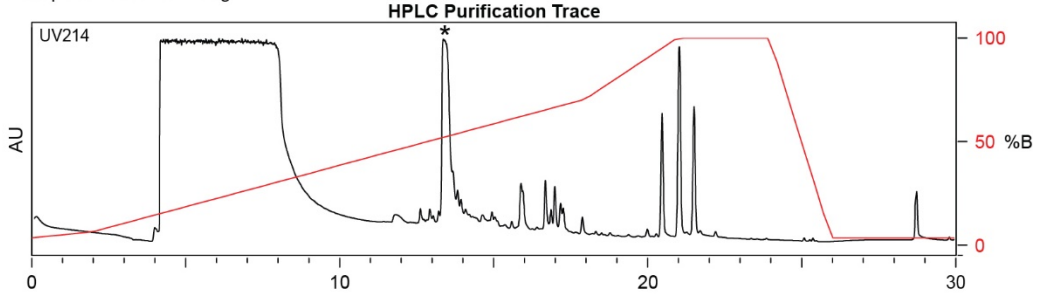

Time (min)	Solvent B (%)
0	2
2	5
18	70
21	100
24	100
26	2
30	2

Flow Rate: 13 mL / min
Phenomenex Kinetex EVO C18 Prep Column
(100 Å, 5 µm, 21.5 mm X 250 mm)

Solvent A: H_2O + 0.1% (v/v) TFA
Solvent B: MeCN + 0.1% (v/v) TFA

LCMS Trace

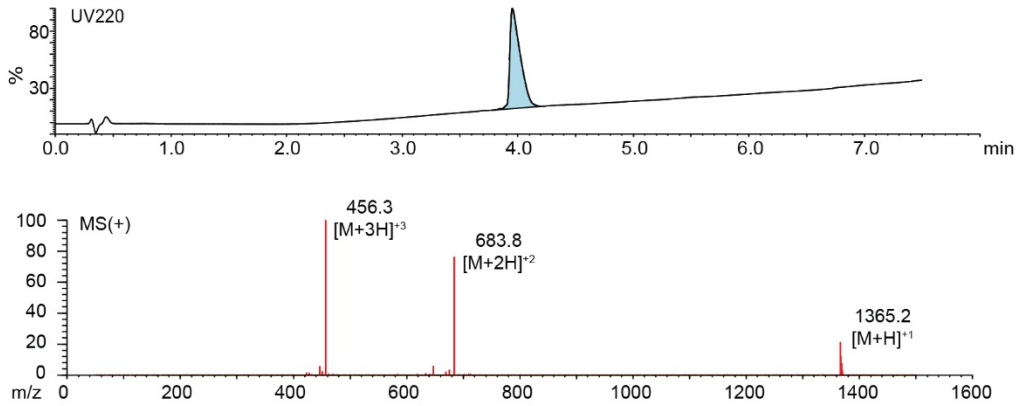

Appendix B-Figure 22. Synthesis summary of **7b**.

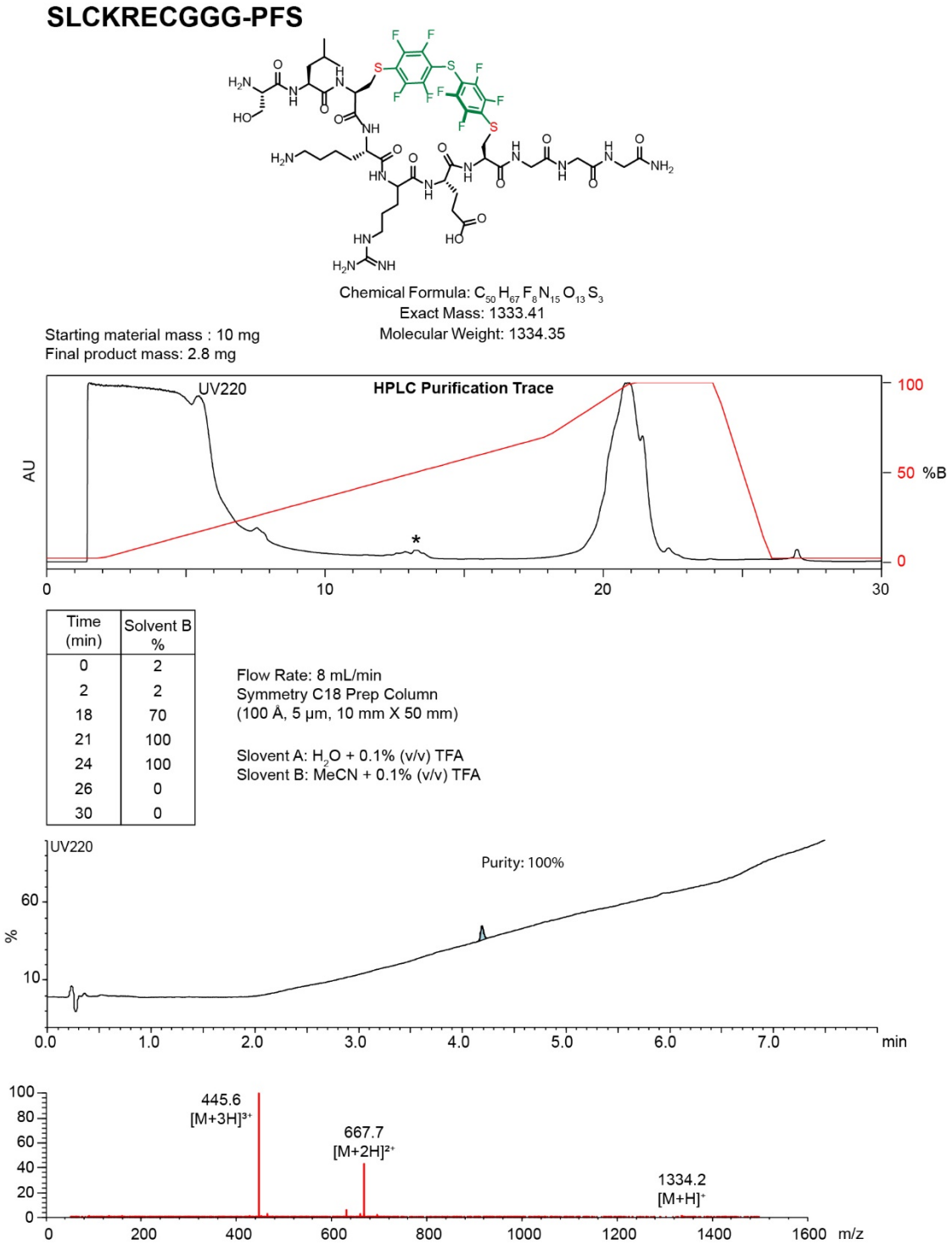

Appendix B-Figure 23. Synthesis summary of **7c**

STCQGECGGG-DFS

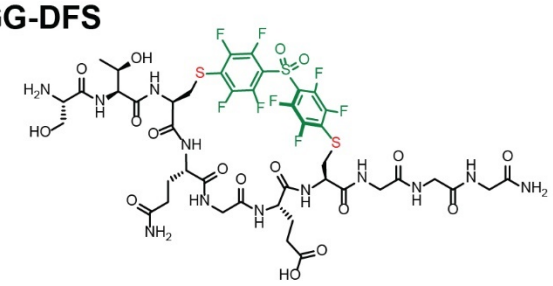

Chemical Formula: $C_{43}H_{50}F_8N_{12}O_{17}S_3$
Exact Mass: 1254.25
Molecular Weight: 1255.11

Starting material mass: 10 mg
Final product mass: 9.4 mg

HPLC Purification Trace

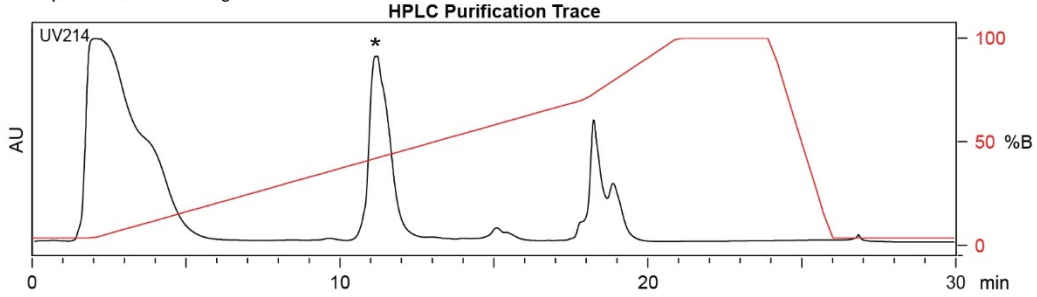

Time (min)	Solvent B (%)
0	2
2	5
21	70
23	100
26	100
29.5	2
30	2

Flow Rate: 13 mL / min
Phenomenex Kinetex EVO C18 Prep Column
(100 Å, 5 µm, 21.5 mm X 250 mm)

Solvent A: H_2O + 0.1% (v/v) TFA
Solvent B: MeCN + 0.1% (v/v) TFA

LCMS Trace

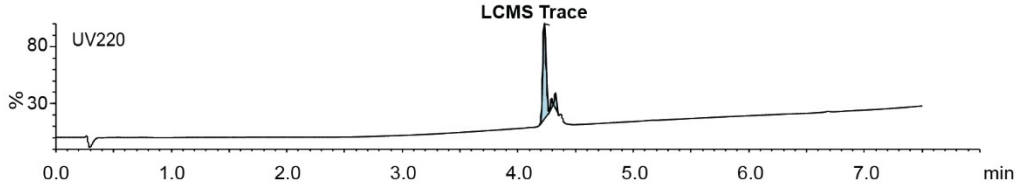

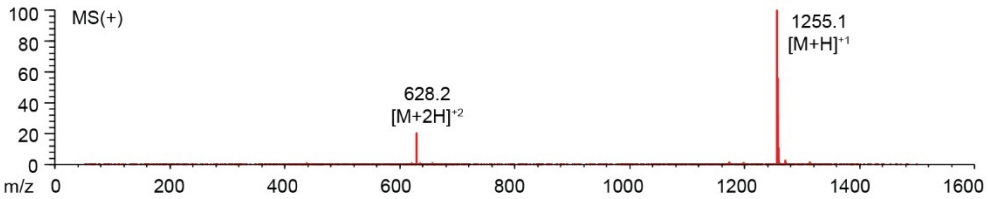

Appendix B-Figure 24. Synthesis summary of **8b**.

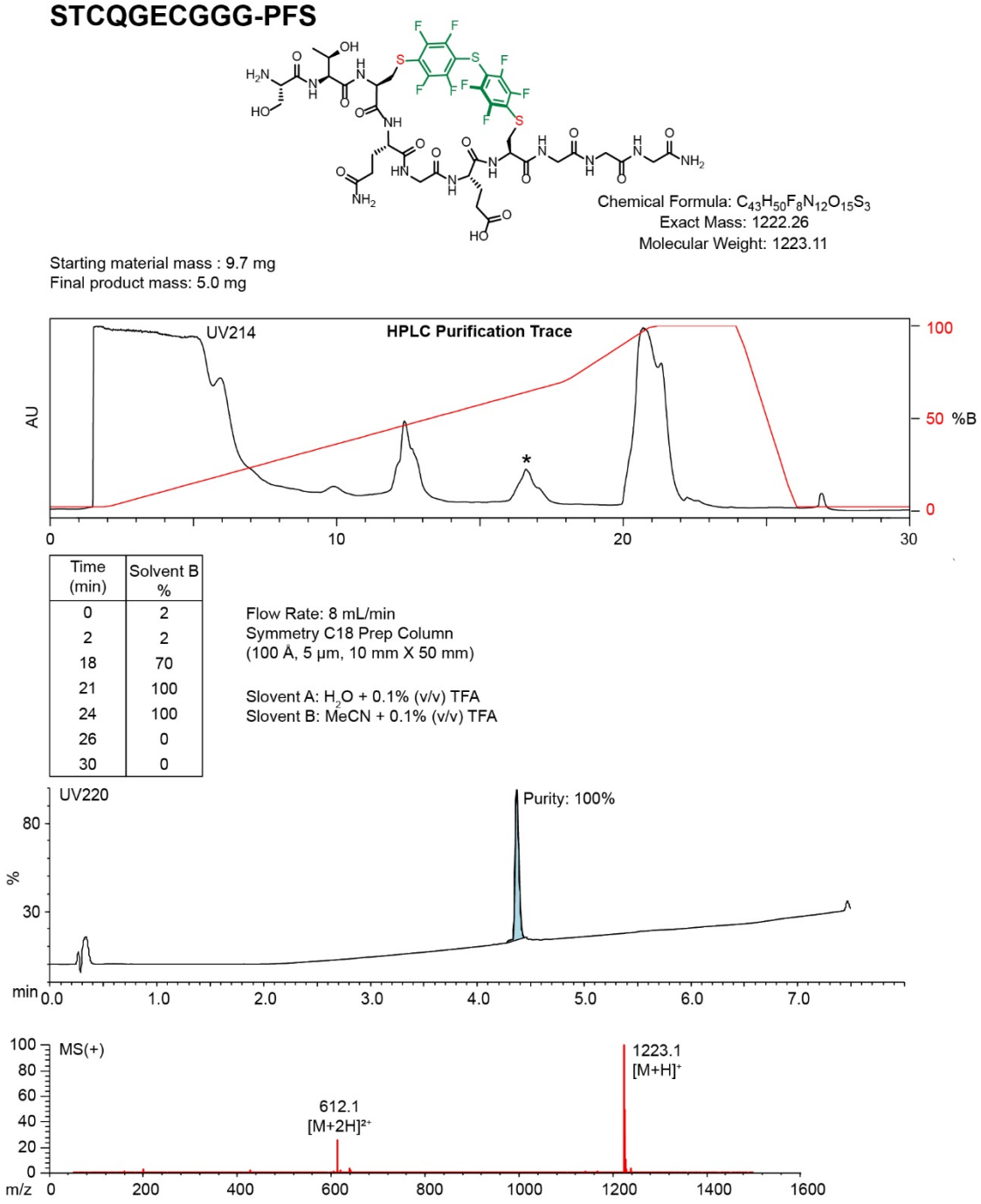

Appendix B-Figure 25. Synthesis summary of **8c**.

SICRFFCGGK-PFS-Bodipy

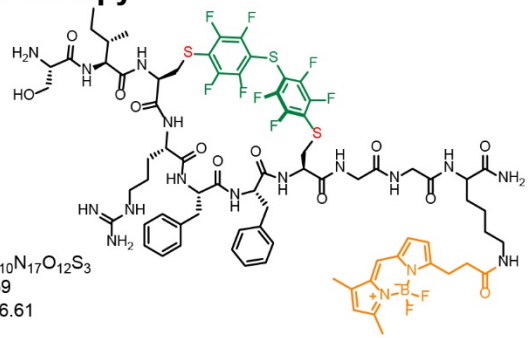

Chemical Formula: $C_{75}H_{88}BF_{10}N_{17}O_{12}S_3$
Exact Mass: 1715.59
Molecular Weight: 1716.61

Starting material mass : 1.2 mg
Final product mass: >0.1 mg

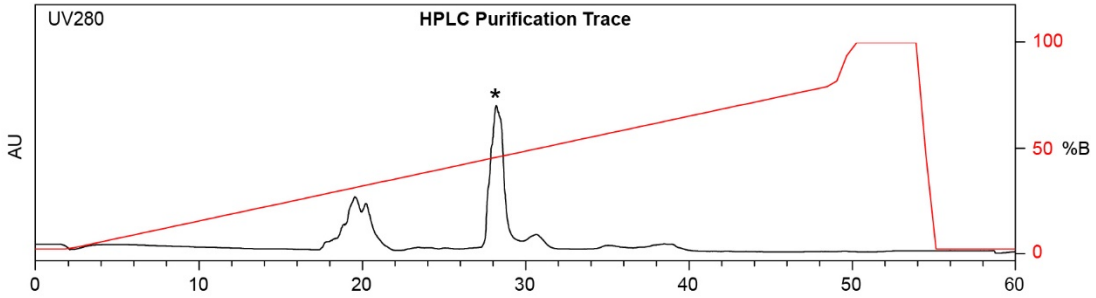

Time (min)	Solvent B %
0	2
2	2
49	80
50	100
54	100
55	2
60	2

Flow Rate: 8 mL/min
Symmetry C18 Prep Column
(100 Å, 5 µm, 10 mm X 50 mm)

Slovent A: H_2O + 0.1% (v/v) TFA
Slovent B: MeCN + 0.1% (v/v) TFA

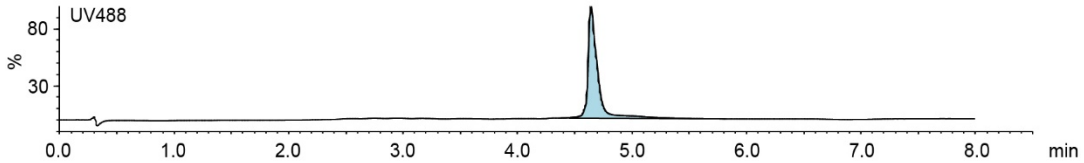

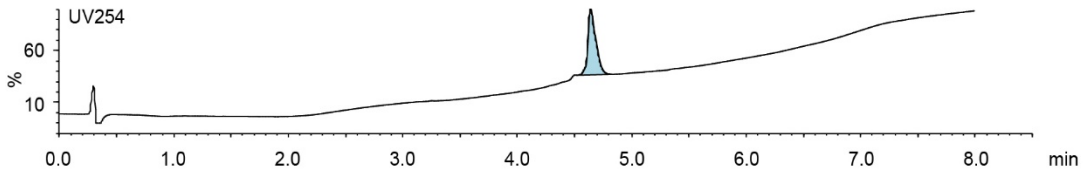

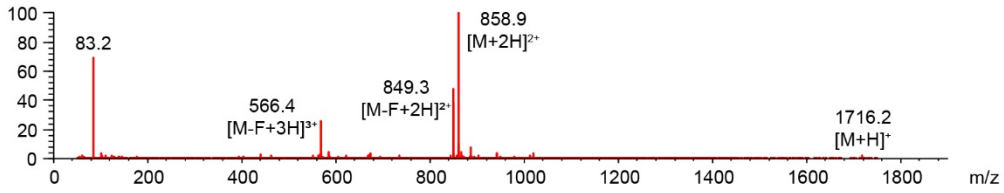

Synthesis summary of C-terminus labeled **5c**-BODIPY**.**

SICRFFCGGG-PFS-BODIPY

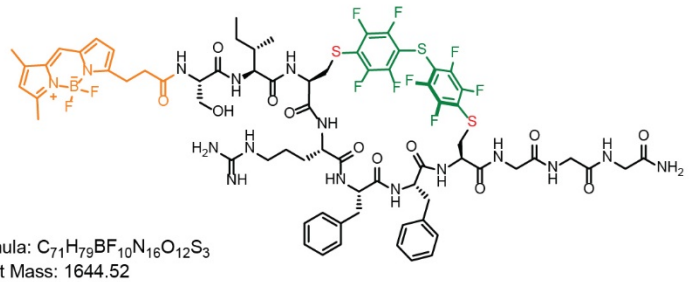

Chemical Formula: $C_{71}H_{79}BF_{10}N_{16}O_{12}S_3$
Exact Mass: 1644.52
Molecular Weight: 1645.49

Starting material mass: 1.6 mg
Final product mass: 1 mg

HPLC Purification Trace

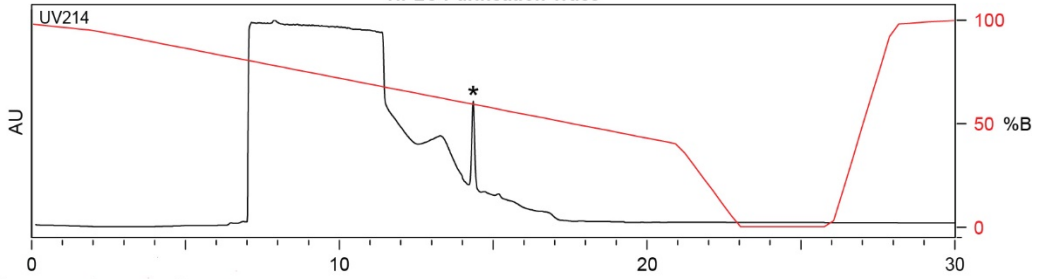

Time (min)	Solvent B (%)
0	98
2	95
21	40
23	0
26	0
28	98
30	98

Flow Rate: 8 mL / min
XBridge BEH Amide OBD Prep Column
(130 Å, 5 µm, 19 mm X 250 mm)

Slovent A: H_2O + 0.1% (v/v) TFA
Slovent B: MeCN + 0.1% (v/v) TFA

LCMS Trace

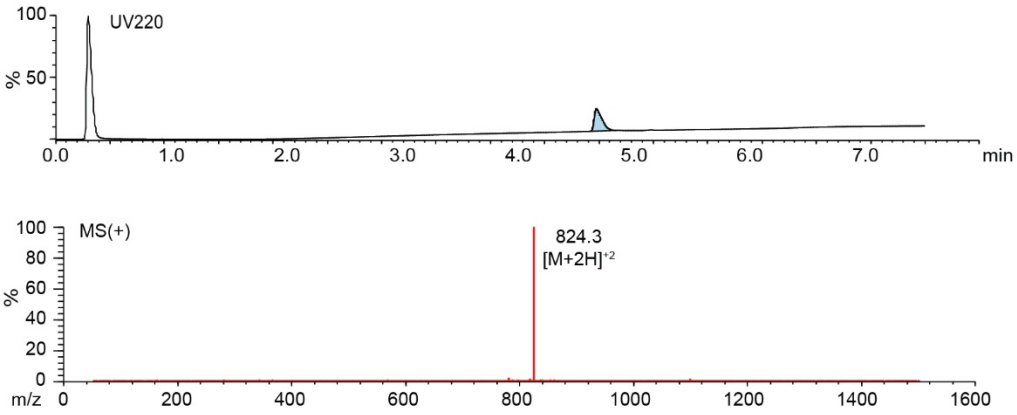

Appendix B-Figure 26. Synthesis summary of N-terminus labeled **5d**-BODIPY

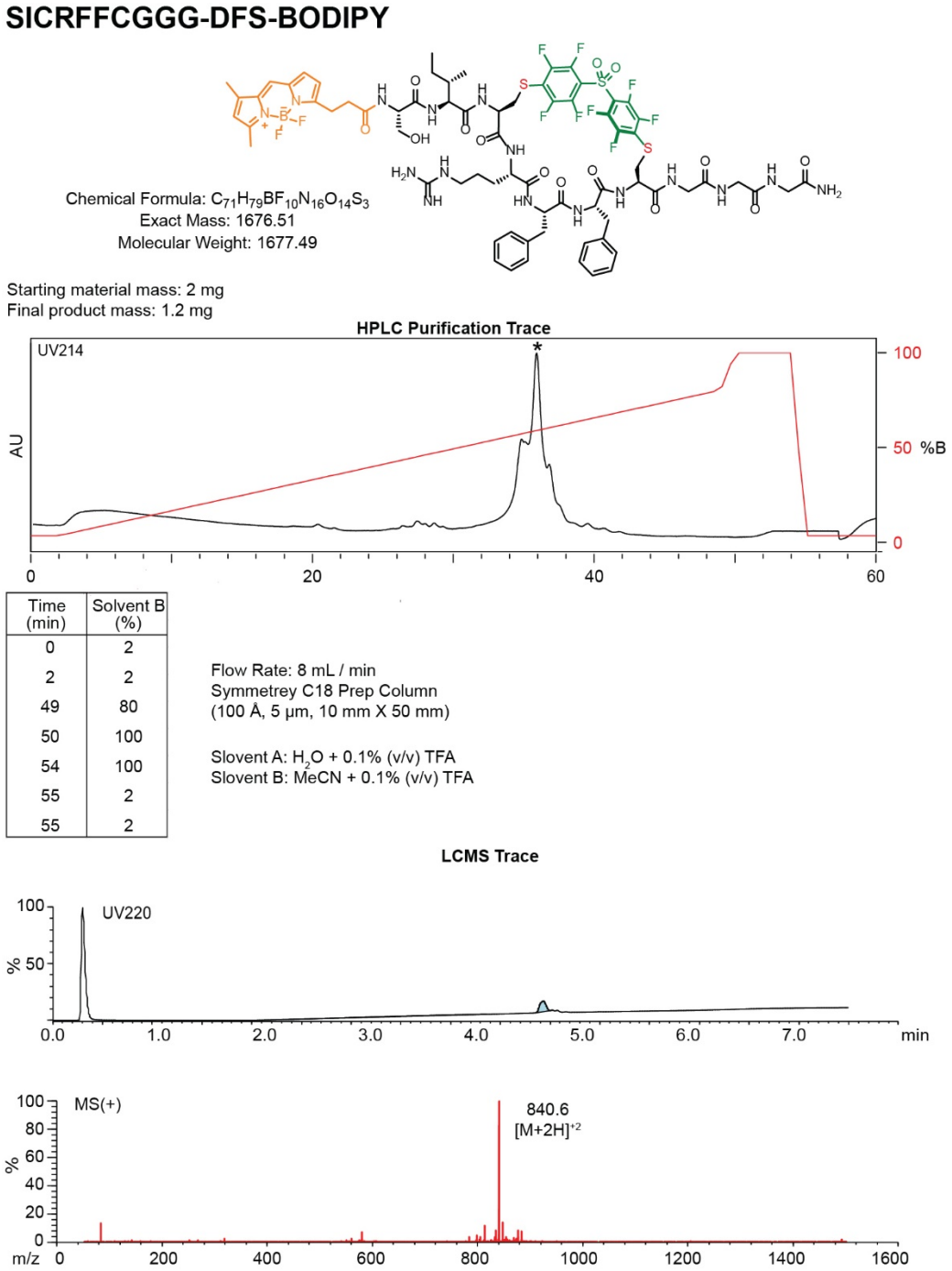

Appendix B-Figure 27. Synthesis summary of N-terminus labeled **5b**-BODIPY

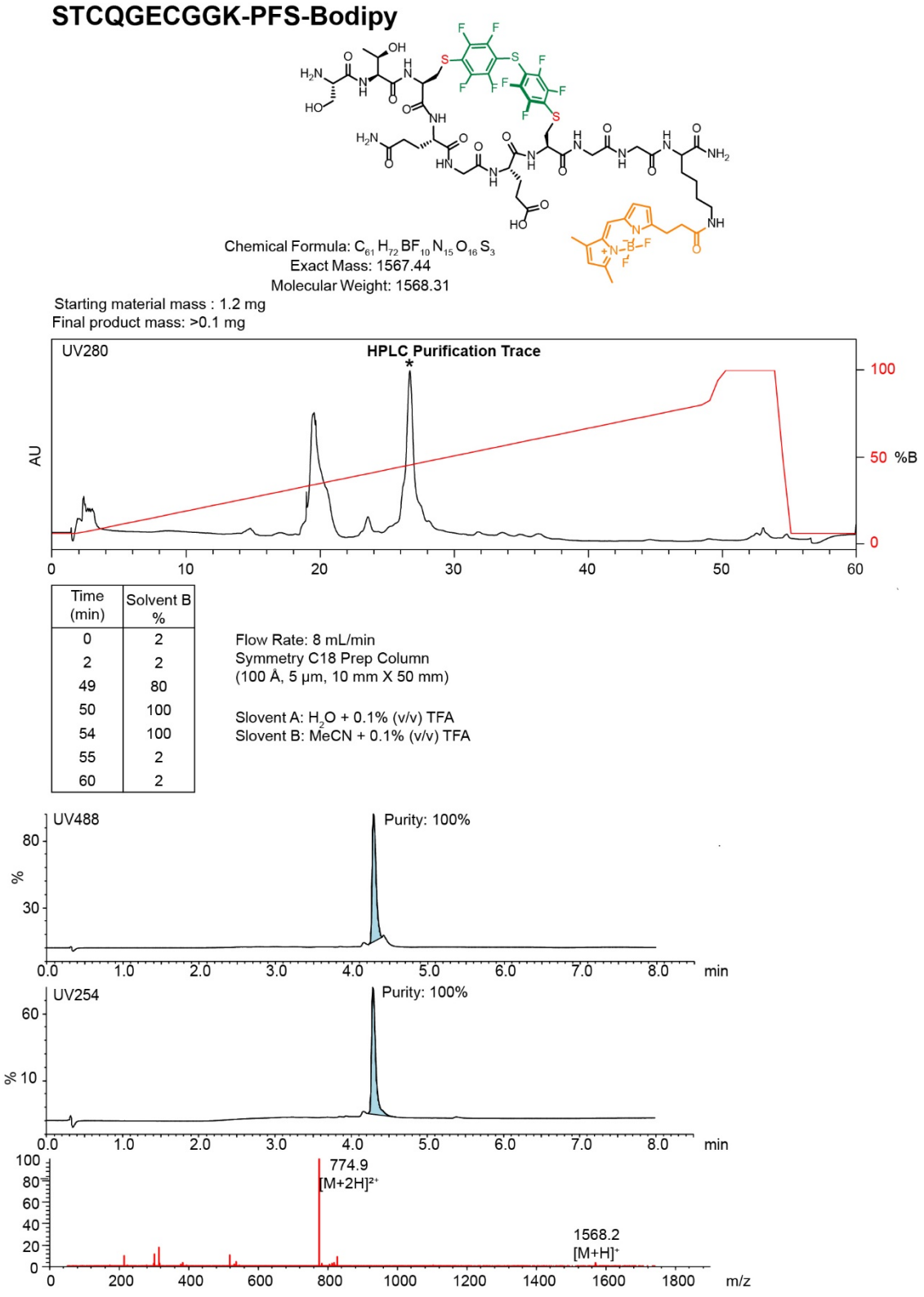

Appendix B-Figure 28. Synthesis summary of C-terminus labeled **8c**-BODIPY.

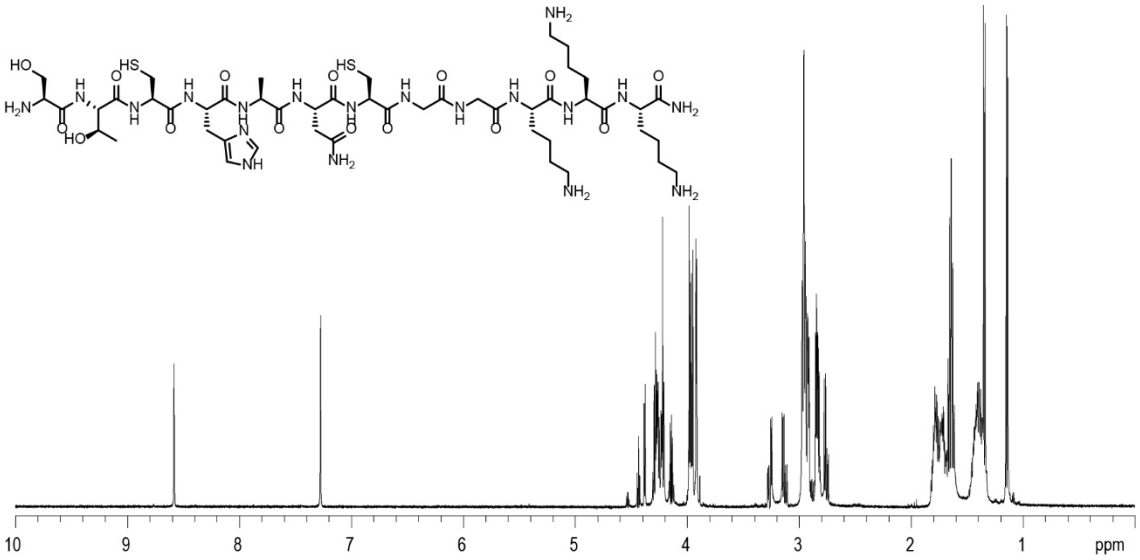

Appendix B-Figure 29. STCHANCGGKKK ^{1}H NMR Spectra in D_2O, 600

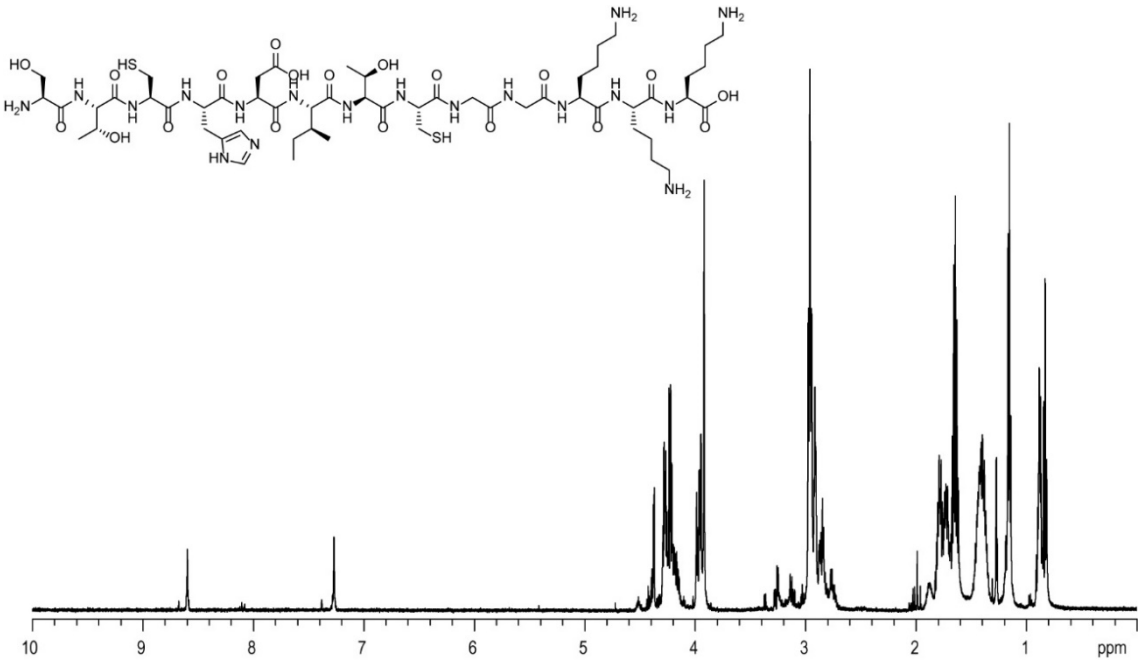

Appendix B-Figure 30. STCHDITCGGKKK ^{1}H NMR Spectra in D_2O, 600

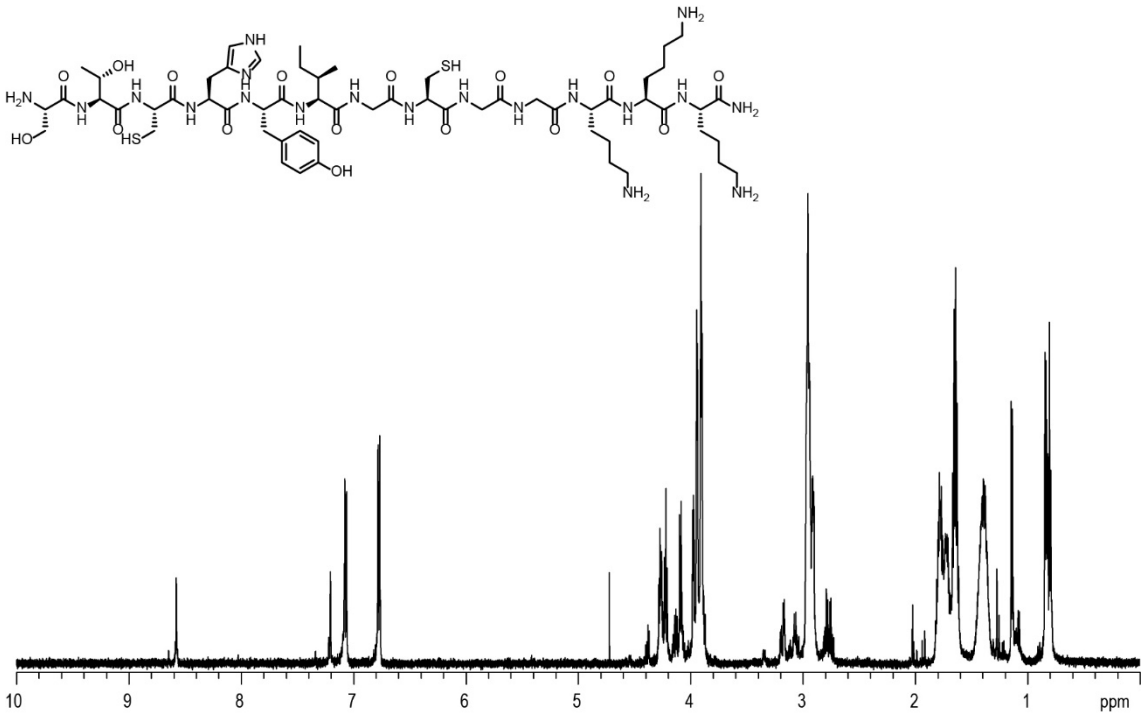

Appendix B-Figure 31. STCHYIGCGGKKK ^{1}H NMR Spectra in D_2O, 600

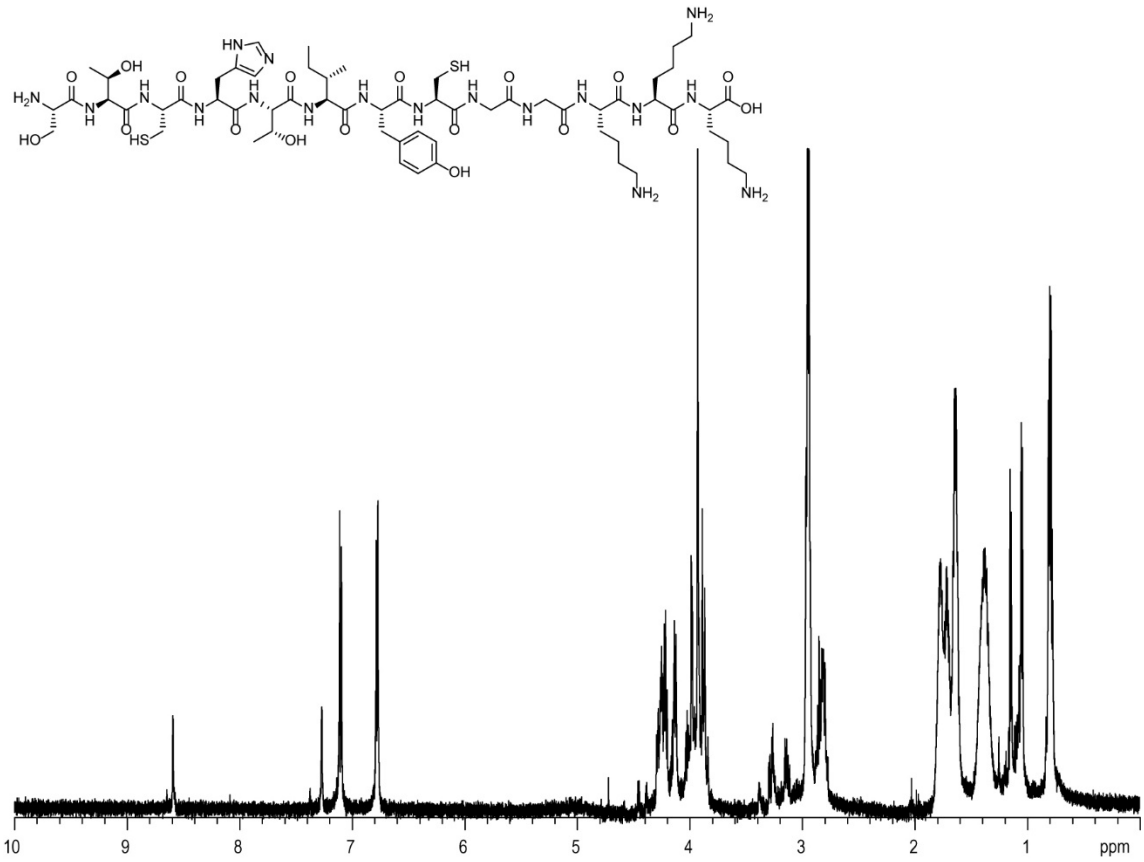

Appendix B-Figure 32. STCHTIYCGGKKK ^{1}H NMR Spectra in D_2O, 600

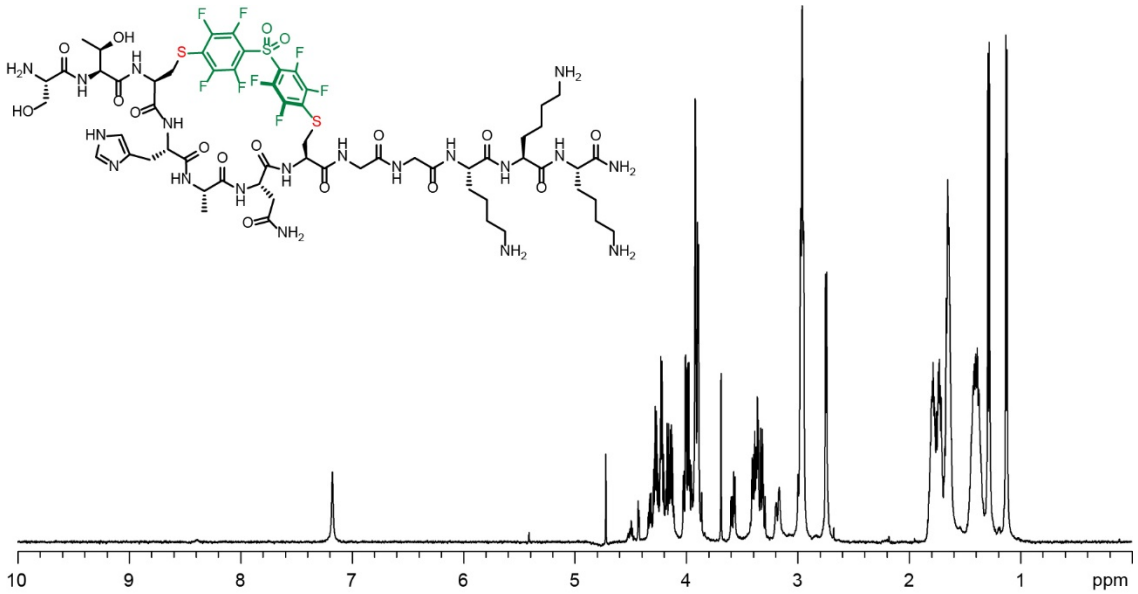

Appendix B-Figure 33. DFS-STCHANCGGKKK ^{1}H NMR Spectra in D_2O, 600

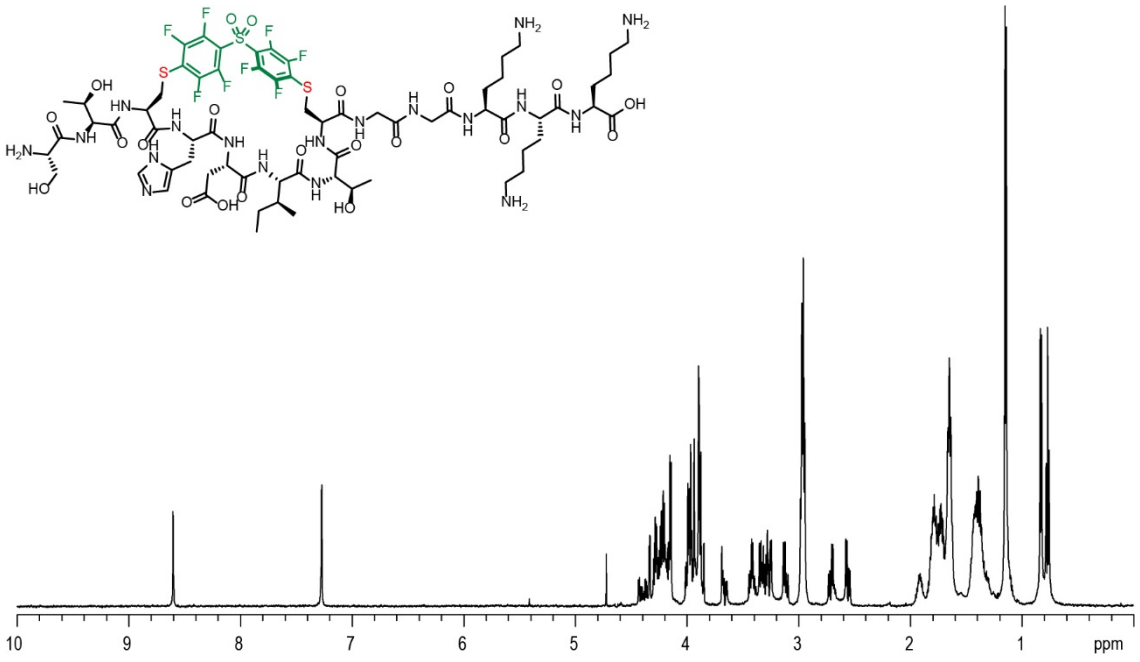

Appendix B-Figure 34. DFS-STCHDITCGGKKK ^{1}H NMR Spectra in D_2O, 600

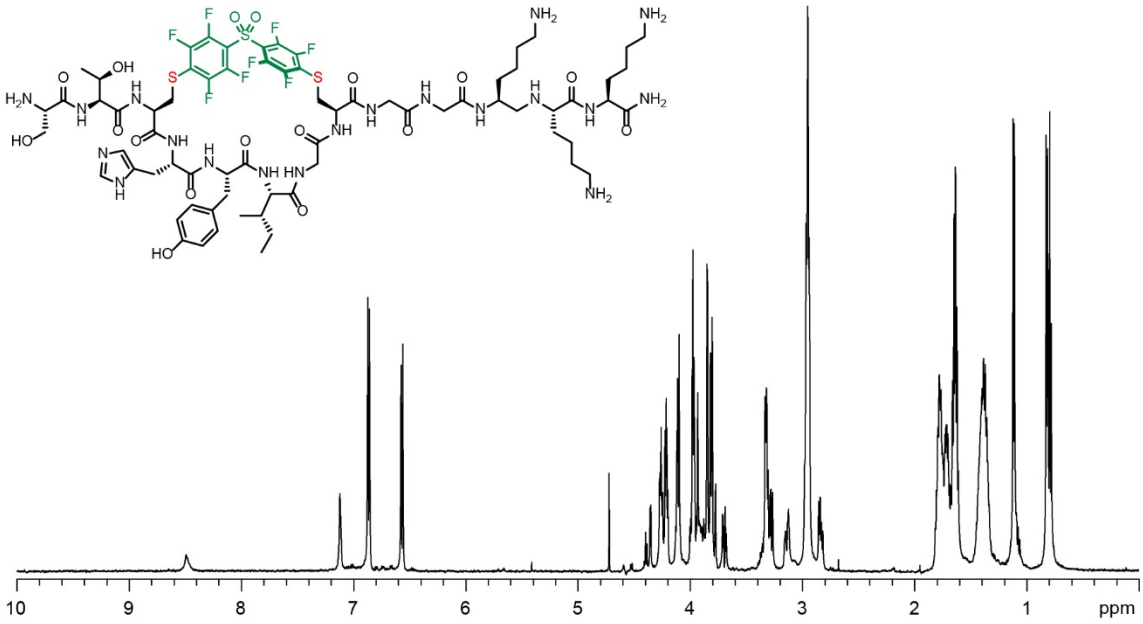

Appendix B-Figure 35. DFS-STCHYIGCGGKKK ^{1}H NMR Spectra in D_2O, 600

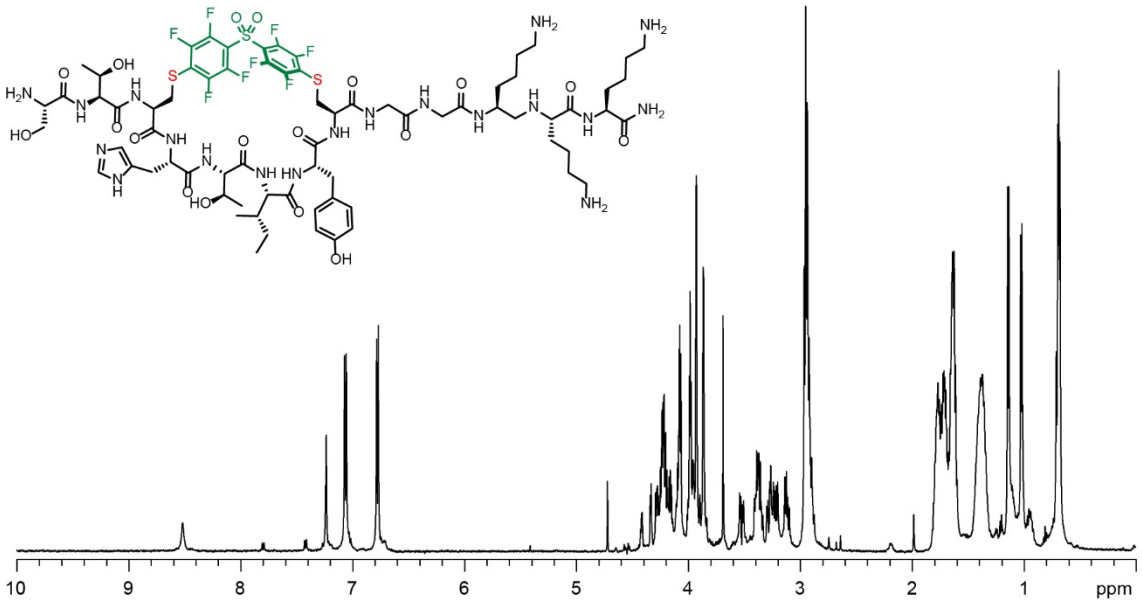

Appendix B-Figure 36. DFS-STCHTIYCGGKKK ^{1}H NMR Spectra in D_2O, 600

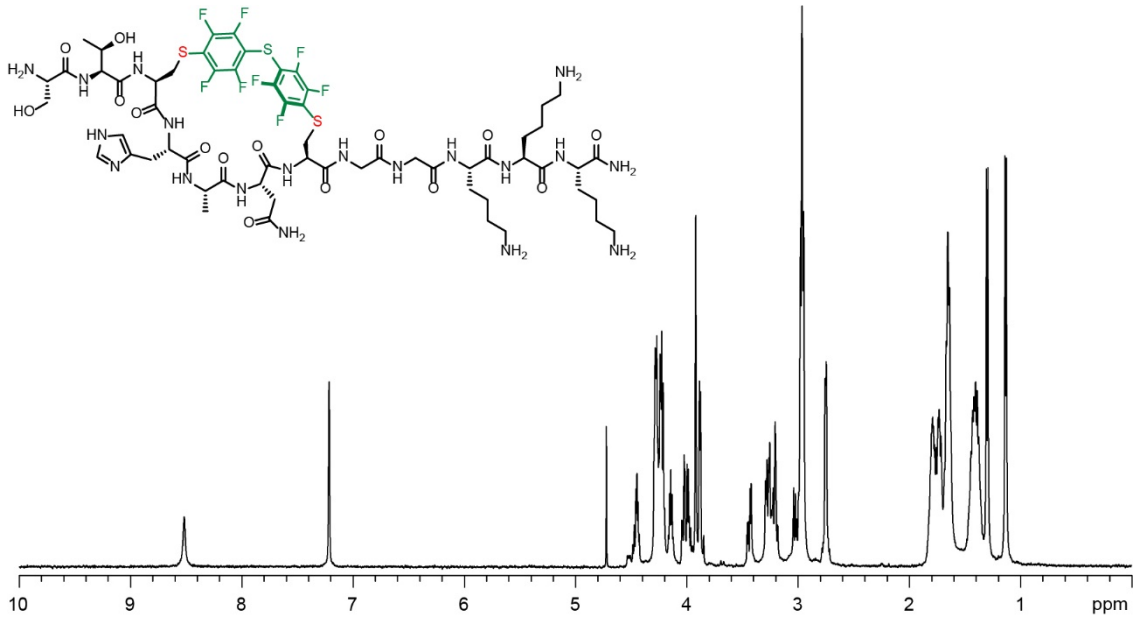

Appendix B-Figure 37. PFS stapled STCHANCGGKKK ^{1}H NMR Spectra in D_2O, 600

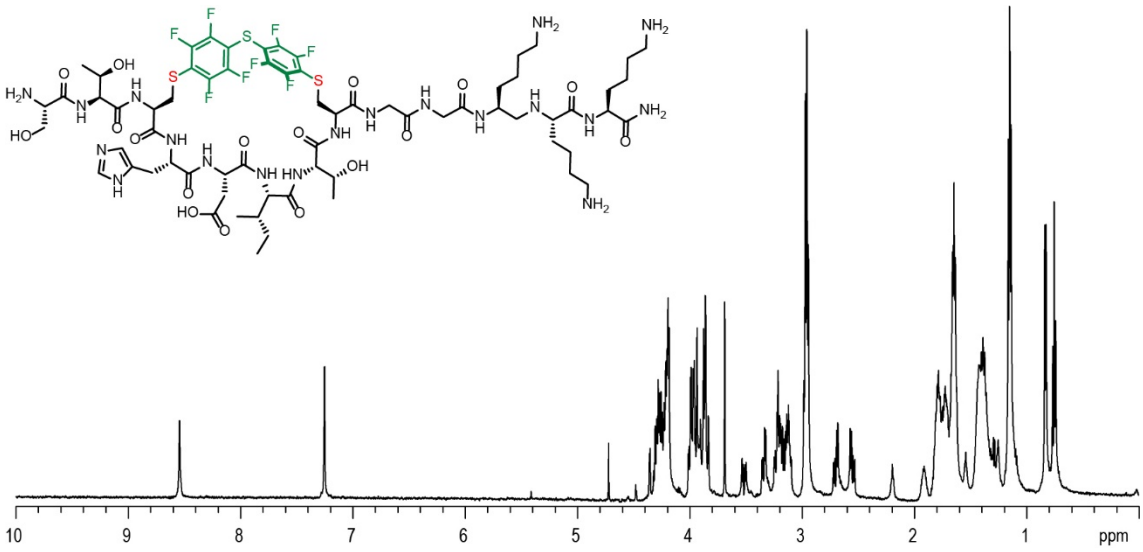

Appendix B-Figure 38. PFS-STCHDITCGGKKK ^{1}H NMR Spectra in D_2O, 600

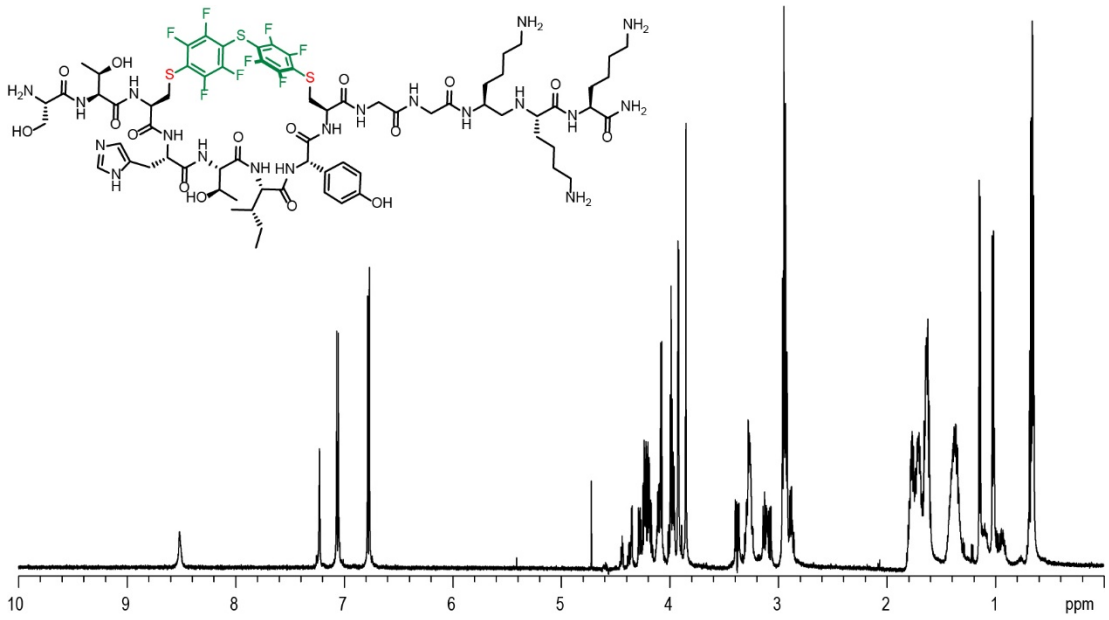

Appendix B-Figure 39. PFS-STCHTIYCGGKKK ^{1}H NMR Spectra in D_2O, 600

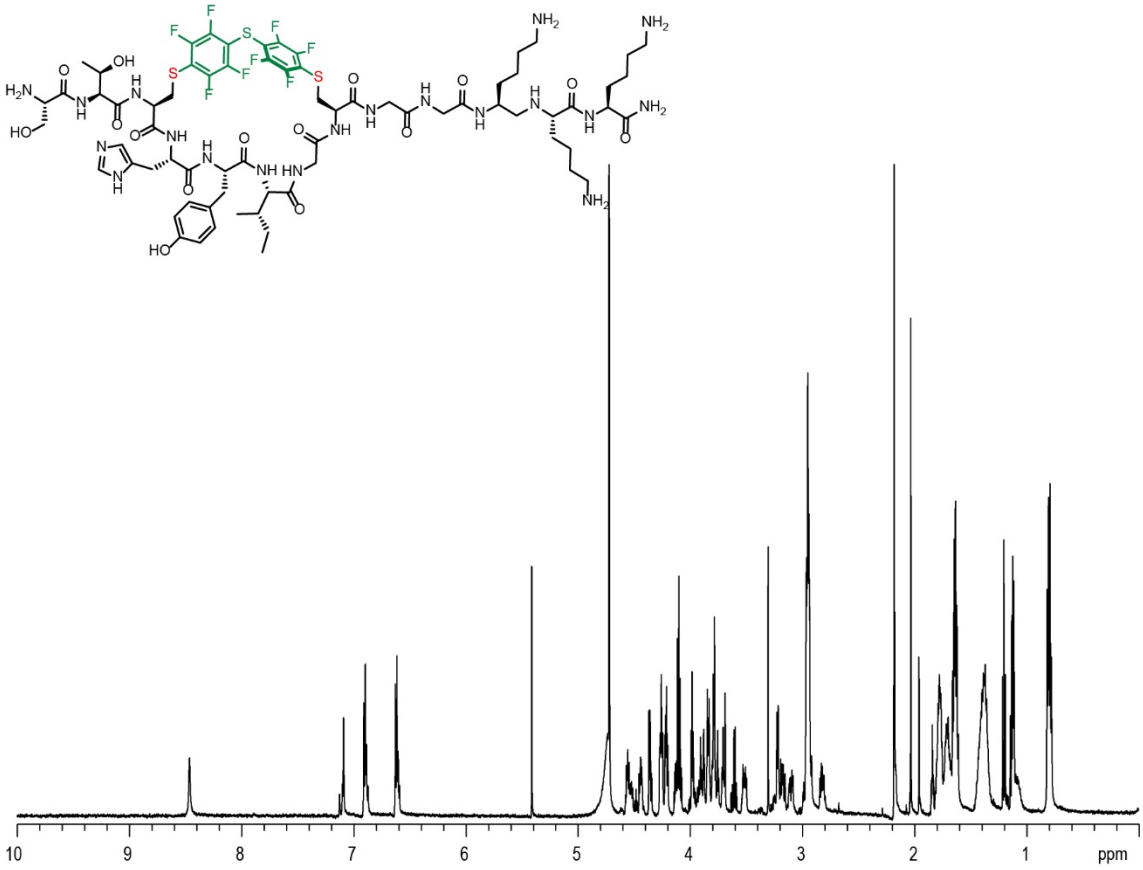

Appendix B-Figure 40. PFS stapled STCHYIGCGGKKK ^{1}H NMR Spectra in D_2O, 600

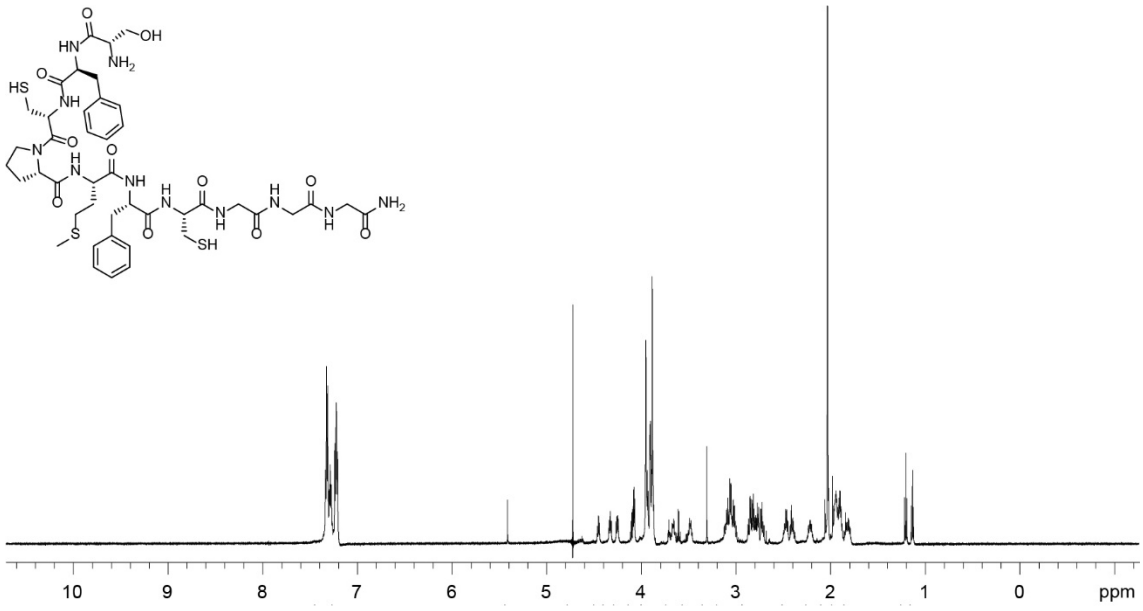

Appendix B-Figure 41. SFCPMFCGGG ^{1}H NMR Spectra in D_2O, 600

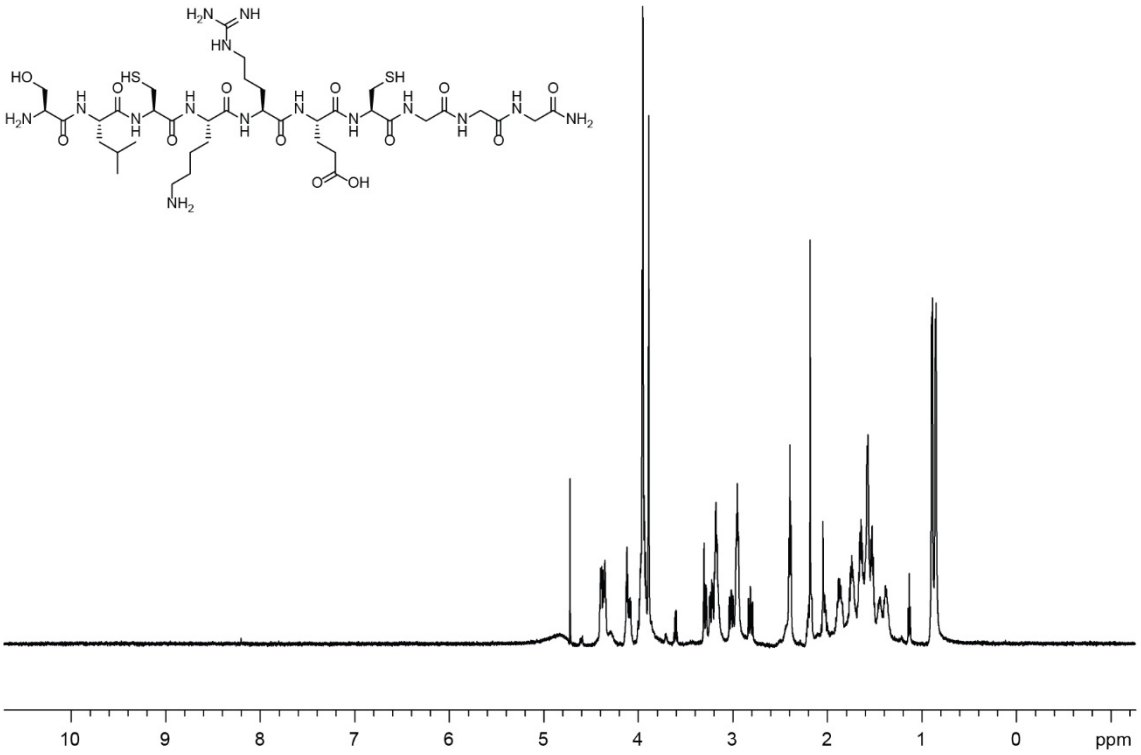

Appendix B-Figure 42. SLCKRECGGG ^{1}H NMR Spectra in D_2O, 600

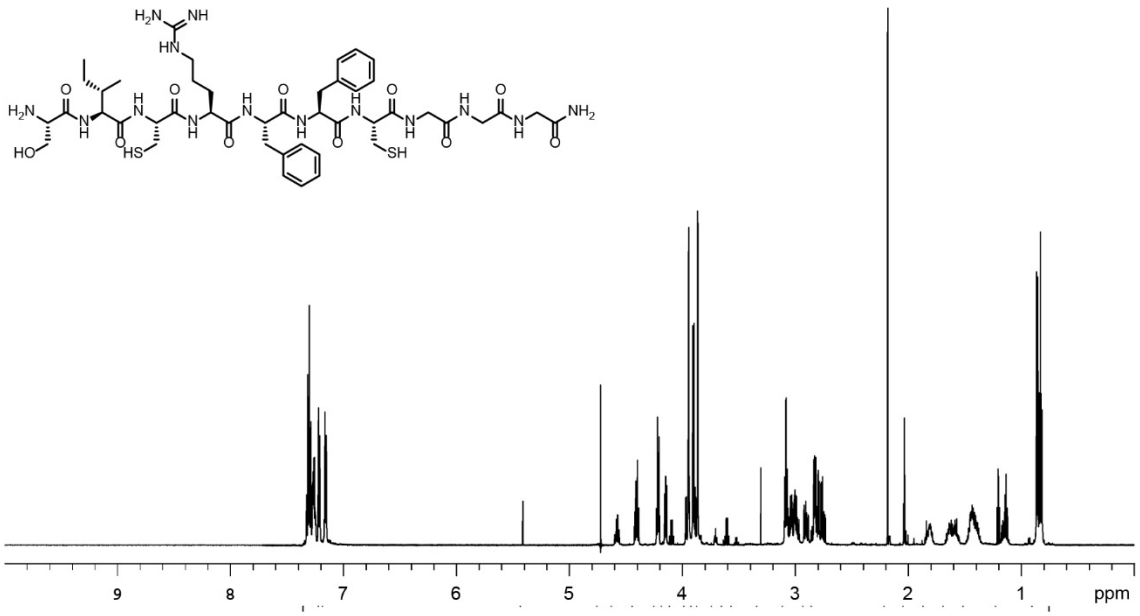

Appendix B-Figure 43. SICRFFCGGG ^{1}H NMR Spectra in D_2O, 600

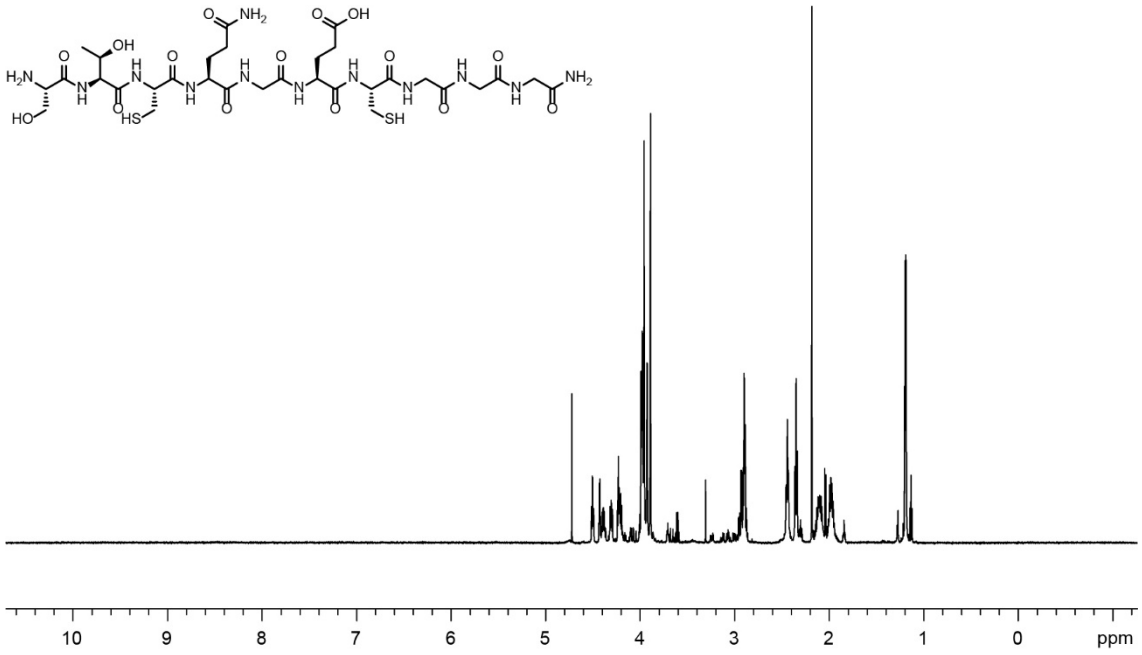

Appendix B-Figure 44. STCQGECGGG ^{1}H NMR Spectra in D_2O, 600

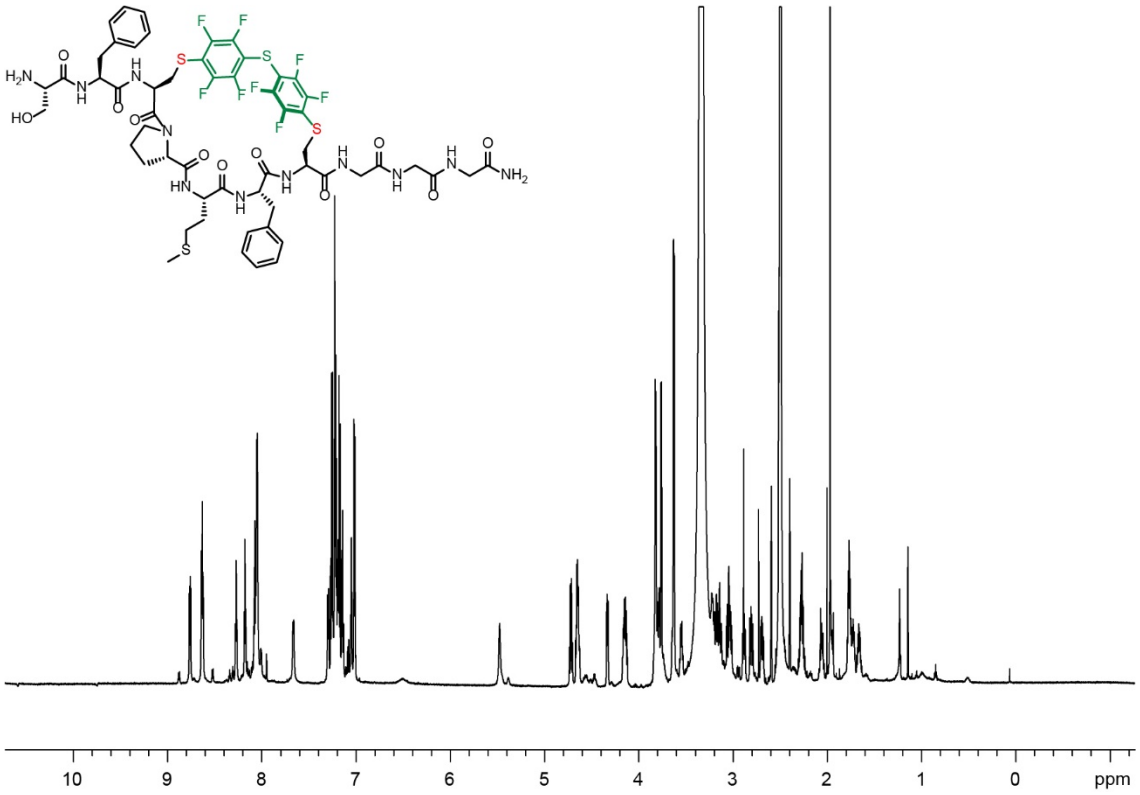

Appendix B-Figure 45. PFS stapled SFCPMFCGGG ^{1}H NMR Spectra in DMSO, 700

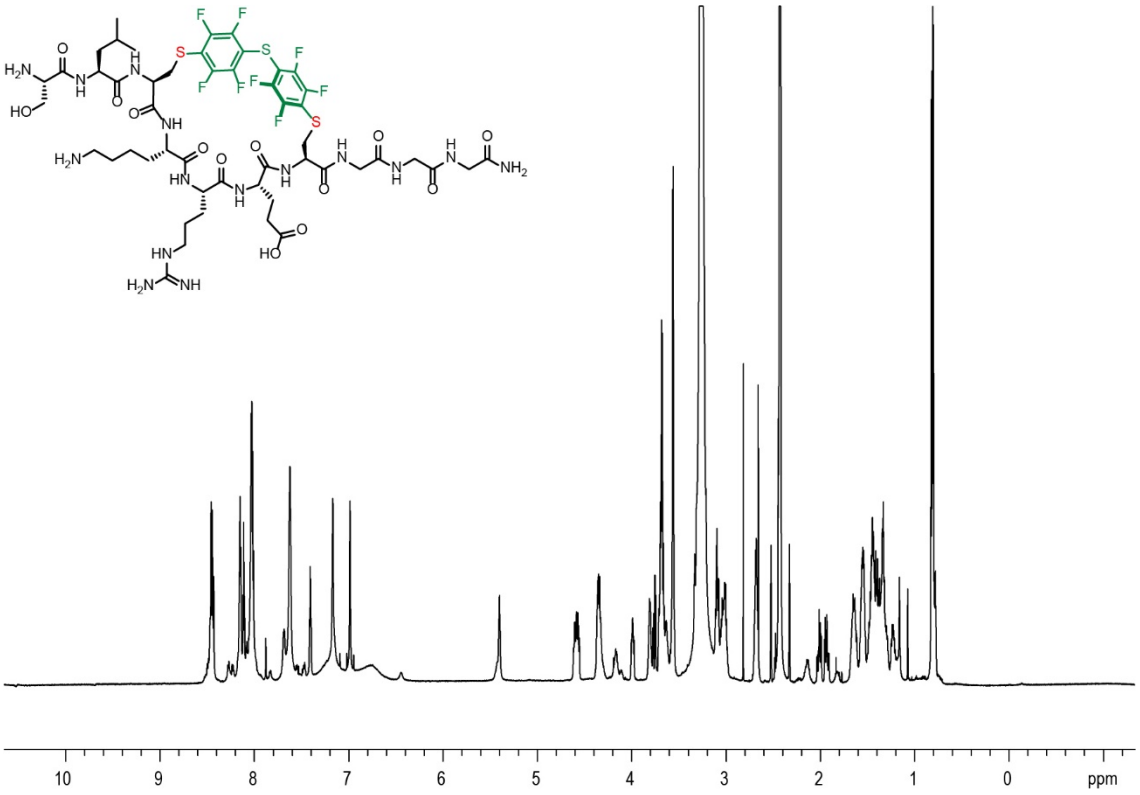

Appendix B-Figure 46. PFS stapled SLCKRECGGG ^{1}H NMR Spectra in DMSO, 700

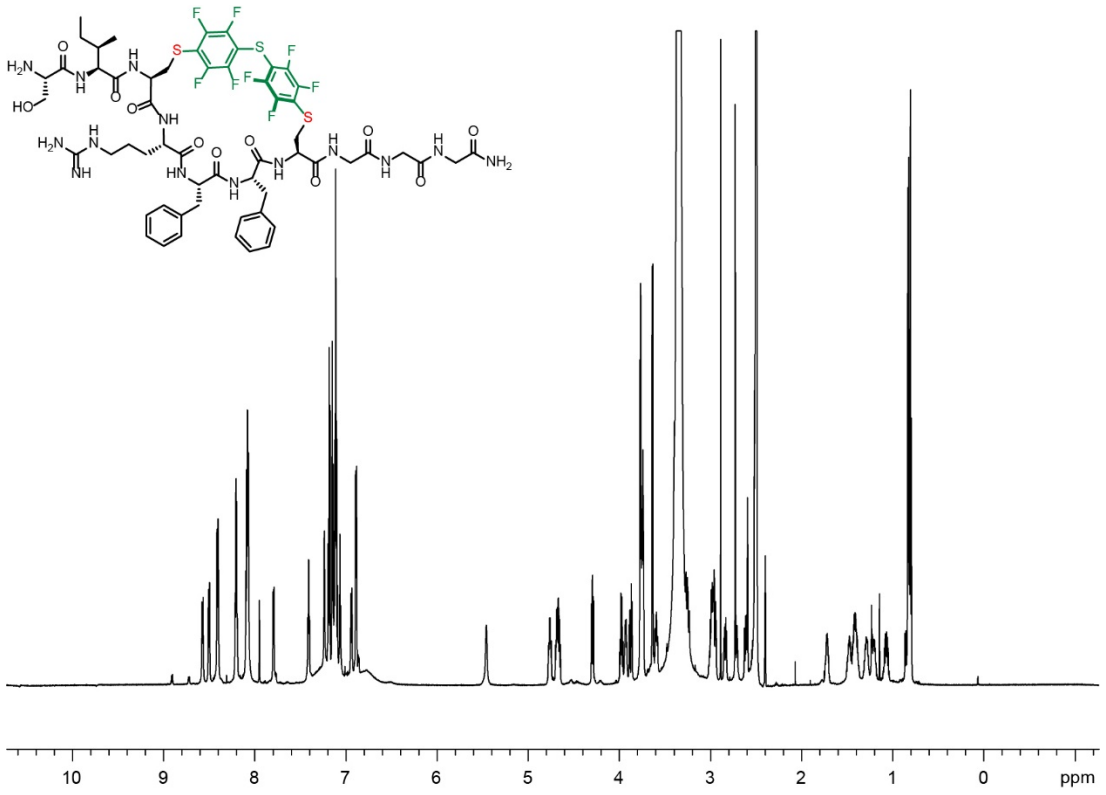

Appendix B-Figure 47. PFS stapled SICRFFCGGG ^{1}H NMR Spectra in DMSO, 700